Geotechnical Investigations of

Wind Turbine Foundations Using

Multichannel Analysis of Surface Waves (MASW)

A Thesis

Submitted in partial fulfillment of the requirements of the degree

of

Master of Science in Engineering Geology

at the

University of Canterbury

by

Malcolm Andrew Hicks

UNIVERSITY OF CANTERBURY

2011

Frontispiece:

Te Rere Hau Windfarm, Palmerston North, New Zealand

Abstract:

The geophysical technique known as Multichannel Analysis of Surface Waves, or MASW (Park et al., 1999) is a relatively new seismic characterisation method which utilises Rayleigh waves propagation. With MASW, the frequency dependent, planar travelling Rayleigh waves are created by a seismic source and then measured by an array of geophone receivers. The recorded data is used to image characteristics of the subsurface.

This thesis explains how MASW was used as a geotechnical investigation tool on windfarms in the lower North Island, New Zealand, to determine the stiffness of the subsurface at each wind turbine site. Shear-wave velocity (V_S) profiles at each site were determined through the processing of the MASW data, which were then used to determine physical properties of the underlying, weathered greywacke.

The primary research site, the Te Rere Hau Windfarm in the Tararua Ranges of the North Island, is situated within the Esk Head Belt of Torlesse greywacke (Lee & Begg, 2002). Due to the high level of tectonic activity in the area, along with the high rates of weathering, the greywacke material onsite is highly fractured and weathering grades vary significantly, both vertically and laterally. MASW was performed to characterise the physical properties at each turbine site through the weathering profile. The final dataset included 1-dimensional MASW shear-wave evaluations from 100 turbine sites. In addition, Poisson's ratio and density values were characterised through the weathering profile for the weathered greywacke. During the geotechnical foundation design at the Te Rere Hau Windfarm site, a method of converting shear-wave velocity profiles was utilised. MASW surveying was used to determine V_S profiles with depth, which were converted to elastic modulus profiles, with the input parameters of Poisson's ratio and density.

This study focuses on refining and improving the current method used for calculating elastic modulus values from shear-wave velocities, primarily by improving the accuracy of the input parameters used in the calculation.

Through the analysis of both geotechnical and geophysical data, the significant influence of overburden pressure, or depth, on the shear wave velocity was identified. Through each of the weathering grades, there was a non-linear increase in shear wave velocity with depth. This highlights the need for overburden pressure conditions to be considered before assigning characteristic shear wave velocity values to different lithologies.

Further to the dataset analysis of geotechnical and geophysical information, a multiple variant non-linear regression analysis was performed on the three variables of shear wave velocity, depth and weathering grade. This produced a predictive equation for determining shear wave velocity within the Esk Head belt 'greywacke' when depth and weathering data are known. If the insitu geological conditions are not comparable to that of the windfarm sites in this study, a set of guidelines have been developed, detailing the most efficient and cost effective method of using MASW surveying to calculate the elastic modulus through the depth profile of an investigation site.

Acknowledgements:

This report takes the form of a thesis, which was supported by the Mason Trust, for which I am thankful. I wish to sincerely thank my thesis supervisors Mr David Bell, Senior Lecturer at the University of Canterbury, Dr Michael Finnemore, Research Associate at the University of Canterbury and Director of Southern Geophysical Ltd, and Mr Dominic Mahoney, Geotechnical Engineer at Aurecon New Zealand Ltd, for their assistance in producing this manuscript. I would specifically like to thank Dr Michael Finnemore and Dominic Mahoney for introducing me to this project and Dr Michael Finnemore for assisting with the collection and processing of data.

I would also like to thank Murray James at New Zealand Windfarms Ltd for allowing me access to the Te Rere Hau Windfarm to perform testing and collect data, along with allowing access to geotechnical investigation information and reports from the windfarm site. In addition, I would again like to thank Dominic Mahoney, lead geotechnical engineer for the Te Rere Hau Windfarm development, for his expert advice and onsite experience.

I would like to thank Mark Omer of Mighty River Power for arranging site access and transporting me around the Turitea Windfarm site, along with assisting me while I performed testing. Your willingness to help and onsite knowledge was much appreciated. In addition, I would also like to thank Mighty River Power for allowing me access to the geotechnical investigation information from the Turitea Windfarm site.

I would like to thank Ewen Robertson of Meridian Energy for arranging access to the West Wind Windfarm, and for allowing me access to the geotechnical investigation information from the site. Mr Alexei Murashev provided exceptional help in my project development and had a critical input in the initial stages of my thesis. He challenged a number of my initial objectives and helped me develop my ideas and focus the scope of my thesis.

The University of Canterbury staff and students were a significant help during my postgraduate studies in Christchurch. I would like to thank Stephen Brown for his help in assisting in my research by performing the XRD analysis on my greywacke samples. Dr James Degnan of the University of Canterbury Maths and Statistics Department was more than willing to give his time to help me with statistical analysis, for which I am very grateful. Brendan Duffy also played a significant role in the initial stages of my thesis, drawing from his expertise using MASW and his recent experience completing his own master's thesis. His patience was much appreciated as

I began to develop an understanding of both research methods and MASW surveying. I would also very much like to thank Allison Roberts and Janet Warburton for their ongoing assistance with all administrative issues during my postgraduate degree. Their ever helpful and understanding approach was always appreciated. In addition, Dr Anekant Wandres was always willing to help with any of my GIS, topography or geological mapping needs, for which I am grateful.

Ryan Nicol, Rob Hunter and the sporadic presence of Hayden McKenzie kept life in our office balanced. It was nice to be reminded from time to time that's others were experiencing similar setbacks, and also breakthroughs as I was. A number of my close friends and training partners have helped me keep the research and life balance in check, whether it was out surfing around Banks Peninsula, or hard training sessions around Hagley Park and in the Port Hills.

Above all, I would finally I would like to thank my parents for encouraging me through my years of both schooling and tertiary study. Without the support of my parents, Kelvin and Marion Hicks, both emotional and financial, I would not have been able to complete this study, or have achieved what I have today.

Table of Contents

FRONTISPIECE……I

ABSTRACT……II

ACKNOWLEDGEMENTS……III

TABLE OF CONTENTS……IV

LIST OF FIGURES……V

LIST OF TABLES……VI

Chapter 1: Introduction……1

1.1 Project Background:……1

1.2 Te Rere Hau Windfarm Project:……3

1.3 Objectives:……4

1.4 Windfarm study sites:……5

1.5 Geological and Tectonic Setting of the Lower North Island:……7

1.6 Multichannel Analysis of Surface Waves:……12

1.7 Determining the elastic condition of weathered 'greywacke':……14

1.8 Thesis Format:……15

Chapter 2: Properties of 'Greywacke' Rock……17

2.1 Introduction:……17

2.2 General 'Greywacke' Lithology:……17

2.2.1 'Greywacke' Lithology……18

2.2.2 'Greywacke' rock mass structure……19

2.2.3 'Greywacke' rock mass strength……20

2.2.4 Summary of 'greywacke' characteristics and properties……20

2.3 In-situ nature of Esk-Head belt 'greywacke':……21

2.4 Weathering:……21

2.4.1 Weathering processes 21
2.4.2 Weathering classification schemes in literature 24
2.4.3 Weathering classification 27
2.4.4 Weathering of the Esk Head belt 'greywacke' 28
2.5 Physical and mechanical properties of 'Greywacke': 32
2.6 Synthesis: 34
Chapter 3: Geotechnical and Engineering Geological Investigations: 35
3.1 Introduction: 35
3.2 Site Engineering Geology: 35
3.2.1 Rock Mass Characterisation 35
3.2.2 Geotechnical classification 37
3.2.3 Face logs 37
3.2.4 Test pit logs 39
3.2.5 Logging of drilled mono-piles 40
3.2.6 Engineering Geological Trends 42
3.3 Rock density characterisation: 45
3.3.1 Introduction 45
3.3.2 Methods 46
3.3.3 Results 48
3.4 Poisson's ratio characterisation: 52
3.4.1 Introduction 52
3.4.2 Method 54
3.4.3 Results 56
3.5 X-Ray Diffraction: 60
3.6 Synthesis: 61
Chapter 4: Surface Wave Velocities: Interpretation and Techniques 62
4.1 Introduction: 62

4.2 Body waves: 62
4.2.1 Compression waves 63
4.2.2 Shear waves 63
4.3 Surface waves: 64
4.3.1 Types of surface waves 64
4.3.2 Rayleigh waves 65
4.4 Dispersion of Surface Waves: 66
4.5 Factors Affecting Surface Wave Velocity and their dispersive characteristics: 67
4.5.1 Determinants of seismic velocity 67
4.5.2 Effects of Poisson's Ratio 71
4.6 Surface wave propagation in anisotropic/ inhomogeneous media: 73
4.7 1D Surface wave inversion limitations: 74
4.8 Synthesis: 75
Chapter 5 MASW Investigations and Data Analysis: 76
5.1 Introduction: 76
5.2 Data collection: 77
5.3 Acquisition Parameters: 78
5.3.1 Survey procedures 78
5.3.2 Source/Receiver Characteristics 80
5.4 Dispersion Curve Extraction: 82
5.5 Surface Wave Inversion: 85
5.6 Results: 87
5.7 Synthesis: 94
Chapter 6 Dataset Analysis and Review: 96
6.1 Introduction: 96
6.2 Weathering grade and V_S variations across the Te Rere Hau Windfarm site: 96
6.3 Combined Analysis of Weathering, Shear Wave Velocity and Depth: 99

6.3.1 Profile Variations 99
6.3.2 Logarithmic Analysis 101
6.4 Non-linear multiple regression analysis: 103
6.4.1 Background 103
6.4.2 Method 103
6.4.3 Results 104
6.5 Limitations of Elastic Moduli Derivation Methodology: 105
6.6 Guidelines for future MASW windfarm investigations: 107
6.6.1 MASW Investigation 107
6.6.2 Density characterisation 110
6.6.3 Poisson's ratio characterisation 110
6.6.4 Dataset Analysis / Prediction modelling 111
6.7 Synthesis: 112
Chapter 7: Summary and Conclusions 113
7.1 Research objectives: 113
7.1.1 Determining physical and mechanical properties of the insitu weathered 'greywacke' 113
7.1.2 Geological controls influencing shear wave velocities 113
7.1.3 Removing errors associated with MASW processing 114
7.1.4 Lateral extrapolation of MASW results 114
7.1.5 Refining the current procedure 114
7.2 Trends highlighted in dataset analysis: 115
7.3 Conclusions: 116
7.4 Recommendations for further research: 116
References: 119
Appendix A: Multichannel Analysis of Surface Waves (MASW) Literature Review 129
Appendix B: Measurement of Elasticity 166
Appendix C: Te Rere Hau Windfarm Testpit Logs and Photos 183

Appendix D: Pile Drilling Logs from Te Rere Hau Windfarm 206

Appendix E: Density Testing Results..... 223

Appendix F: Poisson's Ratio Results and VP and VS Profiles 225

Appendix G: West Wind Windfarm Borehole Logs from sites H03 and K04 250

Appendix H: Turitea Windfarm Borehole Logs 254

Appendix I: MASW survey dispersion curves, velocity models, locations and confidence rankings 260

Appendix J: Dataset Analysis: VS Verses Depth Plots For Each Weathering Grade 352

Appendix K: Logarithmic Dataset Analysis..... 356

Appendix L: Multi Variant Non-Linear Regression Analysis 366

List of Figures:

Figure 1.1: Schematic illustrating a typical Multichannel Analysis of Surface Waves survey set-up (ParkSeismic) 2

Figure 1.2: Locations of the three windfarm research sites utilised in this study 3

Figure 1.3: Site location of the Te Rere Hau Windfarm, Palmerston North, New Zealand (Mahoney, 2010) 5

Figure 1.4: Site layout of the West Wind Windfarm, Wellington, New Zealand (Mason, 2006). 6

Figure 1.5: Turitea Windfarm site layout (proposed), Palmerston North, New Zealand (Coleman, 2006). 7

Figure 1.6: Regional site geology of the Te Rere Hau Windfarm (Mahoney, 2010). 8

Figure 1.7: Geologic legend associated with the geology map in Figure 1.6 above (Lee & Begg, 2002). 9

Figure 1.8: The New Zealand microcontinent and its tectonic setting (Williams, 1991). ... 10

Figure 1.9: Major tectonic geomorphology regions of New Zealand (Williams, 1991)..... 00

Figure 1.10: Digital elevation model of the southern North Island, highlighting the active faults (in red). The Wellington fault (bold) is divided into three parts: W-HV, Wellington–Hutt Valley segment; T, Tararua; and P, Pahiatua sections (after Langridge, Berryman, and Van Dissen, 2005). Inset: Plate tectonic setting of New Zealand, showing North Island dextral fault belt (NIDFB), Alpine Fault (AF), Taupoe Volcanic Zone (TVZ), and BoP, Bay of Plenty. Northern Ohariu Fault (NOF) is located to the west of the Te Rere Hau Windfarm site and the Wellington Fault to the east, defining the boundary of the Tararua Ranges. (Langridge et al., 2011). 12

Figure 1.11: Typical MASW survey setup and 2D MASW V_S profile (ParkSeismic) 13

Figure 2.1: Distribution of New Zealand 'greywacke' rocks (Suggate et al., 1978)..... 18

Figure 2.2: a) Basement (pre-Late Cretaceous) geological map of New Zealand. Units are grouped according to major, rather than sole, rock type. Nomenclature and boundaries of North Island Torlesse and Waipapa terranes are controversial: parts of Morrinsville-Manaia Hill and Pahau units may be correlative. Northland and East Coast Allochthons were emplaced in the Early Miocene; all other units were in mutual juxtaposition by the Late Cretaceous
b) Basement rocks subdivided into tectonostratigraphic terranes for the Wellington area
c) Cartoon cross section through basement rocks of Marlborough/Wellington area illustrating structural style and relationships 22

Figure 2.3: Lateral weathering variations along North Range Road on the Te Rere Hau Windfarm site. Location E 2741787, N 6085957, elevation 466m (WGS 1984) 30

Figure 2.4: Example of the highly variable nature of the Esk Head belt 'Greywacke', displaying both vertical and lateral weathering variations. From a road cut outcrop on the western flanks of the Tararua Ranges at the Te Rere Hau Windfarm. Location E 2741671, N 6086859, elevation 498m (WGS 1984) 30

Figure 2.5: Example of Loess surface material overlying highly and moderately weathered 'greywacke', with shear zones and infilling material. From a road cut outcrop along the North Range Road at the Te Rere Hau Windfarm. Location E 2741976, N 6086260, elevation 474m (WGS 1984) 31

Figure 2.6: Weathering variations from highly to moderately weathered 'greywacke', to slightly-unweathered greywacke. Turbine pad excavation outcrop from turbine site 211 at the Te Rere Hau Windfarm 31

Figure 3.1: Face log from a road cut along Henderson Ave on the Te Rere Hau Windfarm. Location E 2741671, N 6086859, elevation 498m (WGS 1984) 38

Figure 3.2: Face log from a road cut along North Range Road on the Te Rere Hau Windfarm. Location E 2741976, N 6086260, elevation 474m (WGS 1984) 38

Figure 3.3: Face log from a road cut along North Range Road on the Te Rere Hau Windfarm. Location E 2741923, N 6086120, elevation 472m (WGS 1984) 39

Figure 3.4: View of test pit TE11 from the Te Rere Hau Windfarm, with clayey-silty completely weathered 'greywacke' material overlying highly to moderately weathered 'greywacke' rock from 1.7mbgl onwards 40

Figure 3.5: Test pit log from test pit TE11 at the Te Rere Hau Windfarm. Only test pit face logging was performed, without any shear vane, scala penetrometer or other insitu testing utilised (Mahoney, 2010) 41

Figure 3.6: A simplified cross section through the Tararua Ranges, displaying the distribution of loess/loess-colluvium, weathered greywacke and the slightly/unweathered greywacke. 44

Figure 3.7: 100mm diameter sampling tube used to determine a specified volume of completely weathered 'greywacke' at the Te Rere Hau Windfarm site, before weighing and drying are performed in the laboratory..... 46

Figure 3.8: Oil replacement density testing method. Excavation and bagging of material before hole is filled with oil to determine volume and material is dried and weighed in the laboratory to determine mass 47

Figure 3.9: Water immersion method, displaying an irregular shaped rock sample mass being measured while suspended and immersed in water (Standards New Zealand, 1986) 48

Figure 3.10: Averaged dry density testing results from the Te Rere Hau Windfarm with 3rd order polynomial best fit trend line. 50

Figure 3.11: Bulk density variations through the weathering profile from the Hodder and Hetherington (1991) study, undertaken at the Whitehall Quarry, near Cambridge, New Zealand 50

Figure 3.12: Dry density values through the weathering profile from Hodder and Hetherington (1991), Martin & Miller (1974), Raisbeck (1973), along with results from density testing at the Te Rere Hau Windfarm..... 51

Figure3.13: Downhole seismic method for testing P-wave and S-wave velocities (Gadallah & Fisher, 2009)..... 55

Figure 3.14: Shear wave velocity (left) and compression wave velocity (right) profiles from Westwind Windfarm turbine site F01 (Mason, 2006)..... 56

Figure 3.15: Poisson's ratio versus depth for moderately-highly weathered 'greywacke' 57

Figure 3.16: Poisson's ratio versus depth for highly-completely weathered 'greywacke' . 57

Figure 3.17: Plot of compressional P-wave velocity versus Poisson's ratio, which displays no well defined linear relationship (Johnson & De Graff, 1988)..... 58

Figure 3.18: Averaged Poisson's ratio values through the weathering profile, determined from downhole seismic surveying at the West Wind Windfarm..... 59

Figure 4.1: Elastic deformations and ground particle motions associated with the passage of body waves (a) P-wave (b) S-wave, from Bolt (1982) 63

Figure 4.2: Elastic deformations and ground particle motions associated with the passage of surface waves, (a) Rayleigh wave, (b) Love wave, from Bolt (1982) 65

Figure 4.3: Variation in insitu and laboratory seismic velocity with changes in fracture frequency and depth (Turk & Dearman, 1986)..... 68

Figure 4.4: Integration of rock quality Q-V_p-E_{mass} in a model that incorporates depth, porosity and rock strength adjustments. Note that E_{mass} (or M) represents the static modulus of deformation, from plate loading tests and from back-analysis of measured deformations. V_p is the seismic velocity measured from refraction seismic, and from cross-hole seismic tomography, in the case of greater depths (Barton, 2007)..... 70

Figure 4.5: Effect of Poisson's ratio u[on various wave velocities (Richart et al., 1970)..... 71

Figure 4.7: Shear-wave velocity profiles calculated for the same fundamental Rayleigh mode and for different Poisson's ratio values (Karray & Lefebvre, 2008)..... 72

Figure 5.1: A 3-step processing scheme for Multichannel Analysis of Surface Waves data76

Figure 5.2: Schematic illustrating a typical Multichannel Analysis of Surface Waves survey

set-up (ParkSeismic).. 79

Figure 5.3: Experimental dispersion curves from Te Rere Hau Windfarm from 10m source-receiver offset (top), and 22m source-receiver offset (bottom). 81

Figure 5.4: Typical MASW setup with an array of 24 geophones at 1m spacing, from the Te Rere Hau Windfarm. 82

Figure 5.5: Dispersion curve exhibiting sever interference along with being surveyed under poor survey conditions from the undeveloped West Wind Windfarm site H03. This survey was given a confidence ranking of 0. 83

Figure 5.6: An example of dispersion curve extraction using SurfSeis that shows a higher mode adjacent to the fundamental mode causing some erroneous picking of phase velocities. In this instance the pickings would be manually edited (Park & Miller, 2004). 84

Figure 5.7: Relationship between ease of differentiation of fundamental and higher mode Rayleigh waves and the length of geophone string. The longer the array, the easier to visually identify higher mode and body waves. A short 24 channel array (1) shoes very poorly the diverging velocities of fundamental and higher modes compared with a 120 channel array (3) at a similar near offset. A 48 channel array (2) collects significantly more fundamental mode energy, facilitating differentiation and muting..... 85

Figure 5.8: Example of higher modes being present in the data. Fundamental mode dispersion curve has been picked (top), with associated velocity model (bottom) from Te Rere Hau Windfarm Turbine site 2..... 88

Figure 5.9: Dispersion curve (top) and associated velocity model (bottom) for Te Rere Hau Windfarm turbine site 49 89

Figure 5.10: Dispersion curve (top) and associated velocity model (bottom), from Turitea Windfarm, turbine site 6 90

Figure 5.11: Dispersion curves from MASW surveys in both directions at the Turitea Windfarm turbine site 6, showing a good agreement between surveys, suggesting lateral site homogeneity 92

Figure 5.12: Disjointed and undulating dispersion curve (top) and associated velocity model (bottom), from Westwind Windfarm, turbine site K04 93

Figure 6.1: Effects of depth on V_S within the unweathered grade of Esk Head belt 'greywacke', displaying a large scatter of data with an increasing trend of V_S with depth 100

Figure 6.2: Effects of depth on V_S within the highly weathered grade of Esk Head belt 'greywacke' 101

Figure 6.3: Effects of depth on V_S within the moderately weathered grade of Esk Head belt 'greywacke' 101

Figure 6.3: Logarithmic analysis of $LogV_S$ versus Depth (top), V_S versus LogDepth (middle) and $LogV_S$ versus LogDepth (bottom), for the moderately weathered material. All three plots display a relatively good linear relationship 102

Figure 6.4: 3D plot of results from the multiple non-linear regression analysis displaying the relationship between weathering, depth and V_S. The weathering grades of unweathered to completely weathered are represented numerically by the values of 1-9 104

List of Tables:

Table 1.1: Active faults in proximity to the Tararua Ranges. Derived from Lee & Begg (2002). 11

Table 2.1: Comparison of different 'greywacke' weathering classification schemes from literature 26

Table 2.2: A standard 6-fold classification scheme redeveloped from Pender (1971) and Marshall (1974) for this study, used to classify the weathered Esk Head belt 'greywacke' in this study 27

Table 2.3: General soil and rock profile within Esk Head belt 'greywacke' terrain, from combined data based on test pit logging and pile drilling logs from the Te Rere Hau Windfarm 29

Table 2.4: Variation of bulk density and porosity values through the weathering profile. Reproduced from Hodder & Hetherington (1991) 33

Table 2.5: Index properties for grades of highly (4), completely (5) and residually (6) weathered 'greywacke', reproduced from Pender (1971) 33

Table 2.6: Mechanical properties for grades of highly (4), completely (5) and residually (6) weathered 'greywacke', reproduced from Pender (1971) 34

Table 3.1: Rock mass classification scheme for weathered 'greywacke' developed for this study from Pender (1971) and Marshall (1974) 36

Table 3.2: Pile drilling logs from turbine sites on the western flanks of the Tararua Ranges at the Te Rere Hau Windfarm site 43

Table 3.3: Pile drilling logs from turbine sites along the ridge line of the Tararua Ranges at the Te Rere Hau Windfarm site 43

Table 3.4: Pile drilling logs from turbine sites on the eastern flanks of the Tararua Ranges at the Te Rere Hau Windfarm site 44

Table 3.5: Comparison of different density values and ranges through the weathering profile for 'greywacke' 49

Table 3.6: Averaged mass Poisson's ratio values and range in values, through the weathering profile, calculated from 7 downhole seismic surveys at the West Wind Windfarm. The range of values was determined using 1 standard deviation of the dataset higher and lower than the average value 59

Table 3.7: Results of XRD analysis of greywacke rocks from Te Rere Hau Windfarm 60

Table 5.1: Confidence ranking scheme used for MASW surveys to determine data quality78

Table 5.2: Optimum field parameters for MASW surveys for most common soil sites. A seismic source of 4.5kg or heavier sledgehammer and use of recording instrument with 24-bit or higher dynamic range are both assumed. No low-cut analogue filter should be used during the acquisition (Park et al., 1999) 80

Table 5.3: Typical survey parameters used during MASW surveys in this study..... 80

Table 5.4: V_S profiles with depth from Turitea Windfarm turbine site 6, and Te Rere Hau Windfarm turbine sites 2 and 49..... 91

Table 6.1: Pile drilling logs from turbine sites on the western flanks of the Tararua Ranges at the Te Rere Hau Windfarm site..... 97

Table 6.2: Pile drilling logs from turbine sites along the ridge line of the Tararua Ranges at the Te Rere Hau Windfarm site..... 97

Table 6.3: Pile drilling logs from turbine sites on the eastern flanks of the Tararua Ranges at the Te Rere Hau Windfarm site..... 98

Table 6.4: Optimum field parameters for MASW surveys for most common soil sites. A seismic source of 10-lb or heavier sledgehammer and use of recording instrument with 24-bit or higher dynamic range are both assumed. No low-cut analogue filter should be used during the acquisition (Park et al., 1999) 109

Table 6.5: Confidence ranking scheme used for MASW surveys to determine data quality..... 109

Chapter 1: Introduction

1.1 Project Background:

Geotechnical investigations of wind turbine foundations, along with a wide range of other engineering developments, require dynamic soil and rock properties representative of the large-scale, insitu environment. Traditional geotechnical and geological investigation techniques examine very localised volumes and extrapolate between investigation locations, although often it is the broader rock/soil mass properties which are of interest and how they respond to dynamic loading conditions. This evaluation can be achieved by a geophysical technique analysing surface waves.

Multi-channel Analysis of Surface Waves (MASW) is a geophysical seismic exploration method for evaluating velocity profiles in a continuum, which can be used to determine the elastic condition, or stiffness, of the ground. Determining the stiffness of a material involves determining the incremental vertical strain which results from the increase in vertical effective stress (Powrie, 2004), or likewise, the closure of discontinuities that occurs on the application of a load (Wyllie, 1992).

This method was first discovered to have practical uses for engineering projects in the late 1990's. MASW first measures seismic surface waves generated from a seismic source, analyses the propagation velocities of those surface waves, and then finally deduces shear-wave velocity (V_S) variations below the surveyed area. Currently, there is limited understanding about the relationship between seismic velocities in certain material types, and the associated geotechnical properties they represent, especially within complex lithological terrains.

The MASW procedure is summarised in Figure 1.1, and its extensive theory is expounded in Park et al (1999) and Xia et al (1999); Appendix A provides detail of the MASW method and its development into current use in geotechnical engineering. The three main stages of this method are: 1) data acquisition, 2) identification of the fundamental mode dispersion curve, and 3) back-calculating V_S variation with depth.

Seismic velocities are currently being used to represent the elastic modulus of insitu lithology. This is a rough estimation of the elastic condition of subsurface layers, as the elastic modulus is dependent on a range of geotechnical and geological properties, only one of which is its primary lithology. Other factors include weathering, fracturing and groundwater, along with intrinsic material properties, such as density and Poisson's ratio. Hence the shear wave velocities are

being utilised without knowing the full extent of their controls, reducing the accuracy of results when being used as design inputs, or limiting the potential for using shear wave velocities in engineering design, where it is typically used in Finite Element Modelling (FEM).

MASW can be applied in many circumstances. It is being increasingly employed by power companies/electricity providers to determine the elastic condition of proposed turbine sites. This method of investigation has been employed at the New Zealand Windfarm Ltd site, Te Rere Hau Windfarm, in the Tararua Ranges of New Zealand North Island. The weathered greywacke geology on site displays highly variable physical and mechanical properties, with the depth to unweathered material varying from 1.5m depth to below the approximate 15m extent of investigations.

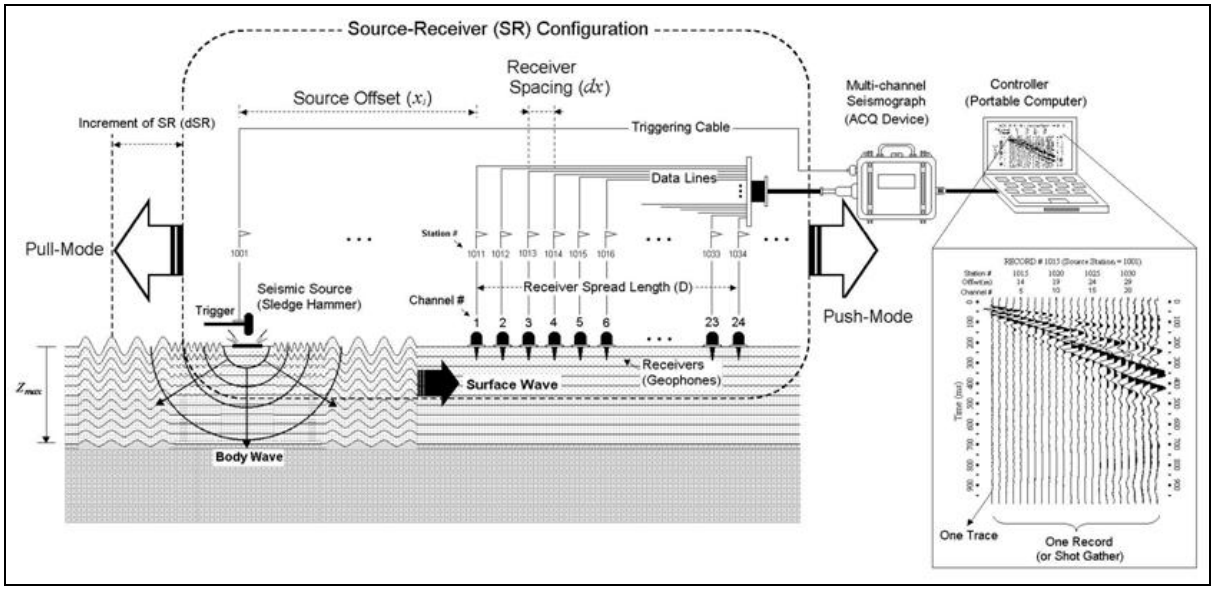

Figure 1.1: Schematic illustrating a typical Multichannel Analysis of Surface Waves survey set-up (ParkSeismic).

Problems can arise when using Multichannel Analysis of Surface Waves in the investigation of wind turbine locations as a single sounding is taken at the proposed location of construction, which is an average across the entire array taken at a point. This produces problems when data is extrapolated laterally, as there is a high possibility for lateral heterogeneity in the subsurface material conditions. Due to a hemisphere of energy being surveyed and represented as a 1-D profile above the centre point of the survey, limitations exist when extrapolating laterally outside the extent of the surveyed area.

This thesis analyses MASW data collected from a wind turbine farm. The MASW data is largely from a dataset gathered by Dr. Michael Finnemore, Director of Southern Geophysical Ltd and Research Associate in the Department of Geological Sciences, University of Canterbury. The data

has been gathered on the Te Rere Hau wind farm site, located in the Tararua Ranges, east of Palmerston North, New Zealand.

1.2 Te Rere Hau Windfarm Project:

As part of the development of the Te Rere Hau wind farm by NZ Windfarms Ltd, elastic modulus profiles of weathered rock at each turbine location were obtained by using Multichannel Analysis of Surface Waves (MASW) for site specific turbine foundation design. The Te Rere Hau windfarm operates 97 New Zealand-made wind turbines. The turbines constructed during Stages 2 to 5 are designed with a 2.4m diameter mono-pile foundation, as opposed to the more traditional shallow concrete pad foundation which was used in the Stage 1 development. Southern Geophysical Ltd was contracted to undertake the MASW surveying of the Stage 2 to 6 development sites, and to provide a surface wave velocity profiles with depth. This velocity profile can be converted to an elastic modulus profile, by a process described in Mahoney & Kupec (2010) and Mahoney (2008), and used as an input in the Finite Element Method (FEM) of analysis for the design of the mono-pile foundation elements.

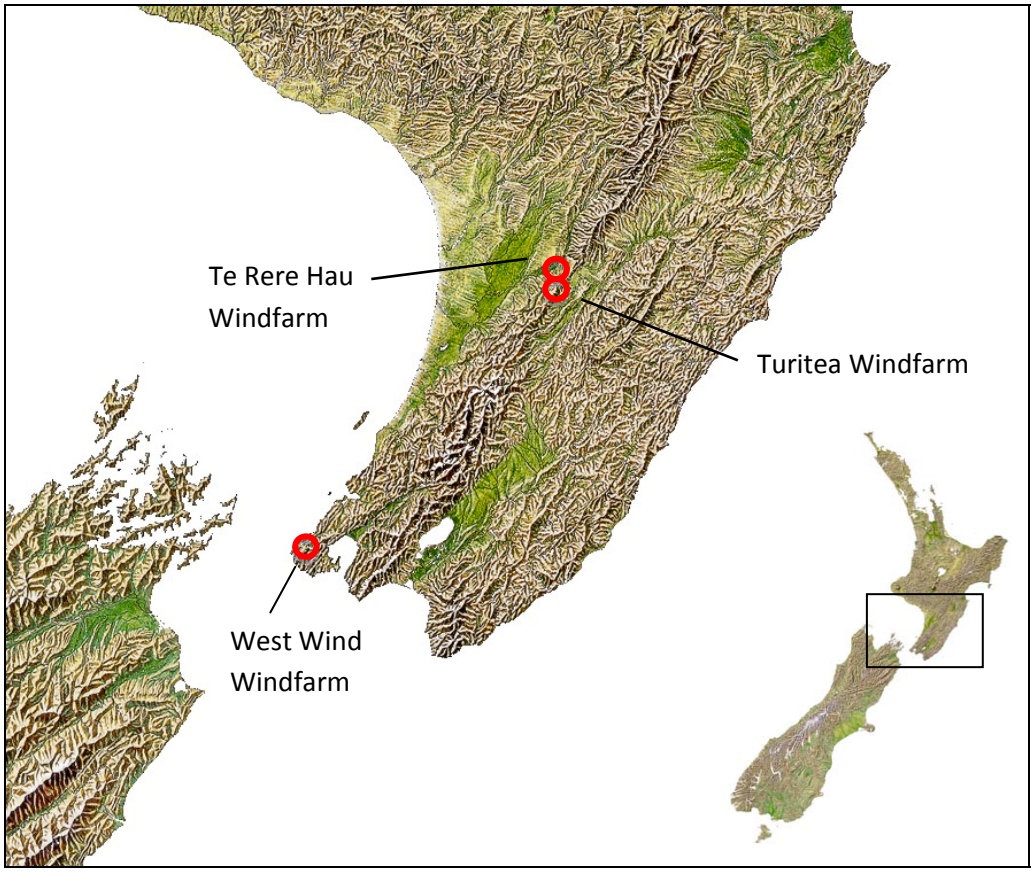

Figure 1.2: Locations of the three windfarm research sites utilised in this study.

A number of factors influenced the use of MASW as a tool for determining the elastic modulus profile, including the highly variable physical and mechanical properties of the underlying Mesozoic greywacke rock, a relatively tight construction schedule, the large number of proposed wind turbines for development, and the difficulty and cost involved in obtaining sufficient undisturbed samples for triaxial testing. The conversion of seismic wave velocity profiles to elastic modulus profiles was done by constraining the results against known and previously determined geotechnical and geological information. The elastic modulus profiles were then used by the nominated structural engineers in their FEM analysis for each turbine location to calculate the required minimum embedment depth for the mono-pile.

This conversion method has only been applied to the local geology at the Te Rere Hau windfarm site, with limited correlation with laboratory tested elastic modulus values. It is believed that this is the first time a correlation of seismic wave velocity profiles with elastic modulus profiles has been applied to wind turbine foundation sites, hence there is a significant potential for refinement of the method and expansion of its applications.

1.3 Objectives:

The objectives of this research fall broadly into two categories:

Firstly, relating directly to Multichannel Analysis of Surface Waves (MASW) method of investigation.

- To develop and refine the current procedure for converting geophysical information to geotechnical information.
- To identify errors associated with the conversion process and the velocity inversion process in the MASW data processing.

Secondly, relating more broadly to the geological site conditions, and the use of shear wave velocities in geotechnical engineering.

- To determine the geological controls which influence surface wave velocities at the wind turbine sites under investigation.
- To determine any correlation between surface wave velocities and geological controls, which are relevant to geotechnical classification schemes.
- To determine a more robust method of investigation when lateral extrapolation is required (with appropriate limits to the method).
- To obtain physical values on the weathered ‘greywacke’ rock found at the Te Rere Hau Windfarm site.

1.4 Windfarm study sites:

The main research site for this study was the Te Rere Hau Windfarm site in the Tararua Ranges to the east of Palmerston North, in New Zealand's North Island (Figure 1.3). The windfarm is situated in the Tararua Ranges, which are formed from highly weathered and deformed 'greywacke'. The 48.5 MW Te Rere Hau Windfarm, is NZ Windfarms Ltd first project, which received resource consent in May 2005, for up to 97 turbines, and was completed in mid 2011.

Stage 1 construction started in January 2006 and consisted of five New Zealand-made, Windflow 500 turbines (2.5 MW capacity each) which operated via a temporary connection into the local PowerCo network. Stage 1 was officially opened on 15 September 2006.

Stage 2 consisted of the installation of an additional 28 turbines, plus the installation of the permanent electrical connection into the national grid, via the Tararua wind farm injection point. Finally, by the end of 2009, Stage 3 was completed with a total of 63 turbines in operation.

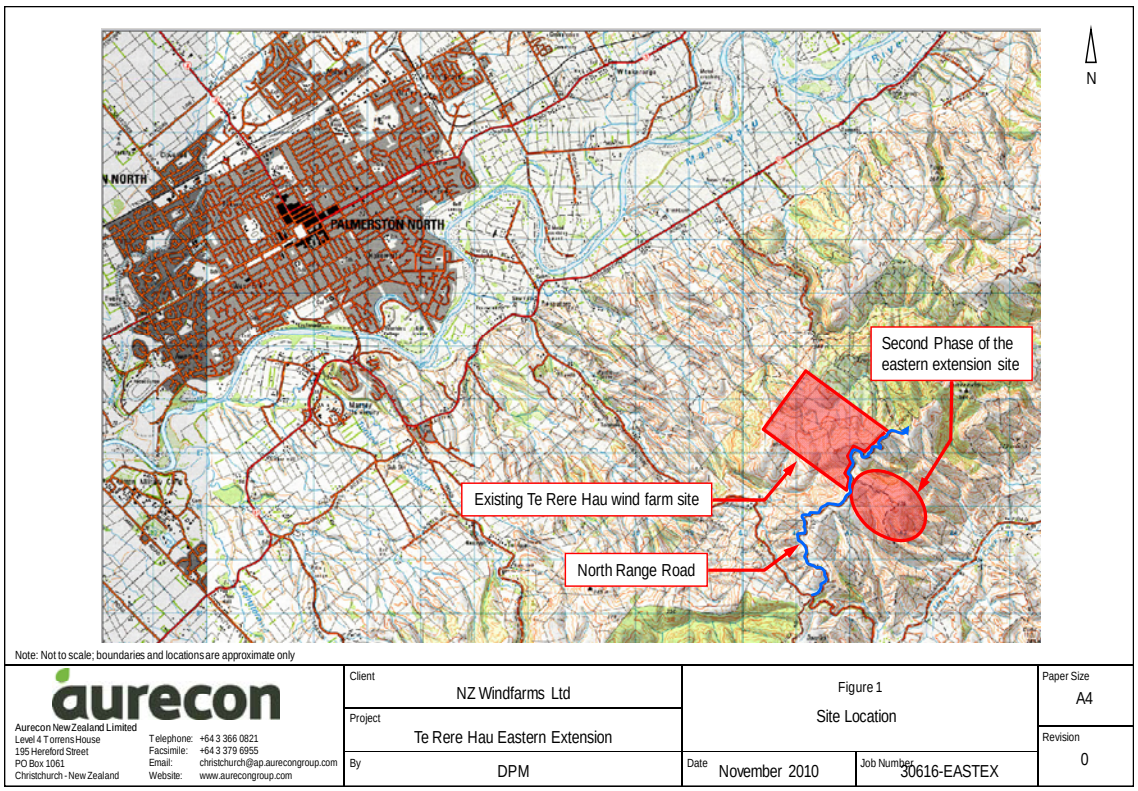

Figure 1.3: Site location of the Te Rere Hau Windfarm, Palmerston North, New Zealand (Mahoney, 2010).

The windfarm site is underlain by Esk Head Belt greywacke rocks, predominantly sandstone and mudstone sequences with a sheared dark argillite matrix (Lee & Begg, 2002). The Esk Head Belt greywacke of the Tararua Ranges is highly weathered through climatic and topographic conditions, and deformed through tectonic movement. Geological investigations (Chapter 3) have shown the weathering grade typically decreases with depth throughout the site, along with a significant level of lateral weathering variability being present.

Two secondary study sites have been utilised, both of which are situated in the Esk Head Belt 'greywacke' rocks of the Lower North Island. Meridian Energy's operational West Wind windfarm in Wellington and also Mighty River Power's proposed Turitea windfarm in Palmerston North's Tararua Ranges, to the south of the Turitea windfarm (Figures 1.4 and 1.5 respectively). Both of these sites provided additional MASW survey locations, along with essential insitu and laboratory geotechnical data which was available for correlation purposes.

In this study, each surveyed site is denoted by the assigned turbine-site number. For example, the site of Te Rere Hau Windfarm turbine site 43 is denoted TRH 43. Likewise the Turitea Windfarm turbine site 5 is denoted T 5, and the West Wind Windfarm turbine site H03 is denoted WW H03.

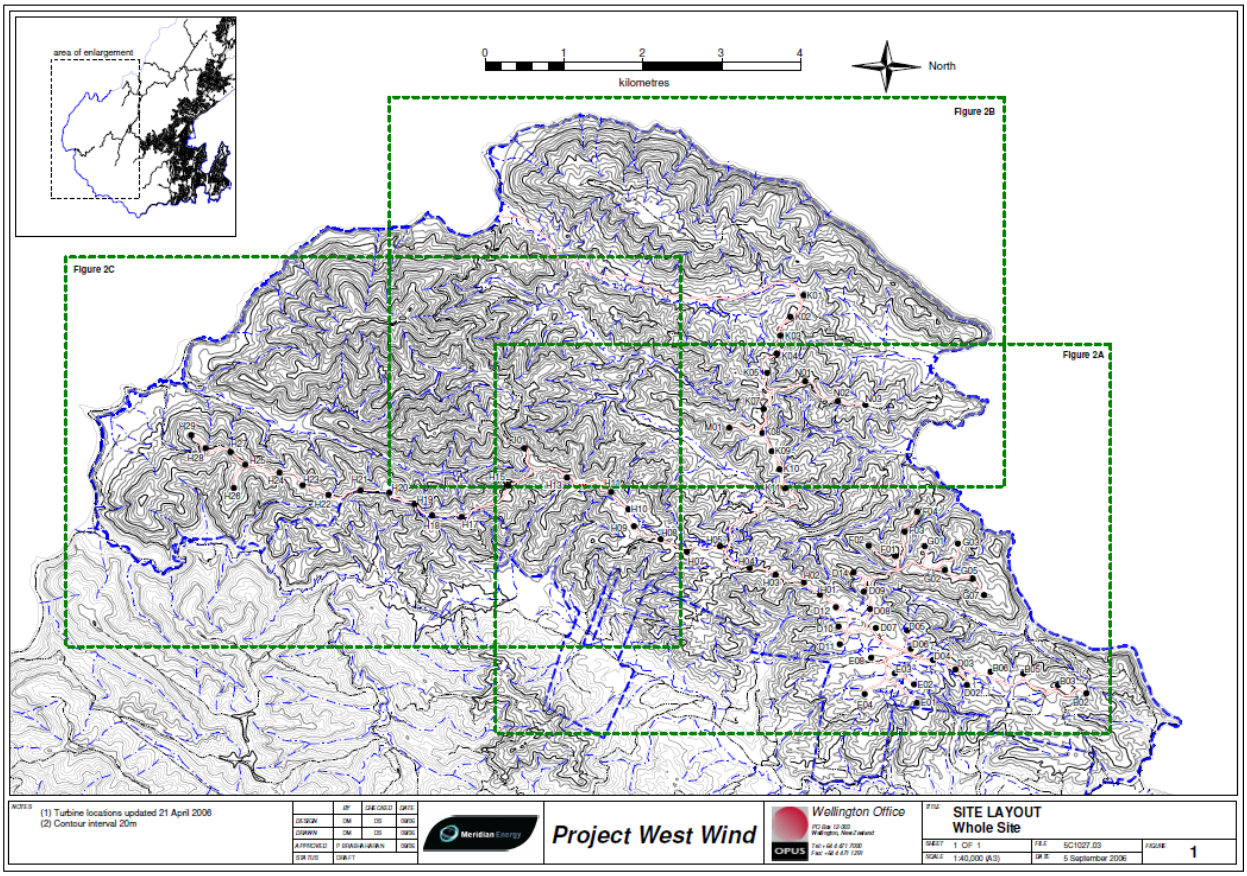

Figure 1.4: Site layout of the West Wind Windfarm, Wellington, New Zealand (Mason, 2006).

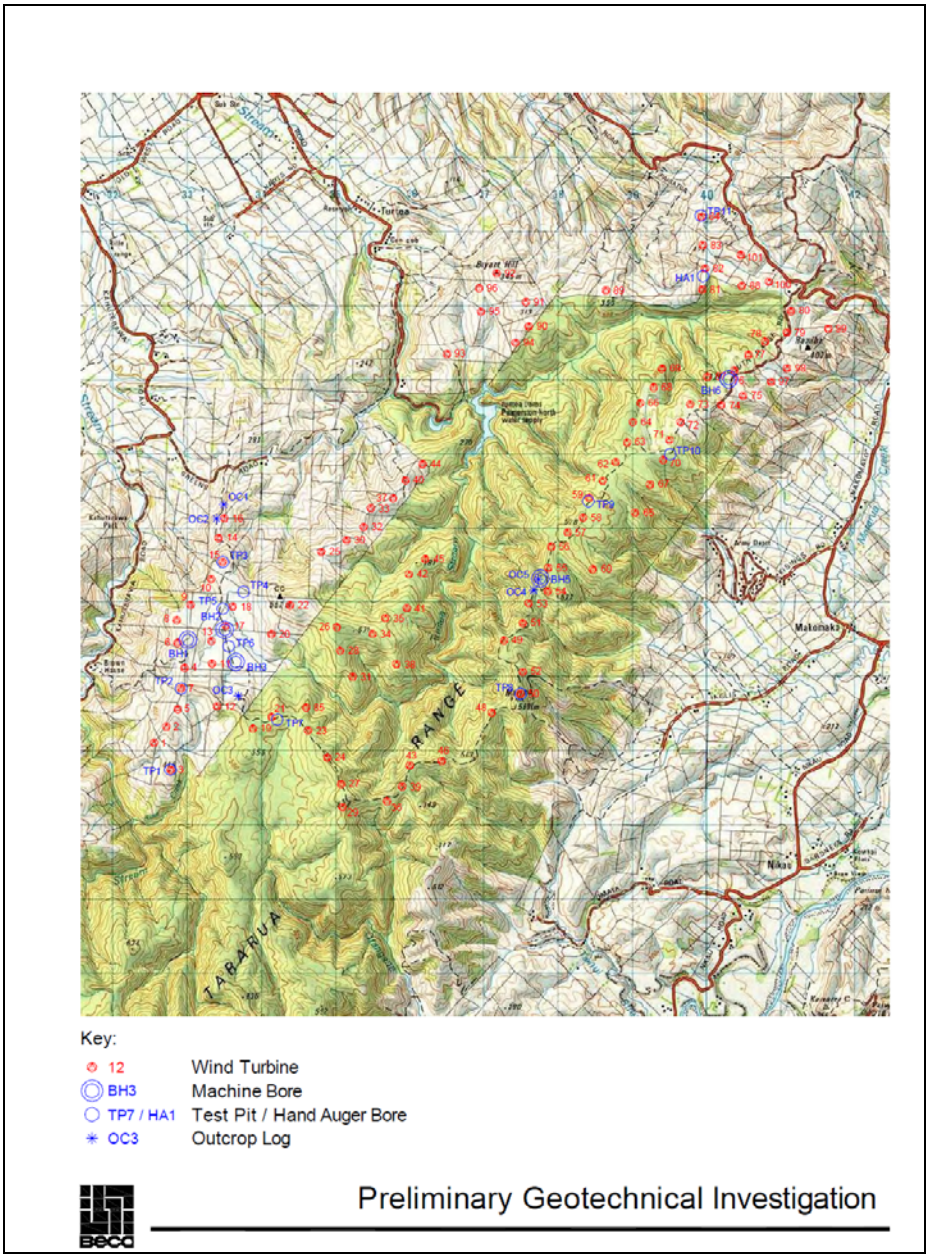

Figure 1.5: Turitea Windfarm site layout (proposed), Palmerston North, New Zealand (Coleman, 2006).

1.5 Geological and Tectonic Setting of the Lower North Island:

New Zealand is a microcontinent across the boundary of the Pacific and Indo-Australian plates. The plate boundary is marked by a broad band of shallow seismicity and a belt of deformation 100-400km wide that transverses diagonally across the country (Williams, 1991). The converging of the two plates operates in opposing directions at opposite ends of the country

(Figure 1.8). In the southwest, New Zealand is dominantly a transform zone, whereas in the northeast it is dominantly a subduction zone (Walcott, 1987).

The most widespread basement lithology throughout New Zealand is the Upper Palaeozoic to Mesozoic age greywacke, belonging to the Torlesse Supergroup (Campbell & Coombs, 1966). This deposit forms the backbone of New Zealand in comprising the Southern Alps and the axial ranges of the North Island. Deformation of these axial ranges has occurred along a northeast trending belt that lies parallel to the Hikurangi trench (Lamb & Vella, 1987).

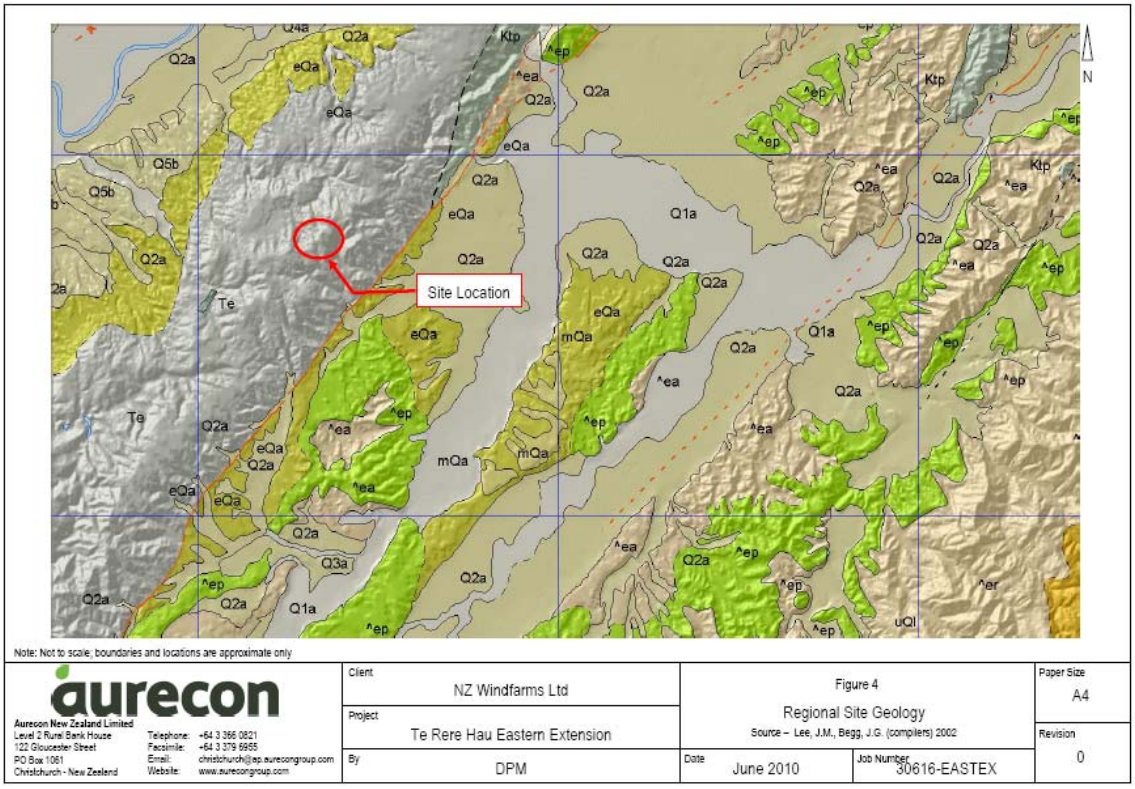

Figure 1.6: Regional site geology of the Te Rere Hau Windfarm (Mahoney, 2010).

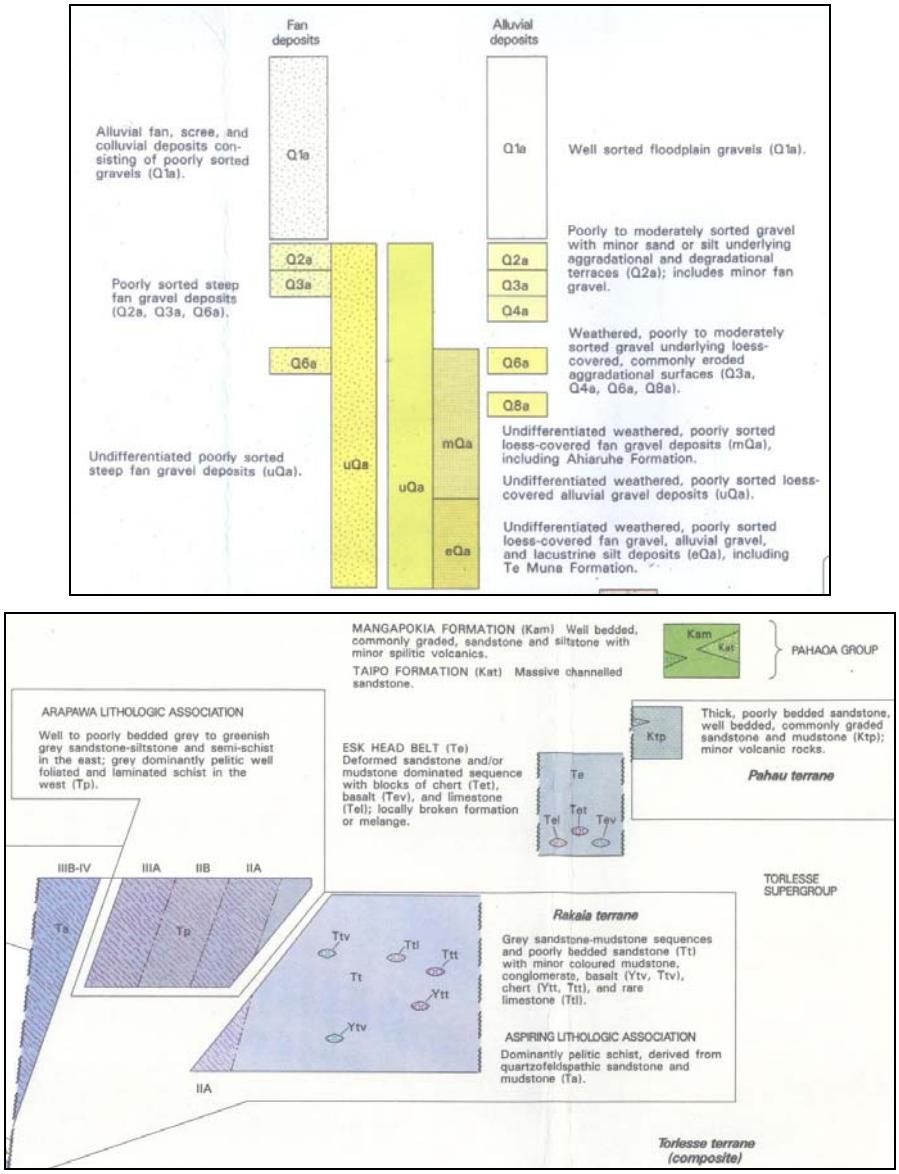

Figure 1.7: Geologic legend associated with the geology map in Figure 1.6 above (Lee & Begg, 2002).

Due to New Zealand being located on an obliquely convergent plate boundary between the Pacific and Australian plates (Figure 1.8), the collision of these plates is caused by the Pacific plate subducting underneath the Australian plate. To the south of the South Island, the situation is reversed, where the Australian plate is subducting underneath the Pacific plate. In the southwest of New Zealand the belt of deformation traversing the country, is dominantly a transform zone, whereas in the northeast it is dominantly a subduction zone (Walcott, 1987). The opposing relative movement results in oblique crustal compression, which is taken up by shearing and uplift (Williams, 1991), the former being expressed in the South Island by the Alpine Fault and the formation of the Southern Alps.

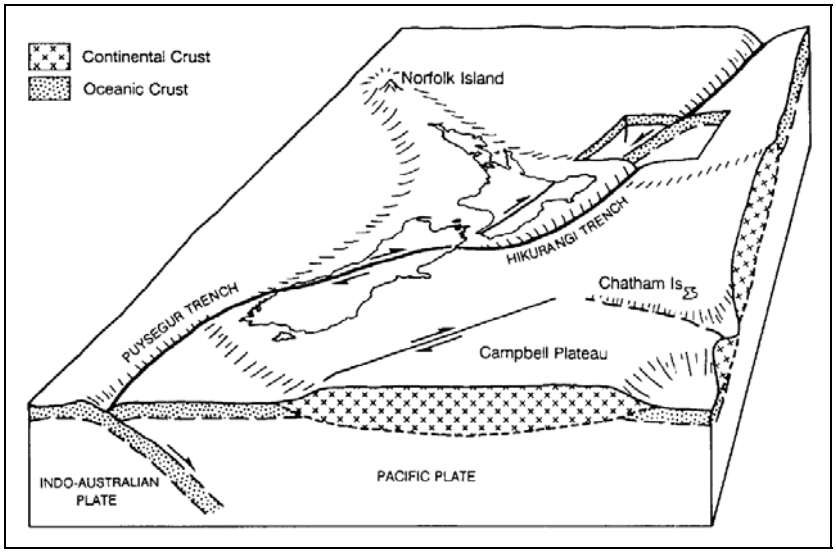

Figure 1.8: The New Zealand microcontinent and its tectonic setting (Williams, 1991).

The Pacific plate is rotating anticlockwise relative to the Australian plate, which causes systematic variation in the deformation style resulting from convergence along the plate boundary. This produces oblique subduction at the Hikurangi Margin and back-arc rifting in the Taupo Rift in the North Island, through to a largely strike-slip transfer zone in the faults of the Marlborough Fault System (MFS) in the north of the South Island. This strike-slip zone of the MFS connects the Hikurangi Margin to the Alpine Fault, where oblique convergence is building the Southern Alps in the central South Island.

During the Rangitata Orogeny, the major mountain-building episode, the Southern Alps were formed through uplift, along with the axial ranges of the North Island, during the Jurassic-Cretaceous time period and underwent severe faulting, folding and shearing in the process (Stewart, 2007).

Historically, the Lower North Island has been a highly active tectonic zone. The Te Rere Hau windfarm, along with both the Turitea and West Wind windfarms, is bounded to the east and west by two northwest-southeast aligned active faults. The Wellington Fault to the west and the Northern Ohariu Fault to the east are responsible for the formation of the Tararua Ranges (Langridge et al., 2011). Details of the two faults are presented in Figure 1.10 and Table 1.1.

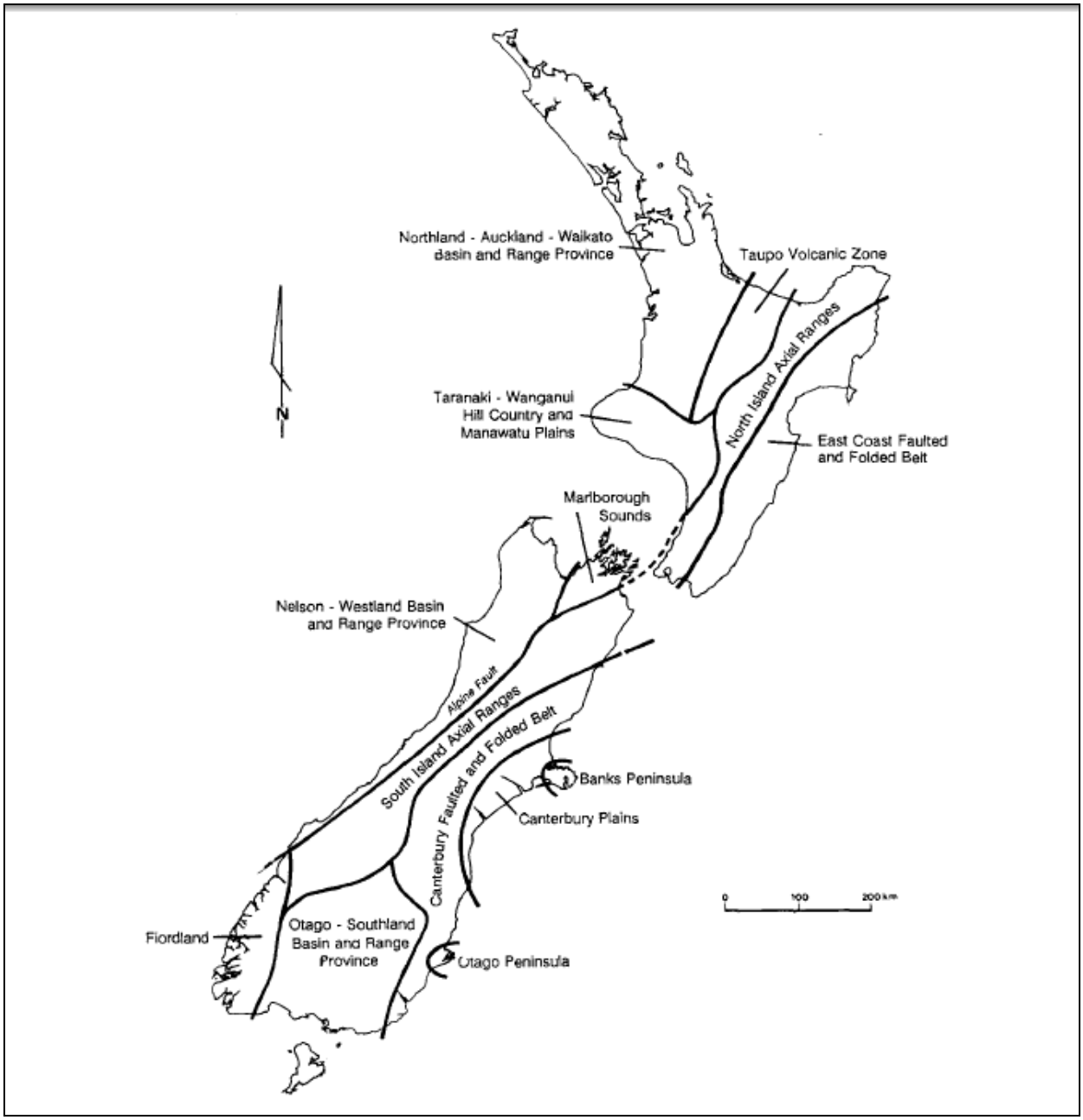

Figure 1.9: Major tectonic geomorphology regions of New Zealand (Williams, 1991).

Fault name	Slip rate (mm/yr)	Estimated single event displacement (m)	Reoccurrence interval (thousand yrs)	Last event (yrs)	Estimated characteristic earthquake magnitude (Mw)
Northern Ohariu	1.0-3.0	3.0-3.5	1.0-4.0	<2000	7.3-7.7
Wellington	6.0-7.6	3.5-5.0	3.0-5.0	<2000	7-7.3

Table 1.1: Active faults in proximity to the Tararua Ranges. Derived from Lee & Begg (2002).

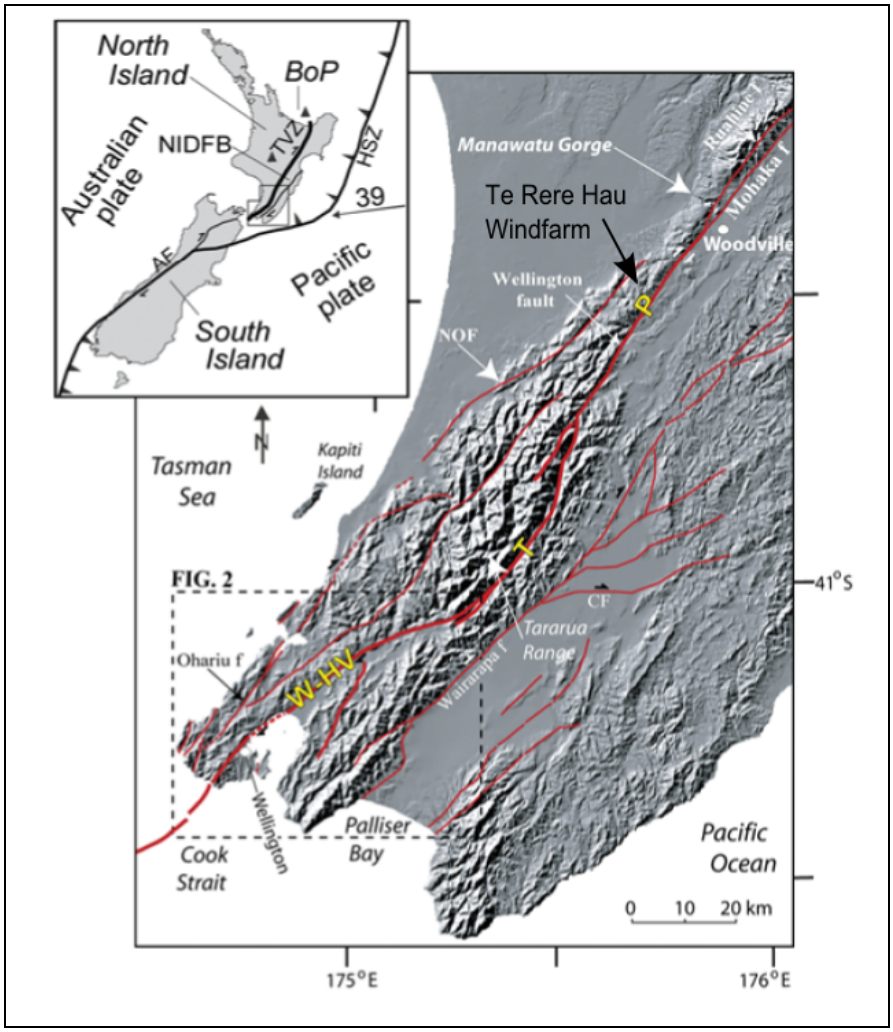

Figure 1.10: Digital elevation model of the southern North Island, highlighting the active faults (in red). The Wellington fault (bold) is divided into three parts: W-HV, Wellington–Hutt Valley segment; T, Tararua; and P, Pahiatua sections (after Langridge, Berryman, and Van Dissen, 2005). Inset: Plate tectonic setting of New Zealand, showing North Island dextral fault belt (NIDFB), Alpine Fault (AF), Taupoe Volcanic Zone (TVZ), and BoP, Bay of Plenty. Northern Ohariu Fault (NOF) is located to the west of the Te Rere Hau Windfarm site and the Wellington Fault to the east, defining the boundary of the Tararua Ranges. (Langridge et al., 2011).

1.6 Multichannel Analysis of Surface Waves:

Surface waves have been utilised and recorded originally by the Spectral Analysis of Surface Waves (SASW) method, and more recently by the Multi-channel Analysis of Surface Waves (MASW) method. The SASW method was the first to harness the valuable information available through the recording of surface waves. SASW uses just two receivers, and varies the distance between them (D) in a highly labour intensive method, which is detailed further in Appendix A. The MASW method adopted a 24 receiver approach, which has long been used in seismic exploration for natural resources. In comparison to body-wave survey methods such as

reflection or refraction, the surface wave seismic method usually has a far greater tolerance in the selection of optimum field parameters. The main reason for this tolerance is that the surface waves have the strongest energy among all other types of seismic waves, ensuring the highest signal-to-noise ratio (Park et al., 1999). This approach, detailed in Park et al (1999), utilises multiple channels for an improved recording of complexities in the subsurface and a much reduced labour intensive method. The MASW procedure is summarised in Figure 1.11, and its extensive theory is expounded in Park et al (1999) and Xia et al (1999).

Surface waves velocities are utilised due to the close relationship to shear-wave velocities (V_S) of earth materials, which is an important geotechnical engineering parameter. MASW measures seismic surface waves which are generated by a man-made seismic source, such as a sledge hammer, through an array of geophones, and is recorded on a seismograph. MASW analyses the propagation velocity of the surface waves and finally deduces a shear-wave velocity profile below the surveyed area, which is most representative of the propagation velocity pattern of the surface waves.

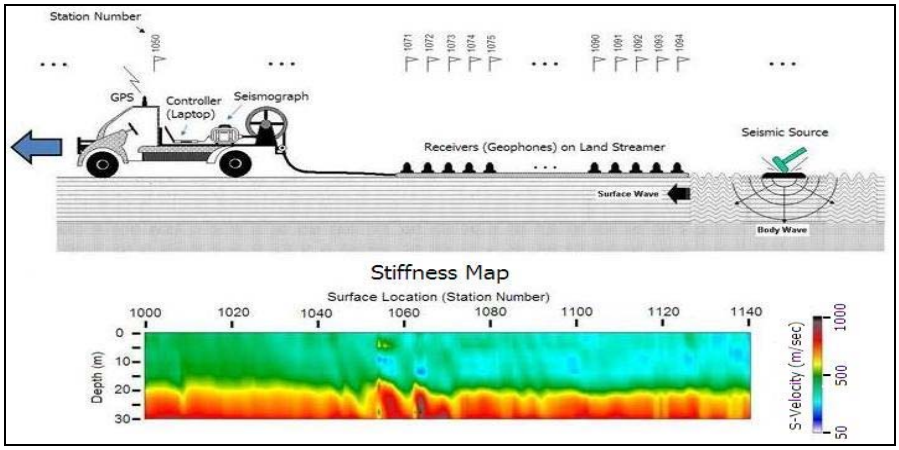

Figure 1.11: Typical MASW survey setup and 2D MASW V_S profile (ParkSeismic).

The MASW method, as discussed, is the method used in this study to determine the elastic condition (stiffness) of wind turbine sites during geotechnical investigations.

MASW can be used to image the subsurface elastic condition in either 1D, 2D or 3D. When determining a stiffness profile below a wind turbine site, a 1D profile is used. This method is based on the assumption that the survey is taking place over a discretely layered, homogenous elastic half-space.

The methodology employed when using MASW is detailed in Chapter 5, and further in Appendix A.

1.7 Determining the elastic condition of weathered 'greywacke':

MASW derived shear wave velocity measurements can be used to calculate the elastic modulus through the depth profile. This section provides a brief overview of the methods and calculations used in the conversion of shear wave velocity data into elastic modulus profiles to determine the stiffness properties of the weathered 'greywacke' onsite at the three windfarms in this study.

For structural foundation design of the wind turbines at the Te Rere Hau Windfarm, an accurate elastic modulus profile of the subsurface at each turbine site was required. To obtain these profiles, MASW was used to determine V_S profiles for each site, from which elastic modulus values were calculated. It is this conversion method which this study aims to refine by improving the accuracy of each input into the calculation.

A two-step computation, detailed in Kramer (1996), relates V_S and shear moduli (G), to compute G and E. Elastic theory states that the small strain shear modulus, G can be determined from:

$$G = \rho V_S^2 \qquad \textbf{Equation 1.1}$$

where ρ is the material density

The small strain shear modulus represents the elastic stiffness of the soils at shear strain (γ) less than 10^{-4} percent. Elastic theory also states that the small strain Young's modulus (Elastic modulus), E is linked to G, as follows:

$$E = 2G(\nu + 1) \qquad \textbf{Equation 1.2}$$

where ν is the Poisson's ratio of the material

Therefore when V_S is directly related to E by the expression:

$$E = 2\rho V_S^2(\nu + 1) \qquad \textbf{Equation 1.3}$$

A full description of the conversion method and its controls, is given in Mahoney & Kupec (2010), and Mahoney (2008). Appendix B details the theory of elasticity and how shear wave velocities can be employed to determine a stiffness profile with depth, or how the strains and displacements of the greywacke vary through the depth profile, as it is loaded and unloaded.

1.8 Thesis Format:

The research objectives and study sites have been outlined in Chapter 1, along with a discussion of the regional geological setting of the lower North Island, and an introduction to MASW, along with the conversion method for calculating elastic moduli from MASW shear wave velocity data.

A review of the geological properties of greywacke rock is presented in Chapter 2, which looks first at typical greywacke rock mass characteristics, then more specifically at the Esk Head Belt 'greywacke'. It then outlines the different weathering processes affecting the windfarm sites in this study, before developing a classification scheme for identifying the different grades of weathered greywacke, and finishes looking at some physical properties available in current literature.

Chapter 3 provides a detailed geotechnical and engineering geological characterisation of the wind farm sites. This includes an engineering geological description of the insitu Esk Head belt 'greywacke' rock, followed by density and Poisson's ratio characterisations through the weathering profiles onsite.

Chapter 4 is focused on the surface wave velocities, their interpretation, and techniques used for acquiring them. Initially, all forms of seismic waves are investigated before focusing on surface waves and the factors which affect their propagation. MASW and the typical field and data processing methodology are also introduced.

Chapter 5 presents the MASW investigations and data analysis from surveys across the three windfarm sites. Acquisition parameters used, discussions on dispersion curve extraction and surface wave inversion are all detailed before an analysis of identified trends within the MASW data.

Chapter 6 presents a data analysis of both the geotechnical and geophysical data. Trends are highlighted, along with their significance to current geotechnical practice. Statistical analysis of the dataset is performed with the process of creating a predictive equation for geotechnical and geophysical properties detailed.

Finally, Chapter 7 presents a general summary of the combined results from this study, and the extent to which the research objectives were achieved. In addition to discussing results from this study, a suggested guideline is detailed for the use of MASW for future investigations on

windfarm developments. Lastly, conclusions are drawn and recommendations are made for further research.

Chapter 2: Properties of 'Greywacke' Rock

2.1 Introduction:

This chapter presents a review of the geological properties of greywacke rock, as an insitu rock-mass, before more specifically detailing the properties of the Esk Head belt 'greywacke'.

Weathering is the major influencing factor which determines both physical and mechanical properties of 'greywacke'. The physical and chemical weathering processes which control the properties of the Esk Head belt 'greywacke' are discussed, along with the methods used in this study to characterise the different weathering grades.

2.2 General 'greywacke' lithology:

'Greywacke' rocks, which are widespread throughout New Zealand, are composed of strong, to extremely strong, sandstones, interbedded sandstones and mudstones, and mudstones. The term 'greywacke' is commonly used to describe the overall rock mass of interbedded sandstone and mudstone rocks, which are mapped as Torlesse Supergroup rocks in the central South Island and the lower North Island (Campbell & Coombs, 1966). Proportions of mudstone and sandstone vary between localities, and in zones of highly deformed 'greywacke' clasts of basalt, chert and limestone are often included (Begg & Johnson, 2000)

The individual sequences of sandstone and mudstone which make up 'greywacke' have been described by Begg and Mazengarb (1996) as:

- Sandstone: Coarse to medium grained, and medium to dark grey. Individual grains are poorly sorted angular quartz and feldspar, plus fragments of metamorphic and igneous rocks. The intergranular filling is clay minerals deposited during induration or slight metamorphism.
- Mudstone: Layers of clay, silt or mud, generally dark grey to black, sometimes red from iron minerals.

Upper Paleozoic to Mesozoic 'greywacke' rocks are widespread throughout New Zealand (Figure 2.1), with a large amount of the nation's infrastructure built in, on or traversing greywacke terrain (Read et al., 1999). These deposits have generally undergone low grade metamorphism and have been subject to multiple phases of uplift and mountain building. Due to

this complex tectonic and geological history, 'greywacke' rocks are commonly closely jointed (6-10mm) rock masses.

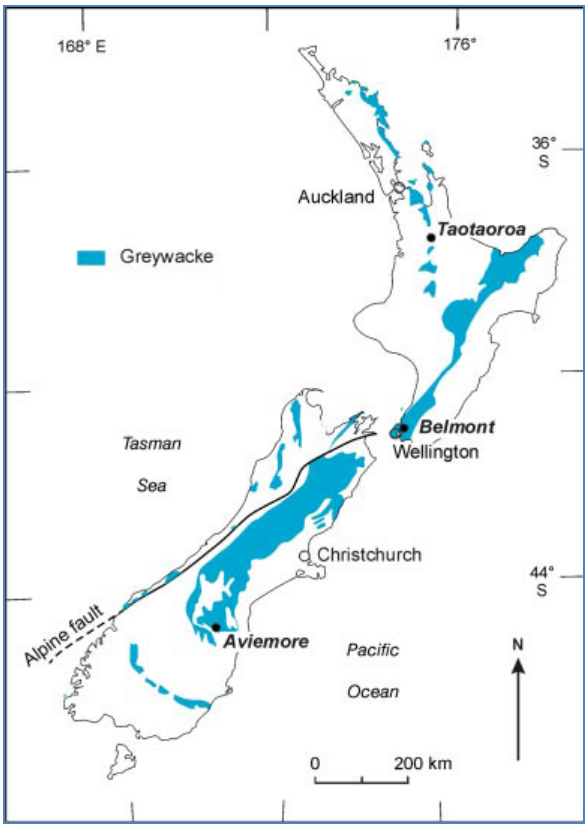

Figure 2.1: Distribution of New Zealand 'greywacke' rocks (Suggate et al., 1978).

2.2.1 'Greywacke' lithology

The term 'greywacke' is used extensively when referring to the indurated sandstones and siltstones of the New Zealand basement rocks. Pender (1971) and the Geological Society of New Zealand (NZGS, 1968) refer to New Zealand greywacke as poorly sorted, well indurated sandstone. Although, greywacke has often been referred to as interbedded siltstone and sandstone sequences (Rowe, 1980; Wellman, 1949), a determination typically only made within the quarrying industry. Greywacke rock is a major source of aggregate for roading and construction, and the individual terms 'siltstone' or 'argillite', and 'sandstone' are used for defining physical properties. The term greywacke has a wide acceptance among New Zealand geologists and more importantly to this study, among New Zealand engineers.

Lithological distinction between sandstone and mudstone can be made in the field where typically muddy sandstones are light coloured and mudstones are dark coloured. Argillite is also occasionally present, generally exhibiting lower intact strengths than greywacke. Proportions of mudstone to sandstones vary from one locality to another. Massive beds of both lithologies (sandstone and mudstone) may be up to tens of metres thick, although more cyclic deposition can result in interbedding with discrete beds <0.5m thick (Read & Richards, 2007). Due to water percolation through fractures, minerals are often found deposited along fractures, including quartz, calcite and zeolite.

At each windfarm site, siltstone, or argillite as it was defined on site, was only present in isolated circumstances. The material was typically logged as dark grey and often found within a zone of high deformation, separating two different grades of weathered 'greywacke'.

The purpose of this study is to determine the insitu elastic properties of the rock-mass below each wind turbine site. Hence, it is of limited benefit to distinguish between sandstone and siltstone lithologies within the insitu rock-mass, as the stiffness properties of each weathering unit are of primary interest, as opposed to the individual properties of individual layers.

For the purpose of this study, the term 'greywacke' will be used synonymously with sandstone and course-grade siltstone, the most common lithology found on site, while the term 'argillite' is used to cover the finer grained siltstones.

2.2.2 'Greywacke' rock mass structure

The 'greywacke' rock masses have a complex geological structure and become highly fractured due to compressional forces. Bedding is often difficult to determine due to the highly deformed nature of insitu 'greywacke', along with commonly having a high fracture density. Joint spacings greater than 750mm are very rare, with the average spacing being 60 to 200mm. Defects with even closer spacing (less then 60mm) are found in crushed and sheared zones (Read et al., 1999).

Defect types found in greywacke include bedding, joints, infilling veins and shear planes. Greywacke rock masses rarely exhibit the regular low fracture density of many other sedimentary rocks. According to Richards and Read (2007), there are often in excess of six defect sets at any one location, and even within the same geological domain there may be several variations. Joints generally comprise over 85% of all defect types and are typically closely spaced. The spacing of joints is normally wider in sandstones than mudstones, with corresponding block sizes small and mostly <0.01 m^3, with joint persistence generally being

<2m and rarely exceeding 10m. Joint apertures are typically <2mm, with the surface roughness of most defects being planar rough or planar smooth using the ISRM (1981) roughness profile classification.

2.2.3 'Greywacke' rock mass strength

The unweathered, intact 'greywacke' rock material is strong to extremely strong, with unconfined strengths of up to 350 MPa, whereas near-surface weathering, to depths of up to 30m, may reduce the strength to that of dense soils (Read et al., 1999). The rocks are often intensely deformed and folded, with subvertical or steep bedding. Using a Rock Mass Rating scheme (RMR) developed by Bieniawski (1976), the unweathered rock masses are generally classified as fair to very poor, with some thick sandstone sequences having a higher rating, or poor to very poor in the Q system (Barton et al., 1974). However, the combination of high intact rock strength and low defect persistence in a closely-jointed rock mass is not well suited to multi-parameter rock mass classification systems like the RMR. According to Read and Richards (2007) the preferred approach is a comprehensive engineering geological description to characterise the 'greywacke' for input to a specifically developed descriptive classification system. This helps provide a direct link to classification systems like the RMR or the Geological Strength Index (GSI), which is based on defect spacing and quality only, a required input into the Hoek-Brown failure criterion.

2.2.4 Summary of 'greywacke' characteristics and properties

'Greywacke' is a complex rock-mass to describe, due to the following factors (Read & Richards, 2007):

- The rock mass has often been subjected to intense geological deformation.
- Mudstone and sandstone lithologies, which are in variable proportions, have different rock mass and material properties.
- The rock mass often has 6 or more defects sets, with variable orientations between structural domains.
- Bedding is generally highly persistent, but joints typically have low persistence.
- Defects are generally very tight, often with offsets at terminations, and the mass is well interlocked.

2.3 In-situ nature of Esk-Head belt 'greywacke':

'Greywacke' forms the basement rocks of much of New Zealand, and is exposed due to uplift. The weakly deformed rocks of the Rakaia and Pahau terranes (see Figure 2.2) are seperated by a belt, up to 20km wide, or more deformed rocks which are referred to as the Rimutaka belt in the southern North Island (Begg & Mazengarb, 1996) and elsewhere as the Esk Head Melange (Bradshaw, 1973), or Esk Head sub-terrane (Silberling et al., 1988). The Esk Head belt of 'greywacke' has a range of degrees of deformation and weathering, from coherent or transposed beds to broken formation and melange (Begg & Johnson, 2000). The Esk Head belt extends from the central South Island up through the axial trace of the Lower North Island, and is found in various stages of weathering, ranging from unweathered (fresh) rock to completely weathered residual soils. Hence although there is limited lithological variation through the Esk Head belt, the physical properties vary significantly through the weathering profile. Zones of highly deformed Esk Head belt include small to large (10-150mm) clasts of basalt, chert and limestone and are regarded as melange (Begg & Johnson, 2000). The Esk-Head belt 'greywacke' is often interbedded with an argillite matrix, which is typically found in zones of shearing.

Rock masses are never homogenous, isotropic bodies. Their properties alter according to the physical, mechanical and chemical interactions they are exposed to throughout their geological history. The Esk Head belt 'greywacke' found on site at the lower North Island windfarms researched in this study displays extensive weathering, with physical and mechanical properties varying both laterally and vertically.

2.4 Weathering:

2.4.1 Weathering processes

Weathering is a set of physical, chemical and biological processes that alter the physical and chemical state of rocks and soil at or near the earth's surface. Rocks and soil are altered physically by disintegration, and chemically by decomposition. The majority of weathering involves water, including processes such as frost-shattering, wetting and drying, salt-weathering, and all chemical weathering is in solution. In addition, one of the dominant factors in weathering is time, although this aspect is not a major contributing factor for locations in the same climate. Due to weathering processes being largely driven by surface and/or atmospheric processes, the intensity of weathering decreases with depth.

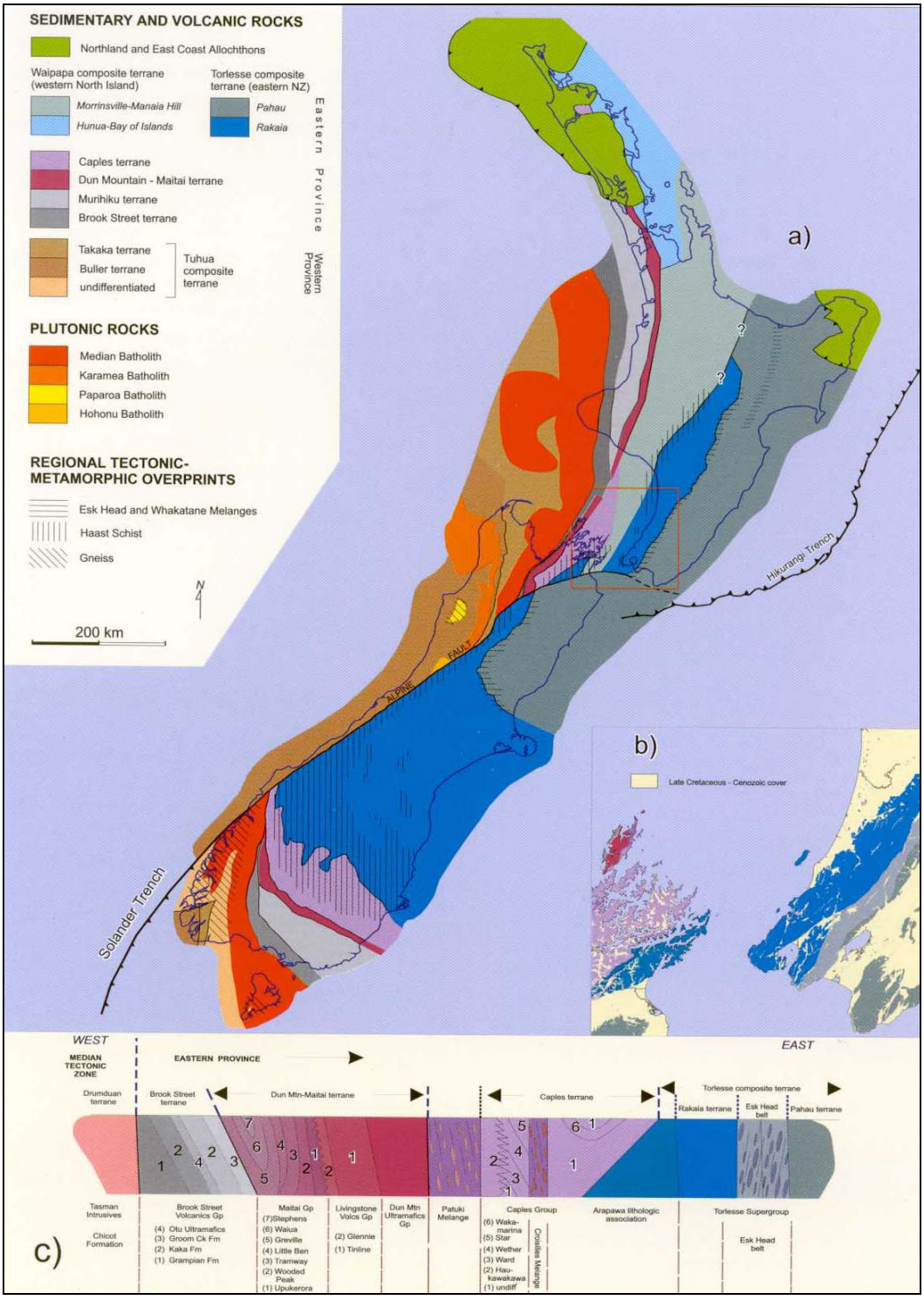

Figure 2.2: a) Basement (pre-Late Cretaceous) geological map of New Zealand. Units are grouped according to major, rather than sole, rock type. Nomenclature and boundaries of North Island Torlesse and Waipapa terranes are controversial: parts of Morrinsville-Manaia Hill and Pahau units may be correlative. Northland and East Coast Allochthons were emplaced in the Early Miocene; all other units were in mutual juxtaposition by the Late Cretaceous.
b) Basement rocks subdivided into tectonostratigraphic terranes for the Wellington area.
c) Cartoon cross section through basement rocks of Marlborough/Wellington area illustrating structural style and relationships.

Factors influencing weathering of all rock types have been listed by Sparks (1960) and Rowe (1980), and include:

- *Mineral composition:* Different minerals will weather at different rates under different physical and chemical weathering conditions.
- *Texture:* Under certain conditions, coarse grained rocks will weather more rapidly than fine grained rocks of the same mineral composition.
- *Effects of minor structures:* Minor structures in greywackes, and especially in argillites, dominate initial weathering patterns once rocks are unconfined. Any features allowing access of chemical weathering agents or increasing surface area also can increase the rates of chemical weathering.
- *Climate:* The climate of the Wellington region is assumed to have been consistent over the period of development of a natural weathering profile (10,000 years) in the greywacke rocks (Rowe, 1980).
- *Time.*

While it is convenient to differentiate between physical and chemical weathering, it is improbable that either physical or chemical processes act alone (Sparks, 1960). Physical weathering processes involve the disintegration of rock by mechanical forces concentrated along rock fractures.

Mechanical, or physical weathering, is the process by which physical forces break down rock, soil and minerals into finer particles (Chesworth, 2008).

- *Frost shattering:* the force of water in rock fractures as it freezes and expands, or is forced into the rock by the pressure of freezing water.
- *Stress release*: exfoliation of a rock mass as it expands in response to the removal of adjacent rock due to the effects of erosion.
- *Salt weathering:* growth of salt crystals in rock fractures with the evaporation of saline groundwater.
- *Hydration*: wetting, swelling and disintegration of soil aggregates and fine grained rocks.
- *Isolation weathering:* expansion and compaction with wetting and drying.

Chemical weathering processes involve the decomposition of rock by chemical reactions which occur in water, especially in soil water and ground water which are rich in dissolved carbon dioxide produced during the decomposition of plants. Hence, chemical weathering occurs as the

mineralogy of the rock adjusts to the surface environment. Chemical weathering processes include:

- *Carbonation (dissolution):* process in which atmospheric carbon dioxide leads to solution weathering.
- *Hydration:* Mineral hydration is a form of chemical weathering that involves the rigid attachment of H+ and OH- ions to the atoms and molecules of a mineral.
- *Oxidation:* Chemical oxidation of a variety of metals occurs. The most commonly observed is the oxidation of Fe^{2+} (iron) and combination with oxygen and water to form Fe^{3+} hydroxides and oxides.
- *Biological:* A number of plants and animals may create chemical weathering through release of acidic compounds.

Weathering is the detrimental physico-chemical alteration of rock. The two main factors influencing this alteration are mineral composition and texture (grain size). Throughout New Zealand the main mineral components of the greywacke rocks are quartz, sodic plagioclase and chlorite with a texture range from gravel to silt size (Rowe, 1979).

Marshall (1974) has shown that chlorite is generally the first of the four main minerals to be altered during weathering, producing clays and iron oxides, with the principle processes being oxidation and hydration. Weathering is also influenced by a range of effects, including the effects of inherent fabric structures, microcracking and preferred orientations, etc.

2.4.2 Weathering classification schemes in literature

There are a number of different classification schemes available to describe both weathered rock, and more specifically weathered 'greywacke', which are all based on visual logging.

One of the most recognised classification schemes is "The logging of rock cores for engineering purposes", a report by the Geological Society Engineering Group Working Party (Anon, 1970). This classification scheme describes the six-fold system of classifying weathered material, and has been used extensively in literature. This scheme is described by Dearman (1986), who details the method of describing the state of weathering of rock material and a scale or weathering grades for rock masses. Similarly, Fookes & Horswill (1969), also used a six-fold classification scheme for the weathering of hard rocks.

Similar schemes which have been reproduced using the 6-fold classification scheme, which focus more specifically on the weathering of 'greywacke'. These include studies by Pender

(1971), who developed a classification scheme specific to a Wellington greywacke site based on visual logging, Marshall (1974), who categorised greywacke weathering based on hand specimen colour changes and strength loss in Auckland greywacke; and a more recent study by Hodder and Hetherington (1991) who produced a quantitative study of the weathering of greywacke and developed a classification scheme specific to New Zealand greywacke based on field appearance and petrography. These papers have demonstrated that it is possible to classify weathered material in the field visually into grades, which may then be confirmed by various physical properties. Each weathering grade can be associated with a characteristic range of values for certain properties such as density, stiffness and modulus values.

Each of these weathering classification schemes utilise the six-fold classification system of describing material: unweathered, slightly weathered, moderately weathered, highly weathered, completely weathered and residually weathered. The grade one material is described as the unweathered material.

Saunders and Fookes (1970) have compared these and other systems in relation to rock weathering and foundation engineering. They discuss and summarise the properties of a range of weathered rocks, and conclude that there is little information available about the properties of weathered greywacke.

A comparison of classification schemes for weathering observations observed in hard rock and more specifically greywacke rocks is shown in Table 2.1.

	Unweathered (fresh)	Slightly Weathered	Moderately Weathered	Highly Weathered	Completely Weathered	Residually weathered
Fookes & Horswill (1969)	Parent rock shows no discolouration, loss of strength or any other effects due to weathering.	Rock slightly discoloured: discontinuities may be open and have slightly discoloured surfaces; intact rock not, as determined in the field, weaker than fresh rock.	Rock discoloured; discontinuities may be open and surfaces have greater discolouration with alteration penetrating inwards; intact rock noticeably weaker, as determined in the field, than fresh rock.	Rock discoloured; discontinuities may be open and fabric of rock near to discontinuities altered; alteration penetrated deeply inwards, lithorelicts still present.	Rock discoloured and externally changed to a soil, but original fabric mainly preserved; properties of the soil depend partly on nature of parent rock.	Rock is discoloured and completely changed to soil with original fabric completely destroyed.
Pender (1971)			Dense, brown, moderately weathered, very closely jointed material. Typical size of pieces ranges from ½ inch upwards; separate pieces break under moderate hammer blow, brown colour extends through the broken pieces but diminishes towards centre.	Light yellow-brown material; broken down to silty sand with moderate to firm finger pressure; occasional much harder lumps; original rock fabric still evident in the undisturbed material by virtue of the clack manganese dioxide along joint planes during weathering; spacing of joints variable, ranging upward from ½ inch and orientation random.	Very similar colour and texture to Grade IV but weathering more advanced; joints in parent material clearly marked; in some cases sandy texture of original rock not so evident as in Grade IV material; Grade V material easily crumbled into sandy silt under light finger pressure.	Dark red, stiff to very stiff homogeneous highly plastic clay; structure of parent rock no longer apparent although there are areas of grey, less weathered material; on drying slightly mottled texture evident.
Marshall (1974)	Dark grey or dark blue-grey. Signs of weathering absent, apart from slight surface staining along open joints and fractures.	Discolouration along joints and fractures. Grey-brown colour penetrates less than 10mm.	Rock decomposition will advance. Weathering aureole around blocks, fresh material at centre of broken fragments. Clay materials form, especially along joint and shear planes. Rock appreciably weakened by weathering – is easily shattered by hammer blow.	Equivalent to "rotten rock" of contractors and farmers. Colour varies from brown, through re-brown and lighter yellow-brown. No fresh material remains. Rock able to be broken by hand. An abundance of clay minerals. Rock retains original structures and is strong enough to maintain a steep cut face.	Material approaches soil in character. Crushes between fingers. Original structure is lost and material will not maintain a steep face.	
Hodder & Hetherington (1999)	Hard grey medium sandstone. Minor hard grey chipwacke containing black argillite ships up to 3mm long, no gradation in grain-size. Open joints, filled with clay gouge limonite or quartz; minimal staining.	Core of fresh material, surrounded by discoloured material (Stokoe et al.) accounting for some 30% of the rock. Discolouration penetrates from edges and small cracks. Open joints filled with clay or quartz. Material does not appear weaker than unweathered material.	Greyish brown rims around slightly less weathered, light grey centre of joint-bound blocks. Open joints, intensity greater than for unweathered material. Can fracture rock with modest force. Material significantly weaker than unweathered material.	Complete discolouration to orange or brown; cores of relict joint-bounded blocks are MW or HW; original fabric apparent, but obvious increase in porosity. Joints closed by expansion.	Relict-joint-bounded blocks; cores of all other grades all original fabric lost; grain size that of fine silt. Joints closed, recognised as relict.	

Table 2.1: Comparison of different 'greywacke' weathering classification schemes from literature.

2.4.3 Weathering classification

The classification scheme for describing the weathering of greywacke, adopted for this study is a combination of that described by Pender (1971) and Marshall (1974). The classification scheme described in Pender (1971) only includes descriptions for grades 3 to 6, hence the Marshall (1974) scheme was adopted to describe grades 1 and 2.

Grade 1 - Unweathered:	Dark grey or dark blue-grey. Signs of weathering absent, apart from slight surface staining along open joints and fractures.
Grade 2 - Slightly Weathered:	Discolouration along joints and fractures with intact rock showing no signs of discolouration. Grey-brown colour penetrates less than 10mm. Weaker than unweathered rock.
Grade 3 - Moderately Weathered:	Dense, brown, moderately weathered, very closely jointed material. Typical size of pieces ranges from 15mm upwards; separate pieces break under moderate hammer blow, brown colour extends through the broken pieces but diminishes towards centre.
Grade 4 - Highly Weathered:	Light yellow-brown material; broken down to silty sand with moderate to firm finger pressure; occasional much harder lumps; original rock fabric still evident in the undisturbed material by virtue of the clack manganese dioxide along joint planes during weathering; spacing of joints variable, ranging upward from 15mm and orientation random.
Grade 5 - Completely Weathered:	Very similar colour and texture to Grade IV but weathering more advanced; joints in parent material clearly marked; in some cases sandy texture of original rock not so evident as in Grade IV material; Grade V material easily crumbled into sandy silt under light finger pressure.
Grade 6 - Residually Weathered:	Dark red, stiff to very stiff homogeneous highly plastic clay; structure of parent rock no longer apparent although there are areas of grey, less weathered material; on drying slightly mottled texture evident.

Table 2.2: A standard 6-fold classification scheme redeveloped from Pender (1971) and Marshall (1974) for this study, used to classify the weathered Esk Head belt 'greywacke' in this study.

A combination of the Pender (1971) and Marshall (1974) classification schemes was used as both schemes were developed specific to the greywacke found in the lower North Island, and both proved to be consistent and accurate when applied to the weathering grades found at the study sites.

The details of the weathering grade classification utilised for this study are detailed in Table 2.2.

2.4.4 Weathering of the Esk Head belt 'greywacke'

The insitu geological material found on the Te Rere Hau windfarm site, along with the West Wind and Turitea windfarm sites, is weathered Esk Head belt 'greywacke'.

The degree of weathering varies significantly, both vertically and laterally due to the uplifted and folded structure and the subsequent steep topography. Therefore, to provide an overall site assessment, the classification scheme described in Section 2.3.3 has been consistently applied to the characterisation of 'greywacke' across all three windfarm sites utilised in this study.

The typical weathering profile found onsite at the Te Rere Hau, Turitea and West Wind Windfarms is detailed below in Table 2.3.

All three windfarm sites provided extensive outcrops for recording and studying, from an extensive network of road cuts at each site. These helped develop an understanding of the level of variability across all three windfarm sites, both laterally and vertically. Figure 2.3 displays an outcrop where the material changes laterally from a red-ionised weathered material to a yellow-brown highly weathered material. Due to the level of tectonic deformation across the windfarm sites, lateral changes in the weathering grade was also evident as beds have been uplifted and folded. Zones of shearing containing dark grey argillite were also frequent, often found within tight folds or between beds which have experienced a high level of movement. Figures 2.4, 2.5 and 2.6 also detail the variability of the subsurface conditions within the Esk Head belt 'greywacke'.

Soil Symbol	Unit	Description	Depth to top of layer (m)	Thickness (m)
	Top Soil	Loose to stiff, gravelly-silty, brown, moist, TOPSOIL.	0	0.1-0.3
	Loess/ Loess-Colluvium	Clayey-SILT, with some Gravel, grey-yellow, moist, plastic.	0.1-0.2	0.3-2.5
	Esk Head belt	Clayey-Gravel, light-grey orange with black staining, moist, completely-weathered GREYWACKE. Gravel fraction is fine to cobble in size and highly weathered.	0.2-2.0	0.5-1.5
	Esk Head belt	Highly-weathered, golden-brown with black staining, GREYWACKE, extremely-very weak, with closely spaced joints.	0.2+	0.5+
	Esk Head belt	Moderately-weathered golden-brown, GREYWACKE with grey-brown colouring on fresh rock surfaces, weak to moderately strong, closely spaced joints. Joints are essentially free of infill material.	0.2+	0.5+
	Esk Head belt	Slightly weathered brown-grey, GREYWACKE, moderately to very strong, closely spaced joints. Joints free of infill material.	0.5+	0.5+
	Esk Head belt	Unweathered, grey, GREYWACKE, very to extremely strong.	2.0+	0.5+

Table 2.3: General soil and rock profile within Esk Head belt 'greywacke' terrain, from combined data based on test pit logging and pile drilling logs from the Te Rere Hau Windfarm.

These changes in weathering grade were readily apparent in hand specimens and outcrops at each study site. It should be noted however, that because the weathering processes depend not only on the nature of the insitu geology, but also on the climate and topography, the following data should not be applied to other 'greywacke' lithologies without considering the geological and climatic differences between sites.

Figure 2.3: Lateral weathering variations along North Range Road on the Te Rere Hau Windfarm site. Location E 2741787, N 6085957, elevation 466m (WGS 1984).

Figure 2.4: Example of the highly variable nature of the Esk Head belt 'Greywacke', displaying both vertical and lateral weathering variations. From a road cut outcrop on the western flanks of the Tararua Ranges at the Te Rere Hau Windfarm. Location E 2741671, N 6086859, elevation 498m (WGS 1984).

Figure 2.5: Example of Loess surface material overlying highly and moderately weathered 'greywacke', with shear zones and infilling material. From a road cut outcrop along the North Range Road at the Te Rere Hau Windfarm. Location E 2741976, N 6086260, elevation 474m (WGS 1984).

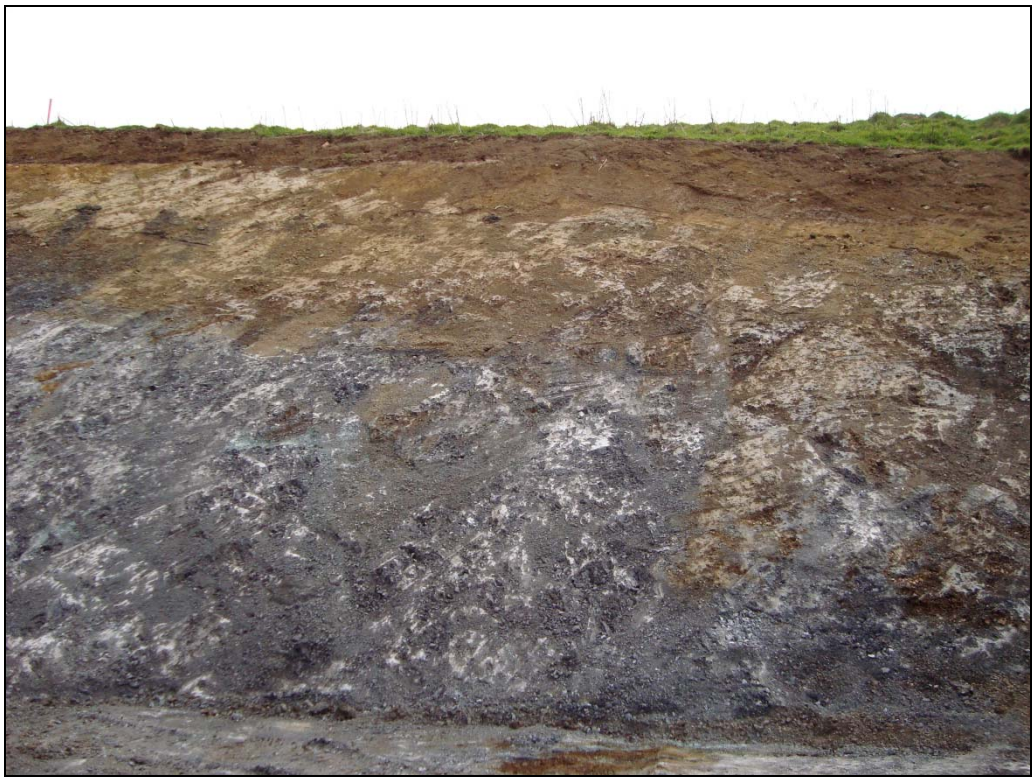

Figure 2.6: Weathering variations from highly to moderately weathered 'greywacke', to slightly-unweathered greywacke. Turbine pad excavation outcrop from turbine site 211 at the Te Rere Hau Windfarm.

2.5 Physical and mechanical properties of 'Greywacke':

Physical properties of unweathered New Zealand 'greywacke' are well established by Geological and Nuclear Sciences (available from their databases), Cook (2001), Marshall (1974) and Rowe (1980). However a very limited amount of literature is available on the physical and mechanical properties of the weathered grades of 'greywacke'.

Well-established density and porosity data for New Zealand's unweathered 'greywackes' is available from a number of studies around New Zealand, and they are generally consistent throughout the whole country (Cook, 2001). The commonly quoted bulk density for New Zealand greywacke of 2670 kg/m^3 (Reilly, 1972) has been widely used for unweathered material. Typically within the quarrying industry, sandstone and siltstone lithofacies are described separately, recording a small difference in bulk density. Cook (2001) has detailed more accurately the densities for unweathered greywacke, with the bulk density for coarse grained sandstone material being 2670-2680 kg/m^3 and for siltstones it ranges between 2700-2730 kg/m^3. The differing density values between sandstone and siltstone are related to composition and proportions of constituent mineral grains in each of the rock types. The higher proportions of phyllosilicates and heavy minerals, and the finer grain size in siltstones make them a denser material compared to the coarser grained sandstones, which dominantly consist of quartz and feldspar, which have lower specific gravities (Rowe, 1980).

Although there is a significant amount of data available on the density of unweathered 'greywacke', the majority of wind turbines at each of the three windfarms Te Rere Hau, Turitea and West Wind, are constructed on a range of weathered materials from completely weathered to slightly weathered. Hodder and Hetherington (1991) produced a quantitative study of the weathering of 'greywacke' from the Whitehall Quarry near Cambridge, New Zealand, and have determined bulk density and porosity values through the weathering profile (Table 2.4). The method used to determine density values was not mentioned in their study.

Rowe (1980) concluded that there is an inverse relationship between porosity and density, providing a scatter of data across numerous grain sizes, but still clearly displaying the mentioned relationship, which is also confirmed in the Hodder and Hetherington (1991) data in Table 2.4.

	Fresh (Unweathered)	Slightly weathered	Moderately weathered	Highly weathered	Completely weathered	Soil
Physical Properties						
Bulk Density	2.69	2.61	2.53	1.78	1.34	1.40
Porosity (%)	1.61	2.58	4.71	29.0	48.2	49.2

Table 2.4: Variation of bulk density and porosity values through the weathering profile. Reproduced from Hodder & Hetherington (1991).

The study by Pender (1971) on the properties of weathered 'greywacke' is one of the most widely quoted studies, and considered an industry standard for weathered 'greywacke' properties, especially for sites in the Wellington region. The study was focused on one particular site in Wellington, New Zealand, where continuous 4 inch diameter undisturbed samples were taken using a triple tube rotary core barrel. The site encountered only 4 grades of weathered greywacke, ranging from residually weathered to moderately weathered 'greywacke'. Pender's study concentrates on the more weathered grades of residually, completely and highly weathered material, on which it is possible to perform soil mechanics classification tests on.

Pender (1971) presents both index and mechanical properties for weathering grades from residually weathered to highly weathered 'greywacke' in Tables 2.5 and 2.6. Both Tables 2.5 and 2.6 present characteristic ranges for most properties, sometimes with overlapping at the transition between weathering grades. Pender suggests that for practical applications, some better means of estimating likely values would be useful, as the spread of ranges for some properties can be fairly wide. This paper identifies the importance of defining a range of values for properties within each weathering grade, as weathering is a gradational scale. However, for geotechnical engineering design or calculations, often a single value is required as an input. In this case, the middle value of the range is typically used as an input.

Grade	Liquid Limit, w_L (%)	Plasticity Index, I_P (%)	% Passing 200 Sieve	% Finer than 2 Microns	Specific Gravity, G	Void Ratio, e
4	35	10	25-55	15	2.70-2.69	0.30-0.55
5	34-60	8-35	55-80	15-40	2.70-2.69	0.50-0.85
6	60-100	30	80	40-60	2.74	0.75-1.4

Table 2.5: Index properties for grades of highly (4), completely (5) and residually (6) weathered 'greywacke', reproduced from Pender (1971).

Grade	Coefficient of Permeability, K	Compression Index, C_C	Preconsolidation Pressure, p_C (kg/m^2)	Angle of Internal Friction, ø
4	10^{-7}	0.1	195000	35
5	$4 \times 10^{-6} - 1 \times 10^{-8}$	0.1-0.35	234000-98000	35-15
6	$3 \times 10^{-8} - 5 \times 10^{-9}$	0.30-0.70	98000	15

Table 2.6: Mechanical properties for grades of highly (4), completely (5) and residually (6) weathered 'greywacke', reproduced from Pender (1971).

2.6 Synthesis:

This chapter detailed the rock mass properties of 'greywacke' rock, including lithology, rock mass structure and strength. Secondly, the insitu characteristics or the Esk Head belt 'greywacke' has been discussed, with a focus on weathering. Both physical and chemical weathering processes acting on the Tararua Ranges site have been detailed, along with the different classification schemes which have been previously used to describe weathered 'greywacke'. The 6-fold classification scheme described in a report by the Geological Society Engineering Group Working Party (Anon, 1970), and further described in Dearman (1986), has been reproduced by a number of subsequent 'greywacke' classification schemes.

The classification scheme utilised in this study is detailed next. This is a 6-fold classification developed from Marshall (1974) and Pender (1971).

Finally, mechanical and physical properties of 'greywacke' are discussed, including data from studies by Cook (2001), Hodder and Hetherington (1991), Marshall (1974), Pender (1971) and Rowe (1980). The lack of information detailing properties of the weathered grades of 'greywacke' is discussed, along with detailing the limited data which is available.

Chapter 3: Geotechnical and Engineering Geological Investigations:

3.1 Introduction:

The principal aims of this geotechnical and engineering geological investigation were to fully characterise the Esk Head belt 'greywacke' from the Te Rere Hau, Turitea and West Wind Windfarms. A full site characterisation allows correlation with geophysical investigation data, and will provide geotechnical input data for the calculation of elastic modulus values through the weathering profile.

The investigative procedures implemented in this study focused on:

1. Engineering geological site characterisation, including rock mass descriptions, test pitting, face logging and logging of drilled piles.
2. Rock mass density characterisation through the weathering profile using Sampling Tube, Oil Replacement and Submersion density testing methods.
3. Poisson's ratio characterisation through the weathering profile using V_P/V_S ratios from downhole seismic surveys.
4. X-Ray Diffraction analysis of the weathered 'greywacke'.

Physical soil and rock properties were determined primarily through insitu geotechnical investigation methods, including downhole seismic testing to determine V_S and V_P profiles, and Sampling Tube, Oil Replacement and Submersion density testing methods. Geotechnical investigations were hampered due to the high fracture density of the insitu 'greywacke'. Due to its high fracture density it was extremely difficult to extract sufficiently sized intact samples of 'greywacke' for laboratory strength testing methods. Therefore, insitu testing was essential for determining physical properties. In addition to this, a number of correlations were made with existing geotechnical and geophysical data.

3.2 Site Engineering Geology:

3.2.1 Rock Mass Characterisation

To accurately classify the material onsite, a classification scheme was applied specific to the geological conditions found onsite. The insitu Esk Head belt 'greywacke' material is in various

stages of decomposition, ranging from unweathered rock to residually weathered soils. Due to the large number of investigation sites across each windfarm, an easily repeatable rock mass classification scheme was developed using a combination of that described by Pender (1971) and Marshall (1974), as detailed in Chapter 2.3.3. Table 3.1 provides a graphical log of a typical weathering profile through the Esk Head belt 'greywacke'.

Grade	Weathering	Description
1	*Unweathered*	Dark grey or dark blue-grey. Shows no discolouration, loss of strength or any other affects due to weathering.
2	*Slightly weathered*	Rock slightly discoloured; discontinuities may be open and have slightly discoloured surfaces; intact rock not, as determined in the field, weaker than unweathered rock.
3	*Moderately weathered*	Dense, discoloured to brown, very closely jointed material. Typical size of pieces ranges from 15mm upwards, brown colour extends through the broken pieces but diminishes towards centre. Discontinuities may be open and surfaces have greater discolouration with alteration penetrating inwards; intact rock noticeably weather, as determined in the field, than unweathered rock.
4	*Highly weathered*	Light yellow-brown material; broken down to silty sand with moderate to firm finger pressure; occasional much harder lumps; original rock fabric still evident in the undisturbed material by virtue of the clack manganese dioxide along joint planes during weathering; spacing of joints variable, ranging upward from 15mm and orientation random.
5	*Completely weathered*	Very similar colour and texture to Grade 4 but weathering more advanced; joints in parent material clearly marked; in some cases sandy texture of original rock not so evident as in Grade 4 material; Grade 5 material easily crumbled into sandy silt under light finger pressure.
6	*Residually weathered*	Dark red, stiff to very stiff homogeneous highly plastic clay; structure of parent rock no longer apparent although there are areas of grey, less weathered material; on drying slightly mottled texture evident.

Table 3.1: Rock mass classification scheme for weathered 'greywacke' developed for this study from Pender (1971) and Marshall (1974).

3.2.2 Geotechnical classification

Classifying the weathered 'greywacke' according to current geotechnical classification systems was difficult due to the nature of the discontinuities in the rock-mass. Chapter 2 detailed the extent of fracturing in the insitu Esk Head belt 'greywacke', with average spacing between joints of between 60 to 200mm, and spacings over 200mm very rare (Read et al., 2000). A high fracture density was apparent through each of the weathering grades of 'greywacke'.

Two commonly used rock mass classification schemes in geotechnical engineering are the Rock Mass Rating (RMR) scheme (Bieniawski, 1976), and the Q system (Barton et al., 1974). Both of these schemes are largely influenced by the Rock Quality Designation (RQD) factor, which is defined as the sum of lengths of rock pieces (intact) or fracture spacings, greater than 10cm, expressed as a total length of the scan line or logged core (Deere, 1963). Due to the fracture density found insitu, unweathered 'greywacke' rock masses are commonly classified as fair to very poor in the Rock Mass Rating (RMR) scheme (Bieniawski, 1976), and poor to very poor in the Q system (Barton et al., 1974), heavily influenced by the RQD value.

Due to the large impact of RQD on both the RMR and the Q system classification schemes, there is little variation between the different weathering grades, as all grades generally fall in the ranges of 'poor rock' for both schemes. Therefore there is minimal benefit in using these geotechnical classification systems for characterising the different grades of weathered 'greywacke' or correlating with changes in shear-wave velocity through the depth and weathering profile.

3.2.3 Face logs

During the initial stages of this study, the extensive network of road cuts across the Te Rere Hau Windfarm site were utilised for familiarisation with the local geology. Road cut faces were logged in an effort to understand the level of variability, both vertically and laterally within the insitu 'greywacke'. This gave an understanding of the contacts between units and their characteristics, along with variability and continuity of the different weathering grades. This method also helped with becoming familiar with the different weathering grades and utilising the classification scheme detailed in Table 3.1.

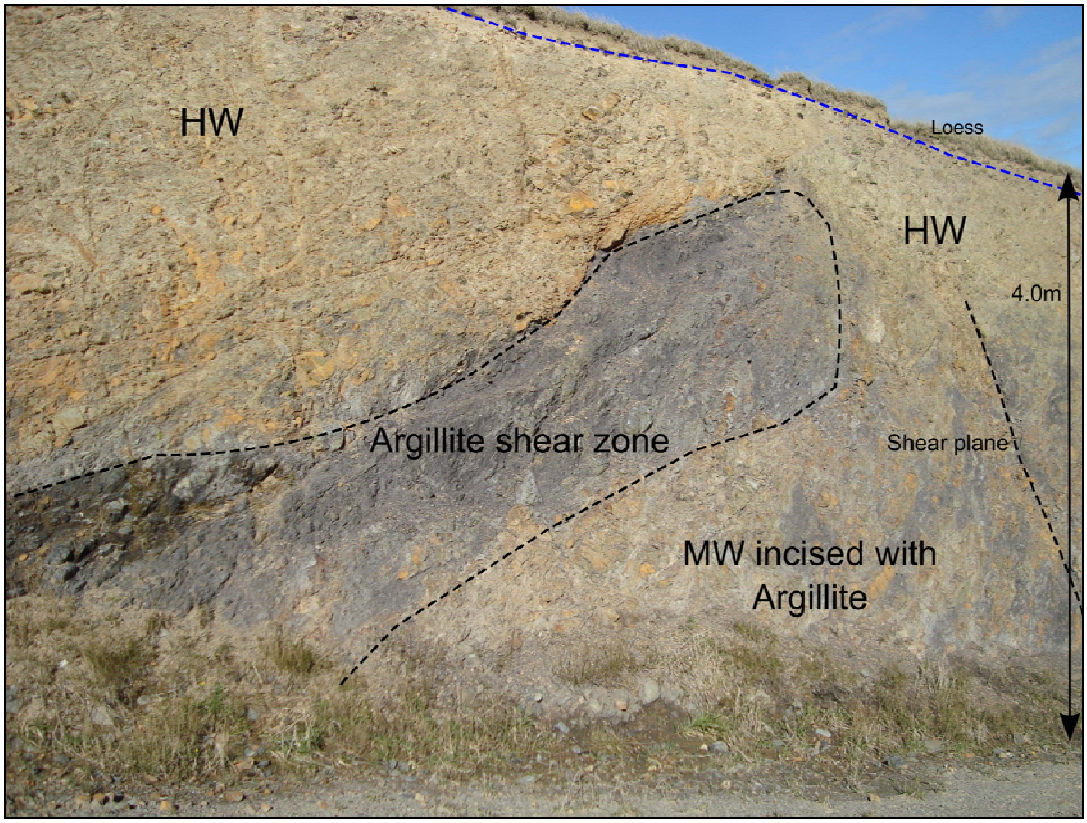

Figure 3.1: Face log from a road cut along Henderson Ave on the Te Rere Hau Windfarm. Location E 2741671, N 6086859, elevation 498m (WGS 1984).

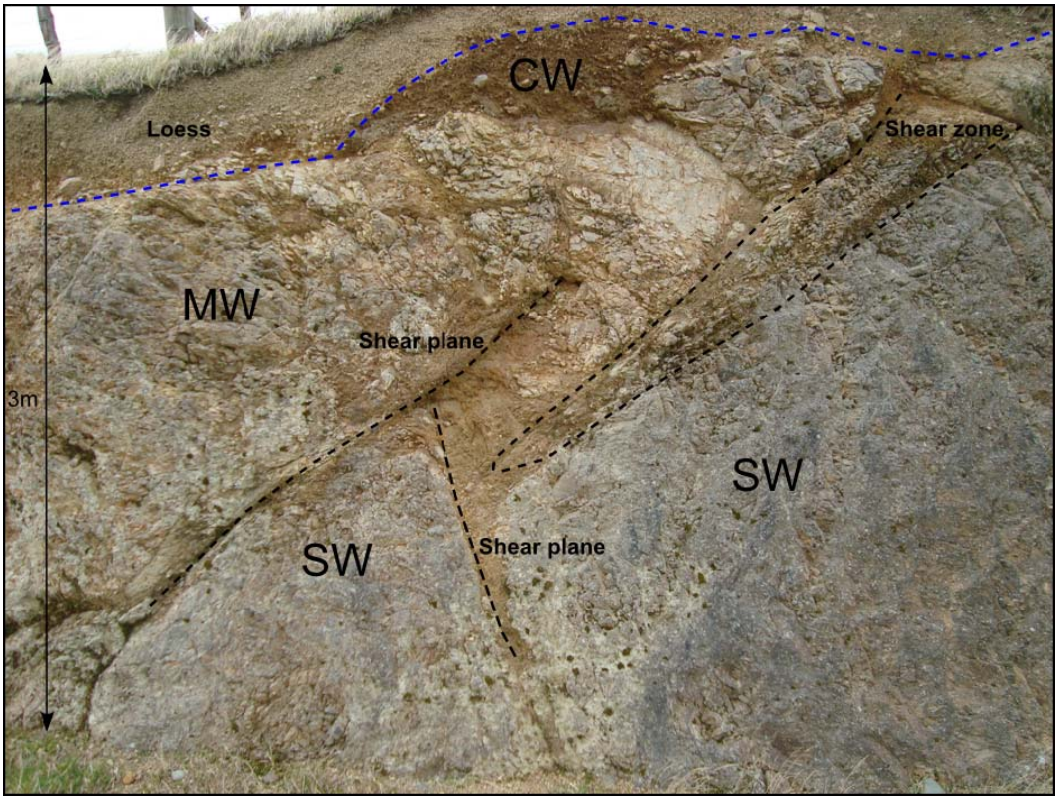

Figure 3.2: Face log from a road cut along North Range Road on the Te Rere Hau Windfarm. Location E 2741976, N 6086260, elevation 474m (WGS 1984).

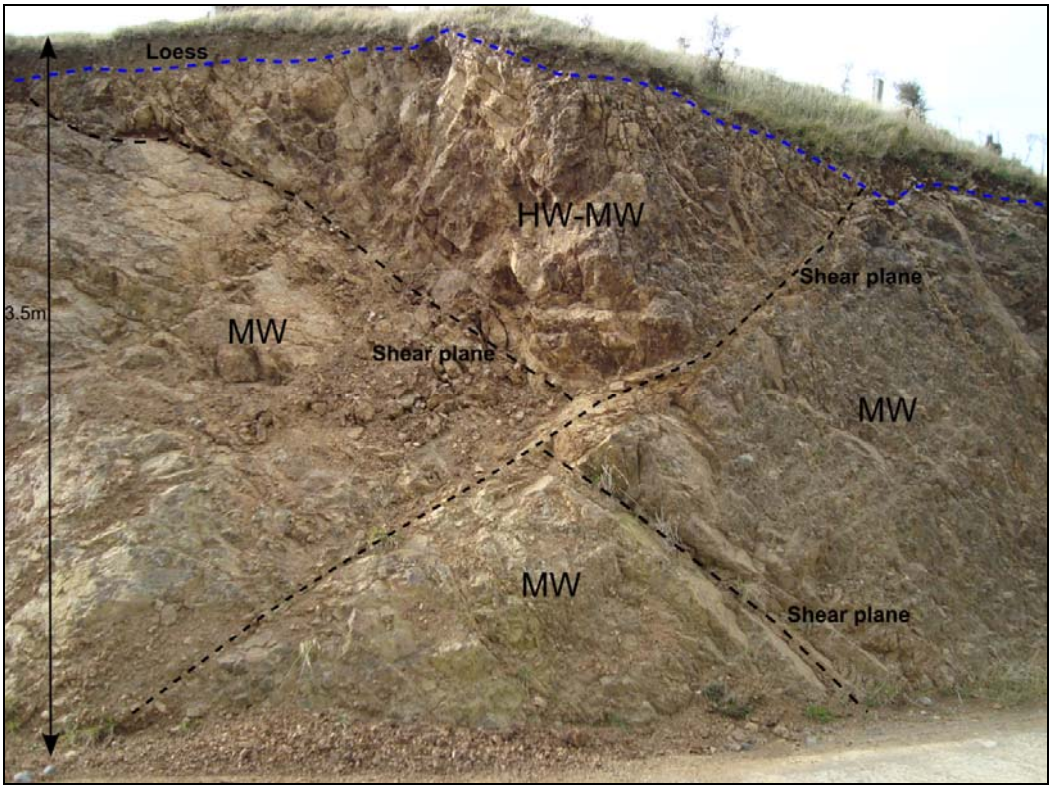

Figure 3.3: Face log from a road cut along North Range Road on the Te Rere Hau Windfarm. Location E 2741923, N 6086120, elevation 472m (WGS 1984).

3.2.4 Test pit logs

Test pitting was performed at the Te Rere Hau Windfarm site during the Eastern Extension geotechnical investigations, where 13 test pits were excavated to an average depth of 1.5m and a maximum depth of 2.5m, and logged by both myself and engineers on site (Figures 3.4 and 3.5). The aim of the test pitting was to determine the depth to competent rock and the depth of overburden to be excavated for construction of the turbine foundations. The excavation of test pits was performed by earth works contractors onsite, using a 20 tonne excavator.

Test pitting provided an opportunity for sampling where fresh insitu material could be visually inspected, and allowed for mapping of subsurface features and conditions. The test pits were logged according to the weathering classification scheme used in this study, described in Table 3.1. The test pit logs presented in this study are those included in the Te Rere Hau Windfarm Eastern Extension Geotechnical Investigation report by Aurecon New Zealand Limited and submitted to New Zealand Windfarms Limited. A full set of test pit logs and photos can be found in Appendix C.

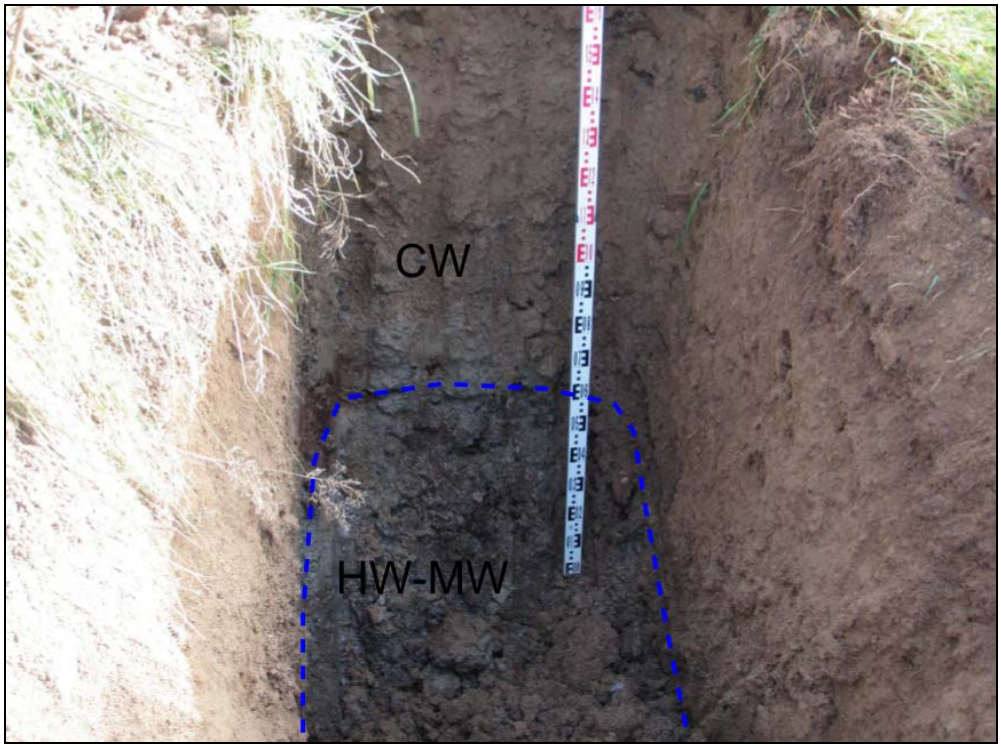

Figure 3.4: View of test pit TE11 from the Te Rere Hau Windfarm, with clayey-silty completely weathered 'greywacke' material overlying highly to moderately weathered 'greywacke' rock from 1.7mbgl onwards.

3.2.5 Logging of drilled mono-piles

Wind turbines on the Te Rere Hau Windfarm were founded on a 2.4m diameter mono-pile foundation up to 10m deep. Without borehole data available for each turbine site at the Te Rere Hau Windfarm, the mono-pile drilling was utilised to characterise the weathering profile at each site. Drilled material was extracted during the drilling process and logged from the disturbed samples at either 1.0 or 1.5m intervals, as specified by the engineers onsite. The extracted material was logged according to the classification scheme described in Table 2.1 above.

Due to the extracted material being in a disturbed and crushed state, a slightly different approach was taken when logging, as some features including geological contacts, shear zones, fracture density and quantity of infilling material were not able to be determined.

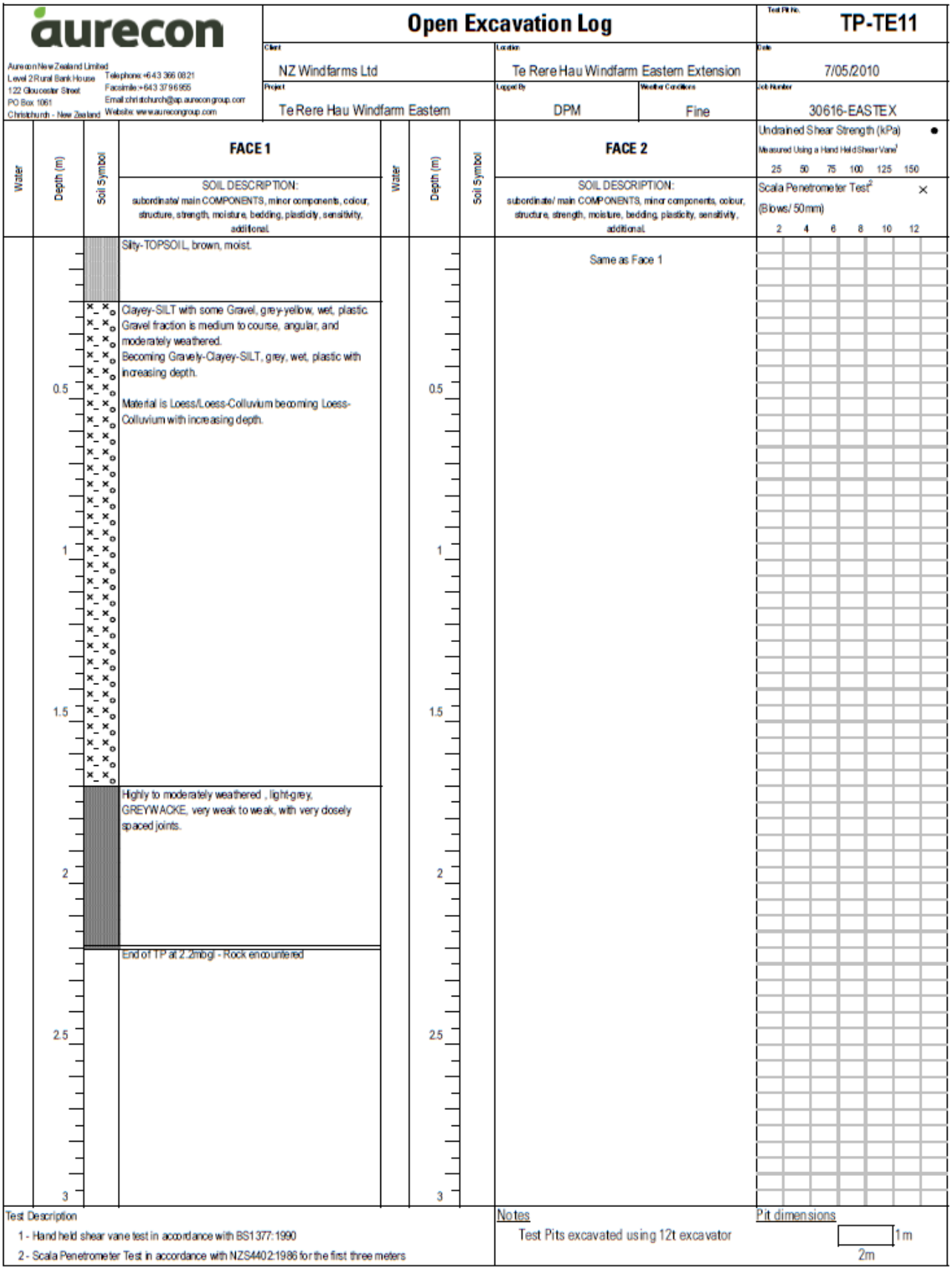

Figure 3.5: Test pit log from test pit TE11 at the Te Rere Hau Windfarm. Only test pit face logging was performed, without any shear vane, scala penetrometer or other insitu testing utilised (Mahoney, 2010).

The importance of colour in establishing both rock type and degree of weathering has long been acknowledged. Classification by rock colour is therefore possible where large colour contrasts exist (Rowe, 1980). In the weathered 'greywacke' the most consistent changes through the weathering profile, identifiable in hand specimen were colour and rock strength, which was determined in the field. In addition to colour and strength determinations, logging was assisted by inspecting the clasts of gravel to determine whether the grains and matrix material were weathered. A full set of logged mono-pile drilled holes can be found in Appendix D.

3.2.6 Engineering Geological Trends

The winds in the Wellington and Manawatu regions are strongly dominated by the prevailing westerly. Because of this, the majority of wind turbines along the Tararua Ranges, at various windfarms, are built on the western flanks of the ranges, taking advantage of the dominant westerly winds.

During the initial stages of development, erecting turbines on the western flanks of the Te Rere Hau Windfarm site was the primary focus. Pile drilling logs from a selection of these sites are displayed in Table 3.2. The majority of these logs show an influence of weathering to depths of approximately 9m, with a gradual change in weathering grade, from residually weathered material at the surface, through to slightly weathered or even unweathered 'greywacke' at depths generally no shallower than 9m. Exceptions do exist where slightly or unweathered material is reached within 4m from the surface.

In comparison to this trend, turbine sites along the ridge line of the Tararua Ranges (Table 3.3) and down onto the eastern flanks (Table 3.4), show unweathered greywacke rock typically being reached at much shallower depths, with a small number of exceptions.

The dominant westerly winds batter the western flanks of the ranges with heavy rain and extremely strong winds, enhancing the rate of weathering, largely due to surface water infiltration, hydration and oxidation. The influence of this climatic condition is also evident in the pile drilling logs from the Te Rere Hau Windfarm.

Determining the depth to competent rock (slightly weathered/unweathered) at each turbine site at the Te Rere Hau Windfarm is essential, as the length of the mono-pile design is dependent on the determination of this boundary.

Western Flanks of the Tararua Ranges									
Turbine 33		**Turbine 47**		**Turbine 53**		**Turbine 73**		**Turbine 84**	
Depth (m)	**Soil Type**	**Depth (m)**	**Soil Type**	**Depth (m)**	**Soil Type**	**Depth (m)**	**Soil Type**	**Depth (m)**	**Soil Type**
1.5	L/LC	1.5	L	1.5	LC	1.5	L/LC	1.5	L/LC
3	CW/HW	3	L/LC	3	HW	3	HW	3	CW
4.5	HW	4.5	HW/MW	4.5	HW/MW	4.5	MW	4.5	CW/HW
6	HW/MW	6	HW/MW	6	MW/SW	6	MW	6	HW
7.5	MW	7.5	MW	7.5	MW/SW	7.5	MW	7.5	HW
9	SW	9	MW/SW	9	SW	9	MW/SW	9	HW/MW
10.5	SW/UW	10.5	SW	10.5	SW	10.5	SW	10.5	MW
11.5	SW/UW	11.5	UW			11.5	SW	11.5	MW/SW

Table 3.2: Pile drilling logs from turbine sites on the western flanks of the Tararua Ranges at the Te Rere Hau Windfarm site.

Ridge line of the Tararua Ranges									
Turbine 210		**Turbine 211**		**Turbine 212**		**Turbine 220**		**Turbine 209**	
Depth (m)	**Soil Type**	**Depth (m)**	**Soil Type**	**Depth (m)**	**Soil Type**	**Depth (m)**	**Soil Type**	**Depth (m)**	**Soil Type**
1	MW/SW	1	LC	1	SW	1	MW	1	MW/SW
2	MW/SW	2	SW	2	SW	2	MW/SW	2	MW/SW
3	SW	3	SW	3	SW/UW	3	SW	3	MW/SW
4	SW	4	SW	4	UW	4	SW	4	MW/SW
5	SW	5	SW	5	UW	5	SW/UW	5	MW/SW
6	SW	6	SW	6	UW	6	SW/UW	6	MW/SW
7	SW/UW	7	SW	7	UW	7	SW/UW	7	MW/SW
8	UW	8	UW	8	UW	8	SW/UW	8	MW/SW
9	UW	9	UW	9	UW	9	SW/UW	9	MW/SW
10	UW	10	UW	10	UW	10	UW	10	MW/SW
11.5	UW	11.5	UW	11.5	UW	11.5	UW	11.5	MW/SW

Table 3.3: Pile drilling logs from turbine sites along the ridge line of the Tararua Ranges at the Te Rere Hau Windfarm site.

Eastern Flanks of the Tararua Ranges									
Turbine 204		**Turbine 205**		**Turbine 202**		**Turbine 203**		**Turbine 240**	
Depth (m)	**Soil Type**	**Depth (m)**	**Soil Type**	**Depth (m)**	**Soil Type**	**Depth (m)**	**Soil Type**	**Depth (m)**	**Soil Type**
1	CW/HW	1	RS	1	MS/SW	1	LC	1	SW
2	MW	2	MW/SW	2	MS/SW	2	LC	2	SW
3	SW	3	MW/SW	3	MS/SW	3	LC	3	SW
4	SW	4	MW/SW	4	MS/SW	4	SW	4	SW
5	SW	5	MW/SW	5	SW	5	SW	5	SW
6	SW	6	SW	6	SW	6	SW	6	SW
7	SW	7	SW/UW	7	SW	7	SW/UW	7	SW
8	SW	8	SW/UW	8	SW/UW	8	SW/UW	8	SW
9	SW	9	SW/UW	9	UW	9	SW/UW	9	SW
10	SW/UW	10	SW/UW	10	UW	10	SW/UW	10	SW/UW
11.5	SW/UW	11.5	UW	11.5	UW	11.5	SW/UW	11.5	SW/UW

Table 3.4: Pile drilling logs from turbine sites on the eastern flanks of the Tararua Ranges at the Te Rere Hau Windfarm site.

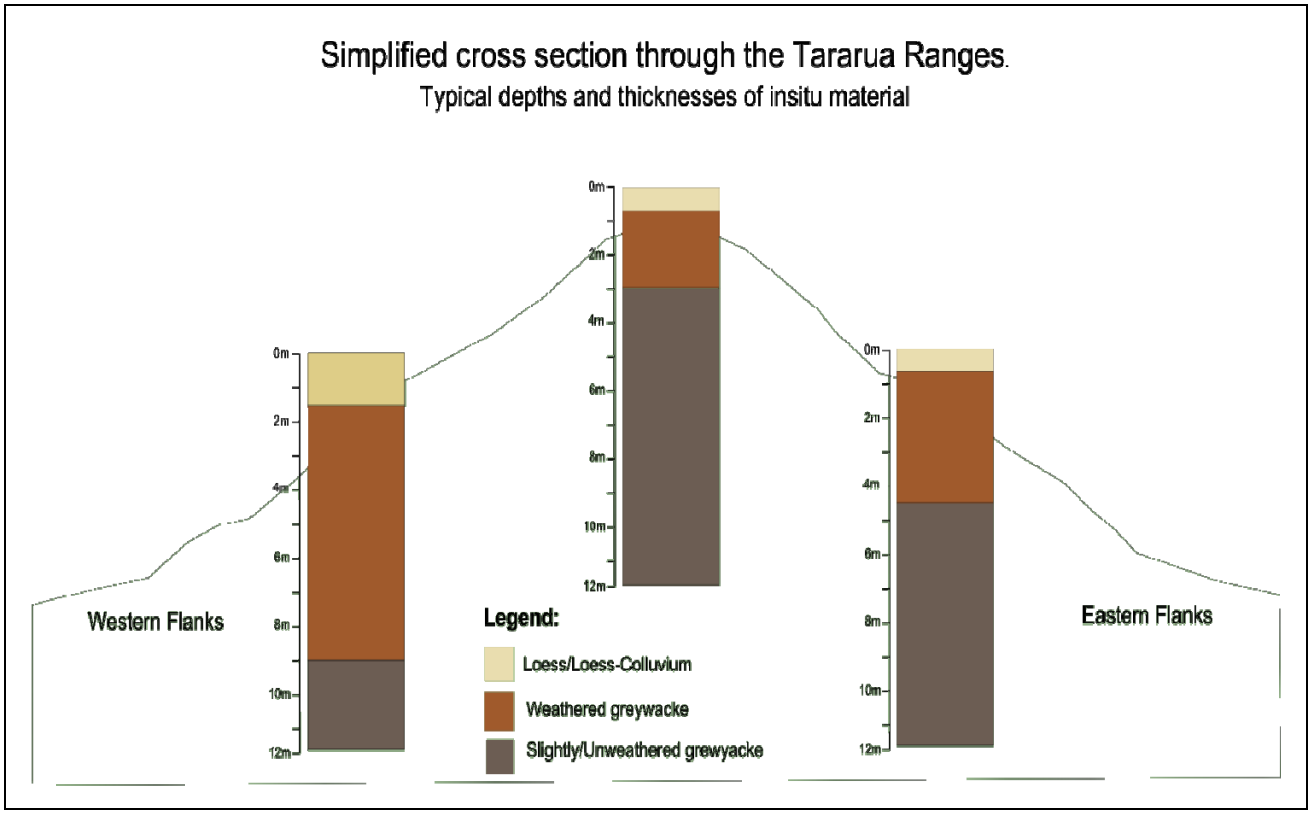

Figure 3.6: A simplified cross section through the Tararua Ranges, displaying the distribution of loess/loess-colluvium, weathered greywacke and the slightly/unweathered greywacke.

3.3 Rock density characterisation:

3.3.1 Introduction

Characterisation of rock mass density values through the weathering profile of the Esk Head belt 'greywacke' rock was required specific to the research sites. Density values were essential to ensure accurate elastic modulus (E) values were calculated from the shear wave velocity (V_S) profiles, as density is an input into this calculation, as detailed in Chapter 1.7. Three different density measurement techniques were employed due to the variation in physical properties of greywacke. The sampling tube method was employed on test sites in the highly weathered to completely weathered grades. The oil displacement method was employed at test sites in the moderately weathered grades, and laboratory submersion methods were employed on slightly weathered to unweathered grades of 'greywacke'. All three methods are detailed in Section 3.3.2 below.

Unweathered greywacke density values in New Zealand are well documented in the literature (Cook, 2001; Marshall, 1974; Read et al., 2000; Reilly, 1972; Rowe, 1980; Stewart, 2007), with the most commonly quoted bulk density value of 2.67 t/m^3 (Reilly, 1972). In contrast to this, density values through the weathering profile of weathered greywacke are less commonly documented in literature. A study by Hodder and Hetherington (1991) details the density values of weathered greywacke through the weathering profile from the Whitehall Quarry, near Cambridge, New Zealand (Figure 3.11). The Whitehall Quarry is situated within the Manaia Hill Group, which the Institute of Geological and Nuclear Sciences New Zealand (2005) determined as part of the Waipapa terrane, whereas this study is focused within the Esk Head Belt greywacke rock of the Torlesse Complex (Institute of Geological and Nuclear Sciences, 2002).

Two earlier studies by Raisbeck (1973), and Martin and Miller (1974) also detail density values through the weathering profile from their studies in the Wellington region. Both studies present a range of dry density values for each weathering grade, representative of the gradational change in physical properties due to weathering displayed in Table 3.6. The exact location of these studies is not available, however it can be assumed they are both located within the Rakaia terrane as is the majority of Wellington.

3.3.2 Methods

Sampling tube method

New Zealand Standard 4402 : 1986. Test 5.1.3

The sampling tube method for the determination of insitu density was used for samples in the highly weathered to completely weathered range. This was due to the sampling tube being relatively easily driven into a horizontally cut face, recovering an accurate insitu sample. A non-corrodible rigid cylindrical sampling tube with a bevelled edge and a diameter of 100mm, was driven into the weathered rock using a mallet. The sampling tube method was only used on highly to completely weathered material because of the ease with which the tube could be driven into the insitu material.

Figure 3.7: 100mm diameter sampling tube used to determine a specified volume of completely weathered 'greywacke' at the Te Rere Hau Windfarm site, prior to extraction and trimming. Then weighing and drying were performed in the laboratory.

Oil displacement method (adapted from the water displacement method)

New Zealand Standard NZ 4402 : 1986. Test 5.1.5

The water displacement method was adapted for this study to use oil as the liquid, replacing water. This was done because of oil's low viscosity, making it less susceptible to being lost down small fractures or absorbing into the soils. This method was applied to the moderately weathered range of insitu material. Due to the combination of blocky rock material along with clay infilling and highly weathered material occupying fractures and joints, neither the sampling

tube method nor the laboratory submersion method was appropriate. In accordance with NZ4402 : 1986 test 5.1.5, the insitu material was removed from a horizontal cut face, gathered in a air tight sample bag for weighing and drying in the laboratory, and the hole filled with oil to a measured and recorded volume.

Figure 3.8: Oil replacement density testing method. Excavation and bagging of material before hole is filled with oil to determine volume and material is dried and weighed in the laboratory to determine mass.

Laboratory submersion method

New Zealand Standard NZ 4402 : 1986. Test 5.1.4

The laboratory submersion method determines the density of a sample using Archimedes' principle. The Archimedes' principle states that a body immersed in a fluid experiences a buoyant force equal to the weight of the fluid it displaces.

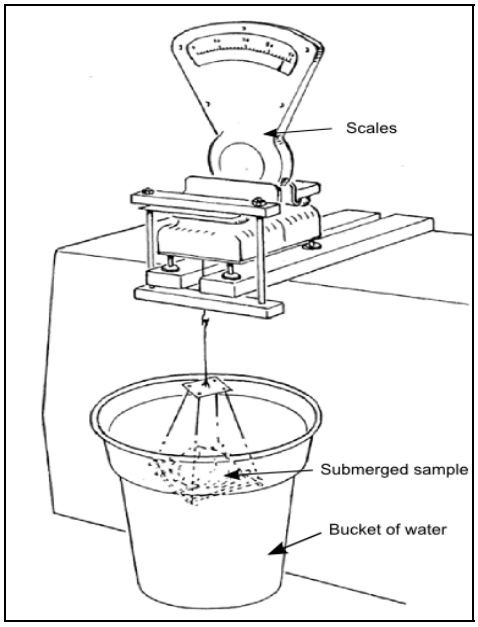

Figure 3.9: Water immersion method, displaying an irregular shaped rock sample mass being measured while suspended and immersed in water (Standards New Zealand, 1986).

The laboratory submersion method involves a dry density measurement and a fully saturated density measurement of irregular shaped samples, and porosity values can be determined from a comparison of these two values. Mass measurements are recorded prior to submersion, next the specimens are placed in a cradle, completely immersed, and an apparent mass of the specimen is taken. The same procedure is repeated after specimens have been left in a densometer for 24 hours until fully saturated.

This method was applied to samples of slightly to unweathered grade material. Due to the irregular shape of the lumps of material and the difficulty associated with volume determinations in the field, the submersion method lended itself appropriately to this grade of rock. This method was also suited to the unweathered grades of material as the samples did not disintegrate once immersed in water or fully saturated in the densometer.

3.3.3 Results

Due to the changing physical properties of 'greywacke' through the weathering profile, different density testing methods were employed. The limitation of using three different testing methods is the introduction of possible inaccuracies when correlating between methods due to inconsistency of procedures. These possible inaccuracies were managed by performing 20 separate density tests over a range of weathering grades, and defining the final density variation results by fitting a 3rd degree polynomial best fit trend line to a scatter plot of all dry density data (Figure 3.10).

The highly weathered material displays the greatest range in density values between the three studies, from 1780 to 2540 kg/m^3. The dry density values from both the Raisbeck (1973) and the Martin & Miller (1974) detail a similar range of dry density values, with Raisbeck's study typically showing a smaller range in values.

The dry density results from the Te Rere Hau Windfarm follow a similar non-linear trend through the weathering profile to the bulk density data from the Hodder & Hetherington (1991) study (Figures 3.10 and 3.11). Both of these profiles present similar values through the less weathered grades, with the Te Rere Hau results showing lower values through the more weathered grades, which is expected due to the results being from dry testing, along with the higher water content of residually weathered to moderately weathered material. The Hodder and Hetherington (1991) results have been adjusted in relation to water content to give dry density results, and have been compared in Figure 3.12 with other dry density values.

Both the Raisbeck (1973) and the Martin & Miller (1974) studies present density values from the Wellington region, which would be considered more representative of the Te Rere Hau Windfarm site than the Whitehall Quarry values. The Wellington studies were undertaken within the Rakaia terrane, which along with the Esk Head belt, is located within the Torlesse Supergroup (Begg & Johnson, 2000). However, significant differences would not be expected between density values of the different geological terranes, as they are both exposed to similar climatic and weathering conditions.

	Unweathered (kg/m^3)	**Slightly weathered (kg/m^3)**	**Moderately weathered (kg/m^3)**	**Highly weathered (kg/m^3)**	**Completely weathered (kg/m^3)**	**Residually weathered (kg/m^3)**
Hodder & Hetherington (1991) *bulk density*	2690	2610	2530	1780	1340	1400
Raisbeck (1973) *dry density*		2243-2450	2082-2243	1794-2082	1490-1794	
Martin & Miller (1974) *dry density*	2540-2570	2320-2450	1930-2420	2020-2540	1500	
Te Rere Hau Windfarm *dry density*	2740	2490	2020	1520	1200	1180

Table 3.5: Comparison of different density values and ranges through the weathering profile for 'greywacke'.

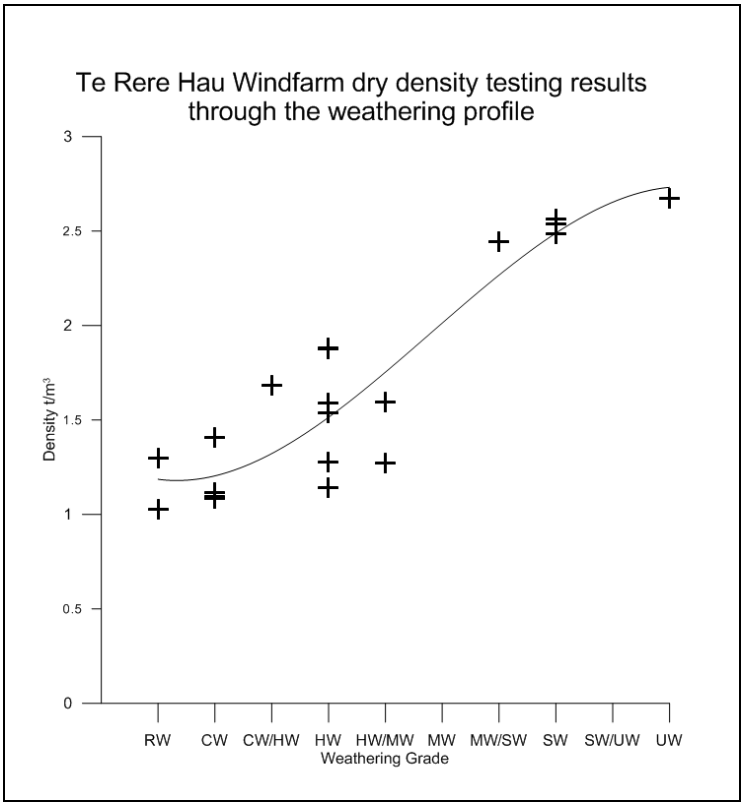

Figure 3.10: Averaged dry density testing results from the Te Rere Hau Windfarm with 3rd order polynomial best fit trend line.

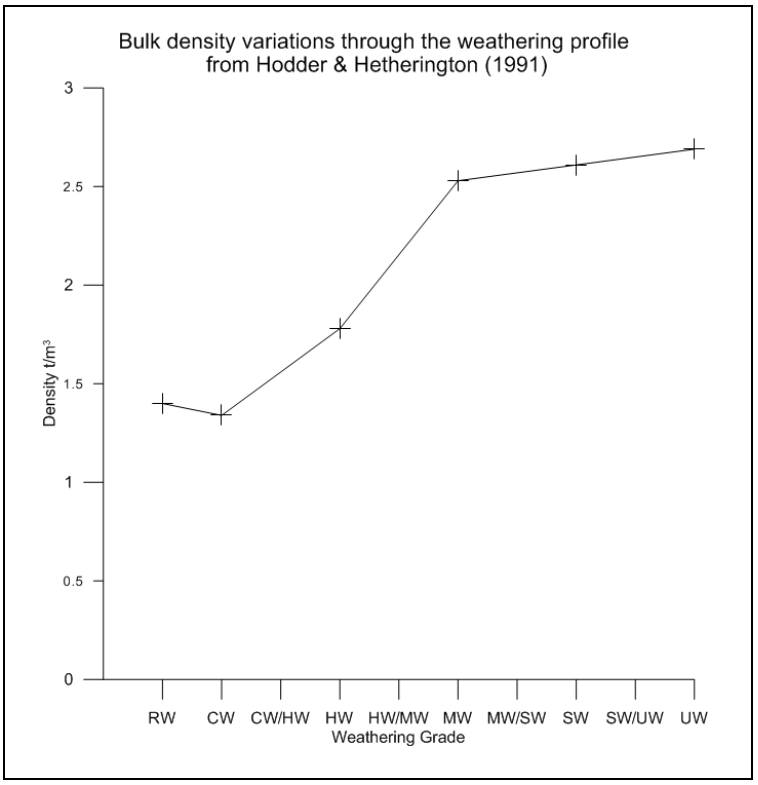

Figure 3.11: Bulk density variations through the weathering profile from the Hodder and Hetherington (1991) study, undertaken at the Whitehall Quarry, near Cambridge, New Zealand.

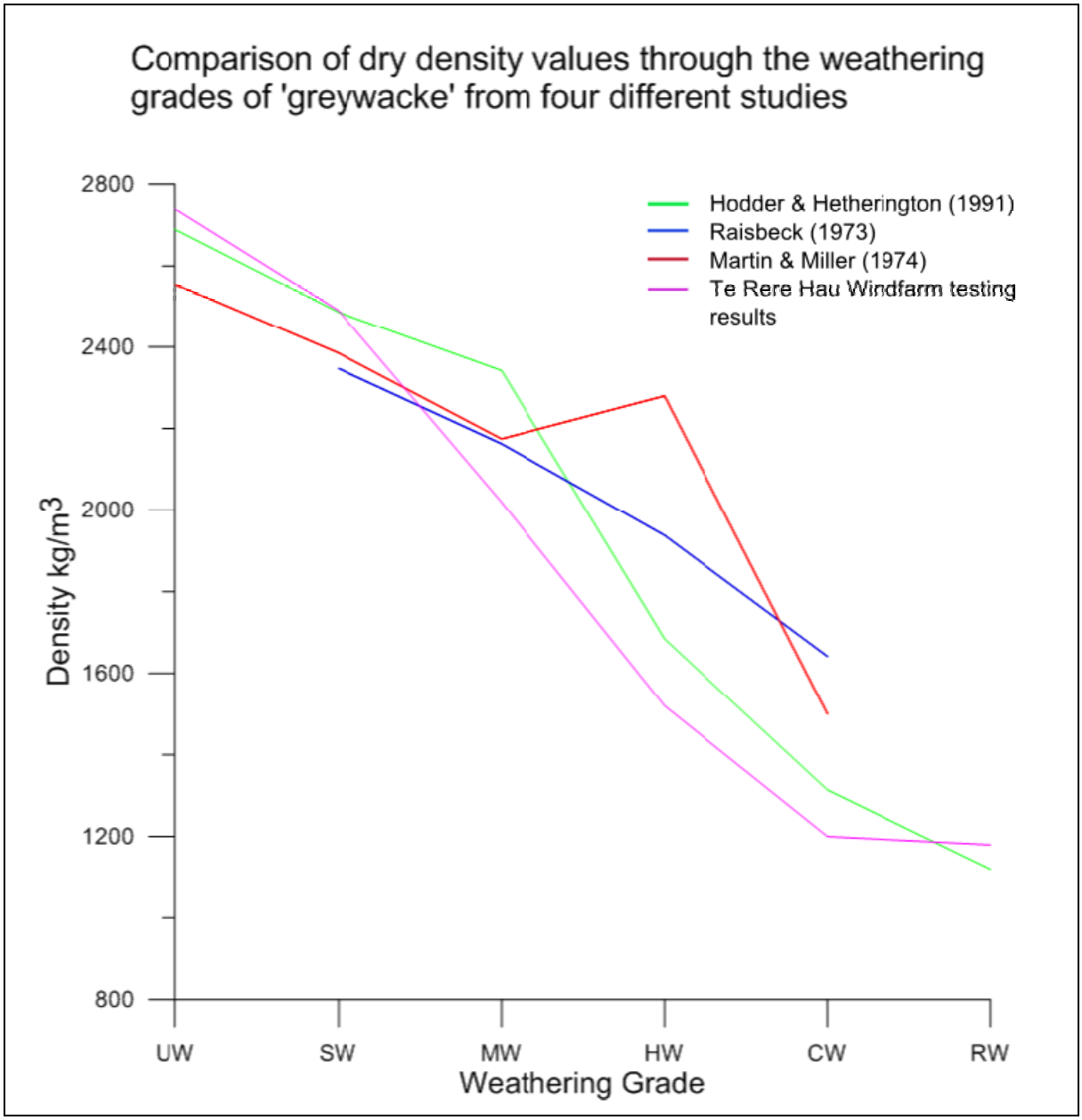

Figure 3.12: Dry density values through the weathering profile from Hodder and Hetherington (1991), Martin & Miller (1974), Raisbeck (1973), along with results from density testing at the Te Rere Hau Windfam.

Figure 3.12 displays the dry density values through the weathering profile from the mentioned studies, along with the results from the testing at the Te Rere Hau Windfarm. The midpoint value has been selected for the ranges in density values, along with a simplistic calculation to determine the dry density values from the bulk density values presented in Hodder and Hetherington (1991). This was calculated using moisture contents determined from the testing performed at the Te Rere Hau Windfarm, which resulted in 0% for unweathered, 4% for slightly weathered, 8% for moderately weathered, 15% for highly weathered, and 25% for completely

and residually weathered. These values also fall within the range of moisture content values presented in Raisbeck (1973).

Significant variations exist between the three studies, especially within the more weathered grades of 'greywacke' where the absolute values do not correlate well with the other studies. However, all three studies display a general trend of increasing density with a decreasing weathering grade. A number of influences could have contributed to the range in density values, the simplest of all being that the physical properties between the sites vary, although a variation this large is unexpected. Sampling tube methods sometimes may entirely fill the tube, leaving unrepresentative voids in the sample, or material can be compressed during sampling. Submersion methods do not include insitu conditions as samples are washed and any highly weathered infilling material disintegrates during the saturation process. However, the most likely source of error is incurred during characterisation of the material. The three studies discussed, along with this study, have used a 6-fold classification scheme to describe the 'greywacke' material, although this is a subjective method. Errors made in the classification of material produce unrepresentative testing results for the classified grade of material, hence a high level of subjectivity can exist.

Possibly another technique needs to be employed in addition to visual logging. Martin and Miller (1974) used direct shear equipment in the classification of different weathered grades of material. The use of a Schmidt Hammer to determine rebound values which can be correlated with visual logging methods can also be used, or as Kingsbury (1987) employed, the use of a cone indenter to determine static hardness, can also be used to identify different grades of material. This aspect has not been integrated in this project.

Because of these inconsistencies, further investigations into the density values within the weathered grades of the Esk Head belt 'greywacke' is required for an accurate determination of density variations with weathering.

Full details and calculations of the density testing can be found in Appendix E.

3.4 Poisson's ratio characterisation:

3.4.1 Introduction

Poisson's ratio characterisation through the weathering profile of weathered greywacke rock was required to ensure accurate elastic modulus (E) values were calculated from the shear

wave velocity (V_S) profiles. Poisson's ratio can be determined seismically if P-wave and S-wave velocities are known.

Poisson's ratio represents the lateral or transverse strain, which occurs along with axial contraction or elongation, and is quoted as a dimensionless ratio (Johnson & De Graff, 1988). The mass Poisson's ratio, which is also referred to as the insitu Poisson's ratio, represents the lateral or transverse strain of the insitu rock-mass, in contrast to the laboratory derived material Poisson's ratio.

The material Poisson's ratio is determined from the following equation for a cylindrical core:

$$v = \frac{\Delta l}{\Delta d} \qquad \textbf{Equation 3.1}$$

Where:
v = Poisson's ratio
Δl = change in length
Δd = change in diameter

Poisson's ratio cannot exceed 0.5, a value obtained from an ideal, incompressible material. Typically, values of Poisson's ratio are inversely proportional to both compressive strength and modulus of elasticity (D'Andrea et al., 1965).

The 'mass Poisson's ratio' can also be determined through small strain seismic testing.

$$\frac{Vp}{Vs} = \sqrt{\frac{2 - 2v}{1 - 2v}} \qquad \textbf{Equation 3.2}$$

$$v = \frac{1}{2}\left[1 - \frac{1}{\left(\frac{V_P}{V_S}\right)^2 - 1}\right] \qquad \textbf{Equation 3.3}$$

(Christensen, 1996)

Often Poisson's ratio is expressed as a V_P/V_S ratio, when calculated from seismic properties, for ease of computation.

An inaccurate Poisson's ratio has a significant influence in the calculation of elastic modulus profiles, as discussed in Chapter 1.7. Converting a V_S profile with depth into an Elastic modulus (E) profile involves Poisson's ratio as an input, using Equation 3.4:

$$E = 2 \rho V_S^{\,2} (\nu + 1) \qquad \textbf{Equation 3.4}$$

For this calculation to produce an accurate elastic modulus profile with depth, Poisson's ratio values are required through the depth profile, associating to either lithological, or the weathering changes with depth.

Unfortunately due to time and budgetary constraints, it was not viable to organise drillholes on the Te Rere Hau Windfarm site for downhole seismic testing. Instead, seismic data from the West Wind Windfarm was used for the determination of Poisson's ratio. The West Wind Windfarm site is also located within the weathered 'greywacke' Torlesse terrane of the lower North Island, and has been exposed to a similar weathering climate to the Te Rere Hau Windfarm site, and similar Poisson's ratio values are expected between the two sites.

3.4.2 Method

The mass Poisson's ratio for each weathering grade was determined from logged drillhole data and downhole seismic testing data performed at the West Wind windfarm site. As discussed, this site is also situated within the weathered 'greywacke' of the lower North Island, and displayed consistent physical and weathering properties with that of the Te Rere Hau Windfarm.

Poisson's ratio was determined using compressional wave velocity (V_P) and shear wave velocity (V_S) data, gathered during downhole seismic surveying from 7 drillhole sites.

$$\nu = \frac{1}{2}\left[1 - \frac{1}{\left(\frac{V_P}{V_S}\right)^2 - 1}\right] \qquad \textbf{Equation 3.5}$$

During the down-hole seismic testing, shear waves (S-waves) were generated using a sledge hammer to strike the ends of a plank, which was held in contact with the ground by parking a loaded vehicle on it. Similarly, compression waves (P-waves) were created by striking the ground vertically. The resulting waves were recorded using a string of six horizontally mounted

geophones suspended down the bolehole, and spaced 0.5m apart, with one geophone mounted vertically. The geophones were individually spring loaded to ensure good contact with the PVC liner, which had been grouted into each drillhole. Each geophone was isolated from the others by a rubber spacer.

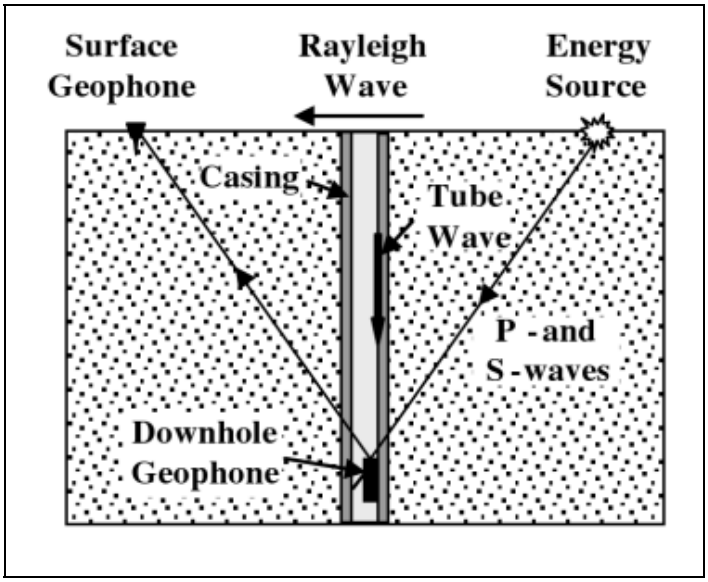

Figure3.13: Downhole seismic method for testing P-wave and S-wave velocities (Gadallah & Fisher, 2009).

Data was recorded using an ABEM digital seismograph. The seismgraph was triggered by the closing of an electrical circuit between the hammer and the steel plates on the ends of the plank. The data were processed to determine the phase velocities of the shear waves over one metre intervals, between geophone elements, using LabView software.

Compression wave velocities were also calculated from the first arrival times from the vertical hits recorded on the vertical geophone element. These velocities were averaged over several metres, dividing the hole into sections was there was obvious changes in velocity.

Poisson's ratio values were calculated through the depth profile from the V_P/V_S ratios, using Equation 3.5, at each of the 7 sites at the West Wind Windfarm. Next, each Poisson's ratio interval was assigned its representative weathering grade. From the drillhole logs at the West Wind Windfarm, the weathering grade profiles were matched with the Poisson's ratio profiles with depth, at each of the 7 sites. From this, Poisson's ratio values for each weathering grade could be collated and graphed in plots of depth verses Poisson's ratio, as displayed in Figure 3.15 and 3.16.

The, along with their associated depth values were then matched with their corresponding borehole log data from each survey site. Poisson's ratio was calculated from the V_P/V_S ratios at each data point, using Equation 3.5. Each Poisson's ratio and its associated depth value was separated into groupings of each weathering grade.

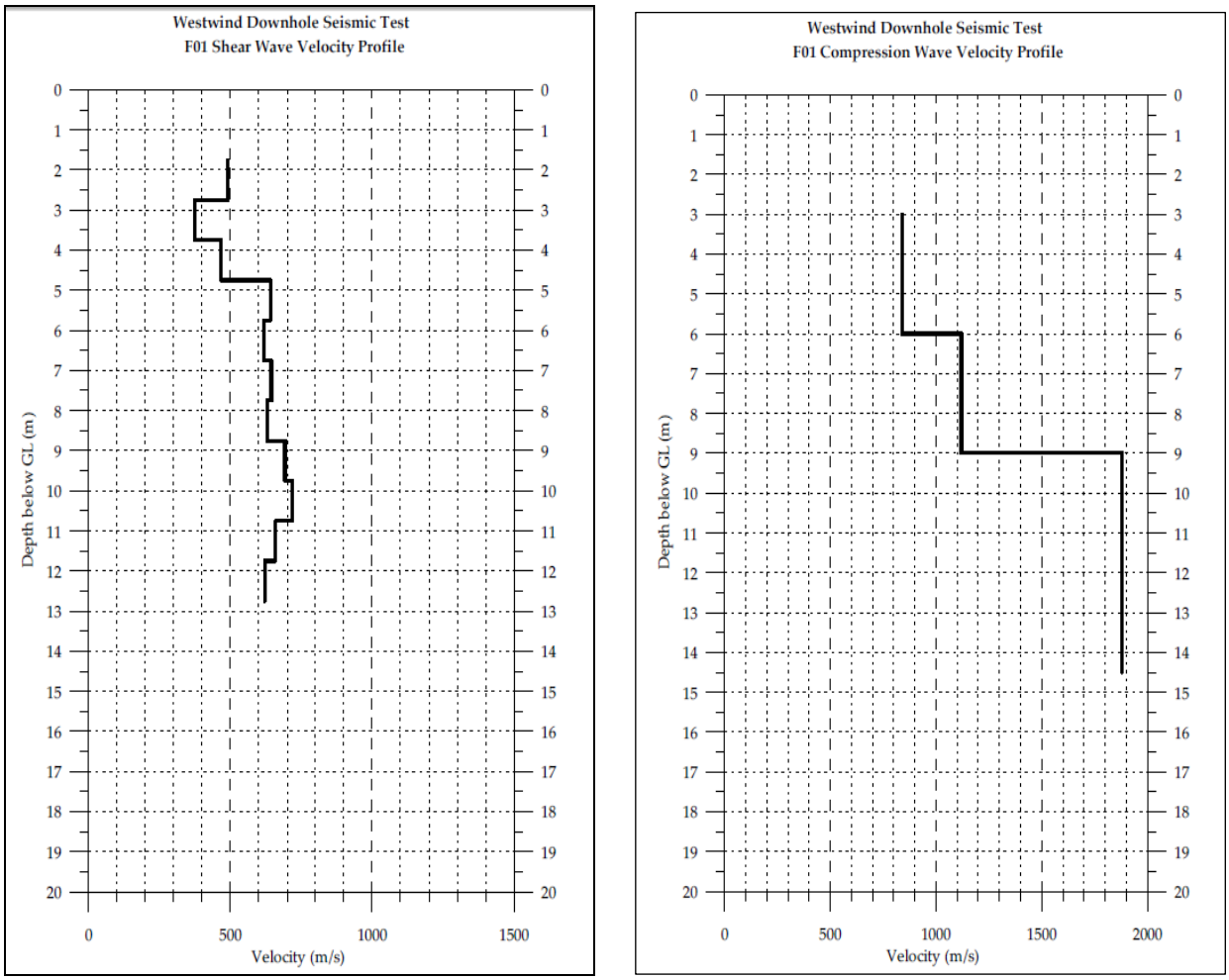

Figure 3.14: Shear wave velocity (left) and compression wave velocity (right) profiles from Westwind Windfarm turbine site F01 (Mason, 2006).

A full set of shear wave and compression wave velocity profiles can be found in Appendix D.

3.4.3 Results

For each weathering grade, the calculated mass Poisson's ratio was plotted against depth. No obvious trends were evident throughout the data set, suggesting that depth had little influence on Poisson's ratio within the same grade of weathered material, as displayed in Figure 3.15 and 3.16. This is in agreement with Johnson and De Graff (1988), who stated that Poisson's ratio shows no well-defined linear relationship with either V_P or V_S (Figure 3.17).

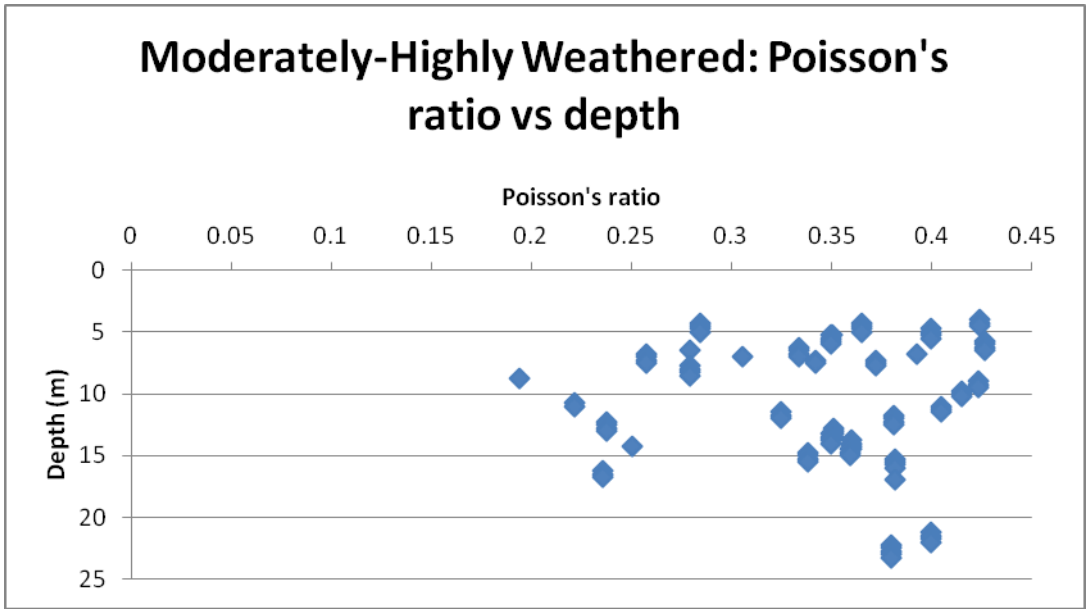

Figure 3.15: Poisson's ratio versus depth for moderately-highly weathered 'greywacke'.

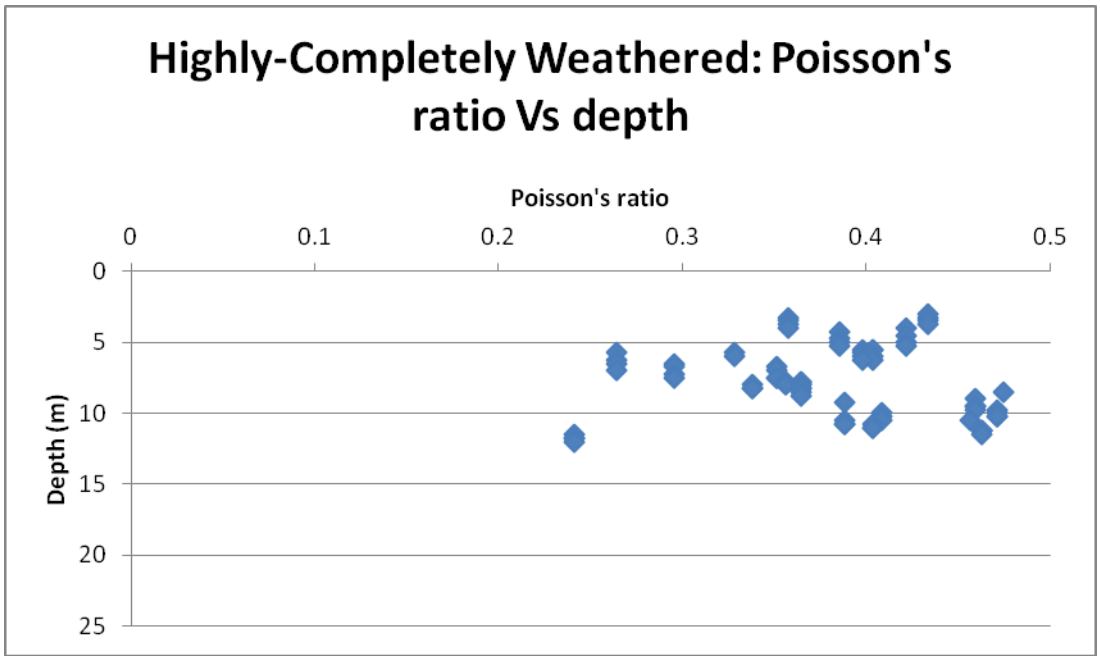

Figure 3.16: Poisson's ratio versus depth for highly-completely weathered 'greywacke'.

This data was averaged for each weathering grade to determine a representative range of values for Poisson's ratio for each weathering grade. Poisson's ratio variation through the weathering profile is detailed in Table 3.4. Figure 3.18 displays the linear trend of the averaged Poisson's ratio values calculated in this study.

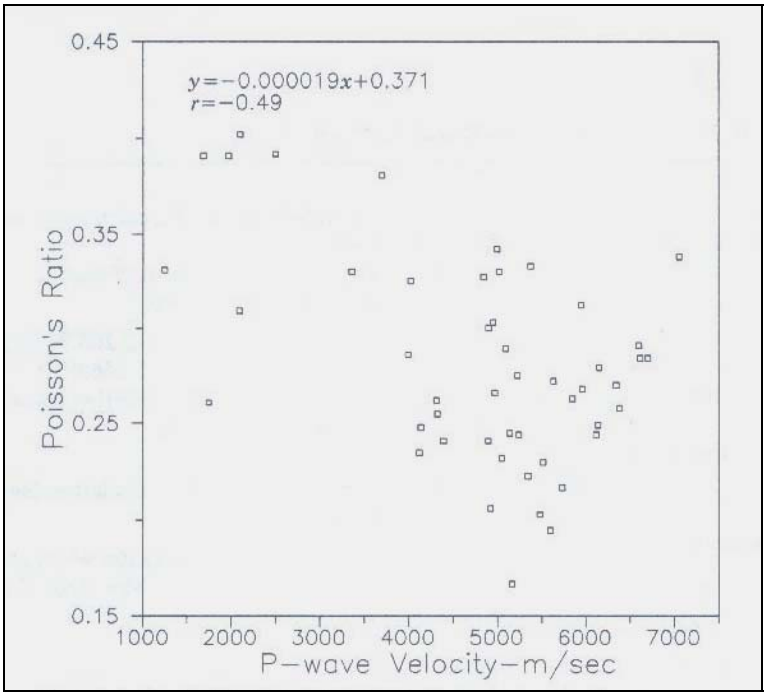

Figure 3.17: Plot of compressional P-wave velocity versus Poisson's ratio, which displays no well defined linear relationship (Johnson & De Graff, 1988).

Although a scatter of Poisson's ratio values is expected, there were also a number of limitations apparent in the Poisson's ratio dataset. These limitations are not associated with the methodology of calculating Poisson's ratio, but the accuracy of the gathered data and the consistency between different datasets. As discussed, a number of different sources of data were used, including borehole logs, V_S and V_P profiles. The boreholes were logged by various engineers during the West Wind Windfarm geotechnical investigation, from which weathering grades were used to characterise and arrange seismic data. In addition, the seismic data was not originally gathered with the intention of determining Poisson's ratio values. The V_P records were averaged over several metres, dividing the profile into sections where there were obvious changes in velocity, possibly excluding important minor detail. This approach was taken by the geophysical contractor conducting the surveys.

For the purposes of this study the methodology used in the calculation of Poisson's ratio is the important focus, especially with the aim of developing a repeatable method. With regard to this study, Poisson's ratio values calculated were not required in any of the data analysis or calculations in this study, only in the calculation for determining elastic modulus from V_S. However, this data would still provide a sound estimation of Poisson's ratio values if required for further investigations within the weathered 'greywacke' of the lower North Island. .

P-wave and S-wave data for unweathered greywacke material was not available, as the 7 boreholes in which downhole seismic testing took place did not extend through to unweathered material. Hence the value for unweathered greywacke has been fixed at 0.21, a commonly used value from the study by Kleffmann et al. (1998).

	CW	CW/HW	HW	HW/MW	MW	MW/SW	SW	SW/UW	UW
Poisson's ratio	0.39	0.38	0.33	0.35	0.34	0.33	0.25		0.21
Range in Poisson's ratio	0.326-0.454	0.316-0.444	0.266-0.394	0.286-0.414	0.276-0.404	0.266-0.394	0.186-0.314		0.146-0.274

Table 3.6: Averaged mass Poisson's ratio values and range in values, through the weathering profile, calculated from 7 downhole seismic surveys at the West Wind Windfarm. The range of values was determined using 1 standard deviation of the dataset higher and lower than the average value.

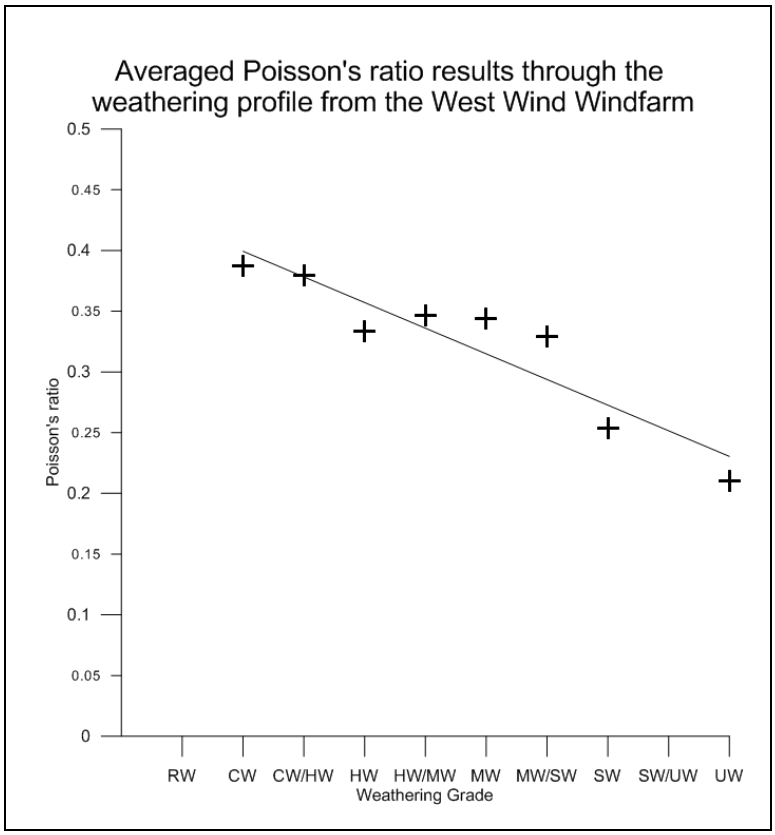

Figure 3.18: Averaged Poisson's ratio values through the weathering profile, determined from downhole seismic surveying at the West Wind Windfarm.

3.5 X-Ray Diffraction:

To ensure a complete characterisation of the site material, four samples of weathered greywacke rock inscriptions were collected and studied using X-Ray Diffraction (XRD) analysis to determine their mineral composition. During the weathering, both physical and chemical processes, alterations occur specific to the parent rock type and the influencing weathering processes. An XRD analysis can determine the type of mineralogy being deposited as a result of weathering. The results of the XRD analysis are displayed in Table 3.7.

Sample	Material Type	Chemical Composition
1	Moderately weathered greywacke rock from Te Rere Hau Windfarm	Quartz (55%), Albite (40%), Kaolinite (5%)
2	Moderately weathered, ironised (red) weathered greywacke rock from Te Rere Hau Windfarm	Quartz (100%)
3	Moderately weathered greywacke rock from Te Rere Hau Windfarm	Quartz (70%), Albite (30%), Kaolinite (trace)
4	Slightly weathered greywacke rock from Te Rere Hau Windfarm	Quartz (65%), Albite (35%)

Table 3.7: Results of XRD analysis of greywacke rocks from Te Rere Hau Windfarm.

The greywacke rock samples were prepared by myself in the University of Canterbury laboratories, where they was crushed into a homogenous fine powder. The samples were then tested by University of Canterbury laboratory technicians using a Phillips PW1820/1710 X-ray powder Diffratometer system.

The clay minerals represented by kaolinite in Table 6.X are a result of alteration of feldspar minerals. The clay minerals usually occur as alteration products, filling the fractures, microfractures and clevages. The kaolinite clay found to be present is likely to have been formed via weathering of feldspathic greywacke sandstone in acidic conditions (Grim, 1968).

However, this analysis only provides an indication of the clay mineralogy present in the Esk Head belt 'greywacke', rather than an accurate percentage content. The larger 'greywacke' particles present in the samples would overprint the clay content, as the clay material is a filling material between fractures in the 'greywacke'. This clay material most likely dried and dispersed from the intact rock samples prior to XRD analysis. Therefore it must be assumed the clay contents indicated are unreliable.

The quartz contents vary between 55-70%, with albite contents varying between 30-40%. These results are typical values for the Torlesse greywacke rocks in New Zealand. Geologists often term greywacke with a high qualtity of albite contents 'dirty sandstones', a term often used for the Torlesse greywacke.

Sample 2 had been exposed to ironisation weathering processes, with 100% Quartz, and had a dark red colour. In these instances iron content is generally less than 1% and often doesn't show up in XRD analysis results, as in the case of Sample 2.

3.6 Synthesis:

This chapter details both the geotechnical and engineering geological investigations across the three windfarm sites. The 'greywacke' rock-mass is detailed and described using a number of investigation techniques, including face logging, test pitting and drillhole logging. These methods helped to characterise the rock-mass and identify engineering geological trends. A significant trend identified from the data was a deeper weathering profile on the western flanks of the Tararua Ranges in comparison to the eastern flanks. It has been suggested that this trend could be due to the climatic conditions, in particular the prevailing westerly winds which could increase the rate of both chemical and physical weathering.

The geotechnical investigations involved both rock-mass density and Poisson's ratio characterisation through the weathering profile. A limited selection of literature was available for density and Poisson's ratio properties through the weathering grades of 'greywacke' for comparisons. The density results displayed a non-linear variation through the weathering profile. This non-linear trend was consistent with other studies detailing density values, although a large scatter exists, which is assumed to be due to the subjectivity of classifying the weathered grades of 'greywacke'. The Poisson's ratio results displayed no trend with depth for the individual weathering grades, but the average values for each grade produced a linear trend of decreasing Poisson's ratio with a decrease in weathering.

Chapter 4: Surface Wave Velocities: Interpretation and Techniques

4.1 Introduction:

When earthquakes occur, 'natural' seismic waves radiate away from the source and travel rapidly through the earth's crust, producing shaking at the ground surface. These waves are a result of an earthquake, explosion or volcanic activity, and produce low frequency acoustic energy. Different types of seismic waves are produced: body waves and surface waves. During an earthquake, both body and surface waves are produced, propagating away from the focus, carrying the energy of the earthquake. The propagation velocity of seismic waves is dependent on the density and elasticity of the medium through which they are travelling. Both surface and body waves can also be induced by a man-made seismic source and the responses measured to reveal dynamic properties of the subsurface. This chapter focuses on seismic waves, in particular surface waves, the influencing factors affecting seismic wave propagation and the limitations resulting from inhomogeneous and anisotropic surveying conditions.

4.2 Body waves:

Wave motion created by a disturbance can be described by two kinds of waves: compression waves and shear waves (Nazarian, 1984). These are collectively called body waves, as they travel within the body of the medium. Compression and shear waves can be distinguished by the direction of particle motion relative to the direction of wave propagation (Figure 4.1).

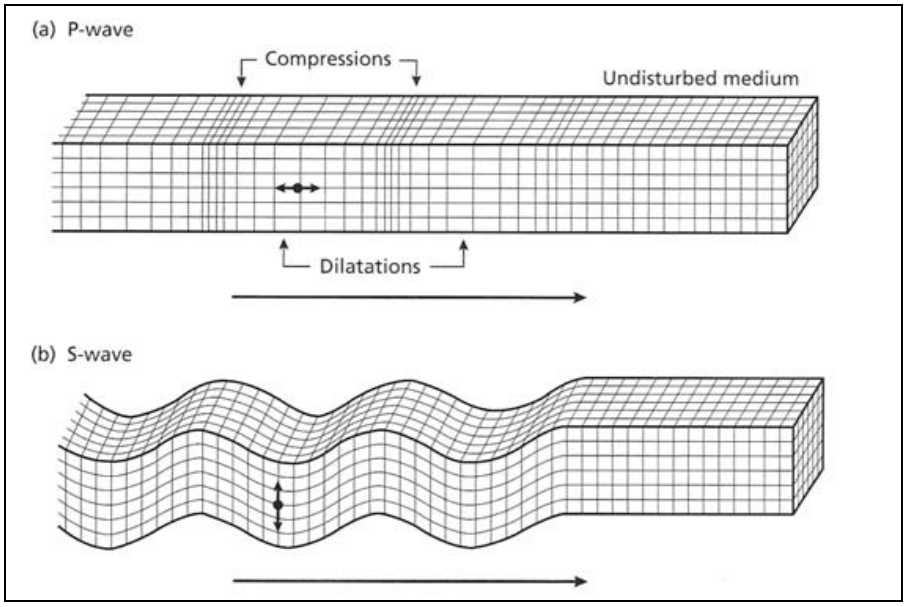

Figure 4.1: Elastic deformations and ground particle motions associated with the passage of body waves (a) P-wave (b) S-wave, from Bolt (1982).

4.2.1 Compression waves

Compression waves (also called Primary or P-waves) are waves that have the same direction of vibration as their direction of travel; hence compression waves exhibit a push-pull motion. They involve successive compression and dilatations (Kramer, 1996), with no rotation of the material they pass through, and they travel at velocity V_P (Equation 4.1). Compression waves are the fastest seismic waves, and appear first in a direct time travel record (Nazarian, 1984).

$$V_P = \sqrt{\frac{G(2-2v)}{\rho(1-2v)}} \qquad \textbf{Equation 4.1}$$

Where: G = Shear modulus (GPa)

v = Poisson's ratio

ρ = Density (kg/m^3) (Kramer, 1996)

4.2.2 Shear waves

Shear waves (also called Secondary or S-waves) are waves that generate shearing motion. A shear wave is a moving wave that consists of oscillations occurring perpendicular to the direction of energy transfer and cause shearing deformations as they travel through a material

(Kramer, 1996). Hence, if a wave is travelling in the x-direction, its oscillations are travelling in the z-y plane. They involve no volume change, and travel at velocity V_S (Equation 4.2). Shear waves travel slower than compression waves (P-waves) and thus appear as the second major wave type in a direct travel time record.

$$V_S = \sqrt{\frac{G}{\rho}}$$ **Equation 4.2**

Where: G = Shear modulus (GPa)

ρ = Density (kg/m^3) (Kramer, 1996)

The velocities of P and S-waves depend on the stiffness, or the resistance to deformation, of the elastic body with respect to the types of deformation induced by each wave. P and S-waves are compared in relation to Poisson's ratio in Equation 4.3:

$$\frac{Vp}{Vs} = \sqrt{\frac{2-2v}{1-2v}}$$ **Equation 4.3**

Where: v = Poisson's ratio (Kramer, 1996)

The P-wave velocity exceeds the S-wave velocity by an amount that is dependent on the compressibility of the body (typically $V_P \approx 2 \times V_S$), which is reflected in Poisson's Ratio, v.

4.3 Surface waves:

4.3.1 Types of surface waves

Surface waves result from the interaction between body waves and the surface, and surficial layers of the earth (Kramer, 1996). Surface wave motion is concentrated in a shallow zone near the free surface (i.e., they travel along the interfaces with velocity contrasts) with amplitudes that decrease approximately exponentially with depth.

The two major types of surface waves are Rayleigh waves and Love waves (see Figure 4.2). Rayleigh waves can be shown to exist in a homogeneous, elastic half-space, whereas Love waves require a surficial layer of lower density and shear modulus than the underlying half-space.

Rayleigh waves are advantageous to engineering investigation and design because they are influenced by the shear strength of the rocks, as well as large fractures and voids. Compared to Rayleigh wave applications, Love waves are not used very often for subsurface V_S imaging. Earlier developed methods such as Spectral Analysis of Surface Waves (SASW), and the more recently developed method of Multichannel Analysis of Surface Waves (MASW), are based around Rayleigh wave measurements. Therefore, a significant amount of development and research has gone into Rayleigh wave use in engineering investigation and design.

Love waves are not widely used because of the assumption that they propagate solely in layers having normally dispersive structures and cannot arise when a thin low velocity layer (LVL) exists at a shallow depth below a stiff superficial layer (Hamimu et al., 2011). however new research is suggesting that Love wave dispersion can be applied for significantly improving V_S imaging, and they may be more sensitive than Rayleigh waves to V_S changes and layer thickness changes (Luo et al., 2010; Safani et al., 2005). Hamimu (Hamimu et al., 2011) has studied in detail the use of Love waves and their advantages in inversion analysis.

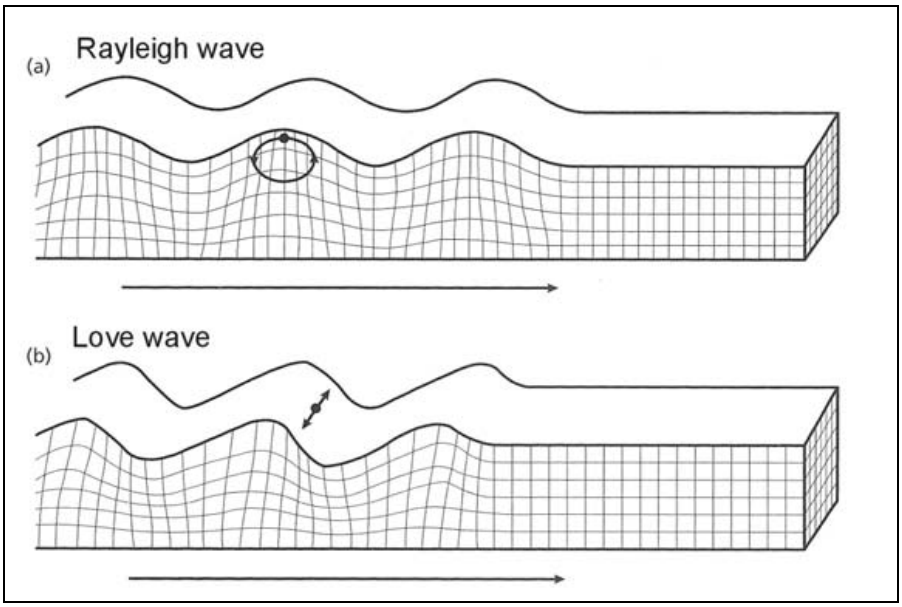

Figure 4.2: Elastic deformations and ground particle motions associated with the passage of surface waves, (a) Rayleigh wave, (b) Love wave, from Bolt (1982).

4.3.2 Rayleigh waves

Rayleigh waves are surface waves that travel along a free surface, such as the earth-air interface. Particle motion of the fundamental mode of Rayleigh waves moving from left to right is elliptical in a counter-clockwise direction (Xia et al., 1999).

Rayleigh waves are the principal component of ground roll and account for up to 70% of the energy in a seismic survey (Park et al., 1999). Ground roll is a particular type of Rayleigh wave that travels along or near the ground surface, and is usually characterised by relatively low velocity, low frequency and high amplitude. The depth of penetration of a Rayleigh-wave depends directly on its wavelength, with the longer wavelengths penetrating deeper (Duffy, 2008). These long wavelength waves are thus more controlled by the elastic properties of the deeper layers and exhibit higher phase velocities. On the other hand, short wavelength waves reflect the elastic properties closer to the surface and travel more slowly. Shorter wavelengths are also sensitive to the physical properties of surficial layers. This property of wavelength-dependent velocity is known as signal dispersion, and is controlled in varying degrees by S-wave velocity, layer thickness, P-wave velocity and density (Xia et al., 1999).

Rayleigh waves propagate as different modes, a mode being a packet of acoustic energy that propagates in one direction whilst confined in the other two directions. In the case of Rayleigh waves they are confined to a surface. Different modes of Rayleigh waves have different motions relative to the travel direction, and therefore different propagation velocities at a given frequency (Duffy, 2008). Of these modes, fundamental mode Rayleigh waves (counter-clockwise motion) are the slowest and so appear closest to the origin in a frequency versus velocity (dispersion) plot.

4.4 Dispersion of Surface Waves:

The frequency dependency of surface wave velocities in a medium is called dispersion, hence surface waves are said to be dispersive. Rayleigh wave velocities are related to the body wave velocities by Poisson's ratio, and since body wave velocities are constant with depth, the Rayleigh wave velocity in a homogeneous half-space is independent of frequency (Kramer, 1996). However, since the properties of earth materials typically display variations with depth, surface wave velocities vary with frequency (Nazarian, 1984).

The depth of penetration for a surface wave is dependent on its wavelength. In non-uniform media, surface waves travel at a velocity dependent on their frequency (Simons et al., 2002), with waves of higher frequencies travelling more slowly than those with lower frequencies. This occurs because a Rayleigh wave with a lower frequency has a relatively longer wavelength. High frequency (short wavelength) Rayleigh waves propagate in shallow zones close to the free surface and are informative about their mechanical properties, whereas low frequency (long wavelength) components involve deeper layers (Foti, 2005).

The property of dispersion allows Rayleigh waves to be used in engineering to determine subsurface stiffness profiles using insitu testing techniques.

4.5 Factors Affecting Surface Wave Velocity and their dispersive characteristics:

4.5.1 Determinants of seismic velocity

The propagation of seismic waves in rock is dependent on the elastic moduli, density and Poisson's ratio. These elastic constants and densities are a function of the geological conditions including rock type, mineralogy, texture, density, stress, confining pressure, porosity, moisture content and temperature.

For weathered greywacke, the most significant factors affecting propagation of surface waves can be grouped as follows:

a) Density (ρ)
b) Porosity
c) Uniaxial compressive strength
d) Depth (confining pressure)
e) Poisson's ratio (v)

$$V_P = \sqrt{\frac{G(2-2v)}{\rho(1-2v)}} \qquad \textbf{Equation 4.1}$$

$$V_S = \sqrt{\frac{G}{\rho}} \qquad \textbf{Equation 4.2}$$

Where: G = Shear modulus (Kramer, 1996)
v = Poisson's ratio
ρ = Density

The propagation velocity of Rayleigh waves (V_R) is related to the propagation velocity of shear waves (V_S) by Equation 4.4 (Rahman & Michelitsch, 2006):

$$V_R \cong \frac{0.87 + 1.12v}{1 + v} V_S$$

Equation 4.4

Each of the geological properties which are used as inputs in the above equations for determining seismic velocities is controlled by the extent of weathering.

Numerous studies have related rock quality and seismic velocities, including Turk and Dearman (1986), who examined the effect of porosity on the seismic velocity of rock masses and determined V_P to be sensitive to changes in porosity, which is a result of weathering.

Turk and Dearman (1986) analysed data from King et el., (1978), concerning V_P and joint frequency measurements from above the water table (in andesite). Specific trends between depth, fracture frequency and seismic velocity were identified, shown in Figure 4.3. Karmis et al (1984), and the effects of fractures on the seismic velocity was also investigated, presenting an increase in F(m^{-1}) (fractures per metre), associated with a decrease in seismic velocity.

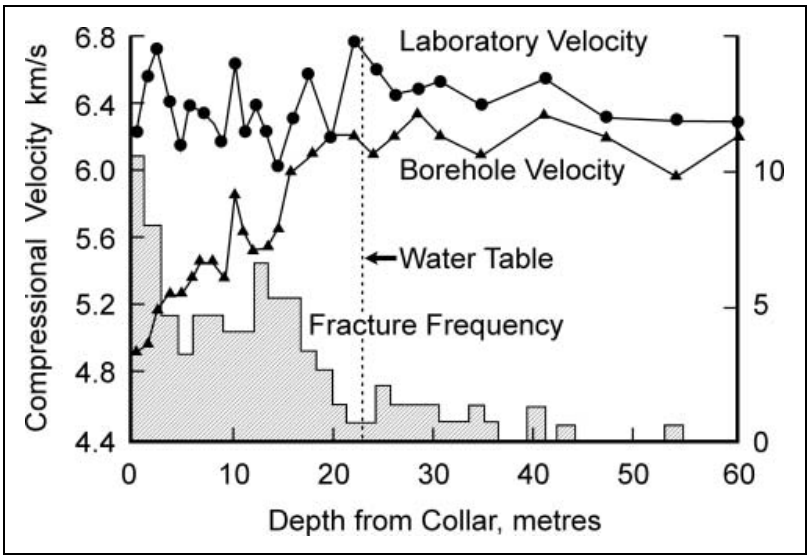

Figure 4.3: Variation in insitu and laboratory seismic velocity with changes in fracture frequency and depth (Turk & Dearman, 1986).

One of the most thorough analyses of seismic refraction measurements was that given by Sjøgren et al (1979) and Sjøgren (1984) with their study of mostly hard, jointed rock environments. The datasets analysed from Sjøgren et al (1979) and Sjøgren (1984) included 113 km of P-wave surveys, 5 km of S-wave surveys and 2.85 km of core from 74 drill holes. They

showed that an increase in the number of joints per metre (also closely measured by RQD) decreases the P-wave velocity.

Sjøgren et al (1979) considered that the insitu velocity of the unjointed rock mass would vary from site to site due to the determining factors, including rock type and mineralogy, porosity, density and uniaxial compressive strength. They also stated that besides the fundamental causes for variation in seismic velocity (stated above), the effects of weathering and depth of measurement was of particular influence.

According to Sjøgren et al (1979), when weathering is present in a rock-mass with the same joint frequency as its unweathered grade, lower seismic velocities will be recorded. This is due to weathering exerting controls on seismic velocities including density, porosity, uniaxial compressive strength, and Poisson's ratio.

In summary, Barton (2007) concluded that seismic velocity (specifically P-wave in this case) were sensitive to variations in rock mass quality, porosity, stress, strength and deformability. Figure 3.4 plots seismic velocity versus the Q-value, which expresses the quality of the rock mass. The Q-value is typically used as a tunnelling index for geotechnical tunnel design and is determined by the Rock Quality Designation (RQD) which is a rough measure of the degree of jointing in a rock mass, the joint set number (J_n), the joint roughness number (J_r), the joint alteration number (J_a), the joint water parameter (J_w) and the stress reduction factor (SRF). In this case the Q-value is used to describe the rock-mass quality, as the majority of the input parameters in this value are controlled by weathering. This diagram displays how the effects of weathering would influence the seismic wave velocities at each of the windfarm sites detailed in this study. As weathering decreases, the number of joint sets reduces, crack closure occurs and lower quantities of water are able to permeate through the rock mass, all contributing to an increased Q-value.

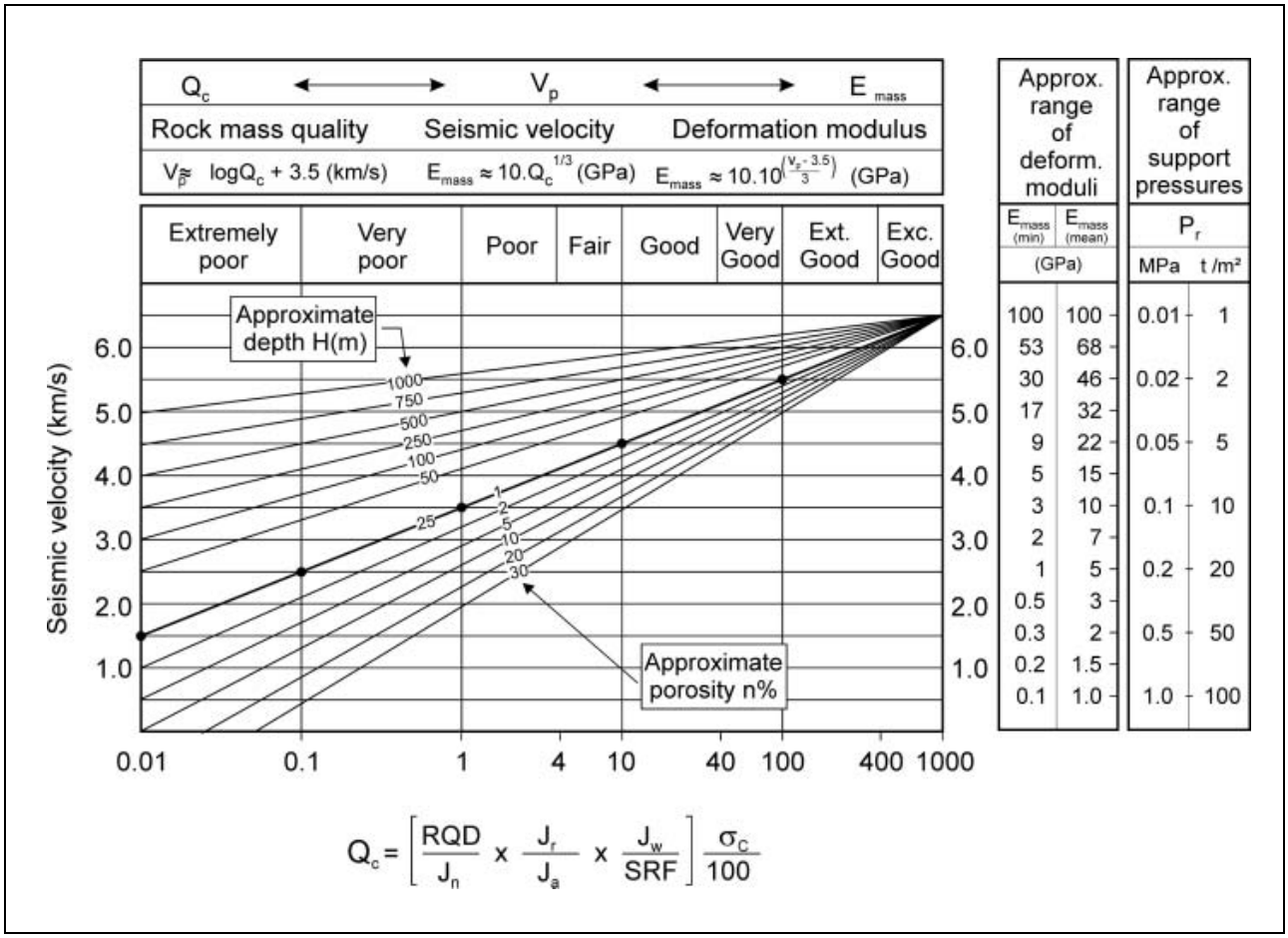

Figure 4.4: Integration of rock quality Q-V_p-E_{mass} in a model that incorporates depth, porosity and rock strength adjustments. Note that E_{mass} (or M) represents the static modulus of deformation, from plate loading tests and from back-analysis of measured deformations. V_p is the seismic velocity measured from refraction seismic, and from cross-hole seismic tomography, in the case of greater depths (Barton, 2007).

Rowe (1980) initiated a study aimed at examining geological aspects of Wellington greywacke rocks for use as an engineering aggregate material. Insitu measurements of ultrasonic velocity were made to better understand the effects of discontinuities in the rock mass. In this study, Rowe identified jointing as being the most prolific form of discontinuity in the Wellington greywacke rocks, along with the associated characteristics of joint spacing, aperture and joint infilling, and has the most significant impact on the velocity at which ultrasonic waves propagate. Issues concerning the representativeness of ultrasonic velocity measurements versus larger scale insitu velocity changes have been discussed by Engelder and Plumb (1984).

4.5.2 Effects of Poisson's Ratio

Poisson's ratio represents the lateral or transverse strain, which occurs along with axial contraction and elongation (Johnson & De Graff, 1988). It is a dimensionless ratio which is determined by the change in length over the change in diameter. Figure 4.5 shows the relationship between P-wave and Rayleigh wave velocities to the S-wave velocity as a function of Poisson's ratio. This figure shows that V_S is independent of the Poisson's ratio of the soil/rock, while V_P is highly dependent upon this value. V_R is only slightly dependent upon Poisson's ratio.

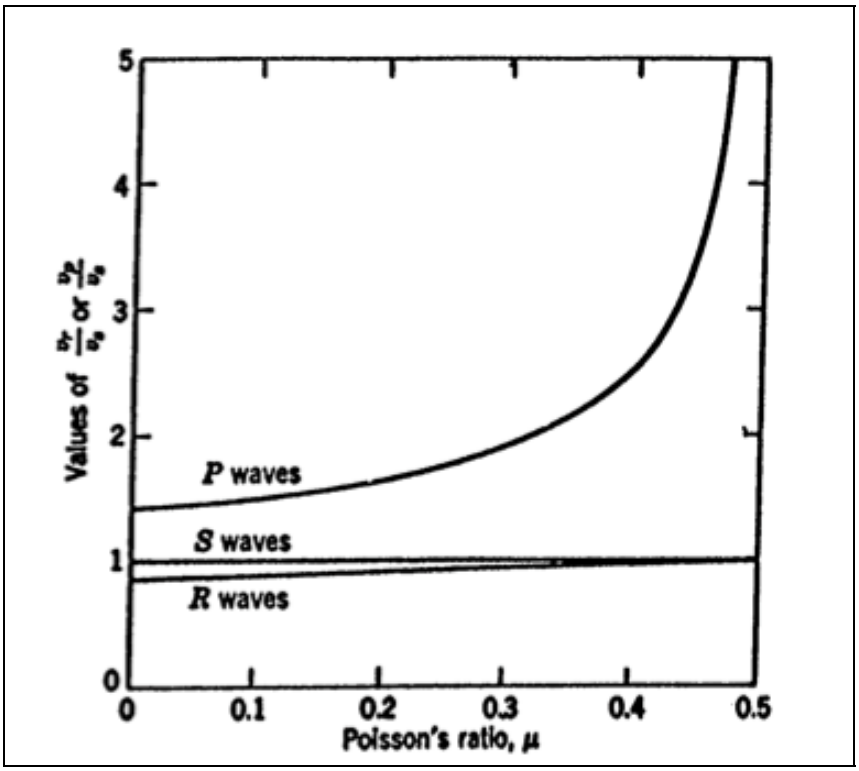

Figure 4.5: Effect of Poisson's ratio u[on various wave velocities (Richart et al., 1970).

Figure 4.5 shows that V_P is only dependent on Poisson's ratio at high Poisson's ratio values. In contrast to this, Johnson and De Graff (1988) state that Poisson's ratio shows no well-defined linear relationship with either V_P or V_S. Figure 3.12 in Chapter 3.4.3 displays the lack of a significant numerical relationship between V_P and Poisson's ratio.

Poisson's ratio has a more significant impact on the calculation of a shear-wave velocity profile, rather than directly impacting the surface wave velocity. Poisson's ratio can be a source of inaccuracy in the construction of a dispersion curve, as its assumed value is used as an input in the inversion process. It is known that the effect of Poisson's ratio is not very important in an elastic, homogeneous, and isotropic medium, however, vertical heterogeneity is almost always prevalent insitu.

Karray and Lefebvre (2008) studied the impact on shear-wave velocity profiles for the same experimental dispersion curve using three different values of Poisson's ratio (0.20, 0.33 and 0.49), with the relative differences of each profile shown in Figure 4.7.

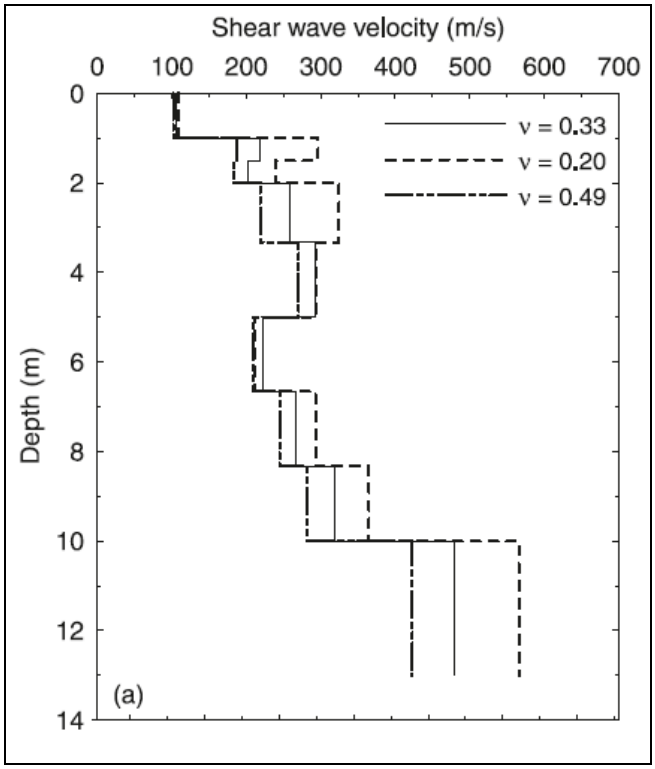

Figure 4.7: Shear-wave velocity profiles calculated for the same fundamental Rayleigh mode and for different Poisson's ratio values (Karray & Lefebvre, 2008).

Karray and Lefebvre (2008) concluded that in the inversion process the impact of Poisson's ratio in construction of the theoretical dispersion curves, for conditions generally encountered in the field, appears to be significantly more important than that demonstrated for homogeneous conditions (Richart et al., 1970) or for a two-layer system (Nazarian, 1984). Both Karray and Lefebvre (2008) and Nazarian (1984) concluded that the effect of Poisson's ratio on construction of the theoretical dispersion curve does not introduce a significant error, if it is reasonably assumed.

Poisson's ratio is an input parameter in the calculation of the elastic modulus (E), and the method used to calculate Poisson's ratio values through for each weathering grade is detailed in Chapter 1.7.

4.6 Surface wave propagation in anisotropic/ inhomogeneous media:

The measureable travel times of seismic events propagating in heterogeneous media depend on the geological scale, the seismic wavelength and the propagation distance.

Lateral heterogeneities were commonly present at the MASW survey sites. These heterogeneities include variations in lithology, porosity, weathering, pore fluid and infilling properties, and conditions of temperature, and stress (Mukerji et al., 1995). They occur over a broad range of scales, from submillimeter grain and pore scale, to the multiple-meter lithological or weathering grade scale.

A fundamental assumption of the MASW data acquisition and processing method is that near-surface materials can be treated implicitly as a layered earth model with no lateral variation in elastic properties, ie: a laterally homogeneous layered earth model. An important issue for interpreting geophysical images in 2-D and 3-D random media is that the seismic wave propagation is itself affected by the heterogeneities.

Park et al. (1999) validate this assumption by recommending the receiver spread for a MASW survey be kept as short as possible. The limitation associated with having a short receiver spread, can create issues with dispersion curve extraction, which is optimized by having a long receiver spread to separate phase velocities of the multiple modes (Ivanov et al., 2001). However, given a suitably short receiver spread and successful dispersion curve extraction, the inherent sensitivity of surface wave velocities to lateral seismic velocity changes renders them useful for identifying structural features characterised by lateral velocity changes in the shallow surface, such as faults (Ivanov et al., 2006).

As shown by Ivanov et al. (2006), the assumption that near-surface materials are treated implicitly as a homogeneous horizontally layered medium, can be used in the investigation of laterally inhomogeneous subsurface features such as faults, underground cavities (Xia et al., 2007; Xu & Butt, 2006) or dipping bedrock strata (Ivanov et al., 2006; Miller et al., 1999). These heterogeneities are used in 2D and 3D imaging to identify such features. Although, when interpreting 1D MASW surveys, these features can cause great difficulty, which was sometimes the case when interpreting 1D MASW wind turbine foundation surveys.

MASW investigation techniques are based on velocity analysis, and since velocities identified in the f-k (frequency-wavenumber) domain are only average velocities of the whole shot line, inaccuracies are inherent when lateral inhomogeneities are present (in 1D imaging). Hence

heterogeneities affect seismic wave propagation in ways that both complicate and aid the interpretation of seismic images.

4.7 1D Surface wave inversion limitations:

As mentioned in Section 3.3, heterogeneous media can cause problems with 1D surface wave profiling. During 1D profiling, the subsurface structure is locally assumed to be horizontally layered. This 1D assumption is often 'violated' by lateral geological or topographic variations (Gabriels et al., 1987), which are frequently encountered in field surveys. It is lateral variations under the recording array which corrupt the wavefield and thus contaminate the inversion.

Bodet et al (2005) used laser-Doppler physical modelling of surface-waves propagation to study the effects of depth penetration, the presence of dipping layers, and the associated limitations and systematic errors propagated in conventional 1D surface-wave inversion. The study concluded that flat-layers models with an active source and linear spread, have a maximum resolvable wavelength of the fundamental mode that is in the order of 40% of the spread length. In the case of a dipping layer, the modelled interface is represented as too shallow in the down-dip direction, and too deep when shooting in the up-dip direction. However, the observed dispersion for the dipping-layer case, correlated well with that calculated for the 'flat average' (or 'central shear-wave velocity profile') over the spread length, except for wavelengths which reach the spread length resolution limit.

To reduce the effects of the presence of heterogeneities, a shorter recording spread can be employed, although this can limit the maximum resolvable wavelength and thus the depth of investigation. Likewise, if the spread length is increased, this can reduce low frequency discrepancies, often called 'near-field effects', but then allowing lateral discontinuity effects to become more influential, voiding the 1D assumption during inversion.

The study highly recommends the method of shooting in both directions along the receiver spread, to help as a reverse check. Without the use of a reverse check, or prior site information for correlation purposes, an interface sloping of only a few degrees can bias the surface-wave inverse problem significantly, 'violating' the 1D results.

4.8 Synthesis:

Up until this point, the term MASW has been introduced and explained, along with details of its use in this study. The method of utilising and recording surface waves for geotechnical investigative purposes has been discussed, along with the close connection between surface wave velocities and shear-wave velocities, of which the latter is very important to geotechnical investigation and design.

This chapter introduces the different types of seismic waves and how they behave under excitation. The requirement that MASW measures a homogenous layered elastic half-space is discussed. This requirement of having a layered half-space is met by the changing weathering grade with depth of the insitu Esk Head belt 'greywacke'. Finally, the requirement of MASW surveys being performed on laterally homogeneous and isotropic material is discussed, the implications behind the presence of lateral heterogeneities, and the methods used to control these limitations.

Chapter 5 MASW Investigations and Data Analysis:

5.1 Introduction:

The method of using MASW to determine the elastic condition of insitu weathered greywacke has previously been used during geotechnical investigations on the Te Rere Hau windfarm site. The MASW investigations at the Te Rere Hau Windfarm were performed by Southern Geophysical Ltd, with which I assisted, and involved determining a V_S profile with depth at each proposed wind turbine location. As explained in Chapter 1, this study aims to refine that method and develop appropriate controls for its future use.

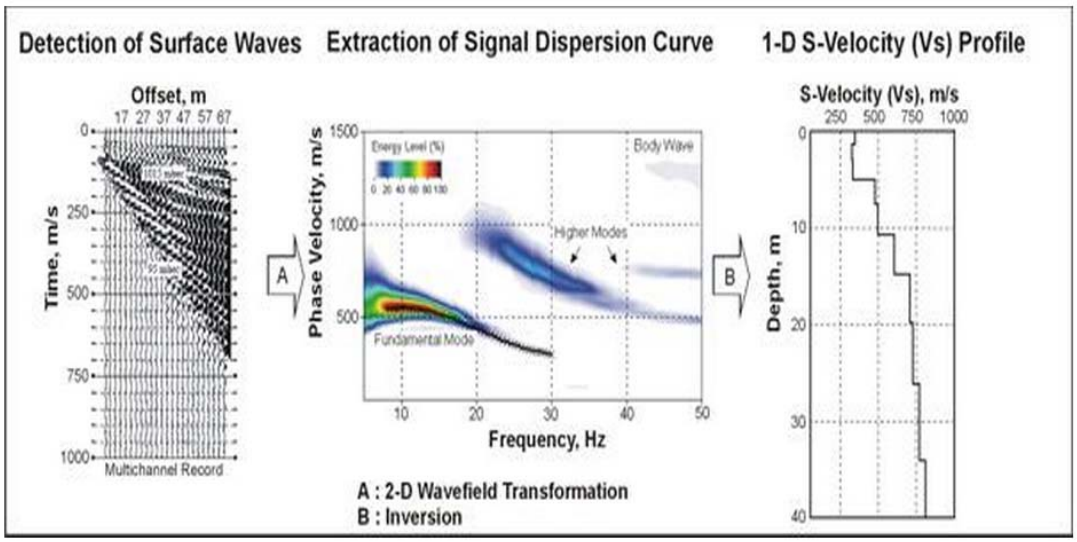

Figure 5.1: A 3-step processing scheme for Multichannel Analysis of Surface Waves data.

The MASW procedure was introduced in Chapter 1 and its extensive theory is expounded in Park et al (1999) and Xia et al (1999) and Appendix A. The three main stages of this method are displayed in Figure 5.1, and include: 1) data acquisition, 2) extraction of a dispersion curve, and 3) back-calculating V_S variation with depth.

Each MASW survey was processed using SurfSeis software. The combined dataset from these three windfarm sites was analysed, determining any consistent trends or characteristics in the data.

A full set of processing results can be found in Appendix X.

5.2 Data collection:

An initial 61 MASW surveys were completed at the Te Rere Hau Windfarm site by Mike Finnemore of Southern Geophysical Ltd, as part of the Stage 2 geotechnical investigation. A further 31 MASW surveys were carried out as part of the geotechnical investigation for Stages 3 to 5 extensions, at the windfarm. In addition to the Te Rere Hau Windfarm surveys, I completed 2 surveys at the West Wind Windfarm in Wellington, which were the only undeveloped turbine sites included in the original geotechnical investigations performed by Opus International Consultants Ltd (Opus), and drillhole data was available at these two sites. I also completed 6 MASW surveys at turbine sites at the proposed Turitea Windfarm in Palmerston North's Tararua Ranges. Drillhole investigations were also performed at these sites, during the Beca International Consultants Ltd (Beca) geotechnical investigation at the proposed Turitea Windfarm site. These 8 surveys were completed between May and August 2010. This brought the total number of MASW surveys available for analysis to 100.

Each survey was run at either a proposed turbine site prior to construction, or an undeveloped turbine site which had been investigated but eventually abandoned as a development site. Each of the survey sites contained geotechnical investigation information, including a combination of drillhole logs, pile drilling logs and test pit logs, along with a number of sites including downhole seismic and laboratory testing data available. The previously assembled geotechnical investigation information used in this study is owned by NZ Windfarms Ltd, Meridian Energy and Mighty River Power at the Te Rere Hau, West Wind and Turitea Windfarms respectively, and was approved for use prior to the commencement of this study.

Each survey, where possible, was centred on the exact turbine location, although in approximately 10% of surveys this was not practical due to difficult terrain or steeply dipping topography. In such cases, the survey centre point was moved to the closest possible position which a reliable MASW survey could be performed, while still ensuring the hemisphere of subsurface surveyed was sufficiently representative of the proposed turbine site.

Survey sites in weathered and fractured greywacke are typically not good candidates for site survey calibration, due to their lateral heterogeneity. In order to overcome this problem, once the survey line had been established, MASW surveys were completed in both directions, i.e. the seismic source was positioned and activated at both ends of the survey line, to complete two separate surveys. In addition to this, surveys were performed perpendicular to the original survey line to provide information on the level of anisotropy at each site. This method provided internal quality checks on the data for any unidentified problems associated with heterogeneities and anisotropy of the subsurface.

Each MASW survey was assigned a confidence ranking of 0 to 5 (including +/- levels of confidence). The confidence ranking was determined by the clarity of the dispersion curve and the strength of the overtone image. Contamination of higher mode Rayleigh waves is common, which is generally a result of lateral inhomogeneities or terrain conditions which are unfavourable for MASW surveying.

Ranking	Description
0	No data or no dispersion curve extractable
1	Poor quality dispersion curve extracted detailed processing. Lowest confidence level.
2	Strong diffractions and scattered wave field. Generally poor coincidence of dispersion curves. Likely to be several significant modal jumps. Likely to be strong lateral contrasts in S-wave velocity. S-wave sounding represents a bulk average only. Use with caution and probably only deepest velocities.
3	Good coincidence of dispersion curves but potential for significant higher mode contamination at a range of depths. Deepest (half space) velocities probably ok, shallower velocities probably excessive.
4	Good coincidence of dispersion curves (or obvious selection of fundamental mode in one and higher mode in the other curve). Possibly inflated velocities close to surface due to higher mode contamination but otherwise confident.
5	Strongly dispersive overtone image. No evidence of higher mode contamination. Highest confidence level.

Table 5.1: Confidence ranking scheme used for MASW surveys to determine data quality.

In order to ensure a high quality dataset, only surveys with a ranking of 3 or higher were used in the data analysis process. This was not purely removing outlying data, but removing the results affected by poor quality survey conditions sometimes encountered onsite, including surveys affected by difficult topography and inhomogeneous subsurface conditions.

5.3 Acquisition Parameters:

5.3.1 Survey procedures

Data acquisition parameters were chosen to optimise recording and ground roll signals. The critical aspects of data acquisition parameters include:

- Source-receiver offset
- Geophone spacing
- Geophone frequency and seismic source

Unlike other seismic methods, acquisition parameters for MASW surveys have quite a wide range of tolerance. This means investigation depths and the subsequent resolution are not highly sensitive to slight changes in acquisition parameters.

When determining the optimal acquisition parameters for a surface wave survey, the most significant difference when compared with conventional body-wave surveys is the enhancement of low frequency energy. Most key acquisition parameters are usually quite tolerant for MASW surveys. Park et al. (1999) have suggested the parameters in Table 5.2 as a guideline. The acquisition parameters used in this study have been adapted to suit the specific conditions encountered onsite to optimise survey quality.

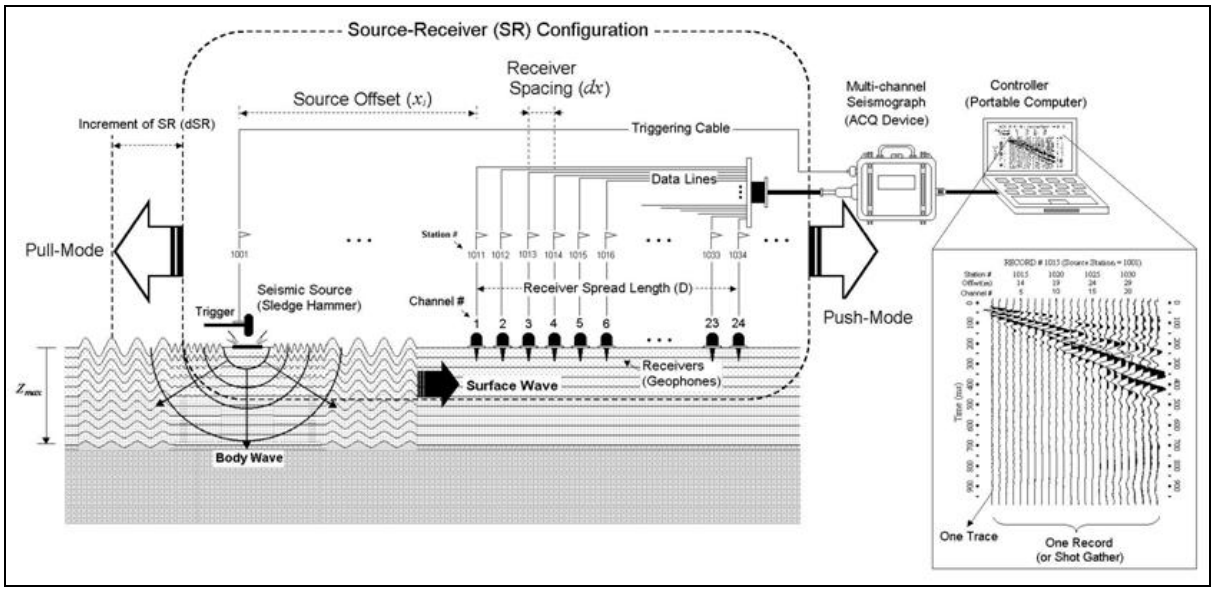

Figure 5.2: Schematic illustrating a typical Multichannel Analysis of Surface Waves survey set-up (ParkSeismic).

Two types of parameters are considered to be the most important when designing a MASW survey: the source-receiver offset and the receiver spacing. The source-receiver offset needs to change in proportion to the intended maximum investigation depth, with a conservative calculation being that the source-receiver offset = half the maximum investigation depth (Park & Miller, 2005).

Receiver (Hz)	Max. Depth (m)	Minimum Offset (m)	Maximum Offset (m)	Receiver Spacing (m)
4.5	50	10	100	1
10	30	10	100	1
40	15	10	100	1

Table 5.2: Optimum field parameters for MASW surveys for most common soil sites. A seismic source of 4.5kg or heavier sledgehammer and use of recording instrument with 24-bit or higher dynamic range are both assumed. No low-cut analogue filter should be used during the acquisition (Park et al., 1999).

Typical acquisition parameters used in this study are detailed in Table 5.3, and these parameters were adjusted according to the site conditions encountered. This involved adjusting the source-receiver offset and receiver spacing, to account for sites with unfavourable topographic conditions, including restricted survey space, and uneven, undulating or steeply dipping slopes along or close by the survey line. Generally the field setup was kept consistent throughout all MASW surveys, although if the conditions required, adjustments were made, while still ensuring target investigation depth and resolution were optimised.

Source	Number of channels	Source-receiver offset	Geophone frequency	Receiver spacing
8kg hammer, 10kg metal plate	24 (48 channel records)	10m	8Hz	1m

Table 5.3: Typical survey parameters used during MASW surveys in this study.

5.3.2 Source/Receiver Characteristics

The surface wave method requires the analysis of horizontally-travelling planar waves of (fundamental-mode) Rayleigh waves, therefore it is important to avoid recording any non-planar components (Park et al., 1999). According to Stokoe et al (1994) and Park et al (1999), surface waves become planar after travelling a certain distance from the source, and this distance is a function of wavelength. Therefore a longer wavelength wave takes a greater distance before it becomes planar. The source-receiver offset spacing controls the degree of contamination by a range of near-field effects, the most significant of which is non-fully developed surface waves if the source is positioned too close to the first receiver. The source-receiver offset also needs to be sufficiently sized to extend to the primary depth range of interest. Since most surface wave inversion methods use a theoretical model that does not include near-field contributions, it is important that data are collected such that near-field effects are minimised (Rosenblad & Cheng-Hsuan, 2011).

To determine the best suited offset for this survey, SurfSeis software was used to check the arrival times and distances of the planar travelling surface waves. From this information, two source-receiver offsets were initially used of 10m and 22m, with a comparison of the processed results. In addition to this, to check the homogeneity of the subsurface, surveys were also shot along a line perpendicular to the original survey. It was eventually determined during the latter stages of processing that the 10m offset consistently provided higher quality dispersion curve results than the 22m offset. The use of the 22m offset was not continued once it had been established that site homogeneity was sufficient for accurate MASW surveying. Therefore, the near-offset spacing used for the majority of the MASW surveys in this study was 10m. This value is in accordance with recommendations of survey parameters made by Park (1999). At selected sites the near offset spacing had to be altered due to constricting topographic conditions encountered, which generally resulted in shortening the near offset spacing to a minimum of 8m.

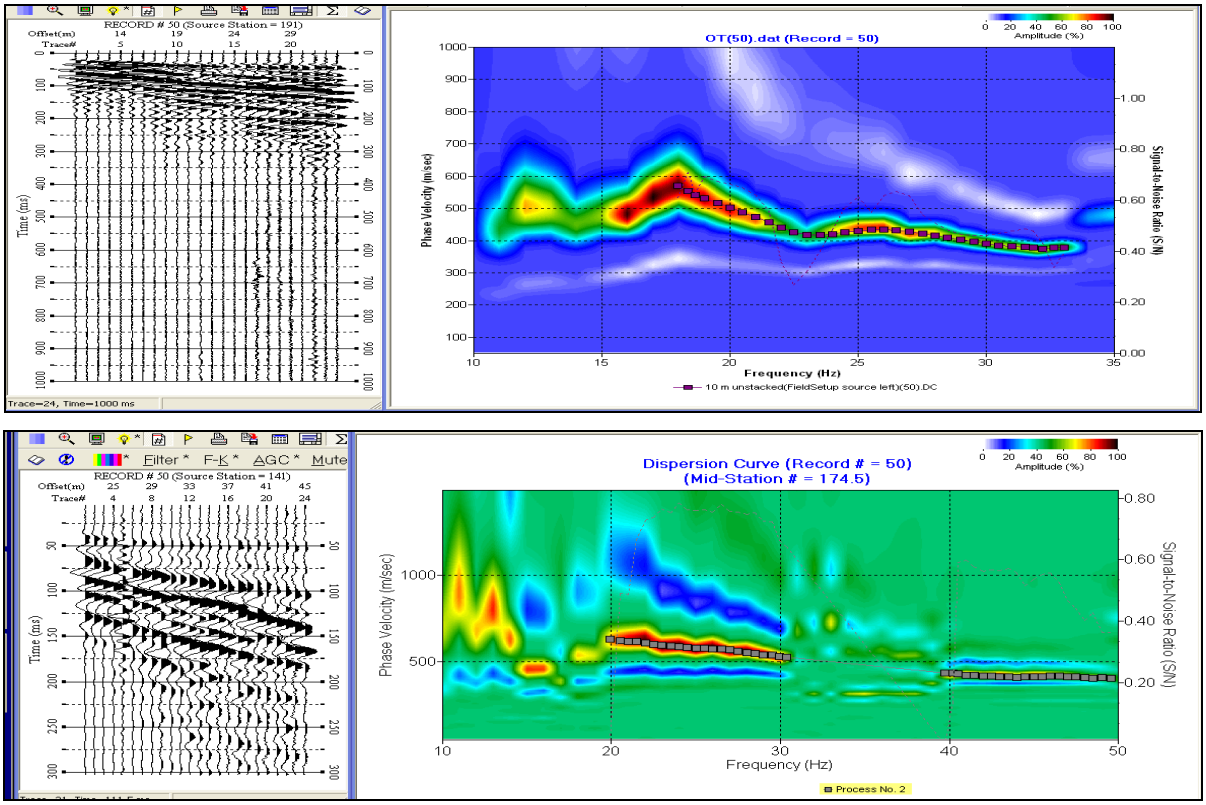

Figure 5.3: Experimental dispersion curves from Te Rere Hau Windfarm from 10m source-receiver offset (top), and 22m source-receiver offset (bottom).

MASW data was collected using 24 channel seismic cables and recorded using a 48 channel NX Stratavisor Seismograph. The geophones used in this survey were 8Hz geophones on a 24

channel array. The array was moved and replanted at each location to make up a 48 channel survey line.

Reducing the geophone spacing can increase the amount of high frequency energy that is collected, although this also decreases the depth of penetration. Surveys in this study were acquired initially with spacings of 1m, although a number of later surveys used 0.5m spacing, again due to topographic constraints. An 8 kg sledgehammer impacting on a 10km steel plate was used to provide the impulse source and an accelerometre on the hammer handle triggered the start of data collection. Between 4 and 8 shots were vertically stacked at each location depending on the signal quality and noise sources present at the time of survey.

Figure 5.4: Typical MASW setup with an array of 24 geophones at 1m spacing, from the Te Rere Hau Windfarm.

5.4 Dispersion Curve Extraction:

Extraction of the fundamental mode dispersion curve is the first major step in the processing of MASW data. Dispersion curve extraction involves the estimation of one or more dispersion curves which are in turn passed into the next step, the inversion process. A dispersion curve is displayed as a function of phase velocity versus frequency. The fundamental mode surface wave

velocities are picked by a user guided automatic picking, followed by manual editing of the selected curve. The fundamental mode (1st harmonic) has the lowest velocity range, and modes that appear at higher velocity ranges are known as higher modes, i.e. 2st harmonic, 3nd harmonic, etc (Ivanov et al., 2001). Accurate dispersion curve extraction is an important element of the MASW method because any error in the dispersion curve can carry forward errors into the inversion process and further again into the Vs profile.

Fundamental mode dispersion curves must reflect the dispersive characteristics of planar propagating fundamental-mode Rayleigh waves only. For the optimal extraction of the surface-wave fundamental mode, several acquisition parameters need to be set properly. A long range receiver spread is essential to separate phase velocity of one mode from those of higher modes. The Park et al (1999) study of higher modes indicated that energy of higher modes tends to become more significant as the source distance becomes greater. Due to unacceptable lateral inhomogeneity in the near surface materials, this requirement is often unable to be met. Therefore multichannel records are generally surveyed with a relatively short (e.g. 8-12m) receiver spread length. At times the interference between different modes of surface waves can be so severe that neither the fundamental mode nor higher mode dispersion curves can be extracted with sufficient confidence (Ivanov et al., 2001), which was sometimes the case in this study.

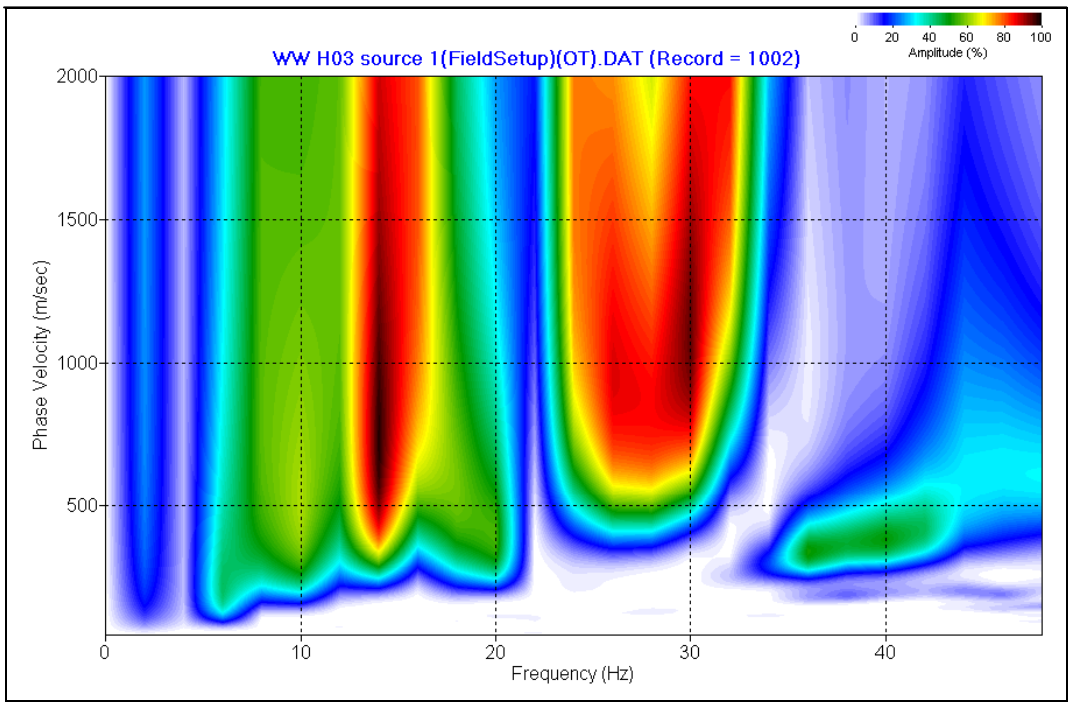

Figure 5.5: Dispersion curve exhibiting sever interference along with being surveyed under poor survey conditions from the undeveloped West Wind Windfarm site H03. This survey was given a confidence ranking of 0.

The majority of field records in this study contained distinct higher modes and other sources of noise, which interfere with the fundamental mode in the offset-time (*x*-*t*) domain. Hence, appropriate filtering techniques were applied to ensure the accuracy of the extracted dispersion curve. A combination of F-K filtering, if the modal velocity fields are not critically overlapping, or offset-time domain muting of higher modes was used (Ivanov et al., 2005).

Often other types of seismic waves can act as noise and interfere with the extraction of an accurate dispersion curve. These include direct waves, refracted waves, guided waves, air waves as well as higher modes of the surface waves (see Figure 5.7)

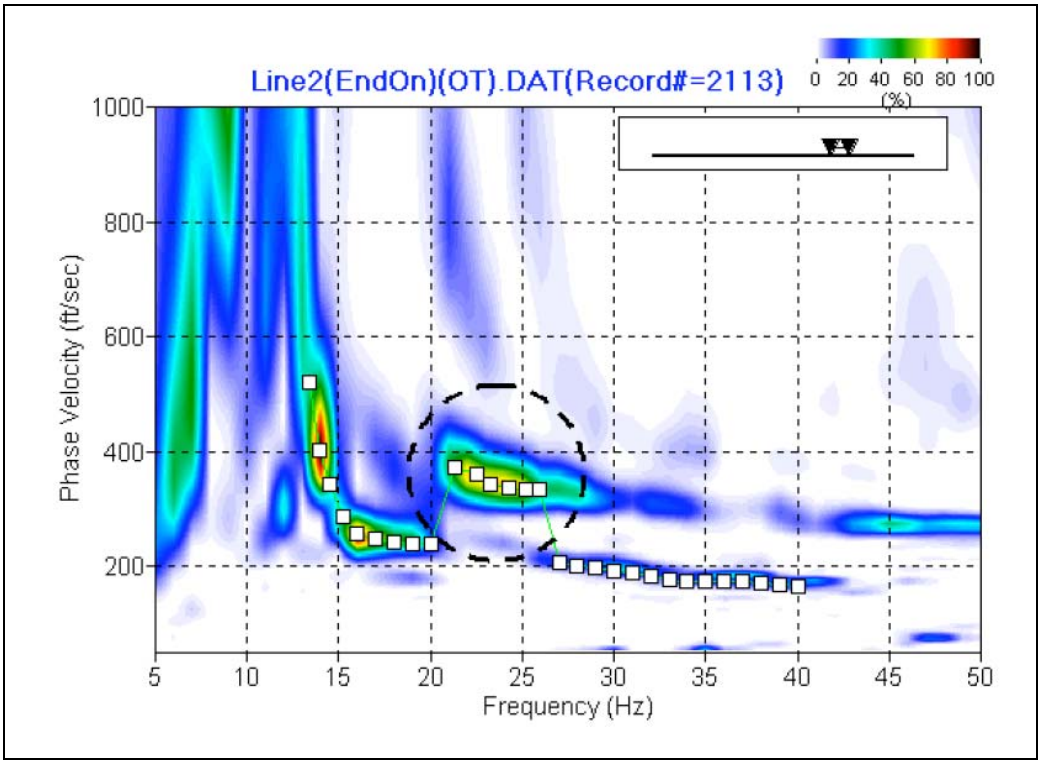

Figure 5.6: An example of dispersion curve extraction using SurfSeis that shows a higher mode adjacent to the fundamental mode causing some erroneous picking of phase velocities. In this instance the pickings would be manually edited (Park & Miller, 2004).

Initially an overtone analysis determines the frequency and velocity ranges of surface waves from the raw shot records. Received bandwidths from this study were variable between 5 Hz and 60 Hz, with most records falling between 20 Hz and 45 Hz. Shot records were velocity filtered to remove body waves, air waves and other sources of noise. In general, surface waves propagate in several modes, which means that the dispersion property may be represented by several curves of different modes. The behaviour of higher mode surface waves is associated

with two parameters: shear-wave velocity structure in the near-surface (<30m) sediments, and the distance of the receiver spread from the source.

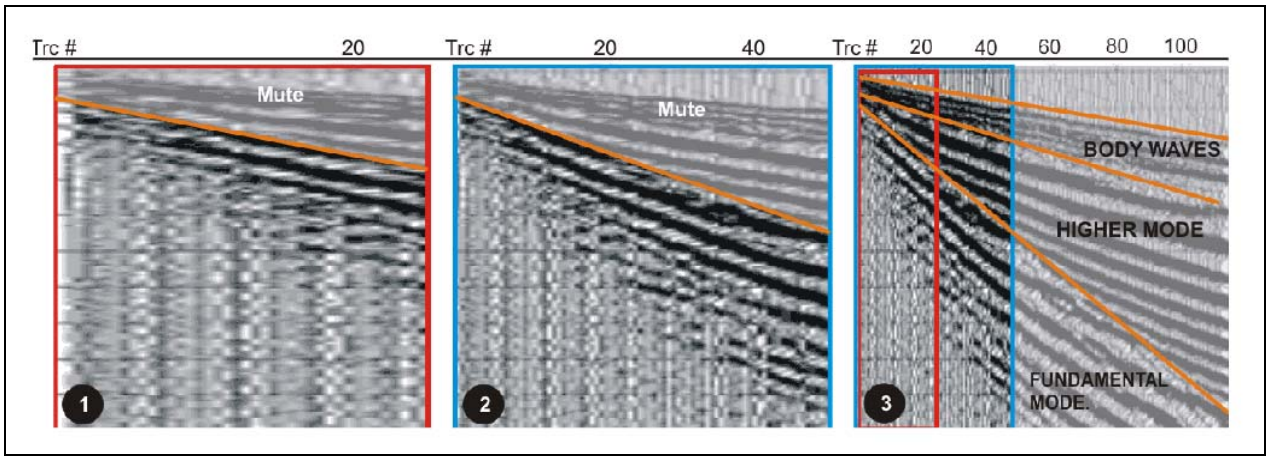

Figure 5.7: Relationship between ease of differentiation of fundamental and higher mode Rayleigh waves and the length of geophone string. The longer the array, the easier to visually identify higher mode and body waves. A short 24 channel array (1) shoes very poorly the diverging velocities of fundamental and higher modes compared with a 120 channel array (3) at a similar near offset. A 48 channel array (2) collects significantly more fundamental mode energy, facilitating differentiation and muting.

Te Rere Hau turbine site 2 clearly shows the fundamental mode (picked curve in Figure 5.8), with a higher mode also present. This survey was given a confidence ranking of 4, due to the lack of interference from higher modes in the dispersion curve. Higher modes typically follow a similar shape to the fundamental mode curve, with a decreased dominance of energy, and at a higher phase velocity and frequency range, shown in Figure 5.8 and 5.9.

5.5 Surface Wave Inversion:

Inversion of S-wave velocities from Rayleigh-wave dispersion curves is the final step in the processing of MASW data. Inversion of the calculated dispersion curve uses the phase velocity with frequency curve as a reference to estimate the vertical S-wave velocity (V_S) structure of the near-surface materials. The inversion algorithm used in SurfSeis software has been adopted from Xia et al (1999).

The inversion of surface waves is an estimation of the Earth's properties from the measured surface wave data. S-wave velocities (V_S) can be derived by inverting Rayleigh-wave dispersion data to fit a layer model with a fixed number of layers applied, Poisson's ration and density. A

layer model is defined as a division of the subsurface into layers of constant velocity, which in turn removes layer thickness as a variable, leaving S-wave velocity as the only remaining variable. A 10-varying-thickness layer model was created at the beginning of the inversion for this study. The number of layers can influence the relative error between the experimental and theoretical dispersion curves, and hence the final V_S profile. Sites with irregular stiffness profiles or strong stiffness contrasts can influence the relative error by the selected number of layers for the V_S profile. By increasing the number of layers, a more realistic inverted model is produced along with computational time increasing (Dal Moro et al., 2007), but generally more than 6 layers describes the first 30m of the site very well.

During the inversion process, only V_S is updated after each iteration, with parameters such as Poisson's ratio, density and thickness of the model remaining unchanged. Inversion of the individual dispersion curves was performed using Surfseis software (Kansas Geological Survey), which produced a 1D vertical V_S profile with depth.

The validity of an inversion of a fundamental mode Rayleigh-wave dispersion curve is primarily dependent on the accuracy of the dispersion curve (O'Neill and Matsuoka, 2005; Xia et al., 2003; Zhang and Chan, 2003). An accurately determined fundamental mode dispersion curve will invert to a model which closely resembles the earth model.

1D profiling was used in this study which produces shear-wave velocity profiles at each turbine site. For this study, fixed Poisson's ratio and density values of 0.3 and 2.0 t/m^3 were assigned for all 10 layers during the inversion process, a method which is common practice. Xia et al (1999) showed that a 25% error in Poisson's ratio or density of all layers only induces a 10% perturbance of the fundamental mode dispersion. Therefore constant Poisson's ratio and density will not significantly affect the inversion results. SurfSeis searches for a V_S profile whose theoretical dispersion curve matches the experimental dispersion curve. The quality of the 'match' between the two curves is evaluated on the root-mean-square error (Xia et al., 1999). The inversion of a dispersion curve using SurfSeis Software is particularly straight forward, as it is a fully automated process that removes any human error being incurred during calculations.

The relative error is an indicator of the match between the theoretical and experimental dispersion curves. Usually a relative error between the experimental and the numerical dispersion curves, which is less than 10%, means that a satisfactory and valid result has been obtained from a practical point of view. Generally if the relative error is between 10% and 20%, the picked dispersion curve is adjusted to reduce the error. The layer model selected for processing, i.e. 10-layers in this study, can influence the relative error between the experimental and theoretical dispersion curves and hence the final V_S profile. Sites with irregular stiffness

profiles or strong stiffness contrasts, which is typically the case, can influence the relative error by the selected number of layers for the V_S profile. By increasing the number of layers a subsurface model is defined more accurately, but generally more than 6 layers describes the first 30m of the site very well. A 10-layer model is used in this study due to the gradational nature of the changes in V_S with depth, providing sufficient detail into the subsurface seismic properties.

5.6 Results:

The results for Te Rere Hau Windfarm turbine sites 2 and 49, and Turitea Windfarm turbine site 6 are displayed below with dispersion curve and velocity inversion images, along with the final V_S profiles. A full set of dispersion curves and velocity models can be found in Appendix I.

Te Rere Hau Windfarm turbine site 2 (Figure 5.8) clearly displays a higher mode present in the dispersion curve. This is a high quality survey due to the lack of higher mode interference, and the ease with which the fundamental mode curve can be picked. Turbine site 49 (Figure 5.8) displayed a similar result with a higher mode present, without interfering with the fundamental mode dispersion curve. The dispersion curve for Turitea Windfarm turbine site 6 (Figure 5.10) is of a high quality with higher modes being filtered out during processing and a consistent change in stiffness properties with depth. All three of these dispersion curves provided a good fit with the theoretical 10-layer velocity models produced during the inversion process.

The average depth of investigation determined by the MASW surveys was between 12 and 25m. Different wavelengths have different penetration depths and propagate with different velocities (Park et al., 1997). The length of the receiver spread (D) is directly related to the longest wavelength (L_{max}) that can be analysed, which in turn determines the maximum depth of investigation (Z_{max}). The receiver spread (D) is usually between 1 and 3 times the depth of investigation (Z_{max}), as shown in Figure 5.2.

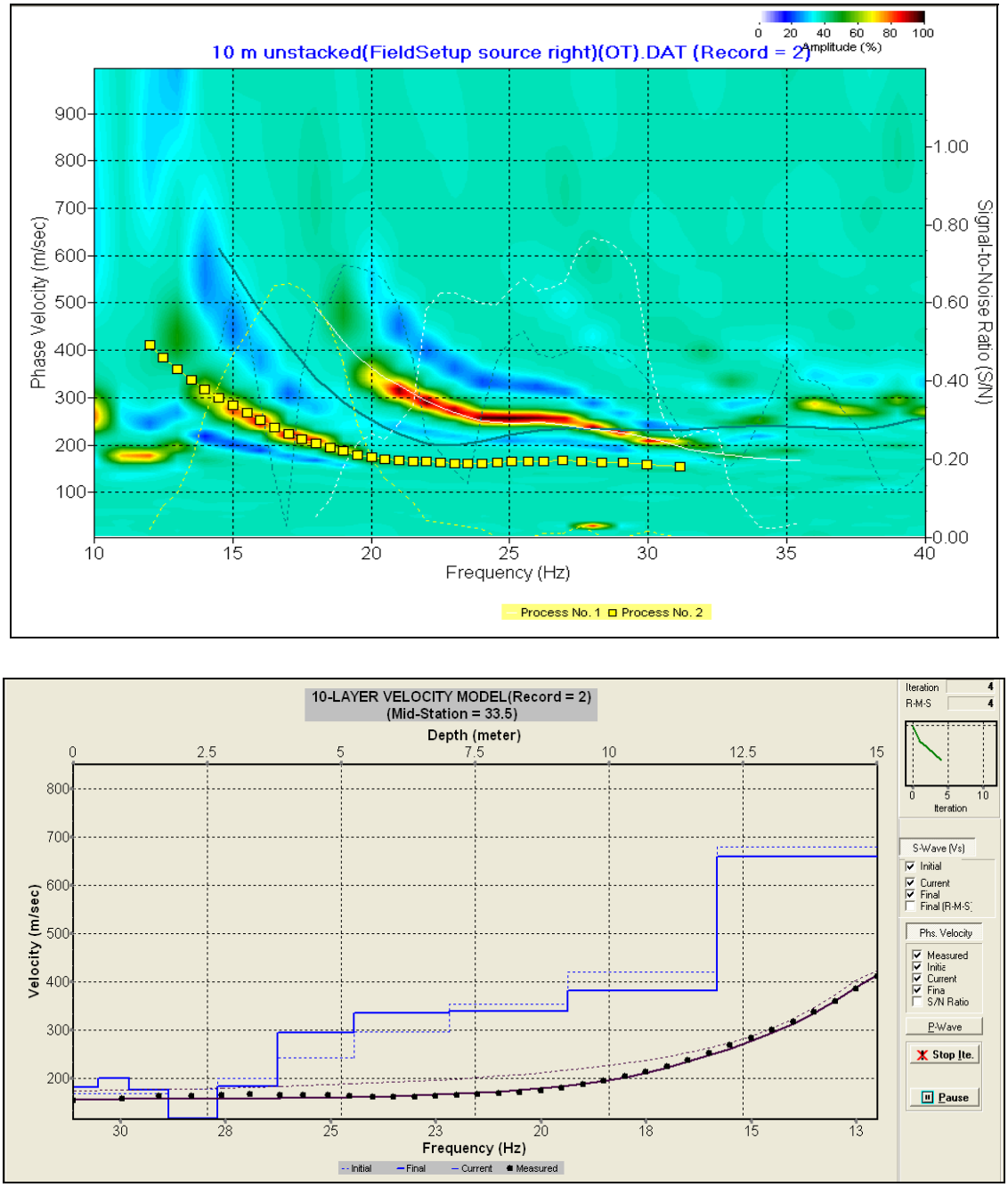

Figure 5.8: Example of higher modes being present in the data. Fundamental mode dispersion curve has been picked (top), with associated velocity model (bottom) from Te Rere Hau Windfarm Turbine site 2.

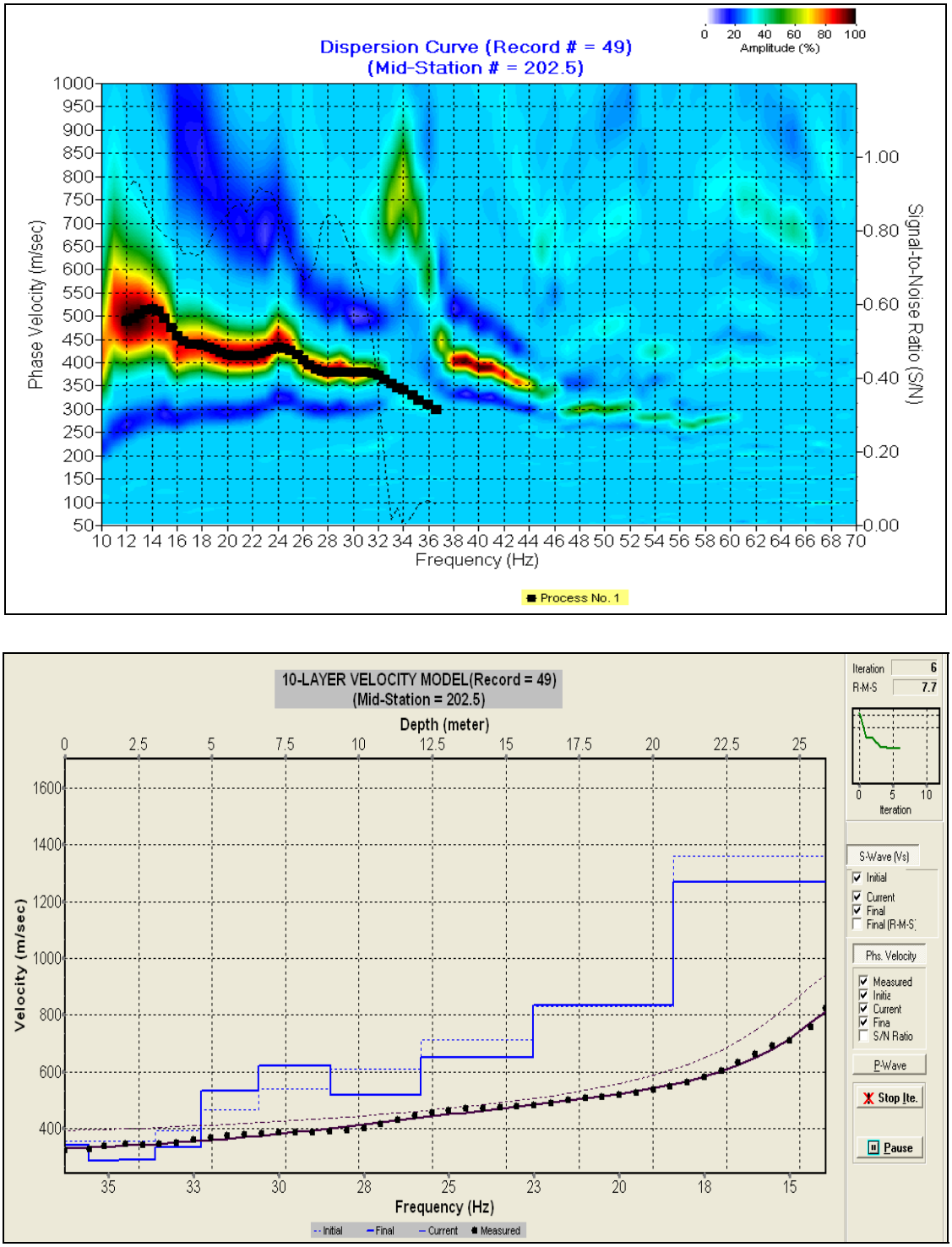

Figure 5.9: Dispersion curve (top) and associated velocity model (bottom) for Te Rere Hau Windfarm turbine site 49.

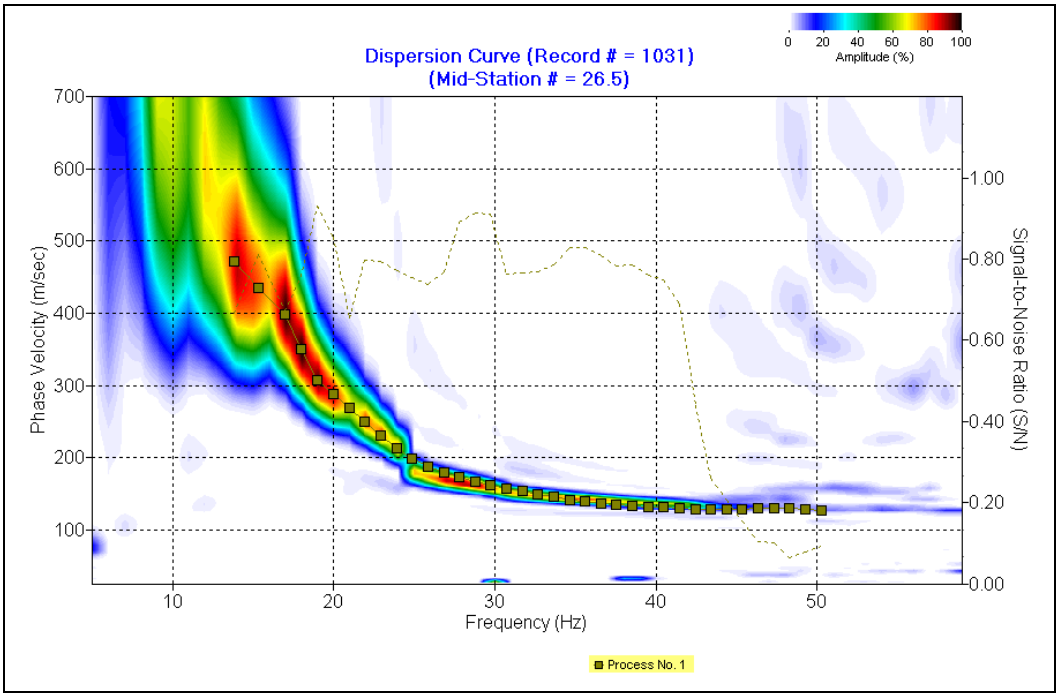

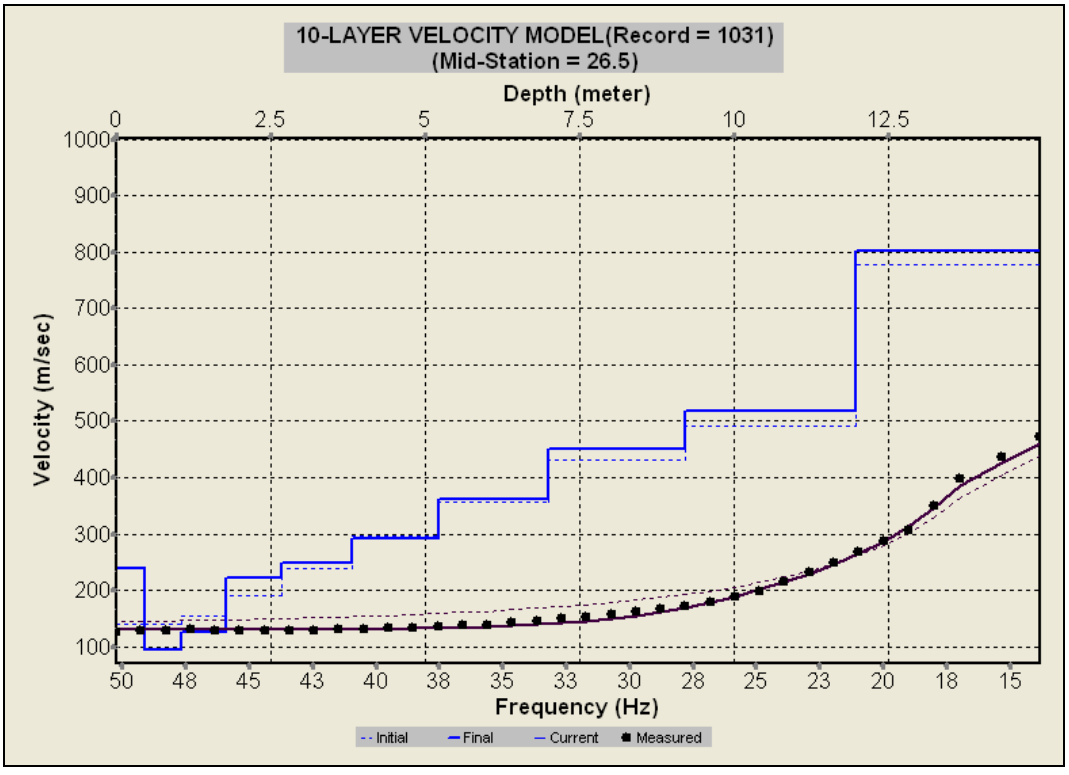

Figure 5.10: Dispersion curve (top) and associated velocity model (bottom), from Turitea Windfarm, turbine site 6.

V_S profiles for turbine sites 6 from Turitea Windfarm and turbine sites 2 and 49 from the Te Rere Hau Windfarm, are displayed in Table 5.4.

Te Rere Hau: Turbine site 2	
Depth (m)	**V_S (m/s)**
0.47	182.79
1.05	200.96
1.78	176.33
2.69	117.91
3.82	184.21
5.24	294.17
7.02	336.01
9.24	339.55
12.02	381.16
12.02	659.95

Te Rere Hau: Turbine site 49	
Depth (m)	**V_S (m/s)**
0.8	344.35
1.81	288.87
3.06	290.25
4.63	334.62
6.59	534.08
9.04	623.25
12.1	519.99
15.93	650.20
20.71	834.62
20.71	1268.00

Turitea: Turbine site 6	
Depth (m)	**V_S (m/s)**
0.463	238.97
1.042	94.38
1.766	125.61
2.671	222.27
3.802	249.84
5.216	292.15
6.984	361.34
9.194	451.43
11.956	517.04
14.945	800.97

Table 5.4: V_S profiles with depth from Turitea Windfarm turbine site 6, and Te Rere Hau Windfarm turbine sites 2 and 49.

Typically, there was a reasonable match between the two surveys in opposite directions (see Figure 5.11). If a survey in one direction produced a poor quality and difficult to extract dispersion curve, the survey in the opposite direction generally produced a dispersion curve of similar quality, which it can be assumed was largely due to subsurface lateral heterogeneities. A discontinuous or irregular dispersion curve may be due to several causes, including ambient noise, other wave types interfering with the signal, or an irregular stiffness profile. Processing the data surveyed in both directions helped limit the influence of disturbances such as those mentioned above. Identification of the cause of these disturbances was sometimes possible, due to the repeated survey and the information about the site and survey conditions which this method provided. Some records had such a poor quality that no dispersion curve could be identified and they were discarded, due to a range of conditions discussed in Section 5.4.

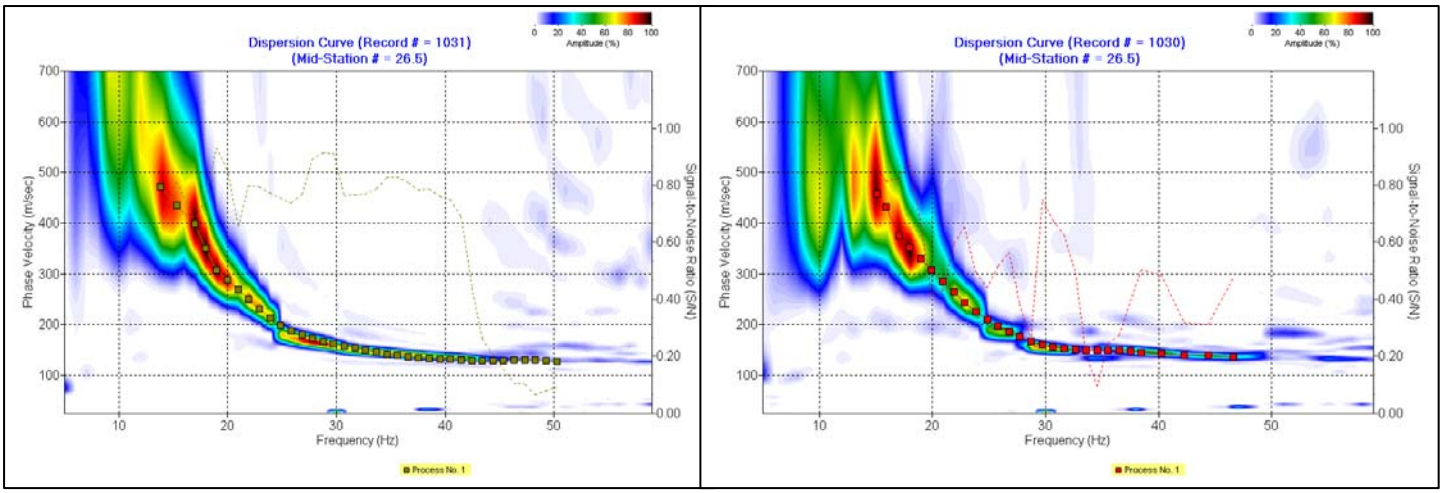

Figure 5.11: Dispersion curves from MASW surveys in both directions at the Turitea Windfarm turbine site 6, showing a good agreement between surveys, suggesting lateral site homogeneity.

Other sites which produced dispersion curves which could not be extracted, similar to that of West Wind Windfarm site H03, included Te Rere Hau Windfarm sites 34, 52, 53 and 80 which were subject to highly unsuitable topographic conditions and insufficient survey area for an appropriately sized source-receiver offset and array length, causing 'near-field effects'. These sites were either investigated further using other geotechnical investigation methods, or abandoned as wind turbine sites due to it not being economically viable for the extra costs associated with geotechnical remedial works or enlarged foundations.

A number of the dispersion curves processed in this study were broken up and did not resemble a smooth curve (Figure 5.12). This makes identifying the fundamental dispersion curve difficult. Due to MASW requiring a planar surveying surface, and the often variable topography encountered on the windfarms, the non-smooth dispersion curves are potentially due to near surface undulations, along with the effects of significant lateral heterogeneity already discussed.

When lateral heterogeneities exist in the subsurface, it is the high frequency imaging which is affected as the waves associated with smaller wavelengths travel through several wave cycles through the length of the array, and with lateral variations on site, waves often image different material at different ends of the array. Whereas with longer wavelengths, ie: lower frequency waves, only one or two wave cycles are completed through the array of receivers. The quality of MASW data and the acceptability of results were determined by the confidence ranking assigned to each survey.

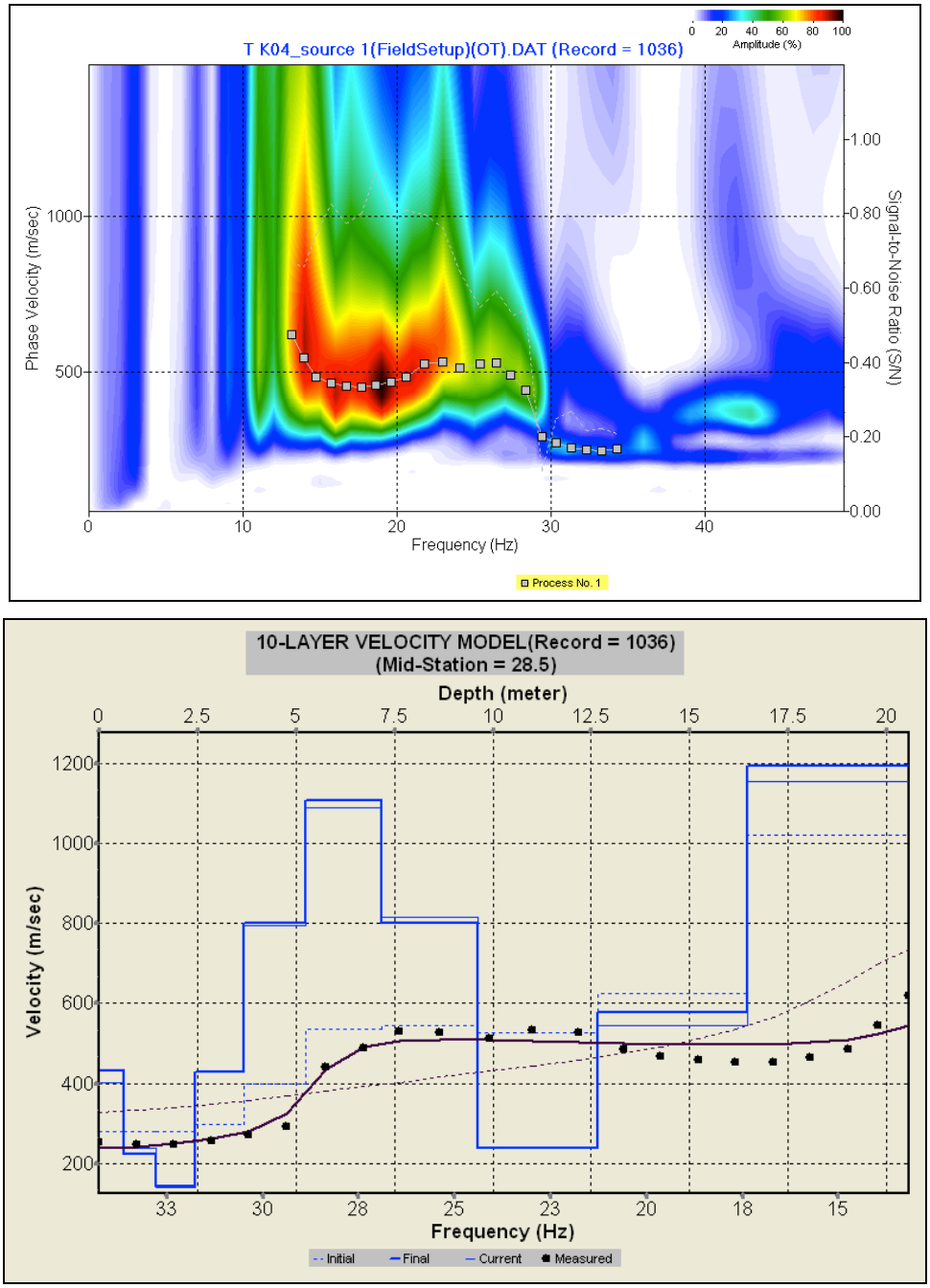

Figure 5.12: Disjointed and undulating dispersion curve (top) and associated velocity model (bottom), from Westwind Windfarm, turbine site K04.

A recurring aspect across all three windfarm sites is a high velocity layer at the surface. This high velocity layer is due to one or a combination of stiff near surface materials (loess/loess-colluvium material), higher mode contamination at higher frequencies, or remnant non-planar waves due to a source-receiver offset fractionally too short. This near-surface high velocity layer is generally confined to the upper 1.5 to 2m, below which the V_S profile increases with depth. Even records of the highest quality all show evidence of a high velocity surface layer (similar to that displayed in Table 5.4). If the source-receiver offset was slightly too short, the remnants of

non-planar travelling surface waves can influence the near surface V_S results. These effects are called near-field effects. Since most surface wave inversion methods use a theoretical model that does not include near-field contributions, it is important that data are collected such that near-field effects are minimised (Rosenblad & Cheng-Hsuan, 2011). Precautions were initially made to ensure non-planar travelling waves were not included in the recordings by adjusting the source-receiver offset. As a method of checking during further surveys on site, it would be of benefit to repeat surveys with a 10m, 11m and 12m offset to compare results. This was not feasible during the majority of MASW surveys on the Te Rere Hau Windfarm site as the work was undertaken in a commercial capacity, hence time and financial constraints were upon the surveyors. In the case of the windfarm development, this high velocity surface layer data did not prove problematic. Whether it was a result of seismic wave behaviour or interference or solely a product of a stiffer surface loess/loess-colluvium material, the top 1.5-3.0m was generally removed as overburden down to the foundation level, meaning this issue could be ignored during time and financially constrained commercial investigations.

The relative error is an indicator of the match between the theoretical and experimental dispersion curves. Usually a relative error between the experimental and the numerical dispersion curves, which is less than 10%, means that a satisfactory and valid result has been obtained. Generally if the relative error is between 10% and 20%, the picked dispersion curve is adjusted to reduce the error.

5.7 Synthesis:

This chapter has detailed the methods used and parameters assigned, for MASW surveying at the wind turbine sites. The methods used to ensure quality data was processed and then used for data analysis in this study include the confidence ranking system, repeating surveys in opposite and perpendicular directions, along with survey parameters including source-receiver offset, array length and geophone spacing. Although a number of parameters and conditions can be altered specific to the survey site, the quality of the survey is eventually at the control of the subsurface conditions. If the fundamental assumption that the survey is performed on a layered, laterally homogenous half-space is not met, which is the 'real' case, survey parameters can only control the influence of these geological conditions.

The method of dispersion curve extraction is explained, along with typical problems encountered, including interference and unfavourable survey conditions. Next the surface wave inversion stage of data processing is explained along with typical errors which can be incurred during this process.

Dispersion curves and velocity models from Te Rere Hau Windfarm turbine sites 2 and 49, along with Turitea Windfarm turbine site 6 are displayed and discussed. Sites which produced results with low confidence rankings and unextractable dispersion curves are discussed, with the reasons behind their exclusion from the final dataset.

Finally the high velocity surface layer found in the majority of MASW surveys is discussed, with the reasons behind this trend assumed to include a stiff surface layer of loess/loess-colluvium, the recording of non-planar travelling surface waves or possibly higher mode contamination at higher frequencies.

Chapter 6 Dataset Analysis and Review:

6.1 Introduction:

This chapter details the analysis of the combined geotechnical and geophysical data from this study. A number of correlations between different variables have been analysed, with significant trends emerging. The MASW data is organised into a dataset which is filtered to include the information only relevant to this study, and correlated with both depth and weathering grade data from pile drilling logs. In addition to this dataset analysis, a number of limitations surrounding the method of calculating elastic moduli values from V_S data are discussed, along with methods for improving the predictive ability of the MASW technique.

A total of 100 sites were surveyed, with 86 sites falling within the required conditions for this study. 58 of these sites produced velocity soundings with confidence levels of 3, 4 or 5, as discussed in Chapter 5.2. This dataset has been filtered to only include 68% of the surveys performed within the required conditions for this study, subjectively removing surveys with low confidence rankings and possibly inaccurate or unrepresentative data. Geophysical surveys are only beneficial if they are performed within the required conditions and bounds of the method itself, and the assumptions made during data processing. Therefore stringent filtering of data is required for a dataset with a high level of confidence.

A full list of the MASW surveys, locations, and their associated confidence rankings are summarised in Appendix I.

6.2 Weathering grade and V_S variations across the Te Rere Hau Windfarm site:

A common trend noticed across the Te Rere Hau windfarm site is typically lower shear wave velocity (V_S) values through the depth profile at turbine sites on the western flanks of the Tararua Ranges (Stage 2 of development), as shown by a representative selection of profiles in Table 6.1. Turbine sites developed later, along the tops and down onto the eastern flanks of the Tararua Ranges, tend to have higher V_S values through the depth profile than those on the western flanks, as shown by a representative selection of profiles in Tables 6.2 and 6.3. An insufficient number of survey sites at the Turitea and West Wind Windfarms were completed to notice characteristic topographic or aspect trends in their V_S profile dataset.

Western Flanks of the Tararua Ranges											
Turbine 33			**Turbine 9**			**Turbine 73**			**Turbine 84**		
Depth (m)	Soil Type	V_S (m/s)	Depth (m)	Soil Type	V_S (m/s)	Depth (m)	Soil Type	V_S (m/s)	Depth (m)	Soil Type	V_S (m/s)
1.5	L/LC	342	1.5	L/LC	422	1.5	L/LC	305	1.5	L/LC	103
3	CW/HW	95	3	HW	267	3	HW	267	3	CW	245
4.5	HW	282	4.5	HW/MW	290	4.5	MW	386	4.5	CW/HW	269
6	HW/MW	368	6	MW	469	6	MW	422	6	HW	386
7.5	MW	430	7.5	MW	562	7.5	MW	461	7.5	HW	440
9	SW	543	9	MW/SW	562	9	MW/SW	537	9	HW/MW	435
10.5	SW/UW	543	10.5			10.5	SW	537	10.5	MW	
11.5	SW/UW	543				11.5	SW	626	11.5	MW/SW	

Table 6.1: Pile drilling logs from turbine sites on the western flanks of the Tararua Ranges at the Te Rere Hau Windfarm site.

Ridge line of the Tararua Ranges											
Turbine 210			**Turbine 211**			**Turbine 212**			**Turbine 209**		
Depth (m)	Soil Type	V_S (m/s)	Depth (m)	Soil Type	V_S (m/s)	Depth (m)	Soil Type	V_S (m/s)	Depth (m)	Soil Type	V_S (m/s)
1	MW/SW	737	1	LC	500	1	SW	593	1	MW/SW	586
2	MW/SW	358	2	SW	247	2	SW	564	2	MW/SW	545
3	SW	236	3	SW	477	3	SW/UW	429	3	MW/SW	343
4	SW	543	4	SW	693	4	UW	369	4	MW/SW	343
5	SW	767	5	SW	693	5	UW	369	5	MW/SW	324
6	SW	898	6	SW	865	6	UW	725	6	MW/SW	727
7	SW/UW	898	7	SW	1312	7	UW	725	7	MW/SW	727
8	UW	1002	8	UW	1312	8	UW	1090	8	MW/SW	940
9	UW	1002	9	UW	1312	9	UW	1090	9	MW/SW	940
10	UW	1598	10	UW	1312	10	UW	1185	10	MW/SW	940
11.5	UW	1598	11.5	UW	1312	11.5	UW	1185	11.5	MW/SW	940

Table 6.2: Pile drilling logs from turbine sites along the ridge line of the Tararua Ranges at the Te Rere Hau Windfarm site.

Eastern Flanks of the Tararua Ranges											
Turbine 204			**Turbine 205**			**Turbine 203**			**Turbine 240**		
Depth (m)	Soil Type	V_S (m/s)	Depth (m)	Soil Type	V_S (m/s)	Depth (m)	Soil Type	V_S (m/s)	Depth (m)	Soil Type	V_S (m/s)
1	CW/HW	428	1	RS	865	1	LC	359	1	SW	409
2	MW	326	2	MW/SW	731	2	LC	312	2	SW	361
3	SW	489	3	MW/SW	731	3	LC	197	3	SW	295
4	SW	674	4	MW/SW	430	4	SW	303	4	SW	295
5	SW	674	5	MW/SW	659	5	SW	508	5	SW	565
6	SW	570	6	SW	659	6	SW	508	6	SW	806
7	SW	570	7	SW/UW	997	7	SW/UW	664	7	SW	806
8	SW	748	8	SW/UW	997	8	SW/UW	664	8	SW	936
9	SW	748	9	SW/UW	864	9	SW/UW	766	9	SW	936
10	SW/UW	748	10	SW/UW	864	10	SW/UW	766	10	SW/UW	936
11.5	SW/UW	1046	11.5	UW	864	11.5	SW/UW	782	11.5	SW/UW	844

Table 6.3: Pile drilling logs from turbine sites on the eastern flanks of the Tararua Ranges at the Te Rere Hau Windfarm site.

As discussed in Chapter 3.2.5 the winds in the Wellington and Manawatu regions are strongly dominated by the prevailing westerly. The geological characteristics through the significant weathering profile at turbine sites on the western flanks have been correlated with V_S profiles. Table 6.1 displays a low velocity down to 10m below ground surface for the four profiles. These show a maximum V_S or 626 m/s at a depth of 11.5m and a minimum V_S value at 11.5m of 543 m/s, which is a typical range for sites on the western flanks. A conservative calculation, involving all pile drilling logs on the western flanks, produced an average depth of 9.0m to slightly weathered or unweathered material. Due to the fact that a number of sites on the western flanks did not reach slightly or unweathered material within the depth of the drilled pile hole, a depth value of 12m was assumed. The pile holes were drilled to 11.5m, therefore assigning a value of 12m to the slightly or unweathered boundary if it had not already been reached, is a conservative assumption.

The geological characteristic trend of a shallow weathering profile at sites along the ridge and down onto the eastern flanks of the Tararua Ranges, has been correlated with V_S profiles in Tables 6.2 and 6.3. The minimum V_S value at 11.5m depth from the 8 profiles displayed in Tables 6.2 and 6.3 is 782 m/s, with a maximum V_S reached of 1598 m/s. These are also typical values for all surveys along the ridge and onto the eastern flanks (a full set of profiles can be found in Appendix D). Again, an average depth to which drill holes reach slightly weathered or unweathered grades was calculated for these sites with an average of 5.3m, with the majority of

sites reaching this grade within the top 3m. Three of the 18 sites located along the ridge and on the eastern flanks did not reach slightly or unweathered material at 11.5m, hence the same 12m assumption discussed above was applied.

The combination of both the pile drilling logs and V_S data confirms that higher weathering grades result in lower V_S values, and vice versa. The distribution of V_S profiles and weathering profiles across the Te Rere Hau site supports the possibility that there is a climatic influence on the rate of weathering with depth on the western flanks, relative to the ridge and eastern flanks (refer to Figure 3.6 for a simplified cross-section of the Tararua Ranges). The westerly winds would result in an increased rainfall on the western flanks, contributing to an increased level of water infiltration, hydration and oxidation. This notion is supported by the Huisman et al (2006) study which details the close relationship between the weathering rates, the slope aspect, and the prevailing wind directions during rainfall events.

6.3 Combined Analysis of Weathering, Shear Wave Velocity and Depth:

6.3.1 Profile Variations

As discussed throughout this study, seismic wave velocity is influenced by a number of factors. During the geotechnical investigations on site, the dominant geological characteristic which changed with depth, and encompassed all of the individual geological controls on V_S, was the weathering grade. Each of the geological characteristics including density, fracture infilling material, and fracture density, are controlled by the weathering grade, as each geological characteristic changes consistently with weathering.

V_S data have often been used to represent geological and geotechnical properties such as density or rock strength, although this method fails to take into account the influence of overburden pressure on seismic velocity (Barton, 2007; Gao & Gibson, 2011; Meglis et al., 1996). Seismic velocities are significantly influenced by overburden pressure, which is often explained by crack closure within the rock. Cracks and fractures within a rock deform under increasing confining pressure, which in turn affects the seismic velocity of a rock. However, at shallow depths (>10m), the influence of vertical stress would typically not exceed approximately 200KPa. The effects of near-surface dilation due to weathering, both chemical and physical, are most likely the major influencing factor. Both effects of overburden pressure

and near-surface dilation are encompassed in the depth value, as they are both expected to influence sites consistently with depth and weathering changes across the whole site.

Therefore, the two factors influencing the V_S profile are depth and weathering grade, each of which takes into account the individual factors influencing V_S discussed above. The V_S profiles determined through MASW surveying were plotted against depth for each individual weathering grade as shown in Figures 6.1, 6.2 and 6.3, with a full set of plots found in Appendix J. These plots clearly indicate that V_S increases with increasing depth within the same grade of weathered material.

Figures 6.2 and 6.3 display a non-linear increase of V_S with depth, although both show a large scatter of data. Figure 6.1 displays the trend of V_S with depth for the unweathered material. Again this data displays a significant amount of scatter, although still displaying a relatively linear trend of increasing V_S with depth. V_S values for the unweathered material between 5 and 10m depth, range from approximately 500 m/s to 1500 m/s. This large range in data for the same unweatehred grade of 'greywacke' is assumed to be an artefact of near-surface dilation. Unweathered material nearer the surface is influenced to a greater level by dilation, resulting in a lower V_S value.

This data identifies the trend of increasing V_S with increasing depth. Therefore it can be deemed unrepresentative to assign V_S values to weathering grades or lithologies without taking into account depth of the material, which encompasses the effects of the overburden conditions and dilation.

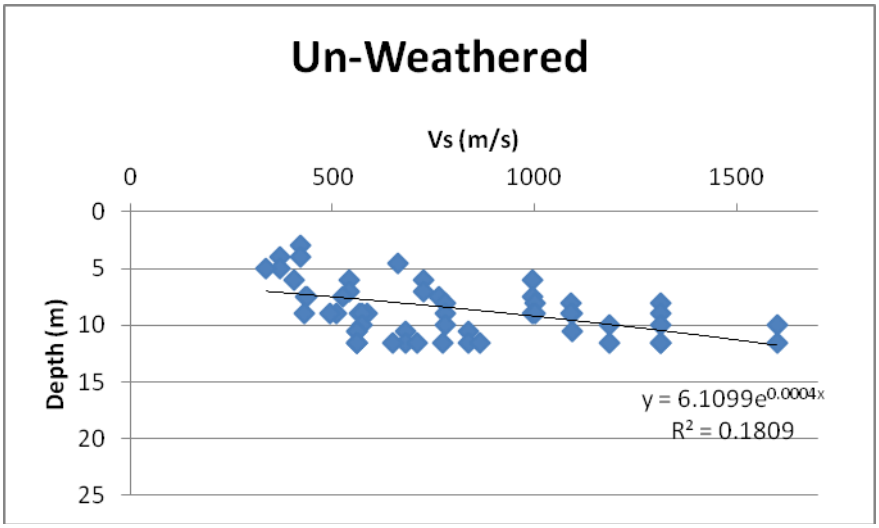

Figure 6.1: Effects of depth on V_S within the unweathered grade of Esk Head belt 'greywacke', displaying a large scatter of data with an increasing trend of V_S with depth.

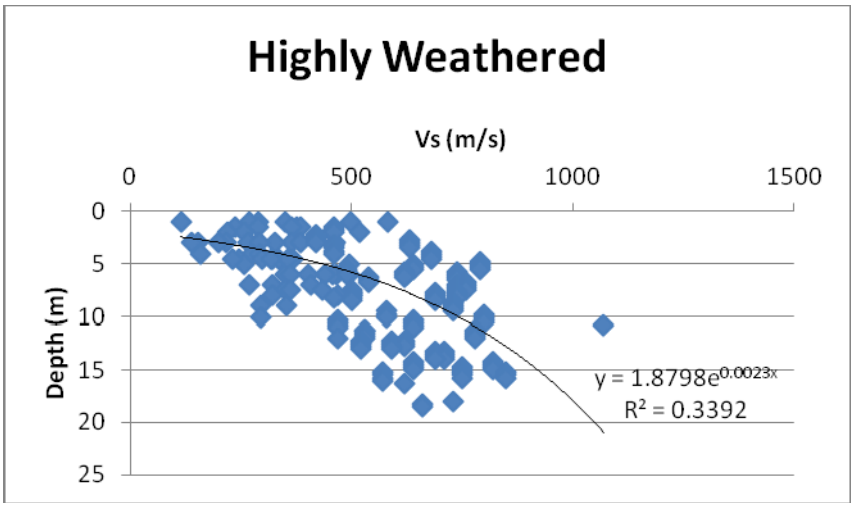

Figure 6.2: Effects of depth on V_S within the highly weathered grade of Esk Head belt 'greywacke'.

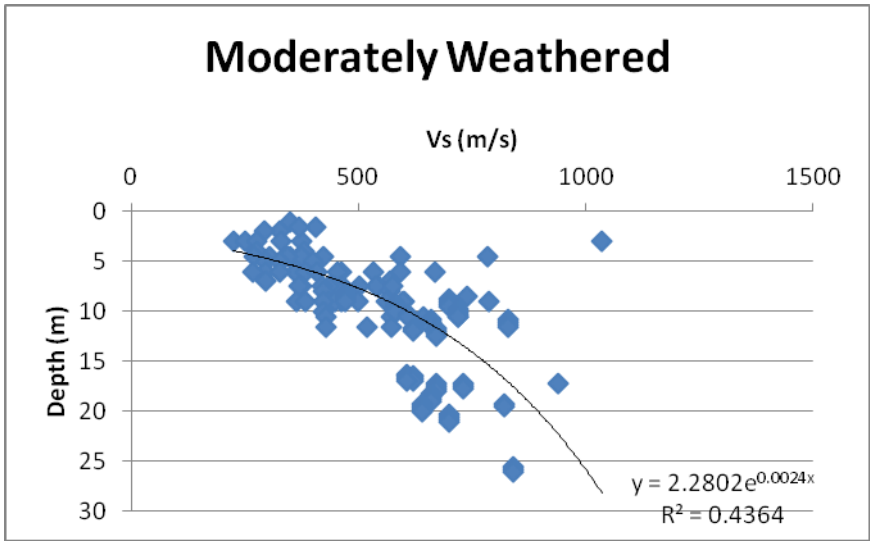

Figure 6.3: Effects of depth on V_S within the moderately weathered grade of Esk Head belt 'greywacke'.

6.3.2 Logarithmic Analysis

An analysis of the impact of the logarithmic mathematical function on both depth and V_S for each weathering grade was also undertaken. The logarithmic function was applied to each of the depth and V_S scales individually, and in combination. This method is typically used to identify the mathematical relationship between two variables, which is important for the regression analysis performed in Section 6.6.

As shown in Figure 6.3 which displays the results for the moderately weathered material, this analysis method failed to reveal a stand-out relationship between the two variables. A clear linear trend was identified from the plots of LogV_S versus Depth, V_S versus LogDepth, and LogV_S versus LogDepth. A full set of plots from the logarithmic analysis can be found in Appendix K.

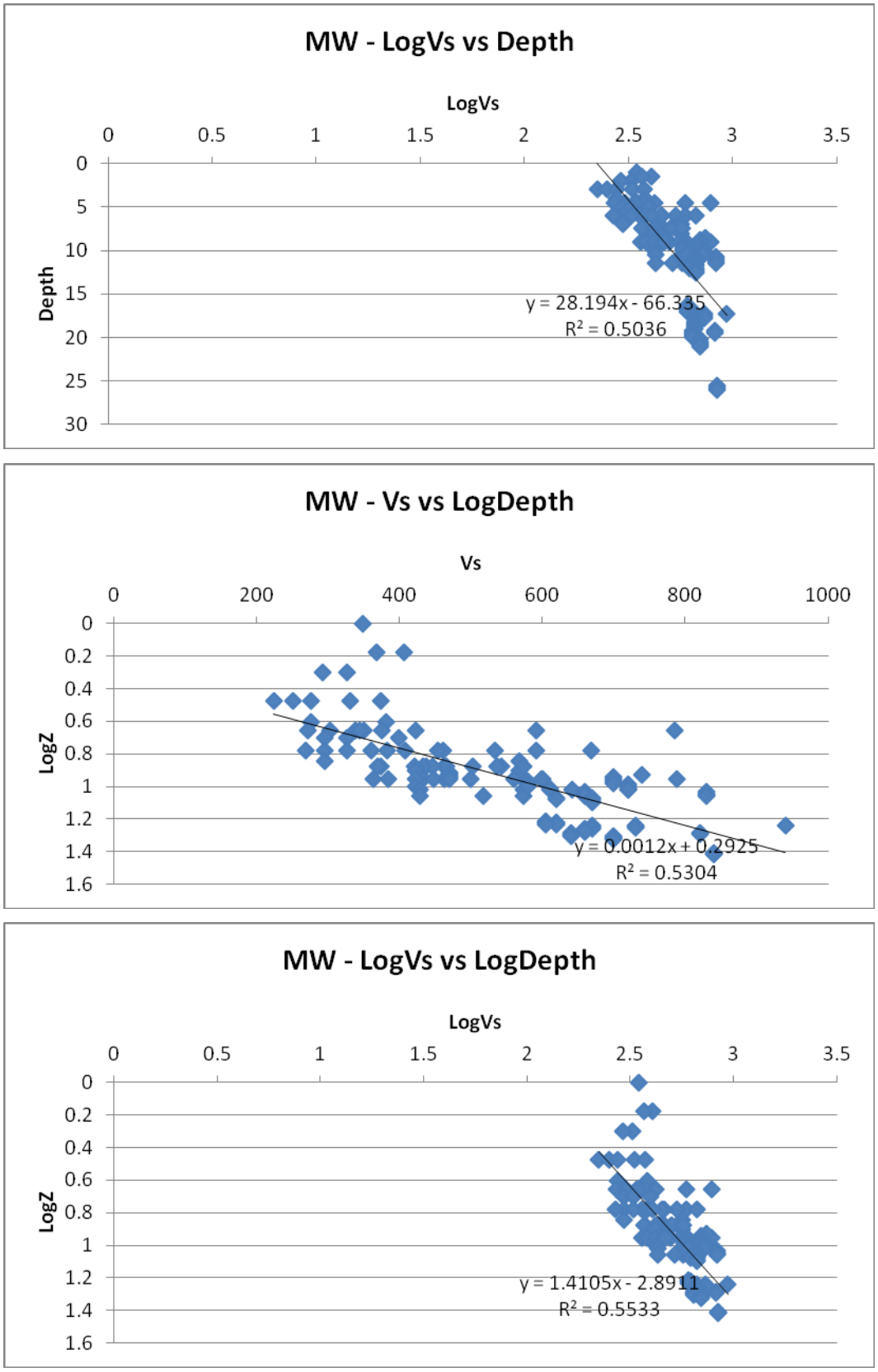

Figure 6.3: Logarithmic analysis of LogV_S versus Depth (top), V_S versus LogDepth (middle) and LogV_S versus LogDepth (bottom), for the moderately weathered material. All three plots display a relatively good linear relationship.

6.4 Non-linear multiple regression analysis:

6.4.1 Background

In order to analyse the entire dataset of V_S, depth and weathering information across all weathering grades, a regression analysis involving multiple variables was performed.

Regression analysis is a technique used for analysing the relationship between the dependent variable and one or more independent variables. During simple linear regression, variations in the dependent variable are attributed to changes in only a single independent variable (Schroeder et al., 1986). In reality, there are usually several factors simultaneously affecting the dependent variable. This is termed multiple regression analysis, which measures the effects of several factors concurrently.

By understanding how the dependent variable relies on the independent variables, predictions can be made as to the result of changing any one variable (Allen, 1997). In relation to this study, by analysing the extensive dataset gathered, the dependent variable, V_S, can be estimated when the independent variables, depth and weathering grade, are known, within the Esk Head belt 'greywacke'.

The multi variable non-linear analysis performed in this study was developed from an extensive dataset. The majority of data was from the Te Rere Hau Windfarm in the Tararua Ranges, with additions to the dataset from Turitea Windfarm also in the Tararua Ranges and the West Wind Windfarm in Wellington.

6.4.2 Method

The regression analysis in this study was performed with the help of Dr James Degnan, Lecturer in the Mathematics and Statistics Department at the University of Canterbury, using the statistical analysis programme, The R Project, commonly called R. The R Project is a language and environment for statistical computing and graphics, and can be used for a wide range of analysis including linear and nonlinear modelling, classical statistical tests, time-series analysis, classification and clustering.

The statistical analysis programme, R, was used to analyse the dataset; procedures and methodology are detailed in Crawley (2007). The entire dataset of V_S, depth and weathering grade data was converted to text file and imported into R. The data was analysed in a 3D format, effectively fitting the data to a non-linear 3D surface. This was performed using a linear model,

or 'lm', along with a 'log' function applied to the V_S data. Using this combination of modelling functions, the data is effectively analysed as a non-linear multi variant model.

Refer to Appendix L for the full regression analysis and a description of the procedure.

6.4.3 Results

The regression analysis calculated the following predictive equation:

$$V_S = EXP(5.771+(0.078*Depth)-0.035*Weathering) \quad \text{Equation 6.1}$$

Due to this being a statistical numerical analysis, the 'weathering grade' had to be classified numerically from 1 to 9 as unweathered to completely weathered respectively, in summarised form as UW (1), SW/UW (2), SW (3), MW/SW (4), MW (5), HW/MW (6), HW (7), CW/HW (8), CW (9).

Therefore to calculate this equation, a value of 1 to 9 representative of the weathering grade is input as 'weathering', and similarly the depth value is input into Equation 6.1.

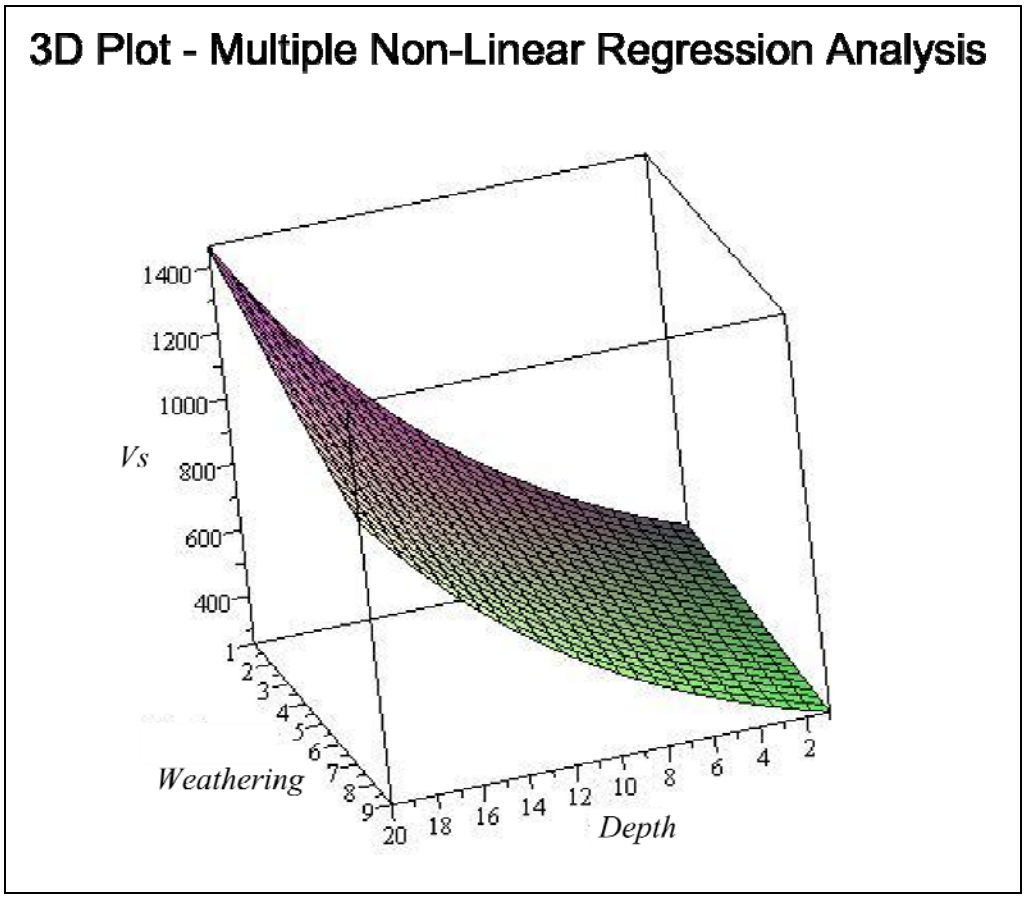

Figure 6.4: 3D plot of results from the multiple non-linear regression analysis displaying the relationship between weathering, depth and V_S. The weathering grades of unweathered to completely weathered are represented numerically by the values of 1-9.

The R^2 value represents the coefficient of determination and is used in statistical models which model future outcomes, and is measured on a scale of 0 to 1. It is the proportion of variability in the dataset that is accounted for by the statistical model (Steel & Torrie, 1960). The adjusted R^2 value is a modification of the R^2 value, which takes into consideration the number of variables in the model.

The R^2 value for this regression model is 0.74, with an adjusted R^2 of 0.70. Hence the R^2 and adjusted R^2 values suggest the regression model makes a good fit with the dataset.

The first requirement for this equation to be applied correctly to other geotechnical investigations, is that the investigation site is located within similar geological terrain and conditions as the research sites in this study. If this requirement is satisfied, V_S can be calculated, within limitations, if weathering and depth data is available. Likewise, with V_S and depth data available, the weathering grade can be predicted, for a completely non-invasive investigation. This method is suitable to be used for further stages of development at the Te Rere Hau Windfarm site, in the development of the Turitea Windfarm (adjacent to the Te Rere Hau site on the Tararua Ranges), or other developments situated along the axial trace of the Tararua Ranges. This predictive method can significantly reduce the costs of insitu investigations, including drilling, geophysical testing, test pitting or other invasive methods measuring physical properties, if it is determined that the calculation can be safely applied to the site under investigation.

Likewise, for further windfarm investigations, where the number of turbine sites can often reach up to 100, a similar process of investigation and calculation can be followed during the initial stages of the geotechnical site investigation. Once a sufficient dataset has been collated, analysed and determined to be representative of the entire site, the calculation of a predictive equation can be performed and applied to the remaining investigations of site development. This would ensure site specific data is being used, along with reducing investigation costs for the latter part of the site development.

6.5 Limitations of Elastic Moduli Derivation Methodology:

During the calculation of elastic modulus from V_S data, detailed in Section 1.7, errors can arise during a number of different stages in the process of MASW surveying, data processing, data analysis. To ensure the accuracy of each step in the process of converting MASW data, in the form of V_S profiles with depth, to elastic modulus profiles with depth, along with the continued development of this method, these errors need to be recognised, minimised and mitigated

where possible. The sources of error are typically derived from the modelling process, as outlined below:

- The MASW method assumes an infinitely flat, discretely layered, half-space. The Te Rere Hau Windfarm site, along with the Turitea and Westwind sites are all situated on steep and variable topography, of which the geology has highly variable physical properties. Hence the conditions on site are not always discretely layered as calculated in the shear wave velocity profiles. These effects can be identified during the processing of the MASW data. Due to these limitations, the confidence ranking scheme was developed and relied on heavily to determine those surveys which were not highly influenced by survey conditions.
- Edge effects caused by steep topography on many of the turbine sites can affect the inversion process. Edge effects can be caused by a steep drop in topography, e.g. off the edge of an excavated turbine pad foundation on an inclined slope. This was mitigated by orientating surveys to best maximise the quality of results from the topography available, by ensuring the survey line is situated on planar topography without significant undulations and/or structural features. Again, the confidence ranking scheme was used to filter out those surveys heavily affected by any edge effects.
- The recording of non-planar surface waves was a possible limitation on the accuracy of the shear wave velocity profiles. This problem was attempted to be eliminated by the determination of an ideal source-receiver offset, ensuring non-planar travelling surface waves were not being recorded, but were still close enough to the geophone array to receive high resolution.
- There are also errors associated with the conversion of shear wave velocity values into elastic modulus values. These errors are associated with the accuracy of the input values into this calculation. Poisson's ratio and density, along with V_S are input into the equation for elastic moduli, and hence the accuracy of the elastic modulus value is dependent on the accuracy of the inputs. This study has significantly improved the accuracy of both density and Poisson's ratio values through insitu testing, replacing the method of assuming these values.
- Due to a lack of available literature on the stiffness of insitu weathered residual greywacke rock, comparisons to established practice were difficult to achieve.
- Due to a lack of available literature on the Poisson's ratio of weathered greywacke rock, comparisons to established information were difficult to achieve. There was

also a very limited amount of information available for comparisons of density values through the weathering profile.

6.6 Guidelines for future MASW windfarm investigations:

A key objective in this study was to develop a set of guidelines to assist with further MASW investigations, focused on determining V_S profiles with depth for the calculation of elastic moduli. This set of guidelines is developed with the intention of having the ability to be adjusted according to the specific requirements of the investigation. MASW survey parameters are frequently required to be adjusted due to topographic conditions, equipment limitations or intended depth of investigation. The suggested methods are intended to assist geophysicists and engineers to extract the most accurate information from the investigation site.

The principles and general features of each step in the investigation process are detailed in the following sections.

6.6.1 MASW Investigation

In the planning and execution of a MASW survey, parameters must be set in accordance with the survey site conditions. The usual steps taken to plan and execute a MASW survey are suggested here, along with additional considerations when performing 1D profiling on a wind turbine site.

- Study of existing information and data, including previous geophysical surveying, drillhole or testpit data, geological maps and previous geotechnical investigations close to the site. From this, develop a survey plan and recommendations for the MASW investigation, i.e. number of survey sites, type of profiling required, intended depth of investigation, etc).

- For the selection of optimal survey acquisition parameters, initially follow the suggested acquisition parameters from Park et al (1999), which are based around the maximum depth of investigation required. These parameters can be adapted according to the level or resolution in relation to the depth of penetration. This is required for the survey, as well as the surveying equipment available (e.g. number of channel seismograph, number of geophones, etc).

- Initially decompose the recorded wavefields into a swept-frequency format, using SurfSeis software. This permits the identification of noise based on frequency content

and offset, identifying the planar surface wave arrival times and distances. From this is it possible to make adjustments during acquisition to minimise noise and maximise signal.

- To improve the accuracy of results, and also to provide a secondary check on results, perform the survey in both directions along the survey line. In addition, initially perform the survey both along the initial survey line and on a secondary line perpendicular to the initial survey line. This helps determine the level of lateral heterogeneity in the subsurface, and will give an indication of the confidence in the results, as homogeneous subsurface conditions will provide a high level of consistency between perpendicular survey results.

- For the continued accuracy of results, it is recommended to keep the acquisition parameters consistent throughout the investigation. However, at times these parameters will need to be adjusted due to the specific topographic conditions at the investigation site. Suggested acquisition parameters from Park et al (1999) are shown in Table 6.4.

- Stacking of data from repeated seismic shots at each site is recommended, depending on the level of interference and the strength of the returned seismic signal (e.g. the signal to noise ratio). If signal strength is weak and the noise level high, shots can be stacked up to 8-10 times, although if the signal to noise ratio is good, only stacking 3-4 shots is necessary. This is at the discretion of the surveyor.

- Identifying the fundamental mode dispersion curve during the dispersion curve extraction stage of processing is essential to the accuracy of results. This involves identifying what is interference of higher modes, and what is the fundamental mode curve. In good quality results, the fundamental mode dispersion curve is easily identifiable, although it often becomes difficult in lesser quality results. Reading Park & Miller (2004) and Park et al (1999) will help with accurate dispersion curve extraction.

Receiver (Hz)	Max. Depth (m)	Minimum Offset (m)	Maximum Offset (m)	Receiver Spacing (m)
4.5	50	10	100	1
10	30	10	100	1
40	15	10	100	1

Table 6.4: Optimum field parameters for MASW surveys for most common soil sites. A seismic source of 10-lb or heavier sledgehammer and use of recording instrument with 24-bit or higher dynamic range are both assumed. No low-cut analogue filter should be used during the acquisition (Park et al., 1999).

- During the inversion stage of processing, the application of a 10 layer model is considered an acceptable approach. The number of layers can influence the relative error between the experimental and theoretical dispersion curves and hence the final V_S profile. Applying a model with less than 6 layers is not recommended.

- Confidence rankings are the best way to ensure poor quality survey data are not used during analysis. Confidence rankings are determined by the quality of the experimental dispersion curve along with knowledge of the site conditions. Generally, unfavourable site topography is an indicator of a poor quality dispersion curve, which is difficult to pick, often with higher mode interference. Confidence rankings of 0 to 5, as used in this study (Table 6.5) are recommended.

Ranking	Description
0	No data or no dispersion curve extractable
1	Poor quality dispersion curve extracted detailed processing. Lowest confidence level.
2	Strong diffractions and scattered wave field. Generally poor coincidence of dispersion curves. Likely to be several significant modal jumps. Likely to be strong lateral contrasts in S-wave velocity. S-wave sounding represents a bulk average only. Use with caution and probably only deepest velocities.
3	Good coincidence of dispersion curves but potential for significant higher mode contamination at a range of depths. Deepest (half space) velocities probably ok, shallower velocities probably excessive.
4	Good coincidence of dispersion curves (or obvious selection of fundamental mode in one and higher mode in the other curve). Possibly inflated velocities close to surface due to higher mode contamination but otherwise confident.
5	Strongly dispersive overtone image. No evidence of higher mode contamination. Highest confidence level.

Table 6.5: Confidence ranking scheme used for MASW surveys to determine data quality.

6.6.2 Density characterisation

Density characterisation of the lithology on site is essential for accurate calculation of elastic moduli. Insitu density testing methods are suggested for accurate characterisation of the insitu density conditions. A number of tests can be performed depending on the geological material and its physical properties, and are detailed below.

Different methods are suited to different soil and rock conditions. Consistency in the testing method used is beneficial for continuous accuracy of results across a site.

The New Zealand Testing Standards for each method are detailed below:

- Sampling Tube Method: *New Zealand Standard 4402 : 1986. Test 5.1.3*
- Sand Cone Replacement Method: *New Zealand Standard 4402 : 1986. Test 5.1.1*
- Oil Replacement Method (adapt from the Water Replacement Method): *New Zealand Standard NZ 4402 : 1986. Test 5.1.5*
- Laboratory Submersion Method: *New Zealand Standard NZ 4402 : 1986. Test 5.1.4*

6.6.3 Poisson's ratio characterisation

As with the determination of density data, Poisson's ratio needs to be characterised through the range of weathering grades or lithologies found at the investigation site.

The most efficient method of determining insitu Poisson's ratio is via small strain seismic testing. This method of testing involves the evaluation of P-wave and S-wave velocities using down-hole seismic surveying. Downhole seismic methods require a PVC cased borehole and down-hole seismic equipment, which ensure geophones have a secure fit against the borehole casing.

Shear waves are generated by using a sledge hammer to strike the ends of a plank (horizontally), which must be held in contact with the ground surface. This is typically done by parking a vehicle on top of the plank. Compression waves are also created by striking the ground surface, or vertically on top of the plank. The resulting shear waves are recorded using a string of horizontally mounted geophones and one vertically mounted geophone, which have good contact with the PVC casing and are isolated from each other, typically using rubber spacers. Shear wave velocities are processed using computer software, and compression wave velocities are also calculated from the first arrival times from the vertical hits recorded on the vertical geophone.

Poisson's ratio is calculated using the V_P/V_S ratio, by the equation:

$$\frac{V_P}{V_S} = \sqrt{\frac{2-2\nu}{1-2\nu}}$$ **Equation 3.2**

$$\nu = \frac{1}{2}\left[1 - \frac{1}{\left(\frac{V_P}{V_S}\right)^2 - 1}\right]$$ **Equation 3.3**

(Christensen, 1996)

Further information, along with survey parameters suggested for this method, can be found in Ivanov et al (2000).

6.6.4 Dataset Analysis / Prediction modelling

Steps involved in dataset analysis and prediction modelling:

- Determining how the different variables of depth and lithology affect V_S.
- Determining the relationship between each lithological unit or weathering grade and V_S.
- Establish whether the trend between V_S and depth is consistent between weathering grades.
- Collate the entire dataset and format ready for analysis. This includes assigning numerical values in the place of weathering grades.
- Performing a multi variant regression analysis.

During the process of analysing the available data, trends will begin to emerge between different variables. The first step in data analysis is determining the influence depth has on V_S for each of the different weathering grades encountered. By producing a scatter plot of depth and V_S data for each grade of geology, trends should emerge showing how profound the effect of near-surface dilation is on V_S within each weathering grade of material. . Trend lines can be applied to the data, either linear or non-linear, determined by whichever produces the best fit and highest R^2 value.

To be able to perform a multi variant regression analysis on the dataset, the trends displayed by depth and V_S plots for each weathering grade or lithology must be consistent throughout all

grades. This consistency is required for an accurate multi variant regression model to be produced.

Before the multi variant regression analysis can be performed, the dataset needs to be correctly formatted. This includes assigning numerical values in the place of lithology, allowing the dataset to be analysed statistically. The regression analysis can be performed in a number of different statistical analysis software packages, including Microsoft Excel and R.

If the dataset used in the regression analysis is deemed to be representative of the entire site, calculations of V_S can be used for further investigations and developments on the site, or nearby sites from within the same geological conditions as the test site.

6.7 Synthesis:

This chapter has combined geotechnical and geophysical datasets, to identify trends within the Esk Head belt "greywacke". Weathering, depth and V_S data have been analysed determining the trend of increasing V_S with increasing depth within the same grade of weathered material. This suggests the need for depth conditions to be taken into account when associating characteristic V_S values for different lithologies or weathering grades in the near surface.

A predictive equation was developed for calculated estimates of V_S values when depth and weathering grade information are known within the Esk Head belt 'greywacke'. This predictive equation will be beneficial for further developments along the Tararua Ranges when seismic information is required, without the time or budget to perform testing.

Lastly, a set of guidelines for further geotechnical investigations, performed with the intent of calculating elastic modulus values from the V_S profiles, is described. These guidelines include MASW data acquisition parameters and how to adjust them to suit the survey conditions, along with methods for determining density and Poisson's ratio through the range of lithologies and weathering grades encountered.

Chapter 7: Summary and Conclusions

7.1 Research objectives:

7.1.1 Determining physical and mechanical properties of the insitu weathered 'greywacke'

Physical properties of the weathered Esk Head Belt 'greywacke' are required for accurate elastic modulus calculations. Both density and Poisson's ratio are properties with minimal literature available for weathered greywacke. Physical properties of unweathered greywacke are extensively published in literature (Cook, 2001; Kleffmann et al., 1998; Reilly, 1972), whereas data through the weathering profile is less extensively published on, with two main studies being utilised in this project, including Martin and Miller (1974) and Raisbeck (1973).

Insitu density testing was performed at the Te Rere Hau Windfarm site, determining characteristics values and ranges of density for each weathered grade of material. The physical properties of the weathered 'greywacke' changed from stiff soils to fractured unweathered rock-masses. The density values determined from the Te Rere Hau Windfarm showed some variances with existing literature, suggesting the need for further testing to be performed. The Poisson's ratio values determined through the weathering profile was established by analysing seismic data previously gathered, in combination with existing geological and geotechnical information.

7.1.2 Geological controls influencing shear wave velocities

As discussed from the results of MASW testing and data analysis, both depth and weathering grade were the two major factors controlling shear wave velocity. The individual geological characteristics and physical properties, including fracture infilling material, fracture spacing, aperture, density and Poisson's ratio, are encompassed in the weathering grade determination, as these properties are consistent within each weathering grade across the site. The influence of near-surface dilation is also encompassed in the depth value and weathering grade. It can be concluded from analysing each of the controls on V_S that rock-masses cannot be assigned representative V_S values without first taking into account the depth conditions which the material is under.

7.1.3 Removing errors associated with MASW processing

In order to limit the number of processing errors incurred during MASW investigations, a method of second checking data was used during this study. Surveys were performed in both directions along the survey line, and initially also in the perpendicular direction to the original survey line.

The perpendicular survey line, in combination with the original survey line data was used to determine the level of lateral heterogeneity at the survey site. If there was a clear agreement between the perpendicular survey line dispersion curves, the MASW data could be used with confidence, as lateral homogeneity is an inherent assumption made during MASW processing.

This method also helped identify any surveying problems encountered in one survey, relative to the second, providing a secondary check on results.

7.1.4 Lateral extrapolation of MASW results

Because of the highly variable nature of the weathered greywacke on site, lateral extrapolation of V_S data outside the survey area of the 1D MASW profile was difficult to perform with confidence. In an ideal half-space, a simple lateral extrapolation could be performed, as subsurface conditions would be laterally homogenous and isotropic. In the weathered 'greywacke' terrain on all three windfarm sites, weathering grade and physical properties frequently varied both vertically and laterally. Therefore, lateral extrapolation would be redundant as there is a high probability that the subsurface conditions have changed from that inside the surveyed area.

7.1.5 Refining the current procedure

With a focus on developing and refining the current procedure for converting geophysical information to geotechnical information, the insitu testing techniques previously used have been replicated in this study to test their accuracy and determine their limitations. Improvements have been made in the physical and mechanical property determinations of the Esk Head belt 'greywacke', and a number of assumptions previously made as part of the elastic moduli modelling process have been replaced with values determined through insitu testing. Mahoney & Kupec (2010) estimated the material properties onsite for residual/weathered lower bounds and weathered/unweathered upper bounds from literature, then linearly varied between these two bounds.

This method has been replaced in this study by actual insitu testing results from the Te Rere Hau Windfarm, assigning accurate physical and mechanical properties as inputs when

calculating the elastic modulus. This data is especially useful for further investigations into the Esk Head belt 'greywacke', as very limited data and literature is currently available. The refining of both density and Poisson's ratio inputs into the elastic modulus calculation has improved both accuracy and consistency of this method for further use.

7.2 Trends highlighted in dataset analysis:

The data analysis process of this study has revealed a number of significant trends, both expected and unexpected.

- The trend of increasing V_S with increasing depth for the same grade of weathered material became evident when plotting V_S versus depth for each individual weathering grade. This is due to the increasing influence of dilation nearer the surface, with a minor influence of increasing overburden pressure with depth. This highlights the requirement for depth conditions to be taken into account when assigning lithological or weathering units a representative V_S value.

- A second trend identified from this study, was the variation in the range of density values through the weathering profile. A clear non-linear trend was evident in the averaged Te Rere Hau Windfarm dry density testing results through the weathering profile. Averages and ranges of dry density values have been presented in this study for each weathering grade, with the need for further testing to be performed for a confident characterisation of the density profile.

- Poisson's ratio values were determined through the weathering profile, calculated from V_S/V_P data from downhole seismic surveying results at the West Wind Windfarm. These values were analysed for each individual weathered grade in relation to V_S. There was a linear trend evident in the average Poisson's ratio values through the weathering profile. No trend was identified between Poisson's ratio and V_S, or Poisson's ratio and depth within each weathering grade.

- The fourth trend revealed from each of the V_S profiles was the occurrence of a high velocity surface layer. The high V_S occurrence in the upper 1.5-2.0m is assumed to be a result of the stiff loess/loess-colluvium surface layer producing high V_S results at the surface. However, this trend could be a result of an insufficiently sized source-receiver offset and the recording of non-planar surface waves, although an attempt was made to avoid this when assigning acquisition parameters.

7.3 Conclusions:

Through this study, surface wave methods have been optimised and analysed to provide detailed geotechnical engineering data. This study has integrated geological, geotechnical and geophysical data to develop MASW as an engineering characterisation tool in the determination of stiffness properties, for a range of weathering grades.

In particular, MASW has proved to be especially effective in determining the influence of depth on the V_S of weathered 'greywacke', which is due to less dilation occurring with increasing confinement. This has led to a more accurate classification of seismic velocities for different lithologies and weathering grades. The identification of the relationship between depth and seismic velocities within the same weathering grade highlights the requirement for depth conditions to be taken into account when assigning characteristic V_S values to different lithologies and weathering grades in the shallow surface, along with the suitability of a range to be quoted.

These advancements have contributed to improvements in the conversion methods from shear-wave velocities to elastic moduli values. The MASW method has proven to provide a low-cost alternative to reduce and supplement the extent of the drilling schedule required during geotechnical investigations.

The method explained in this study for prediction modeling will hopefully help save both time and money for further geotechnical investigations where there is a high amount of repeated testing and large datasets gathered.

The strength of the results and methods outlined in this study are confined by the accuracy of the geophysical testing and interpretation of data. Therefore, with the increase in research and commercial use, the information available and accuracy of the method can only improve.

7.4 Recommendations for further research:

In order to gain a more complete understanding of the MASW method, and further opportunities for its application to geotechnical engineering, especially within the Esk Head Belt 'greywacke' of the Lower North Island, the writer suggests the following work be undertaken:

1. A further evaluate of the accuracy of the predictive calculation developed in this study is required for its continued use. This requires a comparison of insitu MASW determined V_S data with that calculated using the predictive equation, including inputs of depth and

weathering grade from drillhole data. This would help determine the extent to which this predictive equation lends itself to sites within the same geological setting, other than the windfarms in this study.

2. Further research is required to determine the cause of the high shear wave velocity values in the top 1.5-2.0m found across the survey sites. Initially varying the source-receiver offset from 8.0 to 14.0 metres would help identify if the high velocity surface layer is due to the recording of non-planar travelling surface waves or not.

3. Additional density testing is required from within the Esk Head belt 'greywacke' to determine with confidence the density profile through the weathering grades. Variations existed with the values determined in this study with that of existing literature from different 'greywacke' terranes. Therefore further research into density values specific to the Esk Head belt 'greywacke' are required to establish a standard range and provide valuable literature for future research.

4. A full characterisation of Poisson's ratio through the weathering profile of the Esk Head Belt greywacke would further improve the accuracy of values calculated in this study. This would require P and S-wave downhole surveying with the specific intention of calculating Poisson's ratio. This would be of benefit to further investigations within the same geological setting which require Poisson's ratio values for design and calculation inputs, and provide valuable literature for future reference.

5. Further research into the effects of different hammer sizes and plate materials, when used to create the seismic source, would be of benefit to best identify the optimum combination. When using a heavier hammer, more low frequency data is recorded, although this is at the expense of the higher frequency data which is lost, and vice versa with a lighter weighted hammer. By varying the hammer and plate it could be determined which produce the best resolution surface wave recordings within different lithologies or subsurface conditions.

6. Further research into the effects of overburden removal and the changes in the V_S profile resulting from joint dilation and removal of overburden pressures, would identify any changes in the V_S profile during construction. Sites are often surveyed prior to construction and the removal of overburden, after which the physical and mechanical properties may alter due to dilation and stress removal. This would involve performing

MASW surveys prior to overburden removal, then repeating the survey post overburden removal.

References:

Ahrens, T. J. (1995). Rock Physics and Phase Relations: A Handbook of Physical Constants. United States of America, American Geophysical Union.

Allen, M. P. (1997). Understanding Regression Analysis. New York, Plenum Press.

Anon (1970). "The logging of rock cores for engineering purposes." The Quartely Journal of Engineering Geology **3**: 1-24.

ASTM (2010). Standard Test Method for Compressive Strength and Elastic Moduli of Intact Rock Core Specimens under Varying States of Stress and Temperatures. United States of America, ASTM International. **D7012-10**.

Barton, N., Lien, R., et al. (1974). "Engineering classification of jointed rock masses for the design of tunnel support." Rock Mechanics **6**(4): 189-239.

Barton, N. (2007). Rock Quality, Seismic Velocity, Attenuation and Anisotropy. London, Taylor & Francis Group.

Begg, J. G. and Johnson, C. J. (2000). Geology of the Wellington Area, scale 1:250,000. Institute of Geological & Nuclear Siences geological map 22.

Bell, F. G. (2000). Engineering properties of soils and rocks. United Kingdom, Blackwell Science.

Belloti, R., Jamiolkowski, M., et al. (1996). "Anisotropy of small strain stiffness of ticino sand." Geotechnique **46**(1): 115-131.

Bieniawski, Z. T. (1976). Rock mass classification in rock enigneering. Proc. symp. on exploration in rock engineering, Cape Town.

Bodet, L., van Wijk, K., et al. (2005). "Surface-wave inversion limitations from laser-Doppler physical modeling." Journal of Environmental and Engineering Geophysics **10**(2): 151-162.

Bolt, B. A. (1982). Inside the Earth. San Francisco, Freeman.

Bradshaw, J. D. (1973). "Allochthonous Mesozoic fossil locailties in melange in the Torlesse Group of North Canterbury." Journal of the Royal Society of New Zealand **3**: 161-167.

Campbell, J. D. and Coombs, D. S. (1966). "Murihiku Supergroup (Triassic-Jurrassic) of Southland and South Otago." New Zealand Journal of Geology and Geophysics **9**: 393-398.

Chesworth, W. (2008). Encyclopedia of Soil Science. The Netherlands, Springer.

Christensen, N. I. (1996). "Poisson's ratio and crustal seismology." Journal of Geophysical Research **101**(B2).

Coleman, J. (2006). Turitea Wind Farm Preliminary Geotechnical Report, Beca Carter Hollings and Ferner Limited.

Cook, G. K. (2001). Rock mass structure and intact rock strength of New Zealand greywackes. Geology. Christchurch, University of Canterbury. **Master of Science**.

Crawley, M. (2007). The R Book. England, John Wiley & Sons.

D'Andrea, D., Fischer, R. L., et al. (1965). Prediction of compressive strength of rock from other properties., Rep. U.S. Bur. Mines. **Invest. No. 6702**.

Dal Moro, G., Pipan, M., et al. (2007). "Rayleigh wave dispersion curve inversion via genetic algorithms and marginal posterior porbability density estimation." Journal of Applied Geophysics **61**: 39-55.

Dearman, W. R. (1986). "State of Weathering: The Search for a Rational Approach." Geological Society, Engineering Geology Special Publication **2**: 193-198.

Deere, D. U. (1963). "Technical description of rock cores for engineering purposes." Rock Mechanics and Engineering Geology **1**: 18-22.

Donohue, S., Gavin, K., et al. (2003). G_{max} from multichannel analysis of surface waves for Dublin boulder clay. . 13th European Conference on Soil Mechanics and Foundation Engineering (ECSMGE), Prague.

Donohue, S., Long, M., et al. (2004). Use of multichannel analysis of surface waves in determining G_{max} for soft clay. Geotechnical and Geophysical Site Characterisation: 2nd International Conference (ISC-2), Porto, Porto, Millpress.

Drnevich, V. P. (1978). "Resonant Column Testing - Problems and Solutions." Dynamic Geotechnical Testing, ASTM: 384-398.

Duffy, B. G. (2008). Development of multi-channel analysis of surface waves (MASW) for characterising the internal structure of active fault zones as a predictive method of identifying the distribution of ground deformation. Geological sciences. Canterbury, University of Canterbury. **Master of Science**.

Engelder, T. and Plumb, R. (1984). "Changes in insitu ultrasonic properties of rock on strain relaxation." International Journal of Rock Mechanics and Mining Science and Geomechanics Abstracts **21**(2): 75-82.

Fookes, P. G. and Horswill, P. (1969). Discussion on engineering grade zones. Insitu Testing of Soils and Rocks, London, Institution of Civil Engineers.

Foti, S. (2005). Surface Wave Testing for Geotechnical Characterization. Surface Waves in Geomechanics: Direct and Inverse Modelling for Soils and Rocks, CISM Series, Number 481. C. G. Lai and Wilmanski, K. New York, SpringerWein.

Fumal, T. E. (1978). "Correlations between seismic wave velocities and physical properties of near-surface geologic materials in the southern San Francisco Bay region, California." U.S. Geological Survey Open-File Report **78-1067**: 114 p.

Gabriels, P., Snieder, R., et al. (1987). "In situ measurements of shear-wave velocity in sediments with higher-mode Rayleigh waves." Geophysical Prospecting **35**: 187-196.

Gadallah, M. R. and Fisher, R. (2009). Exploration Geophysics. Berlin, Springer.

Gao, K. and Gibson, R. L. (2011). "Pressure-dependent seismic velocities based on unified asperity-deformation model." society of Exploration Geophysicists Extended Abstracts **30**.

Goodman, R. E. (1980). Introduction to Rock Mechanics. United States of America, John Wiley & Sons.

Grim, R. E. (1968). Clay Mineralogy, 2nd Edition. New York, McGraw-Hill.

Hamimu, L., Nawawi, M., et al. (2011). "Utilization of multimode Love wave dispersion curve inversion for geotechnical site investigation." Journal of Geophysics and Engineering **8**: 341–350.

Hardin, B. O. and Drnevish, V. (1972). "Shear Modulus and damping in soils: Design equations and curves." Journal of Soil Mechanics and Foundations Division **98**(7): 667-692.

Harry, D. L., Koster, J. W., et al. (2005). "MASW generated during high-resolution seismic reflection profiling of a fluvial aquifer." Journal of Environmental and Engineering Geophysics **10**(2): 123-134.

Hodder, A. P. W. and R., H. J. (1991). "A quantitative study of the weathering of greywacke." Engineering Geology **31**: 353-368.

Huisman, M., Hack, H. R. G. K., et al. (2006). "Predicting Rock Mass Decay in Engineering Lifetimes: The Influence of Slope Aspect and Climate." Environmental & Engineering Geoscience **XII**(1): 29-51.

ISRM (1981). Rock characterization testing and monitoring: ISRM suggested methods, International Society on Rock Mechanics (ISRM).

Ivanov, J., Park, C. B., et al. (2000). Mapping Poisson's ratio of unconsolidated materials form a joint analysis of surface-wave and refraction events. Symposium on the Application of Geophysics to Engineering and Environmental Problems (SAGEEP 2000), Arlington, VA.

Ivanov, J., Park, C. B., et al. (2001). Modal seperation before dispersion curve extraction by MASW method. SAGEEP Denver, Colorado.

Ivanov, J., Park, C. B., et al. (2005). "Analyzing and filtering surfacewave energy by muting shot gathers." Journal of Environmental and Engineering Geophysics **10**: 307-322.

Ivanov, J., Miller, R. D., et al. (2006). "Delineating a shallow fault zone and dipping bedrock strata using multichannel analysis of surface waves with a land streamer." GEOPHYSICS **71**(5): 39-42.

Johnson, R. B. and De Graff, R. V. (1988). Principles of Engineering Geology. United States of America, John Wiley & Sons.

Karg, C. and Haegeman, W. (2005). Advances Cyclic Triaxial and Bender Element Test Equipment. Innovative Forum Geotechniek. Antwerp.

Karmis, M., Schilizzi, P., et al. (1984). The potential and application of sonic wave methods in engineering rock characterization. Rock Mechanics in Productivity and Protection. I. D. S. E. Evanston, New York: Society of Mining Engineers**:** 1083–1091.

Karray, M. and Lefebvre, G. (2008). "Significance and evaluation of Poisson's ratio in Rayleigh wave testing." Canadian Geotechnical Journal **45**: 624-635.

Kaufmann, R. D., Xia, J., et al. (2005). "Evaluation of MASW data acquired with a hydrophone streamer in a shallow marine environment." Journal of Environmental and Engineering Geophysics **10**(2): 87-98.

King, M. S., Pandit, B. I., et al. (1978). Quality of rock masses by acoustic borehole logging. 3rd IAEG Congress, , Madrid.

Kingsbury, P. A. (1987). Engineering geology investigations, Havelock Area, Marlborough. Geological Sciences. Christchurch, University of Canterbury. **Master of Science**.

Kleffmann, S., Davey, F., et al. (1998). "Crustal structure in the central South Island, New Zealand, from Lake Pukaki seismic experiment." New Zealand Journal of Geology and Geophysics **41**: 39-49.

Kramer, S. (1996). Geotechnical Earthquake Engineering. New Jersey, Prentice Hall.

Lamb, S. H. and Vella, P. (1987). "The last million years of deformation in part of the New Zealand plate-bounday zone." Journal of Structural Geology **9**(7): 877-891.

Langridge, R., Van Dissen, R., et al. (2011). "Five thousand years of surface ruptures on the Wellington Fault, New Zealand: Implications for reoccurance and fault segmentation." Bulliten of the Seismological Society of America **101**(5): 2088-2107.

Lee, J. M. and Begg, J. G. (2002). Geology of the Wairarapa Area. . Lower Hutt, New Zealand, Institute of Geological and Nuclear Sciences, 1:250,000, Geological Map 11.

Long, M. and Donohue, S. (2007). "In Situ Shear Wave Velocity from Multichannel Analysis of Surface Waves (MASW) Tests at Eight Norwegian Research Sites. ." Canadian Geotechnical Journal **44**: 533-544.

Lowrie, W. (2002). Fundamentals of Geophysics. United Kingdom, Cambridge University Press.

Luna, R. and Jadi, H. (2000). Determination of dynamic soil properties using geophysical methods. First International Conference on the Application of Geophysical and NDT Methodologies to Transportation Facilities and Infrastructure, St. Louis, MO.

Luo, Y., Xia, J., et al. (2010). "Finite-difference modeling and dispersion analysis of high-frequency Love waves for near-surface applications." Pure Applied Geophysics **167**(1525-1536).

Mahoney, D. (2008). MASW profiling to obtain elastic moduli models for wind turbine foundation design - Te Rere Hau Windfarm. 8th Young Geotechnical Professionals Conference. Wellington, New Zealand.

Mahoney, D. (2010). Stage 4 - Preliminary Elastic Modulus Modeling for Turbine Foundations, Te Rere Hau Eastern Extension, NZ Windfarms Ltd. Christchurch, New Zealand, Aurecon NZ Limited.

Mahoney, D. and Kupec, J. (2010). "Determining the stiffness of weathered greywacke." IAEG Auckland, New Zealand, September 2010.

Marshall, T. W. (1974). A petrographic investigation of greywacke type aggregates from the Auckland region Geology Dept. Auckland, University of Auckland. **Unpub. M.Sc (hons) thesis:** 125.

Martin, G. R. and Miller, P. J. (1974). Joint strength characteristics of a weathered rock. 3rd International Congress on Rock Mechanics, ISRM, Denver.

Mason, D. (2006). PROJECT WEST WIND GEOTECHNICAL INVESTIGATIONS Stage 2: Site Investigation Report, Opus International Consultants Limited.

Meglis, I. L., Greenfield, R. J., et al. (1996). "Pressure dependence of velocity and attenuation and its relationship to crack closure in crystalline rocks." Journal of Geophysical Research **101**(B8): 17,523-517,533.

Miller, R. D., Xia, J., et al. (1999). "Using MASW to map bedrock in Olathe, Kansas [Exp. Abs.]." Society of Exploration Geophysicists **1**: 433–436.

Mukerji, T., Mavko, G., et al. (1995). "Scale-dependent seismic velocity in heterogeneous media." GEOPHYSICS **60**(4).

Nazarian, S. (1984). In situ determination of elastic moduli of soil deposits and pavement systems by spectral-analysis-of-surface-waves method. Austin, University of Texas. **Doctor of Philosophy**.

NZGS (1968). Report of subcommittee on Greywacke Terminology. **No. 26**.

Park, C. B., Miller, R. D., et al. (1997). Multi-Channel Analysis of Surface Waves (MASW) "A summary report of technical aspects, experimental results, and perspective", Kansas Geological Survey.

Park, C. B., Miller, R. D., et al. (1999). Optimum field parameters. Ext. Abstract, Society of Exploration Geophysicists of Japan. Tokyo.

Park, C. B., Miller, R. D., et al. (1999). "Higher mode observation by the MASW method [Ext. Abs.]." Society of Exploration Geophysicists: 524-527.

Park, C. B., Miller, R. D., et al. (1999). "Multichannel Analysis of Surface Waves." GEOPHYSICS **16**: 800-808.

Park, C. B. and Miller, R. D. (2004). MASW to Map Shear-Wave Velocity of Soil. Lawrence, Kansas, Kansas Geological Survey. **Open-file Report 2004-30**.

Park, C. B. and Miller, R. D. (2005). Seismic Characterization of Wind Turbine Sites in Kansas by the MASW Method. KGS Open-file Report 2005-23, Barr Engineering Company.

Park, C. B. and Miller, R. D. (2005). Seismic Characterisation of Wind Turbine Sites Near Lawton, Oklahoma, by the MASW Method. Kansas Geological urvey Open-File Report 2005-22.

ParkSeismic. "Data Acquisition Parameters for Active MASW Survey." Retrieved 18 February, 2011, from www.masw.com.

Pender, M. J. (1971). Some properties of weathered greywacke. 1st Australia New Zealand Geomechanics Conference, Melbourne.

Powrie, W. (2004). Soil Mechanics. 2nd Editon. New York, Spon Press.

Rahman, M. and Michelitsch, T. (2006). "A note on the formula for the Rayleigh wave speed." Wave Motion **43**: 272-276.

Raisbeck, D. (1973). "Strength parameters for weathered sandstone." New Zealand Engineering **28**(9): 254-260.

Read, S. A. L., Richards, L. R., et al. (1999). Applicability of the Hoek-Brown failure criterion to New Zealand greywacke rocks. 9th ISRM International Congress on Rock Mechanics. Paris**:** 655-660.

Read, S. A. L., Richards, L. R., et al. (2000). Assessment of New Zealand greywacke rock masses with the Hoek-Brown failure criterion. International Conference on Geotechnical & Geological Engineering "GeoEng2000", Melbourne, Australia, Lancaster: Technomic Publishing Company.

Read, S. A. L., Richards, L. R., et al. (2000). Assessment of New Zealand greywacke rock masses with the Hoek Brown failure criterion. Proceedings GeoEng2000 International Conference on Geotechnical and Geological Engineering Melbourne, Rotterdam: Balkema.

Read, S. A. L. and Richards, L. R. (2007). Characteristics and classification of New Zealand greywackes. Rock mechanics: meeting society's challenges and demands. Proceedings of the 1st Canada-US Rock Mechanics Symposium, Vancouver, Canada.

Reilly, W. I. (1972). "New Zealand gravity map series." New Zealand Journal of Geology and Geophysics **15**: 3-15.

Richards, L. R. and Read, S. A. L. (2007). New Zealand greywacke characteristics and influences on rock mass behaviour. 11th congress of the International society for rock mechanics: the second half century of rock mechanics L. R. Sousa, Olalla, C. and Grossmann, N. London, Taylor & Francis Ltd. **2:** 359-364.

Richart, F. E., Hall, J. R., et al. (1970). Vibrations of soils and foundations. New Jersey, Prentice Hall.

Rocha, M., DaSilveira, A., et al. (1966). Determination of the deformability of rock along a borehole. Proceedings of the 1st ISRM Congress, Lisbon.

Rosenblad, B. L. and Cheng-Hsuan, L. (2011). Influence of Poisson's Ratio on Surface Wave Near-Field Effects. Geo-Frontiers 2011: Advances in Geotechnical Engineering, ASCE.

Rowe, G. H. (1979). A method for assessing degradation in New Zealand greywackes, NZ Roading Symp.**:** 1-14.

Rowe, G. H. (1980). Applied Geology for Wellington rocks for aggregate and concrete. Department of Geology. Wellington, Victoria University of Wellington. **Unpublished PhD Thesis**.

Rowe, R. K. (1982). "The determination of rock mass modulus variation with depth for weathered or jointed rock." Canadian Geotechnical Journal **19**(1): 29-43.

Safani, J., O'Neill, A., et al. (2005). "Application of Love wave dispersion for improved shear wave velocity imaging." Journal of Environmental and Engineering Geophysics **10**: 135-150.

Saunders, M. K. and Fookes, P. G. (1970). "A review of the relationship of Rock Weathering and Climate and its significance to Foundation Engineering." Engineering Geology **4**(4): 289-325.

Schneider, J. A., Hoyos, L. J., et al. (1999). Field and laboratory measurements of dynamic shear moduluc of Piedmont residual soils. Behavioral Characteristics of Residual Soils, GSP 92, ASCE. Reston, VA**:** 12-25.

Schroeder, L. D., Sjoquist, D. L., et al. (1986). Understanding Regression Analysis, An Introductory Guide. United States of America, SAGE Publications.

Silberling, N. J., Nichols, K. M., et al. (1988). "Limestone and chert in tectonic blocks from Esk Head subterrane, South Island, New Zealand." Geological Society of America bulletin **100**: 1213-1223.

Simons, N., Menzies, B. K., et al. (2002). A Short Course In Geotechnical Site Investigation. Great Britain, Thomas Telford Limited.

Sjøgren, B., Øfsthus, A., et al. (1979). "Seismic classification of rock mass qualities." Geophysical Prospecting **27**: 409–442.

Sjøgren, B. (1984). Shallow Refraction Seismics. London, Chapman & Hall.

Sparks, B. W. (1960). Geomorphology. London, Longmans.

Standards New Zealand (1986). "Immersion in Water Method." Determination of the Density of Soil. NZS 4402 : 1986 Test 5.1.4.

Steel, R. G. D. and Torrie, J. H. (1960). Principles and Procedures in Statistics. New York, McGraw Hill.

Stewart, S. (2007). Rock Mass Strength and Deformability of Unweathered Closely Jointed New Zealand Greywacke. Civil Engineering. Christchurch, New Zealand, University of Canterbury. **Doctor of Philosophy**.

Stokoe, K. H., Lee, S. H., et al. (1985). Shear moduli measurements under true triaxial stresses. Advances in the art of testing soils under cyclic conditions, ASCE. New York**:** 166-185.

Stokoe, K. H., Wright, G. S., et al. (1994). Characterization of geotechincal sites by SASW method, in Geophysical characterization of sites. ISSMFE Technical Committee #10. R. D. Woods. New Delhi.

Stokoe, K. H., Darendeli, M. B., et al. (1999). Dynamic Soil Properties: Laboratory, Field and Correlation Studies. Themed Lecture, Second International Conference Earthquake Geotechnical Engineering. Lisbon, Portugal. **3:** 811-845.

Suggate, R. P., Stevens, G. R., et al. (1978). The Geology of New Zealand. Wellington, Government Printer.

Thuro, K. and Scholz, M. (2003). Deep Weathering and Alteration in Granites - A Product of Coupled Processes. International Conference on Coupled T-H-M-C Processes in Geosystems: Fundamentals, Modeling, Experiments and Applications. Sweden, Royal Institute of Technology. **1:** 1-6.

Turk, N. and Dearman, W. R. (1986). A suggested approach to rock characterization in terms of seismic velocities. 27th US Symposium on Rock Mechanics. A. H. (Ed.). Tuscaloosa, Society for Mining, Metallurgy and Exploration (SME)**:** 168–175.

Walcott, R. I. (1987). "Geodetic strain and the deformational history of the North Island of New Zealand during the Late Cainozoic." Philosophical Transactions of the Royal Society of London **321**: 163-181.

Wellman, H. W. (1949). "Pillow Lava at Red Rock Point, Wellington." Transactions of the Royal Society of New Zealand **77**(2): 306-312.

Williams, P. W. (1991). "Tectonic geomorphology, uplift rates and geomorphic response in New Zealand." CATENA **18**: 439-452.

Wyllie, D. C. (1992). Foundations on Rock. London, Chapman & Hall.

Xia, J., Miller, R. D., et al. (1999). "Estimation of near-surface shear-wave velocity by inversion of Rayleigh waves." GEOPHYSICS **64**(3): 691-700.

Xia, J., Nyquist, J. E., et al. (2007). "Feasibility of detecting near-surface feature with Rayleigh-wave diffraction." Journal of Applied Geophysics **62**: 244–253.

Xu, C. and Butt, S. D. (2006). "Evaluation of MASW techniques to image steeply dipping cavities in laterally inhomogeneous terrain." Journal of Applied Geophysics **59**: 106– 116.

Zavoral, D. Z. and Campanella, R. G. (1994). Frequency Effects of Damping/Modulus of Cohesive Soil. Dynamic Geotechnical Testing II, ASTM STP 1213. Philadelphia, ASTM**:** 191-201.

Appendix A:

Multichannel Analysis of Surface Waves (MASW) Literature Review

A-1.1 Introduction:

Multichannel Analysis of Surface Waves (MASW) is a seismic exploration method evaluating ground stiffness in 1-D, 2-D, and 3-D formats for various types of geotechnical engineering projects. Since its first introduction in the late 1990s, it has been utilized by many practitioners and researched by many investigators worldwide.

First introduced in the mid 1990's, multichannel analysis of surface waves (MASW) is one of the seismic survey methods evaluating the elastic condition (stiffness) of the ground, often for geotechnical engineering purposes. MASW uses high frequency surface-waves to provide a reliable indication of S-wave velocities in a range of geological settings. MASW first measures seismic surface waves generated from various types of seismic sources (ie. sledge hammer), analyses the propagation velocities of those surface waves, and then finally deduces shear-wave velocity (Vs) variations below the surveyed area that is under investigation. This process is broken down into three main stages:

1. Rayleigh-wave data acquisition,
2. Dispersion curve extraction, and
3. Surface-wave inversion.

Two-thirds of the total seismic energy generated in a seismic survey from a compressional wave source is imparted into Rayleigh waves (Richart et al, 1970), which is the principle component of ground roll. Assuming vertical velocity variation, each frequency component of a surface wave has a different propagation velocity, called the phase velocity (C_f), at each unique frequency (f) component, which has unique characteristic results in a different wavelength for each frequency propagated (Park et al, 1999). This is called dispersion. Generally, ground roll is considered noise on body-wave surveys such as reflection and refraction profiling, but its dispersive properties can be used to infer near-surface elastic properties (Stokoe et al, 1994). By using the dispersive properties of surface waves, a shear-wave velocity (V_s) profile can be constructed by analysis of plane-wave, fundamental-mode Rayleigh waves. These properties of the near surface shear wave velocity (V_s) are commonly used to evaluate near-surface stiffness for geotechnical studies, and are also able to provide information about statics during body wave data processing.

Shear-wave velocity (V_s) is one of the elastic constants and is closely related to Young's modulus. Under most circumstances, V_s is a direct indicator of the ground strength (stiffness) and therefore commonly used to derive load-bearing capacity. After a relatively simple procedure, final V_s information is provided in 1-D, 2-D, and 3-D formats.

A-1.2 Development of MASW:

Historically, most surface wave applications have followed three (3) fundamental steps: Acquisition, Dispersion Analysis and Seeking the layered-earth model (V_s, V_p, h, r, etc.). The main topics of development in recent history have been field procedures (data acquisition) and data processing (dispersion and inversion analyses).

A method used to generate near-surface V_s profiles from wave-propagation was introduced by Nazarian et al (1983), called Spectral Analysis of Surface Waves (SASW), which is considered to be MASW's small-scale predecessor.

The SASW method uses only two receivers for one survey to record propagated surface waves that are generally generated by impact sources such as a sledge hammer. Due to the use of only two receivers, the test needs to be repeated with many different field set ups consisting of different source and receiver spacings, to cover different depths of investigation. Data are analysed in the frequency domain to produce a dispersion curve by calculating the phase difference between each deployment of receiver pairs.

Consequently, the method is time consuming and labour intensive. Furthermore, possible contamination of recorded data is common by the inclusion of body waves (direct, refracted and reflected P-waves) and also by the inclusion of higher modes of surface waves is difficult to detect. The noise incurred during SASW measurements can be controlled by using a set of empirical criteria tailored to suit each investigation site (Stokoe et al, 1994). Determining the optimal criteria is often difficult due to the variation in near-surface materials and their characteristic properties. Further difficulties exist when evaluating and distinguishing signal from noise with only one pair of receivers, therefore the necessity of recording repeated shots into multiple field deployments for a given site increases the manual labour requirements for the survey.

Developed from the SASW method to multichannel analysis of surface waves (MASW) has overcome the few weaknesses associated with the SASW method. Unlike SASW, which is a two-receiver approach, MASW adopted the multichannel concept long used in the history of seismic exploration for natural resources. Hence this method removes the highly labour intensive and time consuming requirements of the SASW method.

In the early 2000s, the MASW method came into popular use among geotechnical engineers. The first documented multichannel approach for surface-wave analysis goes back to the 1980s when investigators in Netherlands used a 24-channel acquisition system to deduce shear-wave velocity structure of tidal flats by analysing recorded surface waves (Gabriels et al, 1987). It

first showed the scientific validity of the multichannel approach in surface wave dispersion analysis and its validity to be used as a routine approach in the future. Then, using uncorrelated vibroseis data, Park et al (1999) highlighted the effectiveness of the approach by detailing advantages with multichannel acquisition and processing concepts most appropriate for the geotechnical engineering applications. A subsequent boom in surface wave applications using the MASW method for various types of geotechnical engineering projects has been observed worldwide since that time.

Further progressions in the use of surface waves involve passive surface wave methods. As the surface-wave method gained in credibility and more diverse applications were attempted and demand for a deeper investigation grew, developers began to utilise surface waves passively generated by natural and cultural activities (Louie, 2001).

Whether a survey is active or passive depends on the ability to control three characteristics of the seismic source:

1. Excitation time,
2. Location (azimuth and distance) relative to the receiver array, and;
3. Impact power.

When these are all strictly controlled, then it is an active survey; otherwise, it is a passive survey.

In specific cases, a passive survey can have partial control when one or more of the characteristics are known to a certain extent. A roadside passive survey is such an example because the type of impact (ie. moving cars) and incoming angle (azimuth) of surface waves are roughly known. Passive MASW surveys are discussed in further detail in Section A-1.5.

A-1.3 Rayleigh Waves:

Surface waves are guided and dispersive. Rayleigh waves are surface waves that travel along a free surface, such as the earth-air interface. Particle motion of the fundamental mode of Rayleigh waves moving from left to right is elliptical in a counter-clockwise direction (Xia et al, 1999).

Rayleigh waves are the principal component of ground roll, and account for up to 70% of the energy in a seismic survey (Park et al, 1999). Ground roll is a particular type of Rayleigh wave that travels along or near the ground surface and is usually characterised by relatively low

velocity, low frequency and high amplitude. The depth of penetration of a Rayleigh-wave depends directly on its wavelength, with the longer wavelengths penetrating deeper (Duffy, 2008). These long wavelength waves are thus more controlled by the elastic properties of the deeper layers and exhibit higher phase velocities. On the other hand, short wavelength waves reflect the elastic properties closer to the surface and travel more slowly. Shorter wavelengths are also sensitive to the physical properties of surficial layers. This property of wavelength dependent velocity is known as signal dispersion and is controlled in varying degrees by S-wave velocity, layer thickness, P-wave velocity and density (Xia et al, 1999).

Rayleigh waves propagate as different modes, a mode being a packet of acoustic energy that propagates in one direction whilst confined in the other two directions. In the case of Rayleigh waves they are confined to the air/earth interface. Different modes of Rayleigh waves have different motions relative to the travel direction and therefore different propagation velocities at a given frequency (Duffy, 2008). Of these modes, fundamental mode Rayleigh waves (counter-clockwise motion) are the slowest and so appear closest to the origin in a frequency versus velocity (dispersion) plot.

A-1.4 Active source MASW:

A-1.4.1 Summary of active MASW surveying:

The common procedure for (1-D, 2-D, and 3-D) MASW surveys consist of three steps:

1. Data Acquisition---acquiring multichannel field records (commonly called shot gathers)
2. Dispersion Analysis---extracting dispersion curves (one from each record)
3. Inversion---back-calculating shear-wave velocity (V_s) variation with depth (called 1-D V_s profile) that gives theoretical dispersion curves closest to the extracted curves (one 1-D V_s profile from each curve).

A 2-D (surface and depth) V_s map is then constructed through an appropriate interpolation scheme by placing each 1-D V_s profile at a surface location corresponding to the middle of the receiver line.

A-1.4.2 Data acquisition:

The active survey is the most common type of MASW survey that can produce a 2-D V_s profile. The overall setup is illustrated in Figure 2 below. The field procedure for passive MASW is different and explained under Passive MASW section 5.0.

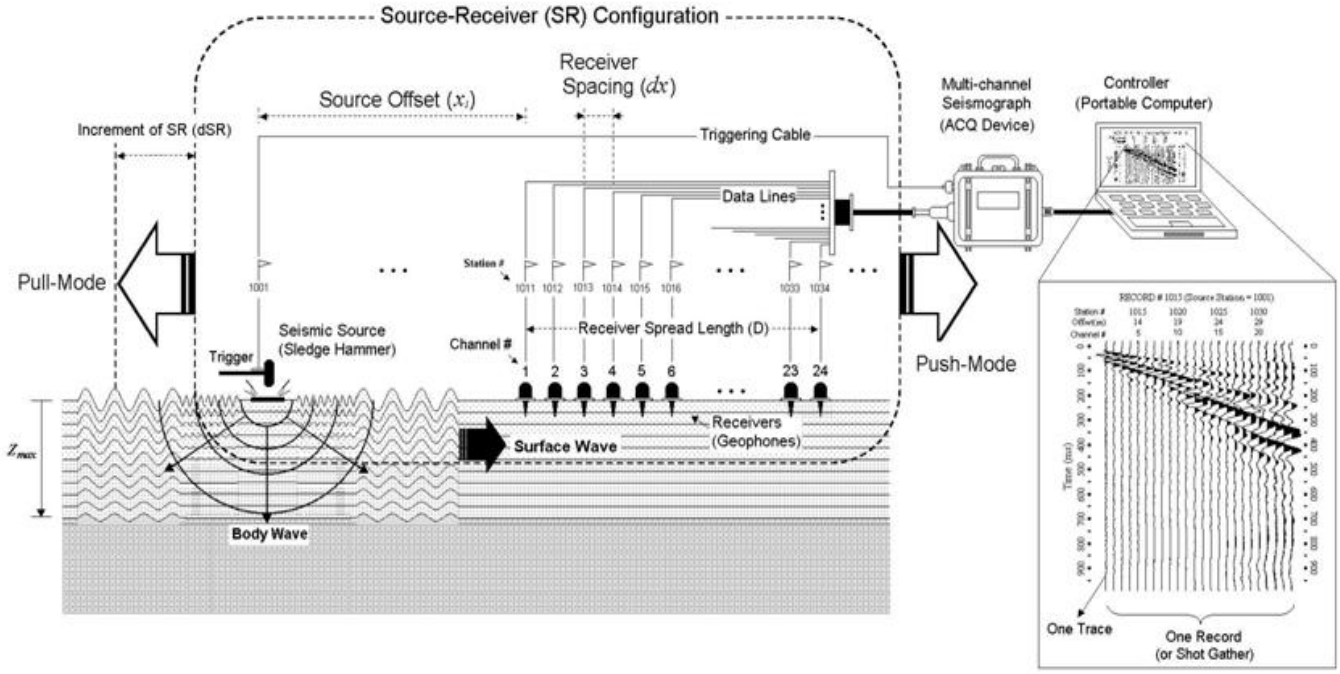

Figure 1: Schematic of the active MASW field survey.

The maximum depth of investigation (Z_{max}) that can be achieved from the survey is usually in the 10-30 m range, but this can vary at each site and is dependent on the type of active sources used. Field procedures and data processing steps are briefly explained in Park et al. (1999). Surface waves are best generated over a 'flat' ground within at least one receiver-spread length (D) shown by Figure 3. If this is the case, then overall topographic variation within an entire survey line should not be critical.

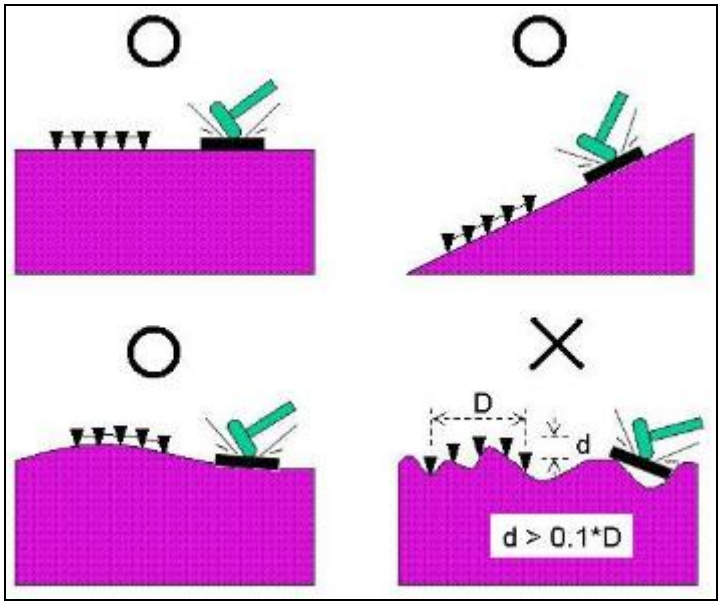

Figure 2: Typical terrain conditions favourable and unfavourable for the MASW survey.

However, any surface relief whose dimension is greater than approximately 10% of D will cause a significant hindrance to surface wave generation.

The following table describes most of the parameters related to data acquisition. A slight variation in any parameter can always be expected. A summary of optimum acquisition parameters for active MASW specifically for soil sites, according to Park et al (2002) are shown by Table 1.

Receiver (Hz)	Max. Depth (m)	Minimum Offset (m)	Maximum Offset (m)	Receiver Spacing (m)
4.5	50	10	100	1
10	30	10	100	1
40	15	10	100	1

Table 1: Optimum field parameters for MASW surveys for most common soil sites. A seismic source of 10-lb or heavier sledgehammer and use of recording instrument with 24-bit or higher dynamic range are both assumed. No low-cut analog filter should be used during the acquisition (Park et al, 2002).

They have been, however, continuously updated by investigators and practitioners, and those most-recently used are listed in Table 2.

Recommended Values in ()

Depth (Z_{max})[1] (ft)	Source (S)[2] (lb)	Receiver (R)[3] (Hz)	Receiver Spread (RS) (ft)				SR Move[6] (dx)			Recording[8]				
			Length[4] (D)	Source Offset[5] (X_1)	Receiver Spacing (dx)		Lateral Resolution[7]			dt[9] (ms)	T[10] (sec)	Vertical Stack[11]		
					24-ch*	48-ch	High	Medium	Low			C	N	VN
≤ 5.0	≤ 1	4.5–100	5–15	1–15	0.2–0.6	0.1–0.3	1–2	2–4	4–12	0.5–1.0	0.5–1.0	1–3	3–5	5–10
	(1)**	(40)	(10)	(2)	(0.3)	(0.2)	(1)	(2)	(4)	(0.5)	(0.5)	(3)	(5)	(10)
5–15	1–5	4.5–40	5–45	1–9	0.2–2.0	0.1–1.0	1–2	2–4	4–12	0.5–1.0	0.5–1.0	1–3	3–5	5–10
	(5)	(10)	(30)	(5)	(1.0)	(0.5)	(1)	(2)	(4)	(0.5)	(0.5)	(3)	(5)	(10)
15–30	5–10	≤ 10	15–90	3–18	0.5–4.0	0.2–2.0	1–2	2–4	4–12	0.5–1.0	0.5–1.0	1–3	3–5	5–10
	(10)	(4.5)	(50)	(10)	(2.0)	(1.0)	(1)	(2)	(4)	(0.5)	(1.0)	(3)	(5)	(10)
30–60	≥ 10	≤ 10	30–180	6–36	1.0–8.0	0.5–4.0	1–2	2–4	4–12	0.5–1.0	1.0–2.0	1–3	3–5	5–10
	(20)	(4.5)	(120)	(30)	(4.0)	(2.0)	(1)	(2)	(4)	(0.5)	(1.0)	(3)	(5)	(10)
60–100	≥ 10	≤ 4.5	60–300	12–60	2–12	1–6	1–2	2–4	4–12	0.5–1.0	1.0–2.0	1–3	3–5	5–10
	(20)	(4.5)	(200)	(40)	(8)	(4)	(1)	(2)	(4)	(1.0)	(1.0)	(3)	(5)	(10)
100–150	≥ 10 (20)	≤ 4.5	100–450	20–90	4–18	2–9	1–2	2–4	4–12	0.5–1.0	1.0–3.0	1–3	3–5	5–10
	or passive	(4.5)	(300)	(60)	(12)	(6)	(1)	(2)	(4)	(1.0)	(1.0))	(3)	(5)	(10)
> 150	≥ 10 (20)	≤ 4.5	> 150	> 30	> 6.0	> 3.0	1–2	2–4	4–12	0.5–1.0	≥ 1.0	1–3	3–5	5–10
	or passive	(4.5)	(450)	(100)	(20)	(10)	(1)	(2)	(4)	(1.0)	(2.0)	(3)	(5)	(10)

++***Values listed here are by no means definitive and required. There can always be a tolerance of, at least, ±20% to the most recommended values.***

[1]maximum depth to be investigated, [2]weight of hammer in pounds, [3]natural frequency of geophone, [4]approximate total length of receiver spread ($D \approx mZ_{max}$ with $1 \le m \le 3$), [5]distance between source and the closest receiver ($X_1 \approx \kappa D$ with $0.2 \le \kappa \le 1.0$), [6]distance in receiver spacing (dx) that the source (S) and receiver (R) setup moves after acquiring data at one location, [7]degree of lateral resolution being sought, [8]recording parameters for seismograph, [9]sampling interval in milliseconds (ms), [10]total recording time in seconds (sec), [11]number of stacking data in seismograph's memory before being saved under different conditions of calm (C), noisy (**N**), and very noisy (**VN**) environment, respectively, [12]acquisition filter (e.g., low-cut, high-cut, etc.), *24-channel acquisition system.

Recommended Values in ()

Depth (Z_{max})[1] (m)	Source (S)[2] (lb)	Receiver (R)[3] (Hz)	Receiver Spread (RS) (m)				SR Move[6] (dx)			Recording[8]				
			Length[4] (D)	Source Offset[5] (X_1)	Receiver Spacing (dx)		Lateral Resolution[7]			dt[9] (ms)	T[10] (sec)	Vertical Stack[11]		
					24-ch*	48-ch	High	Medium	Low			C	N	VN
≤ 1.0	≤ 1	4.5–100	1–3	0.2–3.0	0.05–0.1	0.02–0.05	1–2	2–4	4–12	0.5–1.0	0.5–1.0	1–3	3–5	5–10
	(1)**	(40)	(2.0)	(0.4)	(0.1)	(0.05)	(1)	(2)	(4)	(0.5)	(0.5)	(3)	(5)	(10)
1–5	1–5	4.5–40	1–15	0.2–15	0.05–0.6	0.02–0.3	1–2	2–4	4–12	0.5–1.0	0.5–1.0	1–3	3–5	5–10
	(5)	(10)	(10)	(2)	(0.5)	(0.25)	(1)	(2)	(4)	(0.5)	(0.5)	(3)	(5)	(10)
5–10	5–10	≤ 10	5–30	1–30	0.2–1.2	0.1–0.6	1–2	2–4	4–12	0.5–1.0	0.5–1.0	1–3	3–5	5–10
	(10)	(4.5)	(20)	(4)	(1.0)	(0.5)	(1)	(2)	(4)	(0.5)	(1.0)	(3)	(5)	(10)
10–20	≥ 10	≤ 10	10–60	2–60	0.4–2.5	0.2–1.2	1–2	2–4	4–12	0.5–1.0	1.0–2.0	1–3	3–5	5–10
	(20)	(4.5)	(30)	(10)	(1.5)	(1.0)	(1)	(2)	(4)	(0.5)	(1.0)	(3)	(5)	(10)
20–30	≥ 10	≤ 4.5	20–90	4–90	0.8–3.8	0.4–1.9	1–2	2–4	4–12	0.5–1.0	1.0–2.0	1–3	3–5	5–10
	(20)	(4.5)	(50)	(10)	(2.0)	(1.5)	(1)	(2)	(4)	(1.0)	(1.0)	(3)	(5)	(10)
30–50	≥ 10 (20)	≤ 4.5	30–150	6–150	1.2–6.0	0.6–3.0	1–2	2–4	4–12	0.5–1.0	1.0–3.0	1–3	3–5	5–10
	or passive	(4.5)	(70)	(15)	(3.0)	(2.0)	(1)	(2)	(4)	(1.0)	(1.0)	(3)	(5)	(10)
> 50	≥ 10 (20)	≤ 4.5	> 50	> 10	> 2.0	> 1.0	1–2	2–4	4–12	0.5–1.0	≥ 1.0	1–3	3–5	5–10
	or passive	(4.5)	(150)	(30)	(6.0)	(4.0)	(1)	(2)	(4)	(1.0)	(2.0)	(3)	(5)	(10)

Table 2: Optimum parameters related to data acquisition for active MASW surveys, which have been continuously updated by investigators and practitioners (Park Seismic).

Source:

Maximum investigation depth (Z_{max}) will be determined by the longest wavelength (λ_{max}) of surface waves used for the analysis as $Z_{max} \approx 0.5\ \lambda_{max}$. The maximum wavelength is then governed by the impact power of the seismic source, which can be a controlled type like a sledge hammer in an active survey (or a car moving over a road bump in the case of roadside passive survey). In general, a longer λ_{max} (therefore, a deeper Z_{max}) is achieved with a greater impact power.

A fairly heavy sledge hammer (e.g., 10 kg) is a good choice, although other more-sophisticated sources that can deliver more impact power into ground (e.g., a weight drop) can be an advantage over a sledge hammer because of its potential to generate lower frequencies, and longer wavelengths of surface waves (Park et al, 2002). The gain from using these other sources is often not enough to warrant the cost of the equipment and inconvenience in field operation unless they are carefully designed and built. For example, a mere increase of impact power not accompanied by a careful consideration of energy coupling mechanism many not achieve the goal. Using an impact plate will help the source impact point intrude less into soil. Refer to Table 2 for optimum source for different investigation depth.

Vertical stacking of multiple impacts can suppress ambient noise significantly and is therefore always recommended, especially if the survey takes place in an urban area. The optimum number of stacking impacts can be determined when there is little change in signal-to-noise ratio (S/N) in the displayed seismic record during the stacking. 3-5 vertical stacks are often used. This number, however, should increase as the ambient noise level increases and/or total receiver array length (D) increases.

Receivers:

Vertical phones must be used. Low-frequency geophones (e.g., 4.5 Hz) are generally used, and also provide the greatest depth of investigation (Park et al, 2002). The high end of geophone frequency is not as critical as in the reflection survey where any minor drop in sensitivity may become critical. For instance, recording and analysis of surface waves up to 450 Hz have been reported by using 4.5-Hz geophones (Miller et al., 2000). Effectiveness of somewhat higher-frequency phones (e.g., 10-20 Hz), however, is often comparable to that of much lower-frequency phones. Although spike-coupled geophones always give the highest sensitivity, the coupling provided by a land streamer can be equally efficient and is a significant convenience in field operation (Figure 4). In fact, using a land streamer can speed data acquisition by orders of

magnitude; nowadays, it is becoming one of the routine field apparatus, often operated with a small field vehicle.

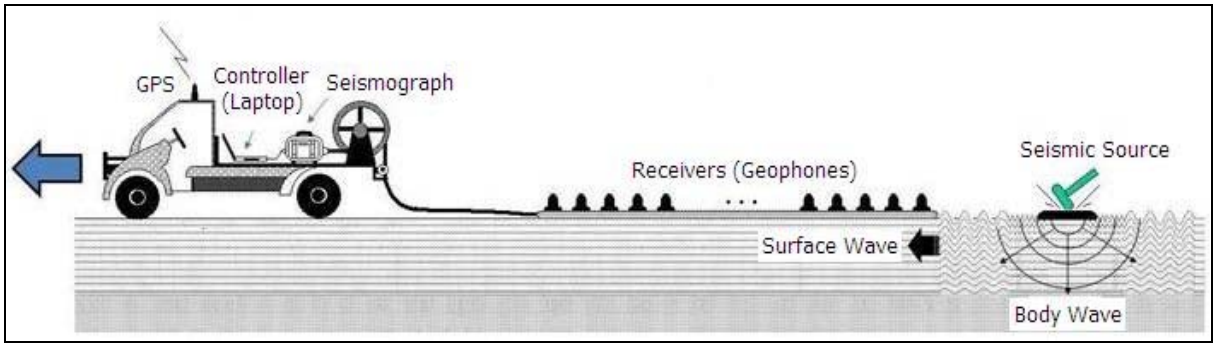

Figure 3: Schematic illustration of receivers on a land streamer (Park Seismic).

Field Geometry:

On-site survey preparation should begin with a full wavefield survey and swept frequency analysis to determine the optimal placement of the array in the wavefield. The near offset x_1 (Figure 5) is a critical parameter as it determines the position of the receiver array in the wavefield and therefore the impact of near or far field effects. Near field effects are caused by cylindrical rather than planar propagation of Rayleigh-waves proximal to the source (Figure 6) and lead to lack of energy and linear coherence in the lower frequency component of a record.

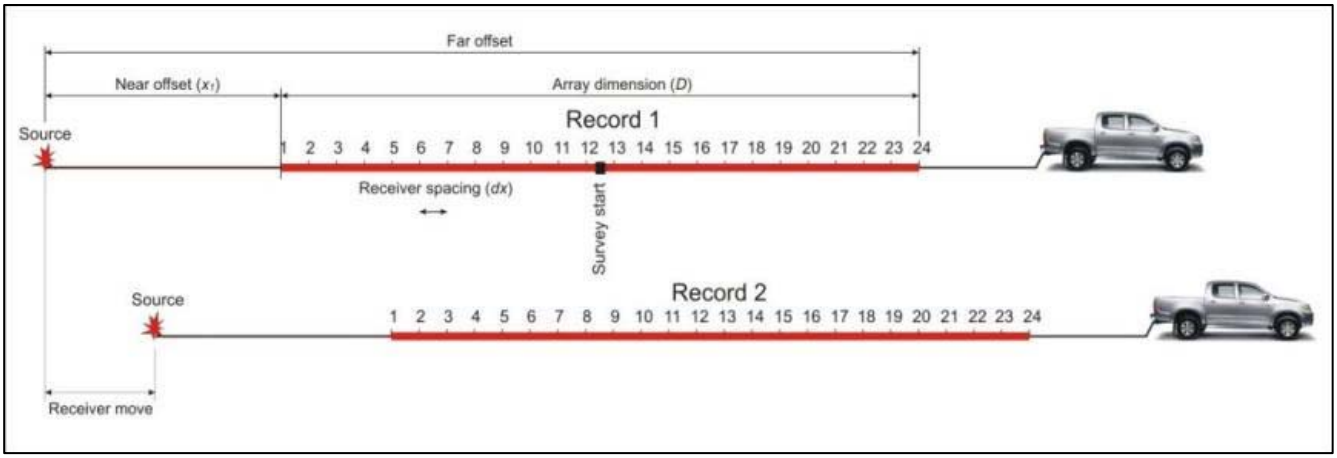

Figure 4: MASW survey geometry using a land streamer. Key acquisition parameters are illustrated and selection of these is discussed in the text (Duffy, 2008).

The longer a wavelength, the further it must travel before becoming planar. The reliable investigation depth is approximately given by $z_{max} = C1 / (2\ f1) = ½\ \lambda_{max}$ where C1 is phase velocity for the lowest frequency analyzed (f_1) and λ_{max} is the maximum wavelength recorded (Rix & Leipski, 1991). Far field effects are caused by contamination of the record due to

attenuation of the higher frequency fundamental mode waves at far offsets (Park et al., 1999). At excessive offsets higher mode surface waves dominate over fundamental mode surface waves and this typically limits the array dimension D (Figure 5). The uppermost frequency reliably imaged is usually given by the velocity and frequency of the highest uncontaminated frequency recorded (f_{max}) (Stokoe et al., 1994) such that:

$$H1 \geq 0.5\lambda_{min} = 0.5Cmin / f_{max}$$

where C_{min} and λ_{min} are phase velocity and wavelength, respectively, which correspond to a particular f_{max}. Although the final inverted S-wave velocity profile may have shallow layers thinner than H_1, any calculated S-wave velocity value for these layers should be considered unreliable.

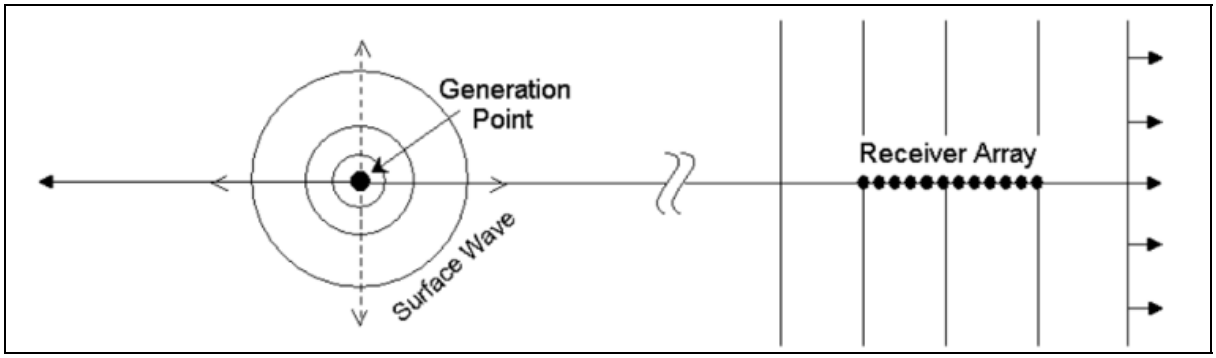

Figure 5: Rayleigh wave propagation away from a generation point. Near to the source the wavefront is cylindrical, whilst further away it becomes planar (Park & Millar, 2006).

By convolving a full wavefield shot gather with a sweeping linear stretch function (Park et al., 1999) and examining the swept frequency record, a near offset can be selected that minimizes near and far field effects over a useful range of wavelengths. As the reliable investigation depth is approximately ½ λ_{max}, optimizing the near offset maximizes the investigation depth.

The source offset (x_1) controls the degree of contamination by the near-field effects that indicate a congregate of all adverse influences (for example, not-fully developed surface waves) on data acquisition because of the source being too close to the receivers. Its optimum value has been a subject of debate. A value of about 20% of D (e.g., x_1=5 m when D=25 m) is suggested as a minimum and 100% as a maximum. A large x_1 value (e.g., > 100 %) and a large D (e.g., > 100 m) will increase the risk of higher-mode domination and reduce the signal to noise ratio for the fundamental mode.

If a MASW receiver spread is too short, the resulting dispersion curve is an apparent dispersion, which may not be purely fundamental mode. A long array dimension D (Figure 5) is therefore

necessary to obtain fundamental mode dispersion. The length required may be even greater at sites where the S-wave velocity does not vary linearly with depth.

Recording Parameters:

A one millisecond of sampling interval (dt=1 ms) is most commonly used with a one second total recording time (T=1 sec). In the case of extremely low velocities (e.g., Vs < 100 m/sec), a longer T (e.g., 2 sec) will be a better choice. A longer T (e.g., 2 sec) is also the preferred option if a long receiver spread (D) (e.g., > 100 m) is used (Park Seismic).

In any case, an excessively long T (e.g., T > 5 sec) is discouraged in an active survey because it can increase the chance of recording ambient noise (e.g., traffic). Usually, 24-channel acquisition will be optimal. If 48-channel acquisition is available, shortening dx is recommended rather than increasing D. Or, combining the two (shorter dx and longer D) is also recommended. The effect of shortening dx when more channels are available will be an increased signal-to-noise ratio (S/N) during data analysis because of the redundancy as well as the possibility of increasing resolution at shallow depths, whereas the effect of increasing D will be an increased Z_{max}.

Swept Frequency record:

A swept frequency record can be obtained either directly by an uncorrelated Vibroseis field record, or indirectly by an impulsive record passed through a stretch function. Three parameters need to be considered when preparing a swept frequency record: the lowest frequency recorded (f_1), the highest frequency recorded (f_2) and the length (T) of frequency-time plot or stretch function (Park et al, 1999).

The lowest frequency (f_1) analysed determines the maximum depth of investigation z_{max}, such that:

$$z_{max} = C_1/(2f_1),$$

Where C_1 is phase velocity for frequency f_1 (Rix & Leipski, 1991). The highest frequency to be analysed (f_2) should be initially higher than the likely necessary, and lowered to the optimal value after noise signals have been removed. Length (T) of the swept-frequency record should be as long as feasible or possible, allowing detailed examination of changes in ground roll frequency. A longer T value is necessary when near-surface properties change rapidly with depth. When f_1 and f_2 are properly selected, a T of no more than 10 seconds should be sufficient (Park et al, 1998). Best practice is to first analyse between 4 and 100 Hz, on a 10-12 second record and then narrow down to optimal values.

A-1.4.3 Dispersion curve extraction:

Generation of a dispersion curve is one of the most critical steps for eventually generating an accurate shear-wave velocity profile. This step is made prior to inversion of the surface wave and must be processed to image the dispersion and to extract the fundamental mode dispersion curves. The goal is to estimate one or more dispersion curves that are in turn passed into the next step of

inversion process, which tries to find a proper layer (shear-velocity, V_s) model whose theoretical dispersion curve matches the measured one as closely as possible. Generally it is the fundamental mode curve which is usually estimated, although curves of higher modes are beginning to be utilised.

Dispersion:

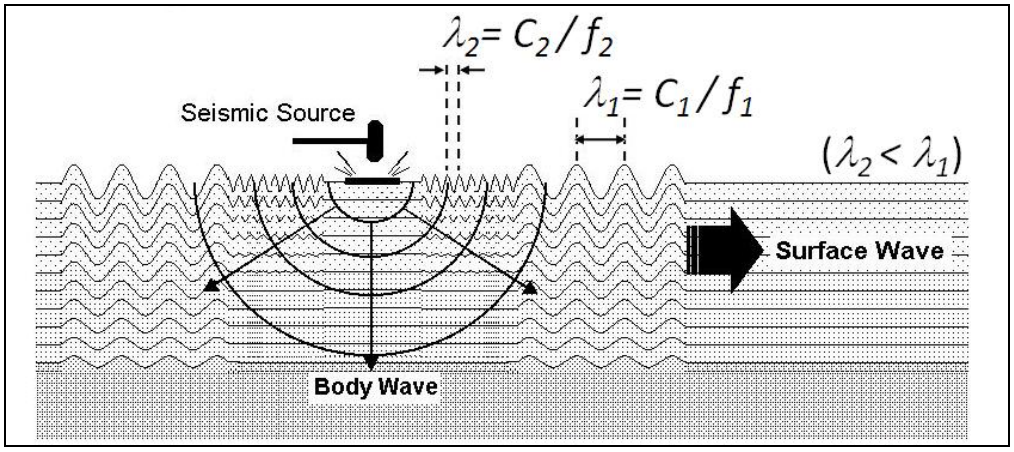

Figure 6: Dispersion of surface waves (Park Seismic).

Figure 7 above shows how a longer wavelength surface wave influences deeper depth of subsurface materials. In the normal case of velocity increasing with depth, the longer wavelength propagates faster as a result. Figure 8 below is a plot of frequency versus propagating velocity (phase velocity) is a dispersion curve. When more than one phase velocity exists for a given frequency is called multi-modal dispersion. The slowest one in this case if called the fundamental mode, and the next fastest is called the first higher mode.

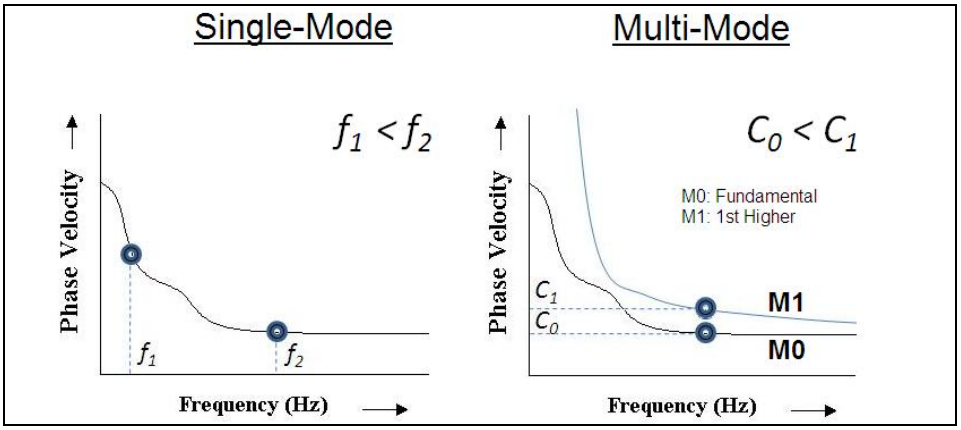

Figure 7: Dispersion curves (Park Seismic).

All types of seismic waves propagating horizontally are imaged if they take any significant energy noticeable from the relative intensity of the image. In this imaging process, a multichannel record in time (t)-space (x) domain is transformed into either frequency (f)-wavenumber (Kx) or frequency (f)-phase velocity (C_f) domain. The traditional f-k method is the former type, whereas the pi-omega transformation (McMechan & Yedlin, 1981) and the phase-shift method (Park et al, 1998) are two instances of the latter type. It is generally known that the f-k method results in the lowest resolution in imaging, whereas the phase-shift method achieves the higher resolution than the pi-omega method (Park et al, 1998)

A wavefield transformation is applied to the data to generate a dispersion (overtone) image. A multichannel coherency measure is applied to a decomposed (swept frequency) record in the offset-frequency domain and used to calculate phase velocity with frequency. These two variables plotted up together make up a dispersion curve (Duffy, 2008). The relationship between phase velocity and frequency can be established by calculating the phase velocity from the linear slope of each component of the swept frequency record.

Fundamental mode dispersion curves must reflect the dispersive character of planar-propagating fundamental-mode Rayleigh waves only. However, the majority of field records contain distinct higher and leaky modes and channel waves, which interfere with the fundamental mode in the offset-time (x-t) domain. Leaky modes are multiply reflected and constructively interfering dispersive waves propagating in a (borehole) waveguide. Part of the energy is reflected each time a compressional wave hits the waveguide wall, while the rest is converted to compressional or shear energy that radiates out of the waveguide, hence the term 'leaky'. A channel wave is a wave that is propagating and confined in a low velocity layer. Such interference causes difficulties because of the imhomogeneity in the subsurface, which requires

the use of a short receiver spread. Interference may therefore be so severe that no dispersion curves can be reliably extracted from the raw shot gather.

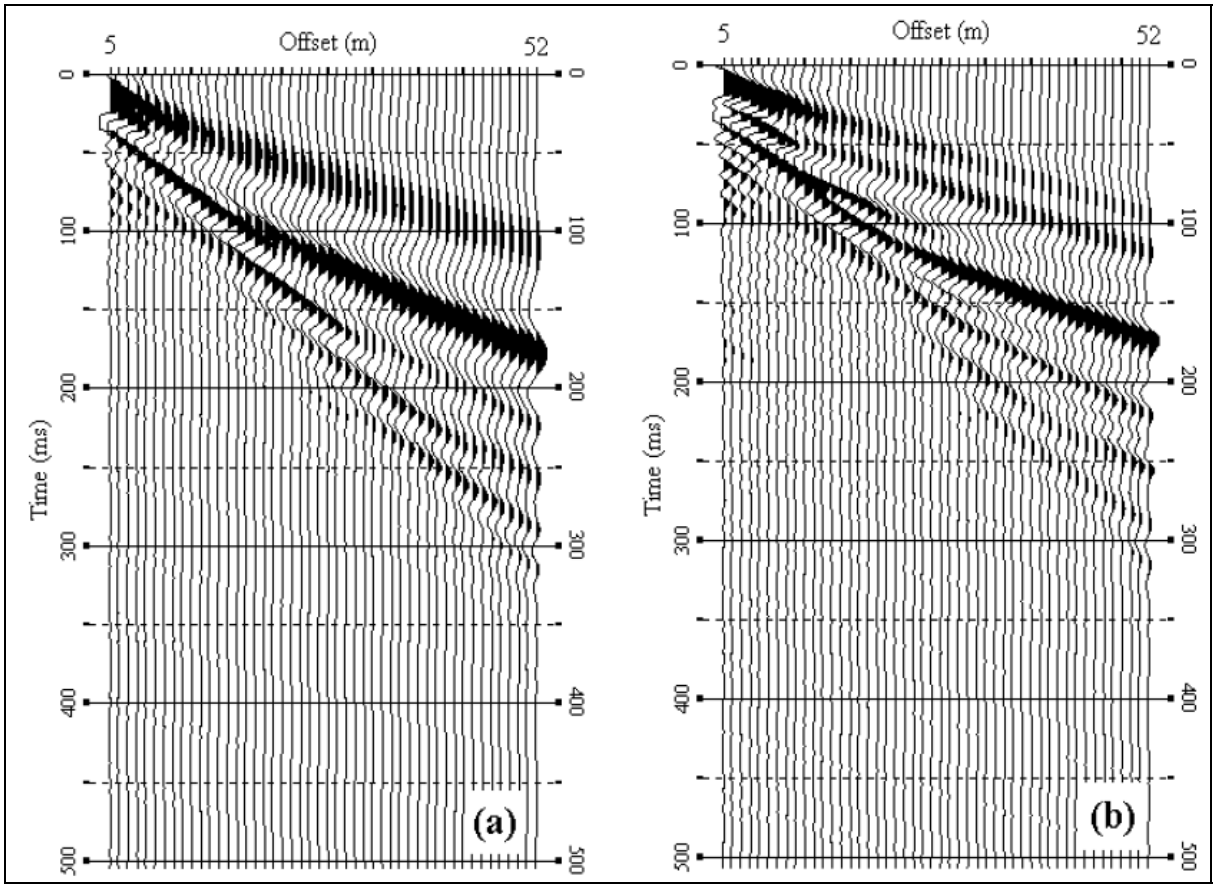

Figure 8: Synthetic shot gathers with a) fundamental mode only and b) fundamental and first higher modes. The low frequency fundamental mode events overlap with the higher mode events, whilst the higher frequencies of fundamental mode inhabit a lower velocity field in the x-t domain (Park et al, 2002).

If fundamental and higher modes are not separable the dispersion curves generated from a raw shot record cannot be interpreted as fundamental mode (Inanov et al, 2001). Under certain circumstances, it may not be possible to separate the fundamental mode of the surface waves from higher modes. Dominant higher surface-wave modes, together with body- and guided waves, can impede the estimation of the fundamental mode. This is especially true when relatively short spread lengths are required for the survey for reasons such as higher lateral-resolution demands or presence of noise at the far offsets (Ivanov et al, 2005).

A simple multichannel processing technique that mutes the interfering seismic waves in the shot records (offset-time (*x*-*t*) domain) can be used to analyze and filter noisy surface-wave modes and thus significantly improve the range and resolution of multimodal dispersion curves in the

phase-velocity–frequency domain. This is demonstrated on both synthetic and real shot gathers. One shortcoming of the muting method is the estimation of artificially high phase-velocity values at low frequencies. This artefact can be countered by employing dispersion-curve estimation in the same low-frequency range using the un-muted shot records.

The method of separation by muting is stipulated by the higher velocities of the higher modes. Higher mode energy appears with smaller slopes than the fundamental mode. The method of muting significantly improves the dispersion curve picking using MASW. Moreover, it allows data to be acquired with smaller spreads and thus significantly increase the horizontal resolution (Ivanov et al 2001).

Figure 10 below displays muting of higher modes in the x-t domain. 'Records' 1 and 2 have been cut from record 3 (Red and blue boxes). The longer the array, the easier to visually identify and mute the velocity fields dominated by higher mode and body waves. Note, however, that the higher mode dominated velocity field will still contain the low frequency (high velocity) component of fundamental mode Rayleigh-waves.

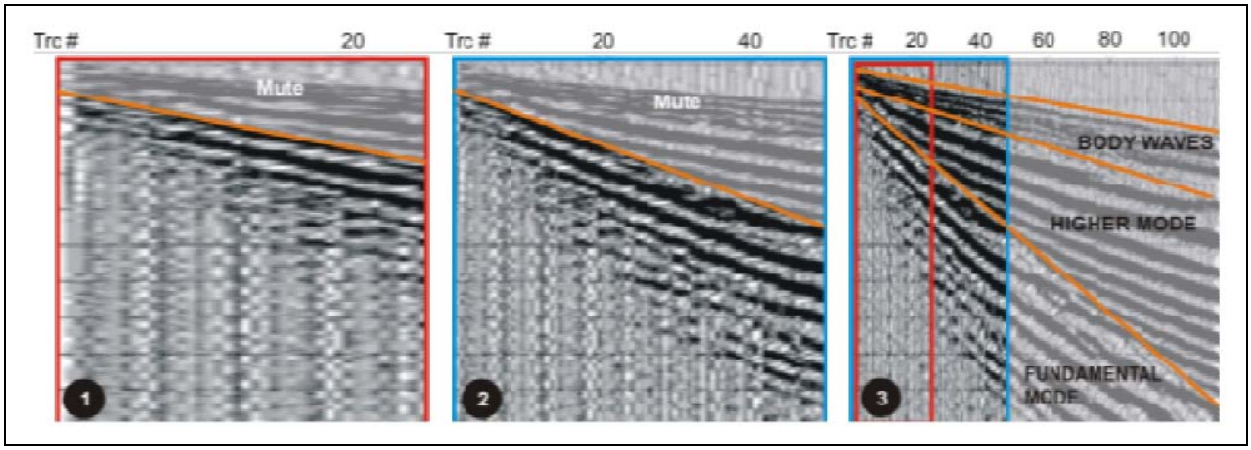

Figure 9: Muting of higher modes in the x-t domain (Duffy, 2008).

Alternatively, modal separation may be undertaken in the frequency-wavenumber (f-k) domain as demonstrated by Park et al (2002). Velocity (or pie-slice or fan) filtering and bow slice filtering are two commonly used methods to filter shot records in the f-k domain. The velocity filter is less than ideal for separation of surface wave modes because the lower frequency fundamental mode commonly has velocities overlapping those of the higher modes. The second method also developed by Park et al (2002), defines the rejecting zone in f-k space by a narrow curved shape (bow-slice) that follows a trajectory in f-k space. The trajectory is predefined using dispersion information of the higher mode, resulting in specific rejection of the higher mode only.

As shown by Figure 11 below, the application of a velocity filter to situation A will remove all but the higher frequency components of the fundamental mode wavefield, due to the overlapping velocities of fundamental and higher modes at low frequencies. The same result from situations A and B can be achieved by muting in the x-t domain. The bow-slice filter, however, is defined by a band around a rejection zone that follows a trajectory in f-k space, thus avoiding the fundamental mode entirely.

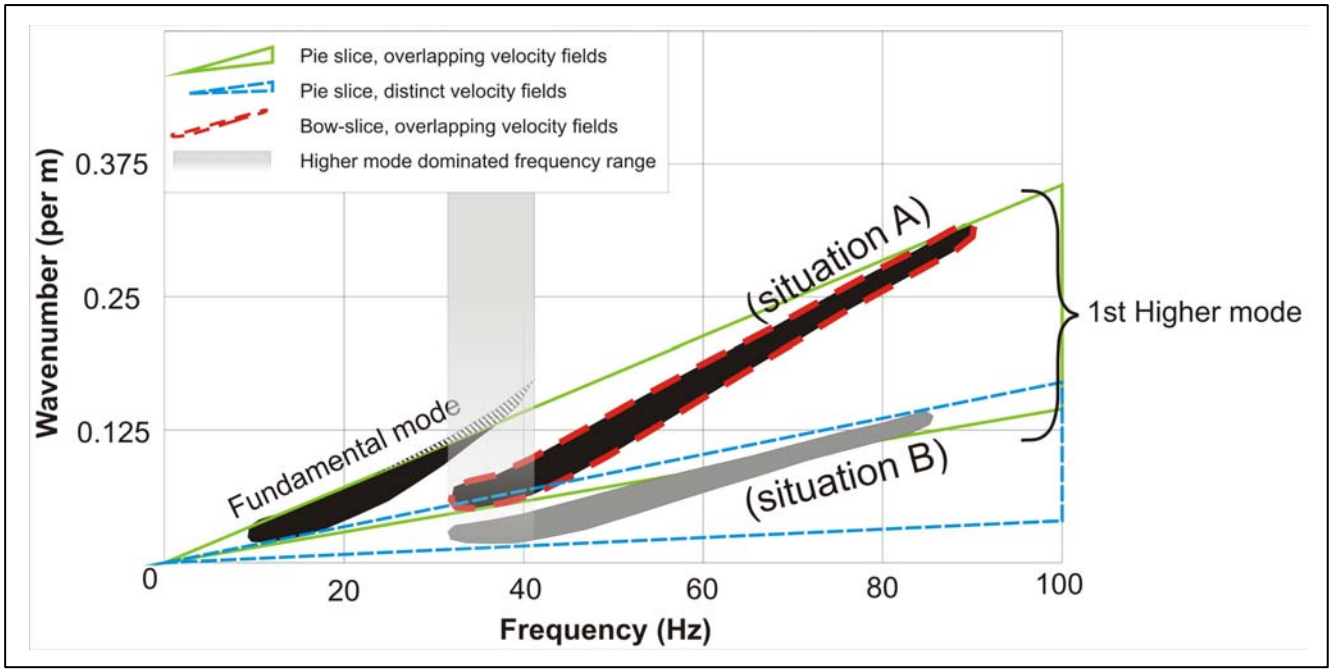

Figure 10: Application of pie-slice and bow-slice filters in the f-k domain (Duffy, 2008).

A-1.4.4 Surface wave inversion:

The primary goal of the field survey and subsequent data processing prior to inversion taking place is to establish the fundamental mode (M0) dispersion curve as accurately as possible. Inversion of S-wave velocities from Rayleigh wave dispersion curves is the final step in the MASW technique. The V_s profiles are calculated using an interactive inversion process that requires the dispersion data and estimations of Poisson's ratio and density (Park et al, 1999). A least-squares approach allows automation of the process (Xia et al, 1999). Generally it is only V_s which are updated after each calculation, as Poisson's Ratio, density and model thickness remain unchanged throughout the inversion process.

The low sensitivity of Rayleigh-wave phase velocity of P-wave velocity and density allows these parameters to be estimated within 25% without significant adverse affect on the convergence of model and inversion. Definition of a layer model by division of the subsurface into layers of

constant velocity removes layer thickness as a variable, leaving S-wave velocity as the only remaining variable. S-wave velocities can thus be derived by inverting Rayleigh-wave dispersion data to fit a layer model with fixed estimates of layer thickness, Poisson's ratio or P-wave velocity and density. Once individual dispersion curves are inverted, the resulting 1-D profiles are interpolates to construct a 2-D S-wave velocity profile.

The accuracy of the curve is the fundamental control on the validity of an inversion of a fundamental mode Rayleigh-wave dispersion curve. Hence, a well picked fundamental mode dispersion curve will invert to a model that closely resembles the earth model, but if the dispersion curve is inaccurate at any point along its length a partly or completely illegitimate S-wave velocity profile can result. The fundamental mode records are susceptible to contamination by body-waves and higher mode Rayleigh-waves, which can affect the dispersion curve over the affected frequency range (Duffy, 2008). This may result in a temporary reversal in the slope of the dispersion curve (Figure 12 B), or a temporary or permanent jump to a higher mode, which may result in dispersion discontinuities (O'neill & Matsuoka, 2005). Of these, the change in slope in Figure 12 is most problematic. This is because an inaccuracy that causes a standard deviation of only 4-5 m/s in Rayleigh-wave phase velocity over a specific frequency range may be unnoticeable but produce an S-wave velocity misfit of 100% compared to the earth model shown in Figure 12 D (Duffy, 2008).

Cross mode mixing of up to 40% at the middle to high frequencies made little difference to the inverted result, but anything more than 5% mixing at low frequencies adversely affected the inverted model (Zhang & Chan, 2003). Mixing of less than 10% dramatically reduces the penetration depth whilst mixing ratios produced similarly reduced penetration depth and significantly higher velocities within those penetration depths (Zhang & Chan, 2003).

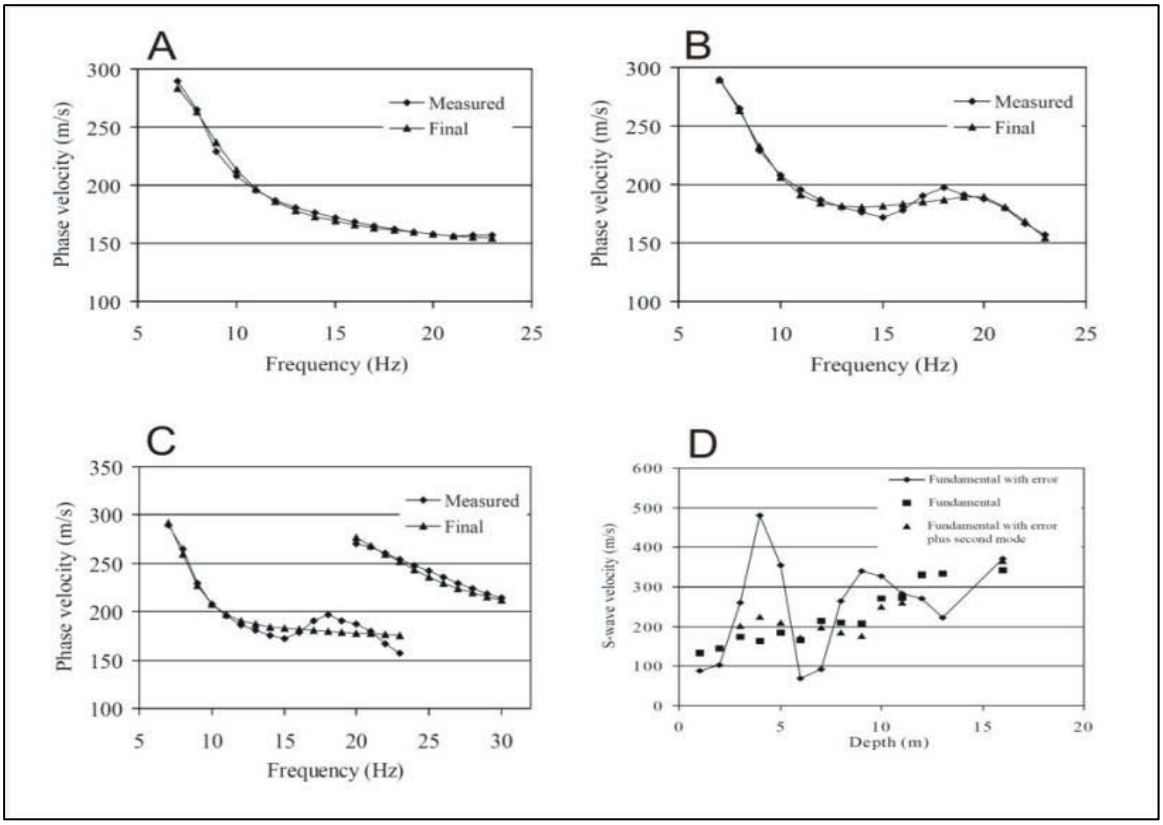

Figure 11: The effect of fundamental dispersion curve error on the inverted model. 'Measured' curves are extracted from the shot record, whilst 'Final' curves are calculated from the final S-wave velocity model. A) Accurate fundamental mode dispersion curve. B) Erroneous fundamental mode dispersion curve with higher mode and body wave contamination deliberately introduced between 13-19 Hz. C) As B but with the inclusion of higher mode data from 20-30Hz. D) The erroneous fundamental mode data produces an irrational profile (diamonds) except where it is supplemented by the higher mode dispersion curve (triangles). In the latter case, the S-wave velocity model closely follows that of the accurate fundamental mode curve (squares). (Xia et al, 2003).

For dealing with errors involved with this problem during fundamental-mode-only inversion Xia et al (2003) suggested to reduce the layering resolution of the model and to avoid over-forcing the fit of the model with potentially inaccurate data. The errors in the inverted S-wave velocities are caused by errors in dispersion data. For any noisy data, it is critical to define an appropriate error level and to terminate the inversion process at or a little above the error level to prevent transferring errors in data into inverted models. In most cases, the best fitting data does not necessarily yield the best inverted result. A choice has to be made between error and resolution of an inverted model. Sacrificing resolution or a trade-off between resolution and error of a model, to obtain stable results is often the best choice. The errors in the inverted S-wave velocity model can be reduced by reducing the resolution of the model (increasing thickness of layers). Reducing the number of layers smoothes out artifacts of the dispersion inaccuracy in the inversion compared with larger numbers of layers. Avoiding over-forcing the

fit of the model with potentially inaccurate data can skew data towards errorneous data if the inversion is forced to conclude at an error that is less than the difference between the inaccurate and accurate data. Therefore the best fit with the [errorenous] dispersion curve does not necessarily produce the best fit with the earth model.

The main proposal from Xia et al (2003), however, was an alternative approach based on inverting both fundamental and higher mode Rayleigh-waves (Figure 12 C). Higher modes Rayleigh-waves are even more strongly dependent on S-wave velocity than are fundamental mode Rayleigh-waves. Therefore a small change in S-wave velocity at a given wavelength produces a many times larger standard deviation in the phase velocity of the higher mode than that of the fundamental mode.
An errorenous fundamental mode dispersion curve forced to terminate inversion with a small error will draw the model towards the errornous data. Although, inclusion of higher modes will increase the overall error as the fundamental mode inversion strays part the true model toward a best fir with the errorneous data. Hence the higher modes stabilise the inversion procedure.

Xia et al (2003) also showed numerically for fundamental and higher mode Rayleigh wave data with the same wavelength, higher modes can ‘‘see’’ deeper than the fundamental mode. And also that higher mode data can increase the resolution of the inverted S-wave velocities.

Displaying MASW data can be done in 1-D, 2-D or 3-D format. In 3-D format, ‘slices’ of MASW survey lines are put together to form a 3-D image, extrapolating laterally between survey lines, producing an image similar to Figure x below.

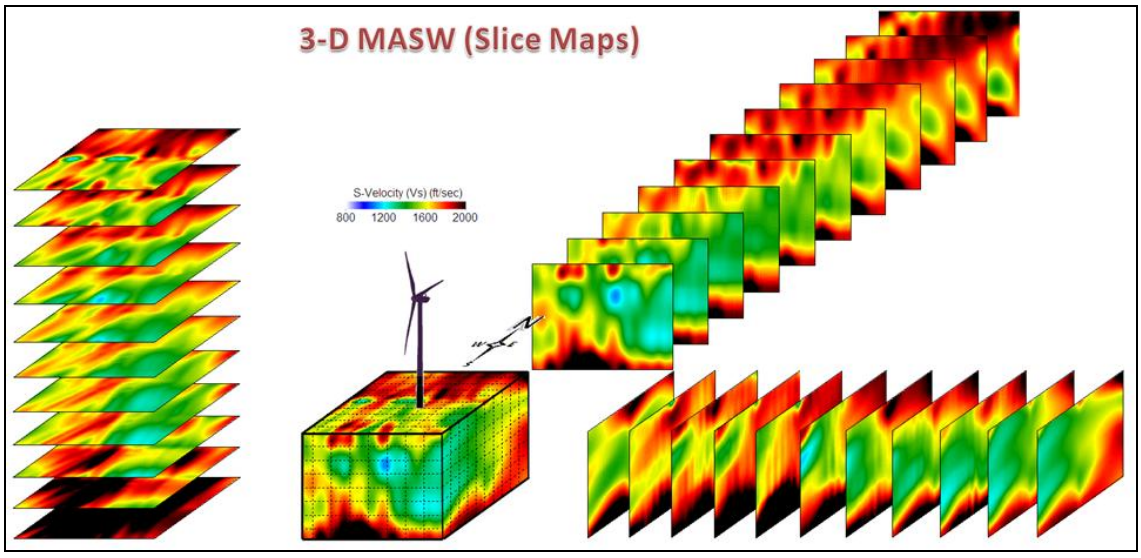

Figure 12: 3-D slice map for a wind turbine foundation site.

A-1.5 Passive MASW:

While the active method using an artificial seismic source, like a sledgehammer, can often achieve the goal of V_s estimation down to a few tens of meters (approximately 30 m) (Park et al, 2005), there are instances where the investigation depth is insufficient due to either elastic properties of the near-surface materials or the unusually deep investigation depth required. Sometimes a heavier active source which provides a more powerful impact can be used, like a heavy weight drop, to overcome this situation, although the depth range gained is often not significant. The impact power required to achieve the required gain in investigation depth needs to be in the order of a few orders of magnitude greater than what can be achieved with most active sources. Such a source, if invented, will not only be expensive but also inconvenient in field operations, which will discourage its use in engineering projects. On the other hand, passive surface waves generated from natural (e.g., tidal motion) or cultural (e.g., traffic) sources are usually of a low-frequency nature, with wavelengths ranging from a few kilometres (natural sources) to a few tens (or hundreds) of meters (cultural), providing a wide range of penetration depths and therefore a strong motivation to utilise them.

Deeper investigation depth requires generation of longer wavelengths (lower frequencies) because the analyzing depth range is directly proportional to the range of the analysable wavelengths. Generation of longer wavelengths, then, requires a larger deformation of the ground surface, requiring a higher impact power. In the case of a passive source (such as a moving truck), it can be assumed that only 10% of the total kinetic energy is consumed to generate surface waves (Park Seismic). This comparison clearly shows that energy from moving cars is greater than that from the active source by a few orders of magnitude.

Weight Drop (V_{max}=10 m/sec)	
Mass (kg)	Energy (J)
5	250
10	500
20	1,000
50	2,500
100	50,000

Truck (*mass = 10,000 kg*)		
Speed (mph)	Total Energy (J)	10% Energy (J)
30	720,000	72,000
40	1,280,000	128,000
50	2,000,000	200,000
60	2,880,000	288,000
70	3,920,000	392,000

Table 3: Comparison of impact energy from typical active and roadside passive surveys (Park Seismic).

There are two main types of passive MASW used today, which are defined on field logistics and type of shear-velocity (Vs) profiles, 1-D or 2-D, which are usually sought: Passive remote surveys which are described in Park et al (2004), and passive roadside surveys which are described in Park & Miller (2006). Passive remote surveys seek a 2-D V_s profile of bulk materials ranging up to a hundred meters along the surface and in depth. Whereas passive roadside surveys can generate a 1D V_s profile covering up to a hundred meters in depth and as much surface distance as the survey is continuously conducted.

A-1.5.1 Passive remote survey:

This method employs a 2-D receiver array such as a cross or circular layout to record passive surface waves. Any type of 2-D receiver array of fairly symmetric shape can be used. Cross and circular arrays generally produce dispersion images with a slightly higher resolution and better definition.

Data acquisition:

According to (Park Seismic) dimension (D) of the array should be at least equal to or greater than the maximum depth of investigation (Zmax):

$$D = mZ_{max} \quad (1 \leq m \leq 3).$$

Then, receiver spacing (dx) is determined by number of channels (N) available. For example, if a circular array of diameter D is to be deployed, then:

$$dx=D*pi/N$$

Once dx is determined (or its minimum size is determined in the case of uneven spacing), then it determines the shallowest depth investigated (Zmin) roughly as:

$$Z_{min}=pdx \ (1/3 \leq p \leq 1.0)$$

Generally the more channels added to the investigation, the greater the resolution of dispersion processing. Forty-eight channels are most desirable for a survey aiming at Z_{max} equal to 100m. A broader-band dispersion image can be constructed by the combination of dispersion image data sets which have been processed separately. When a smaller number of channels are used in the survey (ie: 24), data acquisition can proceed with an array of smaller dimensions (eg: D = 25m), and then with progressively larger dimensions (eg: D = 50m, 75m, etc) to cover a broader range of wavelengths.

Recording parameters:

A sampling interval of 4m/s (ie: dt = 4m/s) and a total recording time of 10 sec (ie: T = 10 sec) are parameters generally used for urban surveys (approximate figures as parameters are always adjusted to the site conditions). Total recording time (T) is determined so that there is at least one occurrence of passive surface wave generation during recording. Therefore, it can be reduced or increased depending on local situations related to the surface wave generation. The longer T is not always better. This is because the chance of recording surface waves generated at different locations (azimuth) on the road increases as well and it will generally degrade the data processing resolution unless those locations are well apart in azimuth (Park Seismic). If the main source point is fixed in location, however, the longer T will be better as multiple generations from the same point will constructively contribute to the dispersion imaging process. A fixed source point of major surface waves is observed when you hear a jolting sound coming from nearly the same spot (azimuth) on the road as vehicles pass over. Vertical stacking during recording is strongly discouraged (unless T is significantly limited) because it will increase the chance of recording multi-azimuth surface waves.

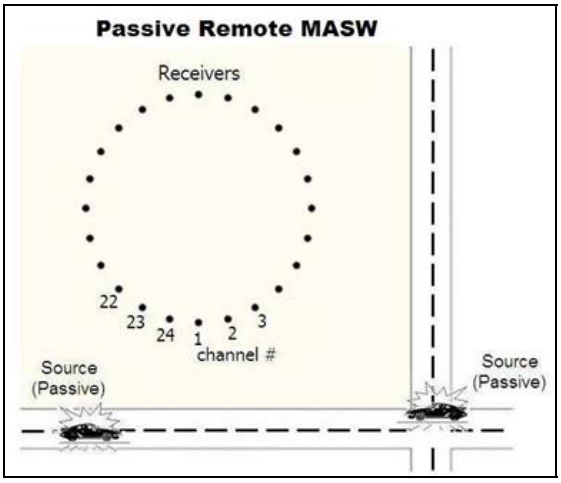

Figure 13: A field layout of a passive remote MASW survey (Park Seismic).

A-1.5.2 Passive roadside survey:

The passive roadside MASW method adopts the conventional linear receiver array and tries mainly to utilize surface waves generated from local traffic. The true 2-D receiver array such as a cross layout is not a practical or possible mode of survey in urban areas populated with buildings which requires an open spacious area, hence, the roadside method which can be

implemented with a conventional 1-D linear receiver array deployed along the roadside is the convenient option (Louie J. , 2001). Using a land streamer (Figure 15) for the array can improve survey speed by as much as a few orders of magnitude. In addition, an active impact (e.g., by using a sledge hammer) can be applied at one end of the array to trigger a long recording (e.g., 10 sec) (Figure 14). This can result in the active-passive combined analysis of surface waves for the purpose of obtaining both shallow (e.g., 1-20 m) and deep (e.g., 20-100 m) V_s information simultaneously.

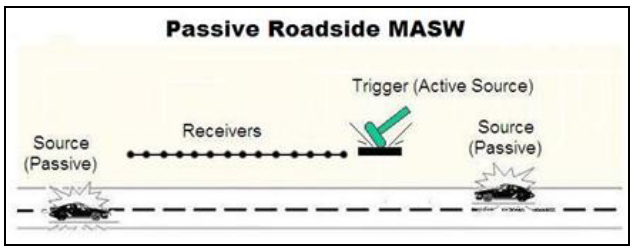

Figure 14: A field layout of a passive roadside MASW survey (Park Seismic)

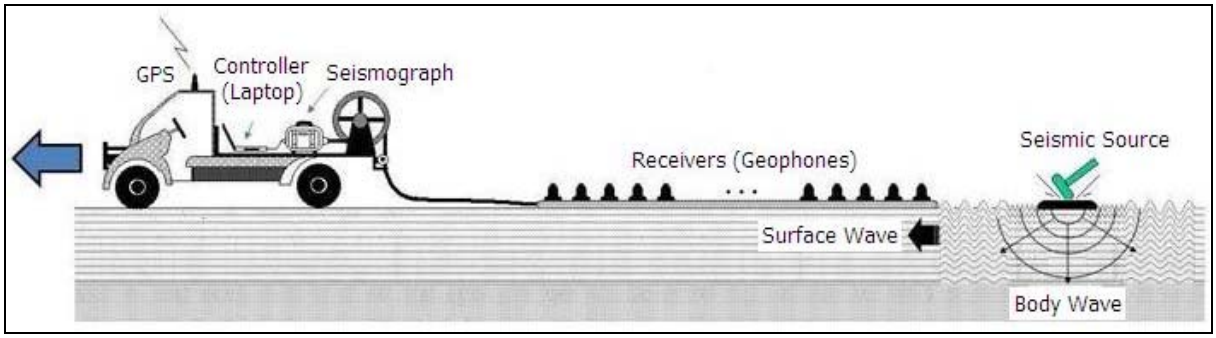

Figure 15: Passive roadside MASW survey with a land-streamer (Park Seismic).

Data acquisition:

The linear receiver array is deployed parallel to the road. The array does not have to be particularly close to the road but it is recommended that the offline distance (the distance between the array and the road centre) to be maintained reasonably constant during the survey. Dimension (D) of the array should be at least equal or greater than the maximum depth of investigation (Z_{max}). Then, receiver spacing (dx) is determined by number of channels (N) available approximately as dx=D/N (Park Seismic). Once dx is determined, then it determines the shallowest depth investigated (Z_{min}) roughly as:

$$Z_{min}=pdx \ (1/3 \leq p \leq 1.0)$$

In any case, more channels are an advantage that can increase the resolution of dispersion processing. Although forty-eight (48) channels are most desirable for a survey aiming at Z_{max} =

100 m, because of the 1-D nature of the array a 24-channel acquisition often may be used with dx = 5 m or so.

Recording Parameters:

Recording parameters used are similar to that of the remote passive MASW method, with sampling interval in the order of 4 ms, and total recording time (T) in the order of 10 sec.

Vertical stacking during recording, like in the remote passive MASW method, is strongly discouraged (unless T is significantly limited) because it will increase the chance of recording multi-azimuth surface waves.

A-1.5.3 Combined active and passive survey:

As discussed above, active surveys using artificial seismic sources can achieve the goal of V_s estimation down to a few tens of meters, which is often not a sufficient depth for the investigation at hand. To overcome this, investigators are turning their attention to those passive waves generated by cultural activities as their wavelengths are long enough to assure the necessary gain below the maximum depth achieved by an active survey. While the active survey provides a dispersion curve in a relatively high-frequency range (eg: 20-50 Hz), the passive survey can fill the dispersion trend at lower frequencies (eg: 5-20 Hz). Traditionally, it was assumed that passive surface waves consist predominantly of fundamental mode Rayleigh waves. However, recent studies aided by the imaging method revealed a strong possibility of frequent higher mode domination (Park et al., 2005). For this reason, Park et al (2005) suggested a combined active/passive survey to be followed by combining dispersion images of both types for a more reliable modal identification.

By combining these two sets of dispersion curves, a dispersion curve of known mode (such as the fundamental mode) is constructed to back calculate a V_s profile for a wide depth range (Park et al, 2005). Therefore, two reasons dispersion images from passive and active data sets are combined are:

1. To enlarge the analyzable frequency (therefore depth) range of dispersion, and;
2. To better identify the modal identity of dispersion trends.

Necessity of separate active survey in passive remote survey, according to Park Seismic:

Because a passive survey usually operates with a larger receiver spacing than normally used in an active survey, a processed dispersion image usually lacks information at shallower depths (higher frequencies). Although in theory this missing information can be filled by multiple surveys of progressively smaller receiver-array dimensions (D's), higher frequency components of passive surface waves may not be recorded effectively because of their relatively rapid attenuation properties. The best way would be to perform a separate active survey, preferably at the passive array centre, using a sledge hammer. Then, two separate dispersion image data sets can be combined to form a broader-band image. Combining active and passive dispersion images can also help modal identification. An alternative approach instead of a separate active survey would be to apply active impact(s) at a place close to (but outside) the passive receiver array during the recording of a passive record. If this is the case, however, followings are to be noted:

1. Analysed shear-velocity (V_s) information at shallow depths can only be associated with those near-surface materials near the impact point.
2. Analysed dispersion trend for those high frequencies generated by the active source can be slightly distorted (up to 10%) because of a violation of the plane-wave assumption.
3. Dispersion images for those low-frequency passive waves can be adversely influenced and result in a degraded definition, or slightly distorted trend, or both.

A-1.6 Geotechnical applications of MASW:

A limited number of publications have focused on the geotechnical applications of MASW, although there is huge potential for further uses in geotechnical engineering investigations. Shallow S-wave velocity structure is an indication of stiffness and is used when estimating site response to shaking. By facilitating construction of an S-wave velocity profile MASW can provide critical information for geotechnical site characterisation.

Seismic methods have often been used as a non destructive testing method that can provide such key geotechnical parameters as shear and bulk moduli from the S-wave (V_s) and P-wave (V_p) velocities of near-surface materials (Park et al, 2005). Surface wave has often been used to infer V_s variation with depth (a V_s profile) of near-surface materials from the measurement of Rayleigh-type surface waves. The V_s profile is a key engineering parameter that can be associated with the stiffness profile in many geotechnical characterisations of soil sites within the depth range of several tens of meters. This is due to that fact that surface waves respond most effectively to various types of near-surface anomalies that are common targets of geotechnical investigation.

It can be used not only for the accurate and detailed characterization of a small area but also for the quick detection of underground anomaly zones from a reconnaissance survey over a large area (Park, 1995). Subsidence and dissolution features such as in karst terrains are often difficult to detect over large areas. With intrusive investigations often being time consuming, costly and providing very limited lateral extrapolation. A MASW survey can provide linear and 3-D profiles of the subsurface velocity profile, identifying anomaly zones over large areas.

MASW surveys must be accompanied with sound geological and geotechnical investigations, as the material properties of the subsurface dictates the seismic parameters. Hence surface wave velocities need to be correlated with measurable rock properties. Although currently there has been limited research into the relationship of surface wave velocities with the geotechnical properties they represent. Geological properties which influence the surface wave velocities within a medium can include weathering, fracturing, fracture spacing, hardness, primary porosity and lithology.

A-1.6.1 Factors affecting rock mass S-wave velocity:

Any surface-wave velocities produced from MASW survey methods must be accompanied by sound geological and geotechnical research. The seismic parameters of a body of material are determined by factors such as its geometry, properties of fracturing and faulting.

An early correlation between seismic wave velocities and physical properties of near-surface geologic materials was undertaken by the United States Geological Survey and reported by Fumal (1978). At each of the 59 sites, they drilled a hole to 30m in a wide range of geological materials to record the site stratigraphy, physical properties and downhole P and S-wave velocities. In order to identify geologic units with distinctly different seismic response for the purposes of seismic zonation, both compressional and shear wave velocities were measured in the boreholes. Several physical parameters, which can be readily determined in the field, were found to correlate with the shear wave velocities and were used to define seismically distinct groups. For the unconsolidated to semiconsolidated sediments, texture, standard penetration resistance and depth were used to define eight seismically distinct groups. In soft rock and alluvium, however, Fumal reported that hardness dominated the S-wave velocities, and a weaker correlation between these physical properties and P-wave velocities. For the bedrock materials, fracture spacing and hardness were used to differentiate ten distinct categories. Fracturing dramatically reduces the elastic moduli, often without significantly changing the porosity so that, in well-cemented lithologies, fracture spacing exerts a greater influence on S-wave velocity than does lithology, hardness or primary porosity. Fumal (1978) found hardness to be a proxy for weathering in bedrock material, in which fracturing dominated S-wave velocities.

Fumal (1978) typically observed three weathering-related velocity zones in his well logs. With increasing depth, these were a layer of unconsolidated residual material, an underlying zone of moderately to deeply weathered bedrock, and relatively fresh bedrock. His results show a close correlation on almost every well log between these weathering zones and the corresponding interval velocities. More significantly, from the point of view of distinguishing lithologies based on S-wave velocities, the thickness of individual weathering zones varied between geological units in a given area. Fumal compared the effect of moderate weathering on S-wave velocity for a variety of lithologies. By plotting the velocity reduction for weathered rock against the fresh rock velocity at the same site over a range of lithologies, Fumal showed that the velocity drop due to weathering is a direct function of the strength of the fresh rock. Weak rocks will exhibit a greater absolute velocity drop for an equal degree of weathering than will equivalently weathered strong rocks.

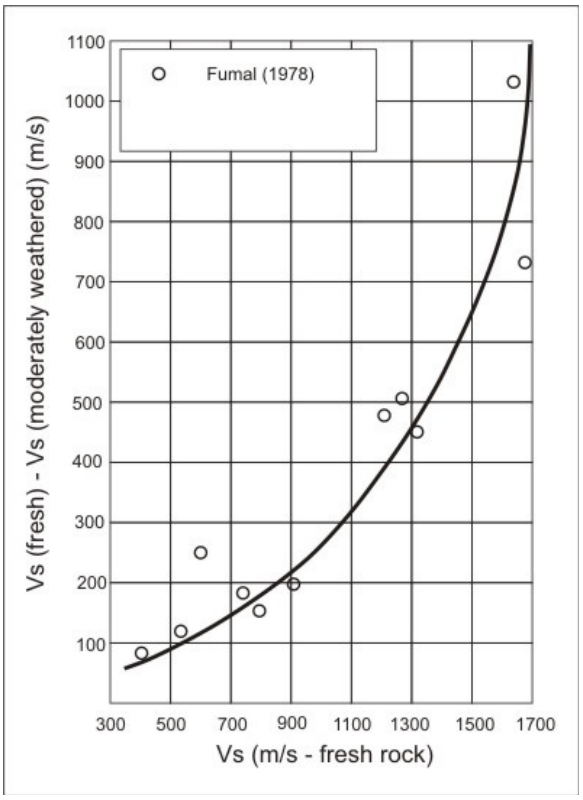

Figure 16: Reduction in S-wave velocity attributable to moderate weathering, graphed as a function of the fresh rock S-wave velocity (Fumal, 1978).

Geotechnical interpretation of S-wave behaviour in a geological medium must be guided by an understanding of the physical relationships between S-wave propagation and rock mass character. A waveform propagating through a fractured medium is delayed and the high frequencies are filtered, so that the peak frequency in the received signal is observed as a lower frequency. As a wave propagates, an apparent attenuation accumulates because reflections from individual fractures interfere with the propagating wave (Boadu & Long, 1996). This seismic response to fracturing provides a means of inferring fracture density from variations in seismic velocity in and otherwise homogenous medium. Boadu & Long (1996) incorporate linear fracture density into their equations for estimating velocity and attenuation in a fractured medium.

As weathering is only one of the parameters affecting surface wave velocity, many other parameters have been used to attempt to quantify the condition and mechanical state of a fractured rock mass. Boadu (1997) modelled the effect of fractures on seismic waves, correlated S-wave velocity strongly with linear fracture density and rock quality designation among other parameters. Although his correlation did not take into account the effects of weathering.

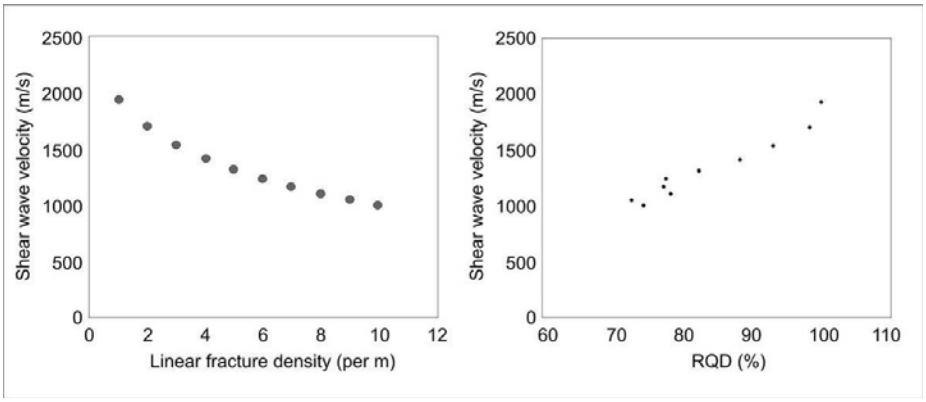

Figure 17: Variations of S-wave velocity with fractured rock mass parameters for the model of Boadu (1997). Both parameters exhibit a strong correlation with S-wave velocity.

Currently there is very little control on what the surface wave velocities are reflecting when used to determine stiffness parameters in geotechnical investigations. At present they are being used to represent the shear modulus of lithologies, but the shear modulus is a result of a range of geological characteristics, as aforementioned. Hence the shear wave velocities are being used without knowing the full extent of their controls, and further research is needed to fully determine the effects of these controls and their interactions.

A-1.6.2 Further applications of MASW:

Active and passive surface wave testing can be used to obtain V_S profiles for:

- Earthquake site response
- Seismic microzonation
- Liquefaction analysis
- Soil compaction control
- Mapping subsurface stratigraphy
- Locating potentially weak zones in earthen embankments and levees

A-1.7 Case Studies:

A-1.7.1 National Hazard Earthquake Reduction Programme (NHERP) soil classification and estimation of 1-D site effect of Dehradun fan deposits using shear wave velocity. (Mahajan, 2009)

Dehradun city is located in India in a sub Himalayan mountain exit, and is mainly covered by fan deposits which are a product of weathering, erosion, and deposition over a long period of time.

Shear wave velocity of the near surface soil at nearly 50 sites was determined using Multi-channel Analysis of Surface Waves (MASW). Efforts of deriving shear wave velocity profiles down to a depth of 30–40 m will help sedimentologists in understanding the sedimentary architecture and basin evolution. The data is useful for the prediction of the ground motion response to earthquakes in areas where significant soil cover overlays the firm bedrock and the information can be used to derive the stiffness factor of any site. The structure of the unconsolidated materials of young sedimentary basins can have a profound effect on the spatial distribution of ground amplification and dynamic site period, resulting in large variation in the severity of damage to buildings, transportation corridors and other lifeline infrastructures.

Factors which deem the city of Dehradun to be in a critical situation include the regions high seismicity, the close proximity of major thrust faults and seismic regions, the growing urbanisation of the city and variation in thickness of sediments from north to south.

The objective of this shallow subsurface study was to derive a shear wave velocity map of Dehradun city and to understand the one dimensional site effect, including the amplification and dynamic period of different sites within the Dehradun city itself.

It was found that the amplification function of the ground motion decreases from northeast to southwest across the study area. This trend of decreasing ground motion amplification is due to the increased depth to bedrock and the subsequent increase in attenuation (i.e., deamplification).
In the northern part of the city, the relatively high shear wave velocities do not attenuate the bed rock-induced motions to the extent that it does in the central part of the city.

This study will be useful in ground motion hazard maps that are based on site class. Since, the Dehradun city is under development stage, the above study will also be useful in land use

planning if one considers the one dimensional site effect while designing new engineering structure in the city considering future earthquakes.

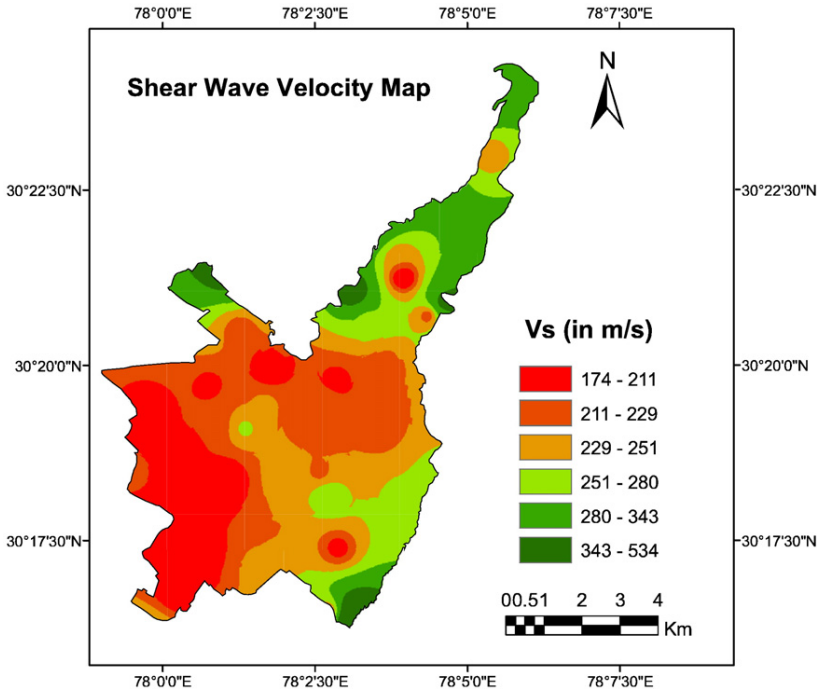

Figure 18: Shear-wave velocity map of the Dehradun city (Mahajan, 2009)

A-1.7.2 Feasibility of Using the MASW Method to Define a Sinkhole Impact Area at Calvert Cliffs Nuclear Power Plant, Maryland. (Xia at el, 2001)

A sinkhole developed at Calvert Cliffs Nuclear Power Plant, Maryland. The subsurface drainage system is a possible cause of the sinkhole. The original groundwater level was 15 to 20 ft above the sea level in the plant area; however, a permanent pipe drainage system surrounding the plant maintains the groundwater below 10 ft above sea level. At the same time that the drainage system lowers the groundwater level, soil may wash away so that over time void(s) may develop.

Approximately 700 tons of soil was used to fill in the sinkhole to prevent further damage. Although the refilling reduced the velocity contrast in the sinkhole impact area, the new soil was much less compacted than surrounding materials so the sinkhole impact area still showed anomalies with a lower S-wave velocity. A high-frequency surface-wave survey was conducted to define the sinkhole impact area. Acquisition of surface-wave data was in an extremely noisy

environment, and was conducted at a noise level 50-100 times higher than a normal environment for a shallow seismic survey. The S-wave velocity field calculated from surface-wave data showed chimney-shaped low-velocity anomalies that were directly related to the sinkhole. Based on S-wave velocity field maps, a potential sinkhole impact area was tentatively defined. S-wave velocity field maps also revealed, depending on the acquisition geometry, one side of the water tunnel of the power plant.

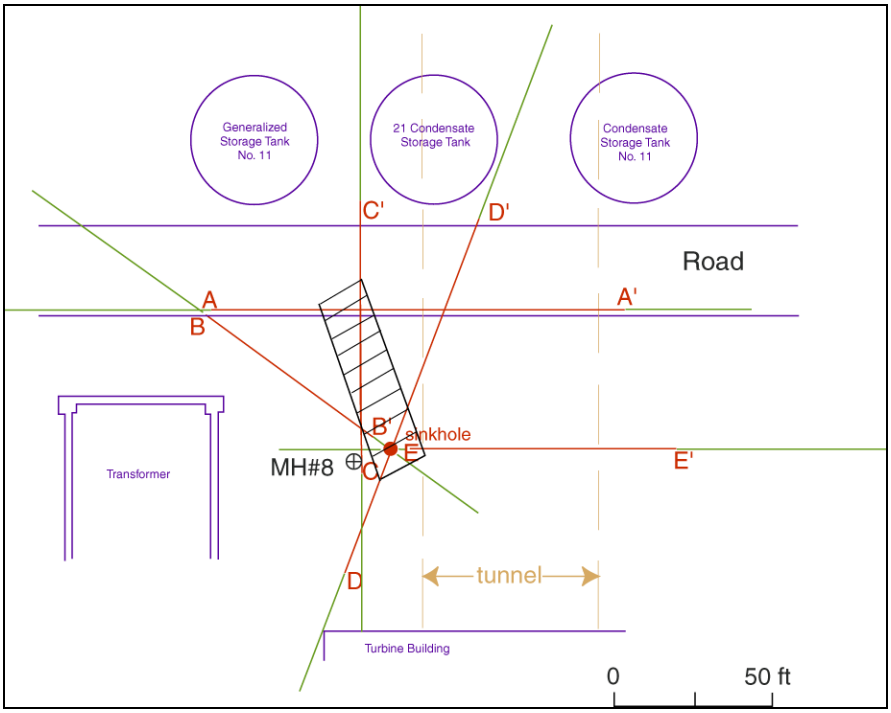

Figure 19: The sinkhole impact area (shaded) interpreted from surface-wave data, survey lines shown in red (Xia et al, 2001).

The S-wave velocity field calculated from surface-wave data delineated a possible sinkhole impact area. This meant that calculated estimations could be made as to remediation measures to further stabilise the ground, and the full vertical and lateral extent of the sinkhole could be determined.

A-1.8 Conclusion:

When ground roll is acquired using a multichannel recording method and displayed in a swept-frequency format, different frequency components of Rayleigh waves can be identified by distinctive and simple coherency. The MASW seismic surface-wave method provides a useful non-invasive tool, where information about elastic properties or near-surface materials can be effectively determined. This is due to the integrity of each single Rayleigh wave frequency, which can be readily examined for contamination by noise, and making adjustments is possible to improve the signal to noise ratio during data acquisition and processing. Also, a highly accurate dispersion curve can be obtained and then inverted to produce a V_s profile with a high level of accuracy using ground roll recorded on a single shot gather.

Three major components of MASW surveying which are beneficial to subsurface modelling include:

1. Many different depths can be investigated simultaneously during one survey
2. A fast method which requires a reduced level of labour compared to earlier methods and other seismic methods, and
3. Non-destructive method of investigation

This surface-wave technique also provides a high level of flexibility of surveying to the investigation site conditions. If an active MASW survey cannot be conducted due to the urban nature of a site, passive methods can be used to determine a V_s profile from a roadside survey.

Geotechnical application of this method is almost endless. It can be used not only for the accurate and detailed characterisation of a small or large area but also for the quick detection of underground anomaly zones from a reconnaissance survey over a large area.

A-1.9 References:

Boadu, F. K. (1997). Fractured rock mass characterisation parameters and seismic properties. *Journal of Applied Geophysics* , v. 37, p. 1-19.

Boadu, F. K., & Long, L. T. (1996). Effects of fractures on seismic-wave velocity and attenuation. *Geophysical Journal International* , v. 127, p. 86-110.

Duffy, B. G. (2008). *Development of multi-channel analysis of surface waves (MASW) for characterising the internal structure of active fault zones as a predictive method of identifying the distribution of ground deformation .* University of Canterbury Masters Thesis.

Fumal, T. E. (1978). Correlations between seismic wave velocities and physical properties of near-surface geological materials in the southern San Francisco Bay region, California. *U.S Geological Survey* .

Gabriels, P., Snider, R., & Nolet, G. (1987). In situ measurements of shear-wave velocity in desiments with higher mode Rayleigh waves. *Geophysical Prospecting* , 35, 187-196.

Ivanov, J., Park, C. B., Miller, R. D., & Xia, J. (2005). Analyzing and Filtering Surface-Wave Energy By Muting Shot Gathers. *Journal of Environmental & Engineering Geophysics* , v. 10, p. 307-322.

Ivanov, J., Park, C., Miller, R., Xia, J., & Overton, R. (2001). Modal separation before dispersion curve extraction by MASW method. *Proceedings of the SAGEEP.* Denver, Colorado.

Louie, J. (2001). Faster, better: shear-wave velocity to 100 meters depth from refraction microtremor arrays. *Bulletin of the Seismological Society of America* , v. 91, n. 2, p. 347-364.

Mahajan, A. K. (2009). NEHRP soil classification and estimation of 1-D site effect of Dehradun fan deposits using shear wave velocity. *Engineering Geology* , v. 104, p. 232–240.

McMechan, G., & Yedlin, M. (1981). Analysis of dispersive waves by wave field transformation. *Geophysics* , v. 46, n. 6, p. 869-874.

Miller, R. D., Xia, J., Park, C. B., & Ivanov, J. M. (1999). Multichannel analysis of surface waves to map bedrock, Kansas Geological Survey. *The Leading Edge* , p. 1392 - 1396.

Nazarian, S., Stokoe, K. H., & Hudson, W. R. (1983). Use of spectral analysis of surface waves method for determinination of moduli and thicknesses of pavement systems. *Transport. Res. Record.* , 930, 38-45.

O'neill, A., & Matsuoka, T. (2005). Dominant higher surface-wave modes and possible inversion pitfalls. *Jounral of Environmental and Engineering Geophysics* , v. 10, p. 185-201.

Park Seismic. (n.d.). Retrieved October 2, 2009, from Multichannel Analysis of Surface Waves (MASW): http://www.masw.com/ACQParaTables.html

Park, C. B. (1995). Characterisation of Geotechnical Sites by Multi-Channel Analysis of Surface Waves. *Kansas Gological Survey* .

Park, C. B., & Miller, R. D. (2006). Roadside passive MASW. *Proceedings of the SAGEEP.* Seattle, Washington.

Park, C. B., Miller, R. D., & Miura, H. (2002). Optimum field parameters. *Ext. Abstract, Society of Exploration Geophysicists of Japan, Tokyo* , 22-23 May.

Park, C. B., Miller, R. D., & Xia, J. (1999). Multichannel analysis of surface waves. *GEOPHYSICS* , Vol 16, p. 800-808.

Park, C. B., Miller, R. D., Xia, J., & Ivanov, J. (2005). Seismic Characterization of Geotechnical Sites By Multichannel Analysis of Surface Waves (MASW) Method. *Kansas Geological Survey* .

Park, C., Miller, R., & Xia, J. (1998). Imaging dispersion curves of surface waves on multi-channel record. *68th Annual International Meeting of Society of Exploration Geophysicists*, (pp. 1377-1380).

Park, C., Miller, R., Laflen, D., Cabrillo, N., Ivanov, J., Bennett, B., et al. (2004). Imaging dis-persion curves of passive surface waves. *Society Exploration Geophysics* , p. 1357-1360.

Park, C., Miller, R., Ryden, N., Xia, J., & Ivanov, J. (2005). Combined use of active and passive surface waves. *Journal of Environmental & Engineering Geophysics* , v. 10, no. 3, p. 323-334.

Richart, F. E., Hall, J. R., & Woods, R. D. (1970). *Vibrations of Soils and Foundations.* Prentice-Hall.

Rix, G. J., & Leipski, E. A. (1991). Accuracy and resolution of surface wave inversion. *Geotechnical Special Publication* , p. 17-32.

Stokoe, K. H., Wright, G. S., Bay, J. A., & Roesset, J. M. (1994). Characterization of geotechincal sites by SASW method, in Geophysical characterization of sites. *ISSMFE Technical Committee #10, edited by R. D. Woods.* New Delhi: Oxford Publishers.

Xia, J., Miller, R. D., & Park, C. B. (1999). Estimation of near-surface shear-wave velocity by inversion of Rayleigh waves. *Geophysics* , v. 64, p. 691-700.

Xia, J., Miller, R. D., & Park, C. B. (2001). Feasibility of Using the MASW Method to Define a Sinkhole Impact Area at Calvert Cliffs Nuclear Power Plant, Maryland. *Kansas Geological Survey* , .

Xia, J., Miller, R., Park, C., & Tian, G. (2003). Inversion of high frequency surface. *Journal of Applied Geophysics* , v. 52, p. 45-57.

Zhang, S., & Chan, L. (2003). Possible effects of misidentified mode number on Rayleigh wave inversion. *Journal of Applied Geophysics* , v. 53, p. 17-29.

Appendix B:

Measurement of Elasticity

A-2 Measurement of Elasticity:

A-2.1 Introduction:

This chapter details the principles of mechanics in civil engineering and how they are utilised in geology, particularly soil and rock mechanics. Material responses to applied stresses and strains can provide a basis for understanding qualitative and quantitative aspects of engineering geology, and important engineering properties used in geotechnical design (Johnson & De Graff, 1988). This chapter provides a review of methods used for determining elastic parameters at varying scales, both high and low strain methods, from the hand-specimen to insitu.

A-2.2 Theory of Elasticity:

A-2.2.1 Stress and Strain:

Natural forces that act on soil and rock masses can cause deformation and ultimately failure of soil and rock. Force, however, is not a measureable quantity, as it varies proportionally with the surface area to which the force is applied. Stress on the other hand, is not dependent on differences in area. Stress is defined as force per unit area and is synonymous with pressure.

Strain acting on a material is related to the above discussion on stress. Without the application of forces on a material, there would be no strain. Whereas stresses are analysed at a point at a given instant, strains are defined as changes in relative positions of particles in a body at two different times (Johnson & De Graff, 1988).

Stress:

Stress is defined as load per unit area and is synonymous with pressure. Stress is a vector quantity and is analysed independently of material physical properties. A stress vector acting on the surface is typically resolved into normal and parallel (shear) components relative to the surface. For a elemental cube of unit dimensions in an equilibrium state, the sum of forces acting on the surfaces and their moments equals zero (Johnson & De Graff, 1988).

Strain:

Strain, or deformation of a material, is closely related to stress. Without the application of forces on a material, there would be no strain. Strains are defined as changes in relative positions of particles in a body at two different times. The term displacement is often useful in defining strain. The displacement of a given particle from its initial position must be such that it cannot correspond to the movement of the whole body, i.e. the body must be deformed or distorted in shape rather than just moved as a rigid body (Johnson & De Graff, 1988).

A-2.2.2 Elastic modulus:

When a force is applied to a material, it deforms. This means the particles of the material are displaced from their original positions. These displacements are reversible, provided the forces applied do not exceed a critical value, and the material particles return to their original positions once the force is removed, with no permanent deformation. This is called *elastic behaviour.*

Elasticity refers to the property of reversibility of deformation when subjected to a load. The elastic modulus is the mathematical description of an object's tendency to be deformed elastically when force is applied to it. The Elastic Modulus, (E), of an object is defined as the slope of its stress-strain curve in the elastic deformation region.

$$E = \frac{\text{Stress}}{\text{Strain}}$$ **Equation 1**

For elastic behaviour, the strain in a body is proportional to the stress applied to it; therefore the load is proportional to deformation. This linear relationship is called Hooke's Law, which forms the basis of elastic theory (Lowrie, 2002). As shown by Figure 4.2, beyond a certain value of stress, called the proportionality limit, Hooke's Law no longer applies. Although the material is still elastic, the stress-strain relationship is no longer linear. If the material is deformed beyond a certain point, known as the elastic limit, it will not recover its original shape when stress is removed. Deformation in this range is said to be plastic.

For a further discussion on stress and strain and the theory of elasticity, read Johnson and De Graff (1988) chapter on the Mechanics Fundamentals.

If a stress-strain curve is plotted for a perfectly elastic solid, the result will be a straight line and its slope which represents the elastic modulus, E, will be the same for all stress levels. Although this is not the case for rocks, as the stress-strain curve is not linear but a shape determined by constituent material (Rowe, 1980). Thus, the slope of the curve, E, varies at different strain levels.

E can be represented at any point on the curve in different ways. The two most common methods are: the tangential modulus E_t, as a tangent at a point, and secondly as the secant modulus, E_s, as a secant from the origin through the point. At any point on the near linear portion of the curve, the tangential modulus will be the truest representation of E.

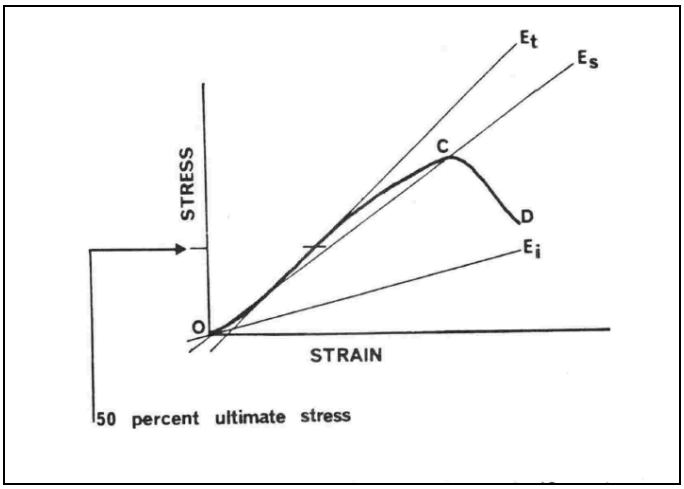

Figure 1: A complete stress-strain curve for rock (Rowe, 1980).

A-2.2.3 Elastic Parameters:

Specifying how stress and strain are to be measured, including directions, allows for many types of elastic moduli to be defined. The three primary ones are:

- Young's Modulus: also known as the tensile modulus, is a measure of the stiffness of an isotropic elastic material. It is the tendency of an object to deform along an axis when opposing forces are applied along that axis. It is defined as the ratio of the uniaxial stress over the uniaxial strain.

$$\mathbf{E = 2\,G\,(v + 1)}$$ **Equation 2**

- Shear Modulus: also known as the modulus of rigidity, is defined as the ratio of shear stress to the shear strain. It is the tendency of an object to shear (deformation of shape at constant volume) when acted upon by opposing forces.

$$G = \rho V_S^2$$

Equation 3

- Bulk Modulus: describes the volumetric elasticity. It measures a substance's resistance to uniform compression, or the tendency of an object to deform in all directions when uniformly loaded in all directions. It is defined as the volumetric stress over volumetric strain.

$$K = \frac{\lambda}{2(\lambda + \mu)}$$

Equation 4

(Kramer, 1996)

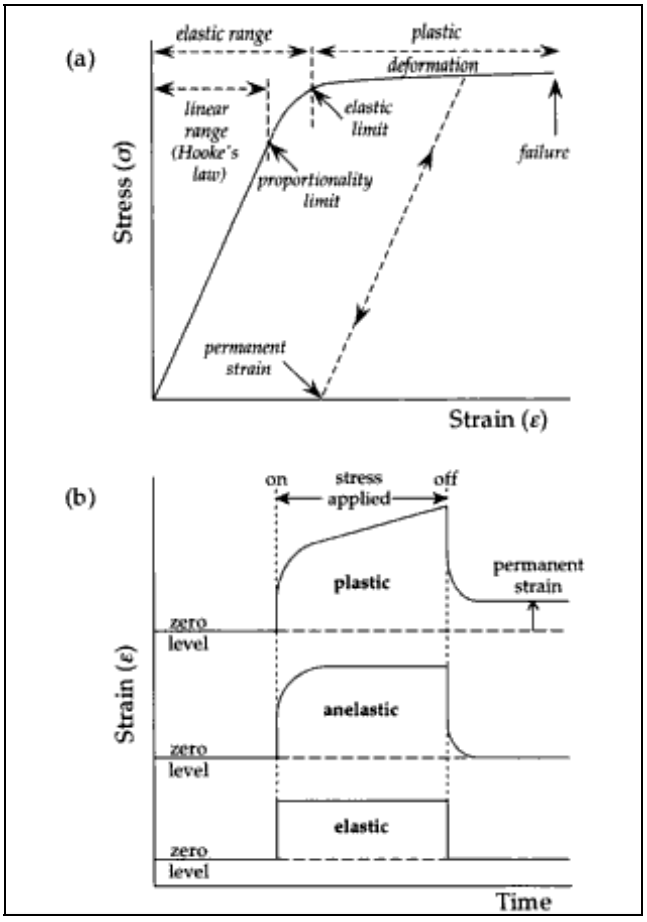

Figure 2: (a) The stress-strain relation for a hypothetical solid is linear (Hooke's Law) until the proportionality limit, and the material deforms elastically until it reaches the elastic limit; plastic

deformation produces further strain until failure occurs. (b) Variations of elastic, anelastic and plastic strains with time, during and after application of a stress. (Lowrie, 2002).

A perfectly elastic material is one that follows the same path during both the loading and unloading cycles; that is, hysteresis is zero and all the energy stored in the rock during loading is released during unloading. An elastic material is one that returns to zero strain at the end of the unloading cycle, although the loading and unloading cycles may follow different paths indicating that some energy is dissipated in the rock mass during the loading and unloading cycles (Wyllie, 1992).

Most rocks display elasticity at the hand-specimen scale. Although, when considering an insitu rock-mass there a number of contributing factors which influence its elastic behaviour. Insitu rock-masses contain fractures, fissures, bedding planes, shear zones and mineral alterations, all of which will influence the elastic reaction of the rock-mass to applied forces. This highlights the importance of insitu testing during geotechnical investigations for foundation design.

A-2.3 Determination of Elastic Modulus at Hand Specimen Scale:

Hand specimen samples of rock can be tested to determine the elastic modulus using either low strain methods, or high strain method. Low strain methods induce shear strains lower than 10^{-4} % and can be used to compute the G_{max} using the expression:

$$G_{max} = \rho V_S \qquad \textbf{Equation 5}$$

where: ρ is the mass density of the material, measured in kg/m^3.

There are two laboratory based testing methods used to determine low strain elastic constants on hand specimen samples. The first is the bender element test, which determines V_S in the laboratory, from which G_{max} can be calculated using Equation 1. This test consists of two sheets of piezoelectric material bonded together in such a way that a voltage applied to their faces causes one to expand while the other contracts, causing the entire element to bend. One of the bender elements acts as the shear wave transmitter and the other bender element as the receiver. By measuring the time travel of the wave, the wave velocity V_S is determined.

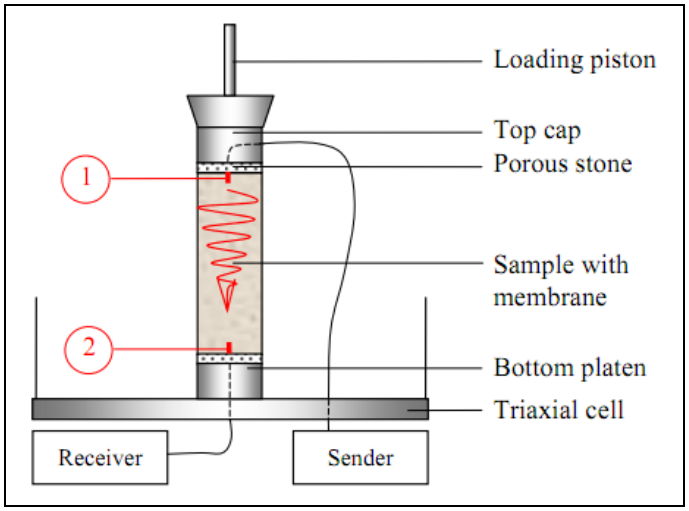

Figure 3: Bender element test setup, The generated signal is amplified to a peak-topeak amplitude of 20 V and sent to the top cap bender element (1). Caused by the electrical signal the top cap element bends in horizontal direction. This bending generates a shear wave propagating towards the bottom of the soil sample where the arriving wave generates bending of the bottom bender element (2), annotated from Karg &Haegeman (2005).

The second low strain test is the resonant column test which employs wave propagation to determine modulus and damping in cylindrical specimens of soil and rock (Drnevich, 1978). This method subjects specimens to harmonic torsional or axial loading by an electromagnetic loading system (Kramer, 1996). The loading system usually applies harmonic loads for which the frequency and amplitude can be controlled. In this test the frequency of the applied force is adjusted until resonance occurs. This frequency plus the magnitude of applied force and the magnitude of the resulting motion are used to calculate the modulus, damping, and strain amplitude (Drnevich, 1978), and V_S is calculated using Equation 4.2, from which G_{max} can be calculated using Equation 1.

$$V_s = \frac{2\omega_n h}{\pi} = 4\, f_n\, h$$

Equation 6

(Kramer, 1996)

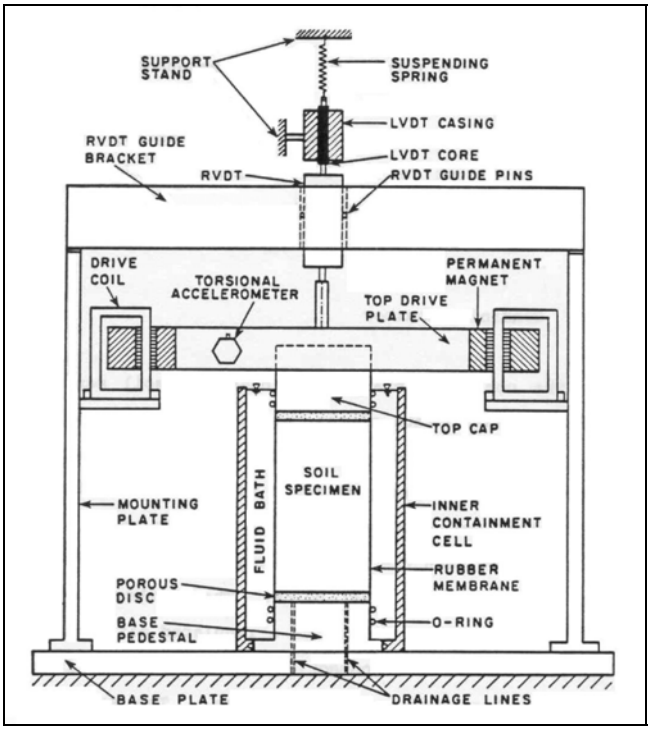

Figure 4: Cylindrical specimen undergoing resonant column test (Zavoral & Campanella, 1994).

High strain tests determine the relationship between stress and strain under particular levels of loading, and will indicate whether the soil or rock will be 'brittle' (a clear breaking or shearing point), 'elastic' (shape recoverable on unloading) or 'plastic' (shape not recoverable on unloading). The tangent or secant slope of the stress/strain curve (see Figure 1) designates the elastic modulus (E) and can be determined using either triaxial or uniaxial compressive strength testing methods for rock. These testing methods determine the intact strength of a rock sample, while its response to stress and strain is measured during the test to determine the elastic modulus.

In a conventional triaxial compression test, a cylindrical core sample is loaded axially to failure, at constant confining pressure. The peak value of the axial stress is taken as the confined compressive strength of the sample, while in addition to axial stress, axial and radial strains can be monitored during this test, for the determination of elastic constants. In order to replicate the field conditions, this test needs to confine and consolidate the soil sample back to the state of stress from which the sample was under insitu. Generally a range of confining pressures is performed during triaxial testing, from very low confining pressures to beyond the expected insitu effective stress conditions.

Compressive strength testing of intact rock can be readily measured using either a uniaxial compression machine, which required cylindrical sample of specific dimensions, or a point load tester, which can perform compression tests on unprepared core and irregular pieces of rock. The sample of rock is loaded in compression until the material fails completely which is recorded as the compressive strength of the material. During the compression test, there is a linear relationship between stress and strain which is considered the elastic response of the material, before permanent deformation occurs. Like in triaxial testing, the elastic modulus can be calculated as described by Equation 1.2. Compression testing is performed under unconfined conditions, which is unrepresentative of the insitu conditions. Hence care must be taken when applying compressive strength test results to insitu rock masses

A-2.4 Determination of Insitu Elastic Modulus:

Insitu testing is always required for full analysis and prediction of shear strength for foundation design of structures. The limitations of laboratory testing on hand specimen samples is apparent when dealing with highly fractures rock masses where acquiring intact samples of sufficient size and quantity is difficult. While the modulus of intact rock can be determined in the laboratory on pieces of core, the modulus of fractured rock masses is dependent on both the strain of intact rock and closure of the fractures, which must be determined by insitu methods (Wyllie, 1992). Both low and high-strain testing can be used insitu with a range of benefits for both methods.

There are number of different type of ground conditions where insitu testing is essential due to a range of difficulties associated with hand specimen scale testing. Very soft or sensitive soils and clays are problematic when trying to obtain undisturbed samples for laboratory testing. Gravelly soils, sands and gravels and are also problematic when trying to obtain samples for testing, with the quality of samples typically compromised during extraction due to disturbance. Therefore in situ testing is commonly used in granular soils.

Weak and fractured rock, like that of the Esk Head belt “greywacke” found at the windfarm sites in this study, are also difficult to test under hand specimen scale. The strength and compressibility of a fractured rock mass is controlled by the discontinuities (joints, fissures, faults) within it. Hence when accurate values of compressibility and elastic constants are required, insitu testing is the only option. Two high strain insitu tests which can be used to determine the elasticity of rock masses are plate load testing and pressuremeter testing.

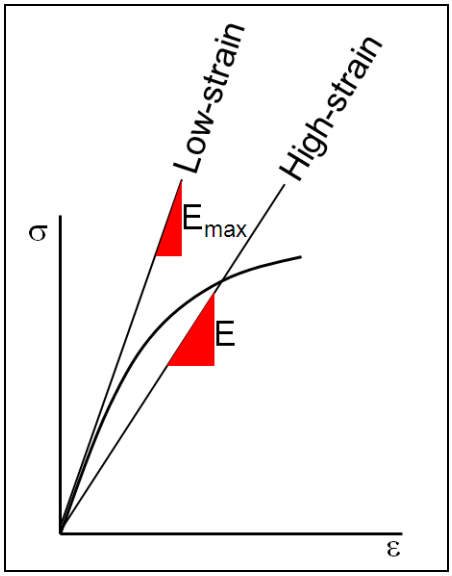

Figure 5: Difference in elastic modulus calculation, determined from a stress vs strain graph, between low-strain (E_{max}) and high-strain (E) methods.

The deformability of rock may be measured in the field by loading a rock surface and monitoring the resulting deformation. The plate load test comprises application of a compressive stress normal to the rock surface and measuring the deformation during the loading process. A relatively flat rock surface is sculptured and levelled to receive bearing plates between 50cm to 1m in diameter (Goodman, 1980). The depth of the rock volume affected by the loading is directly proportional to the diameter of the loaded area. Although with greater plate diameters it becomes difficult to apply the required compressive stresses.

Loads are applied to the plate incrementally, with a set period of time between each load cycle (usually 60min). The majority of deformation occurs in the first few minutes after loading, hence displacements are measured on a integer square basis, to ensure a greater amount of data is collected in the early stages of each load increment.

The pressuremeter test, or also referred to as the dilatometer test, is a borehole expansion experiment which exerts a uniform radial pressure on the walls of the borehole by means of a rubber sleeve. The expansion of the borehole is measured by the oil or gas flow into the sleeve as the pressure is raised (Goodman, 1980), or by potentiometers or linear variable differential transformers built inside the sleeve (Rocha et al., 1966).

As the applied pressure increases, the borehole walls deform. The pressure is held constant for a given period and the increase in volume required for maintaining the constant pressure is recorded. A load-deformation diagram and soil characteristics can be deduced by measurement of the applied pressure and change in the volume of the expanding membrane.

A-2.4.1 MASW surveying to determine insitu elastic modulus

Dynamic properties, including the elastic condition of soil and rock, can be determined insitu by induced low strain methods such as MASW. The MASW method operates at strain levels that are not large enough to induce significant nonlinear stress-strain behaviour, determining the low strain insitu elastic condition of a site. This method operates on the basis of wave propagation in linear materials, and involves the development of surface wave velocities which can be related to the low-strain modulus.

A seismic source is used to excite a pulse of waves, whose times of arrival are measured at evenly spaced receivers. The seismic source will produce P-waves, S-waves and surface waves, with the relative amplitude of each dependent on the method used to generate the impulse.

Surface wave methods are the most commonly used method for determining the insitu elastic condition of an engineering site. MASW is the most advanced method of geophysical surveying using surface waves, which replaced its predecessor Spectral Analysis of Surface Waves (SASW), and as discussed in Chapter 4, is the method of investigation used in this study. Further information regarding the MASW method can be found in Appendix A.

As dicussed in Chapter 4, MASW is a nondestructive and noninvasive seismic method to evaluate shear wave velocity, dynamic properties, material boundaries and special variations in the ground. MASW evaluates the velocity profile of the subsurface in a 1D, 2D or 3D format. MASW first measures the frequency dependant seismic surface waves (also known as Rayleigh waves) generated from various types of seismic sources, such as a sledge hammer. It then analyses the propagation velocities of those surface waves, and finally deduces shear-wave velocity (Vs) variations below the surveyed area that is most responsible for the analysed propagation velocity pattern of surface waves. As shear-wave velocity (V_S) is representative of the insitu elasticity and closely related to Young's modulus, the V_S profiles produced can be used to derive elastic conditions, or stiffness, of the subsurface.

The MASW technique investigates a hemisphere of the subsurface which is representative of the large scale insitu environment, taking into account all influencing factors, including fracturing, joint spacing, infilling and weathering variations with depth. During 1D profiling, like that used during the wind turbine investigations in this study, provide detail on the elastic condition of the large scale rock mass below the centre of the survey array, rather than the isolated properties surrounding a borehole or other type of penetrative testing technique. Therefore, the measured shear wave velocity is generally considered the most reliable means to obtain the G_{max} and subsequently E_{max} for a soil or rock deposit.

A-2.5 Influence of Confinement on Strength and Elastic Modulus:

Seismic wave velocity is strongly dependent on confining pressure, which in turn, is a product of density, gravity and depth. The confining pressure exerted at a point below the surface, acts equally in all directions, opposing the opening of fractures, and therefore increasing rock mass density.

Rowe (1982) has shown that weathering and the variation in frequency and tightness of joints results in an increase in mass modulus with depth. This increase in the modulus will continue until a depth is reached where the rock behaves as an intact mass, below which the modulus will be relatively constant with depth. This is due to joint spacing increasing and joint aperture decreasing with depth (Wyllie, 1992), which is also associated with a decrease in weathering grade. It is clearly shown in Figure 6 that density increases with a decrease in weathering grade. Along with decreasing density, weathering also leads to a decrease in strength. This is primarily due to the development of fractures in the initial stages of weathering which subsequently increases permeability (Bell, 2000).

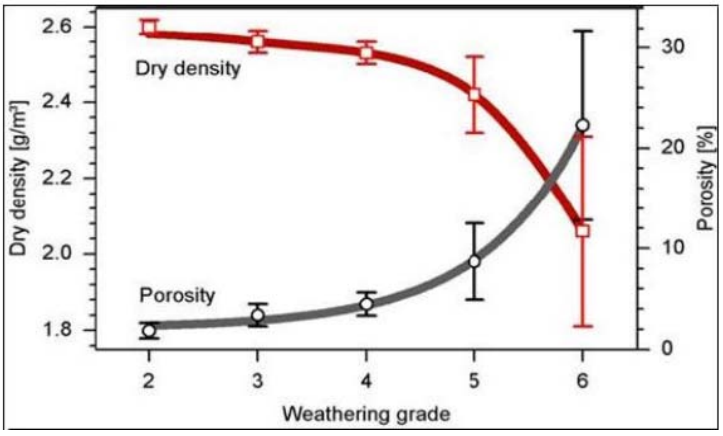

Figure 6: Correlation of weathering grade with dry density and porosity. Density decrease and porosity increased as weathering grade increased (Thuro & Scholz, 2003).

Confining pressure also has a strong influence on intact rock strength and elastic modulus. Triaxial testing of rock in the confined state is performed by uniformly applying confining stresses equally in both principal stress directions by hydraulic pressure acting on the

specimen. Triaxial testing of rock permits evaluation of rock properties under conditions which are designed to duplicate insitu confinement (Johnson & De Graff, 1988).

Rock strength increases with increasing confining stress. Figure 7 illustrates the relatively linear relationship between compressive strength (axial stress) and confining stress. Increase confinement of a specimen also will subsequently result in increased values for elastic modulus (Johnson & De Graff, 1988), as shown by Figure 8. The Mohr diagram another means which is commonly employed to graphically present the influence of confining pressure on rock strength.

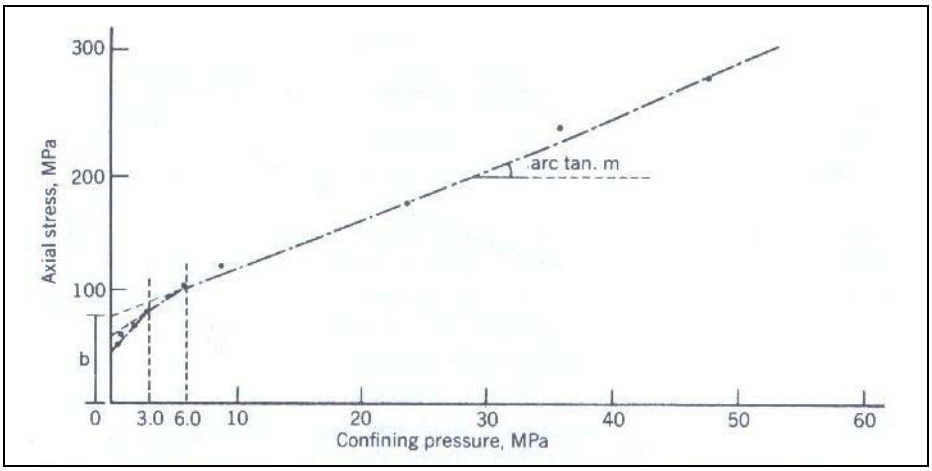

Figure 7: Influence of confining pressure on compressive strength where m = slope angle and b = cohesion (Johnson & De Graff, 1988).

A number of studies have focused on the state of effective stress in soil or rock and the impact it has on V_S (Belloti et al., 1996; Hardin & Drnevish, 1972; Stokoe et al., 1985). Effective stress represents the average stress carried by a soil skeleton, and it determined by the total stress (σ) minus the pore water pressure (υ). Basically, effective stress is the difference between confining pressure and pore pressure (Ahrens, 1995). These studies concluded that the insitu shear wave velocity increases with an increase in the state of stress.

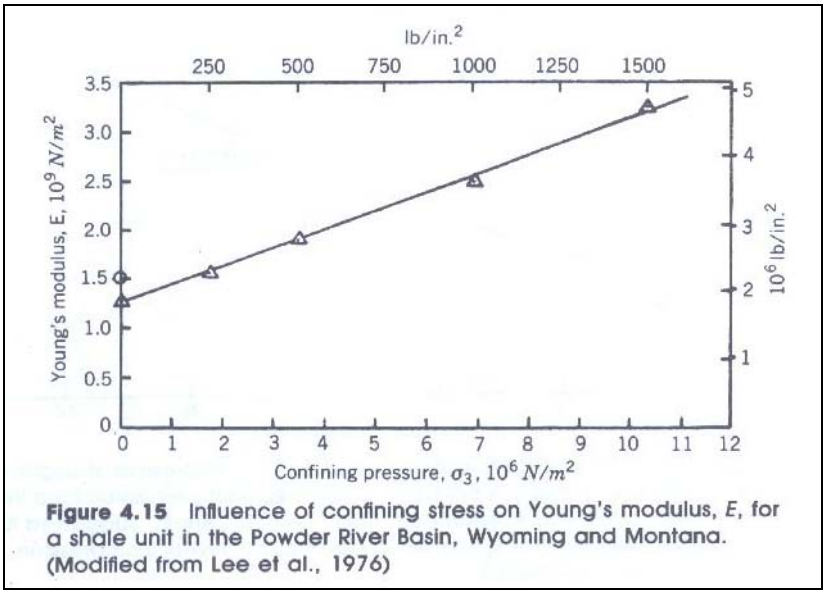

Figure 4.15 Influence of confining stress on Young's modulus, *E*, for a shale unit in the Powder River Basin, Wyoming and Montana. (Modified from Lee et al., 1976)

Figure 8: Influence of confining pressure on Young's modulus, E, for a shale unit (Johnson & De Graff, 1988).

Often in geotechnical problems, it is convenient to idealise a rock mass as being an elastic material. The suitability of this idealisation depends on the type and condition of the rock as well as the proposed loading conditions. In the case of weathered greywacke, the rock is both jointed and weathered, and its response to loading is dependent upon the insitu stresses. Under these circumstances, assigning elastic modulus values with depth must be determined through insitu testing as weathered greywacke does not present homogeneous properties.

Rock profiles may be idealised as having a linear increase in elastic modulus with depth between the surface and some depth, z_c, and a relatively constant modulus below this point.

A-2.6 Evaluation of Insitu and Laboratory Elastic Modulus Testing:

Laboratory measurements have long been the reference standard for determining the properties of geomaterials. To develop a greater confidence in the results of insitu tests, it is essential to compare field results to conventional laboratory tests. In the laboratory, parameters such as shear strain, confining pressure, frequency, number of loading cycles, void ratio and over-consolidation ratio (OCR) can be varied to analyse soil and rock response, and to try and replicate the insitu conditions (Schneider et al., 1999).

The key difference between laboratory and field measured dynamic properties is that insitu geological conditions are measured during field testing, whereas laboratory testing can only attempt to replicate these conditions. Insitu geological conditions which laboratory testing cannot replicate include fracturing, fracture spacing, infilling and wreathing profiles with depth, which are important factors which can control deformation and responses to loading. Field measured elastic moduli, or insitu testing, measures the insitu rockmass, rather than testing an intact sample in the laboratory, taken from an isolated locality, which is assumed to be representative of a much larger insitu volume. Hence, laboratory testing only gives stiffness information which is representative of a localised volume very near the drillhole or sampling site (Park & Miller, 2004). Therefore, laboratory testing values for intact hand specimens must be employed with proper judgment in engineering applications (ASTM, 2010).

Different test equipment and methods result in various stress and strain levels, so both strain dependency and stress levels must be taken into account in comparing moduli provided from different test methods, both at hand specimen and insitu scales. All tests or test procedures that characterize soil behaviour need to apply the initial stress conditions as best as possible. Insitu testing methods have the advantage that the state of stress is inherently included in the procedure. Laboratory testing at hand specimen scale need to confine and consolidate the sample, like during triaxial testing, back to the state of stress found insitu. The geophysical field tests have the advantage of testing undisturbed soil in the actual field condition with the actual effective stress and drainage conditions, additionally, what is being tested is a volume or average condition of the material between the source and receiver (Luna & Jadi, 2000).

The balanced schedule of geotechnical investigation using of both hand specimen scale laboratory testing methods along with insitu testing methods is the most practical and cost-effective way to determine strength and stiffness parameters over an entire site.

A-2.7 Elastic modulus calculations from shear wave velocity data:

The purpose of using MASW extensively at the Te Rere Hau Windfarm site during the geotechnical investigation was to determine the elastic condition of each prospective wind turbine site. Shear wave velocity (V_S) profiles determined through MASW testing were used in the calculation of elastic modulus (E) profiles, determined for their use in Finite Element Modelling (FEM) during geotechnical foundation design.

A two-step computation, detailed in Kramer (1996), relates V_S and shear moduli (G), to compute G and E. Elastic theory states that the small strain shear modulus, G can be determined from:

$$G = \rho V_S^2 \qquad \textbf{Equation 1.1}$$

where ρ is the material density

The small strain shear modulus represents the elastic stiffness of the soils at shear strain (γ) less than 10^{-4} percent. Elastic theory also states that the small strain Young's modulus (Elastic modulus), E is linked to G, as follows:

$$\mathbf{E = 2\,G\,(\nu + 1)} \qquad \textbf{Equation 1.2}$$

where ν is the Poisson's ratio of the material

Therefore when V_S is directly related to E

$$\mathbf{E = 2\,\rho\,V_S^{\,2}\,(\nu + 1)} \qquad \textbf{Equation 1.3}$$

The elastic moduli value is dependent on both density (ρ) and Poisson's ratio (ν). As discussed in Chapter 1.6, E is dependent on density (ρ) and Poisson's ratio (ν) values, which are in turn dependent on the intrinsic material properties. These material properties are strongly influenced by weathering and jointing, which are highly prevalent within weathered Greywacke. In order to derive accurate E profiles for each site, appropriate ρ and ν values that are representative of the extent of rock weathering must be selected.

A number of researchers and publications have detailed the relationship between G and V_S (Fumal, 1978; Kramer, 1996; Long & Donohue, 2007). The use of measured shear wave velocities is generally the most reliable means of evaluating the insitu value of G for a particular site. More recently, several researchers have shown that V_S (and hence, G) can be obtained most reliably and also most cost effectively by using the multichannel analysis of surface waves (MASW) technique (Donohue et al., 2003; Donohue et al., 2004; Harry et al., 2005; Kaufmann et al., 2005; Park et al., 1999).

This method of calculating E values from V_S data was developed and employed during the design of the Te Rere Hau Windfarm. Mahoney (2008; 2010) details this conversion method and its previous use at the Te Rere Hau Windfarm. Park and Miller (2005) and Park and Miller (2005) used MASW to seismically characterise the Blue Canyon Wind Mill Farm, near Lawton,

Oklahoma. These two investigations have used MASW to determine the V_S profile with depth for each turbine sites, and hence the calculation of dynamic properties at each site (of which is beyond the scope of the two reports).

Appendix C:

Te Rere Hau Windfarm Testpit Logs and Photos

aurecon
Aurecon New Zealand Limited
Level 2 Rural Bank House Telephone:+64 3 366 0821
122 Gloucester Street Facsimile:+64 3 379 6955
PO Box 1061 Email:christchurch@ap.aurecongroup.com
Christchurch - New Zealand Website: www.aurecongroup.com

Open Excavation Log

Test Pit No. **TP-TE1**

Client: NZ Windfarms Ltd	Location: Te Rere Hau Windfarm Eastern Extension		Date: 7/05/2010
Project: Te Rere Hau Windfarm Eastern	Logged By: DPM	Weather Conditions: Fine	Job Number: 30616-EASTEX

Water	Depth (m)	Soil Symbol	FACE 1 SOIL DESCRIPTION: subordinate/ main COMPONENTS, minor components, colour, structure, strength, moisture, bedding, plasticity, sensitivity, additional.
	0		Silty-TOPSOIL, brown, moist.
	0.5		Clayey-SILT, grey-yellow, moist, plastic. Material is Loess
	1		
	1.5		Clayey-SILT with some Gravel, light-grey, moist, plastic. Gravel fraction is fine to medium, angular. Material is Loess-Colluvium.
	2		
	2.5		End of TP at 2.5mbgl - 0.5m below finished construction pad level
	3		

Water	Depth (m)	Soil Symbol	FACE 2 SOIL DESCRIPTION: subordinate/ main COMPONENTS, minor components, colour, structure, strength, moisture, bedding, plasticity, sensitivity, additional.
	0		Same as Face 1
	0.5		
	1		
	1.5		
	2		
	2.5		
	3		

Undrained Shear Strength (kPa) ●
Measured Using a Hand Held Shear Vane
25 50 75 100 125 150

Scala Penetrometer Test[2] ×
(Blows/ 50mm)
2 4 6 8 10 12

Test Description
1 - Hand held shear vane test in accordance with BS1377:1990
2 - Scala Penetrometer Test in accordance with NZS4402:1986 for the first three meters

Notes
Test Pits excavated using 12t excavator

Pit dimensions
1m
2m

aurecon
Aurecon New Zealand Limited
Level 2 Rurel Bank House
122 Gloucester Street
PO Box 1061
Christchurch - New Zealand
Telephone:+64 3 366 0821
Facsimile:+64 3 379 6955
Email:christchurch@ap.aurecongroup.com
Website: www.aurecongroup.com

Open Excavation Log

Test Pit No. **TP-TE5**

Client: NZ Windfarms Ltd	Location: Te Rere Hau Windfarm Eastern Extension		Date: 7/05/2010
Project: Te Rere Hau Windfarm Eastern	Logged By: DPM	Weather Conditions: Fine	Job Number: 30616-EASTEX

Water	Depth (m)	Soil Symbol	FACE 1 SOIL DESCRIPTION: subordinate/ main COMPONENTS, minor components, colour, structure, strength, moisture, bedding, plasticity, sensitivity, additional.
	0		Gravely-Sandy-SILT, yellow-grey, moist, plastic. Gravel fraction is fine, and angular. Sand fraction is fine to course.
			Material is Loess-Colluvium.
	0.5		
			Highly weathered becoming moderately weathered, golden brown light-grey, GREYWACKE, weak, with closely spaced joints.
	1		
			End of TP at 1.1mbgl - Rock encountered.
	1.5		
	2		
	2.5		
	3		

Water	Depth (m)	Soil Symbol	FACE 2 SOIL DESCRIPTION: subordinate/ main COMPONENTS, minor components, colour, structure, strength, moisture, bedding, plasticity, sensitivity, additional.
	0		Same as Face 1
	0.5		
	1		
	1.5		
	2		
	2.5		
	3		

Undrained Shear Strength (kPa) ●
Measured Using a Hand Held Shear Vane
25 50 75 100 125 150

Scala Penetrometer Test[2] ×
(Blows/ 50mm)
2 4 6 8 10 12

Test Description
1 - Hand held shear vane test in accordance with BS1377:1990
2 - Scala Penetrometer Test in accordance with NZS4402:1986 for the first three meters

Notes
Test Pits excavated using 12t excavator

Pit dimensions
1m
2m

aurecon
Aurecon New Zealand Limited
Level 2 Rural Bank House
122 Gloucester Street
PO Box 1061
Christchurch - New Zealand
Telephone:+64 3 366 0821
Facsimile:+64 3 379 6955
Email:christchurch@ap.aurecongroup.com
Website: www.aurecongroup.com

Open Excavation Log

Test Pit No. **TP-TE6**

Client: NZ Windfarms Ltd	Location: Te Rere Hau Windfarm Eastern Extension		Date: 7/05/2010
Project: Te Rere Hau Windfarm Eastern	Logged By: DPM	Weather Conditions: Fine	Job Number: 30616-EASTEX

Water	Depth (m)	Soil Symbol	FACE 1 SOIL DESCRIPTION: subordinate/ main COMPONENTS, minor components, colour, structure, strength, moisture, bedding, plasticity, sensitivity, additional.	Water	Depth (m)	Soil Symbol	FACE 2 SOIL DESCRIPTION: subordinate/ main COMPONENTS, minor components, colour, structure, strength, moisture, bedding, plasticity, sensitivity, additional.
	0		Silty-TOPSOIL, brown, moist.		0		Same as Face 1
	0.5		Moderately weathered, golden-brown with black staining, GREYWACKE, weak, with closely spaced joints.		0.5		
	1		End of TP at 1mbgl - Rock encountered		1		
	1.5				1.5		
	2				2		
	2.5				2.5		
	3				3		

Undrained Shear Strength (kPa) ●
Measured Using a Hand Held Shear Vane
25 50 75 100 125 150

Scala Penetrometer Test[2] ×
(Blows/ 50mm)
2 4 6 8 10 12

Test Description
1 - Hand held shear vane test in accordance with BS1377:1990
2 - Scala Penetrometer Test in accordance with NZS4402:1986 for the first three meters

Notes
Test Pits excavated using 12t excavator

Pit dimensions
1m
2m

aurecon
Aurecon New Zealand Limited
Level 2 Rural Bank House
122 Gloucester Street
PO Box 1061
Christchurch - New Zealand
Telephone:+64 3 366 0821
Facsimile:+64 3 379 6955
Email:christchurch@ap.aurecongroup.com
Website: www.aurecongroup.com

Open Excavation Log

Test Pit No. **TP-TE7**

Client: NZ Windfarms Ltd	Location: Te Rere Hau Windfarm Eastern Extension		Date: 7/05/2010
Project: Te Rere Hau Windfarm Eastern	Logged By: DPM	Weather Conditions: Fine	Job Number: 30616-EASTEX

Water	Depth (m)	Soil Symbol	FACE 1 SOIL DESCRIPTION: subordinate/ main COMPONENTS, minor components, colour, structure, strength, moisture, bedding, plasticity, sensitivity, additional.	Water	Depth (m)	Soil Symbol	FACE 2 SOIL DESCRIPTION: subordinate/ main COMPONENTS, minor components, colour, structure, strength, moisture, bedding, plasticity, sensitivity, additional.
	0		Gravely-Silty-TOPSOIL, brown, moist. Gravel fraction is fine to medium.		0		Same as Face 1
	0.5		Moderately weathered with highly weathered seams, golden-brown with black staining, GREYWACKE, very weak to weak, with closely spaced joints.		0.5		
	1				1		
	1.5		End of TP at 1.3mbgl - Rock encountered		1.5		
	2				2		
	2.5				2.5		
	3				3		

Undrained Shear Strength (kPa) ●
Measured Using a Hand Held Shear Vane
25 50 75 100 125 150

Scala Penetrometer Test[2] ×
(Blows/ 50mm)
2 4 6 8 10 12

Test Description
1 - Hand held shear vane test in accordance with BS1377:1990
2 - Scala Penetrometer Test in accordance with NZS4402:1986 for the first three meters

Notes
Test Pits excavated using 12t excavator

Pit dimensions
1m
2m

aurecon
Aurecon New Zealand Limited
Level 2 Rural Bank House
122 Gloucester Street
PO Box 1061
Christchurch - New Zealand
Telephone:+64 3 366 0821
Facsimile:+64 3 379 6955
Email:christchurch@ap.aurecongroup.com
Website: www.aurecongroup.com

Open Excavation Log

Test Pit No. **TP-TE8**

Client: NZ Windfarms Ltd	Location: Te Rere Hau Windfarm Eastern Extension		Date: 7/05/2010
Project: Te Rere Hau Windfarm Eastern	Logged By: DPM	Weather Conditions: Fine	Job Number: 30616-EASTEX

Water	Depth (m)	Soil Symbol	FACE 1 — SOIL DESCRIPTION: subordinate/ main COMPONENTS, minor components, colour, structure, strength, moisture, bedding, plasticity, sensitivity, additional.	Water	Depth (m)	Soil Symbol	FACE 2 — SOIL DESCRIPTION: subordinate/ main COMPONENTS, minor components, colour, structure, strength, moisture, bedding, plasticity, sensitivity, additional.
	0		Gravely-Silty-TOPSOIL, brown, moist. Gravel fraction is fine to medium, angular.		0		Same as Face 1
	0.5		Moderately weathered golden-brown, GREYWACKE, weak to moderately strong, with very closely spaced joints. The joints are essentially free of infill material.		0.5		
	1		End of TP at 1.1mbgl - Rock encountered		1		
	1.5				1.5		
	2				2		
	2.5				2.5		
	3				3		

Undrained Shear Strength (kPa) ●
Measured Using a Hand Held Shear Vane
25 50 75 100 125 150

Scala Penetrometer Test[2] ×
(Blows/ 50mm)
2 4 6 8 10 12

Test Description
1 - Hand held shear vane test in accordance with BS1377:1990
2 - Scala Penetrometer Test in accordance with NZS4402:1986 for the first three meters

Notes
Test Pits excavated using 12t excavator

Pit dimensions
1m
2m

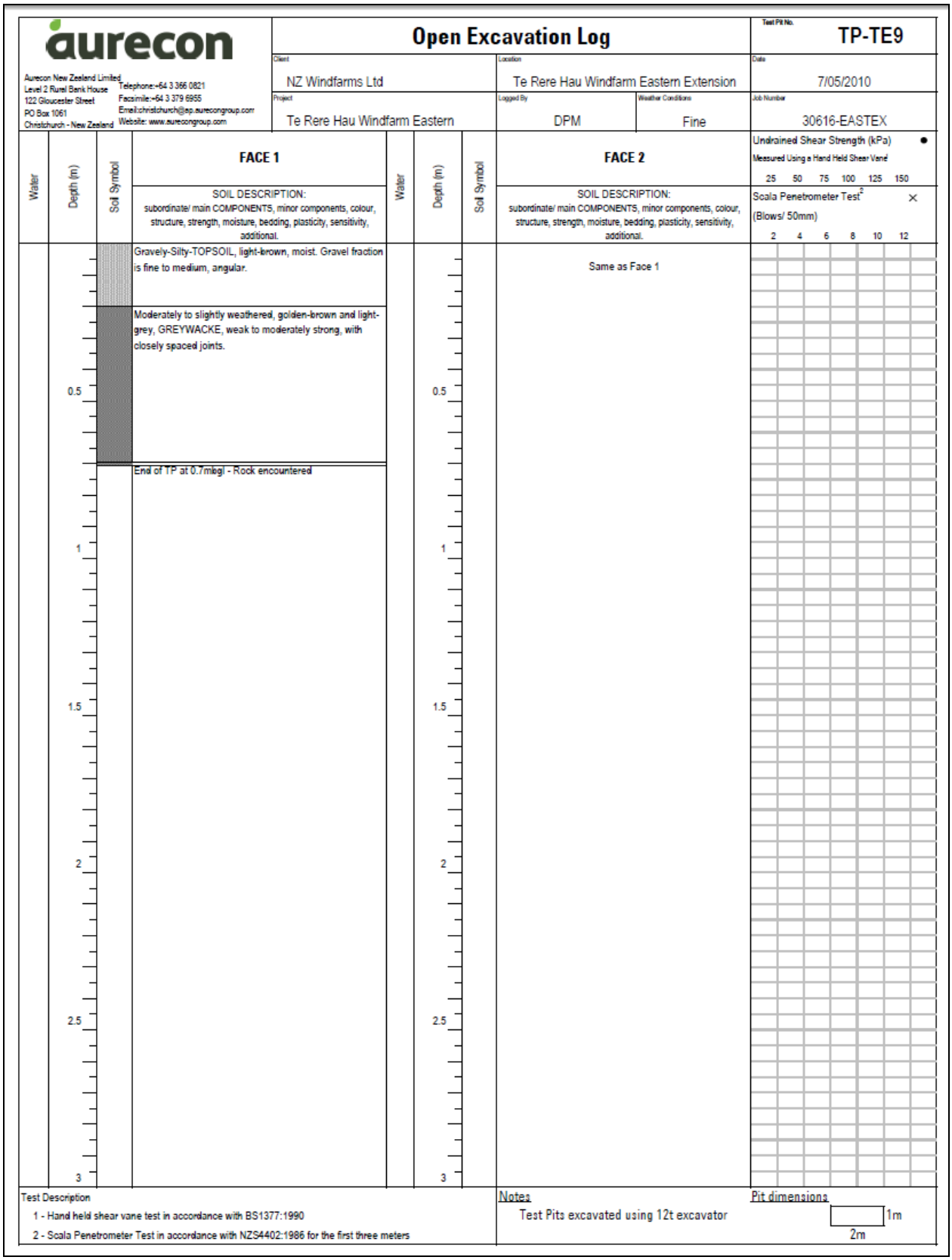

aurecon

Aurecon New Zealand Limited
Level 2 Rural Bank House
122 Gloucester Street
PO Box 1061
Christchurch - New Zealand
Telephone:+64 3 366 0821
Facsimile:+64 3 379 6955
Email:christchurch@ap.aurecongroup.com
Website: www.aurecongroup.com

Open Excavation Log

Test Pit No. **TP-TE9**

Client: NZ Windfarms Ltd	Location: Te Rere Hau Windfarm Eastern Extension		Date: 7/05/2010
Project: Te Rere Hau Windfarm Eastern	Logged By: DPM	Weather Conditions: Fine	Job Number: 30616-EASTEX

Water	Depth (m)	Soil Symbol	FACE 1 — SOIL DESCRIPTION: subordinate/ main COMPONENTS, minor components, colour, structure, strength, moisture, bedding, plasticity, sensitivity, additional.	Water	Depth (m)	Soil Symbol	FACE 2 — SOIL DESCRIPTION: subordinate/ main COMPONENTS, minor components, colour, structure, strength, moisture, bedding, plasticity, sensitivity, additional.
	0		Gravely-Silty-TOPSOIL, light-brown, moist. Gravel fraction is fine to medium, angular.		0		Same as Face 1
	0.5		Moderately to slightly weathered, golden-brown and light-grey, GREYWACKE, weak to moderately strong, with closely spaced joints.		0.5		
			End of TP at 0.7mbgl - Rock encountered				
	1				1		
	1.5				1.5		
	2				2		
	2.5				2.5		
	3				3		

Undrained Shear Strength (kPa) ●
Measured Using a Hand Held Shear Vane
25 50 75 100 125 150

Scala Penetrometer Test[2] ×
(Blows/ 50mm)
2 4 6 8 10 12

Test Description
1 - Hand held shear vane test in accordance with BS1377:1990
2 - Scala Penetrometer Test in accordance with NZS4402:1986 for the first three meters

Notes
Test Pits excavated using 12t excavator

Pit dimensions
1m
2m

aurecon

Aurecon New Zealand Limited
Level 2 Rurel Bank House
122 Gloucester Street
PO Box 1061
Christchurch - New Zealand
Telephone:+64 3 366 0821
Facsimile:+64 3 379 6955
Email:christchurch@ap.aurecongroup.com
Website: www.aurecongroup.com

Open Excavation Log

Test Pit No. **TP-TE10**

Client: NZ Windfarms Ltd	Location: Te Rere Hau Windfarm Eastern Extension		Date: 7/05/2010
Project: Te Rere Hau Windfarm Eastern	Logged By: DPM	Weather Conditions: Fine	Job Number: 30616-EASTEX

Water	Depth (m)	Soil Symbol	FACE 1 — SOIL DESCRIPTION: subordinate/ main COMPONENTS, minor components, colour, structure, strength, moisture, bedding, plasticity, sensitivity, additional.
	0		Silty-TOPSOIL, brown, moist.
	0.5		Clayey-SILT with some Gravel, yellow-grey, moist, plastic. Gravel fraction is fine to course, angular, and slightly to un-weathered. Material is Loess-Colluvium.
	1		
	1.5		Moderately to slightly weathered, golden-brown, GREYWACKE, weak to moderately strong, with closely spaced joints.
	2		End of TP at 1.5mbgl - Rock encountered
	2.5		
	3		

Water	Depth (m)	Soil Symbol	FACE 2 — SOIL DESCRIPTION: subordinate/ main COMPONENTS, minor components, colour, structure, strength, moisture, bedding, plasticity, sensitivity, additional.
	0		Same as Face 1
	0.5		
	1		
	1.5		
	2		
	2.5		
	3		

Undrained Shear Strength (kPa) ●
Measured Using a Hand Held Shear Vane
25 50 75 100 125 150

Scala Penetrometer Test[2] ×
(Blows/ 50mm)
2 4 6 8 10 12

Test Description
1 - Hand held shear vane test in accordance with BS1377:1990
2 - Scala Penetrometer Test in accordance with NZS4402:1986 for the first three meters

Notes
Test Pits excavated using 12t excavator

Pit dimensions
1m
2m

aurecon
Aurecon New Zealand Limited
Level 2 Rural Bank House
122 Gloucester Street
PO Box 1061
Christchurch - New Zealand
Telephone:+64 3 366 0821
Facsimile:+64 3 379 6955
Email:christchurch@ap.aurecongroup.com
Website: www.aurecongroup.com

Open Excavation Log

Test Pit No. **TP-TE11**

Client	Location	Date
NZ Windfarms Ltd	Te Rere Hau Windfarm Eastern Extension	7/05/2010
Project	**Logged By** / **Weather Conditions**	**Job Number**
Te Rere Hau Windfarm Eastern	DPM / Fine	30616-EASTEX

Water	Depth (m)	Soil Symbol	FACE 1 — SOIL DESCRIPTION: subordinate/ main COMPONENTS, minor components, colour, structure, strength, moisture, bedding, plasticity, sensitivity, additional.
	0		Silty-TOPSOIL, brown, moist.
	0.5		Clayey-SILT with some Gravel, grey-yellow, wet, plastic. Gravel fraction is medium to course, angular, and moderately weathered. Becoming Gravely-Clayey-SILT, grey, wet, plastic with increasing depth. Material is Loess/Loess-Colluvium becoming Loess-Colluvium with increasing depth.
	1		
	1.5		
	2		Highly to moderately weathered , light-grey, GREYWACKE, very weak to weak, with very closely spaced joints.
	2.5		End of TP at 2.2mbgl - Rock encountered
	3		

Water	Depth (m)	Soil Symbol	FACE 2 — SOIL DESCRIPTION: subordinate/ main COMPONENTS, minor components, colour, structure, strength, moisture, bedding, plasticity, sensitivity, additional.
	0		Same as Face 1
	0.5		
	1		
	1.5		
	2		
	2.5		
	3		

Undrained Shear Strength (kPa) ●
Measured Using a Hand Held Shear Vane
25 50 75 100 125 150

Scala Penetrometer Test[2] ×
(Blows/ 50mm)
2 4 6 8 10 12

Test Description

1 - Hand held shear vane test in accordance with BS1377:1990

2 - Scala Penetrometer Test in accordance with NZS4402:1986 for the first three meters

Notes

Test Pits excavated using 12t excavator

Pit dimensions

1m
2m

aurecon
Aurecon New Zealand Limited
Level 2 Rural Bank House
122 Gloucester Street
PO Box 1061
Christchurch - New Zealand
Telephone:+64 3 366 0821
Facsimile:+64 3 379 6955
Email:christchurch@ap.aurecongroup.com
Website: www.aurecongroup.com

Open Excavation Log

Test Pit No. **TP-TE12**

Client: NZ Windfarms Ltd	Location: Te Rere Hau Windfarm Eastern Extension		Date: 7/05/2010
Project: Te Rere Hau Windfarm Eastern	Logged By: DPM	Weather Conditions: Fine	Job Number: 30616-EASTEX

Undrained Shear Strength (kPa) ●
Measured Using a Hand Held Shear Vane
25 50 75 100 125 150
Scala Penetrometer Test[2] ×
(Blows/ 50mm)
2 4 6 8 10 12

Water	Depth (m)	Soil Symbol	FACE 1 — SOIL DESCRIPTION: subordinate/ main COMPONENTS, minor components, colour, structure, strength, moisture, bedding, plasticity, sensitivity, additional.
	0		Silty-TOPSOIL, brown, moist.
	0.5		Gravely-SILT with occasional Cobbles, grey-yellow, moist. Gravel fraction is fine to medium, angular, and moderately weathered. Boulders are angular, and moderately weathered. Material is Loess-Colluvium or possibly completely weathered Greywacke rock.
	1		Moderately weathered, golden-brown, GREYWACKE, weak, with very closely spaced to closely spaced joints.
	1.5		End of TP at 1.1mbgl - Excavator struggling to rip
	2		
	2.5		
	3		

Water	Depth (m)	Soil Symbol	FACE 2 — SOIL DESCRIPTION: subordinate/ main COMPONENTS, minor components, colour, structure, strength, moisture, bedding, plasticity, sensitivity, additional.
	0		Same as Face 1
	0.5		
	1		
	1.5		
	2		
	2.5		
	3		

Test Description
1 - Hand held shear vane test in accordance with BS1377:1990
2 - Scala Penetrometer Test in accordance with NZS4402:1986 for the first three meters

Notes
Test Pits excavated using 12t excavator

Pit dimensions
1m
2m

aurecon
Aurecon New Zealand Limited
Level 2 Rurel Bank House
122 Gloucester Street
PO Box 1061
Christchurch - New Zealand
Telephone:+64 3 366 0821
Facsimile:+64 3 379 6955
Email:christchurch@ap.aurecongroup.com
Website: www.aurecongroup.com

Open Excavation Log

Test Pit No. **TP-TE13**

Client: NZ Windfarms Ltd	Location: Te Rere Hau Windfarm Eastern Extension	Date: 7/05/2010	
Project: Te Rere Hau Windfarm Eastern	Logged By: DPM	Weather Conditions: Fine	Job Number: 30616-EASTEX

Water	Depth (m)	Soil Symbol	FACE 1 SOIL DESCRIPTION: subordinate/ main COMPONENTS, minor components, colour, structure, strength, moisture, bedding, plasticity, sensitivity, additional.	Water	Depth (m)	Soil Symbol	FACE 2 SOIL DESCRIPTION: subordinate/ main COMPONENTS, minor components, colour, structure, strength, moisture, bedding, plasticity, sensitivity, additional.
	0		Silty-TOPSOIL with some Gravel, brown, moist. Gravel fraction is fine to medium, and angular.		0		Same as Face 1
	0.5		Clayey-GRAVEL, light-grey orange with black staining, moist. Gravel fraction is fine to cobble in size, and highly weathered. Material is completely-weathered Greywacke rock.		0.5		
	1				1		
	1.5		End of TP at 1.5mbgl - 0.3m below finished construction pad level		1.5		
	2				2		
	2.5				2.5		
	3				3		

Undrained Shear Strength (kPa) ●
Measured Using a Hand Held Shear Vane
25 50 75 100 125 150

Scala Penetrometer Test[2] ×
(Blows/ 50mm)
2 4 6 8 10 12

Test Description
1 - Hand held shear vane test in accordance with BS1377:1990
2 - Scala Penetrometer Test in accordance with NZS4402:1986 for the first three meters

Notes
Test Pits excavated using 12t excavator

Pit dimensions
1m
2m

aurecon

Aurecon New Zealand Limited
Level 2 Rural Bank House
122 Gloucester Street
PO Box 1061
Christchurch - New Zealand
Telephone:+64 3 366 0821
Facsimile:+64 3 379 6955
Email:christchurch@ap.aurecongroup.com
Website: www.aurecongroup.com

Open Excavation Log

Test Pit No. **TP-TE14**

Client: NZ Windfarms Ltd	Location: Te Rere Hau Windfarm Eastern Extension		Date: 7/05/2010
Project: Te Rere Hau Windfarm Eastern	Logged By: DPM	Weather Conditions: Fine	Job Number: 30616-EASTEX

Water	Depth (m)	Soil Symbol	FACE 1 — SOIL DESCRIPTION: subordinate/ main COMPONENTS, minor components, colour, structure, strength, moisture, bedding, plasticity, sensitivity, additional.
	0		Silty-TOPSOIL, brown, moist.
	0.5		Clayey-SILT with occasional boulders, orange-brown, moist, plastic. Material is Loess
	1		Highly weathered, golden-brown with black staining, GREYWACKE, very weak, with closely spaced joints.
	1.5		End of TP at 1.4mbgl - Rock encountered
	2		
	2.5		
	3		

Water	Depth (m)	Soil Symbol	FACE 2 — SOIL DESCRIPTION: subordinate/ main COMPONENTS, minor components, colour, structure, strength, moisture, bedding, plasticity, sensitivity, additional.
	0		Same as Face 1
	0.5		
	1		
	1.5		
	2		
	2.5		
	3		

Undrained Shear Strength (kPa) ●
Measured Using a Hand Held Shear Vane
25 50 75 100 125 150

Scala Penetrometer Test[2] ×
(Blows/ 50mm)
2 4 6 8 10 12

Test Description
1 - Hand held shear vane test in accordance with BS1377:1990
2 - Scala Penetrometer Test in accordance with NZS4402:1986 for the first three meters

Notes
Test Pits excavated using 12t excavator

Pit dimensions
1m
2m

aurecon
Aurecon New Zealand Limited
Level 2 Rural Bank House
122 Gloucester Street
PO Box 1061
Christchurch - New Zealand
Telephone:+64 3 366 0821
Facsimile:+64 3 379 6955
Email:christchurch@ap.aurecongroup.com
Website: www.aurecongroup.com

Open Excavation Log

Test Pit No. **TP-TE14**

Client	Location	Date
NZ Windfarms Ltd	Te Rere Hau Windfarm Eastern Extension	7/05/2010
Project	**Logged By** / **Weather Conditions**	**Job Number**
Te Rere Hau Windfarm Eastern	DPM / Fine	30616-EASTEX

Water	Depth (m)	Soil Symbol	FACE 1 — SOIL DESCRIPTION: subordinate/ main COMPONENTS, minor components, colour, structure, strength, moisture, bedding, plasticity, sensitivity, additional.
	0		Silty-TOPSOIL, brown, moist.
	0.5		Clayey-SILT with occasional boulders, orange-brown, moist, plastic. Material is Loess
	1		Highly weathered, golden-brown with black staining, GREYWACKE, very weak, with closely spaced joints.
	1.5		End of TP at 1.4mbgl - Rock encountered
	2		
	2.5		
	3		

Water	Depth (m)	Soil Symbol	FACE 2 — SOIL DESCRIPTION: subordinate/ main COMPONENTS, minor components, colour, structure, strength, moisture, bedding, plasticity, sensitivity, additional.
	0		Same as Face 1
	0.5		
	1		
	1.5		
	2		
	2.5		
	3		

Undrained Shear Strength (kPa) ●
Measured Using a Hand Held Shear Vane
25 50 75 100 125 150

Scala Penetrometer Test[2] ×
(Blows/ 50mm)
2 4 6 8 10 12

Test Description
1 - Hand held shear vane test in accordance with BS1377:1990
2 - Scala Penetrometer Test in accordance with NZS4402:1986 for the first three meters

Notes
Test Pits excavated using 12t excavator

Pit dimensions
1m
2m

aurecon

Aurecon New Zealand Limited
Level 2 Rural Bank House
122 Gloucester Street
PO Box 1061
Christchurch - New Zealand
Telephone:+64 3 366 0821
Facsimile:+64 3 379 6955
Email:christchurch@ap.aurecongroup.com
Website: www.aurecongroup.com

Open Excavation Log

Test Pit No. **TP-TE20**

Client	Location	Date
NZ Windfarms Ltd	Te Rere Hau Windfarm Eastern Extension	7/05/2010
Project	**Logged By** / **Weather Conditions**	**Job Number**
Te Rere Hau Windfarm Eastern	DPM / Fine	30616-EASTEX

Water	Depth (m)	Soil Symbol	FACE 1 — SOIL DESCRIPTION: subordinate/ main COMPONENTS, minor components, colour, structure, strength, moisture, bedding, plasticity, sensitivity, additional.
	0		Silty-TOPSOIL, brown, moist.
	0.5		Moderately to slightly weathered, golden-brown orange, GREYWACKE, weak to moderately strong, with closely spaced defects.
	1		End of TP at 0.9mbgl - Excavator struggling to rip due to site topography
	1.5		
	2		
	2.5		
	3		

Water	Depth (m)	Soil Symbol	FACE 2 — SOIL DESCRIPTION: subordinate/ main COMPONENTS, minor components, colour, structure, strength, moisture, bedding, plasticity, sensitivity, additional.
	0		Same as Face 1
	0.5		
	1		
	1.5		
	2		
	2.5		
	3		

Undrained Shear Strength (kPa) ●
Measured Using a Hand Held Shear Vane
25 50 75 100 125 150

Scala Penetrometer Test[2] ×
(Blows/ 50mm)
2 4 6 8 10 12

Test Description

1 - Hand held shear vane test in accordance with BS1377:1990

2 - Scala Penetrometer Test in accordance with NZS4402:1986 for the first three meters

Notes

Test Pits excavated using 12t excavator

Pit dimensions

1m
2m

aurecon
Aurecon New Zealand Ltd
Level 4 Torens House
195 Hereford Street
PO Box 1061
Christchurch - New Zealand
Telephone: +64 3 366 0821
Facsimile: +64 3 379 6955
Email: christchurch@ap.aurecongroup.com
Website: www.aurecongroup.com

Job No: 30616-EASTEX

Job Name: Te Rere Hau Winfarm Eastern Extension

PHOTO: 1
NARRATIVE: View of test pit at TE1 with clayey-silty surfical soil encountered to depth.

PHOTO: 2
NARRATIVE: View from TE5 showing the approximate positions of TE2, TE3, and TE4 which were inaccessible with a 12t excavator during the time of the geotechnical site investigation. Therefore no test pit excavations were undertaken. DPM

aurecon
Aurecon New Zealand Ltd
Level 4 Tomens House
195 Hereford Street
PO Box 1061
Christchurch - New Zealand
Telephone: +64 3 366 0821
Facsimile: +64 3 379 6955
Email: christchurch@ap.aurecongroup.com
Website: www.aurecongroup.com

Job No: 30616-EASTEX

Job Name: Te Rere Hau Winfarm Eastern Extension

PHOTO: 3
NARRATIVE: View of test pit TE5 with highly weathered becoming moderately weathered Greywacke rock encountered from 0.7mbgl onwards.

PHOTO: 4
NARRATIVE: View of test pit TE6 with moderately weathered Greywacke rock encountered form 0.3mbgl onwards.

DPM
Creation date:10/5/2010

aurecon
Aurecon New Zealand Ltd
Level 4 Torrens House
195 Hereford Street
PO Box 1061
Christchurch - New Zealand
Telephone: +64 3 366 0821
Facsimile: +64 3 379 6955
Email: christchurch@ap.aurecongroup.com
Website: www.aurecongroup.com

Job No: 30616-EASTEX

Job Name: Te Rere Hau Winfarm Eastern Extension

PHOTO: 5
NARRATIVE: View of test pit TE7 with moderately weathered Greywacke rock encountered from 0.2mbgl onwards.

PHOTO: 6
NARRATIVE: View of test pit TE8 with moderately weathered Greywacke rock encountered from 0.2mbgl onwards.

DPM
Creation date:10/5/2010

aurecon
Aurecon New Zealand Ltd
Level 4 Tomens House
195 Hereford Street
PO Box 1061
Christchurch - New Zealand
Telephone: +64 3 366 0821
Facsimile: +64 3 379 6955
Email: christchurch@ap.aurecongroup.com
Website: www.aurecongroup.com

Job No: 30616-EASTEX

Job Name: Te Rere Hau Winfarm Eastern Extension

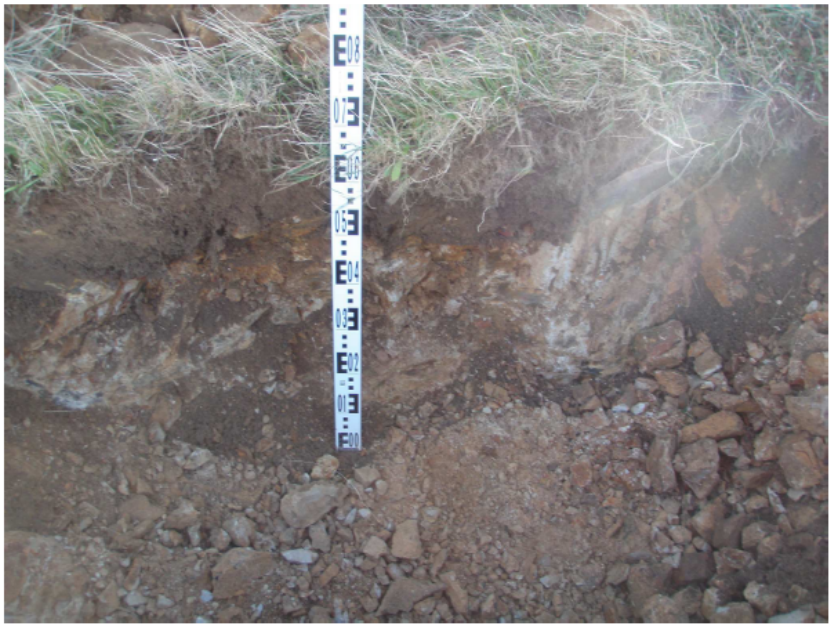

PHOTO: 7
NARRATIVE: View of test pit TE9 with moderately to slightly weathered Greywacke rock from 0.2mbgl onwards.

PHOTO: 8
NARRATIVE: View of test pit TE10 with clayey-silty material overlying moderately to slightly weathered Greywacke rock from 1.1mbgl onwards.

DPM
4
Creation date: 10/5/2010

aurecon
Aurecon New Zealand Ltd
Level 4 Torens House
195 Hereford Street
PO Box 1061
Christchurch - New Zealand
Telephone: +64 3 366 0821
Facsimile: +64 3 379 6955
Email: christchurch@ap.aurecongroup.com
Website: www.aurecongroup.com

Job No: 30616-EASTEX

Job Name: Te Rere Hau Winfarm Eastern Extension

PHOTO: 9
NARRATIVE: View of test pit TE11 with clayey-silty material overlying highly to moderately weathered Greywacke rock from 1.7mbgl onwards.

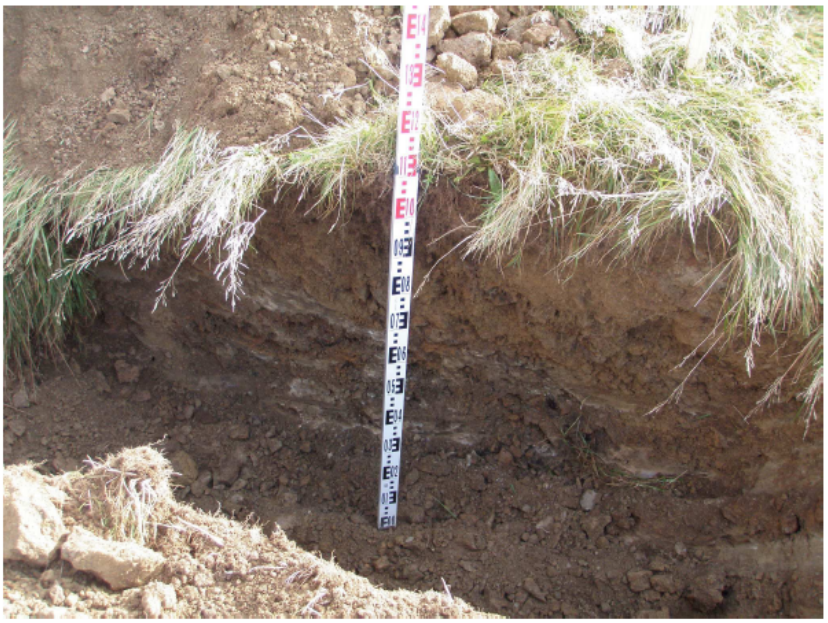

PHOTO: 10
NARRATIVE: View of test pit TE12 with gravely-silty material overlying moderately weathered Greywacke rock from 0.7mbgl onwards.

DPM
Creation date:10/5/2010

aurecon
Aurecon New Zealand Ltd
Level 4 Torrens House
195 Hereford Street
PO Box 1061
Christchurch - New Zealand
Telephone: +64 3 366 0821
Facsimile: +64 3 379 6955
Email: christchurch@ap.aurecongroup.com
Website: www.aurecongroup.com

Job No: 30616-EASTEX

Job Name: Te Rere Hau Winfarm Eastern Extension

PHOTO: 11
NARRATIVE: View of test pit TE13 with clayey-gravel material underlying the site to depth.

PHOTO: 12
NARRATIVE: View of test pit TE14 with clayey-silty soil overlying highly weathered Greywacke rock from 0.8mbgl onwards.

aurecon
Aurecon New Zealand Ltd
Level 4 Torrens House
195 Hereford Street
PO Box 1061
Christchurch - New Zealand
Telephone: +64 3 366 0821
Facsimile: +64 3 379 6955
Email: christchurch@ap.aurecongroup.com
Website: www.aurecongroup.com

Job No: 30616-EASTEX

Job Name: Te Rere Hau Winfarm Eastern Extension

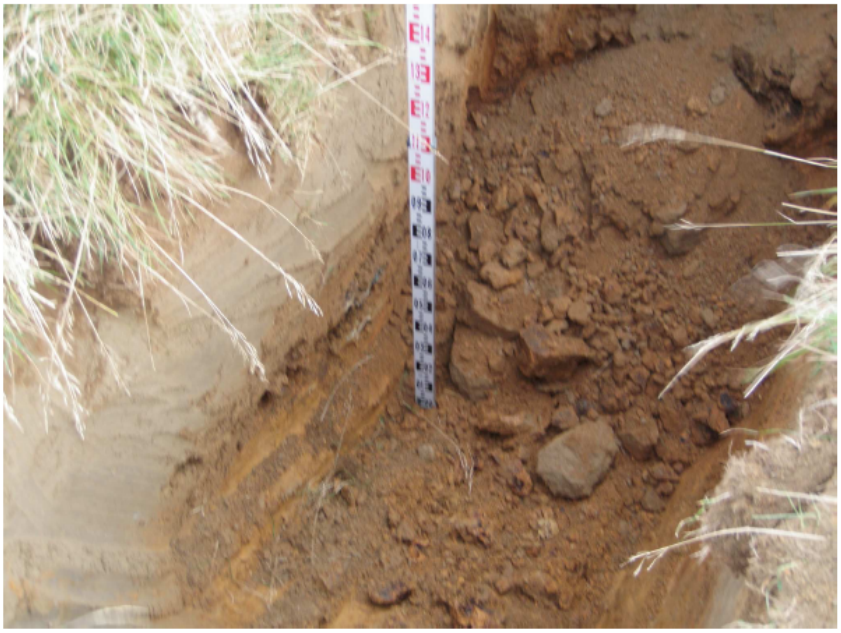

PHOTO: 13
NARRATIVE: View of test pit TE19 silt and silty-sandy material being underlain by highly weathered Greywacke rock from 1.2mbgl onwards.

PHOTO: 14
NARRATIVE: View of test pit TE20 directly underlain by moderately to slightly weathered Greywacke rock.

DPM
Creation date:10/5/2010

aurecon
Aurecon New Zealand Ltd
Level 4 Torrens House
195 Hereford Street
PO Box 1061
Christchurch - New Zealand
Telephone: +64 3 366 0821
Facsimile: +64 3 379 6955
Email: christchurch@ap.aurecongroup.com
Website: www.aurecongroup.com

Job No: 30616-EASTEX

Job Name: Te Rere Hau Winfarm Eastern Extension

PHOTO: 15
NARRATIVE: View of western side of the TE8 site.

PHOTO: 16
NARRATIVE: View of the northern approach to TE8 looking south.

aurecon
Aurecon New Zealand Ltd
Level 4 Tomens House
195 Hereford Street
PO Box 1061
Christchurch - New Zealand
Telephone: +64 3 366 0821
Facsimile: +64 3 379 6955
Email: christchurch@ap.aurecongroup.com
Website: www.aurecongroup.com

Job No: 30616-EASTEX

Job Name: Te Rere Hau Winfarm Eastern Extension

PHOTO: 17
NARRATIVE: Composite view of TE8 site with the possible collapse feature to the east (LHS).

PHOTO: 18
NARRATIVE: Composite view of the possible collapse feature at TE8.

DPM
Creation date:10/5/2010

Appendix D:

Pile Drilling Logs from Te Rere Hau Windfarm

Turbine 1	Spillite		
Depth (m)	**Soil Type**	**E (GPa)**	**Vs**
1.5	Volcanic Rock	Volcanic Rock	
3			
4.5			
6			
7.5			
9			
10.5			
11.5			

Turbine 2	Has churt / red argilite		
Depth (m)	**Soil Type**	**E (GPa)**	**Vs**
1.5	MW	0.1	**200**
3	MW/SW	0.2	**118**
4.5	MW/SW	0.4	**184**
6	SW	0.6	**294**
7.5	SW	0.6	**336**
9	SW/UW	0.6	**336**
10.5	SW/UW	0.8	**339**
11.5			

Turbine 3	Highly fractured red argilite		
Depth (m)	**Soil Type**	**E (GPa)**	**Vs**
1.5	HW	0.1	**492**
3	MW	0.3	**114**
4.5	MW	0.7	**265**
6	MW	1.2	**367**
7.5	MW/SW	1.2	**438**
9	SW	1.9	**411**
10.5			
11.5			

Turbine 4			
Depth (m)	**Soil Type**	**E (GPa)**	**Vs**
1.5	SW	No Accurate E Profile	
3	SW		
4.5	UW		
6	UW		
7.5	UW		
9			
10.5			
11.5			

Turbine 5			
Depth (m)	**Soil Type**	**E (GPa)**	**Vs**
1.5	HW	0.1	
3	HW	0.3	
4.5	HW	0.7	
6	HW	1.2	
7.5			
9			
10.5			
11.5			

Turbine 6			
Depth (m)	**Soil Type**	**E (GPa)**	**Vs**
1.5	L/LC	0.1	**422**
3	HW	0.2	**267**
4.5	HW/MW	0.2	**290**
6	MW	0.4	**469**
7.5	MW	0.7	**562**
9	MW/SW	0.7	**562**
10.5			
11.5			

Turbine 7	**Argillite at base**		
Depth (m)	**Soil Type**	**E (GPa)**	**Vs**
1.5	HW/MW	0.2	**261**
3	MW	0.2	**254**
4.5	MW	0.4	**271**
6	MW	0.7	**271**
7.5	MW	1.2	**359**
9	UW	1.7	**438**
10.5			
11.5			

Turbine 8			
Depth (m)	**Soil Type**	**E (GPa)**	**Vs**
1.5	HW/MW	0.5	**315**
3	MW	0.55	**315**
4.5	MW	0.7	**358**
6	SW	0.7	**350**
7.5	SW	0.9	**395**
9			
10.5			
11.5			

Turbine 9			
Depth (m)	**Soil Type**	**E (GPa)**	**Vs**
1.5	SW	0.4	
3	SW	0.5	
4.5	SW	0.5	
6	UW	2.8	
7.5	UW	5	
9			
10.5			
11.5			

Turbine 10			
Depth (m)	Soil Type	E (GPa)	**Vs**
1.5	HW/MW	0.5	
3	MW	0.9	
4.5	MW	1	
6	MW/SW	1	
7.5	SW	1.5	
9	SW/UW	1.5	
10.5	UW	2.5	
11.5	UW	2.5	

Turbine 11			
Depth (m)	**Soil Type**	**E (GPa)**	**Vs**
1.5	L/LC	Empirical	
3	L	Empirical	
4.5	L/LC	Empirical	
6	HW/MW	Empirical	
7.5	HW/MW	Empirical	
9	HW/MW	Empirical	
10.5	HW/MW	Empirical	
11.5	HW/MW	Empirical	

Turbine 17			
Depth (m)	Soil Type	E (GPa)	**Vs**
1.5	HW	0.4	**376**
3	HW	0.4	**273**
4.5	MW	0.7	**365**
6	MW	1.3	**591**
7.5	SW	2	**591**
9	SW	2	**591**
10.5	UW	3	**550**
11.5	UW	3	**550**

Turbine 23			
Depth (m)	**Soil Type**	**E (GPa)**	**Vs**
1.5		Empirical	
3		Empirical	
4.5		Empirical	
6		Empirical	
7.5		Empirical	
9		Empirical	
10.5		Empirical	
11.5		Empirical	

Turbine 24			
Depth (m)	**Soil Type**	**E (GPa)**	**Vs**
1.5		Empirical	
3		Empirical	
4.5		Empirical	
6		Empirical	
7.5		Empirical	
9		Empirical	
10.5		Empirical	
11.5		Empirical	

Turbine 25			
Depth (m)	**Soil Type**	**E (GPa)**	**Vs**
1.5		Empirical	
3		Empirical	
4.5		Empirical	
6		Empirical	
7.5		Empirical	
9		Empirical	
10.5		Empirical	
11.5		Empirical	

Turbine 26			
Depth (m)	**Soil Type**	**E (GPa)**	**Vs**
1.5		Empirical	
3		Empirical	
4.5		Empirical	
6		Empirical	
7.5		Empirical	
9		Empirical	
10.5		Empirical	
11.5		Empirical	

Turbine 27			
Depth (m)	**Soil Type**	**E (GPa)**	**Vs**
1.5		Empirical	
3		Empirical	
4.5		Empirical	
6		Empirical	
7.5		Empirical	
9		Empirical	
10.5		Empirical	
11.5		Empirical	

Turbine 28			
Depth (m)	Soil Type	E (GPa)	**Vs**
1.5	MW	0.25	**346**
3	MW/SW	0.5	**330**
4.5	UW	0.5	**330**
6	UW	0.8	**315**
7.5	UW	1.5	**382**
9	UW	1.5	**485**
10.5			
11.5			

Turbine 29			
Depth (m)	**Soil Type**	**E (GPa)**	**Vs**
1.5	L	0.1	
3	HW	0.1	
4.5	HW/MW	0.7	
6	MW	1.3	
7.5	MW	1.3	
9	MW	1.6	
10.5			
11.5			

Turbine 30			
Depth (m)	**Soil Type**	**E (GPa)**	**Vs**
1.5	L	0.1	
3	L	0.1	
4.5	L/LC	0.1	
6	HW	0.7	
7.5	MW	1.3	
9	MW	1.3	
10.5	MW/SW	1.6	
11.5	SW	1.6	

Turbine 31			
Depth (m)	**Soil Type**	**E (GPa)**	**Vs**
1.5	L/LC	0.25	
3	L/LC	0.25	
4.5	MW	0.6	
6	MW/SW	0.8	
7.5	MW/SW	1.35	
9			
10.5			
11.5			

Turbine 32			
Depth (m)	**Soil Type**	**E (GPa)**	**Vs**
1.5	HW	0.4	
3	HW/MW	0.6	
4.5	MW	0.6	
6	MW	0.8	
7.5	MW	1.3	
9	MW/SW	1.3	
10.5	SW	1.7	
11.5	UW	1.7	

Turbine 33			
Depth (m)	**Soil Type**	**E (GPa)**	**Vs**
1.5	L/LC	0.1	**342**
3	CW/HW	0.2	**95**
4.5	HW	0.4	**282**
6	HW/MW	0.9	**368**
7.5	MW	1.5	**430**
9	SW	2.8	**543**
10.5	SW/UW	2.8	**543**
11.5	SW/UW	2.8	**543**

Turbine 34			
Depth (m)	**Soil Type**	**E (GPa)**	**Vs**
1.5	L	0.1	**721**
3	L/LC	0.5	**403**
4.5	MW/SW	0.8	**314**
6	SW	2.6	**457**
7.5	SW	2.6	**1046**
9	SW/UW	2.6	
10.5	UW	2.6	
11.5	UW	2.6	

Turbine 35			
Depth (m)	**Soil Type**	**E (GPa)**	**Vs**
1.5	L	0.2	**234**
3	C	0.3	**209**
4.5	CSW	0.75	**279**
6	SW	1.2	**279**
7.5	SW/UW	1.5	**334**
9	UW	2.1	**376**
10.5			
11.5			

Turbine 36			
Depth (m)	**Soil Type**	**E (GPa)**	**Vs**
1.5	LC	0.2	**684**
3	MW	0.4	**755**
4.5	MW	1.1	**829**
6	MW/SW	2.2	**816**
7.5	MW/SW	2.8	**816**
9	SW	2.8	**633**
10.5	SW/UW	3.6	**402**
11.5			

Turbine 37			
Depth (m)	**Soil Type**	**E (GPa)**	**Vs**
1.5	LC	0.3	**427**
3	LC	0.9	**344**
4.5	MW	4	**504**
6	MW	2.9	**785**
7.5	HW/MW	2.7	**669**
9			
10.5			
11.5			

Turbine 38			
Depth (m)	**Soil Type**	**E (GPa)**	**Vs**
1.5	L	0.1	**418**
3	C	0.2	**411**
4.5	HW	0.4	**369**
6	HW/MW	0.6	**367**
7.5	SW	0.8	**480**
9	SW	1.1	**480**
10.5	UW	1.1	**571**
11.5	UW	1.1	**571**

Turbine 52			
Depth (m)	**Soil Type**	**E (GPa)**	**Vs**
1.5	C	0.2	**417**
3	HW/MW	0.5	**859**
4.5	MW	0.5	**387**
6	MW/SW	1.1	**387**
7.5	SW	2	**263**
9	SW	2.3	**773**
10.5			
11.5			

Turbine 53			
Depth (m)	**Soil Type**	**E (GPa)**	**Vs**
1.5	LC	0.1	**680**
3	HW	0.25	**720**
4.5	HW/MW	0.6	**748**
6	MW/SW	0.8	**748**
7.5	MW/SW	1.1	**628**
9	SW	1.7	**289**
10.5	SW	4.8	**289**
11.5			

Turbine 54			
Depth (m)	**Soil Type**	**E (GPa)**	**Vs**
1.5	C	0.2	**626**
3	MW	0.2	**1035**
4.5	SW	1	**619**
6	UW	3.8	**405**
7.5	UW	7.7	**405**
9	UW	7.7	**762**
10.5	UW	7.7	**1093**
11.5			

Turbine 55			
Depth (m)	**Soil Type**	**E (GPa)**	**Vs**
1.5	LC	0.2	**265**
3	HW	0.2	**222**
4.5	MW	0.5	**218**
6	SW	1	**303**
7.5	SW	1.5	**412**
9	SW	1.5	**492**
10.5	SW	1.9	**492**
11.5	SW/UW	1.9	**548**

Turbine 56			
Depth (m)	**Soil Type**	**E (GPa)**	**Vs**
1.5	CW	0.1	
3	CW	0.1	
4.5	CW	0.2	
6	HW	0.3	
7.5	MW/SW	0.3	
9	SW	0.4	
10.5	UW	0.5	
11.5			

Turbine 57			
Depth (m)	**Soil Type**	**E (GPa)**	**Vs**
1.5	RS/L	0.1	
3	RS	0.1	
4.5	MW	0.2	
6	MW	0.3	
7.5	M/SW	0.3	
9	SW/UW	0.4	
10.5			
11.5			

Turbine 58			
Depth (m)	**Soil Type**	**E (GPa)**	**Vs**
1.5	LC	0.4	**385**
3	MW	0.8	**385**
4.5	MW/SW	0.8	**374**
6	MW/SW	0.9	**383**
7.5	SW	0.9	**395**
9	SW	1.2	**395**
10.5			
11.5			

Turbine 59			
Depth (m)	**Soil Type**	**E (GPa)**	**Vs**
1.5	CW	0.5	**327**
3	HW	0.5	**310**
4.5	MW	0.8	**326**
6	SW	0.9	**375**
7.5	UW	1.1	**375**
9	UW	2.1	**436**
10.5			
11.5			

Turbine 46			
Depth (m)	**Soil Type**	**E (GPa)**	**Vs**
1.5	LC	0.06	**162**
3	CW	0.16	**178**
4.5	HW	0.28	**213**
6	HW/MW	0.46	**265**
7.5	MW	0.67	**320**
9	MW	1.94	**373**
10.5	MW		
11.5	MW		

Turbine 47			
Depth (m)	**Soil Type**	**E (GPa)**	**Vs**
1.5	L	0.07	**145**
3	L/LC	0.23	**230**
4.5	HW/MW	0.32	**262**
6	HW/MW	0.34	**264**
7.5	MW	No E profile	
9	MW/SW	No E profile	
10.5	SW	No E profile	
11.5	UW	No E profile	

Turbine 48			
Depth (m)	**Soil Type**	**E (GPa)**	**Vs**
1.5	HW	Empirical	
3	HW	Empirical	
4.5	MW/SW	Empirical	
6	MW/SW	Empirical	
7.5	MW/SW	Empirical	
9	MW/SW	Empirical	
10.5	SW	Empirical	
11.5	SW	Empirical	

Turbine 49			
Depth (m)	**Soil Type**	**E (GPa)**	**Vs**
1.5	HW	0.2	**344**
3	HW	0.42	**290**
4.5	HW/MW	0.59	**334**
6	MW	1.84	**334**
7.5	MW/SW	2.25	**534**
9	MW/SW	2.51	**623**
10.5	SW/UW	1.75	**623**
11.5	UW	1.75	**623**

Turbine 50			
Depth (m)	**Soil Type**	**E (GPa)**	**Vs**
1.5	MW	0.4	**409**
3	SW	0.8	**397**
4.5	SW	0.8	**384**
6	SW	0.9	**376**
7.5	UW	1.1	**406**
9	UW	1.3	**432**
10.5	UW	1.7	**432**
11.5	UW	1.7	**516**

Turbine 51			
Depth (m)	**Soil Type**	**E (GPa)**	**Vs**
1.5	L	0.18	**288**
3	LC	0.42	**272**
4.5	CW/HW	0.67	**319**
6	MW/SW	1.00	**393**
7.5	MW/SW	1.23	**449**
9	SW	1.57	**449**
10.5	UW	1.70	**494**
11.5	UW	2.00	**494**

Turbine 65			
Depth (m)	**Soil Type**	**E (GPa)**	**Vs**
1.5	L		
3	RS		
4.5	RS		
6	RS		
7.5	RS		
9	-		
10.5	-		
11.5	-		

Turbine 72			
Depth (m)	**Soil Type**	**E (GPa)**	**Vs**
1.5	HW/MW	0.15	**241**
3	SW/UW	1.63	**241**
4.5	UW	2.24	**502**
6	UW	2.83	**502**
7.5	UW	4.12	**662**
9	UW	4.50	**662**
10.5	UW	4.50	**995**
11.5	UW	4.50	**995**

Turbine 73			
Depth (m)	**Soil Type**	**E (GPa)**	**Vs**
1.5	L/LC	0.04	**305**
3	Hw	0.42	**267**
4.5	MW	0.95	**386**
6	MW	1.2	**422**
7.5	MW	1.53	**461**
9	MW/SW	1.86	**537**
10.5	SW	2.48	**537**
11.5	SW	2.53	**626**

Turbine 74			
Depth (m)	**Soil Type**	**E (GPa)**	**Vs**
1.5	L	0.07	**115**
3	L	0.19	**203**
4.5	CW	0.32	**243**
6	CW/HW	0.41	**275**
7.5	HW/MW	0.51	**311**
9	MW	0.72	**311**
10.5	MW	1.05	**363**
11.5	MW	1.1	**363**

Turbine 75			
Depth (m)	**Soil Type**	**E (GPa)**	**Vs**
1.5	L	0.09	**116**
3	L	0.29	**216**
4.5	HW	0.3	**247**
6	HW/MW	0.73	**365**
7.5	MW	1.09	**365**
9	MW	1.13	**433**
10.5	HW/MW	1.13	**433**
11.5	HW/MW	1.12	**433**

Turbine 76			
Depth (m)	**Soil Type**	**E (GPa)**	**Vs**
1.5	L	0.12	**225**
3	L	0.15	**232**
4.5	CW/HW	0.36	**271**
6	HW	0.64	**347**
7.5	HW	0.66	**347**
9	HW	0.67	**350**
10.5	HW/MW	0.67	
11.5	HW/MW		

Turbine 77			
Depth (m)	**Soil Type**	**E (GPa)**	**Vs**
1.5	L/LC	0.11	**168**
3	HW	0.33	**270**
4.5	CW/HW	0.47	**268**
6	HW/MW	0.92	**328**
7.5	HW/MW		
9	HW/MW		
10.5	CW/HW		
11.5	HW		

Turbine 78			
Depth (m)	**Soil Type**	**E (GPa)**	**Vs**
1.5	L	0.08	**105**
3	L	0.21	**206**
4.5	CW/HW	0.33	**209**
6	HW/MW	0.63	**278**
7.5	MW	0.73	**354**
9	MW	0.78	**369**
10.5	MW	0.83	**369**
11.5	MW	-	

Turbine 79			
Depth (m)	**Soil Type**	**E (GPa)**	**Vs**
1.5	L	0.06	106
3	L	0.3	361
4.5	HW	0.42	272
6	HW	1.05	298
7.5	CW/HW	1.55	457
9	CW/HW	2.1	529
10.5	HW/MW	2.1	529
11.5	HW/MW	2.1	529

Turbine 80			
Depth (m)	**Soil Type**	**E (GPa)**	**Vs**
1.5		Empirical	
3		Empirical	
4.5		Empirical	
6		Empirical	
7.5		Empirical	
9		Empirical	
10.5		Empirical	
11.5		Empirical	

Turbine 84			
Depth (m)	**Soil Type**	**E (GPa)**	**Vs**
1.5	L/LC	0.1	**103**
3	CW	0.2	**245**
4.5	CW/HW	0.5	**269**
6	HW	1	**386**
7.5	HW	1.15	**440**
9	HW/MW	1.2	**435**
10.5	MW	No E profile	
11.5	MW/SW	No E profile	

Turbine 85			
Depth (m)	**Soil Type**	**E (GPa)**	**Vs**
1.5	L/LC	0.02	**77**
3	L/LC	0.5	**289**
4.5	MW	0.65	**344**
6	SW	0.9	**400**
7.5	SW	1.55	**400**
9	UW	Red Argillite	**491**
10.5	UW		**595**
11.5	UW		

Turbine 86			
Depth (m)	**Soil Type**	**E (GPa)**	**Vs**
1.5	L/LC	0.05	**184**
3	CW/HW	0.15	**184**
4.5	HW	0.4	**257**
6	HW	0.7	**335**
7.5	HW/MW	0.95	**401**
9	MW	1.25	**401**
10.5	MW/SW	1.6	**448**
11.5	HW/MW	1.75	**448**

Turbine 87			
Depth (m)	**Soil Type**	**E (GPa)**	**Vs**
1.5	HW	0.1	**284**
3	HW	0.28	**236**
4.5	HW/MW	0.6	**267**
6	MW	1.2	**403**
7.5	MW	1.5	**454**
9	MW	2	**421**
10.5	SW	2.4	**421**
11.5	SW/UW	2.7	**499**

Turbine 88			
Depth (m)	**Soil Type**	**E (GPa)**	**Vs**
1.5	CW/HW	0.1	**299**
3	HW/MW	0.28	**198**
4.5	HW/MW	0.6	**271**
6	HW/MW	1.2	**392**
7.5	HW/MW	1.5	**484**
9	MW	2	**484**
10.5	SW	2.4	**559**
11.5	SW	2.7	**559**

Turbine 96			
Depth (m)	**Soil Type**	**E (GPa)**	**Vs**
1.5m	LC	Empirical	**90**
3.0m	CW	Weathered Spilite	**331**
4.5m	CW		**277**
6.0m	CW		**363**
7.5m	CW/HW		**363**
9.0m	HW		**499**
10.5m	MW	Empirical	
11.5m	MW/SW	Empirical	

Turbine 97			
Depth (m)	**Soil Type**	**E (GPa)**	**Vs**
1.5m	L	0.05	**210**
3.0m	LC	0.27	**213**
4.5m	HW	0.58	**292**
6.0m	HW/MW	0.95	**355**
7.5m	MW	1.41	**423**
9.0m	MW	1.73	**502**
10.5m	MW	2.12	**502**
11.5m	MW	2.12	**573**

Turbine 103			
Depth (m)	**Soil Type**	**E (GPa)**	**Vs**
1.5	HW	0.15	**366**
3	MW	0.3	**147**
4.5	MW/SW	1.3	**251**
6	SW	1.55	**466**
7.5	UW	1.75	**519**
9	UW	1.8	**519**
10.5	-	-	
11.5	-	-	

Turbine 104			
Depth (m)	**Soil Type**	**E (GPa)**	**Vs**
1.5	HW	Empirical	**412**
3	MW	Empirical	**384**
4.5	MW/SW	Empirical	**384**
6	SW/UW	Empirical	**383**
7.5	UW	Empirical	**458**
9	UW	Empirical	**458**
10.5			
11.5			

Turbine 201			
Depth (m)	**Soil Type**	**E (GPa)**	**Vs**
1	RS	Empirical	
2	CW	Empirical	
3	CW	Empirical	
4	CW/HW	Empirical	
5	HW/MW	Empirical	
6	HW/MW	Empirical	
7	MW	Empirical	
8	MW	Empirical	
9	MW/SW	Empirical	
10	SW	Empirical	
11.5	SW	Empirical	

Turbine 202			
Depth (m)	**Soil Type**	**E (GPa)**	**Vs**
1	MS/SW	Empirical	
2	MS/SW	Empirical	
3	MS/SW	Empirical	
4	MS/SW	Empirical	
5	SW	Empirical	
6	SW	Empirical	
7	S	Empirical	
8	SW/UW	Empirical	
9	UW	Empirical	
10	UW	Empirical	
11.5	UW	Empirical	

Turbine 203			
Depth (m)	**Soil Type**	**E (GPa)**	**Vs**
1	LC	0.05	359
2	LC	0.15	312
3	LC	0.18	197
4	SW	0.36	303
5	SW	0.69	508
6	SW	1.67	508
7	SW/UW	2.15	664
8	SW/UW	2.85	664
9	SW/UW	3.01	766
10	SW/UW	3.79	766
11.5	SW/UW	3.79	782

Turbine 204			
Depth (m)	**Soil Type**	**E (GPa)**	**Vs**
1	CW/HW	0.1	428
2	MW	0.2	326
3	SW	0.96	489
4	SW	1.53	674
5	SW	1.9	674
6	SW	2	570
7	SW	2.1	570
8	SW	2.55	748
9	SW	3.61	748
10	SW/UW	3.61	748
11.5	SW/UW	9.5	1046

Turbine 205			
Depth (m)	**Soil Type**	**E (GPa)**	**Vs**
1	RS	0.19	865
2	MW/SW	0.56	731
3	MW/SW	0.93	731
4	MW/SW	1.11	430
5	MW/SW	1.95	659
6	SW	2.8	659
7	SW/UW	4.98	997
8	SW/UW	6.43	997
9	SW/UW	5	864
10	SW/UW	5	864
11.5	UW	5	864

Turbine 206			
Depth (m)	**Soil Type**	**E (GPa)**	**Vs**
1	MW/SW	Empirical	
2	MW/SW	Empirical	
3	MW/SW	Empirical	
4	SW	Empirical	
5	SW	Empirical	
6	S	Empirical	
7	S	Empirical	
8	S	Empirical	
9	SW/US	Empirical	
10	SW/US	Empirical	
11.5	SW/US	Empirical	

Turbine 207			
Depth (m)	**Soil Type**	**E (GPa)**	**Vs**
1	RS	Empirical	
2	MW	Empirical	
3	MW	Empirical	
4	MW	Empirical	
5	MW/SW	Empirical	
6	MW/SW	Empirical	
7	SW	Empirical	
8	SW	Empirical	
9	SW/UW	Empirical	
10	UW	Empirical	
11.5	UW	Empirical	

Turbine 208			
Depth (m)	**Soil Type**	**E (GPa)**	**Vs**
1	MW	0.33	348
2	MW	3	292
3	MW/SW	3.5	244
4	MW/SW	3.76	419
5	SW	2.7	720
6	SW	1.04	762
7	SW	1.25	762
8	SW/UW	3.44	762
9	SW/UW	3.44	762
10	SW/UW	-	762
11.5	SW/UW	-	762

Turbine 209			
Depth (m)	**Soil Type**	**E (GPa)**	**Vs**
1	MW/SW	0.12	586
2	MW/SW	0.36	545
3	MW/SW	0.58	343
4	MW/SW	0.63	343
5	MW/SW	0.54	324
6	MW/SW	1.46	727
7	MW/SW	3.42	727
8	MW/SW	3.9	940
9	MW/SW	5.72	940
10	MW/SW	5.72	940
11.5	MW/SW	3.6	940

Turbine 210			
Depth (m)	**Soil Type**	**E (GPa)**	**Vs**
1	MW/SW	0.06	737
2	MW/SW	0.19	358
3	SW	0.25	236
4	SW	1.75	543
5	SW	3.43	767
6	SW	4.34	898
7	SW/UW	5.22	898
8	UW	6	1002
9	UW	6.5	1002
10	UW	10	1598
11.5	UW	16.5	1598

Turbine 211			
Depth (m)	**Soil Type**	**E (GPa)**	**Vs**
1	LC	0.1	500
2	SW	0.3	247
3	SW	0.32	477
4	SW	3.11	693
5	SW	4.8	693
6	SW	7.42	865
7	SW	11	1312
8	UW	11	1312
9	UW	11	1312
10	UW	11	1312
11.5	UW	11	1312

Turbine 212			
Depth (m)	**Soil Type**	**E (GPa)**	**Vs**
1	SW	0.1	593
2	SW	0.3	564
3	SW/UW	0.7	429
4	UW	3.4	369
5	UW	5.07	369
6	UW	7.68	725
7	UW	7.68	725
8	UW	7.68	1090
9	UW	9.07	1090
10	UW	9.07	1185
11.5	UW	9.07	1185

Turbine 213			
Depth (m)	**Soil Type**	**E (GPa)**	**Vs**
1	HW	0.02	497
2	HW	0.06	454
3	HW	0.1	463
4	HW	0.13	160
5	HW	0.28	258
6	HW	0.66	625
7	HW/MW	2.52	625
8	HW/MW	2.74	788
9	MW	4.01	788
10	SW	4.01	788
11.5	SW	4.3	832

Turbine 214			
Depth (m)	**Soil Type**	**E (GPa)**	**Vs**
1	HW	0.04	288
2	HW	0.1	257
3	HW	0.32	152
4	HW	0.4	276
5	HW	0.5	496
6	HW	0.53	496
7	HW	0.53	321
8	HW	0.45	321
9	HW	0.43	294
10	HW	3.79	294
11.5	HW/MW	3.79	765

Turbine 219			
Depth (m)	**Soil Type**	**E (GPa)**	**Vs**
1	HW	0.07	350
2	HW/MW	0.14	330
3	MW	0.27	276
4	MW	0.38	276
5	MW	0.4	296
6	MW	0.43	296
7	MW	0.8	296
8	MW	1.06	422
9	MW	1.26	422
10	MW	1.73	422
11.5	MW	1.73	518

Turbine 220			
Depth (m)	**Soil Type**	**E (GPa)**	**Vs**
1	MW	Empirical	
2	MW/SW	Empirical	
3	SW	Empirical	
4	SW	Empirical	
5	SW/UW	Empirical	
6	SW/UW	Empirical	
7	SW/UW	Empirical	
8	SW/UW	Empirical	
9	SW/UW	Empirical	
10	UW	Empirical	
11.5	UW	Empirical	

Turbine 232			
Depth (m)	**Soil Type**	**E (GPa)**	**Vs**
1	SW	0.07	466
2	SW	0.21	481
3	UW	0.35	421
4	UW	0.49	421
5	UW	0.58	336
6	UW	0.92	540
7	UW	1.88	540
8	UW	2.54	780
9	UW	3.93	780
10	UW	3.93	780
11.5	UW	3.25	709

Turbine 234			
Depth (m)	**Soil Type**	**E (GPa)**	**Vs**
1	L	0.02	116
2	L/LC	0.05	120
3	CW	0.17	204
4	CW	0.29	245
5	CW/HW	0.32	253
6	MW	0.34	268
7	HW	0.35	268
8	HW/MW	1.04	434
9	HW/MW	1.03	
10	HW/MW	-	
11.5	HW/MW	-	

Turbine 238			
Depth (m)	**Soil Type**	**E (GPa)**	**Vs**
1	HW	0.12	583
2	MW/SW	0.36	559
3	MW/SW	0.6	496
4	MW/SW	0.84	496
5	MW/SW	1	415
6	MW/SW	1.1	416
7	SW	1.1	416
8	SW	1.33	573
9	UW	1.12	573
10	UW	2.12	573
11.5	UW	3.8	771

Turbine 240			
Depth (m)	**Soil Type**	**E (GPa)**	**Vs**
1	SW	0.09	409
2	SW	0.37	361
3	SW	1.58	295
4	SW	2.3	295
5	SW	4.2	565
6	SW	4.38	806
7	SW	5.66	806
8	SW	5.66	936
9	SW	4.99	936
10	SW/UW	4.6	936
11.5	SW/UW	4.6	844

Turbine 241			
Depth (m)	**Soil Type**	**E (GPa)**	**Vs**
1	MW	Empirical	
2	MW/SW	Empirical	
3	SW	Empirical	
4	SW	Empirical	
5	SW	Empirical	
6	SW	Empirical	
7	SW	Empirical	
8	SW	Empirical	
9	SW	Empirical	
10	SW	Empirical	
11.5	SW	Empirical	

Turbine 242			
Depth (m)	**Soil Type**	**E (GPa)**	**Vs**
1	CW/HW	0.07	407
2	CW/HW	0.21	418
3	HW	0.35	291
4	HW	0.42	291
5	MW	0.49	327
6	MW	0.55	327
7	MW	1.21	568
8	MW	2.09	568
9	MW	2.07	560
10	SW	2.03	560
11.5	MW/SW	2.03	626

Turbine 243			
Depth (m)	**Soil Type**	**E (GPa)**	**Vs**
1	HW	0.04	269
2	HW	0.09	221
3	HW/MW	0.25	381
4	MW	0.81	381
5	MW	0.89	399
6	MW	0.93	408
7	HW	0.97	408
8	MW/SW	1.17	510
9	SW	1.68	510
10	SW	1.68	510
11.5	SW	2.3	600

Turbine 244			
Depth (m)	**Soil Type**	**E (GPa)**	**Vs**
1	HW	0.4	115
2	HW	0.15	519
3	HW	0.3	200
4	HW/MW	0.39	203
5	HW/MW	0.75	369
6	MW/SW	1.69	519
7	SW	1.84	519
8	SW	2.31	598
9	MW/SW	2.31	598
10	SW/UW	4.89	870
11.5	SW/UW	4.89	870

Turbine 246			
Depth (m)	**Soil Type**	**E (GPa)**	**Vs**
1	MW	Empirical	
2	MW/SW	Empirical	
3	MW/SW	Empirical	
4	SW	Empirical	
5	SW/UW	Empirical	
6	SW/UW	Empirical	
7	UW	Empirical	
8	UW	Empirical	
9	UW	Empirical	
10	UW	Empirical	
11.5	UW	Empirical	

Turbine 247			
Depth (m)	**Soil Type**	**E (GPa)**	**Vs**
1		Empirical	
2		Empirical	
3		Empirical	
4		Empirical	
5		Empirical	
6		Empirical	
7		Empirical	
8		Empirical	
9		Empirical	
10		Empirical	
11.5		Empirical	

Turbine 248			
Depth (m)	**Soil Type**	**E (GPa)**	**Vs**
1		Empirical	
2		Empirical	
3		Empirical	
4		Empirical	
5		Empirical	
6		Empirical	
7		Empirical	
8		Empirical	
9		Empirical	
10		Empirical	
11.5		Empirical	

Turbine 249			
Depth (m)	**Soil Type**	**E (GPa)**	**Vs**
1		Empirical	
2		Empirical	
3		Empirical	
4		Empirical	
5		Empirical	
6		Empirical	
7		Empirical	
8		Empirical	
9		Empirical	
10		Empirical	
11.5		Empirical	

Turbine 250			
Depth (m)	**Soil Type**	**E (GPa)**	**Vs**
1		Empirical	
2		Empirical	
3		Empirical	
4		Empirical	
5		Empirical	
6		Empirical	
7		Empirical	
8		Empirical	
9		Empirical	
10		Empirical	
11.5		Empirical	

Turbine 251			
Depth (m)	**Soil Type**	**E (GPa)**	**Vs**
1		Empirical	
2		Empirical	
3		Empirical	
4		Empirical	
5		Empirical	
6		Empirical	
7		Empirical	
8		Empirical	
9		Empirical	
10		Empirical	
11.5		Empirical	

Turbine 252			
Depth (m)	**Soil Type**	**E (GPa)**	**Vs**
1		Empirical	
2		Empirical	
3		Empirical	
4		Empirical	
5		Empirical	
6		Empirical	
7		Empirical	
8		Empirical	
9		Empirical	
10		Empirical	
11.5		Empirical	

Appendix E:

Density Testing Results

Density Testing: Submersion Method

	Bulk Mass	Saturated surface Dry Mass	Grain Weight/Dry Mass	Submerged Mass	Water Density	Pore Volume	Bulk Volume	Dry Density	Weathering Grade
	M (grams)	Msat (grams)	Ms (grams)	Msub (grams)	Pw (kg/m^3)	Vv (cm^3)	V (cm^3)	(kg/m^3)	
Test 1	2125.4	2156.2	2116.6	1330.59	1000	0.0396	825.61	**2560**	SW
Test 2	3104.8	3176.6	3094.6	1930.5	1000	0.082	1246.1	**2480**	SW (red argillite)
Test 3	1959.8	1992.4	1955.3	1221.2	1000	0.0371	771.2	**2540**	SW
Test 4	2621.3	2695.4	2611.5	1627.3	1000	0.0839	1068.1	**2440**	MW/SW

Density Testing: Sampling Tube and Oil Replacement Methods

	Insitu volume	Metal tray + insitu sample mass	Metal tray + dry sample	Tray mass	Insitu mass	Dry mass	Insitu Density	Dry Density	Weathering grade
	(mL)	(grams)	(grams)	(grams)	(grams)	(grams)	(kg/m^3)	(kg/m^3)	
Test 5	918.915	1346.4	1064.4	13.77	1332.63	1050.63	1450	**1140**	HW
Test 6	918.915	1463.0	1186.5	13.9	1449.1	1172.6	1580	**1280**	HW
Test 7	2000	4575.0	4300	1113	3462	3187	1730	**1590**	HW-MW
Test 8	918.915	1589.7	1305.4	14.02	1575.68	1291.38	1710	**1410**	CW (red argillite)
Test 9	915	1399.7	1177.2	13.91	1385.79	1163.29	1510	**1270**	HW-MW
Test 10	918.915	1448.2	1037.5	14.2	1434	1023.3	1560	**1110**	CW
Test 11	918.915	1451.1	1017.7	13.02	1438.08	1004.68	1560	**1090**	CW
Test 12	975	2390.9	2105.8	557.71	1833.19	1548.09	1880	**1590**	HW
Test 13	918.915	1477.0	1011.2	13.13	1463.87	998.07	1590	**1090**	CW
Test 14	1340	3583.3	3195.9	1135.3	2448	2060.6	1830	**1540**	HW

Appendix F:

Poisson's Ratio Results and V_P and V_S Profiles

Poisson's ratio was calculated using the following equation from Christensen (1996):

$$\nu = \frac{1}{2}\left[1 - \frac{1}{\left(\frac{V_P}{V_S}\right)^2 - 1}\right]$$

Completely Weathered					
Borehole	**Depth**	**V_S**	**V_P**	**V_P/V_S**	**Poisson's Ratio**
D06 - Vs	3	480	910	1.895833333	0.307
F01-Vs	3	380	830	2.184210526	0.367
D06 - Vs	3.25	460	910	1.97826087	0.328
F01-Vs	3.25	380	830	2.184210526	0.367
D06 - Vs	3.5	460	910	1.97826087	0.328
F01-Vs	3.5	380	830	2.184210526	0.367
H13-Vs	9.25	530	1170	2.20754717	0.371
H13-Vs	9.5	530	1170	2.20754717	0.371
H13-Vs	9.75	530	1170	2.20754717	0.371
H13-Vs	10	530	1170	2.20754717	0.371
H13-Vs	10.25	500	1170	2.34	0.388
K07-Vs	13.75	600	2400	4	0.467
K07-Vs	14	600	2400	4	0.467
K07-Vs	14.25	600	2400	4	0.467
K07-Vs	14.5	600	2400	4	0.467
				Average	**0.387**

Highly-Completely Weathered					
Borehole	**Depth**	**V_S**	**V_P**	**V_P/V_S**	**Poisson's Ratio**
H13-Vs	1.25	400	1170	2.925	0.434
H18-Vs	1.25	480	1020	2.125	0.358
H13-Vs	1.5	400	1170	2.925	0.434
H18-Vs	1.5	480	1020	2.125	0.358
H13-Vs	1.75	400	1170	2.925	0.434
H18-Vs	1.75	480	1020	2.125	0.358
H13-Vs	2	400	1170	2.925	0.434
H18-Vs	2	480	1020	2.125	0.358
H13-Vs	2.25	430	1170	2.720930233	0.422
H18-Vs	2.25	440	1020	2.318181818	0.386
H13-Vs	2.5	430	1170	2.720930233	0.422
H18-Vs	2.5	440	1020	2.318181818	0.386
H13-Vs	2.75	430	1170	2.720930233	0.422
H18-Vs	2.75	440	1020	2.318181818	0.386
H13-Vs	3	430	1170	2.720930233	0.422

H18-Vs	3	440	1020	2.318181818	0.386
H13-Vs	3.25	470	1170	2.489361702	0.404
H18-Vs	3.25	420	1020	2.428571429	0.398
H13-Vs	3.5	470	1170	2.489361702	0.404
H18-Vs	3.5	420	1020	2.428571429	0.398
D06 - Vs	3.75	460	910	1.97826087	0.328
F01-Vs	3.75	470	830	1.765957447	0.264
H13-Vs	3.75	470	1170	2.489361702	0.404
H18-Vs	3.75	420	1020	2.428571429	0.398
D06 - Vs	4	460	910	1.97826087	0.328
F01-Vs	4	470	830	1.765957447	0.264
H13-Vs	4	470	1170	2.489361702	0.404
H18-Vs	4	420	1020	2.428571429	0.398
D06 - Vs	4.25	490	910	1.857142857	0.296
F01-Vs	4.25	470	830	1.765957447	0.264
H13-Vs	4.25	560	1170	2.089285714	0.351
D06 - Vs	4.5	490	910	1.857142857	0.296
F01-Vs	4.5	470	830	1.765957447	0.264
H13-Vs	4.5	560	1170	2.089285714	0.351
D06 - Vs	4.75	490	910	1.857142857	0.296
H13-Vs	4.75	560	1170	2.089285714	0.351
D06 - Vs	5	490	910	1.857142857	0.296
H13-Vs	5	560	1170	2.089285714	0.351
D06 - Vs	5.25	430	910	2.11627907	0.356
H13-Vs	5.25	540	1170	2.166666667	0.365
D06 - Vs	5.5	430	910	2.11627907	0.356
H13-Vs	5.5	540	1170	2.166666667	0.365
D06 - Vs	5.75	430	910	2.11627907	0.356
H13-Vs	5.75	540	1170	2.166666667	0.365
D06 - Vs	6	430	910	2.11627907	0.356
H13-Vs	6	540	1170	2.166666667	0.365
D06 - Vs	6.25	450	910	2.022222222	0.338
H13-Vs	6.25	540	1170	2.166666667	0.365
D06 - Vs	6.5	450	910	2.022222222	0.338
H13-Vs	6.5	540	1170	2.166666667	0.365
D06 - Vs	6.75	450	910	2.022222222	0.338
H13-Vs	6.75	540	1170	2.166666667	0.365
D06 - Vs	7	450	2050	4.555555556	0.475
H13-Vs	7	540	1170	2.166666667	0.365
D06 - Vs	7.25	560	2050	3.660714286	0.460
H13-Vs	7.25	500	1170	2.34	0.388
D06 - Vs	7.5	560	2050	3.660714286	0.460
D06 - Vs	7.75	560	2050	3.660714286	0.460
D06 - Vs	8	560	2050	3.660714286	0.460
D06 - Vs	8.25	480	2050	4.270833333	0.471
D06 - Vs	8.5	480	2050	4.270833333	0.471

H13-Vs	8.5	460	1170	2.543478261	0.409
D06 - Vs	8.75	480	2050	4.270833333	0.471
H13-Vs	8.75	460	1170	2.543478261	0.409
D06 - Vs	9	480	2050	4.270833333	0.471
H13-Vs	9	460	1170	2.543478261	0.409
D06 - Vs	9.25	580	2050	3.534482759	0.456
H13-Vs	10.5	500	1170	2.34	0.388
H13-Vs	10.75	500	1170	2.34	0.388
H13-Vs	11	500	1170	2.34	0.388
H13-Vs	11.25	470	1170	2.489361702	0.404
H13-Vs	11.5	470	1170	2.489361702	0.404
H13-Vs	11.75	470	1170	2.489361702	0.404
K07-Vs	12.75	630	2400	3.80952381	0.463
K07-Vs	13	630	2400	3.80952381	0.463
K07-Vs	13.25	630	2400	3.80952381	0.463
K07-Vs	13.5	630	2400	3.80952381	0.463
H18-Vs	18.25	800	1370	1.7125	0.241
H18-Vs	18.5	800	1370	1.7125	0.241
H18-Vs	18.75	800	1370	1.7125	0.241
H18-Vs	19	800	1370	1.7125	0.241
				Average	**0.379**

Highly Weathered					
Borehole	**Depth**	**V_S**	**V_P**	**V_P/V_S**	**Poisson's Ratio**
K07-Vs	3	630	1200	1.904761905	0.310
H23-Vs	3.25	460	1040	2.260869565	0.378
K07-Vs	3.25	630	1200	1.904761905	0.310
H23-Vs	3.5	460	1040	2.260869565	0.378
K07-Vs	3.5	630	1200	1.904761905	0.310
H23-Vs	3.75	460	1040	2.260869565	0.378
K07-Vs	3.75	680	1200	1.764705882	0.264
H23-Vs	4	460	1040	2.260869565	0.378
K07-Vs	4	680	1200	1.764705882	0.264
K07-Vs	4.25	680	1200	1.764705882	0.264
K07-Vs	4.5	680	1200	1.764705882	0.264
K07-Vs	4.75	790	1200	1.518987342	0.118
K07-Vs	5	790	1200	1.518987342	0.118
K07-Vs	5.25	790	1200	1.518987342	0.118
H18-Vs	5.5	490	1020	2.081632653	0.350
K07-Vs	5.5	790	1200	1.518987342	0.118
H18-Vs	5.75	490	1020	2.081632653	0.350
K07-Vs	5.75	740	1200	1.621621622	0.193
F01-Vs	6	620	1120	1.806451613	0.279
H18-Vs	6	490	1020	2.081632653	0.350
K07-Vs	6	740	1200	1.621621622	0.193

F01-Vs	6.25	620	1120	1.806451613	0.279
H18-Vs	6.25	540	1020	1.888888889	0.305
K07-Vs	6.25	740	1200	1.621621622	0.193
H18-Vs	6.5	540	1020	1.888888889	0.305
K07-Vs	6.5	740	1200	1.621621622	0.193
H18-Vs	6.75	540	1020	1.888888889	0.305
K07-Vs	6.75	760	1200	1.578947368	0.165
B02-Vs	7	740	1760	2.378378378	0.393
K07-Vs	7	760	2400	3.157894737	0.444
B02-Vs	7.25	740	1760	2.378378378	0.393
K07-Vs	7.25	760	2400	3.157894737	0.444
B02-Vs	7.5	740	1760	2.378378378	0.393
H13-Vs	7.5	500	1170	2.34	0.388
K07-Vs	7.5	760	2400	3.157894737	0.444
B02-Vs	7.75	690	1760	2.550724638	0.409
H13-Vs	7.75	500	1170	2.34	0.388
H18-Vs	7.75	500	1020	2.04	0.342
K07-Vs	7.75	740	2400	3.243243243	0.447
B02-Vs	8	690	1760	2.550724638	0.409
H13-Vs	8	500	1170	2.34	0.388
H18-Vs	8	500	1020	2.04	0.342
H23-Vs	8	470	1040	2.212765957	0.372
K07-Vs	8	740	2400	3.243243243	0.447
B02-Vs	8.25	690	1760	2.550724638	0.409
H13-Vs	8.25	460	1170	2.543478261	0.409
H23-Vs	8.25	500	1040	2.08	0.350
K07-Vs	8.25	740	2400	3.243243243	0.447
B02-Vs	8.5	690	1760	2.550724638	0.409
H23-Vs	8.5	500	1040	2.08	0.350
B02-Vs	8.75	730	1760	2.410958904	0.396
B02-Vs	9	730	1760	2.410958904	0.396
B02-Vs	9.25	730	1760	2.410958904	0.396
B02-Vs	9.5	730	1760	2.410958904	0.396
D06 - Vs	9.5	580	2050	3.534482759	0.456
B02-Vs	9.75	800	1760	2.2	0.370
D06 - Vs	9.75	580	2050	3.534482759	0.456
B02-Vs	10	800	1760	2.2	0.370
D06 - Vs	10	580	2050	3.534482759	0.456
B02-Vs	10.25	800	1760	2.2	0.370
D06 - Vs	10.25	640	2050	3.203125	0.446
H23-Vs	10.25	470	1040	2.212765957	0.372
B02-Vs	10.5	800	1760	2.2	0.370
D06 - Vs	10.5	640	2050	3.203125	0.446
H23-Vs	10.5	470	1040	2.212765957	0.372
B02-Vs	10.75	1070	1760	1.644859813	0.207
D06 - Vs	10.75	640	2050	3.203125	0.446

H23-Vs	10.75	470	1040	2.212765957	0.372
D06 - Vs	11	640	2050	3.203125	0.446
H23-Vs	11	470	1040	2.212765957	0.372
D06 - Vs	11.25	780	2050	2.628205128	0.415
H18-Vs	11.25	530	1020	1.924528302	0.315
H23-Vs	11.25	530	1040	1.962264151	0.325
D06 - Vs	11.5	780	2050	2.628205128	0.415
H18-Vs	11.5	530	1020	1.924528302	0.315
D06 - Vs	11.75	780	2050	2.628205128	0.415
H18-Vs	11.75	530	1020	1.924528302	0.315
D06 - Vs	12	780	2050	2.628205128	0.415
H13-Vs	12	470	1170	2.489361702	0.404
H18-Vs	12	530	1020	1.924528302	0.315
D06 - Vs	12.25	780	2050	2.628205128	0.415
F01-Vs	12.25	620	1890	3.048387097	0.440
H13-Vs	12.25	520	1170	2.25	0.377
H18-Vs	12.25	590	1020	1.728813559	0.249
F01-Vs	12.5	620	1890	3.048387097	0.440
H13-Vs	12.5	520	1170	2.25	0.377
H18-Vs	12.5	590	1020	1.728813559	0.249
F01-Vs	12.75	620	1890	3.048387097	0.440
H13-Vs	12.75	520	1170	2.25	0.377
H18-Vs	12.75	590	1020	1.728813559	0.249
H13-Vs	13	520	1170	2.25	0.377
H18-Vs	13	590	1020	1.728813559	0.249
H13-Vs	13.25	710	1170	1.647887324	0.209
H18-Vs	13.25	690	1020	1.47826087	0.078
H13-Vs	13.5	710	1170	1.647887324	0.209
H18-Vs	13.5	690	1020	1.47826087	0.078
H13-Vs	13.75	710	1170	1.647887324	0.209
H18-Vs	13.75	690	1020	1.47826087	0.078
H13-Vs	14	710	1170	1.647887324	0.209
H18-Vs	14	690	1020	1.47826087	0.078
H13-Vs	14.25	640	1170	1.828125	0.287
H13-Vs	14.5	640	1170	1.828125	0.287
H13-Vs	14.75	640	1170	1.828125	0.287
K07-Vs	14.75	750	2400	3.2	0.446
H13-Vs	15	640	1170	1.828125	0.287
K07-Vs	15	750	2400	3.2	0.446
H13-Vs	15.25	570	1170	2.052631579	0.344
K07-Vs	15.25	750	2400	3.2	0.446
H13-Vs	15.5	570	1170	2.052631579	0.344
K07-Vs	15.5	750	2400	3.2	0.446
H13-Vs	15.75	570	1170	2.052631579	0.344
K07-Vs	15.75	750	2400	3.2	0.446
H13-Vs	16	570	1170	2.052631579	0.344

H13-Vs	16.25	620	1170	1.887096774	0.305
H13-Vs	18	730	1170	1.602739726	0.181
H13-Vs	18.25	660	1170	1.772727273	0.267
H13-Vs	18.5	660	1170	1.772727273	0.267
				Average	**0.333**

Moderately-Highly Weathered					
Borehole	**Depth**	**V_S**	**V_P**	**V_P/V_S**	**Poisson's Ratio**
B02-Vs	4	640	1760	2.75	0.424
B02-Vs	4.25	640	1760	2.75	0.424
H18-Vs	4.25	560	1020	1.821428571	0.284
H23-Vs	4.25	480	1040	2.166666667	0.365
B02-Vs	4.5	640	1760	2.75	0.424
H18-Vs	4.5	560	1020	1.821428571	0.284
H23-Vs	4.5	480	1040	2.166666667	0.365
B02-Vs	4.75	720	1760	2.444444444	0.400
H18-Vs	4.75	560	1020	1.821428571	0.284
H23-Vs	4.75	480	1040	2.166666667	0.365
B02-Vs	5	720	1760	2.444444444	0.400
H18-Vs	5	560	1020	1.821428571	0.284
H23-Vs	5	480	1040	2.166666667	0.365
B02-Vs	5.25	720	1760	2.444444444	0.400
H18-Vs	5.25	490	1020	2.081632653	0.350
H23-Vs	5.25	500	1040	2.08	0.350
B02-Vs	5.5	720	1760	2.444444444	0.400
H23-Vs	5.5	500	1040	2.08	0.350
B02-Vs	5.75	630	1760	2.793650794	0.427
H23-Vs	5.75	500	1040	2.08	0.350
B02-Vs	6	630	1760	2.793650794	0.427
H23-Vs	6	500	1040	2.08	0.350
B02-Vs	6.25	630	1760	2.793650794	0.427
H23-Vs	6.25	520	1040	2	0.333
B02-Vs	6.5	630	1760	2.793650794	0.427
F01-Vs	6.5	620	1120	1.806451613	0.279
H23-Vs	6.5	520	1040	2	0.333
B02-Vs	6.75	740	1760	2.378378378	0.393
F01-Vs	6.75	640	1120	1.75	0.258
H23-Vs	6.75	520	1040	2	0.333
F01-Vs	7	640	1120	1.75	0.258
H18-Vs	7	540	1020	1.888888889	0.305
H23-Vs	7	520	1040	2	0.333
F01-Vs	7.25	640	1120	1.75	0.258
H18-Vs	7.25	500	1020	2.04	0.342

H23-Vs	7.25	470	1040	2.212765957	0.372
F01-Vs	7.5	640	1120	1.75	0.258
H18-Vs	7.5	500	1020	2.04	0.342
H23-Vs	7.5	470	1040	2.212765957	0.372
F01-Vs	7.75	620	1120	1.806451613	0.279
H23-Vs	7.75	470	1040	2.212765957	0.372
F01-Vs	8	620	1120	1.806451613	0.279
F01-Vs	8.25	620	1120	1.806451613	0.279
F01-Vs	8.5	620	1120	1.806451613	0.279
F01-Vs	8.75	690	1120	1.623188406	0.194
F01-Vs	9	690	1890	2.739130435	0.423
F01-Vs	9.25	690	1890	2.739130435	0.423
F01-Vs	9.5	690	1890	2.739130435	0.423
F01-Vs	9.75	720	1890	2.625	0.415
F01-Vs	10	720	1890	2.625	0.415
F01-Vs	10.25	720	1890	2.625	0.415
H18-Vs	10.75	610	1020	1.672131148	0.222
B02-Vs	11	1070	2670	2.495327103	0.404
H18-Vs	11	610	1020	1.672131148	0.222
B02-Vs	11.25	1070	2670	2.495327103	0.404
B02-Vs	11.5	1070	2670	2.495327103	0.404
H23-Vs	11.5	530	1040	1.962264151	0.325
B02-Vs	11.75	1170	2670	2.282051282	0.381
H23-Vs	11.75	530	1040	1.962264151	0.325
B02-Vs	12	1170	2670	2.282051282	0.381
H23-Vs	12	530	1040	1.962264151	0.325
B02-Vs	12.25	1170	2670	2.282051282	0.381
H23-Vs	12.25	610	1040	1.704918033	0.238
B02-Vs	12.5	1170	2670	2.282051282	0.381
H23-Vs	12.5	610	1040	1.704918033	0.238
B02-Vs	12.75	1280	2670	2.0859375	0.351
H23-Vs	12.75	610	1040	1.704918033	0.238
B02-Vs	13	1280	2670	2.0859375	0.351
H23-Vs	13	610	1040	1.704918033	0.238
B02-Vs	13.25	1280	2670	2.0859375	0.351
H23-Vs	13.25	500	1040	2.08	0.350
B02-Vs	13.5	1280	2670	2.0859375	0.351
H23-Vs	13.5	500	1040	2.08	0.350
B02-Vs	13.75	1250	2670	2.136	0.360
H23-Vs	13.75	500	1040	2.08	0.350
B02-Vs	14	1250	2670	2.136	0.360
H23-Vs	14	500	1040	2.08	0.350
B02-Vs	14.25	1250	2670	2.136	0.360
H23-Vs	14.25	600	1040	1.733333333	0.251
B02-Vs	14.5	1250	2670	2.136	0.360
H23-Vs	14.5	600	1280	2.133333333	0.359

B02-Vs	14.75	1320	2670	2.022727273	0.338
H23-Vs	14.75	600	1280	2.133333333	0.359
B02-Vs	15	1320	2670	2.022727273	0.338
H23-Vs	15	600	1280	2.133333333	0.359
B02-Vs	15.25	1320	2670	2.022727273	0.338
H23-Vs	15.25	560	1280	2.285714286	0.382
B02-Vs	15.5	1320	2670	2.022727273	0.338
H23-Vs	15.5	560	1280	2.285714286	0.382
H23-Vs	15.75	560	1280	2.285714286	0.382
H23-Vs	16	560	1280	2.285714286	0.382
H18-Vs	16.25	600	1020	1.7	0.235
H18-Vs	16.5	600	1020	1.7	0.235
H18-Vs	16.75	600	1020	1.7	0.235
H18-Vs	17	600	1370	2.283333333	0.381
H23-Vs	21.25	650	1590	2.446153846	0.400
H23-Vs	21.5	650	1590	2.446153846	0.400
H23-Vs	21.75	650	1590	2.446153846	0.400
H23-Vs	22	650	1590	2.446153846	0.400
H23-Vs	22.25	700	1590	2.271428571	0.380
H23-Vs	22.5	700	1590	2.271428571	0.380
H23-Vs	22.75	700	1590	2.271428571	0.380
H23-Vs	23	700	1590	2.271428571	0.380
H23-Vs	23.25	700	1590	2.271428571	0.380
				Average	**0.346**

Moderately Weathered					
Borehole	**Depth**	**V_S**	**V_P**	**V_P/V_S**	**Poisson's Ratio**
K07-Vs	8.5	740	2400	3.243243243	0.447
H23-Vs	8.75	500	1040	2.08	0.350
K07-Vs	8.75	700	2400	3.428571429	0.454
H23-Vs	9	500	1040	2.08	0.350
K07-Vs	9	700	2400	3.428571429	0.454
H23-Vs	9.25	480	1040	2.166666667	0.365
K07-Vs	9.25	700	2400	3.428571429	0.454
H23-Vs	9.5	480	1040	2.166666667	0.365
K07-Vs	9.5	700	2400	3.428571429	0.454
H23-Vs	9.75	480	1040	2.166666667	0.365
K07-Vs	9.75	720	2400	3.333333333	0.451
H23-Vs	10	480	1040	2.166666667	0.365
K07-Vs	10	720	2400	3.333333333	0.451
K07-Vs	10.25	720	2400	3.333333333	0.451
F01-Vs	10.5	720	1890	2.625	0.415
K07-Vs	10.5	720	2400	3.333333333	0.451
F01-Vs	10.75	660	1890	2.863636364	0.431
K07-Vs	10.75	830	2400	2.891566265	0.432

F01-Vs	11	660	1890	2.863636364	0.431
K07-Vs	11	830	2400	2.891566265	0.432
F01-Vs	11.25	660	1890	2.863636364	0.431
K07-Vs	11.25	830	2400	2.891566265	0.432
F01-Vs	11.5	660	1890	2.863636364	0.431
K07-Vs	11.5	830	2400	2.891566265	0.432
F01-Vs	11.75	620	1890	3.048387097	0.440
K07-Vs	11.75	670	2400	3.582089552	0.458
F01-Vs	12	620	1890	3.048387097	0.440
K07-Vs	12	670	2400	3.582089552	0.458
K07-Vs	12.25	670	2400	3.582089552	0.458
K07-Vs	12.5	670	2400	3.582089552	0.458
H23-Vs	16.25	605	1280	2.115702479	0.356
H13-Vs	16.5	620	1170	1.887096774	0.305
H23-Vs	16.5	605	1280	2.115702479	0.356
H13-Vs	16.75	620	1170	1.887096774	0.305
H23-Vs	16.75	605	1280	2.115702479	0.356
H13-Vs	17	620	1170	1.887096774	0.305
H23-Vs	17	605	1280	2.115702479	0.356
H13-Vs	17.25	730	1170	1.602739726	0.181
H18-Vs	17.25	940	1370	1.457446809	0.055
H23-Vs	17.25	670	1280	1.910447761	0.311
H13-Vs	17.5	730	1170	1.602739726	0.181
H23-Vs	17.5	670	1280	1.910447761	0.311
H13-Vs	17.75	730	1170	1.602739726	0.181
H23-Vs	17.75	670	1280	1.910447761	0.311
H23-Vs	18	670	1280	1.910447761	0.311
H23-Vs	18.25	660	1280	1.939393939	0.319
H23-Vs	18.5	660	1280	1.939393939	0.319
H23-Vs	18.75	660	1280	1.939393939	0.319
H23-Vs	19	660	1280	1.939393939	0.319
H18-Vs	19.25	820	1370	1.670731707	0.221
H23-Vs	19.25	640	1280	2	0.333
H18-Vs	19.5	820	1370	1.670731707	0.221
H23-Vs	19.5	640	1590	2.484375	0.403
H23-Vs	19.75	640	1590	2.484375	0.403
H23-Vs	20	640	1590	2.484375	0.403
H23-Vs	20.25	700	1590	2.271428571	0.380
H23-Vs	20.5	700	1590	2.271428571	0.380
H23-Vs	20.75	700	1590	2.271428571	0.380
H23-Vs	21	700	1590	2.271428571	0.380
H18-Vs	25.5	840	1370	1.630952381	0.199
H18-Vs	25.75	840	1370	1.630952381	0.199
H18-Vs	26	840	1370	1.630952381	0.199
				Average	**0.344**

Slightly-Moderately Weathered					
Borehole	**Depth**	**V_S**	**V_P**	**V_P/V_S**	**Poisson's Ratio**
H18-Vs	22.25	740	1370	1.851351351	0.294
H18-Vs	22.5	740	1370	1.851351351	0.294
H18-Vs	22.75	740	1370	1.851351351	0.294
H18-Vs	23	740	1370	1.851351351	0.294
H18-Vs	23.25	620	1370	2.209677419	0.371
H18-Vs	23.5	620	1370	2.209677419	0.371
H18-Vs	23.75	620	1370	2.209677419	0.371
H18-Vs	24	620	1370	2.209677419	0.371
H18-Vs	24.25	730	1370	1.876712329	0.302
				Average	**0.329**

Slightly Weathered					
Borehole	**Depth**	**V_S**	**V_P**	**V_P/V_S**	**Poisson's Ratio**
H18-Vs	24.5	730	1370	1.876712329	0.302
H18-Vs	24.75	730	1370	1.876712329	0.302
H18-Vs	25	730	1370	1.876712329	0.302
H18-Vs	25.25	840	1370	1.630952381	0.199
H18-Vs	26.25	810	1370	1.691358025	0.231
H18-Vs	26.5	810	1370	1.691358025	0.231
H18-Vs	26.75	810	1370	1.691358025	0.231
H18-Vs	27	810	1370	1.691358025	0.231
				Average	**0.254**

Unweathered (Fixed Value)	
	0.21

Westwind Downhole Seismic Test
B02 Shear Wave Velocity Profile

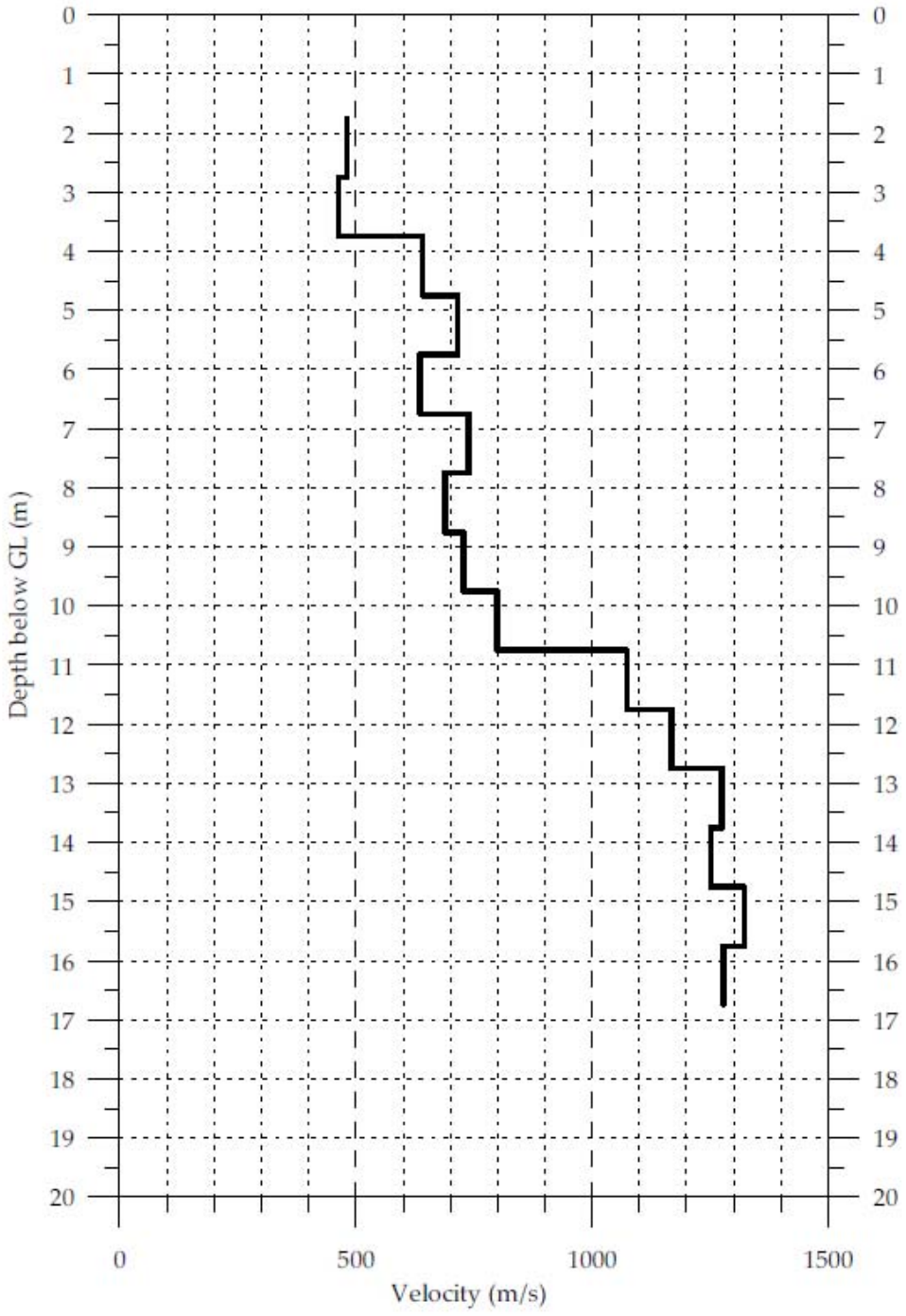

Westwind Downhole Seismic Test
B02 Compression Wave Velocity Profile

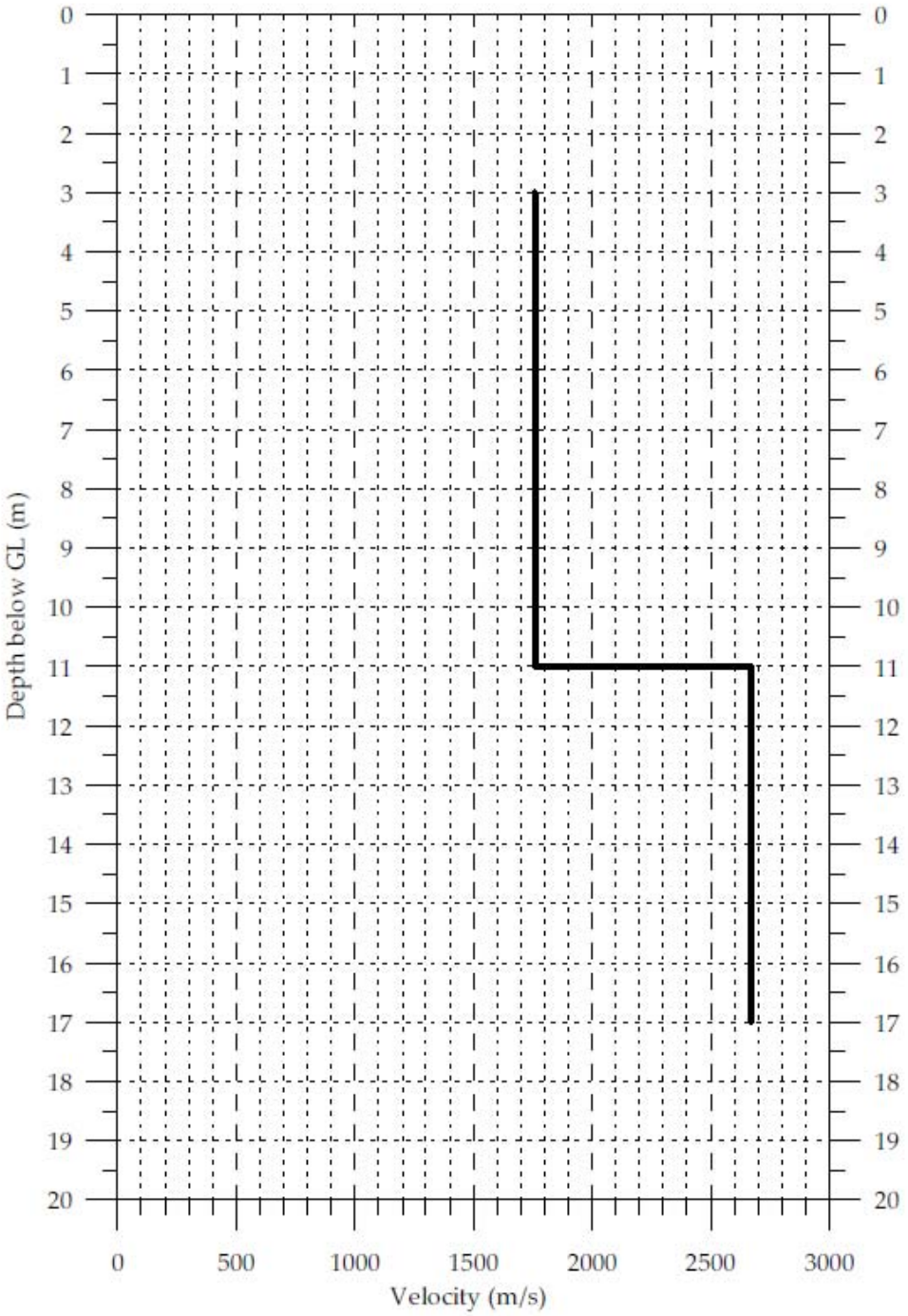

Westwind Downhole Seismic Test
D06 Shear Wave Velocity Profile

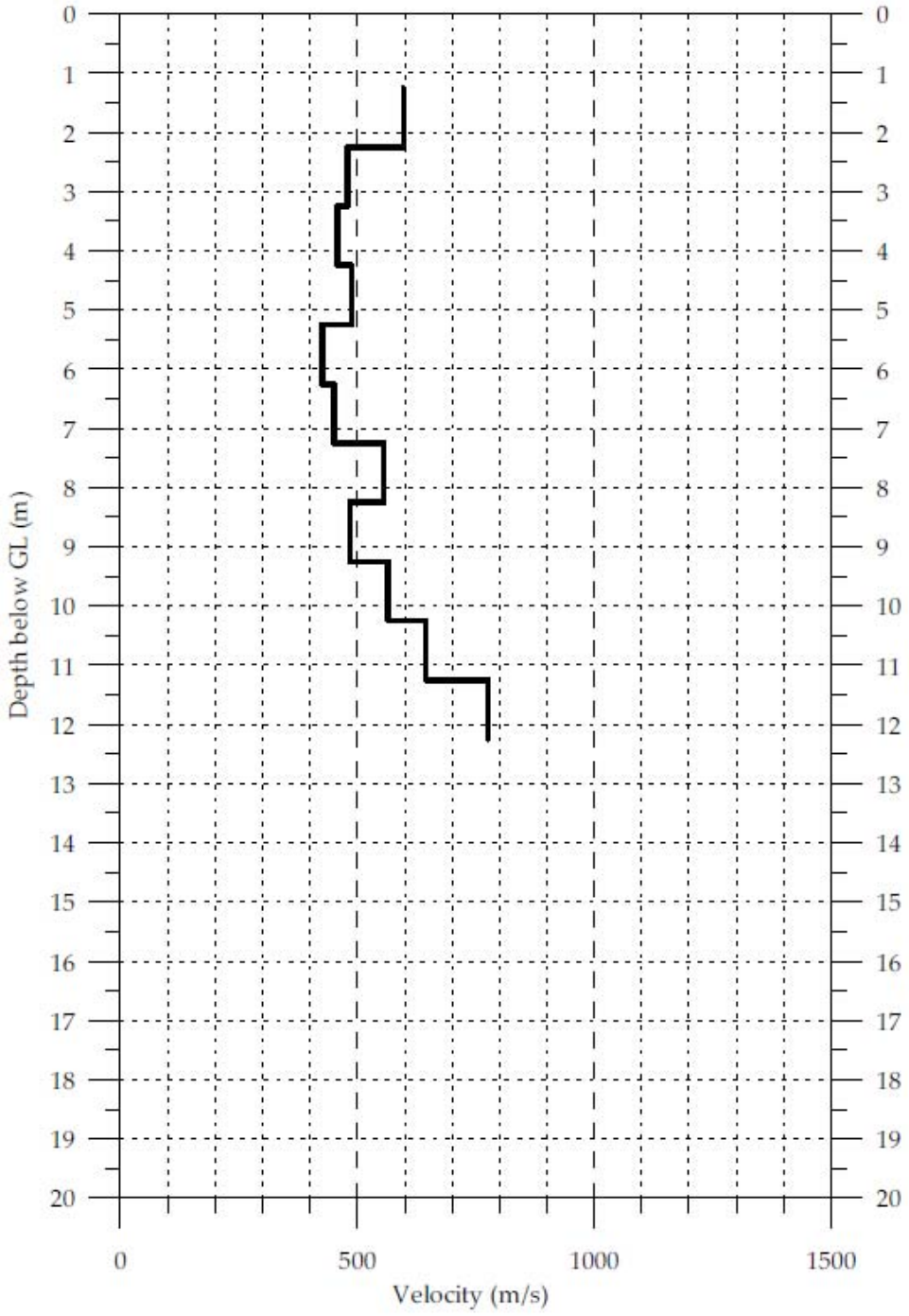

Westwind Downhole Seismic Test
D06 Compression Wave Velocity Profile

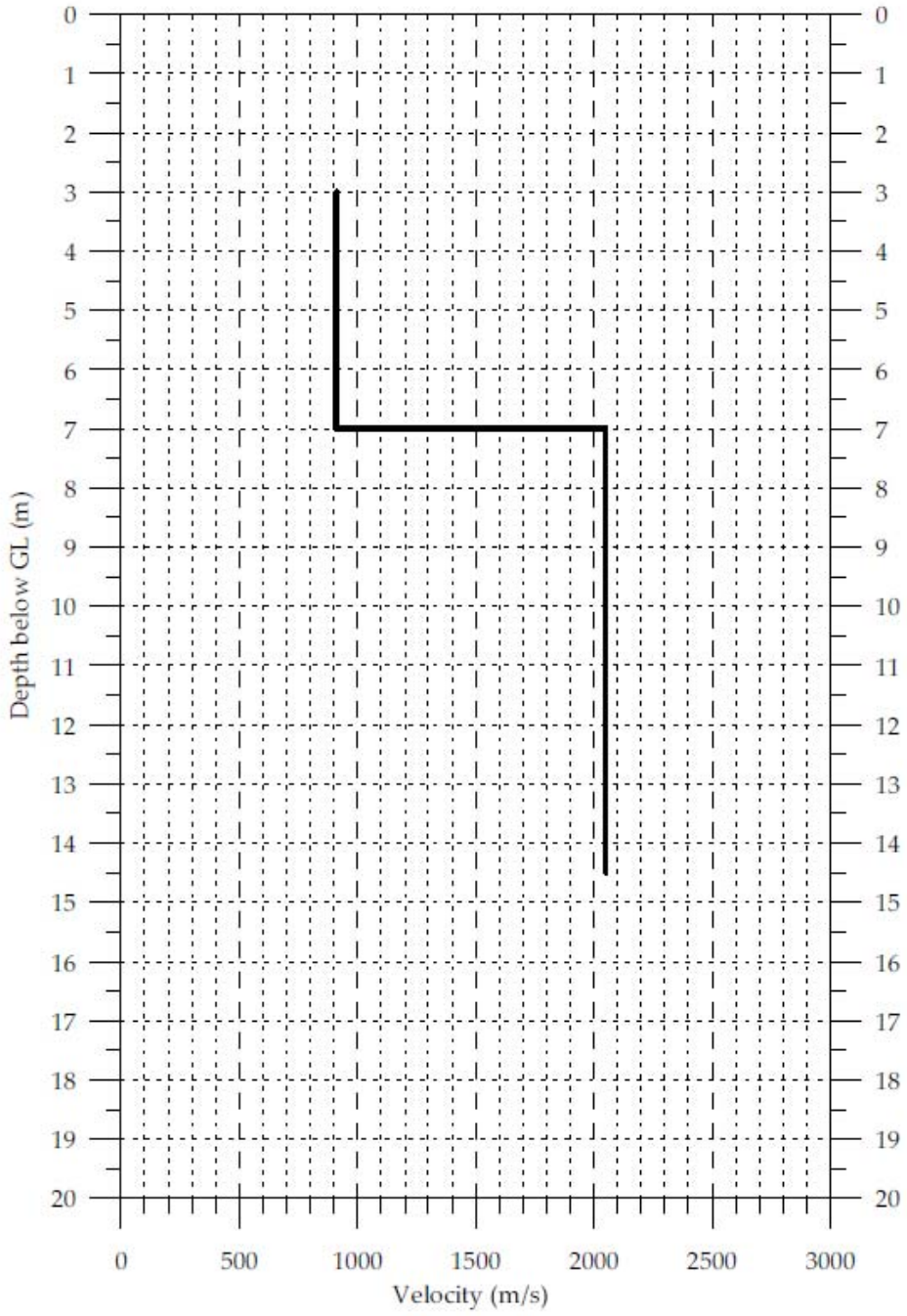

Westwind Downhole Seismic Test
F01 Shear Wave Velocity Profile

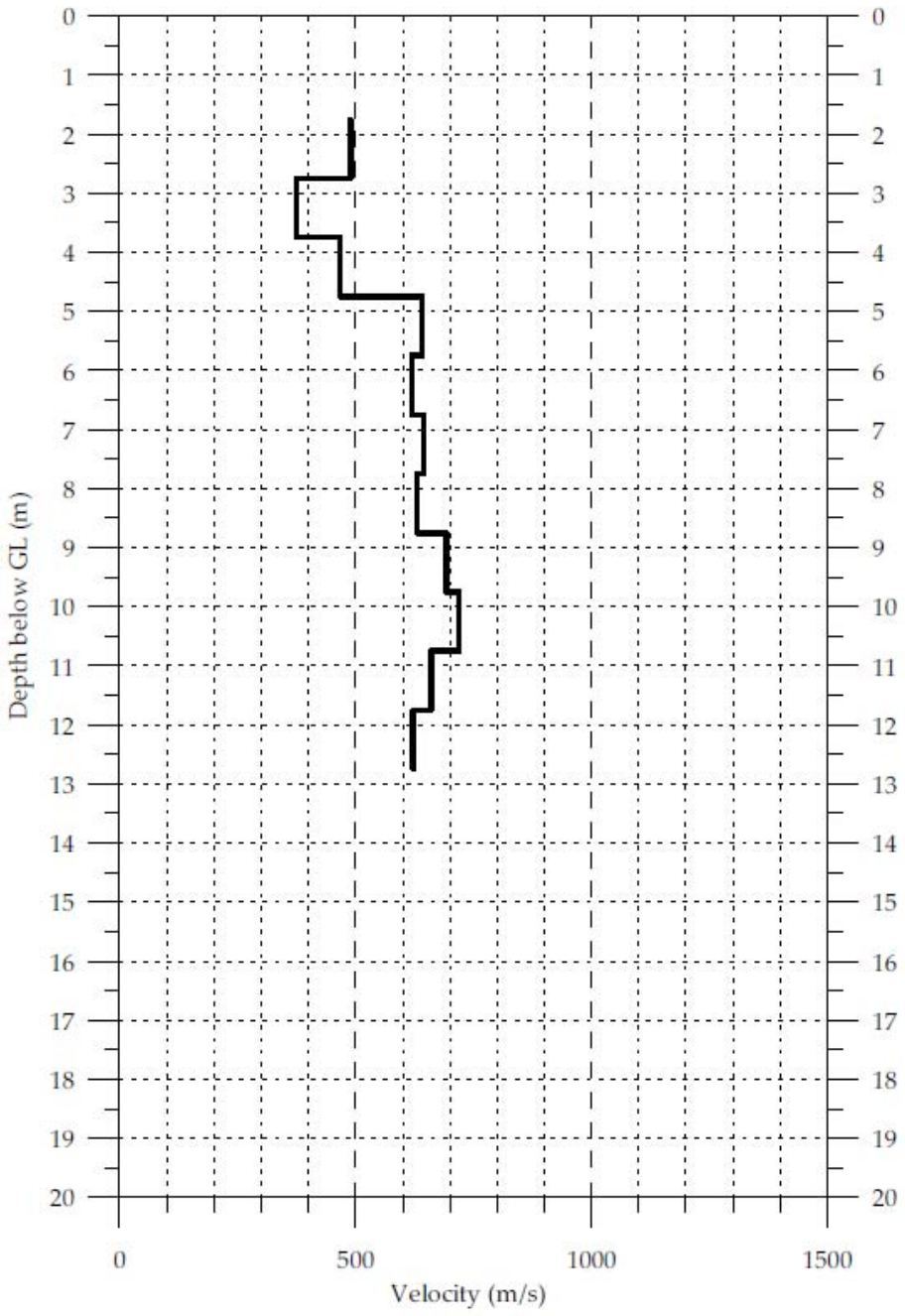

Westwind Downhole Seismic Test
F01 Compression Wave Velocity Profile

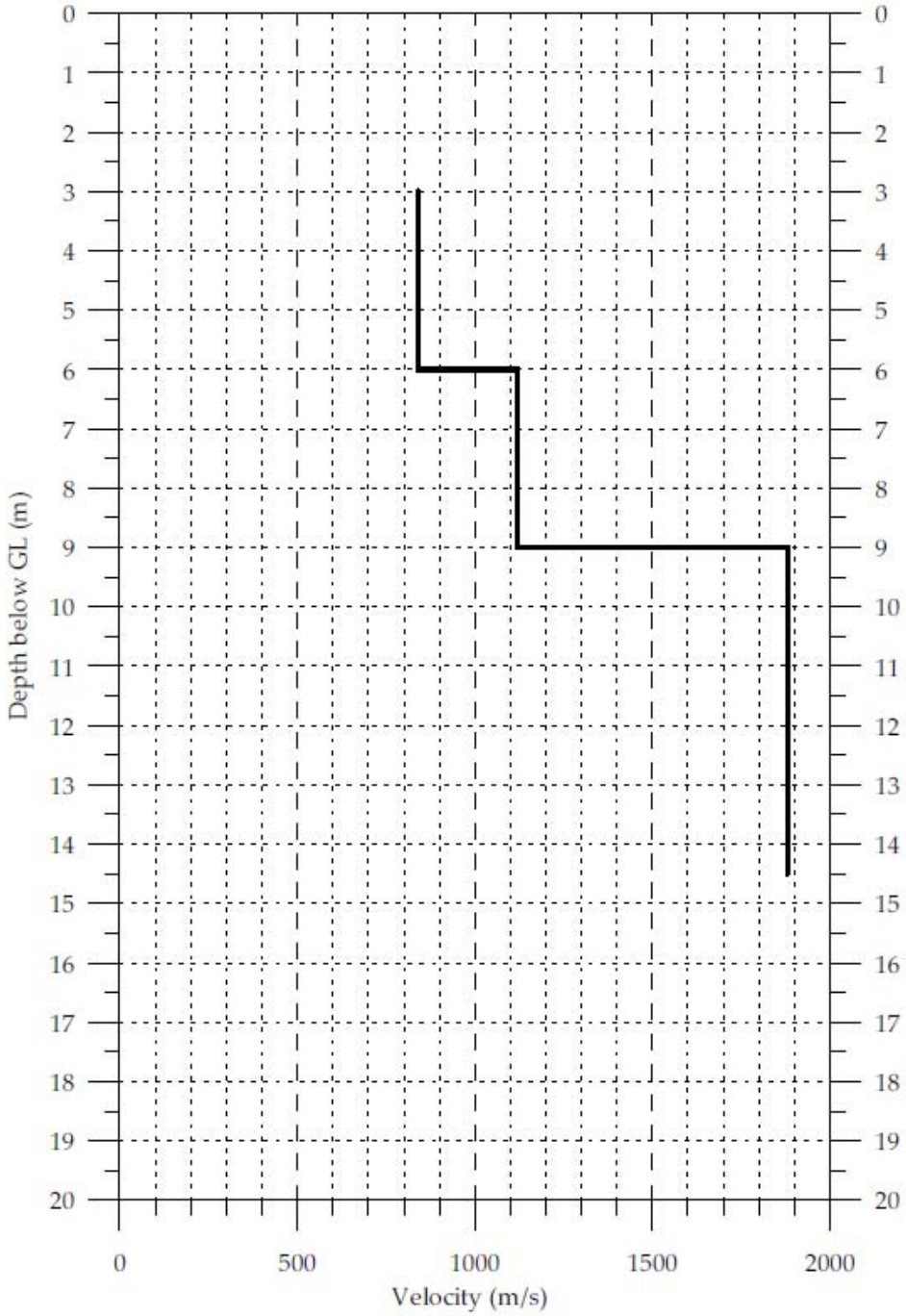

Westwind Downhole Seismic Test
H13 Shear Wave Velocity Profile

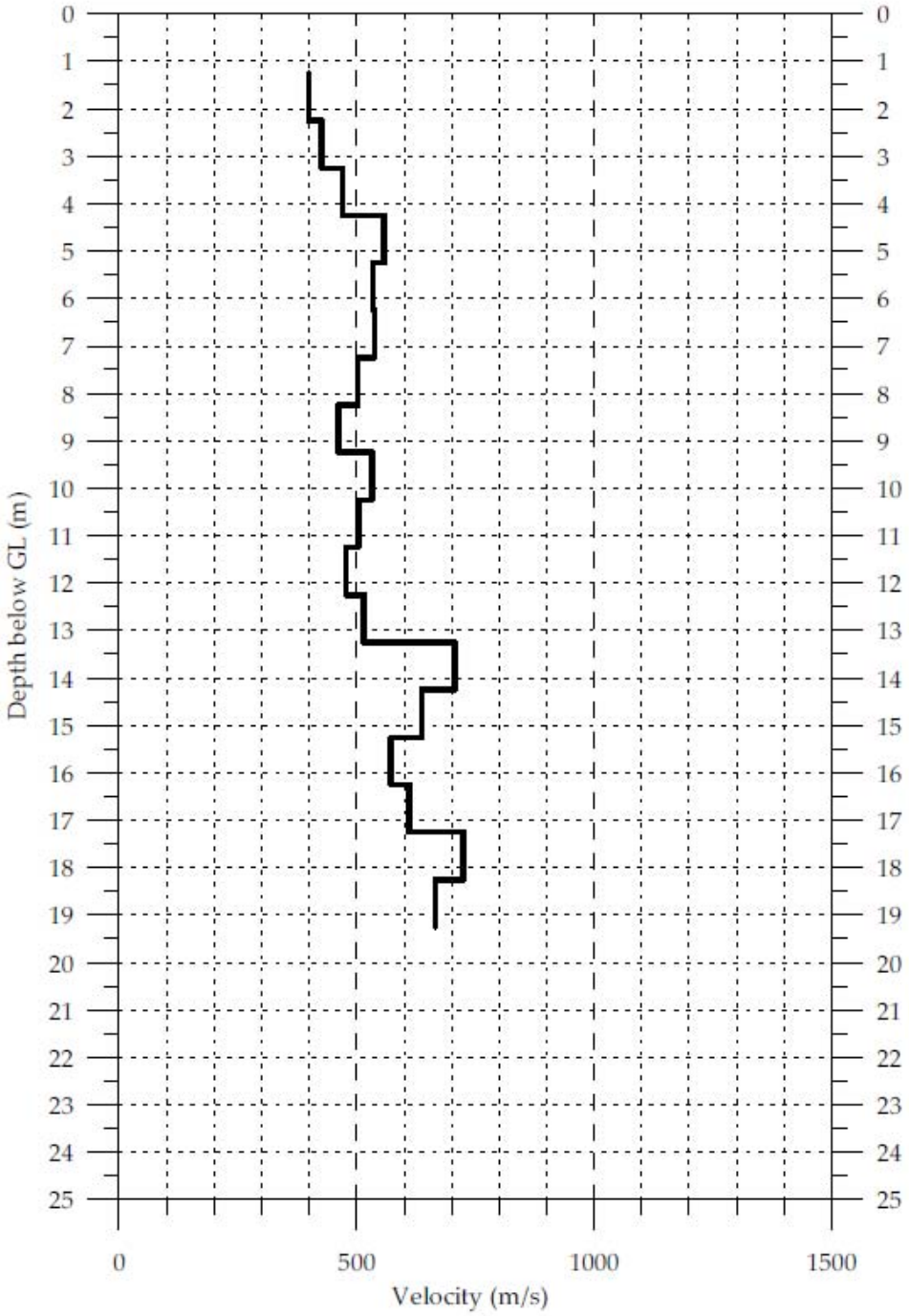

Westwind Downhole Seismic Test
H13 Compression Wave Velocity Profile

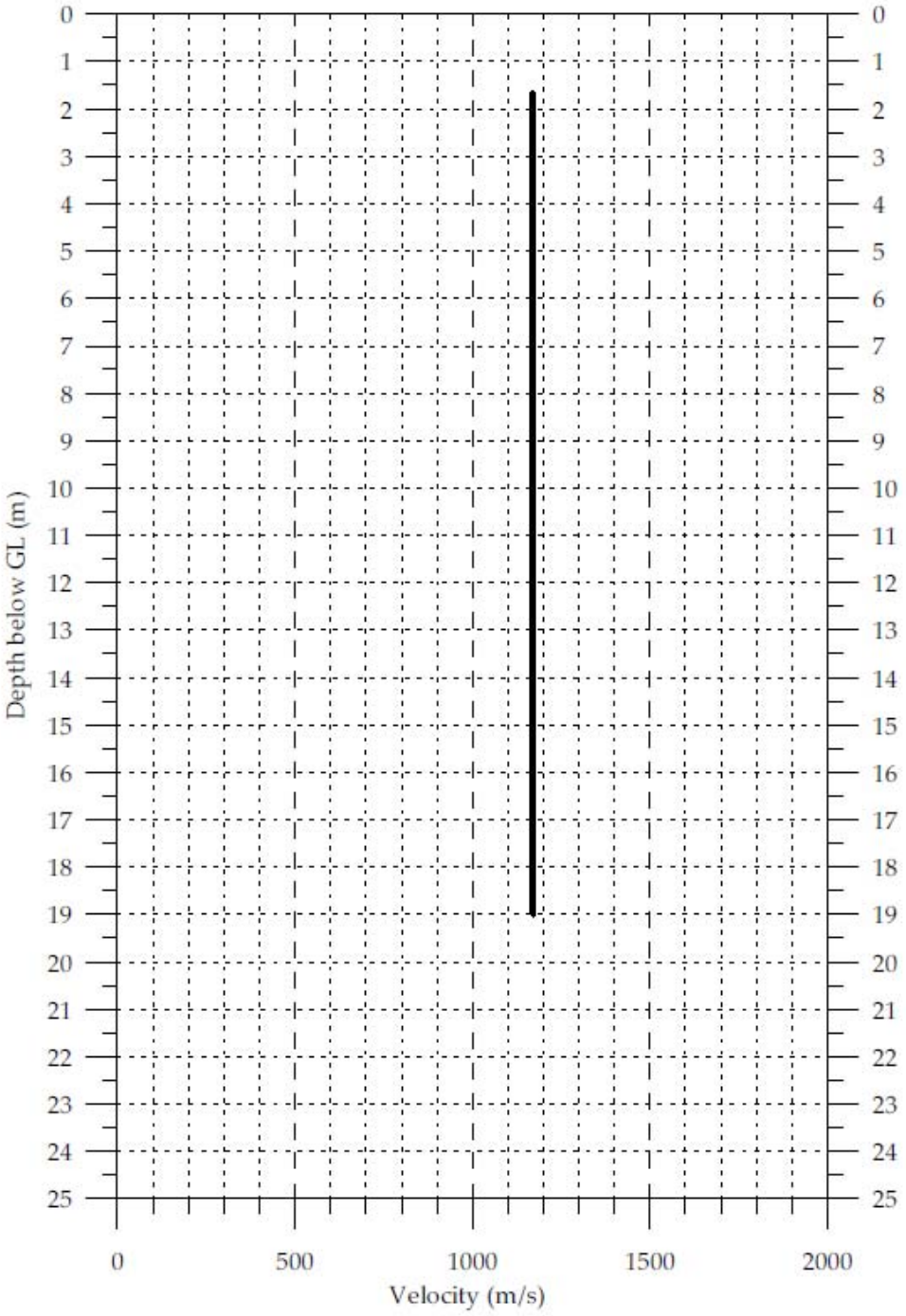

Westwind Downhole Seismic Test
H18 Shear Wave Velocity Profile

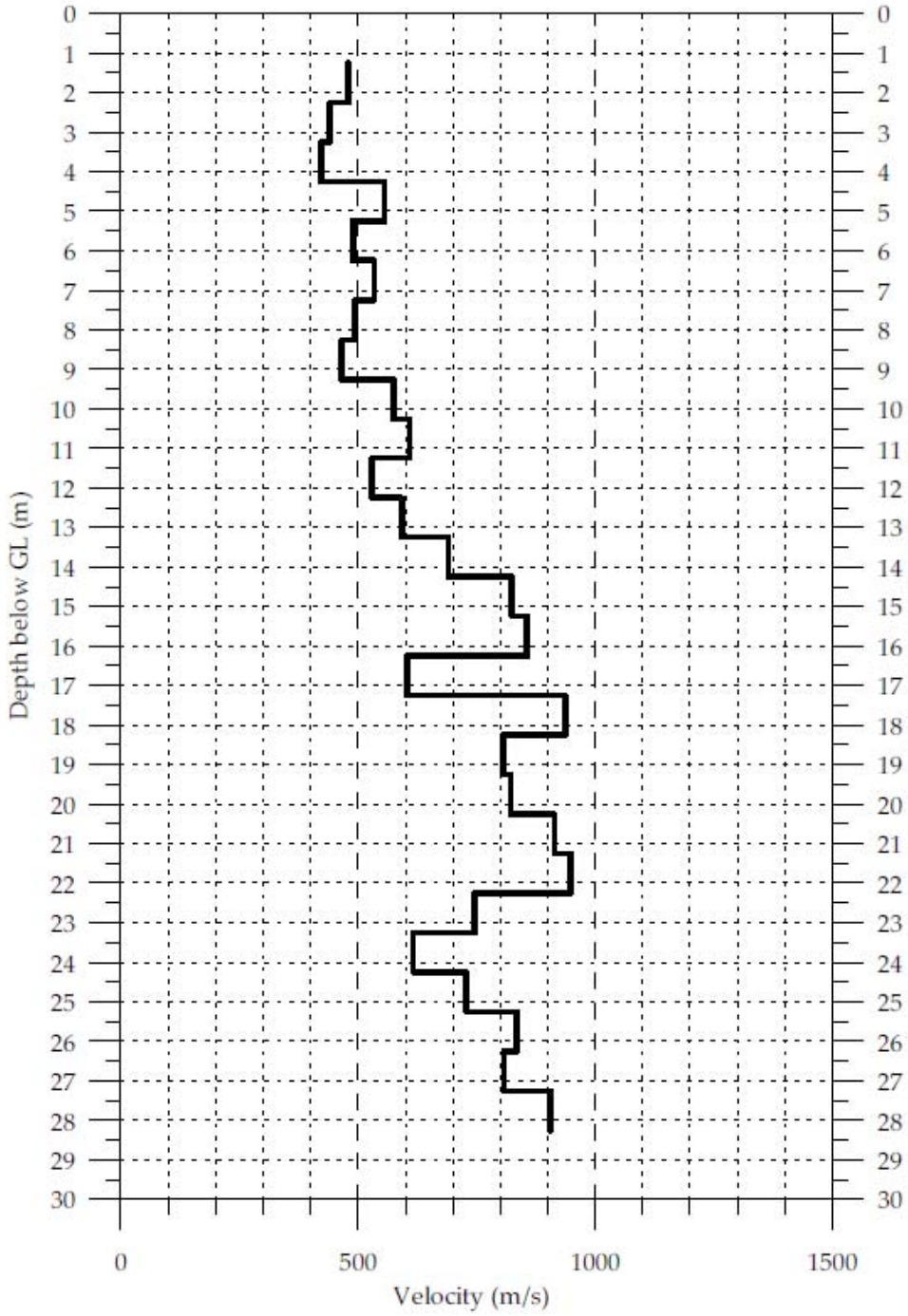

Westwind Downhole Seismic Test
H18 Compression Wave Velocity Profile

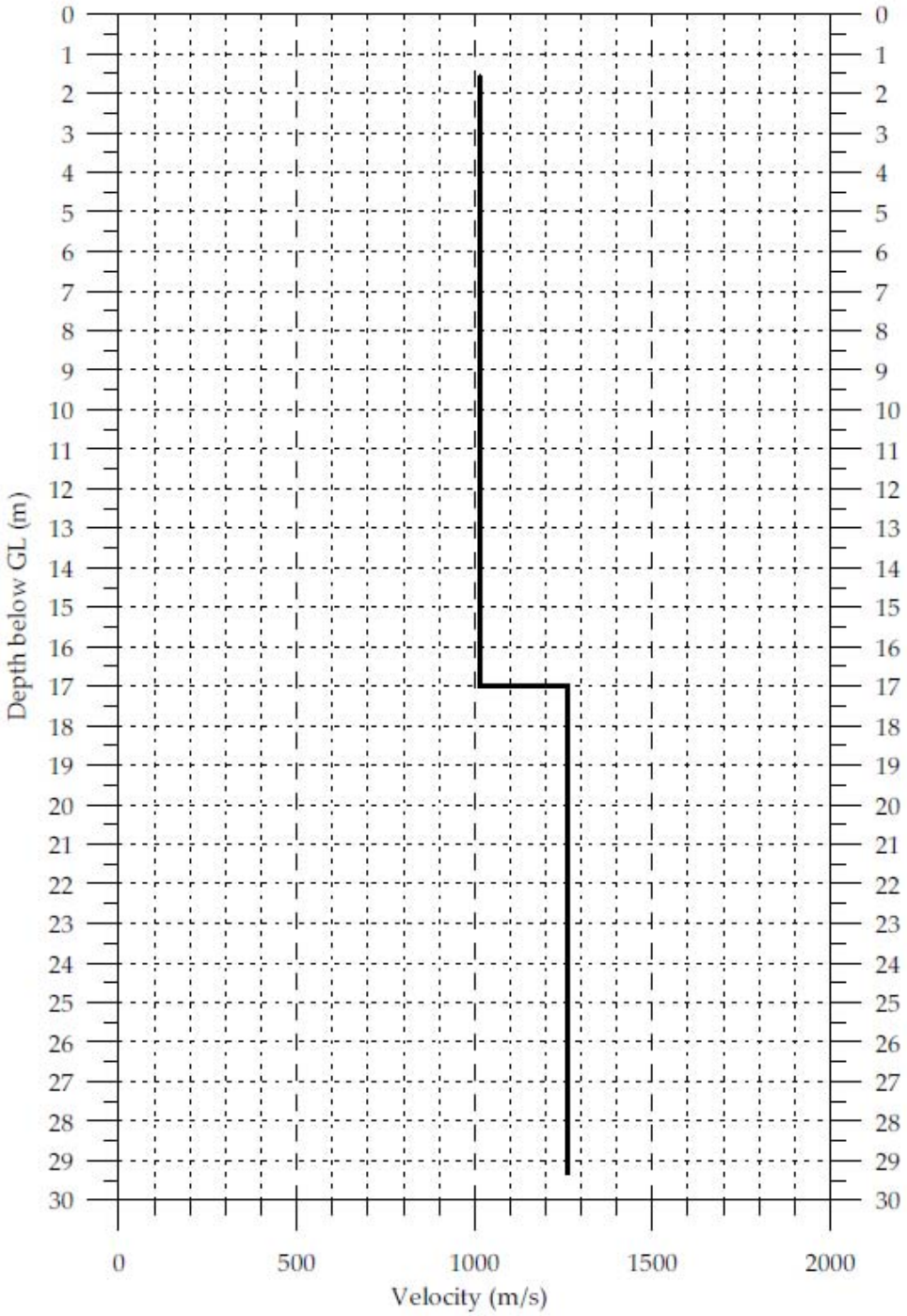

Westwind Downhole Seismic Test
H23 Shear Wave Velocity Profile

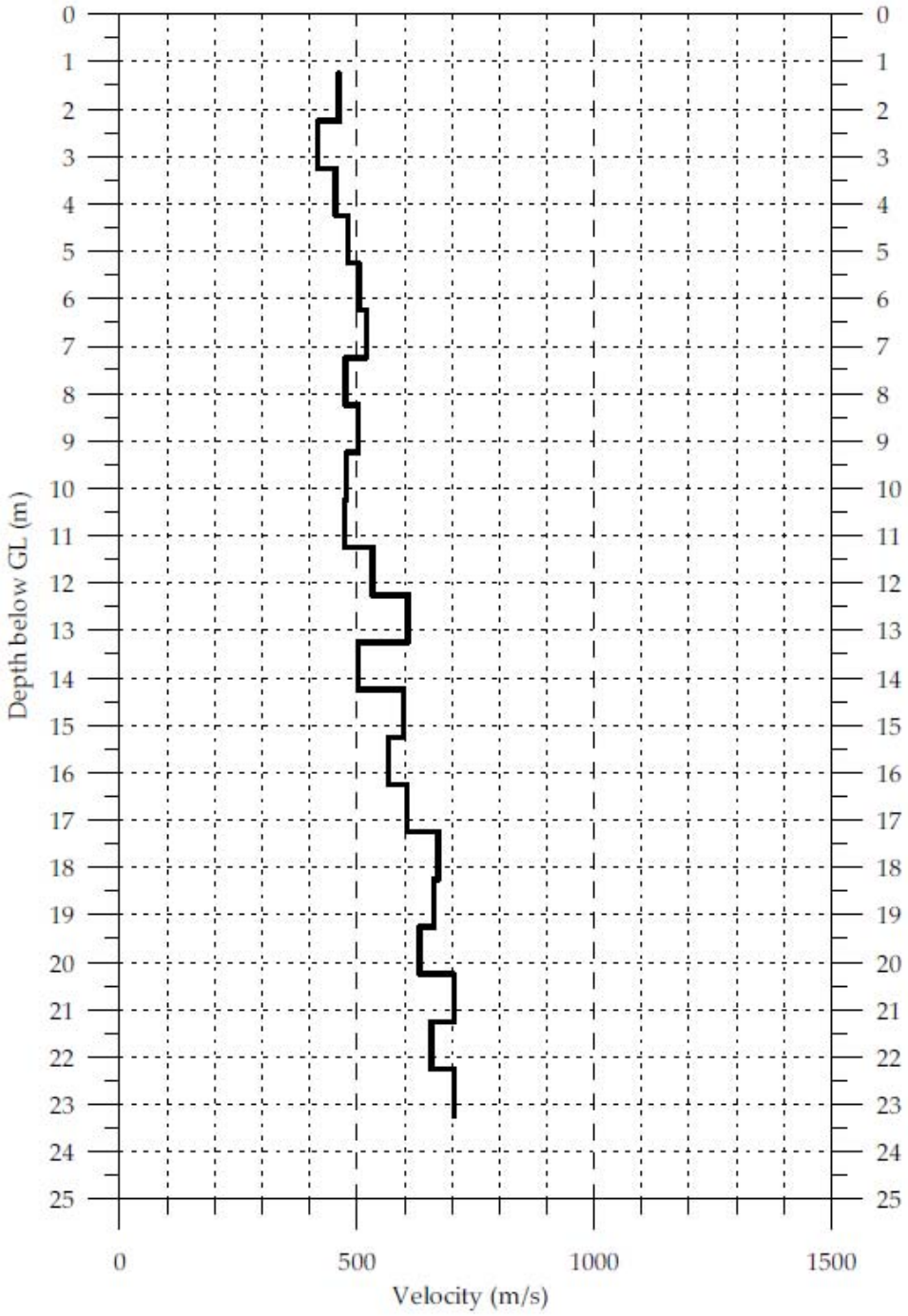

Westwind Downhole Seismic Test
H23 Compression Wave Velocity Profile

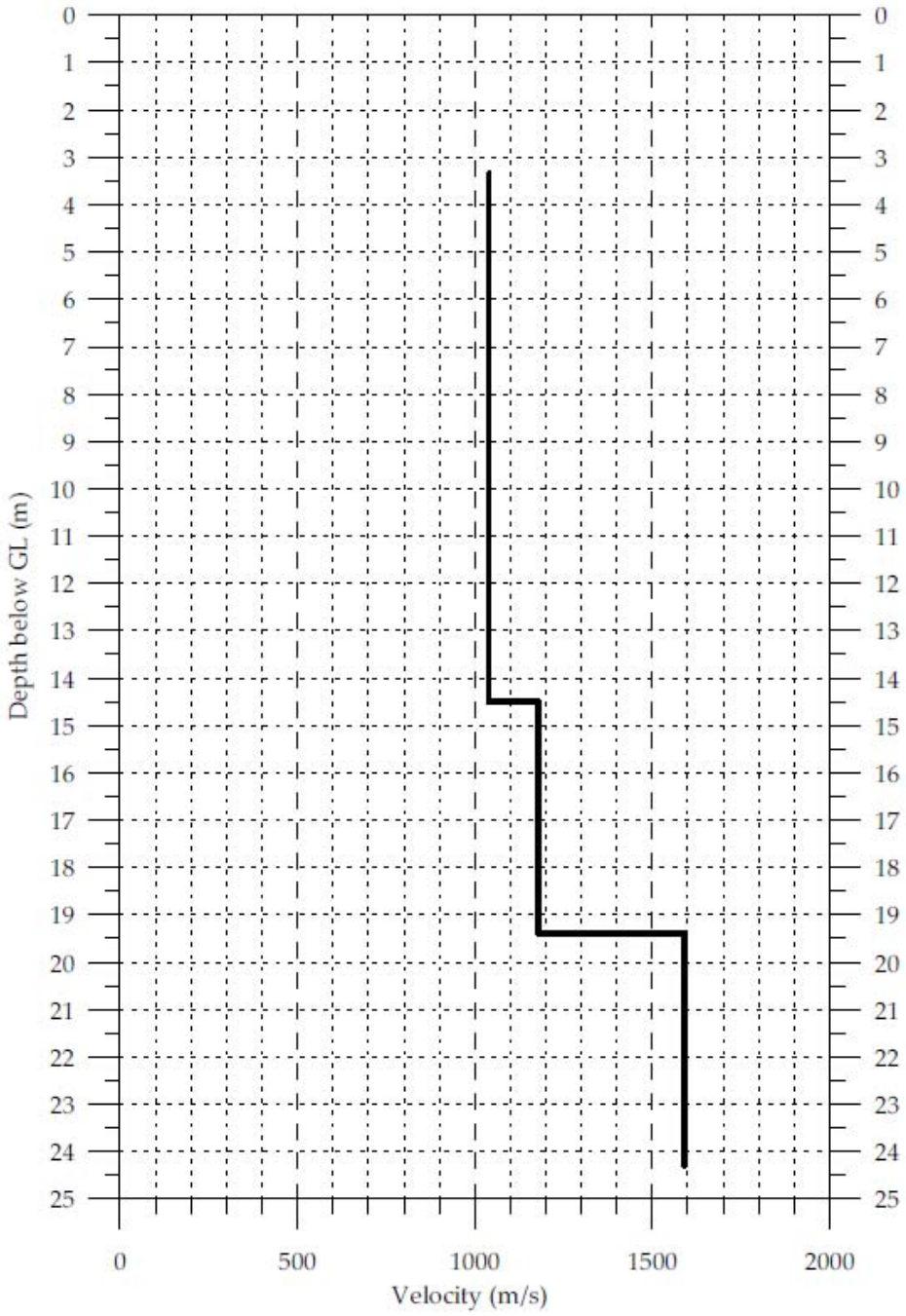

Westwind Downhole Seismic Test
K07 Shear Wave Velocity Profile

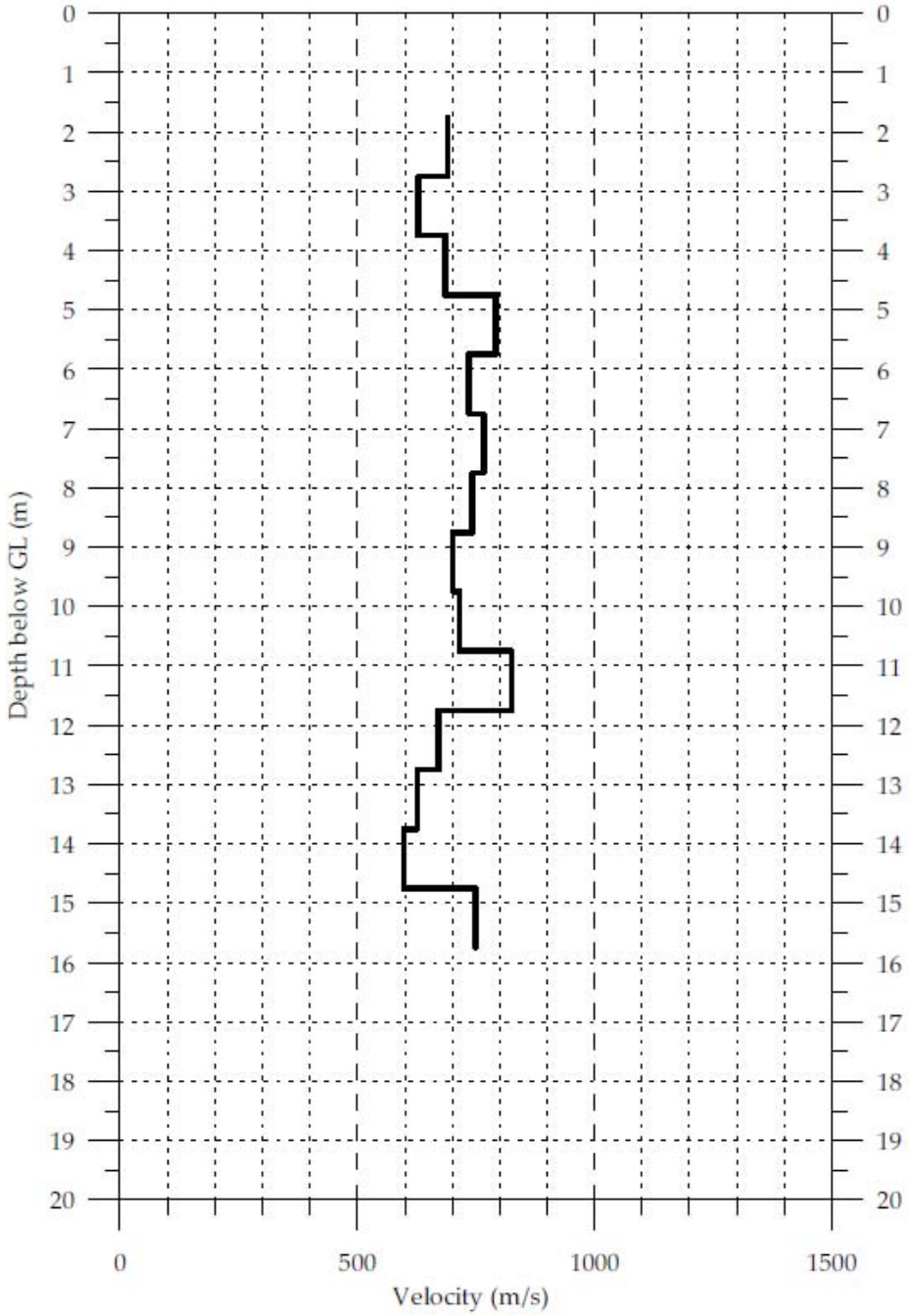

Westwind Downhole Seismic Test
K07 Compression Wave Velocity Profile

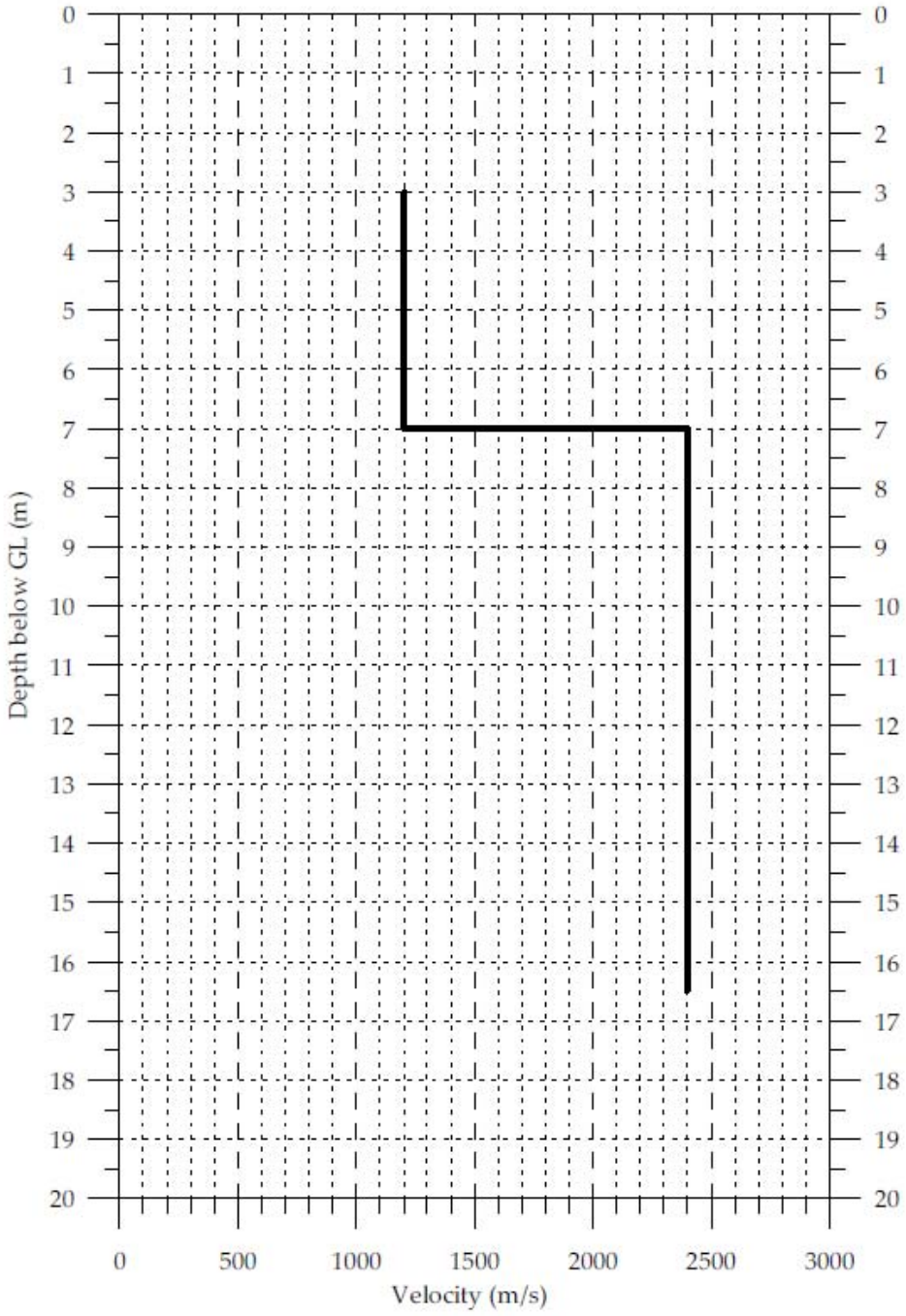

Appendix G:

West Wind Windfarm Borehole Logs from sites H03 and K04

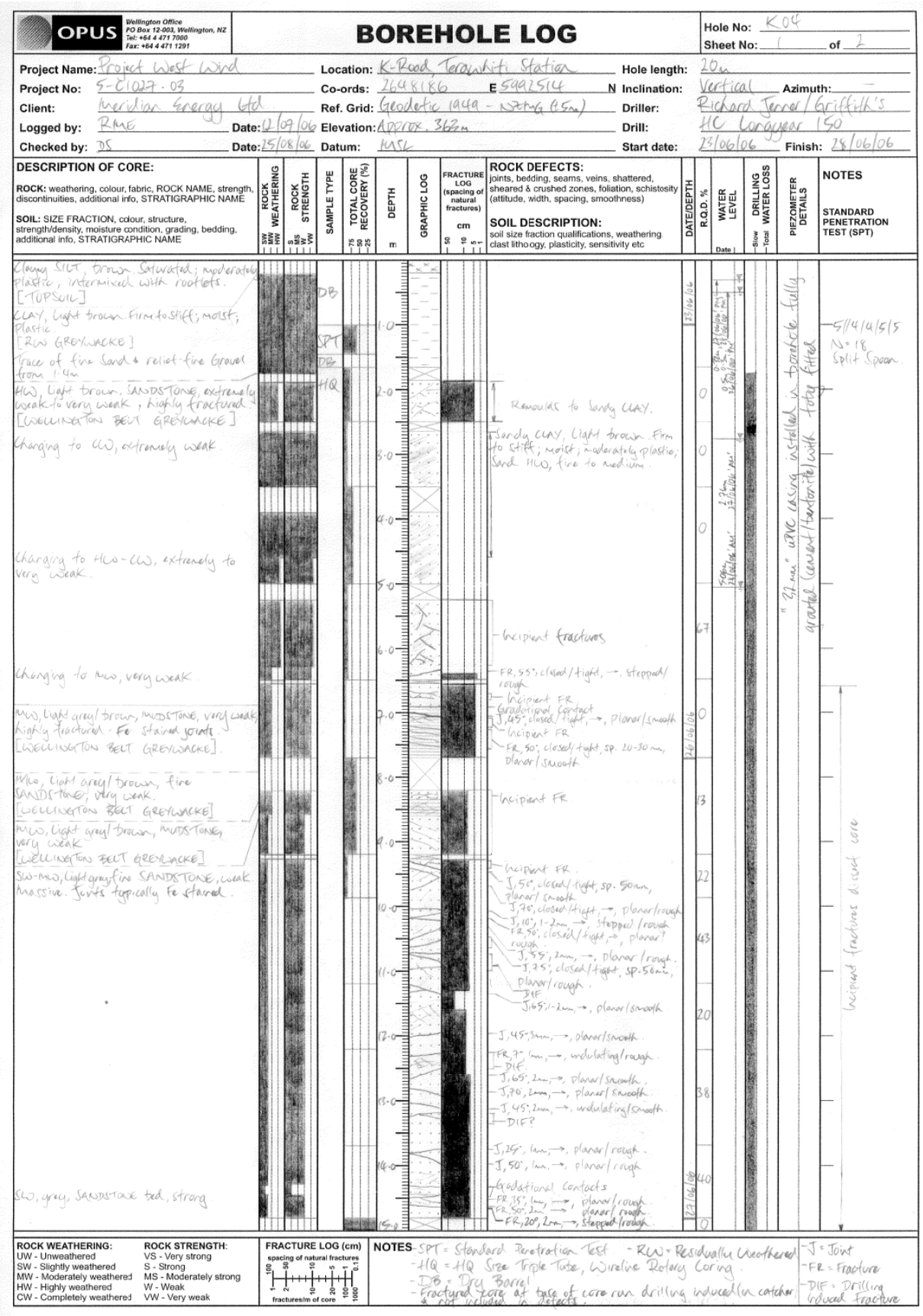

OPUS Wellington Office, PO Box 12-003, Wellington, NZ, Tel: +64 4 471 7000, Fax: +64 4 471 1291

BOREHOLE LOG

Hole No: K04
Sheet No: 1 of 2

Project Name:	Project West Wind	Location:	K-Road, Terawhiti Station	Hole length:	20m
Project No:	5-C1027.03	Co-ords:	2648186 E 5992514 N	Inclination:	Vertical Azimuth: -
Client:	Meridian Energy Ltd	Ref. Grid:	Geodetic 1949 - NZTM (15m)	Driller:	Richard Jerrel / Griffith's
Logged by:	RWE Date: 12/09/06	Elevation:	Approx. 362m	Drill:	HC Longyear 150
Checked by:	DS Date: 25/08/06	Datum:	MSL	Start date:	23/06/06 Finish: 28/06/06

DESCRIPTION OF CORE:

ROCK: weathering, colour, fabric, ROCK NAME, strength, discontinuities, additional info, STRATIGRAPHIC NAME

SOIL: SIZE FRACTION, colour, structure, strength/density, moisture condition, grading, bedding, additional info, STRATIGRAPHIC NAME

ROCK WEATHERING: UW, SW, MW, HW
ROCK STRENGTH: S, MS, W, VW
SAMPLE TYPE
TOTAL CORE RECOVERY (%): 75, 90, 95
DEPTH (m)
GRAPHIC LOG
FRACTURE LOG (spacing of natural fractures) cm: 50, 10, 5

ROCK DEFECTS:
joints, bedding, seams, veins, shattered, sheared & crushed zones, foliation, schistosity (attitude, width, spacing, smoothness)

SOIL DESCRIPTION:
soil size fraction qualifications, weathering clast lithology, plasticity, sensitivity etc

DATE/DEPTH
R.Q.D. %
WATER LEVEL: Date
DRILLING WATER LOSS: Slow, Total
PIEZOMETER DETAILS
NOTES: STANDARD PENETRATION TEST (SPT)

Clayey SILT, brown. Saturated; moderately plastic, intermixed with rootlets. [TOPSOIL]

CLAY, light brown. Firm to stiff; moist; plastic. [RW GREYWACKE]

Trace of fine Sand & relict fine Gravel from 1.4m

HW, light brown, SANDSTONE, extremely weak to very weak, highly fractured. [WELLINGTON BELT GREYWACKE]

Changing to CW, extremely weak

Changing to HCW - CW, extremely to very weak.

Changing to MW, very weak

MW, light grey/brown, MUDSTONE, very weak, highly fractured. Fe stained joints [WELLINGTON BELT GREYWACKE].

MW, light grey/brown, fine SANDSTONE, very weak. [WELLINGTON BELT GREYWACKE]

MW, light grey/brown, MUDSTONE, very weak. [WELLINGTON BELT GREYWACKE]

SW-MW, light grey fine SANDSTONE, weak massive. Joints typically Fe stained.

SW, grey, SANDSTONE bed, strong

DB
SPT
DB
HQ

Remoulds to Sandy CLAY.

Sandy CLAY, light brown. Firm to stiff; moist; moderately plastic; Sand HCW, fine to medium.

Incipient fractures

FR, 55°, closed/tight, →, stepped/rough

Incipient FR

Gradational Contact

J, 45°, closed, tight, →, planar/smooth

Incipient FR

FR, 50°, closed/tight, SP. 20-30mm, planar/smooth

Incipient FR

Incipient FR

J, 50°, closed/tight, sp. 50mm, planar/smooth

J, 70°, closed/tight, →, planar/rough

J, 10°, 1-2mm, → stepped/rough

FR, 50°, closed/tight, →, planar/rough

J, 55°, 2mm, →, planar/rough.

J, 75°, closed/tight, SP. 50mm, planar/rough.

DIF

J, 65°, 1-2mm, →, planar/smooth

J, 45°, 3mm, →, planar/smooth

FR, 7°, 1mm, →, undulating/rough

DIF

J, 65°, 2mm, →, planar/smooth.

J, 70°, 2mm, →, planar/smooth

J, 45°, 2mm, →, undulating/smooth

DIF?

J, 25°, 1mm, →, planar/rough.

J, 50°, 1mm, →, planar/rough

Gradational Contacts

FR, 35°, 1mm, →, planar/rough

FR, 50°, 2mm, →, planar/rough

FR, 20°, 2mm, →, stepped/rough

"27mm" uPVC casing installed in borehole fully grouted (cement/bentonite) with fotag fitted

Incipient fractures discontinuous core

5/4/4/5/5
N = 18
Split Spoon

ROCK WEATHERING:
UW - Unweathered
SW - Slightly weathered
MW - Moderately weathered
HW - Highly weathered
CW - Completely weathered

ROCK STRENGTH:
VS - Very strong
S - Strong
MS - Moderately strong
W - Weak
VW - Very weak

FRACTURE LOG (cm)
spacing of natural fractures
100, 50, 20, 10, 5, 2, 1, 0.1
fractures/m of core
1, 2, 5, 10, 20, 100, 1000

NOTES: SPT = Standard Penetration Test - RW = Residually Weathered
- HQ = HQ Size Triple Tube, Wireline Rotary Coring.
- DB = Dry Boring
- Fractured zone at base of core run drilling induced (in catcher & not included in defects).

J = Joint
FR = Fracture
DIF = Drilling Induced Fracture

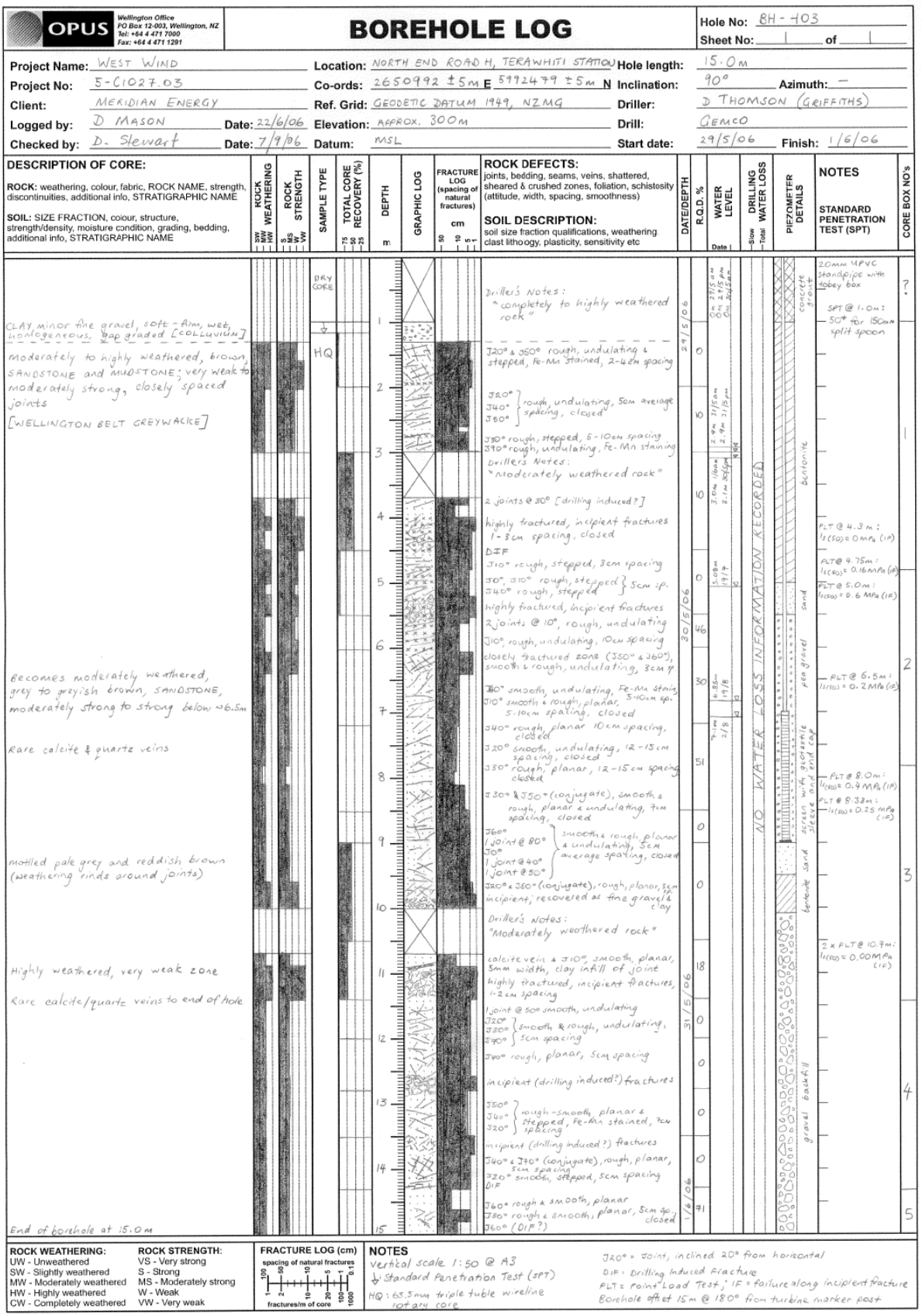

OPUS Wellington Office PO Box 12-003, Wellington, NZ Tel: +64 4 471 7000 Fax: +64 4 471 1291

BOREHOLE LOG

Hole No: BH-403
Sheet No: 1 of 1

Project Name: WEST WIND
Project No: 5-C1027.03
Client: MERIDIAN ENERGY
Logged by: D MASON Date: 22/6/06
Checked by: D. Stewart Date: 7/9/06

Location: NORTH END ROAD H, TERAWHITI STATION
Co-ords: 2650992 ±5m E 5992479 ±5m N
Ref. Grid: GEODETIC DATUM 1949, NZMG
Elevation: APPROX. 300m
Datum: MSL

Hole length: 15.0m
Inclination: 90° Azimuth: –
Driller: D THOMSON (GRIFFITHS)
Drill: GEMCO
Start date: 29/5/06 Finish: 1/6/06

DESCRIPTION OF CORE:

ROCK: weathering, colour, fabric, ROCK NAME, strength, discontinuities, additional info, STRATIGRAPHIC NAME

SOIL: SIZE FRACTION, colour, structure, strength/density, moisture condition, grading, bedding, additional info, STRATIGRAPHIC NAME

ROCK WEATHERING: UW SW MW HW CW
ROCK STRENGTH: VS S MS W VW
SAMPLE TYPE
TOTAL CORE RECOVERY (%): 75 50 25
DEPTH: m
GRAPHIC LOG
FRACTURE LOG (spacing of natural fractures): cm 50 10 5 1

ROCK DEFECTS: joints, bedding, seams, veins, shattered, sheared & crushed zones, foliation, schistosity (attitude, width, spacing, smoothness)

SOIL DESCRIPTION: soil size fraction qualifications, weathering clast lithology, plasticity, sensitivity etc

DATE/DEPTH
R.Q.D. %
WATER LEVEL Date
DRILLING WATER LOSS: Slow / Total
PIEZOMETER DETAILS
NOTES: STANDARD PENETRATION TEST (SPT)
CORE BOX NO's

CLAY, minor fine gravel, soft - firm, wet, homogeneous, bag graded [COLLUVIUM]

DRY CORE

HQ

moderately to highly weathered, brown, SANDSTONE and MUDSTONE; very weak to moderately strong, closely spaced joints
[WELLINGTON BELT GREYWACKE]

becomes moderately weathered, grey to greyish brown, SANDSTONE, moderately strong to strong below ~6.5m

Rare calcite & quartz veins

mottled pale grey and reddish brown (weathering rinds around joints)

Highly weathered, very weak zone

Rare calcite/quartz veins to end of hole

End of borehole at 15.0m

Driller's Notes: "completely to highly weathered rock"

J20° & J50° rough, undulating & stepped, Fe-Mn stained, 2-4cm spacing

J20° } J40° } J80° } rough, undulating, 5cm average spacing, closed

J80° rough, stepped, 5-10cm spacing
J90° rough, undulating, Fe-Mn staining

Driller's Notes: "Moderately weathered rock"

2 joints @ 30° [drilling induced?]

highly fractured, incipient fractures 1-3cm spacing, closed

DIF

J10° rough, stepped, 3cm spacing
J0°, J10° rough, stepped } 5cm sp.
J40° rough, stepped }

highly fractured, incipient fractures

2 joints @ 10°, rough, undulating

J10° rough, undulating, 10cm spacing

closed fractured zone (J50° & J60°), smooth & rough, undulating, 3cm sp.

J80° smooth, undulating, Fe-Mn stain
J10° smooth & rough, planar, 5-10cm sp. 5-10cm spacing, closed

J40° rough, planar 10cm spacing, closed

J20° smooth, undulating, 12-15cm spacing, closed

J80° rough, planar, 12-15cm spacing closed

J30° & J50° (conjugate), smooth & rough, planar & undulating, 7cm spacing, closed

J60° 1 joint @ 80° J0° 1 joint @ 40° 1 joint @ 50° } smooth & rough, planar & undulating, 5cm average spacing, closed

J20° & J60° (conjugate), rough, planar, 5cm incipient, recovered as fine gravel & clay

Driller's Notes: "Moderately weathered rock"

calcite vein & J10° smooth, planar, 5mm width, clay infill of joint

highly fractured, incipient fractures, 1-2cm spacing

1 joint @ 50° smooth, undulating

J20° J80° J90° } smooth & rough, undulating, 5cm spacing

J90° rough, planar, 5cm spacing

incipient (drilling induced?) fractures

J50° J40° J20° } rough-smooth, planar & stepped, Fe-Mn stained, 7cm spacing

incipient (drilling induced?) fractures

J40° & J70° (conjugate), rough, planar, 5cm spacing
J20° smooth, stepped, 5cm spacing
DIF

J60° rough & smooth, planar
J80° rough & smooth, planar, 5cm sp. closed
J60° (DIF?)

29/5/06
30/5/06
31/5/06
1/6/06

0m 27/5/06
0m 29/5/06
0m 30/5/06

3.5m 16/6m
2.1m 30/5pm

5.08m 31/5

6.85m 1/6

7.4m 2/6

NO WATER LOSS INFORMATION RECORDED

2.0mm UPVC standpipe with lobey box
concrete
bentonite
sand
pea gravel
screen with geotextile sleeve
bentonite sand
gravel backfill

SPT @ 1.0m: 50* for 150mm split spoon

PLT @ 4.3m: $I_{s(50)}$ = 0MPa (I/F)
PLT @ 9.75m: $I_{s(50)}$ = 0.16MPa (I/F)
PLT @ 5.0m: $I_{s(50)}$ = 0.6 MPa (I/F)
PLT @ 6.5m: $I_{s(50)}$ = 0.2MPa (I/F)
PLT @ 8.0m: $I_{s(50)}$ = 0.4 MPa (I/F)
PLT @ 8.38m: $I_{s(50)}$ = 0.25 MPa (I/F)
2 x PLT @ 10.9m: $I_{s(50)}$ = 0.00MPa (I/F)

CORE BOX NO's: ? 1 2 3 4 5

ROCK WEATHERING:
UW - Unweathered
SW - Slightly weathered
MW - Moderately weathered
HW - Highly weathered
CW - Completely weathered

ROCK STRENGTH:
VS - Very strong
S - Strong
MS - Moderately strong
W - Weak
VW - Very weak

FRACTURE LOG (cm)
spacing of natural fractures
100 50 20 10 5 2 1 0.1
1 2 5 10 20 50 100 1000
fractures/m of core

NOTES
Vertical scale 1:50 @ A3
Standard Penetration Test (SPT)
HQ: 63.5mm triple tube wireline rotary core

J20° = Joint, inclined 20° from horizontal
DIF = Drilling Induced Fracture
PLT = Point Load Test, I/F = failure along incipient fracture
Borehole offset 15m @ 180° from turbine marker post

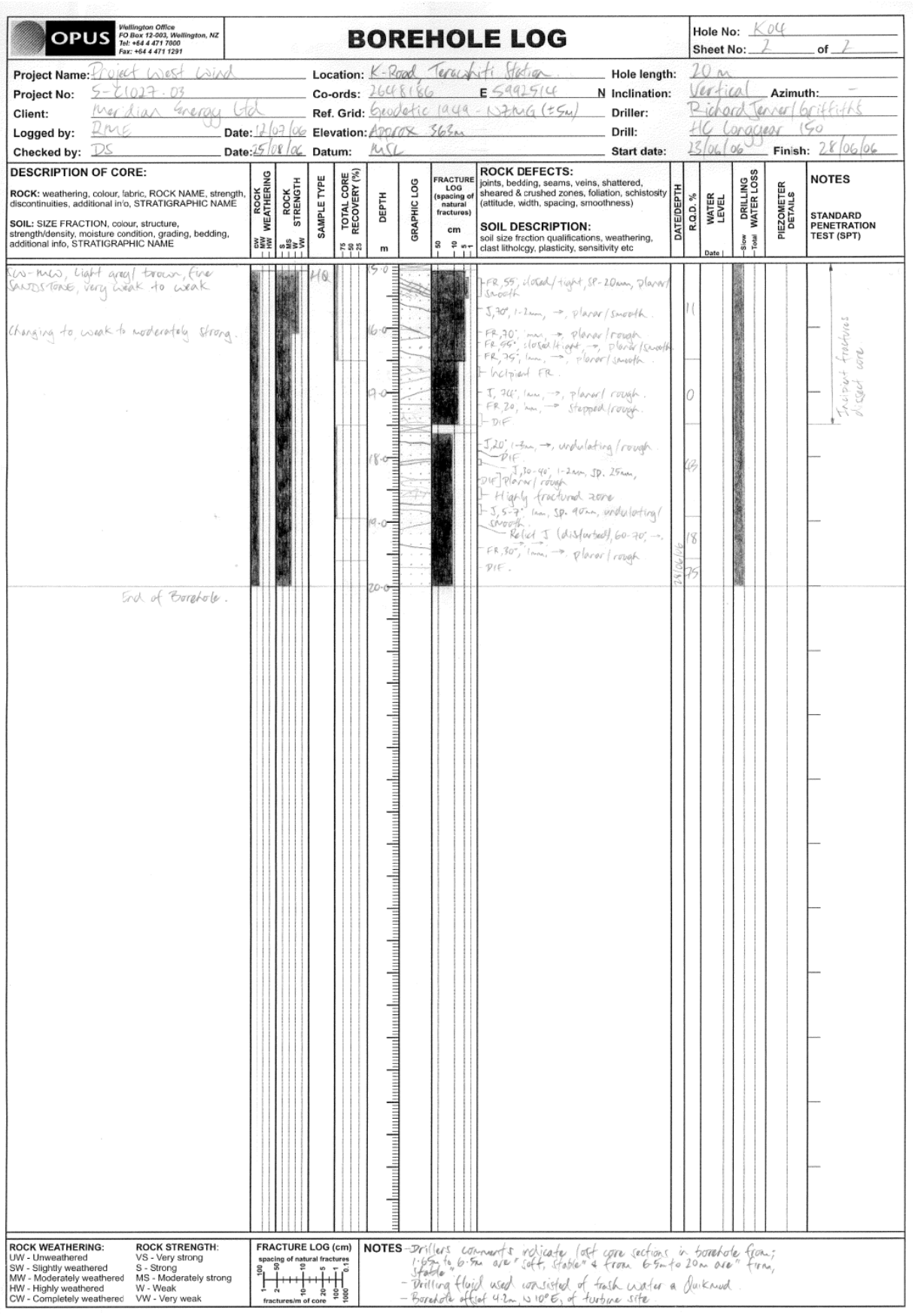

OPUS — Wellington Office, PO Box 12-003, Wellington, NZ, Tel: +64 4 471 7000, Fax: +64 4 471 1291

BOREHOLE LOG

Hole No: K04
Sheet No: 1 of 1

Project Name: Project West Wind
Project No: S-21027.03
Client: Meridian Energy Ltd
Logged by: RMC Date: 12/07/06
Checked by: DS Date: 25/08/06

Location: K-Road, Terawhiti Station
Co-ords: 2648186 E 5492514 N
Ref. Grid: Geodetic 1949 - NZMG (±5m)
Elevation: Approx 568m
Datum: MSL

Hole length: 20 m
Inclination: Vertical Azimuth: -
Driller: Richard Jenner / Griffiths
Drill: HC Carogear 150
Start date: 23/06/06 Finish: 28/06/06

DESCRIPTION OF CORE:

ROCK: weathering, colour, fabric, ROCK NAME, strength, discontinuities, additional info, STRATIGRAPHIC NAME

SOIL: SIZE FRACTION, colour, structure, strength/density, moisture condition, grading, bedding, additional info, STRATIGRAPHIC NAME

ROCK WEATHERING: CW MW HW
ROCK STRENGTH: S MS W VW
SAMPLE TYPE: HQ
TOTAL CORE RECOVERY (%): 75 50 25
DEPTH: m
GRAPHIC LOG
FRACTURE LOG (spacing of natural fractures): cm 50 10 1

ROCK DEFECTS:
joints, bedding, seams, veins, shattered, sheared & crushed zones, foliation, schistosity (attitude, width, spacing, smoothness)

SOIL DESCRIPTION:
soil size fraction qualifications, weathering, clast litholcgy, plasticity, sensitivity etc

DATE/DEPTH
R.Q.D. %
WATER LEVEL Date
DRILLING WATER LOSS: Slow / Total
PIEZOMETER DETAILS

NOTES
STANDARD PENETRATION TEST (SPT)

0.0–16.0 m: XW - MW, light grey / brown, fine SANDSTONE, very weak to weak
16.0–20.0 m: changing to, weak to moderately strong.
20.0 m: End of Borehole.

FR, 55°, closed / tight, SR - 20mm, planar / smooth
J, 70°, 1-2mm, →, planar / smooth
FR, 70°, 1mm, →, planar / rough
FR, 65°, closed / tight, →, planar / smooth
FR, 75°, 1mm, →, planar / smooth
Incipient FR.
J, 76°, 1mm, →, planar / rough.
FR, 20°, 1mm, → stepped / rough.
DIF
J, 20°, 1-3mm, →, undulating / rough
DIF.
J, 30-40°, 1-2mm, SP. 25mm, DIF] planar / rough
Highly fractured zone
J, 5-7°, 1mm, SP. 90mm, undulating / smooth.
Relict J (disturbed), 60-70°, →,
FR, 30°, 1mm, → planar / rough
DIF.

11
0
48
18
75
24/06/06

Frequent fractures in core

ROCK WEATHERING:
UW - Unweathered
SW - Slightly weathered
MW - Moderately weathered
HW - Highly weathered
CW - Completely weathered

ROCK STRENGTH:
VS - Very strong
S - Strong
MS - Moderately strong
W - Weak
VW - Very weak

FRACTURE LOG (cm)
spacing of natural fractures
100 50 10 5 1 0.1
1–2 10 20 100–1000
fractures/m of core

NOTES – Drillers comments indicate lost core sections in borehole from; 1.65m to 6.5m are "soft, stable" & from 6.5m to 20m are "firm, stable"
– Drilling fluid used consisted of fresh water & Quikwood
– Borehole offset 4.2m N 10°E, of turbine site.

Appendix H:

Turitea Windfarm Borehole Logs

Beca Carter Hollings & Ferner Ltd

BOREHOLE LOG KEY SHEET

WATER

Water level on date shown

METHOD

shows drilling method

OB	open barrel
Wash	wash boring
TT	triple tube
UT	thin walled undisturbed tube
SPT	standard penetration test
MA	machine auger
PS	piston sampler

SAMPLES

Dx	Disturbed sample, number x
Bx	Bulk sample, number x
Ux(d)	Undisturbed sample, number x, tube diameter d in mm
Wx	Water sample, number x

MOISTURE

D	Dry, looks and feels dry
M	Moist, no free water on hand when remoulding
W	Wet, free water on hand when remoulding
S	Saturated, soil below water table

CONSISTENCY

Cohesive Soils

		Undrained Shear Strength (kPa)
VS	Very soft	<12
S	Soft	12 to 25
F	Firm	25 to 50
St	Stiff	50 to 100
VSt	Very stiff	100 to 200
H	Hard	>200

CLASSIFICATION

Based on USBR Unified Soil Classification System

SOIL AND ROCK DESCRIPTIONS

Soil and Rock Descriptions are generally as described in the "Guidelines for the Field Description of Soils and Rocks in Engineering Use" by the NZ Geotechnical Society (1988)

Vane Shear Strength measurements in accordance with the NZ Geotechnical Society "Guideline for hand held shear vane test", dated August 2001.

IN-SITU TESTS

SV	= 40/10	Insitu shear strength and remoulded shear strength respectively, as measured by Pilcon Shear Vane
τ	= 50/12	Vane shear strength and remoulded vane shear strength respectively, corrected to BS1377
UTP	=	Unable To Penetrate with Shear Vane
N	= 15	SPT uncorrected blow count for 300mm penetration

S Laboratory Test(s) carried out:

AL	Atterberg limits
UU	Unconsolidated undrained triaxial
PSD	Particle size
CU	Consolidated undrained triaxial
CONS	Consolidation
COMP	Compaction
UCS	Unconfined compression

WEATHERING

CW	Completely weathered
HW	Highly weathered
MW	Moderately weathered
SW	Slightly weathered
UW	Unweathered

Non-cohesive Soils

		SPT - Uncorrected
VL	Very loose	0 to 4
L	Loose	4 to 10
MD	Medium dense	10 to 30
D	Dense	30 to 50
VD	Very dense	>50

GRAPHIC LOG (1 or a combination of the following)

Organic material

Clay

Silt

Sand

Mudstone

Siltstone

Sandstone

Volcanic Rock

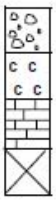

Gravel

Shells

Limestone

No Core

P:\320\32000000\EXCEL\GEOHOLE.XLS
Revised October 2001

Beca Carter Hollings & Ferner Ltd

BOREHOLE No: **BH5**

MACHINE BOREHOLE LOG

SHEET 1 of 1

PROJECT:	Turitea Windfarm	JOB NUMBER:	2310848/220
SITE LOCATION:	Turitea, Palmerston North	CLIENT:	Mighty River Power
BOREHOLE LOCATION:	Turbine 54		
COORDINATES:	N 6,080,318.00 m E 2,737,762.00 m	R L: DATUM:	520 m MSL

GEOLOGICAL UNIT	DRILLING: FLUID LOSS	DRILLING: WATER LEVEL	DRILLING: CORE RECOVERY	DRILLING: METHOD	DRILLING: RQD	DRILLING: CASING	IN-SITU TESTS: SV (kPa)	IN-SITU TESTS: τ (kPa)	IN-SITU TESTS: SPT 'N'	SAMPLES	R L (m)	DEPTH (m)	GRAPHIC LOG	CLASSIFICATION	MOISTURE	CONSISTENCY	SOIL / ROCK DESCRIPTION	INSTRUMENTATION
Topsoil			100 %	OB										ML	M	VSt	Very stiff brown GRAVELLY SILT, minor sand, trace clay, trace organics; moist, slightly plastic. Gravels are HW angular greywacke < 20 mm.	
Esk Head Belt		27/4	54 %	TT	21 %										M	VW	Very weak to moderately strong HW to MW grey GREYWACKE; moist. Fractures are closely spaced lined with < 2 mm of brown silt (Fe and Mn), subhorizontal to steeply dipping, undulating, rough to smooth, and planar.	
											519	1						
															M	EW	Extremely weak HW grey brown sheared SILTSTONE; moist. Trace greywacke gravel < 80 mm. Contact is rough and disturbed during drilling. Slickensided surface at 1.2 m, dipping 66 degrees.	
			50 %	TT	0 %										M	W	Weak HW-MW grey GREYWACKE; moist. Fractures are extremely closely spaced, lined with brown silt (Fe and Mn), rough and undulating .	
			0 %	SPT					50 for 120 mm N=50+		518	2			M	W	Weak grey sheared SILTSTONE with gravels of greywacke and dark red argillite < 70 mm lining bedding planes. Shear zones are steeply dipping (56 degrees) subparallel to bedding planes.	
			63 %	TT	0 %													
			100 %	TT	55 %										M	W	Weak to moderately strong grey fine SANDSTONE. Orange Fe and black Mn silt lining fractures, trace thin white calcite veins. Fractures are closely spaced, steeply dipping. Minor dark red brown chert gravels < 10 mm.	
			99 %	TT	0 %						517	3			M	W	Weak to moderately strong grey sheared SILTSTONE; moist. Gravels of < 5 mm (dark red argillite) to 60 mm (greywacke) lining bedding planes, boudinage structure.	
			0 %	SPT					50 for 100 mm N=50+								From 3.15m to 3.4m crush zone.	
			43 %	TT	0 %						516	4					Subvertical contact between grey fine greywacke and dark grey argillite. Fractures are closely spaced, rough, undulating. Stickensided contact lining interface.	
			0 %	SPT					50 for 25 mm N=50+								End of Borehole 4.525m.	

DATE STARTED:	26/4/06	DRILLED BY:	Pro-Drill
DATE FINISHED:	27/4/06	DRILL TYPE:	Gemco HP7
LOGGED BY:	JZC	DRILL METHOD:	Rotary
PILCON VANE No:	DR 3969	DRILL FLUID:	Water/polymer

COMMENTS: Shear strengths (SV) measured in end of core barrel. Coordinates taken from handheld gps unit. Elevations assumed from Topographic map. Mn=Manganese, Fe= Iron.

REVIEWED BY:

FOR EXPLANATION OF SYMBOLS AND ABBREVIATIONS SEE KEY SHEET

BCHF_MB P:\2311\2310848\TGETURITE~1.GPJ BCHFMB2.GDT 21/05/06

Beca Carter Hollings & Ferner Ltd

BOREHOLE No: **BH6**

MACHINE BOREHOLE LOG

SHEET 1 of 3

PROJECT: Turitea Windfarm — JOB NUMBER: 2310848/220

SITE LOCATION: Turitea, Palmerston North — CLIENT: Mighty River Power

BOREHOLE LOCATION: Turbine 76

COORDINATES: N 6,083,006.00 m — R L: 420 m

E 2,740,298.00 m — DATUM: MSL

GEOLOGICAL UNIT	DRILLING: FLUID LOSS	DRILLING: WATER LEVEL	DRILLING: CORE RECOVERY	DRILLING: METHOD	DRILLING: RQD	DRILLING: CASING	IN-SITU TESTS: SV (kPa)	IN-SITU TESTS: τ (kPa)	IN-SITU TESTS: SPT 'N'	SAMPLES	R L (m)	DEPTH (m)	GRAPHIC LOG	CLASSIFICATION	MOISTURE	CONSISTENCY	SOIL / ROCK DESCRIPTION	INSTRUMENTATION
Topsoil			76 %	OB										OL	M	St	Stiff dark brown ORGANIC SILT, trace clay; moist, slightly plastic.	
Quaternary Deposits			100 %	OB			95/36	152/57						ML	M	St	Grades to stiff yellow brown SILT, trace clay, trace orange flecks; moist, slightly plastic.	
			100 %	OB													Trace ironstained organics, trace sand, trace fine gravel < 3 mm.	
			100 %	OB			76/16	120/24			419	1		MH			Minor clay; moderately plastic.	
			100 %	SPT			51/16	80/24	1 6 5 N=11					SM	M	MD	Medium dense yellow brown SILTY SAND, trace fine greywacke gravel < 5 mm; moist, non plastic.	
CW Esk Head Belt														MH	M	St	Stiff yellow brown SILT, minor clay, trace fine gravel < 5 mm, trace decomposing organics; moist, moderately plastic.	
			47 %	OB							418	2		ML	M	MD	Medium dense yellow brown mottled grey SILT, some sand, minor HW angular greywacke gravel < 5 mm; moist, non plastic. Poor recovery.	
HW Esk Head Belt (Sandstone)		27/4/06	100 %	SPT			UTP	UTP	11 21 32 N=50+		417	3		ML	M	VD	Very dense yellow mottled orange dark brown SANDY SILT; moist, non plastic. Trace black Mn and orange Fe streaks lining relict fractures cross cutting core.	
			0 %	TT													Lost sample.	
			100 %	TT							416	4			M	EW	Extremely weak HW yellow mottled orange and grey GREYWACKE; moist. Fractures very closely spaced, angular and stepped. Medium dense SILT; moist, non plastic.	
									10					ML	M	MD	Medium dense yellow mottled orange SILT, minor angular greywacke gravel < 10 mm.	

DATE STARTED: 27/4/06 — DRILLED BY: Pro-Drill

DATE FINISHED: 28/4/06 — DRILL TYPE: Gemco HP7

LOGGED BY: JZC — DRILL METHOD: Rotary

PILCON VANE No: DR 3969 — DRILL FLUID: Water/polymer

COMMENTS: Shear strengths (SV) measured in end of core barrel. Coordinates taken from handheld gps unit. Elevations assumed from Topographic map. Mn=Manganese, Fe= Iron.

REVIEWED BY:

FOR EXPLANATION OF SYMBOLS AND ABBREVIATIONS SEE KEY SHEET

BCHF_MB P:\2311\2310848\TGT\TURITE~1.GPJ BCHFMB2.GDT 25/05/06

Beca Carter Hollings & Ferner Ltd

BOREHOLE No: **BH6**

MACHINE BOREHOLE LOG

SHEET 2 of 3

PROJECT: Turitea Windfarm — JOB NUMBER: 2310848/220

SITE LOCATION: Turitea, Palmerston North — CLIENT: Mighty River Power

BOREHOLE LOCATION: Turbine 76

COORDINATES: N 6,083,006.00 m — R.L: 420 m

E 2,740,298.00 m — DATUM: MSL

GEOLOGICAL UNIT	DRILLING: FLUID LOSS	DRILLING: WATER LEVEL	DRILLING: CORE RECOVERY	DRILLING: METHOD	DRILLING: RQD	DRILLING: CASING	IN-SITU TESTS: SV (kPa)	IN-SITU TESTS: T (kPa)	IN-SITU TESTS: SPT 'N'	SAMPLES	R.L (m)	DEPTH (m)	GRAPHIC LOG	CLASSIFICATION	MOISTURE	CONSISTENCY	SOIL / ROCK DESCRIPTION	INSTRUMENTATION
HW Esk Head Belt (Sandstone)			100 %	SPT					11 16 N=27					ML	M	MD	Medium dense orange brown mottled dark orange and grey SANDY SILT, minor MW greywacke gravel < 20 mm. Relict fractures are steeply dipping and lined with black Mn, smooth and planar.	
			60 %	TT							414	6			M	EW	Extremely weak HW yellow brown mottled orange SILTSTONE; moist. Fractures are very closely spaced; smooth and stepped, lined with dark orange Fe silt. Some dark red brown argillite gravels < 50 mm.	
			0 %	SPT					28 35 15 for 60 mm N=50+								No sample, solid SPT.	
			66 %	TT							413	7			M	EW	Extremely weak HW orange SILTSTONE; moist. Minor light grey clay-silt laminations and HW dark red brown argillite gravels < 30 mm lining bedding planes. Slickensided surfaces, 36 degrees, lined with dark brown Mn and Fe, undulating lining bedding planes.	
			100 %	TT													From 7.5m to 8m, crush zone. Light grey and orange brown steeply dipping laminations. Sheared surfaces dipping 32 to 50 degrees.	
			100 %	SPT					13 30 20 for 75 mm N=50+		412	8		MH	M	H	Hard dark grey speckled white SILT, minor clay, trace fine gravel; moist, moderately plastic.	
														MH	M	H	Hard grey SANDY SILT, minor clay; some fine angular siltstone gravel; moist, moderately plastic.	
			100 %	TT										MH	M	VD	Very dense dark grey mottled white SILTY SAND, minor clay, minor HW argillite angular gravel < 10 mm; moist, moderately plastic.	
			0 %	TT							411	9					Lost sample.	
MW Esk Head Belt			100 %	SPT					50 for 105 mm N=50+						M	EW	Extremely weak MW dark grey sheared SILTSTONE, trace silt, trace clay; moist. Steeply dipping slickensided surfaces lined with trace clay. Driller comment that material is similar to drilling through fault gouge.	
			70 %	TT														

DATE STARTED: 27/4/06 — DRILLED BY: Pro-Drill

DATE FINISHED: 28/4/06 — DRILL TYPE: Gemco HP7

LOGGED BY: JZC — DRILL METHOD: Rotary

PILCON VANE No: DR 3969 — DRILL FLUID: Water/polymer

COMMENTS: Shear strengths (SV) measured in end of core barrel. Coordinates taken from handheld gps unit. Elevations assumed from Topographic map. Mn=Manganese, Fe= Iron.

REVIEWED BY:

FOR EXPLANATION OF SYMBOLS AND ABBREVIATIONS SEE KEY SHEET

BCHF_MB P:\2310\2310848\BTGEL\TURITE~1.GPJ BCHFMB2.GDT 25/05/06

Beca Carter Hollings & Ferner Ltd

BOREHOLE No: **BH6**

MACHINE BOREHOLE LOG

SHEET 3 of 3

PROJECT:	Turitea Windfarm	JOB NUMBER:	2310848/220
SITE LOCATION:	Turitea, Palmerston North	CLIENT:	Mighty River Power

BOREHOLE LOCATION: Turbine 76

COORDINATES: N 6,083,006.00 m E 2,740,298.00 m

R L: 420 m DATUM: MSL

GEOLOGICAL UNIT	DRILLING: FLUID LOSS	DRILLING: WATER LEVEL	DRILLING: CORE RECOVERY	DRILLING: METHOD	DRILLING: RQD	DRILLING: CASING	IN-SITU TESTS: SV (kPa)	IN-SITU TESTS: τ (kPa)	IN-SITU TESTS: SPT 'N'	SAMPLES	R L (m)	DEPTH (m)	GRAPHIC LOG	CLASSIFICATION	MOISTURE	CONSISTENCY	SOIL / ROCK DESCRIPTION	INSTRUMENTATION
MW Esk Head Belt			70 %	TT													Poor recovery.	
			15 %	TT													Lost sample.	
SW Esk Head Belt			C %	SPT					50 for 35 mm N=50+		409 11				M	EW	Extremely weak SW grey speckled white interbedded GREYWACKE and ARGILLITE; moist. Subvertical, thinly bedded. Broken into gravels by drilling action.	
			61 %	TT														
			0 %	TT							408 12						Poor recovery. Trace thin white veins cross cutting core.	
			48 %	TT														
			C %	SPT					52 for 50 mm N=50+									
			100 %	TT													Dark grey subvertically bedded greywacke gravel < 60 mm (boudins) in sheared argillaceous matrix.	
			100 %	TT							407 13						Steeply dipping slickensided surfaces. Fractures are very closely spaced, rough and stepped.	
			67 %	TT											W		Weak to moderately strong, greywacke gravels < 60 mm. Fractures lined with sheared argillaceous material. Inclination of slickensided surface at 34 degrees, corresponding to bedding dip.	
			0 %															
			C %	SPT					50 for 50 mm N=50+		406 14						End of Borehole 13.95m.	

DATE STARTED:	27/4/06	DRILLED BY:	Pro-Drill
DATE FINISHED:	28/4/06	DRILL TYPE:	Gemco HP7
LOGGED BY:	JZC	DRILL METHOD:	Rotary
PILCON VANE No:	DR 3969	DRILL FLUID:	Water/polymer

COMMENTS: Shear strengths (SV) measured in end of core barrel. Coordinates taken from handheld gps unit. Elevations assumed from Topographic map. Mn=Manganese, Fe= Iron.

REVIEWED BY:

FOR EXPLANATION OF SYMBOLS AND ABBREVIATIONS SEE KEY SHEET

CHF_MB P:\2312310848\TGEITURITE~1.GPJ BCHFM82.GDT 25/05/06

Appendix I:

MASW survey dispersion curves, velocity models, locations and confidence rankings

Location	Turbine number	Confidence Ranking	Relative
Te Rere Hau	1	4	-
Te Rere Hau	2	4	
Te Rere Hau	3	3	-
Te Rere Hau	4	2	
Te Rere Hau	5	3	
Te Rere Hau	7	4	+
Te Rere Hau	8	4	-
Te Rere Hau	9	4	
Te Rere Hau	10	4	+
Te Rere Hau	17	5	-
Te Rere Hau	28	2	
Te Rere Hau	29	4	+
Te Rere Hau	31	4	-
Te Rere Hau	33	4	
Te Rere Hau	34	1	+
Te Rere Hau	34	4	+
Te Rere Hau	35	4	
Te Rere Hau	36	1	
Te Rere Hau	36	3	
Te Rere Hau	37	4	
Te Rere Hau	38	2	+
Te Rere Hau	38	3	
Te Rere Hau	45	5	-
Te Rere Hau	46	4	+
Te Rere Hau	47	3	+
Te Rere Hau	49	4	
Te Rere Hau	50	4	
Te Rere Hau	51	4	
Te Rere Hau	52	1	+
Te Rere Hau	52	5	
Te Rere Hau	53	1	+
Te Rere Hau	53	5	-
Te Rere Hau	54	3	-
Te Rere Hau	55	5	

Te Rere Hau	56	4	+
Te Rere Hau	58	4	
Te Rere Hau	59	4	
Te Rere Hau	60	5	+
Te Rere Hau	72	3	-
Te Rere Hau	73	4	+
Te Rere Hau	74	5	
Te Rere Hau	75	5	
Te Rere Hau	76	4	+
Te Rere Hau	77	5	
Te Rere Hau	78	5	
Te Rere Hau	79	5	
Te Rere Hau	80	2	-
Te Rere Hau	84	4	+
Te Rere Hau	85	5	
Te Rere Hau	86	5	
Te Rere Hau	87	4	+
Te Rere Hau	88	4	+
Te Rere Hau	89	4	-
Te Rere Hau	91	4	+
Te Rere Hau	94	4	-
Te Rere Hau	95	5	
Te Rere Hau	96	5	+
Te Rere Hau	97	5	+
Te Rere Hau	103	4	+
Te Rere Hau	104	2	
Te Rere Hau	201	4	-
Te Rere Hau	202	2	+
Te Rere Hau	203	5	-
Te Rere Hau	204	3	+
Te Rere Hau	205	3	+
Te Rere Hau	206	3	+
Te Rere Hau	207	2	+
Te Rere Hau	208	4	+
Te Rere Hau	209	4	+
Te Rere Hau	210	3	-
Te Rere Hau	211	3	-
Te Rere Hau	212	4	-

Te Rere Hau	213	4	-
Te Rere Hau	214	3	+
Te Rere Hau	219	4	+
Te Rere Hau	220	3	+
Te Rere Hau	232	4	+
Te Rere Hau	234	5	
Te Rere Hau	238	3	-
Te Rere Hau	240	4	-
Te Rere Hau	241	3	-
Te Rere Hau	242	4	+
Te Rere Hau	243	4	-
Te Rere Hau	244	3	
Te Rere Hau	245	2	-
Te Rere Hau	245	0	
Turitea	1	3	+
Turitea	2	4	-
Turitea	3	4	
Turitea	5	3	+
Turitea	6	4	+
Westwind	K04	4	
Westwind	H03	1	

Table I.1: Confidence ranking for each MASW survey at turbine sites across the Te Rere Hau, Turitea and West Wind Windfarms.

SITE NUMBER: T1 (4-)

Site description

No marker found, bedrock to surface at what is believed to be turbine site. Probe >1.3 m.

Field file numbers

203-22, 204-10, 205-10.

Site photographs

Shot record and dispersion curve (10 m)

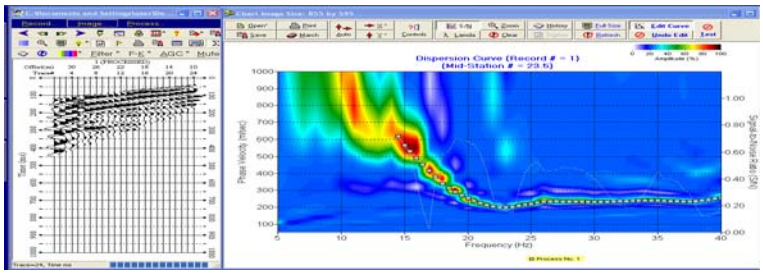

Shot record and dispersion curve (22 m)

No curve extracted

Shot record and dispersion curve (36 m FRW)

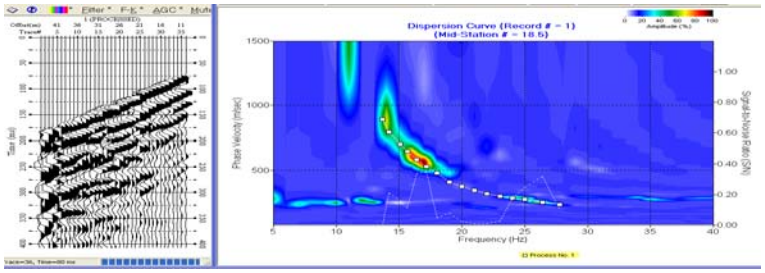

Velocity model from walkaway record

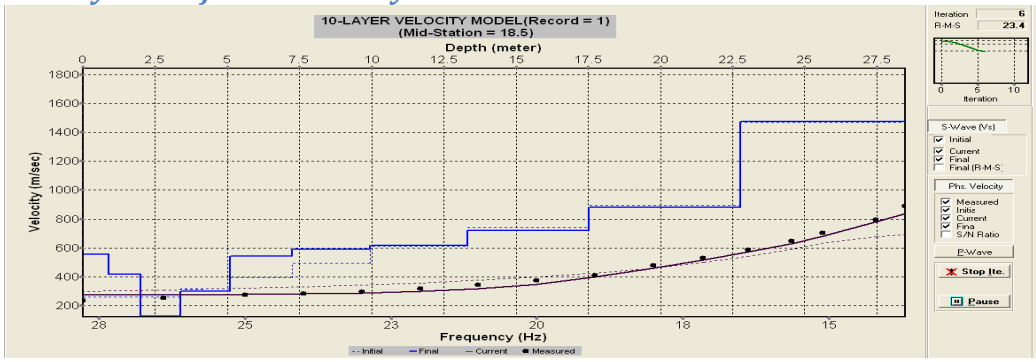

SITE NUMBER: T2 (4)

Site description

Under T2 mark, Torlesse bedrock to surface, weathered but generally intact. Probe >1.3m

Field file numbers

201-22, 202-10

Site photographs

Shot record and dispersion curve (10 m)

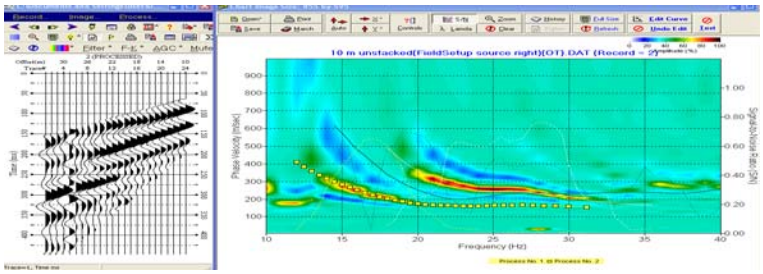

Shot record and dispersion curve (22 m)

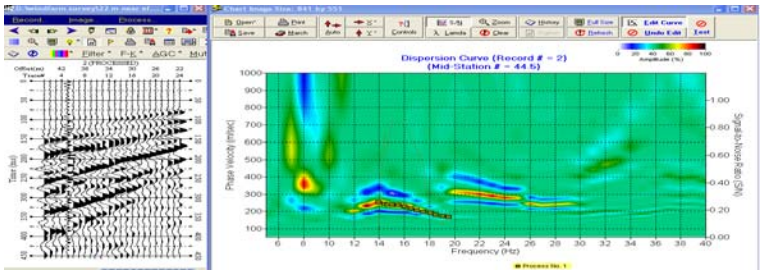

Velocity model from 10 m record

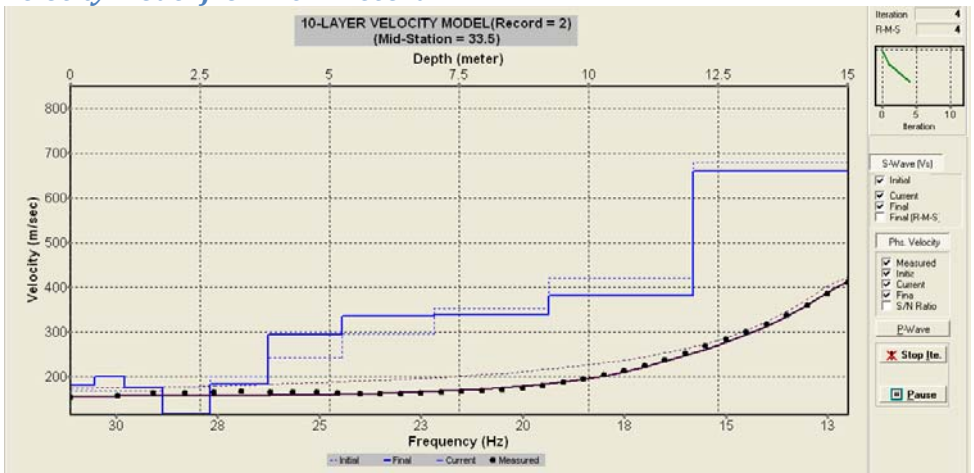

SITE NUMBER: T3 (3-)

Site description

Depth to bedrock approximately 1 m. Outcrop 5 m from peg.

Field file numbers

208-22, 209-10, (later 349, 350 and 351 – all 10 m)

Site photographs

Shot record and dispersion curve (10 m)

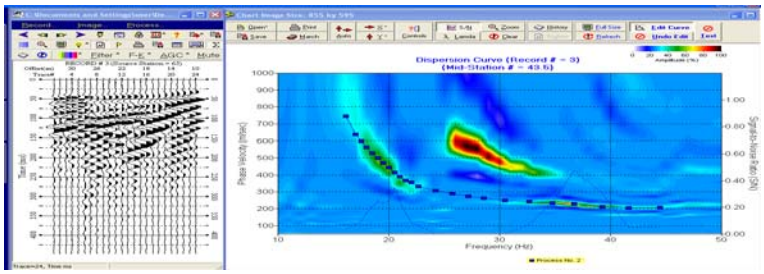

Shot record and dispersion curve (22 m)

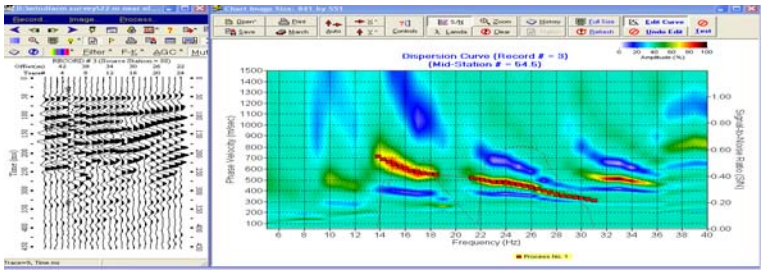

Velocity model from 10 m record

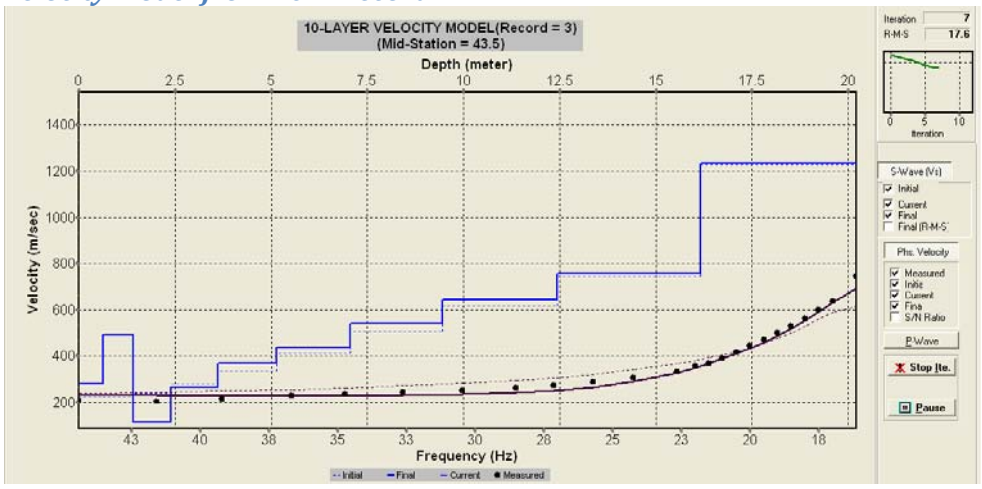

SITE NUMBER: T4 (2)

Site description

Sited on bedrock

Field file numbers

212-22, 213-10

Site photographs

Shot record and dispersion curve (10 m)

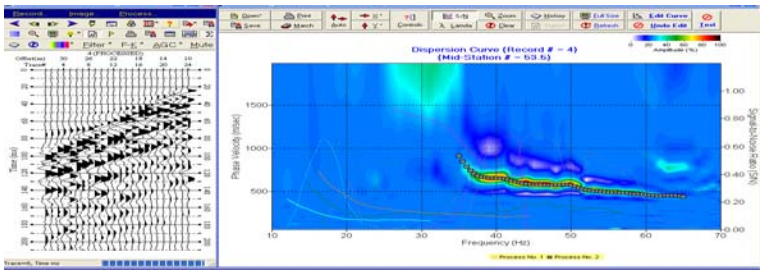

Shot record and dispersion curve (22 m)

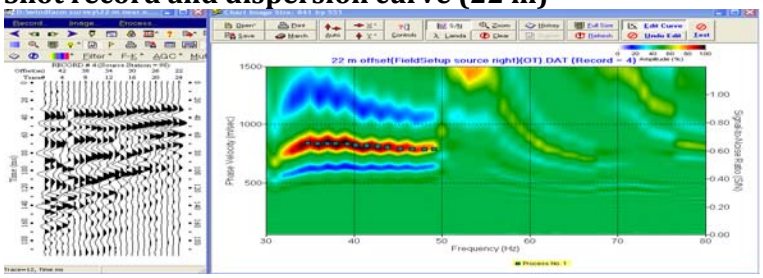

Velocity model from 10 m record

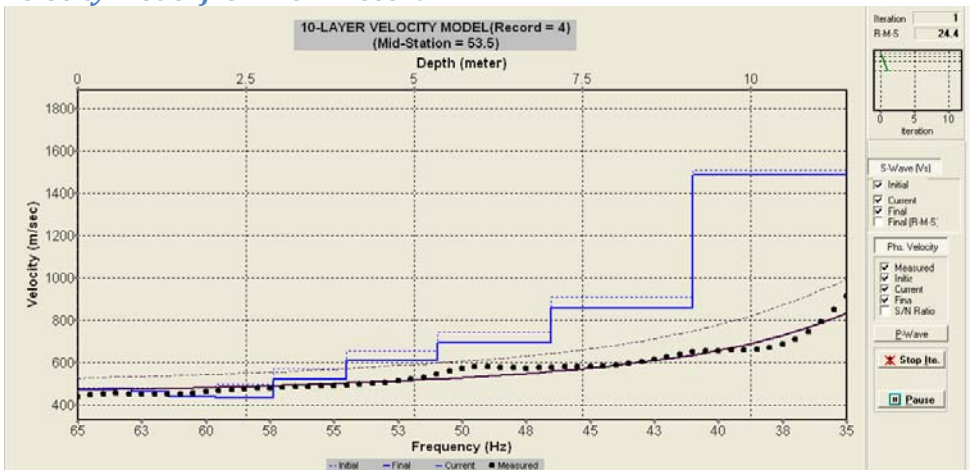

SITE NUMBER: T5/6 (3)

Site description

Bedrock to surface along geophone line

Field file numbers

214-22, 215-10

Site photographs

Shot record and dispersion curve (10 m)

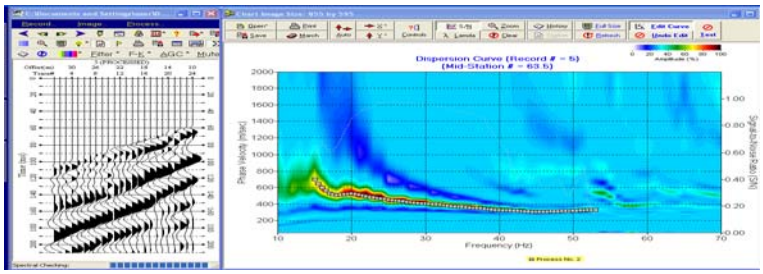

Shot record and dispersion curve (22 m)

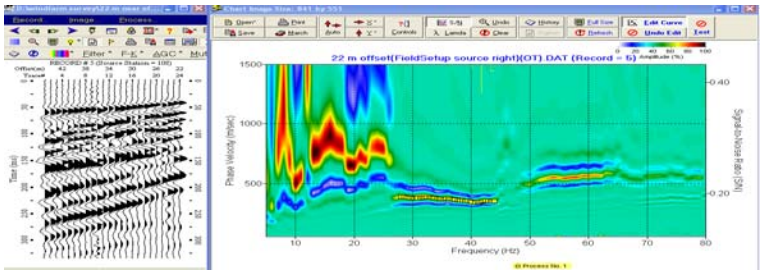

Velocity model from 10 m record

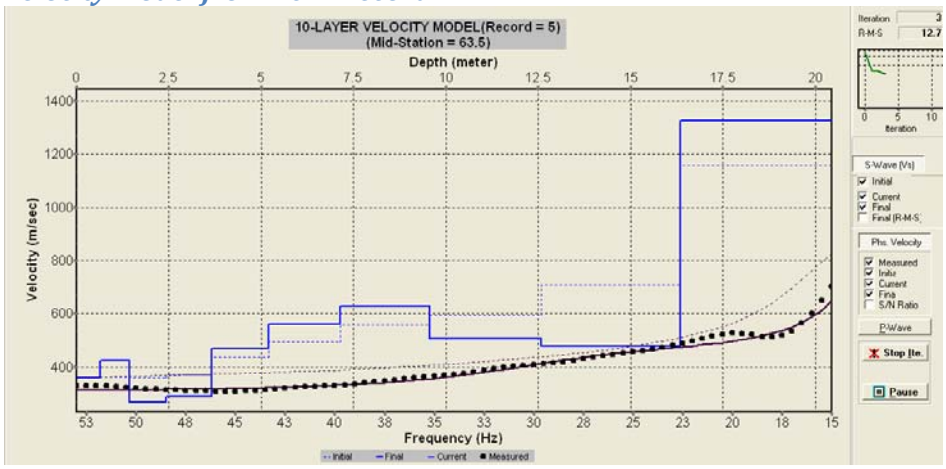

SITE NUMBER: T7 (4+)

Site description

0.5m soil over weathered bedrock

Field file numbers

216-22, 217-10

Site photographs

Shot record and dispersion curve (10 m)

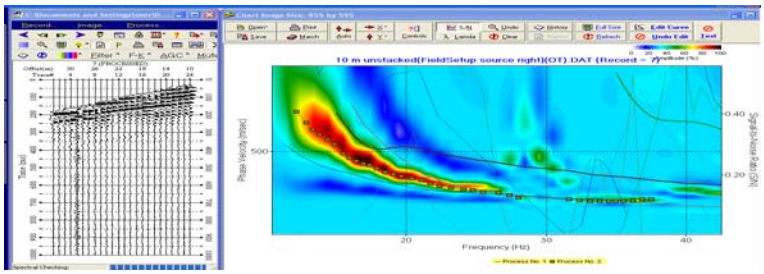

Shot record and dispersion curve (22 m)

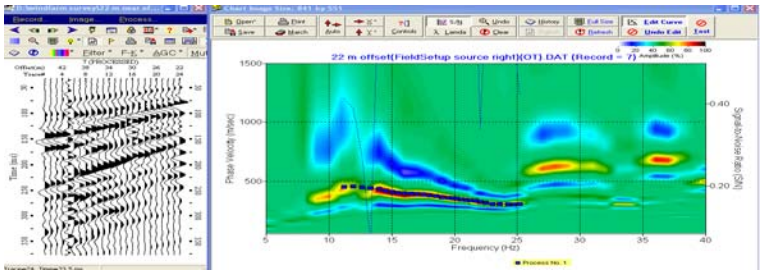

Velocity model from 10 m record

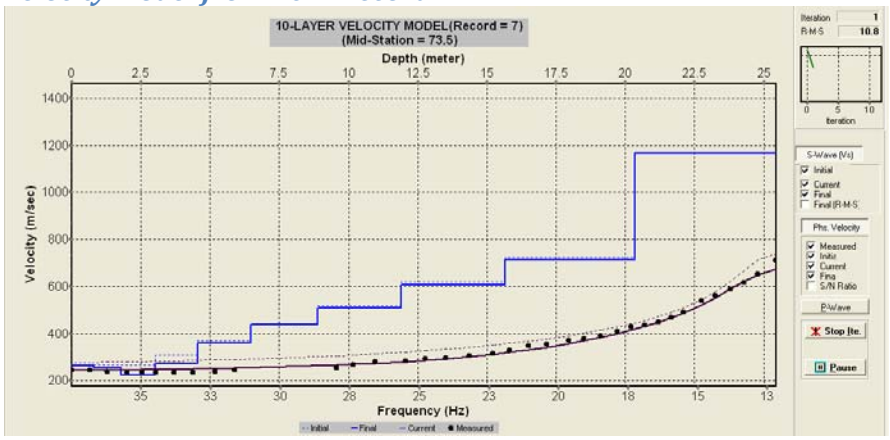

SITE NUMBER: T8 (4-)

Site description

Bedrock 0.4 m below surface

Field file numbers

218-22, 219-10

Site photographs

Shot record and dispersion curve (10 m)

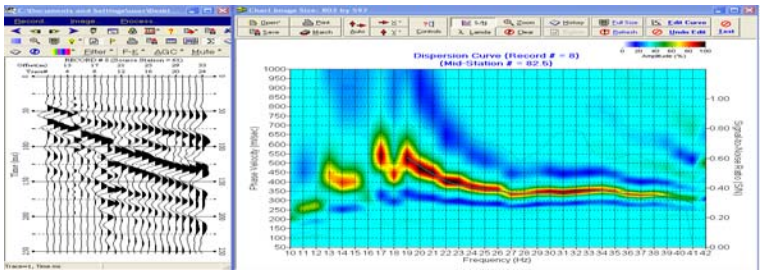

Shot record and dispersion curve (22 m)

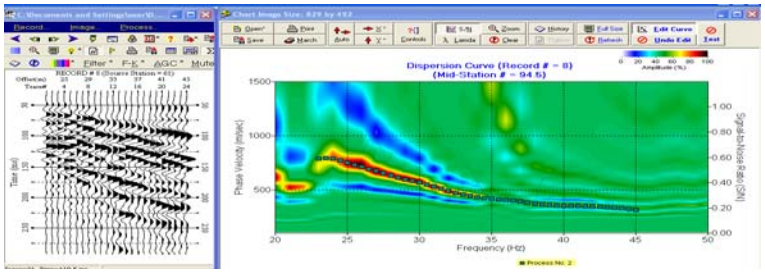

Velocity model from 10 m record

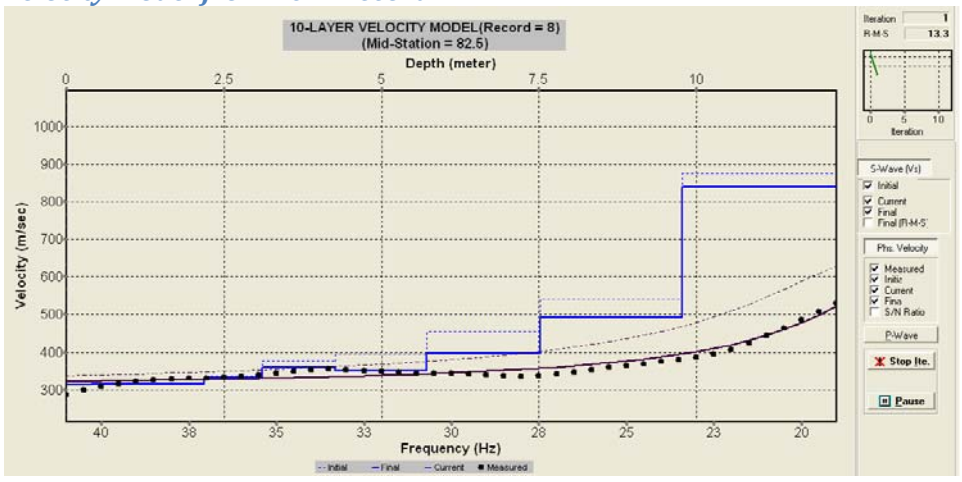

SITE NUMBER: T10 (0)

Site description

Cutting into bedrock

Field file numbers

354-10, 355-10

Site photographs

Shot record and dispersion curve (10 m)

Velocity model

SITE NUMBER: T17 (5-)

Site description

Cutting on hillside, bedrock visible at 1 m below top of cutting. Bench cut into bedrock.

Field file numbers

352-6 (stacked) 353-6

Site photographs

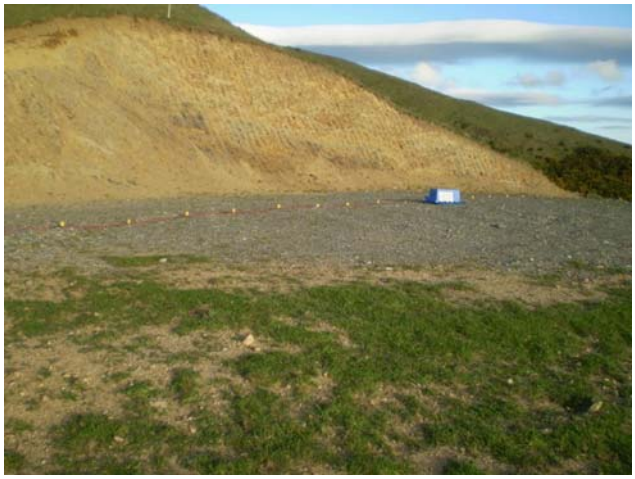

Shot record and dispersion curve (6 m)

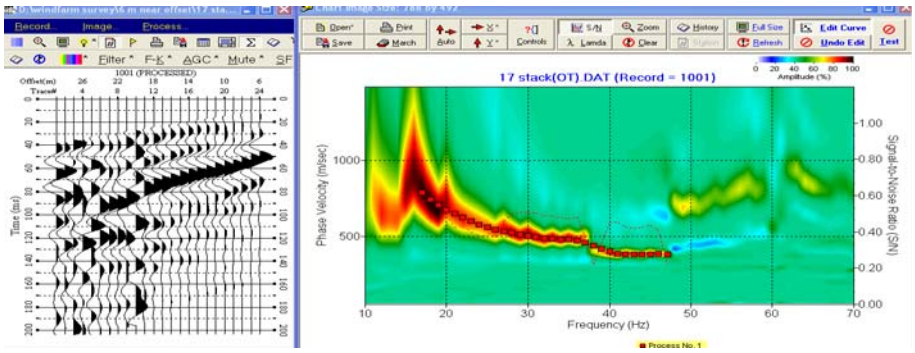

Velocity model from 6 m record

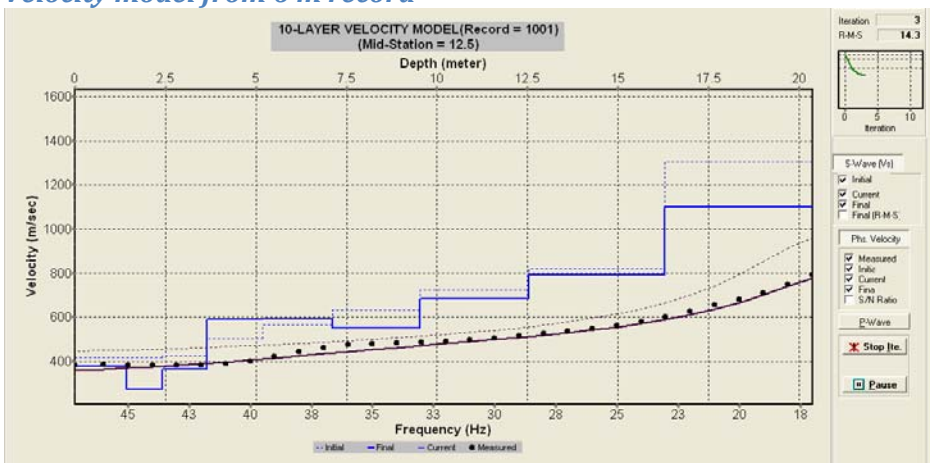

SITE NUMBER: T28 (2)

Site description

Bedrock to surface. Probe under array <1 m, probe under mark ~0.5 m

Field file numbers

222-22, 223-10

Site photographs

Shot record and dispersion curve (10 m)

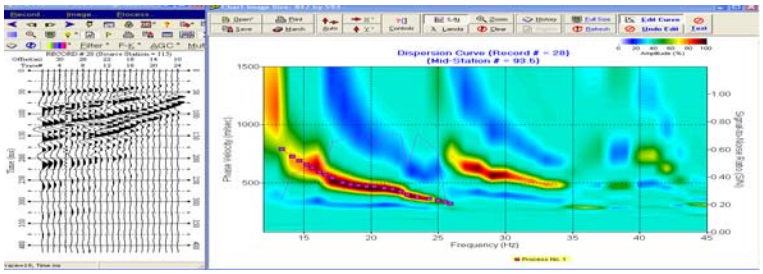

Shot record and dispersion curve (22 m)

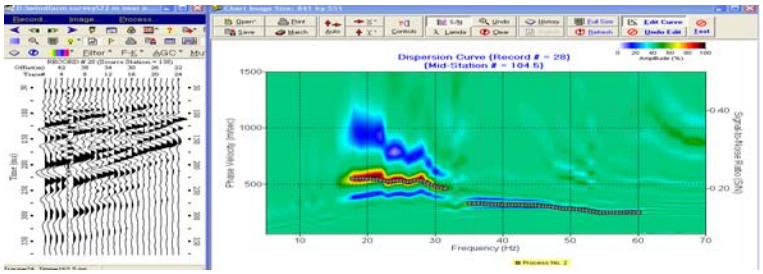

Velocity model from 10 m record

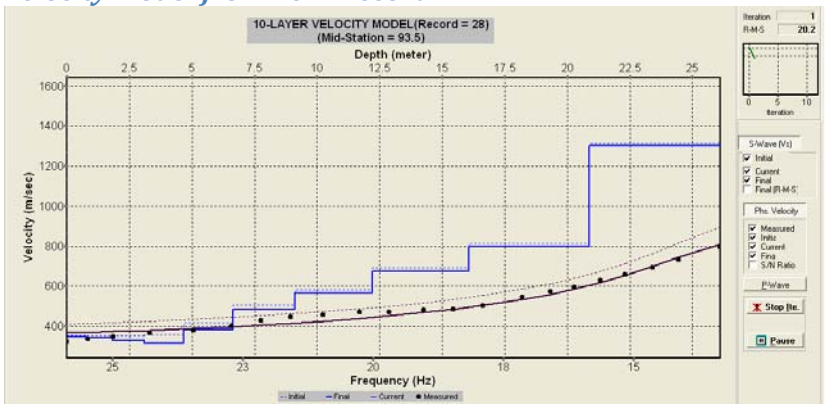

SITE NUMBER: T29/30 (4+)

Site description

>1m cover, no outcrop.

Field file numbers

226-22, 227-10

Site photographs

Shot record and dispersion curve (10 m)

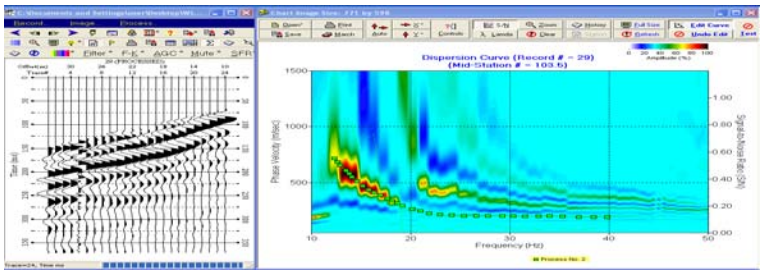

Shot record and dispersion curve (22 m)

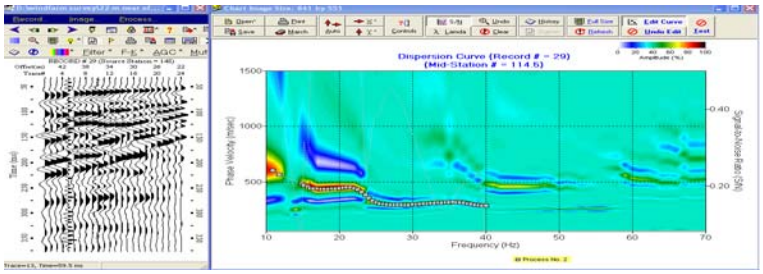

Velocity model from 10 m record

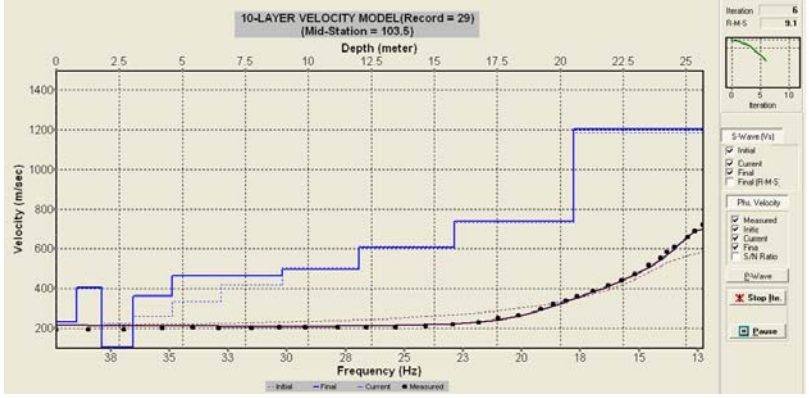

SITE NUMBER: T31/32 (4-)

Site description

No outcrop, probe under array to >1 m

Field file numbers

228-22, 229-10

Site photographs

Shot record and dispersion curve (10 m)

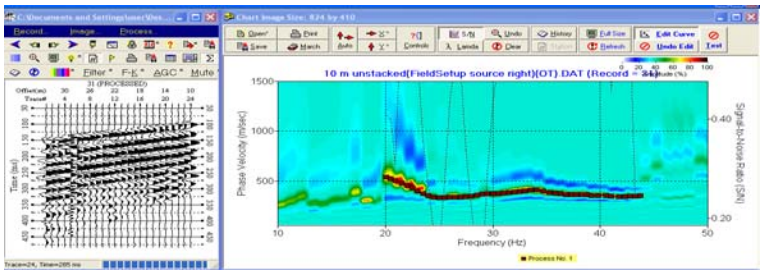

Shot record and dispersion curve (22 m)

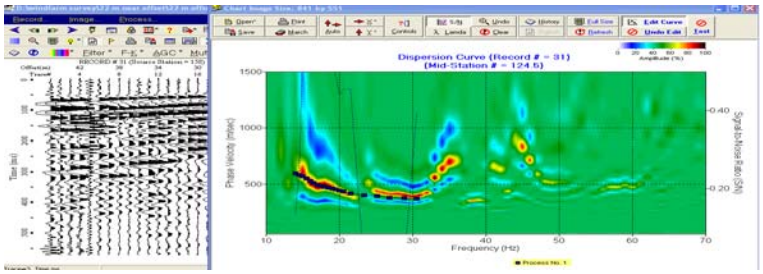

Velocity model from 22m record

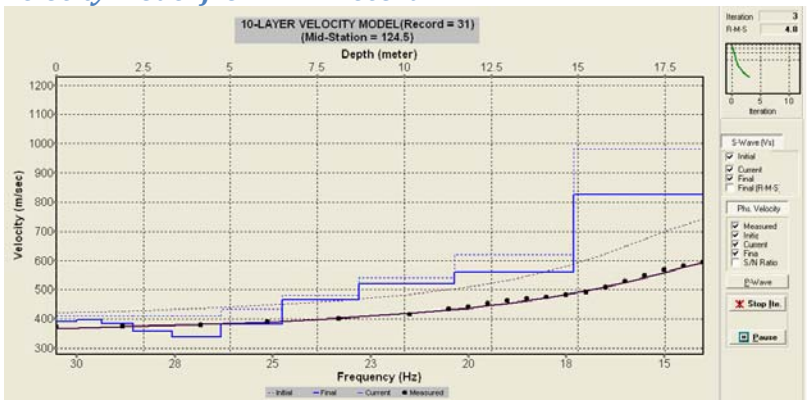

SITE NUMBER: T33 (4)

Site description

Outcrop at pad, probe along array to >1 m

Field file numbers

231-22, 232-10

Site photographs

Shot record and dispersion curve (10 m)

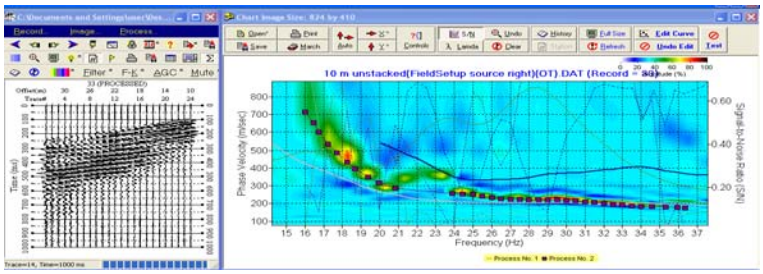

Shot record and dispersion curve (22 m)

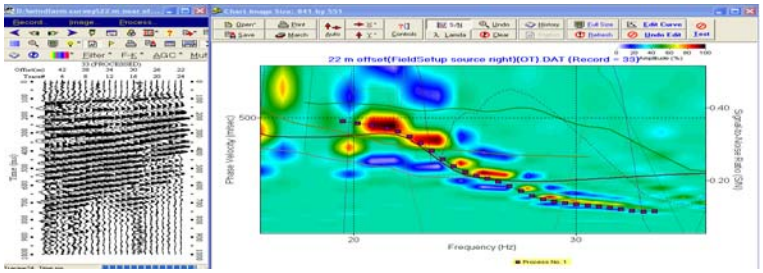

Velocity model from 10 m record

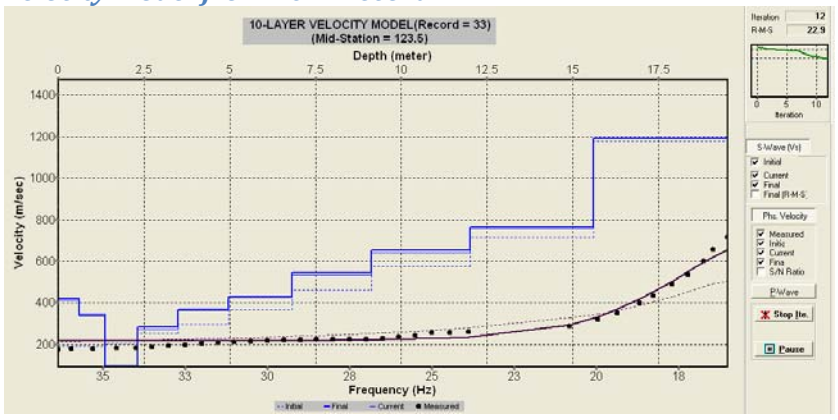

SITE NUMBER: T34 (1+)

Site description

Light grey mudstone seen in pad, probe to 0.8 m under array.

Field file numbers

233-22, 234-22 stacked, 235-10 stacked, 236-10

Site photographs

Shot record and dispersion curve (10 m)

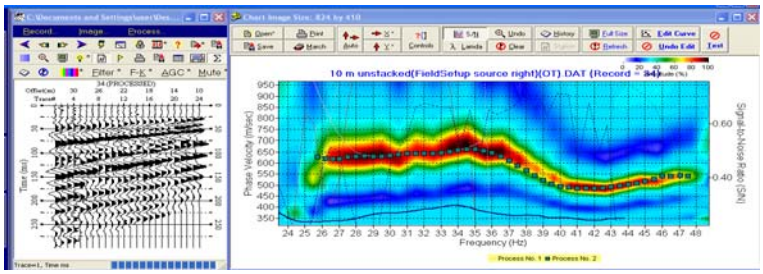

Shot record and dispersion curve (22 m)

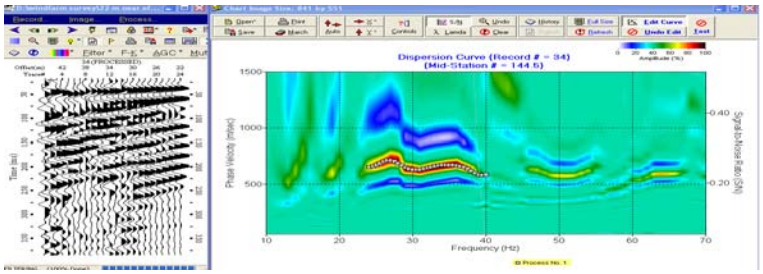

Velocity model from 10 m record

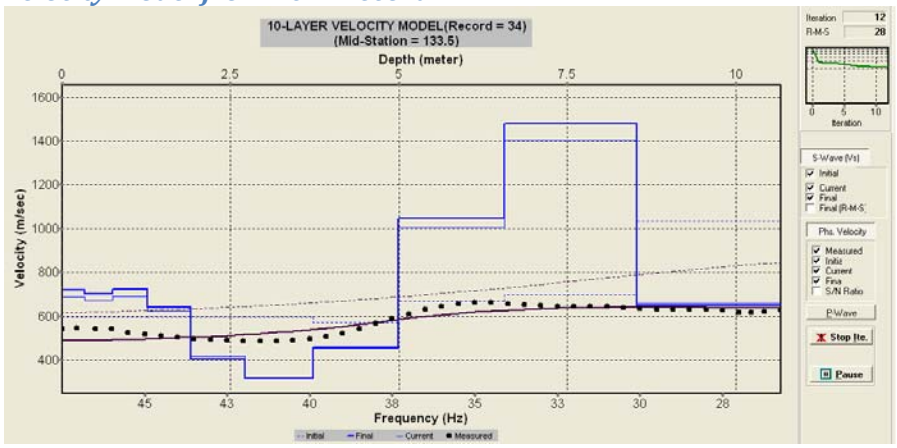

SITE NUMBER: T35 (4+)

Site description

Bedrock 0.5 m in road next to pad. Probe 0.5 m along array, >1.3m at array. Marker located in small gulley.

Field file numbers

237-22 stacked, 238-10 stacked, 239-10

Site photographs

Shot record and dispersion curve (10 m)

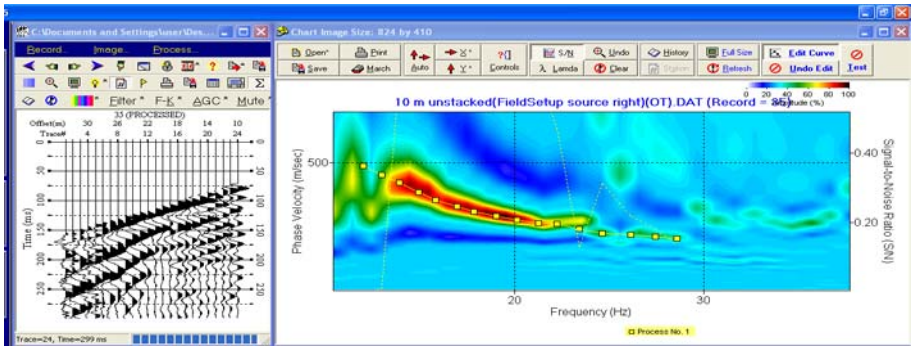

Shot record and dispersion curve (22 m)

Missing file

Velocity model from 10 m record

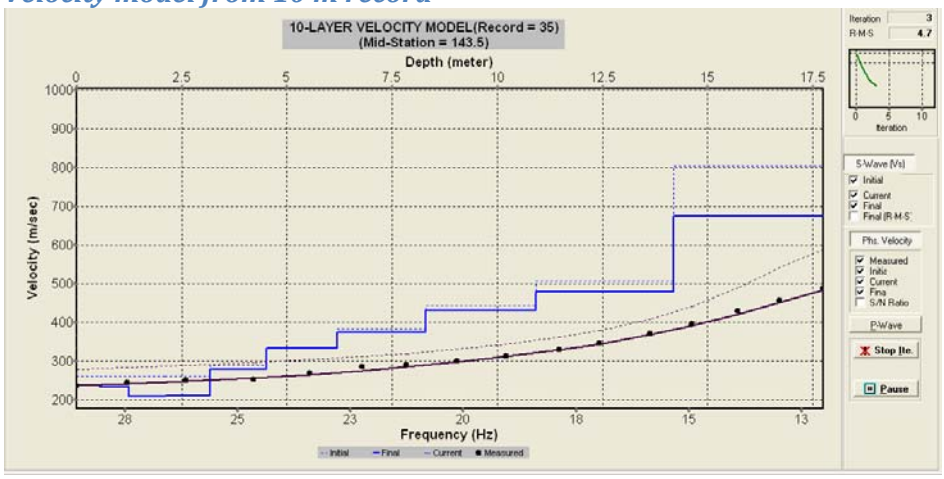

SITE NUMBER: T36 (1)

Site description

Highly fractured Torlesse with talus slope material under 1-2 m of clayey soil

Field file numbers

240-22 stacked, 241-10 stacked, 242-10

Site photographs

Shot record and dispersion curve (10 m)

No dispersion curve extractable

Shot record and dispersion curve (22 m)

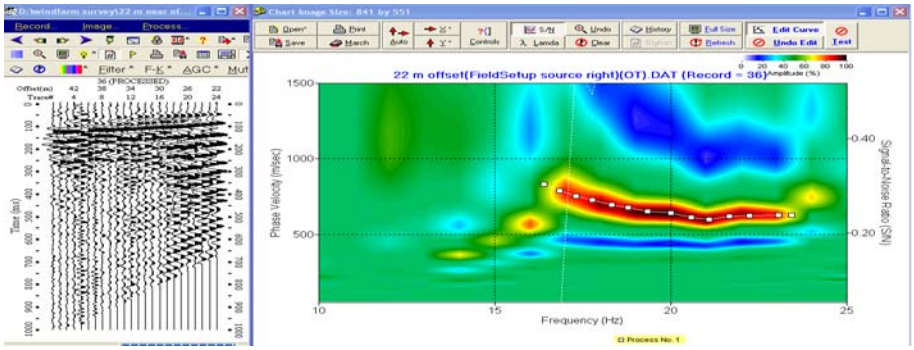

Velocity model from 22 m record

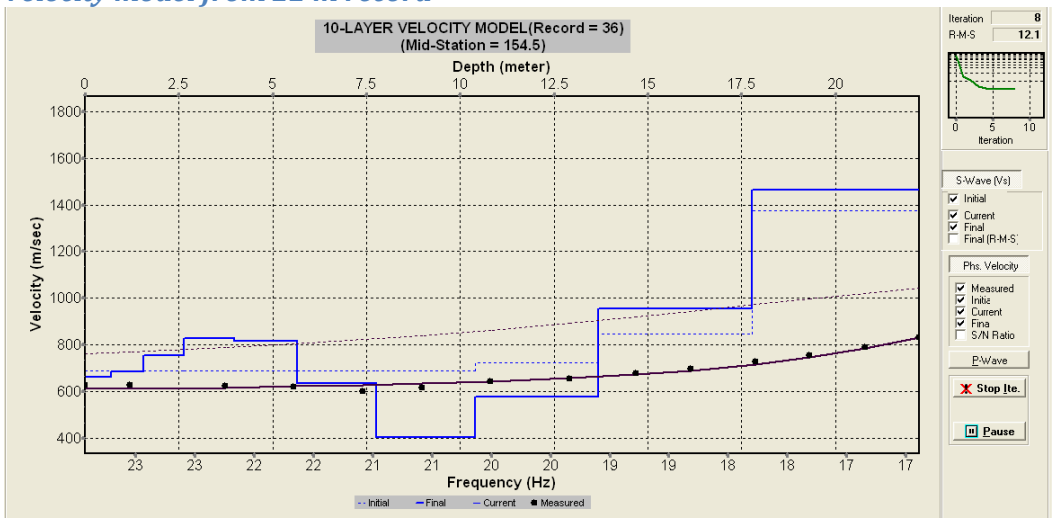

SITE NUMBER: T37 (4)

Site description

Bedrock to surface with gravel veneer

Field file numbers

243-10 stacked, 244-10

Site photographs

Shot record and dispersion curve (10 m)

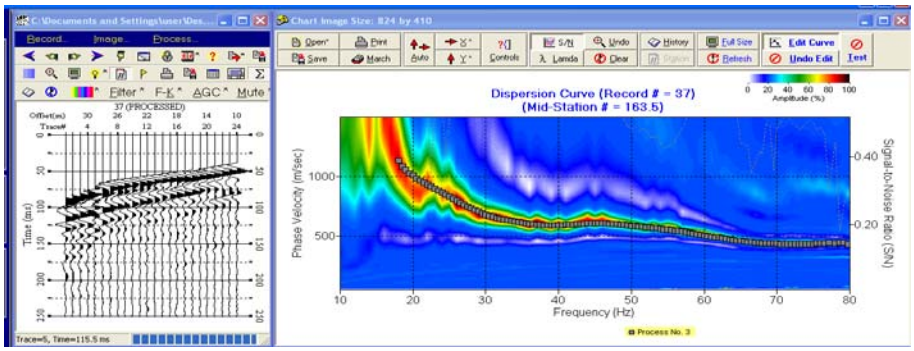

Velocity model

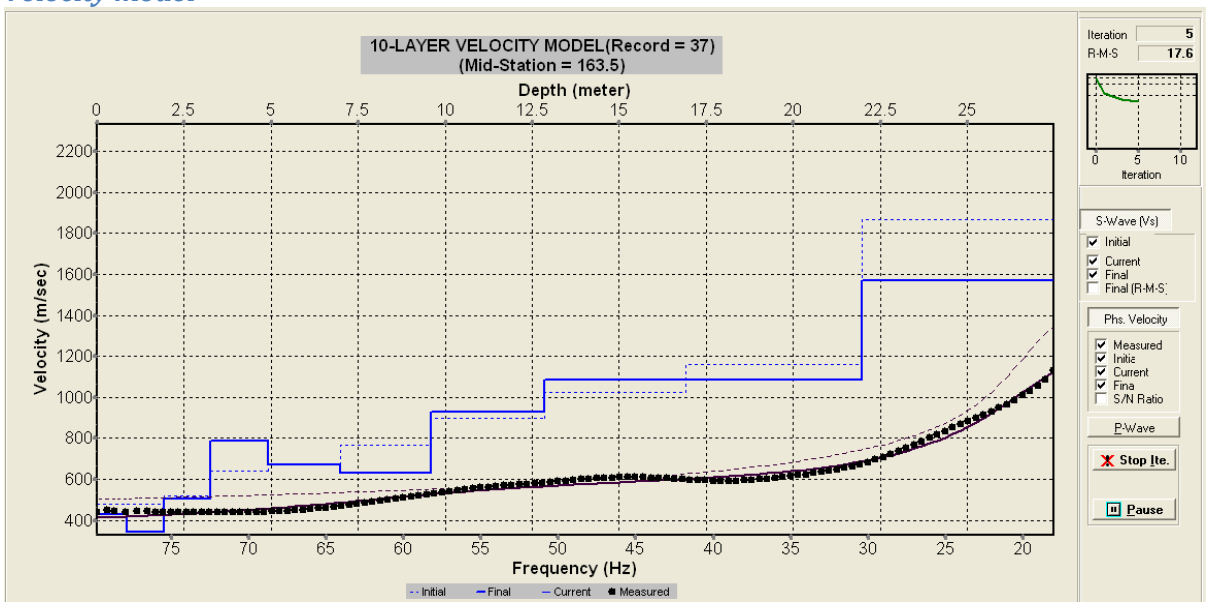

SITE NUMBER: T38 (2++)

Despite the difficulty obtaining a dispersion curve, the result looks more like a **4**

Site description

Probe at marker to 0.2 m. Probe along array to 0.5 m. Soil on fractured bedrock. Very steep array.

Field file numbers

245-10 (weak), 246-10 stacked, 247-10

Site photographs

Shot record and dispersion curve (10 m)

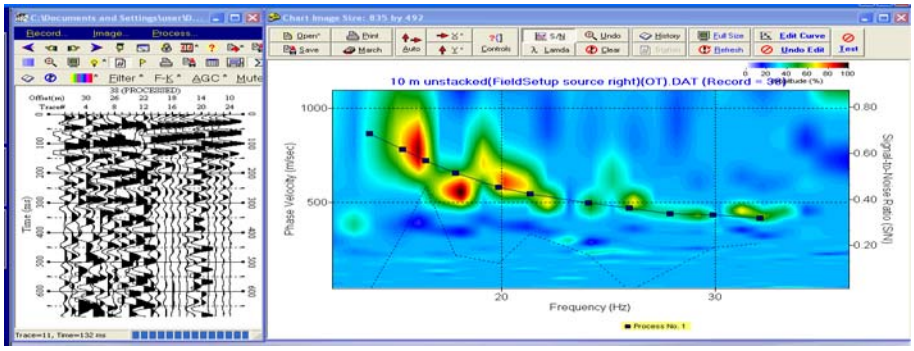

Velocity model

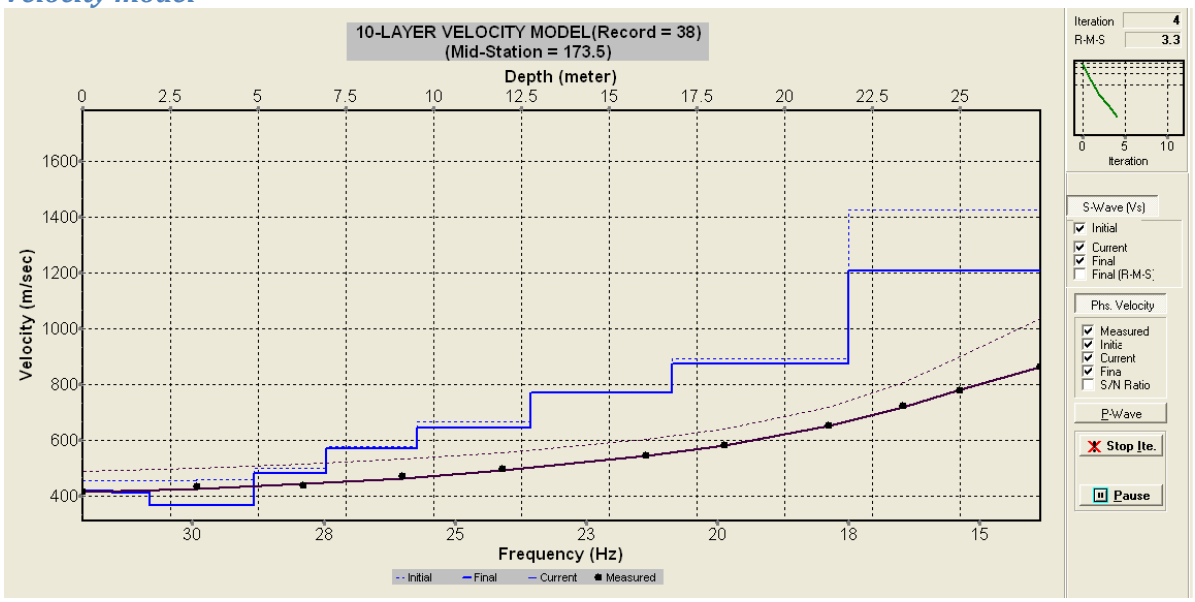

SITE NUMBER: T45 (4+/5)

Site description

Top of spur, hummocky grassed slope.

Field file numbers

332-10, 333-10

Site photographs

No photographs

Shot record and dispersion curve (10 m)

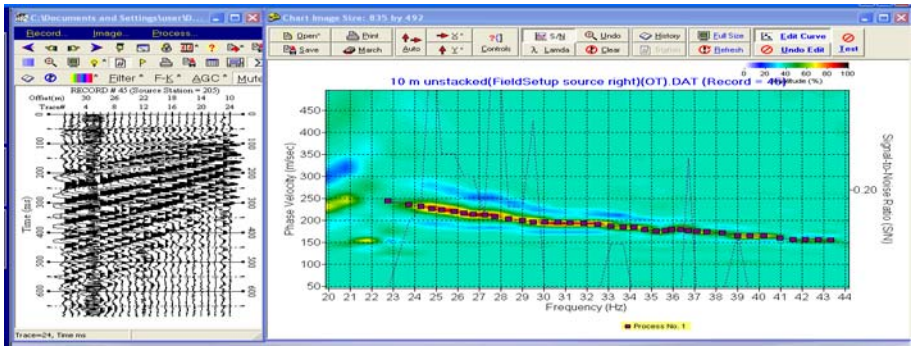

Velocity model

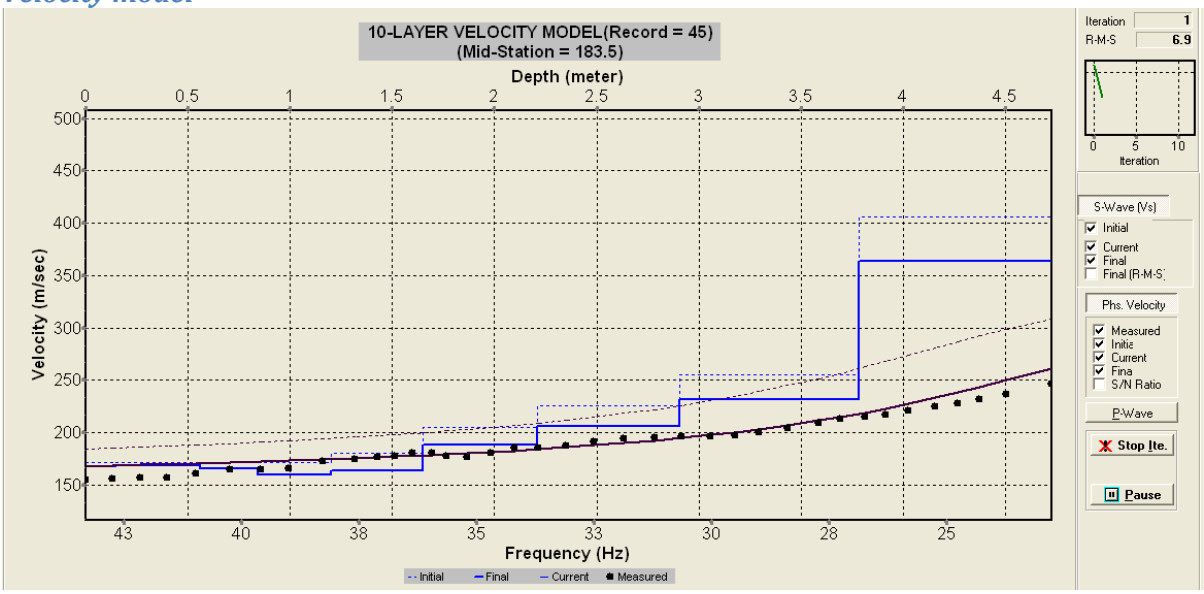

Note that the extremely low velocities recorded here and the absence of lower frequencies resulted in poor penetration. A 22 m shot was not possible but may have produced a better result. It is unlikely that the halfspace has such a low velocity

SITE NUMBER: T46 (4+)

Site description

Steep hummocky hillside, no outcrop, probed to 1.3 m with no bedrock.

Field file numbers

330-10 stacked, 331-10

Site photographs

No photograph

Shot record and dispersion curve (10 m)

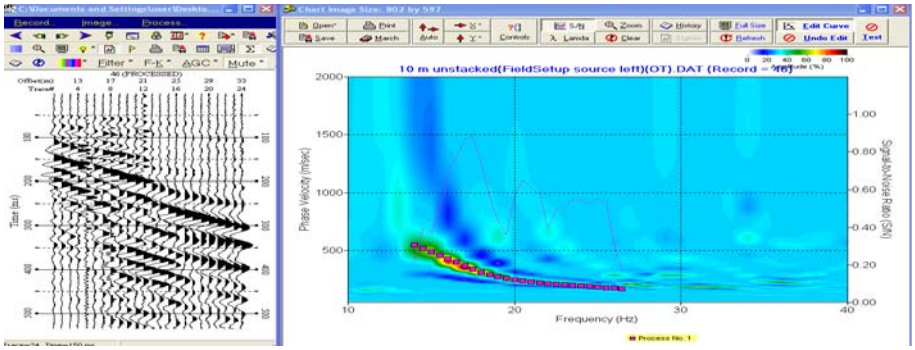

Shot record and dispersion curve (22 m)

No record

Velocity model from 10 m record

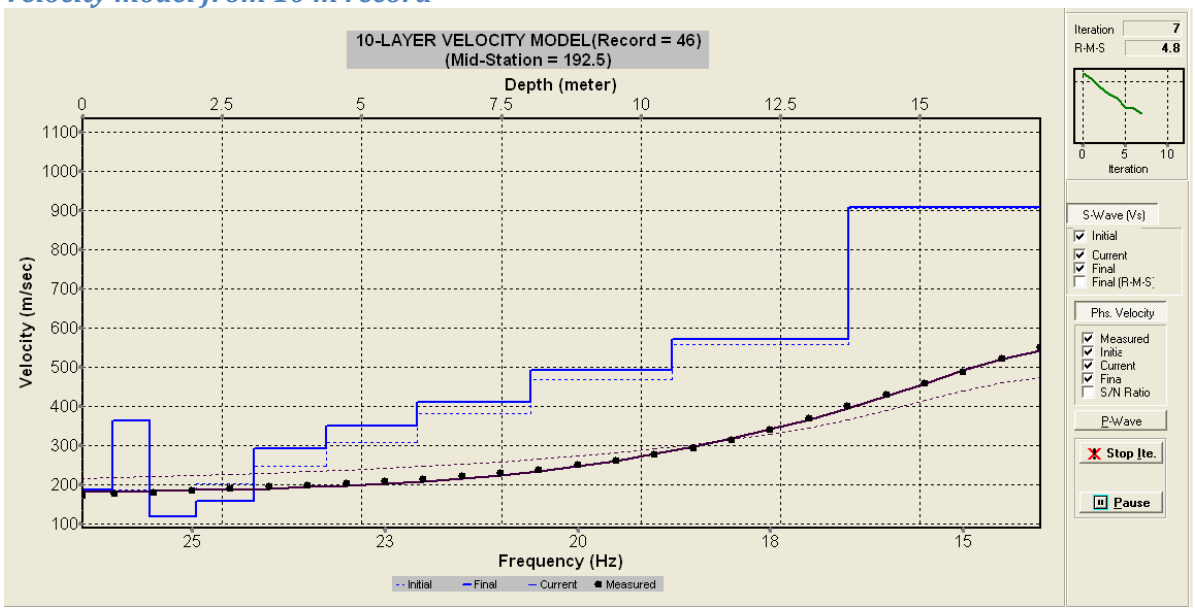

SITE NUMBER: T47 (3+)

Site description

Grass covered spur, no bedrock on probe to >1.3 m

Field file numbers

260-10 stacked, 26-10, 262-10 reduced gain

Site photographs

Shot record and dispersion curve (10 m)

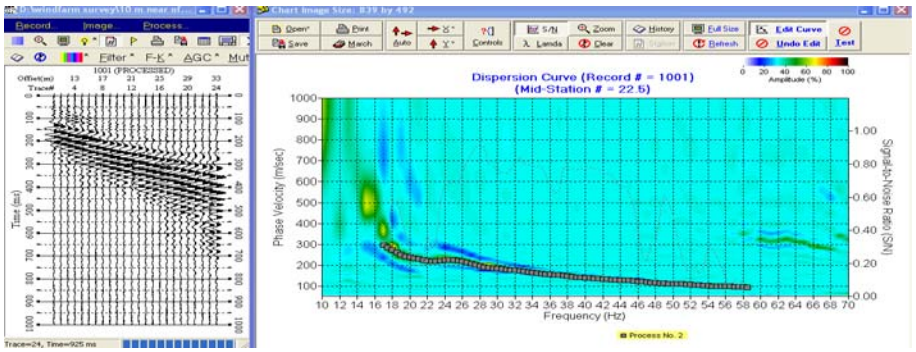

Velocity model

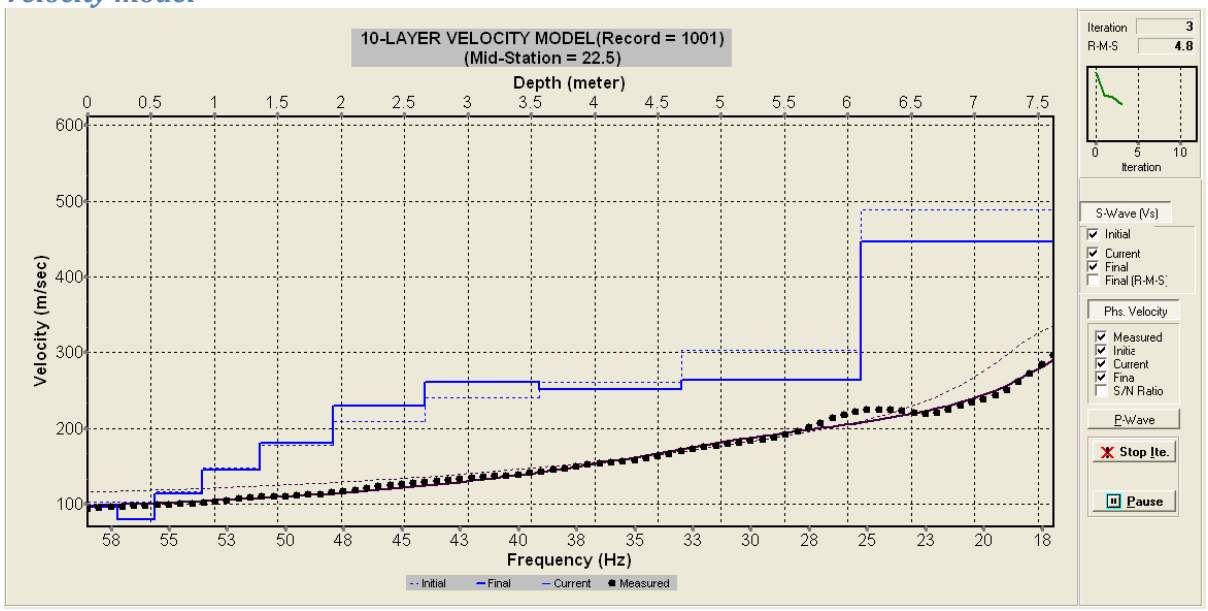

SITE NUMBER: T49 (4)

Site description

Grass covered spur, boulders at surface, probe suggested approx 0.9m to bedrock

Field file numbers

257-22 stacked, 258-10 stacked, 259

Site photographs

Shot record and dispersion curve (10 m)

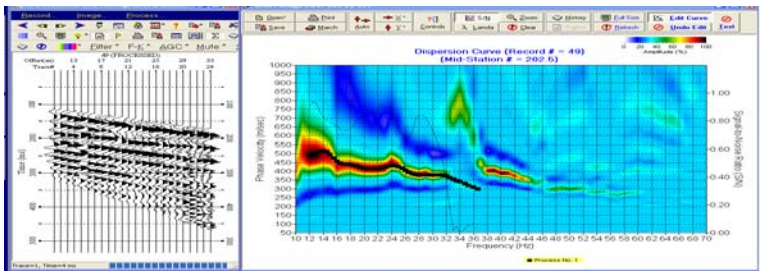

Shot record and dispersion curve (22 m)

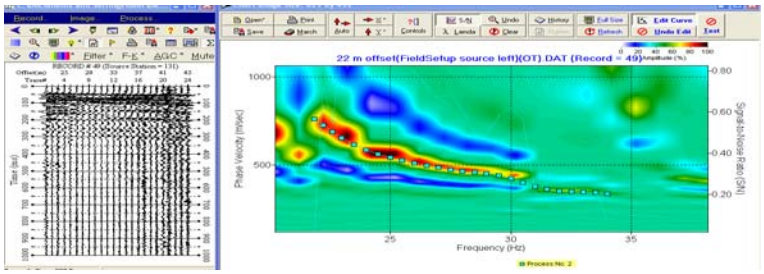

Velocity model from 10 m record

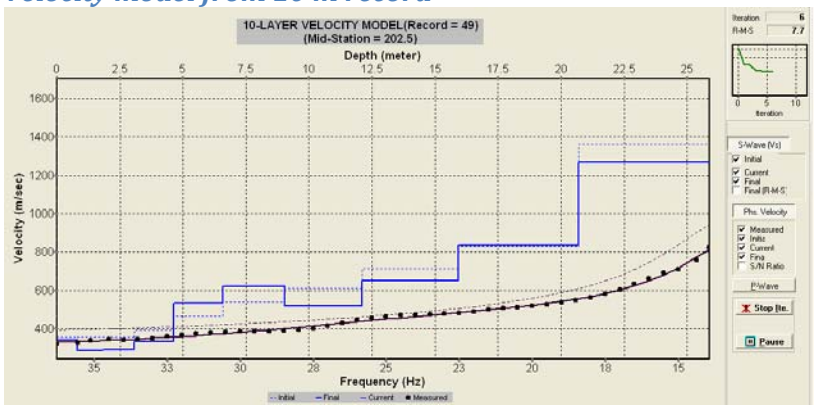

SITE NUMBER: T50 (4)

Site description

Grass covered track, boulders at surface, probe hit bedrock at 0.4m, located on top surface of spur.

Field file numbers

254-22 stacked, 255-10 stacked, 256-10

Site photographs

Shot record and dispersion curve (10 m)

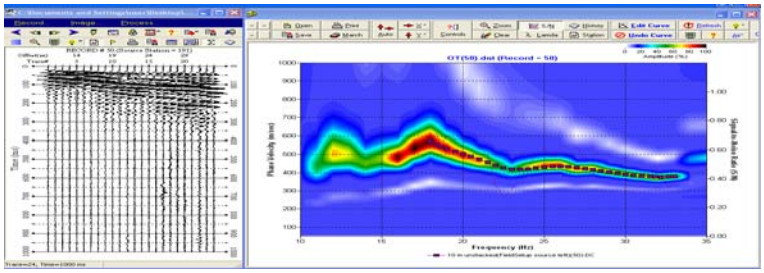

Shot record and dispersion curve (22 m)

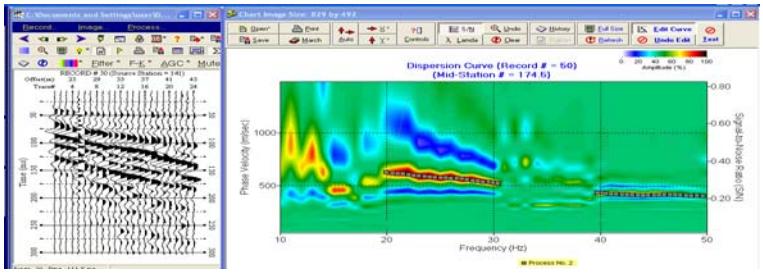

Velocity model from 10 m record

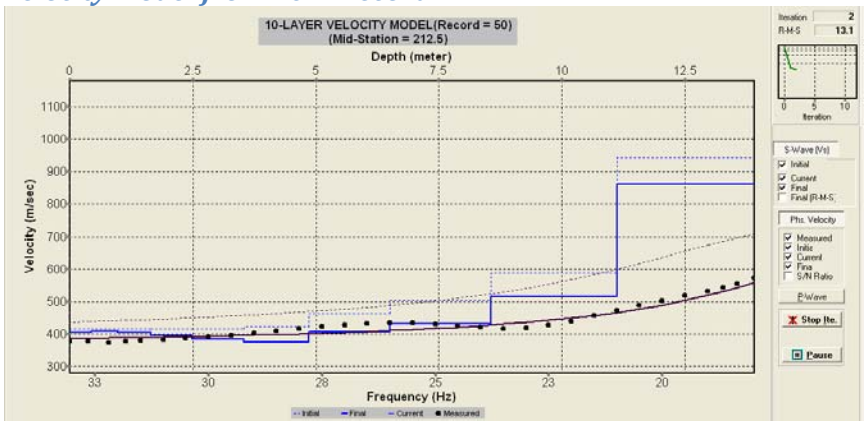

These velocities seem ok but there is virtually no coincidence between the dispersion curves

SITE NUMBER: T51 (4)

Site description

Grass track, no outcrop, probe penetrated to ~1 m.

Field file numbers

251-22 (4 stack), 252-10 (4 stack), 253-10

Site photographs

Shot record and dispersion curve (10 m)

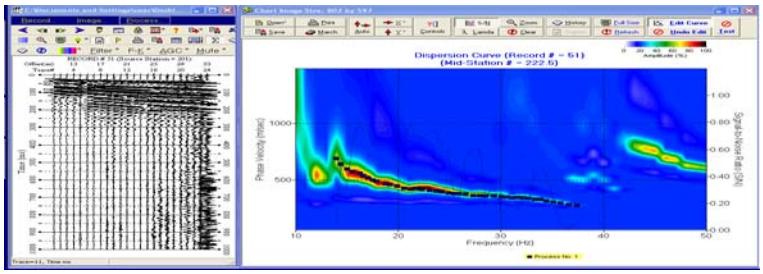

Shot record and dispersion curve (22 m)

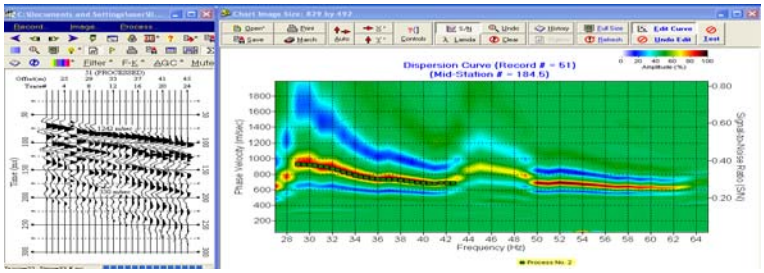

Velocity model from 10 m record

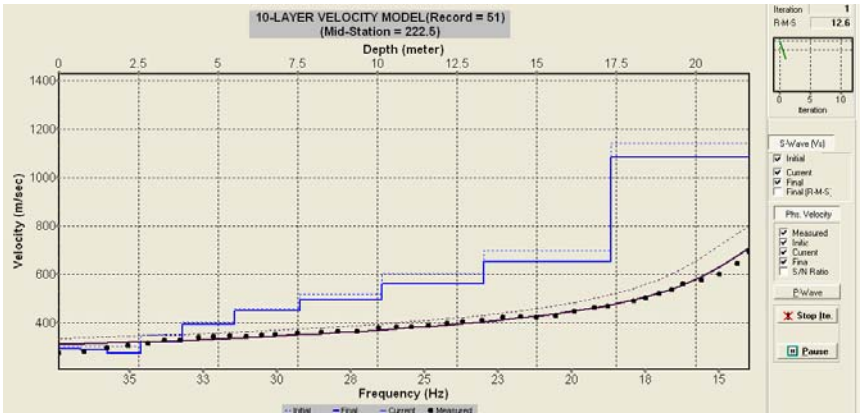

SITE NUMBER: T52 (1+)

Site description

No outcrop. Probe at peg to 0.5 m, probe along array to 1 m and >1.3 m

Field file numbers

248-22 (4 stack), 249-10 (4 stack), 250-10

Site photographs

Shot record and dispersion curve (10 m)

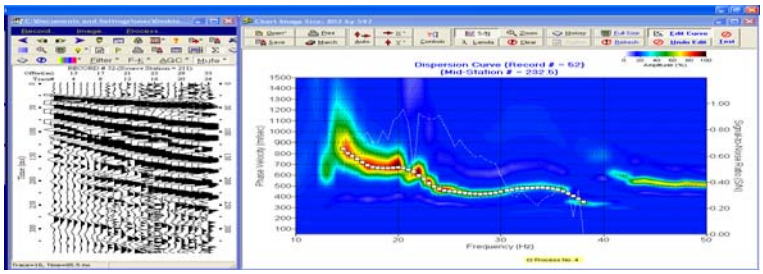

Shot record and dispersion curve (22 m)

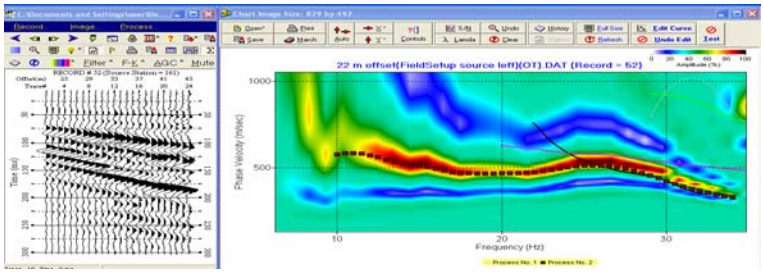

Minor surface wave diffraction evident at start of array. Possible fault? (See also 53)

Velocity model from 10 m record

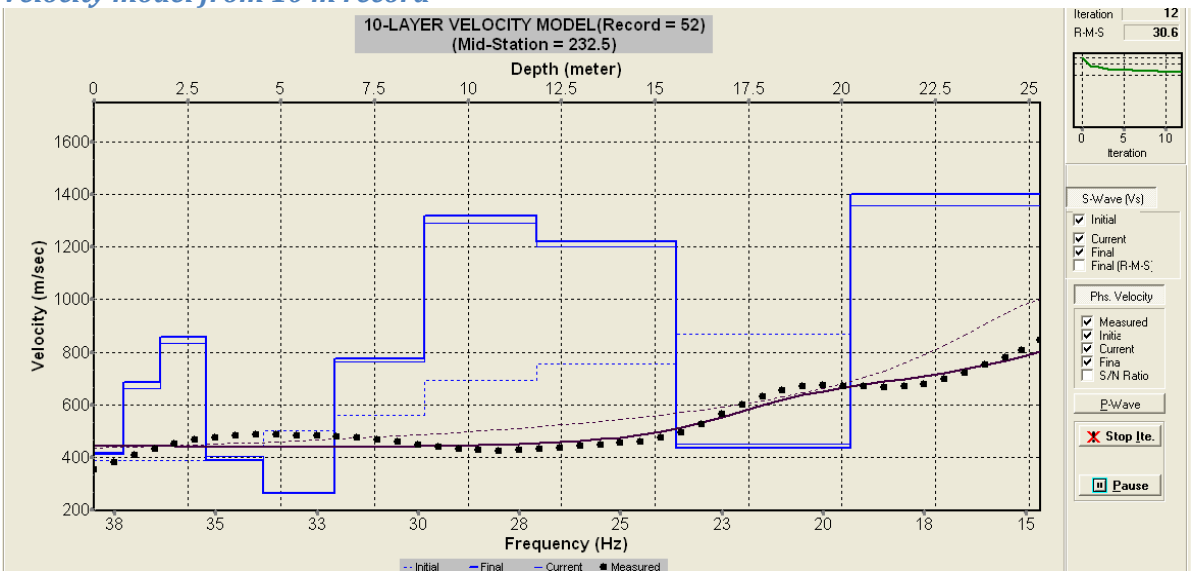

and 22 m record

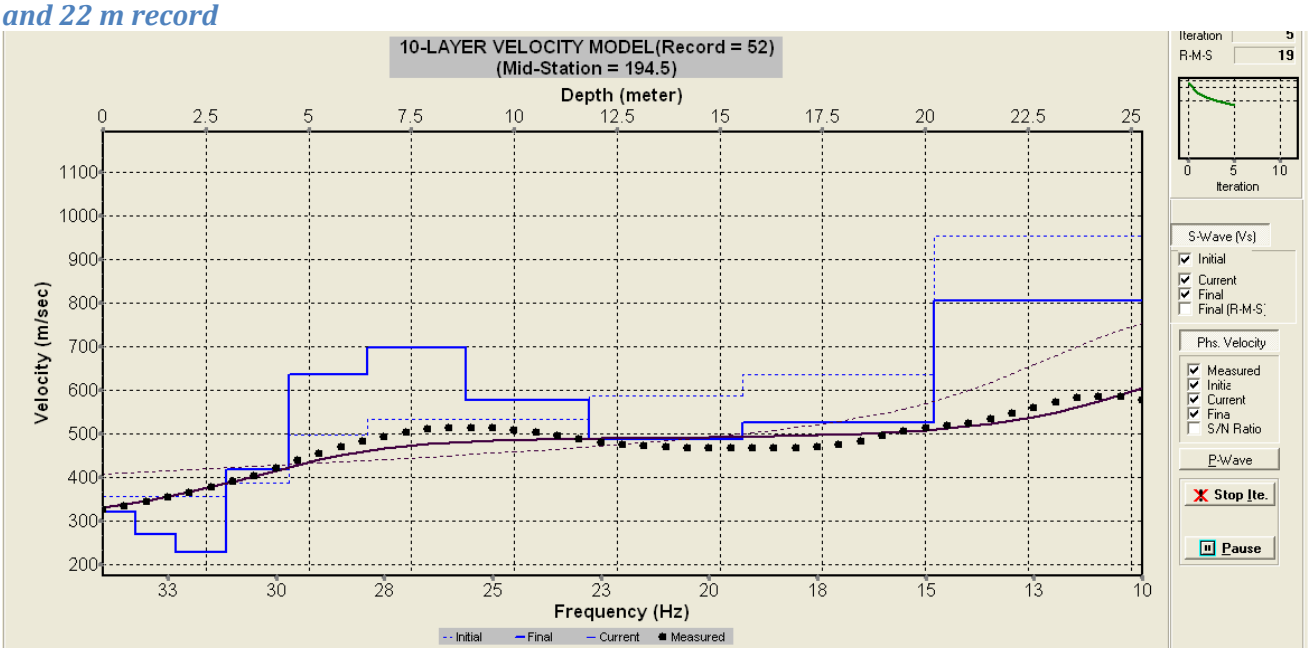

SITE NUMBER: T53 (1+)

Site description

Fractured Torlesse seen at cutting approximately 1 m below surface. Track appears to be cut into bedrock.

Field file numbers

328-10 (4 stack), 329-10

Site photographs

Shot record and dispersion curve (10 m)

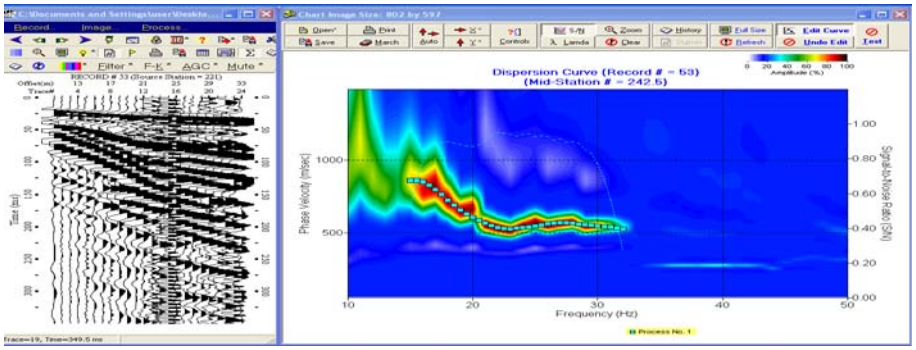

Major surface wave diffraction evident at start of array. Possible fault? (See also 52)

Velocity model

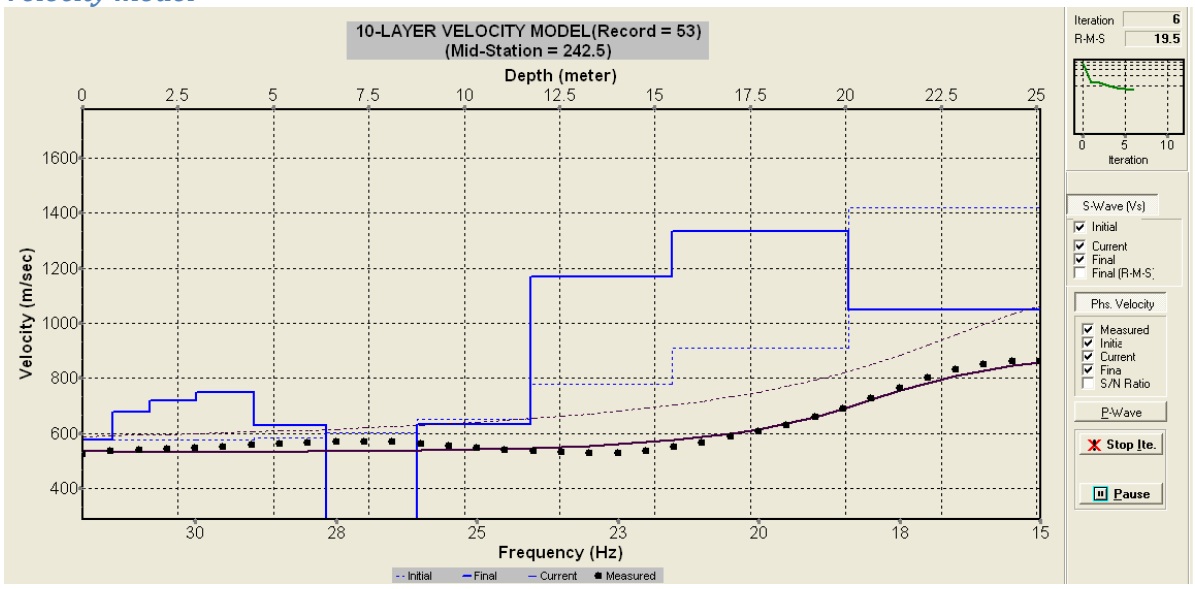

SITE NUMBER: T54 (3-)

Site description

Cut into fractured torlesse. Note, drain under geophone 19 @ 0.5-1 m deep. Probe bedrock to surface with max 0.2m gravel veneer

Field file numbers

326-10 stacked, 327-10

Site photographs

Shot record and dispersion curve (10 m)

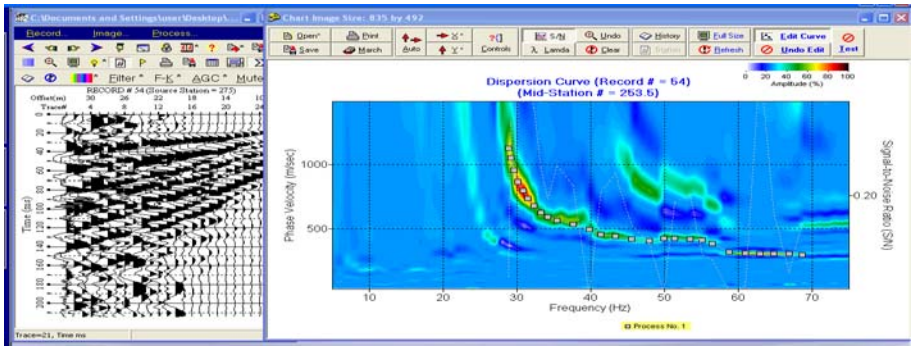

Velocity model

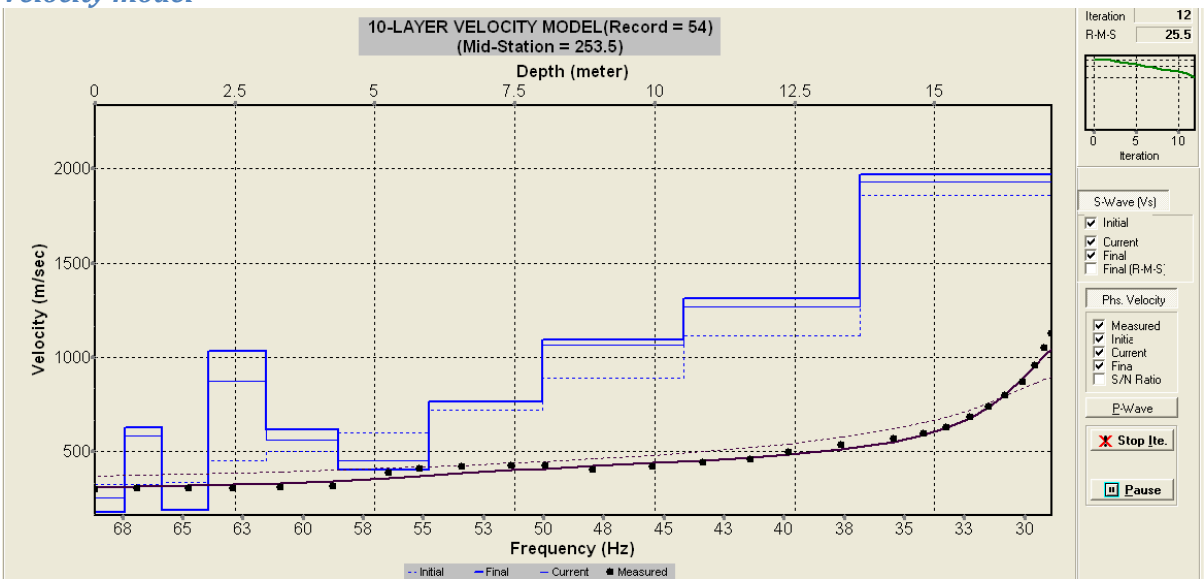

SITE NUMBER: T55 (5)

Site description

Bottom of gulley. Bedrock outcrop seen in cutting 20 m east. No surface outcrop. Saddle between gullies Probe >1.3 m.

Field file numbers

293-22 (4 stack), 294-10 (4 stack), 295-10

Site photographs

Shot record and dispersion curve (10 m)

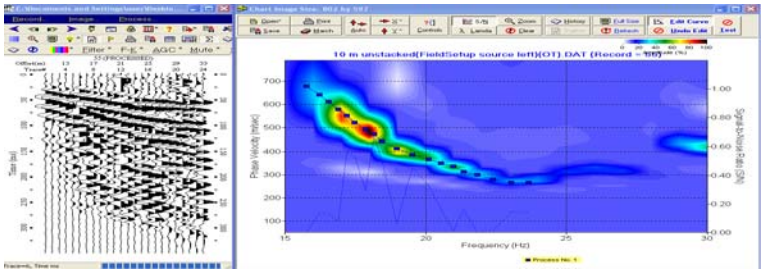

Shot record and dispersion curve (22 m)

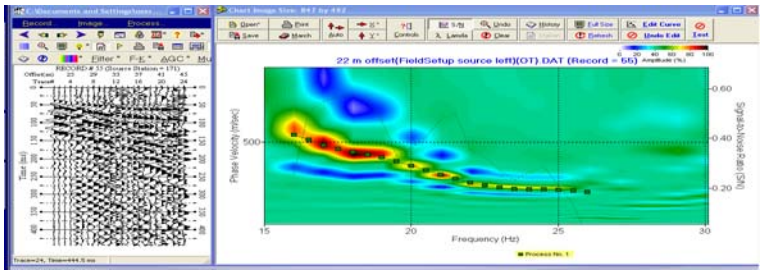

Velocity model from 22 m record

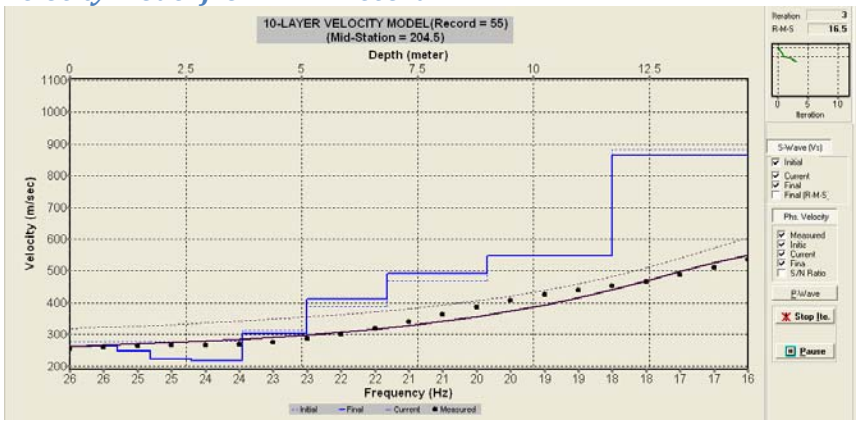

SITE NUMBER: T56/7 (4+)

Site description

> 1 m loess cover. No outcrop. Top of spur probe >1.3 m

Field file numbers

296-22 (4 stack), 297-10 (4 stack), 298-10

Site photographs

Shot record and dispersion curve (10 m)

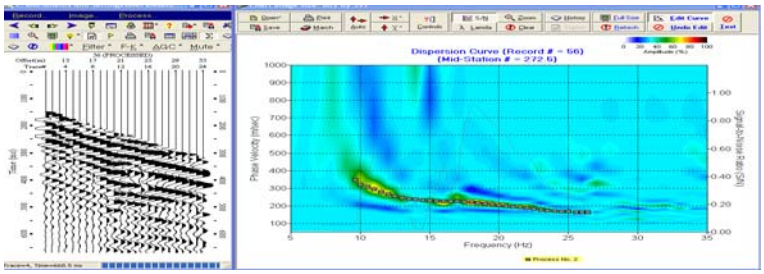

Shot record and dispersion curve (22 m)

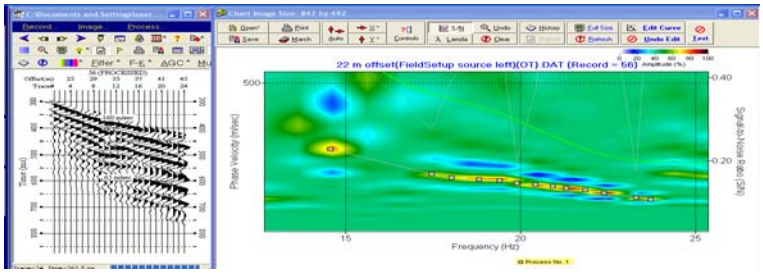

Velocity model from 10 m record

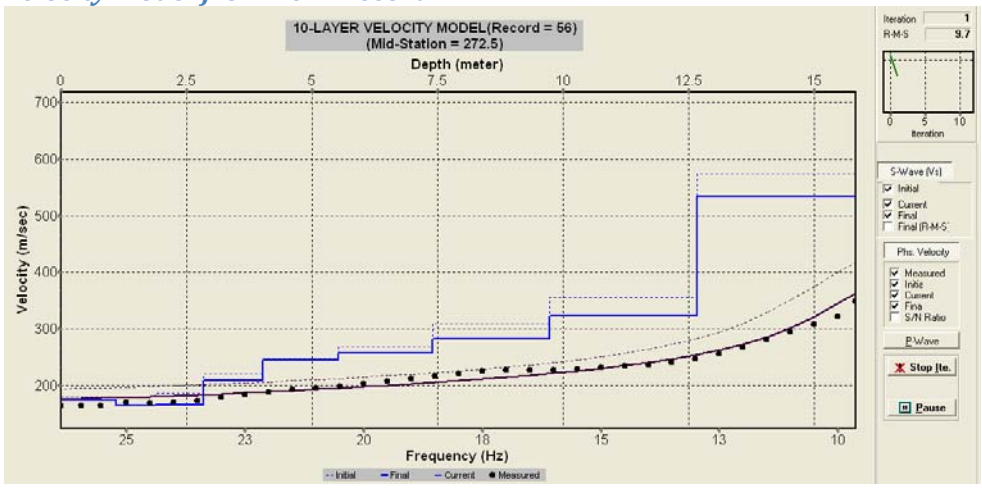

SITE NUMBER: T58 (4)

Site description

Highly fractured torlesse to near surface. 0-0.5 m loess cover.

Field file numbers

301-22, 302-10 (4 stack), 303-10

Site photographs

Shot record and dispersion curve (10 m)

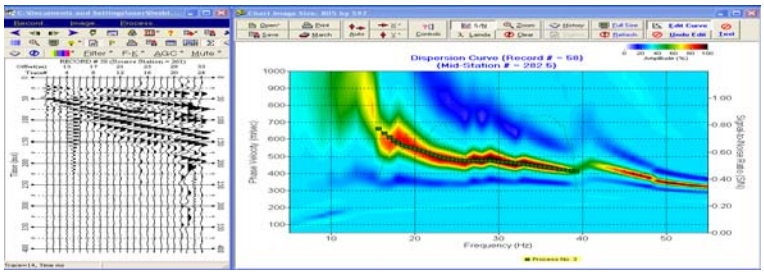

Shot record and dispersion curve (22 m)

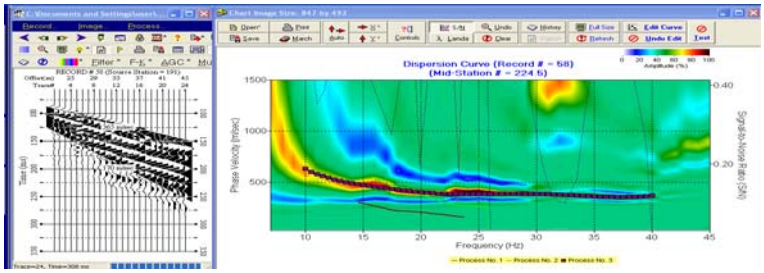

Velocity model from 22 m record

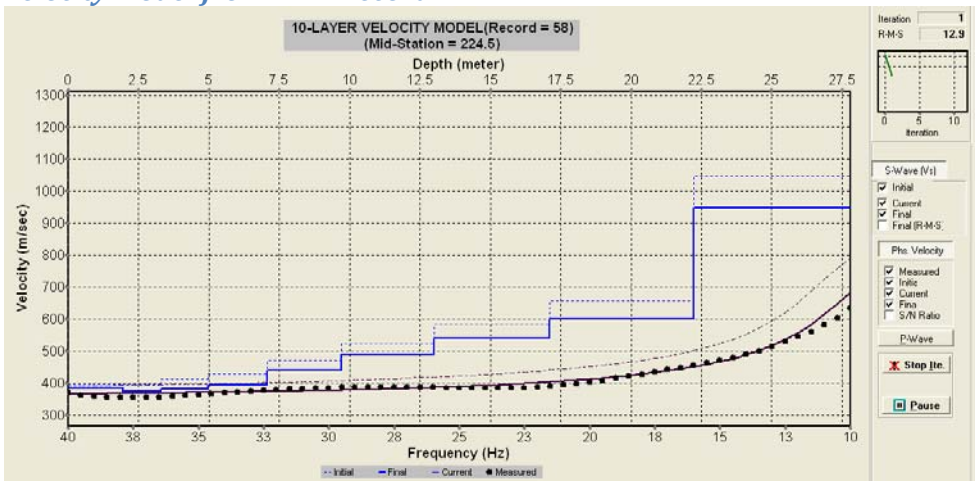

SITE NUMBER: T59 (4)

Site description

Spur, gently sloping, bedrock outcrop in cutting by T59. Probe bedrock 0.2-1.0 m

Field file numbers

304-22, 305-10 stacked, 306-10

Site photographs

Shot record and dispersion curve (10 m)

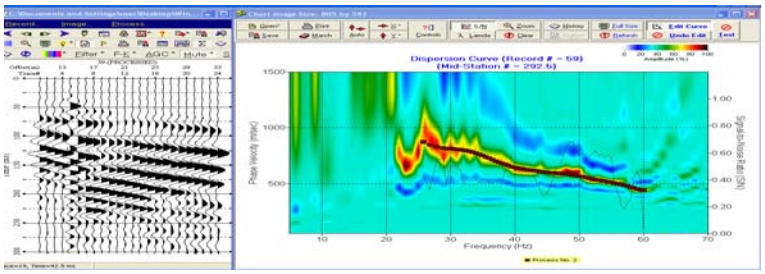

Shot record and dispersion curve (22 m)

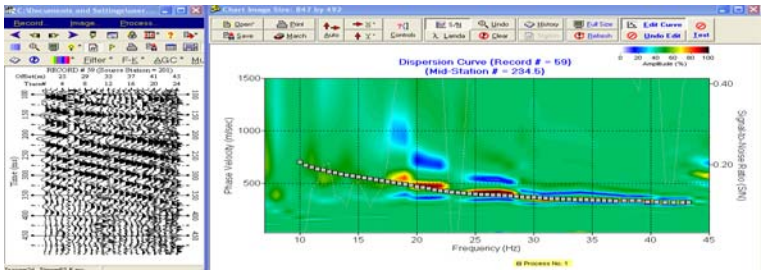

Velocity model from 22 m record

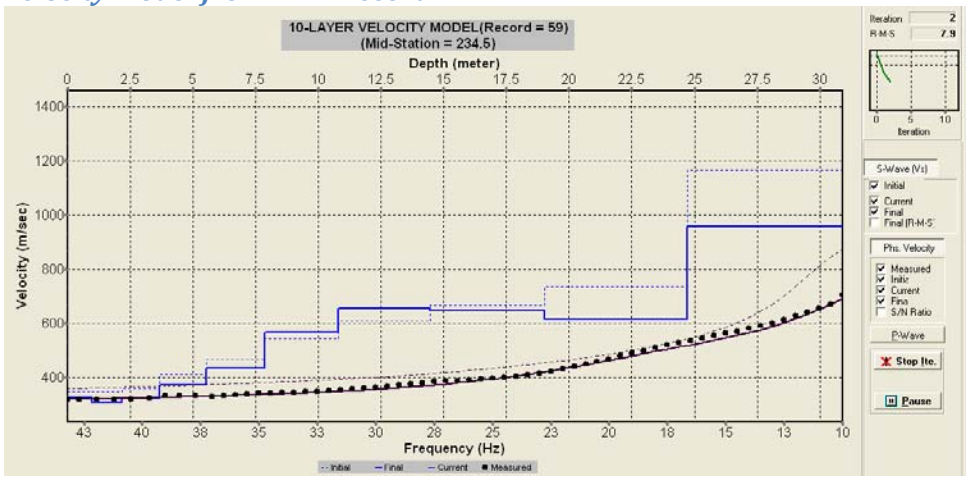

SITE NUMBER: T60 (5+)

Site description

Undulating slope with small hillocks, no outcrop

Field file numbers

290-22, 291-10 stacked, 292

Site photographs

Shot record and dispersion curve (10 m)

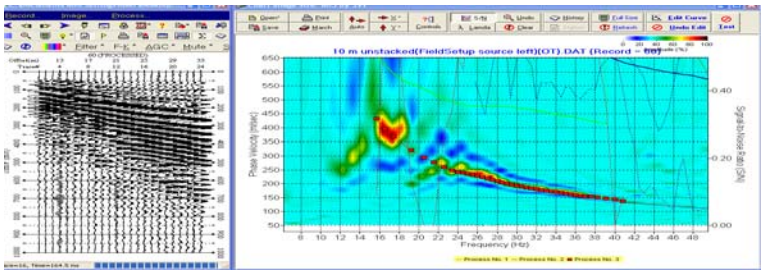

Shot record and dispersion curve (22 m)

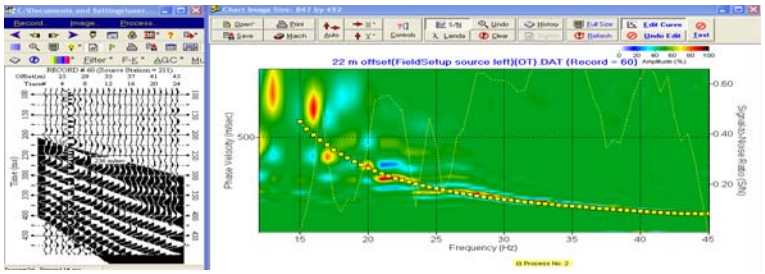

Velocity model from 10 m record

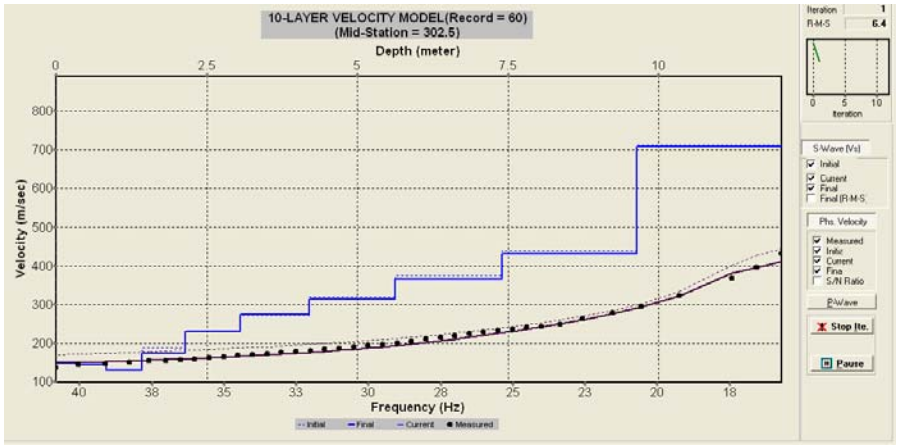

SITE NUMBER: T72 (3-)

Site description

Undulating with small hillocks. Bouldery surface. Probe hitting boulders 0.2-1 m

Field file numbers

287-22, 288-10 (4 stack), 289-10

Site photographs

Shot record and dispersion curve (10 m)

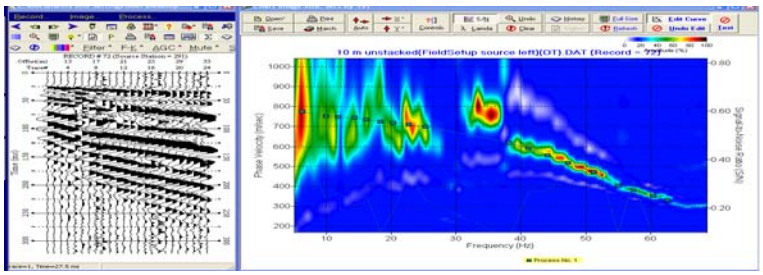

Shot record and dispersion curve (22 m)

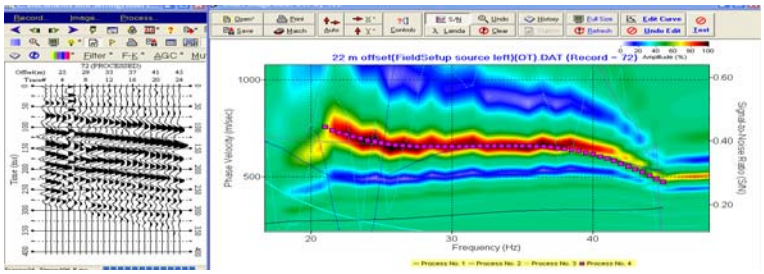

Velocity model from 10 m record

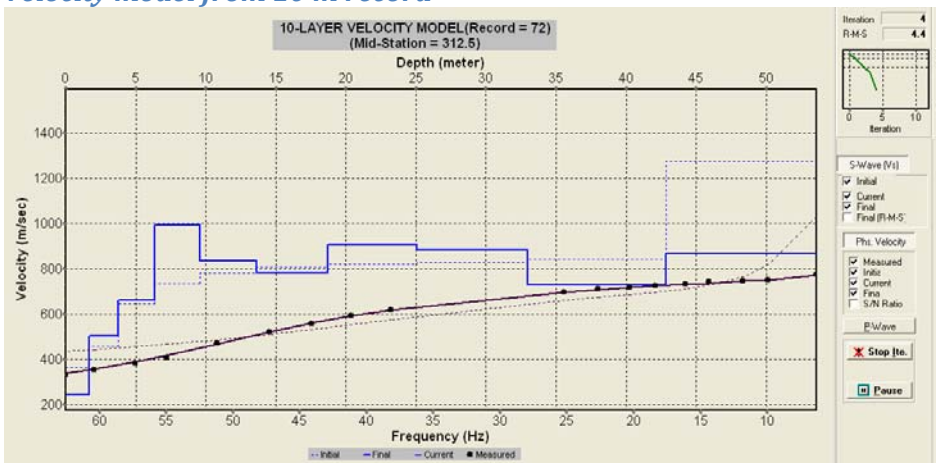

SITE NUMBER: T73 (4+)

Site description

Undulating small hillocks, no outcrop

Field file numbers

284-22 stacked, 285-10 stacked, 286-10

Site photographs

Shot record and dispersion curve (10 m)

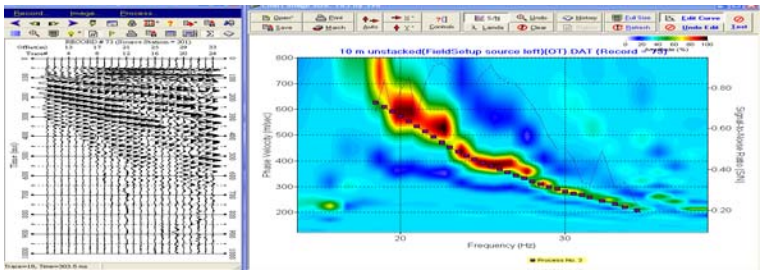

Shot record and dispersion curve (22 m)

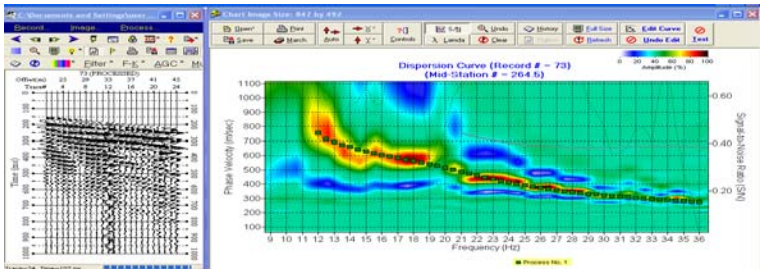

Velocity model from 10 m record

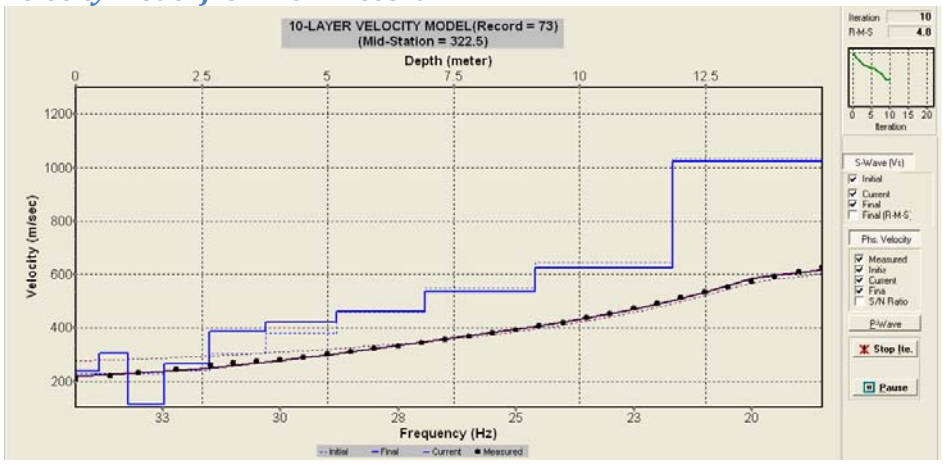

SITE NUMBER: T74 (5)

Site description

Undulating small hills, no outcrop, Probe >1.3 m

Field file numbers

281-22 stacked, 282-10 stacked, 283-10

Site photographs

Shot record and dispersion curve (10 m)

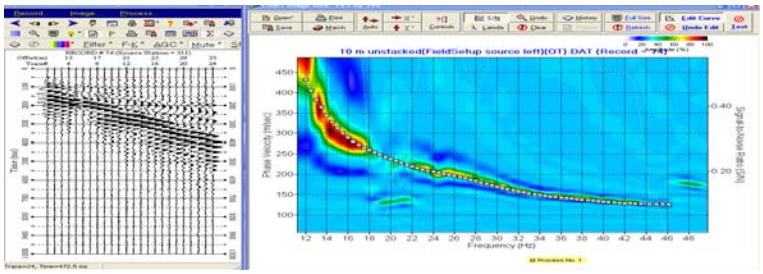

Shot record and dispersion curve (22 m)

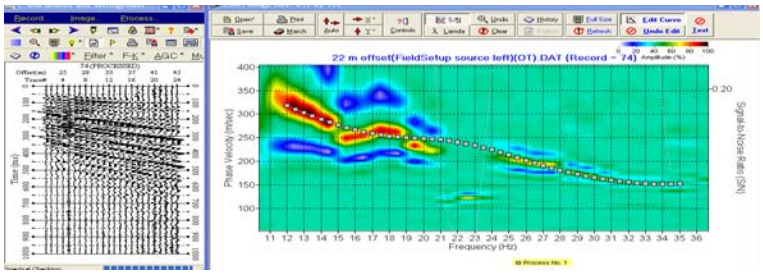

Velocity model from 10 m record

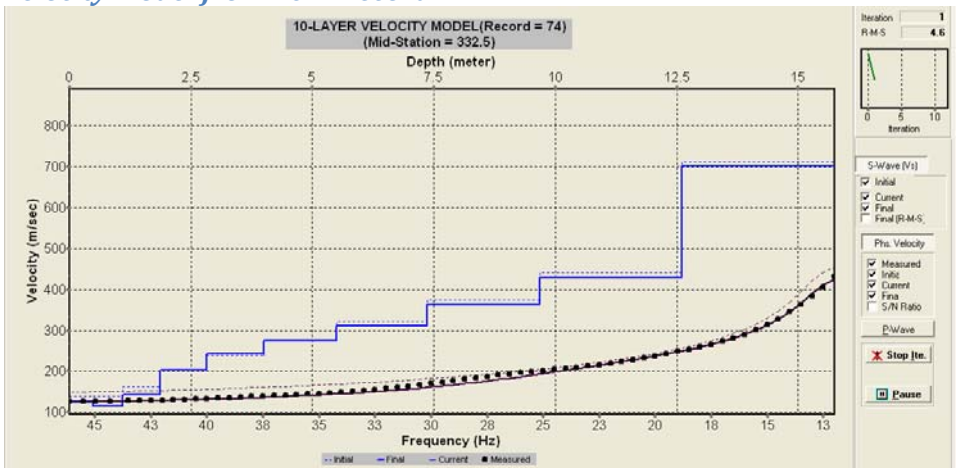

SITE NUMBER: T75 (5)

Site description

Flat grassed area, no outcrop

Field file numbers

278-22 stacked, 279-10 stacked, 280-10

Site photographs

Shot record and dispersion curve (10 m)

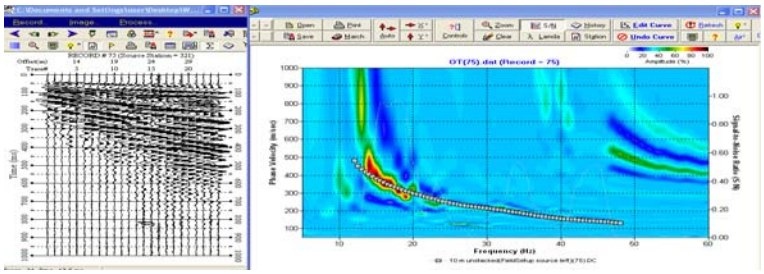

Shot record and dispersion curve (22 m)

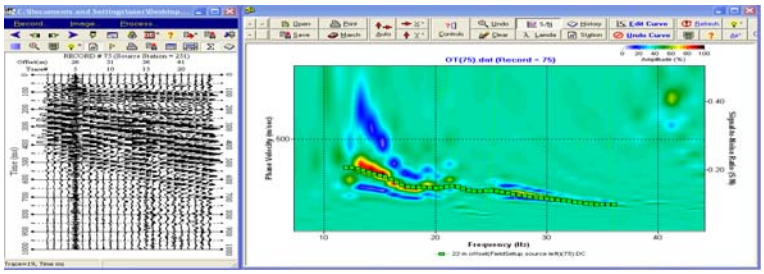

Velocity model from 10 m record

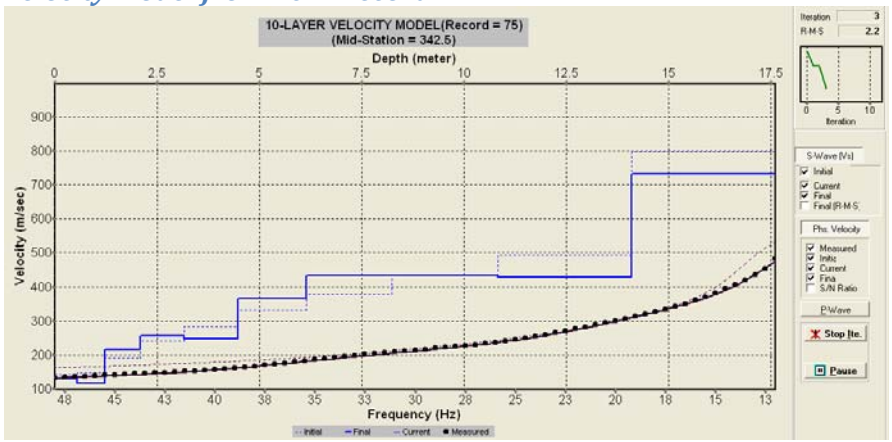

SITE NUMBER: T76 (4+)

Site description

Flat grassed area, no outcrop, probe to >1.3 m hit clay.

Field file numbers

275-22, 276-10 (4 stack), 277-10

Site photographs

No photographs

Shot record and dispersion curve (10 m)

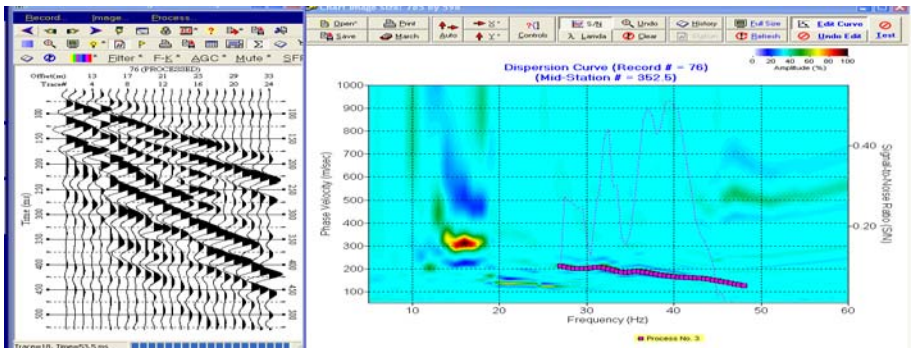

Shot record and dispersion curve (22 m)

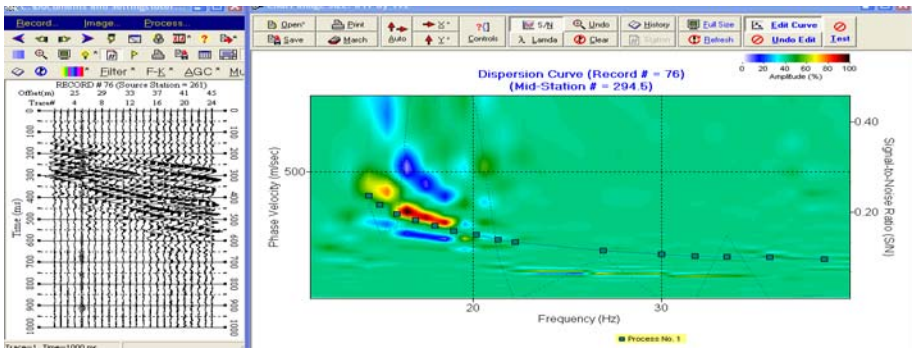

Velocity model using combined curve

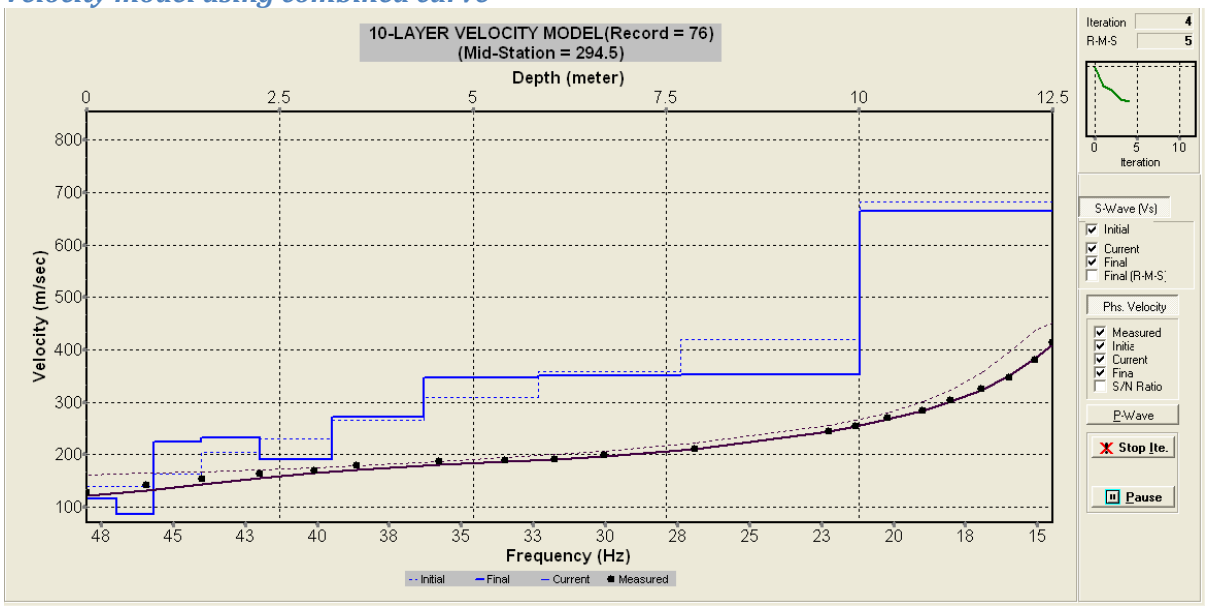

SITE NUMBER: T77 (5)

Site description

Flat grassed paddock, no outcrop, Probe to > 1.3m clay.

Field file numbers

273-10 stacked, 274-10

Site photographs

Shot record and dispersion curve (10 m)

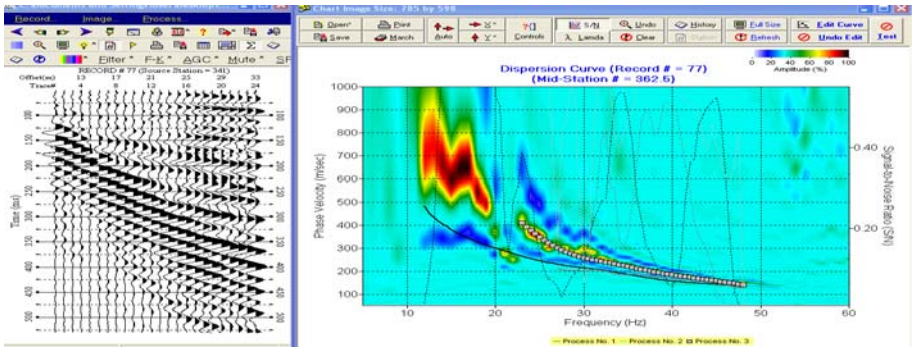

Velocity model

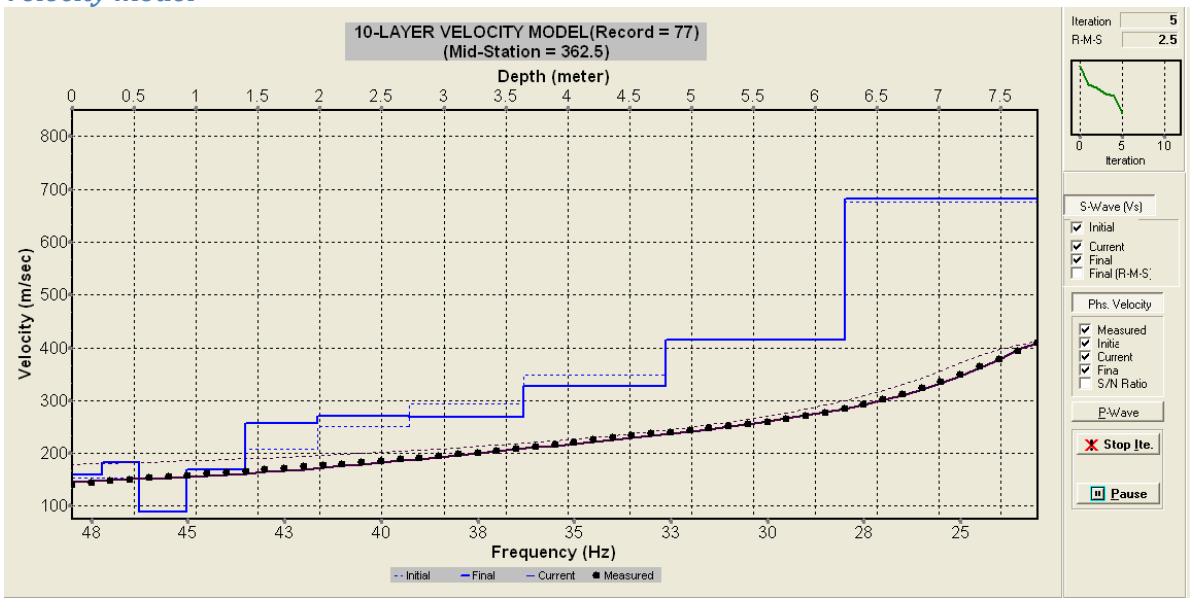

SITE NUMBER: T78 (5)

Site description

Flat grassed paddock, no outcrop, Probe to > 1.3m clay.

Field file numbers

269-22 stacked, 270-10 stacked, 271-10

Site photographs

Shot record and dispersion curve (10 m)

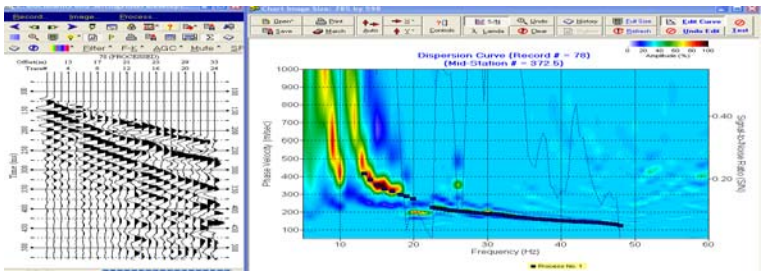

Shot record and dispersion curve (22 m)

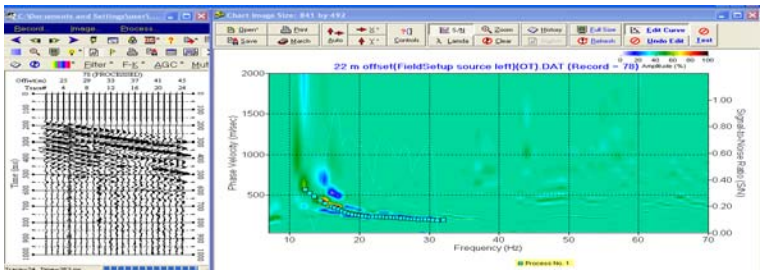

Velocity model from 10 m record

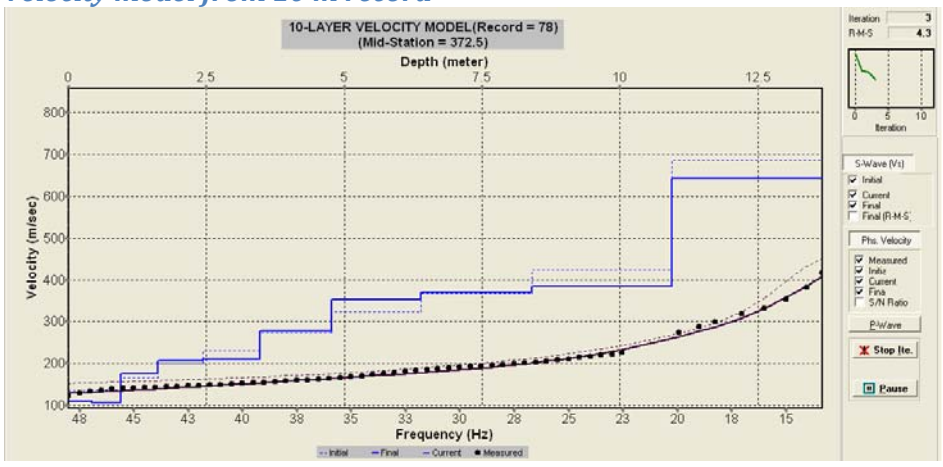

SITE NUMBER: T79 (5)

Site description

Flat surface, no outcrop, probe to >1.3 m

Field file numbers

263-22 stacked, 264-10 stacked, 265-10

Site photographs

Shot record and dispersion curve (10 m)

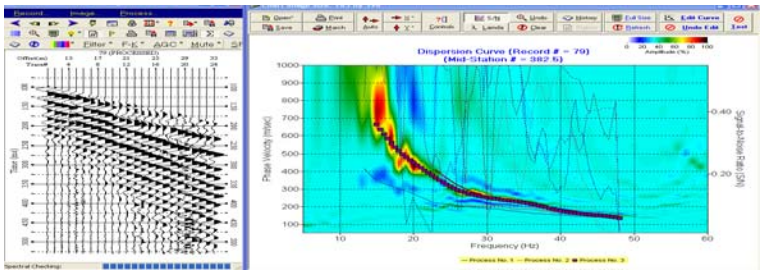

Shot record and dispersion curve (22 m)

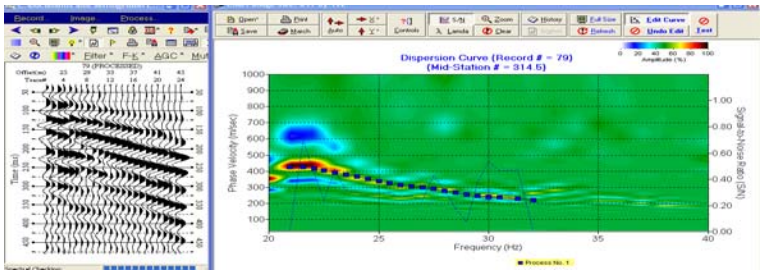

Velocity model from 10 m record

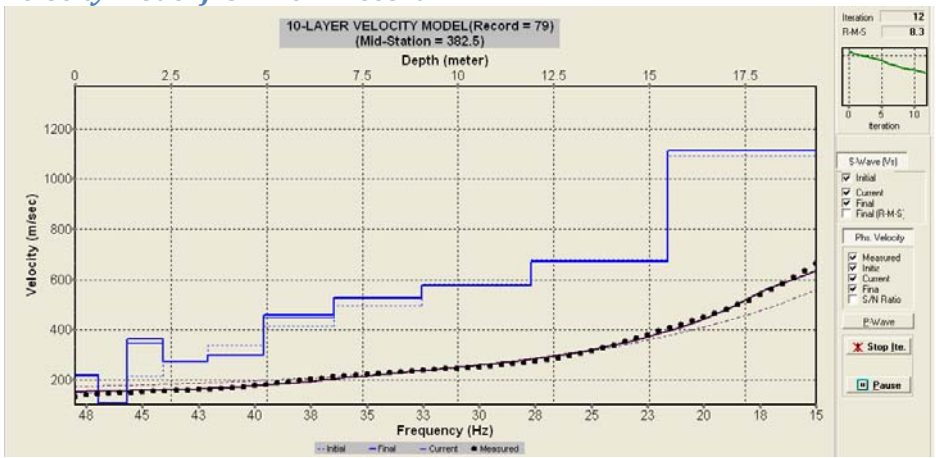

SITE NUMBER: T80 (2-)

Site description

Run parallel to small scarp. Grass covered boulder strewn surface.

Field file numbers

266-22, 267-10 (4 stack), 268-10

Site photographs

Shot record and dispersion curve (10 m)

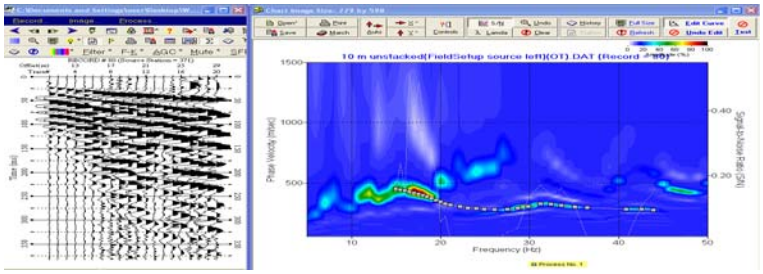

Shot record and dispersion curve (22 m)

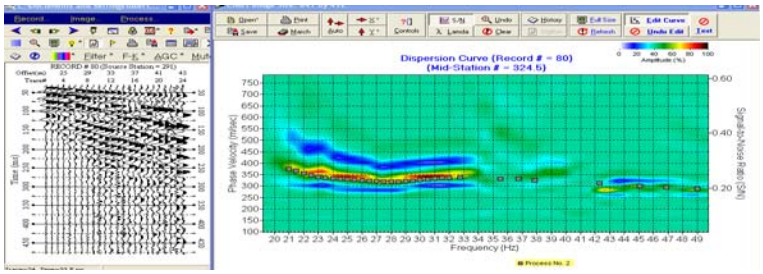

Velocity model

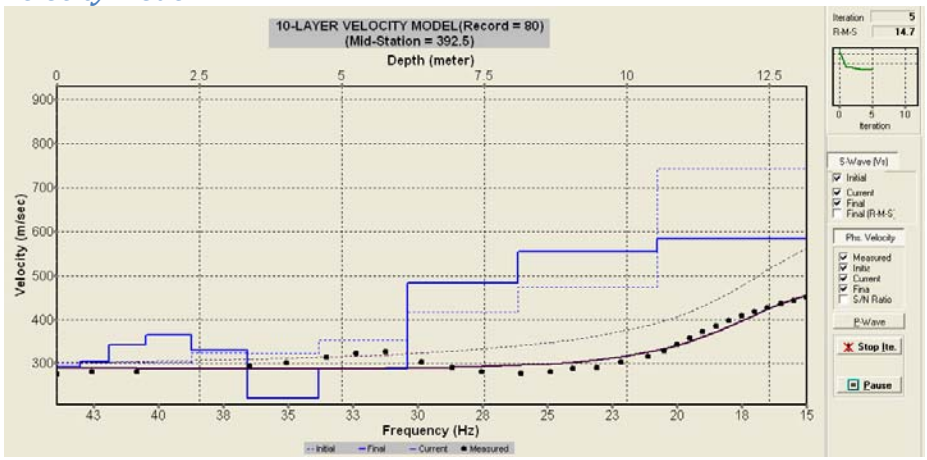

SITE NUMBER: T83 (0)

Site description

No flat surface available.

Field file numbers

Site photographs

Shot record and dispersion curve (10 m)

Shot record and dispersion curve (22 m)

Velocity model

SITE NUMBER: T84 (4+)

Site description

Gently sloping grassed hillside, no outcrop. Probe >1.3m. Probably old forest. Very windy.

Field file numbers

324-10 (4 stack), 325-10

Site photographs

Shot record and dispersion curve (10 m)

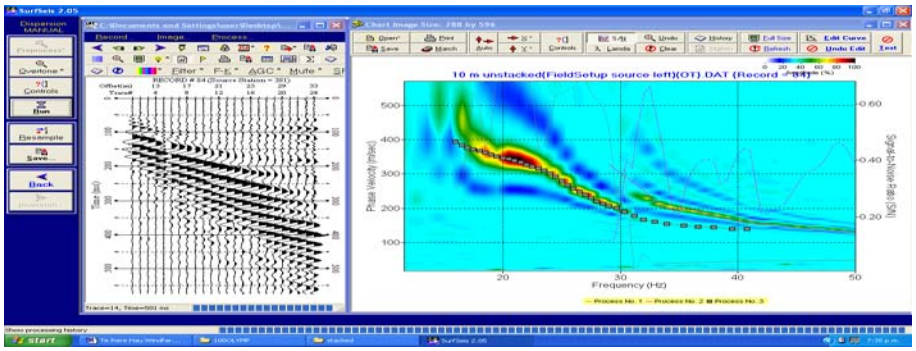

Velocity model

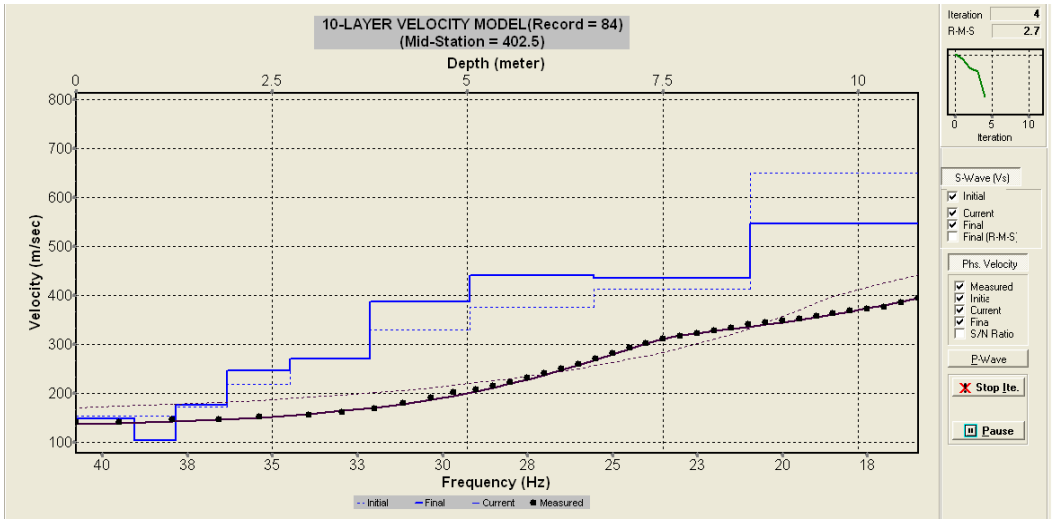

SITE NUMBER: T85 (5)

Site description

Bottom of small grassed gulley, some small surface boulders, bedrock seen in outcrop at edge of gulley. Probe >1.3m

Field file numbers

321-22, 322-10 (4 stack), 323-10

Site photographs

Shot record and dispersion curve (10 m)

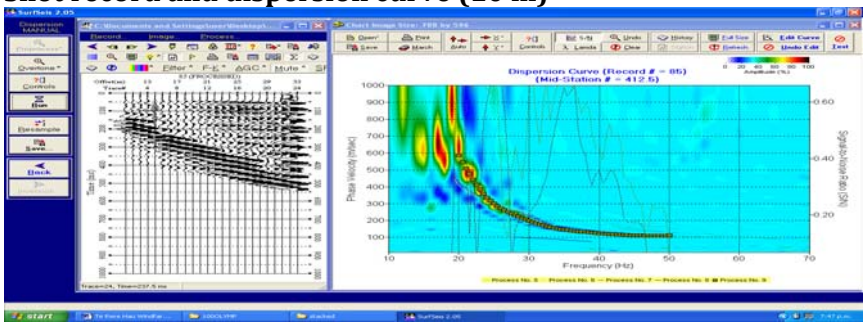

Shot record and dispersion curve (22 m)

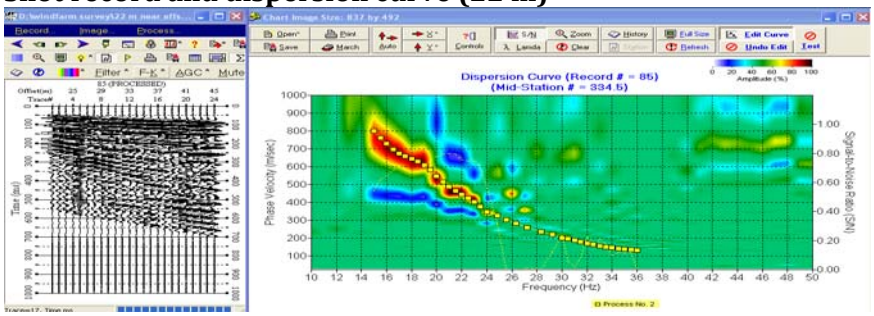

Velocity model

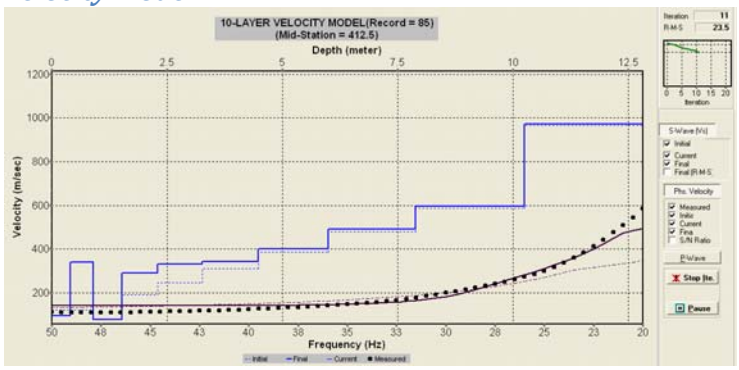

SITE NUMBER: T86 (5)

Site description

High flat plateau, grass covered, no outcrop. Probe >1.3m

Field file numbers

318-22, 319-10 (4 stack), 320-10

Site photographs

Shot record and dispersion curve (10 m)

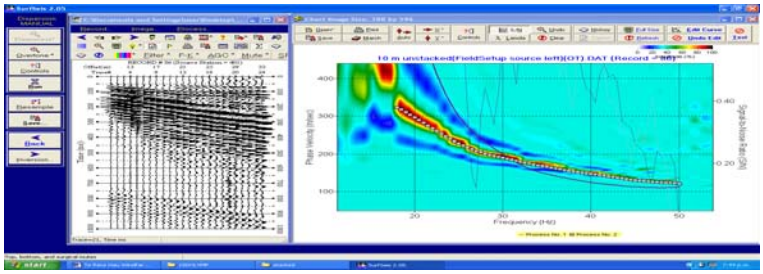

Shot record and dispersion curve (22 m)

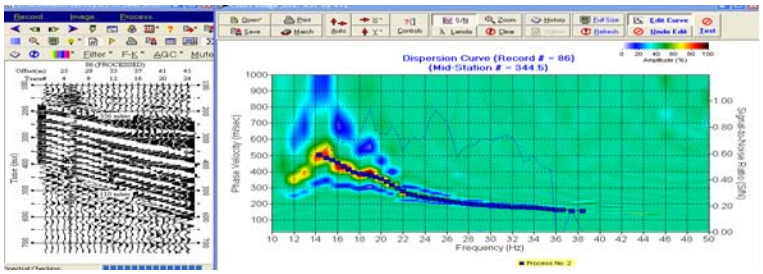

Velocity model

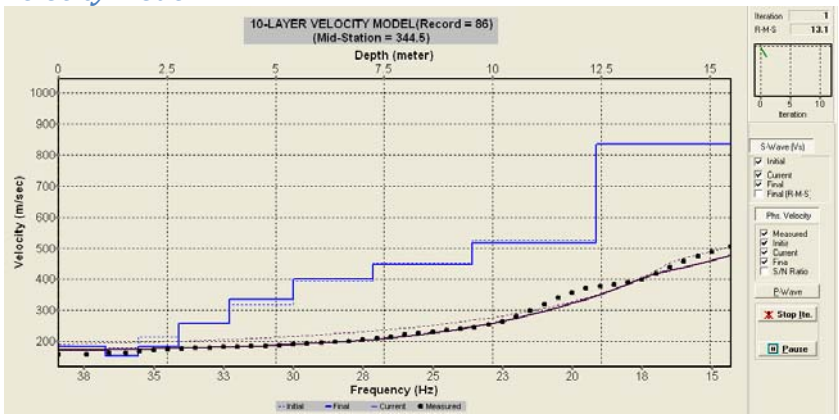

SITE NUMBER: T87 (4+)

Site description

Gentle hummocky slope grass covered, no outcrop

Field file numbers

315-22, 316-10 (4 stack), 317-10

Site photographs

Shot record and dispersion curve (10 m)

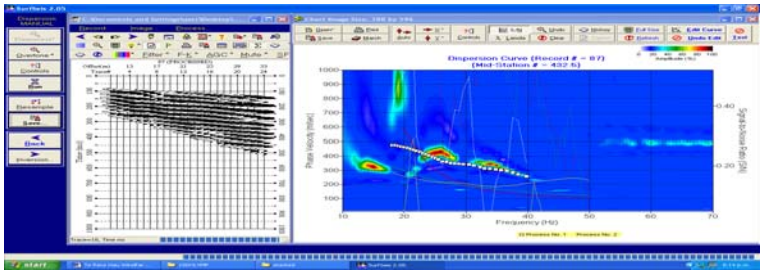

Shot record and dispersion curve (22 m)

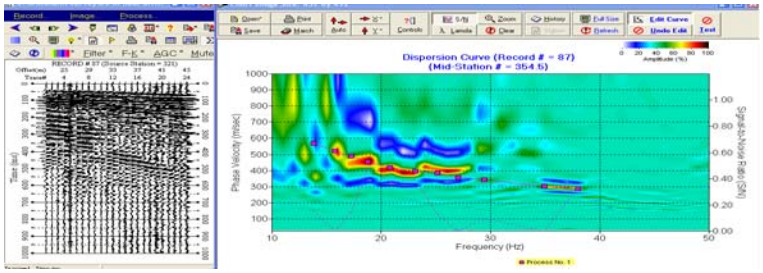

Velocity model

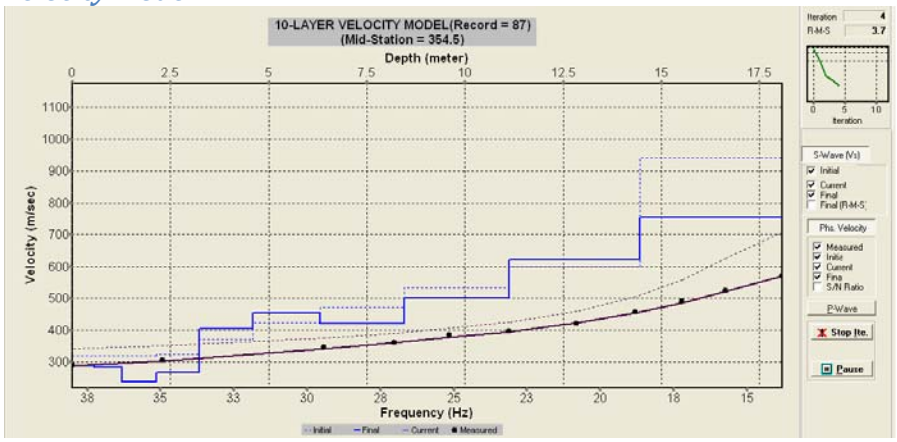

Very noisy records but practically identical curves.

SITE NUMBER: T88 (4+)

Site description

Sloping hillside, small hummocks, no outcrop.

Field file numbers

312-10 (4stack), 313-10 4stack, 314-10

Site photographs

Shot record and dispersion curve (10 m)

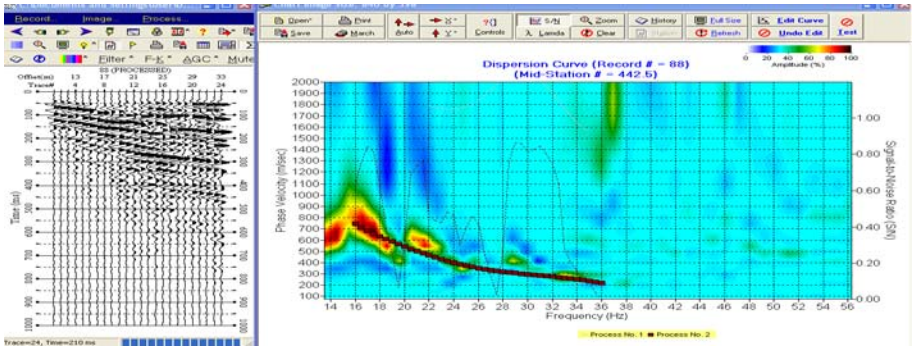

Velocity model

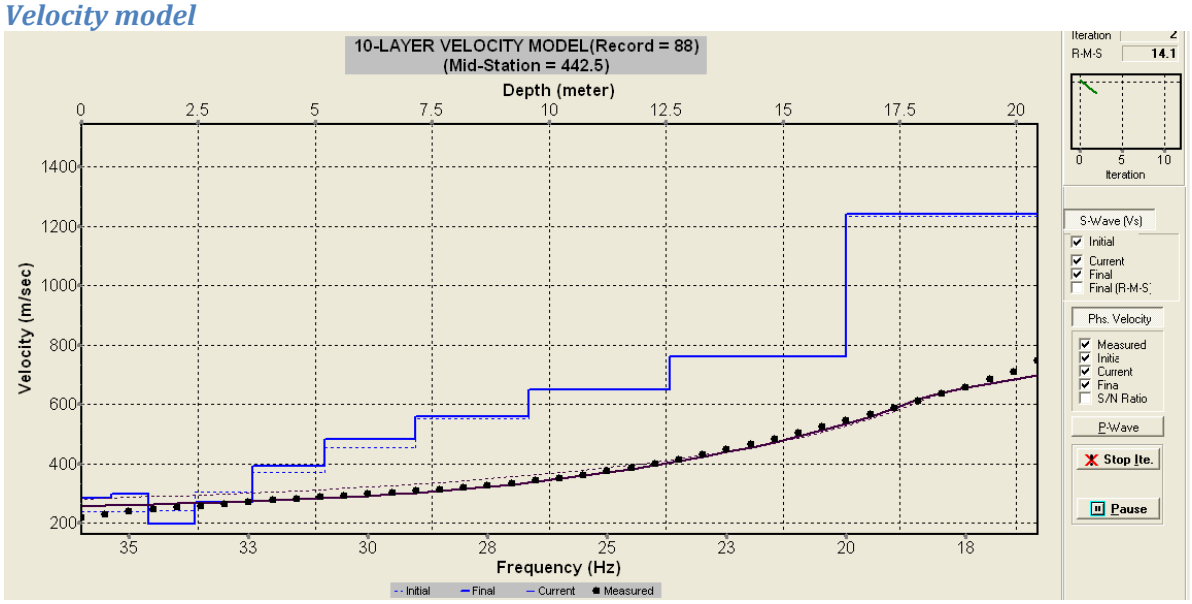

SITE NUMBER: T89 (4-)

Site description

Top of spur, flat grassed area, no outcrop, probe >1.3 m

Field file numbers

345-10 (stacked) 346-10

Site photographs

Shot record and dispersion curve (10 m)

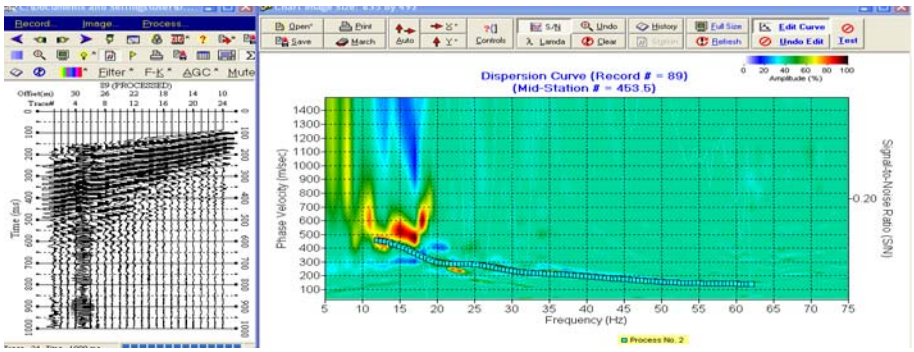

Velocity model

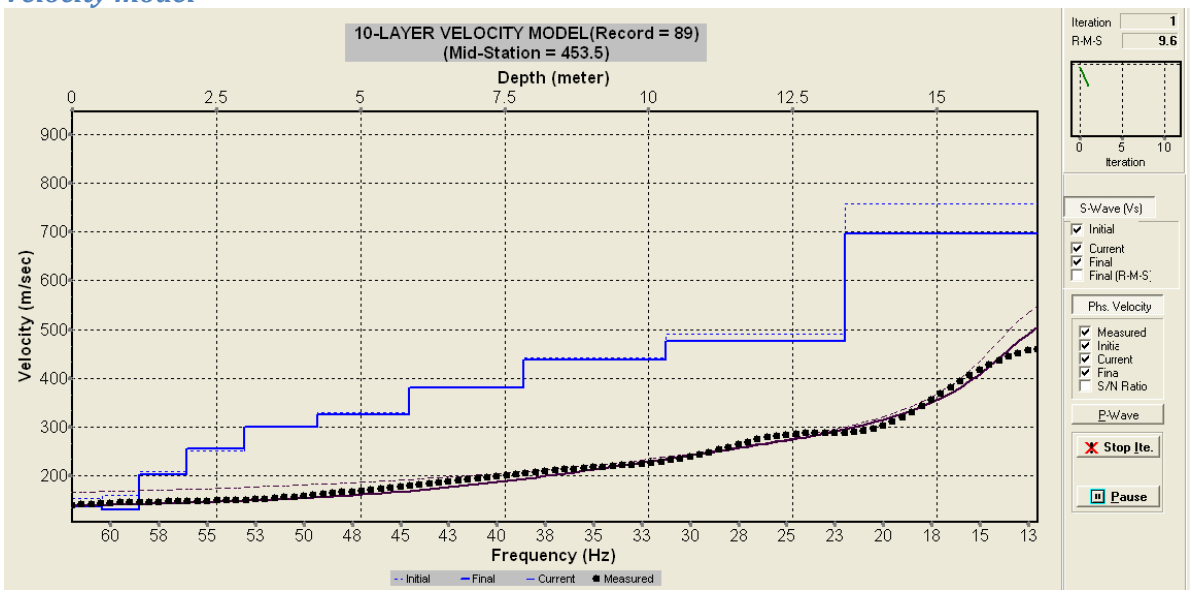

SITE NUMBER: T91 (4+)

Site description

Steep slope, bouldery surface. Probe to bedrock (?) variable 0.1-1.0 m

Field file numbers

347-10 (4 stack), 348-10

Site photographs

Shot record and dispersion curve (10 m)

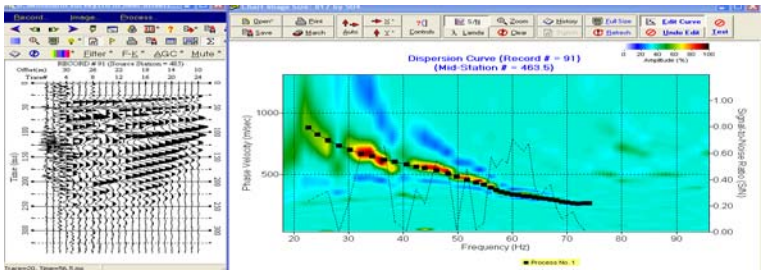

Velocity model

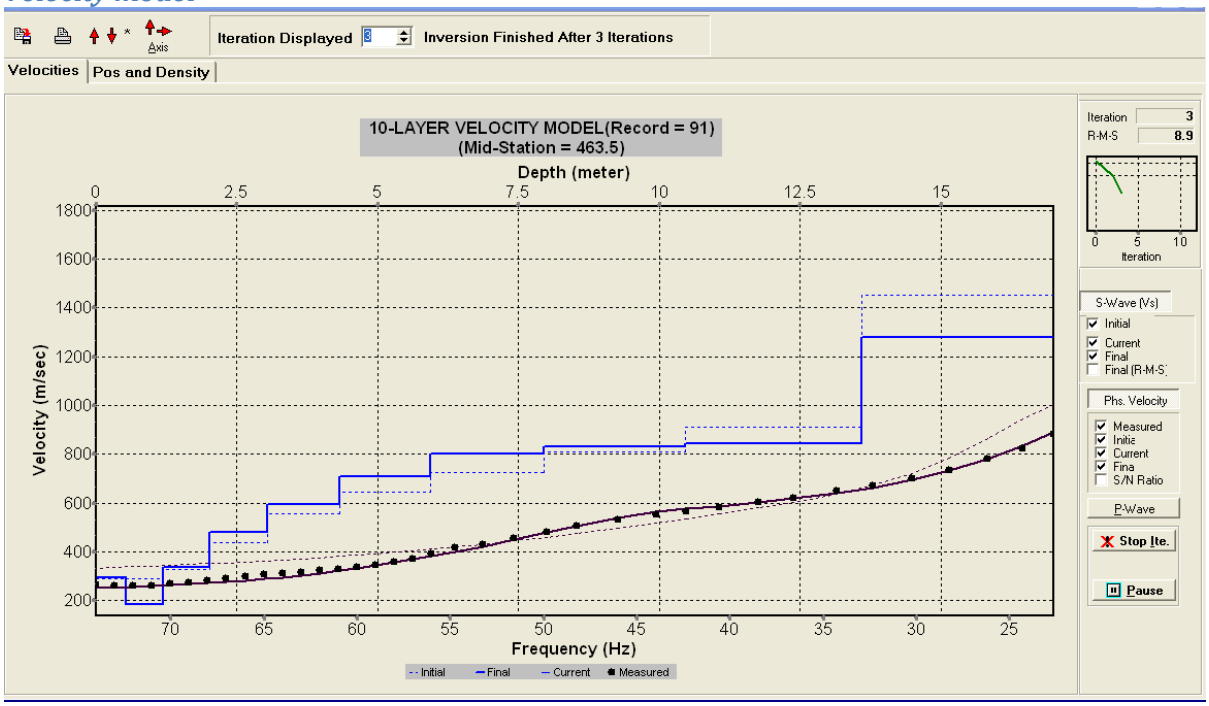

SITE NUMBER: T94 (4-)

Site description

Steep hummocky slope, no outcrop. Probe >1.3 m

Field file numbers

342-22 (stacked), 343-10 (stacked), 344-10

Site photographs

Shot record and dispersion curve (10 m)

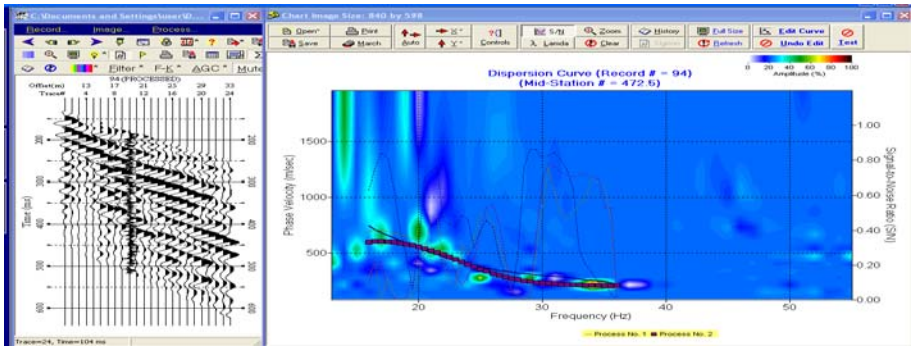

Shot record and dispersion curve (22 m)

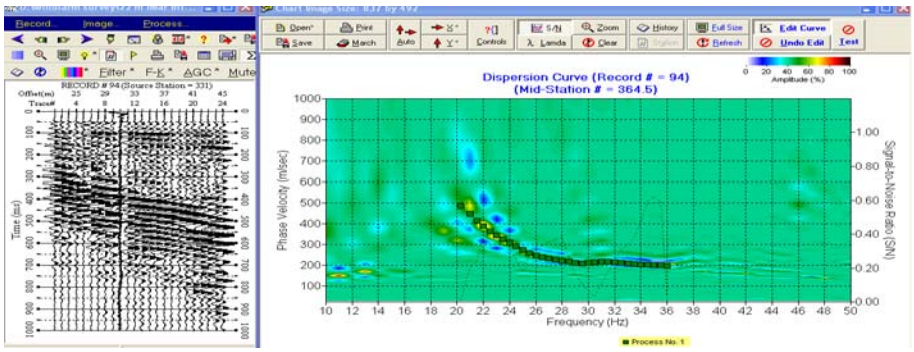

Velocity model from 22 m record

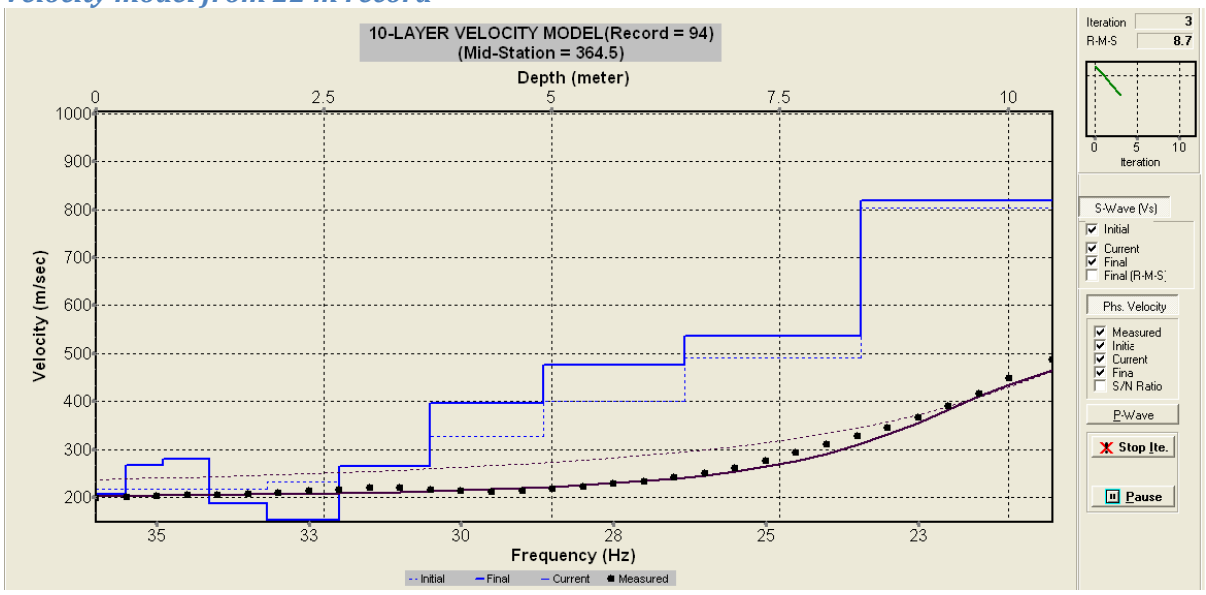

SITE NUMBER: T95 (5)

Site description

Steep hummocky slope, no outcrop. Probe >1.3 m (soft)

Field file numbers

340-10 (4 stack), 341-10

Site photographs

Shot record and dispersion curve (10 m)

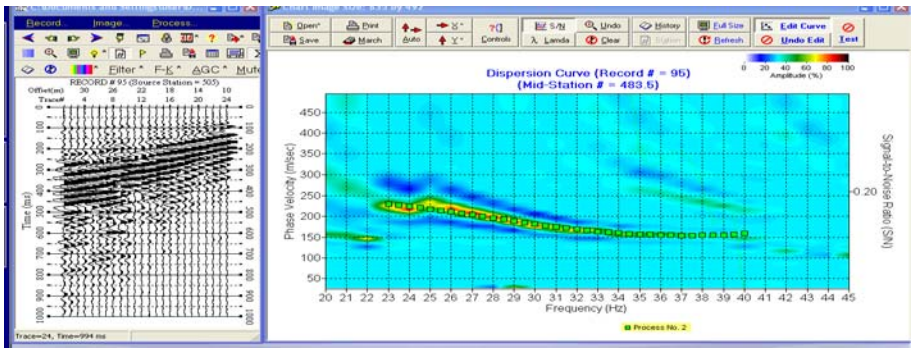

Velocity model

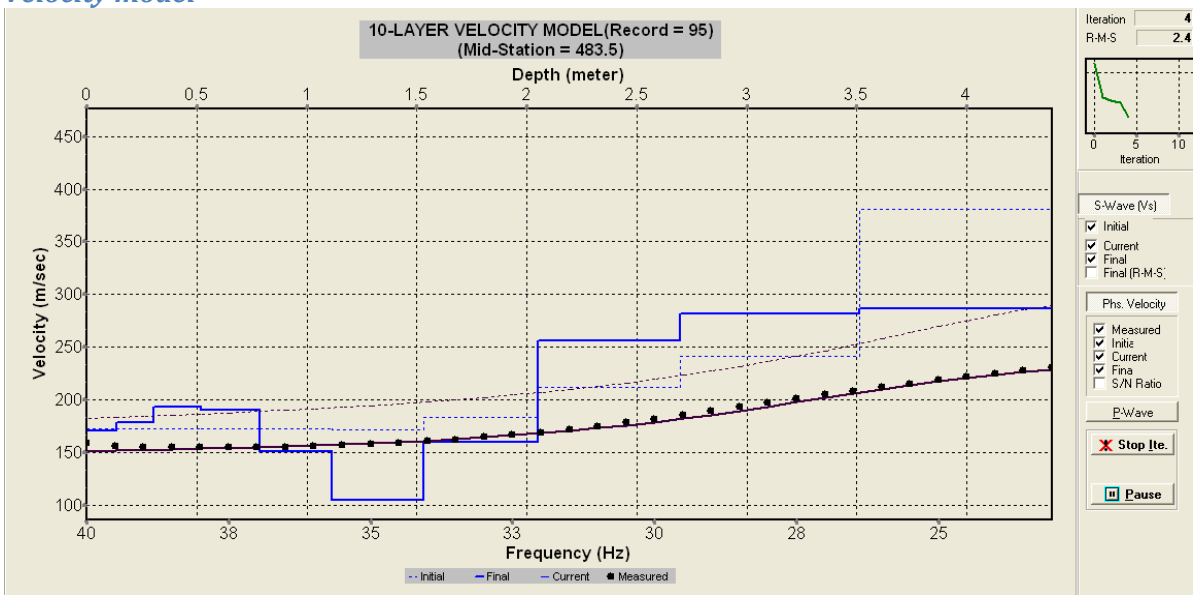

SITE NUMBER: T96 (5+)

Site description

Top of spur, hummocky no outcrop. Probe >1.3 m, dry very soft.

Field file numbers

334-22 (stacked), 335-10 (stacked), 336-10

Site photographs

Shot record and dispersion curve (10 m)

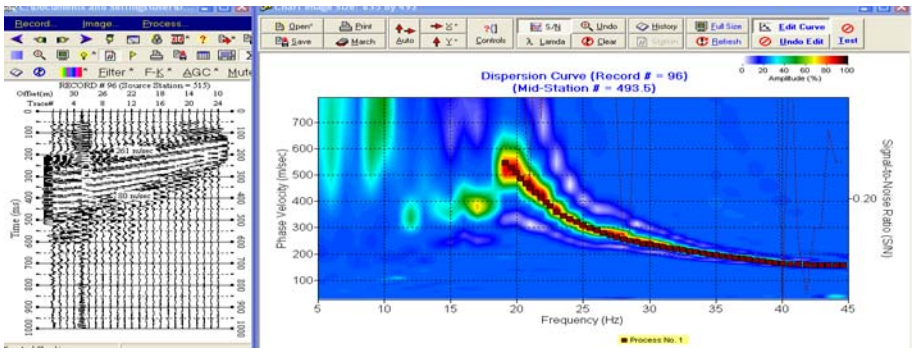

Shot record and dispersion curve (22 m)

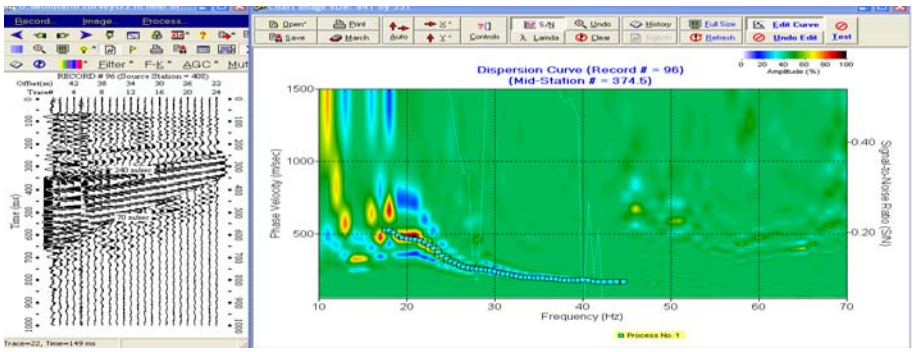

Velocity model

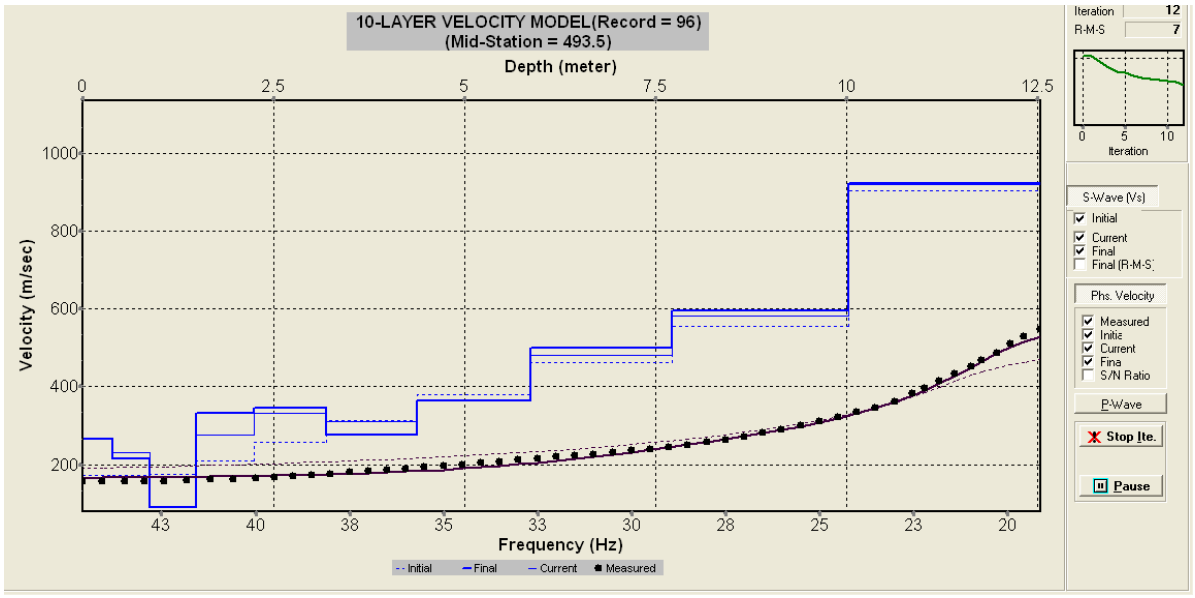

SITE NUMBER: T97 (5+)

Site description

Top of spur, hummocky no outcrop. Probe >1.3 m, dry very soft.

Field file numbers

337-22 (4 stack), 338-10 (stacked), 339-10

Site photographs

Shot record and dispersion curve (10 m)

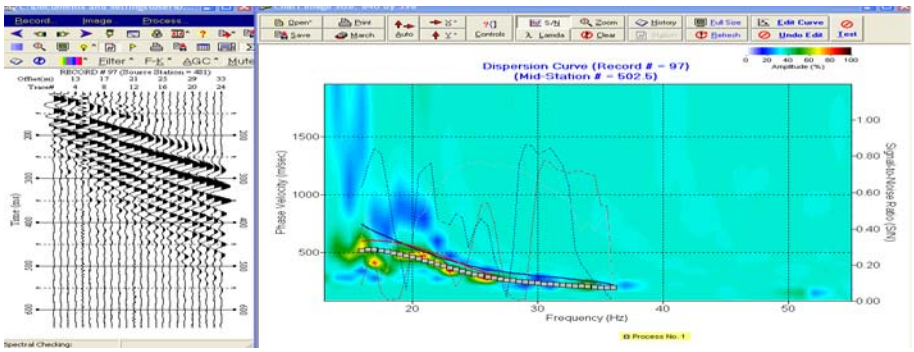

Shot record and dispersion curve (22 m)

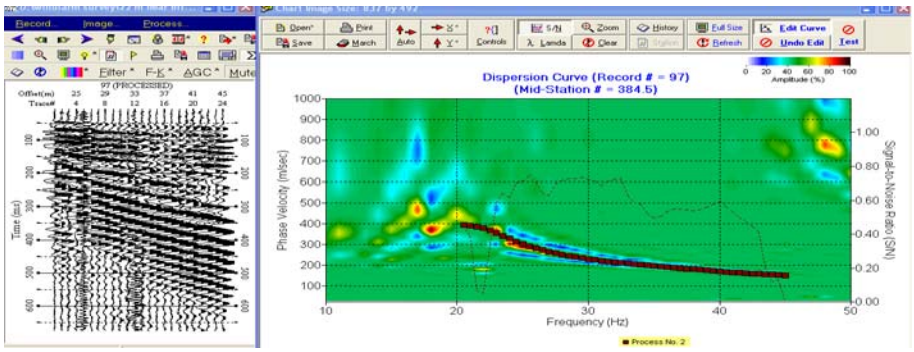

Velocity model from combined curve

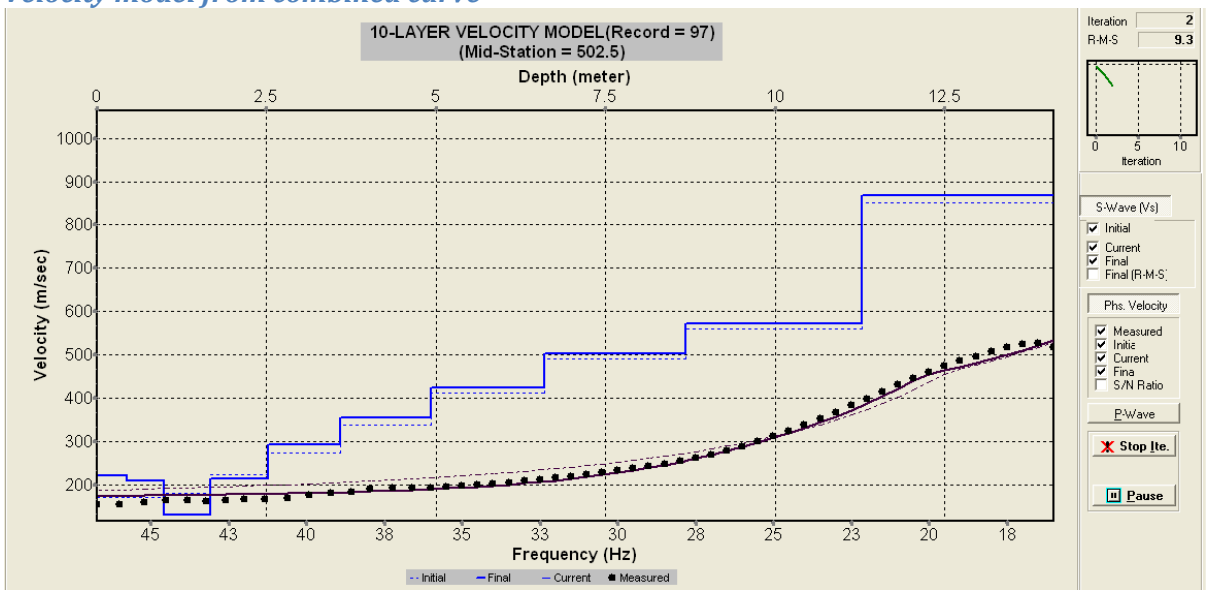

SITE NUMBER: T103 (4+)

Site description

Grassy spur, small hummocks, no outcrop.

Field file numbers

309-22 (4 stack), 310-10 (4 stack), 311-10

Site photographs

Shot record and dispersion curve (10 m)

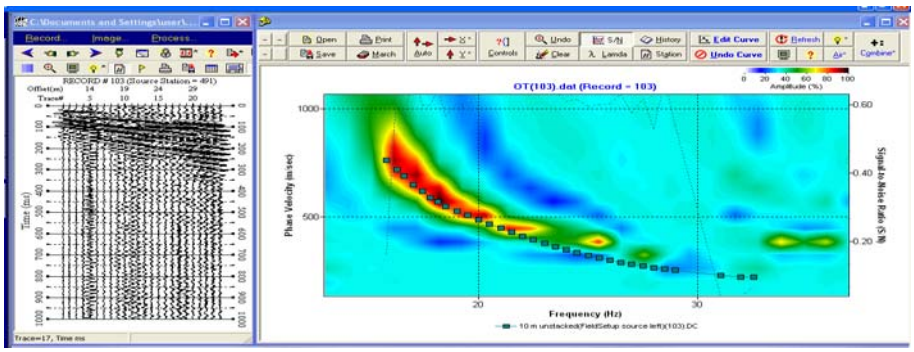

Shot record and dispersion curve (22 m)

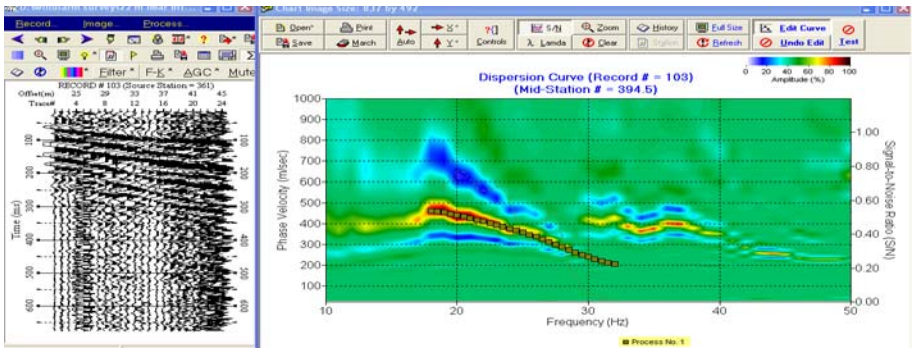

Velocity model from 10 m record

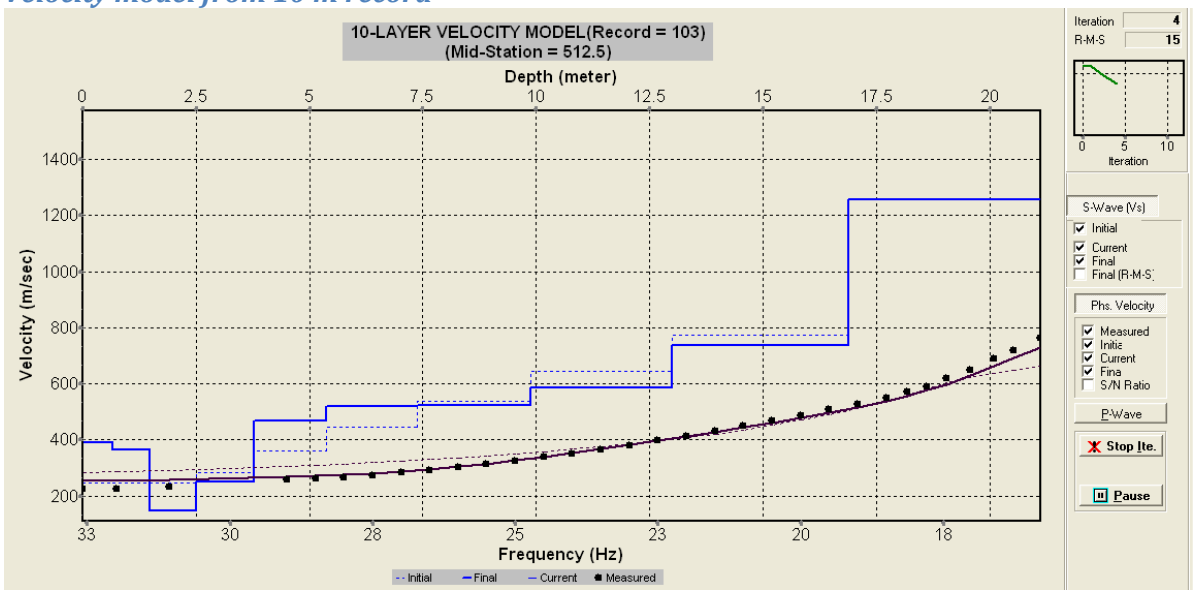

SITE NUMBER: T104 (2)

Site description

Grass covered hummocky hillslope, no outcrop, Probe >1.3 m gravels.

Field file numbers

307-10 (4 stack), 308-10

Site photographs

Shot record and dispersion curve (10 m)

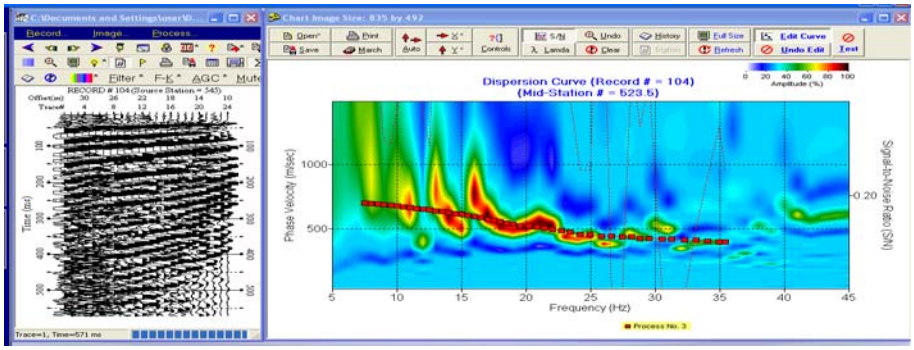

Velocity model

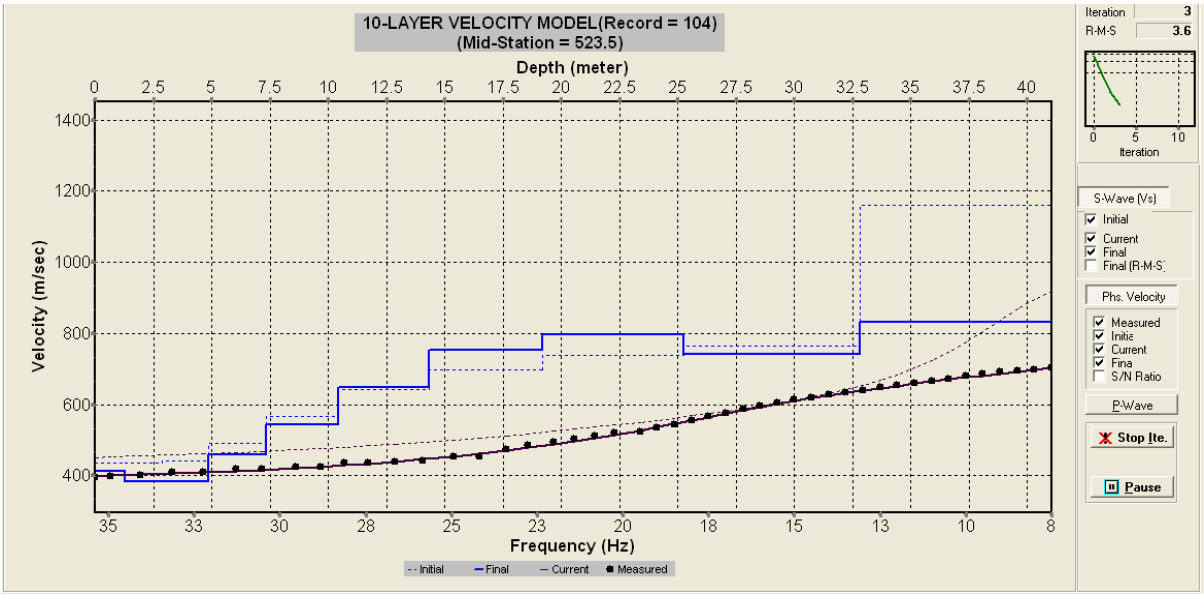

SITE NUMBER: 201(4+)

Site description: Grass covered hill slope. Light wind.
Photographs of site:

Field file numbers:

FF 100-103, -8 m offset, 4 stacks, 1/2 m spacing, 48 geophones, 24 dB gain.

Dispersion curves:

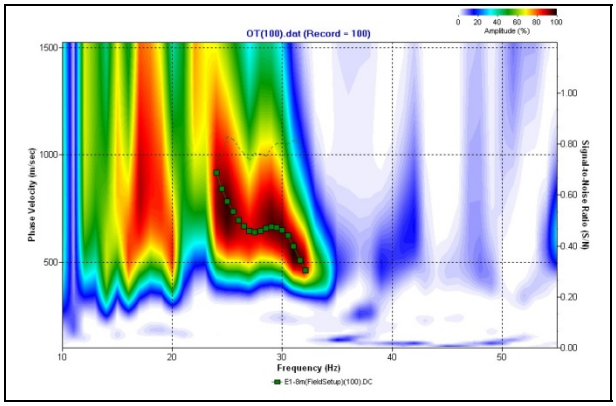

Velocity model:

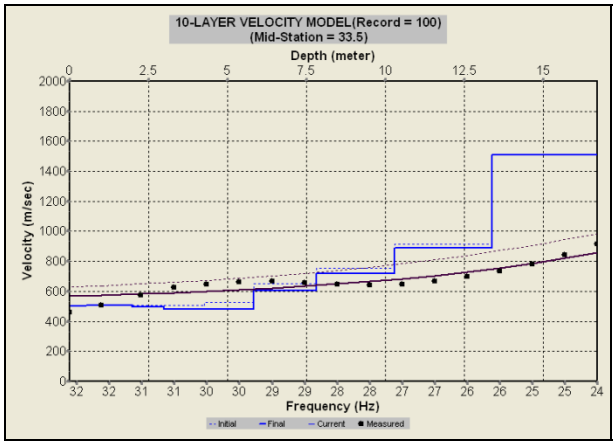

SITE NUMBER: 209(4+)

Site description: Grass covered hill slope. Light wind.

Photographs of site:

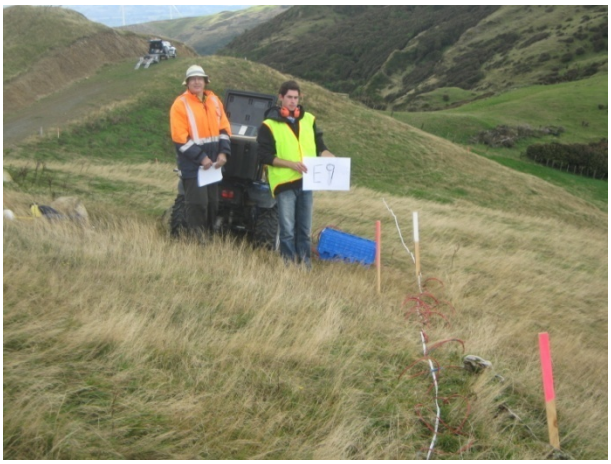

Field file numbers:

FF 109-110, 8 m offset, 4 stack, 1/2 m spacing, 48 geophones, gain 24 dB.

Dispersion curves:

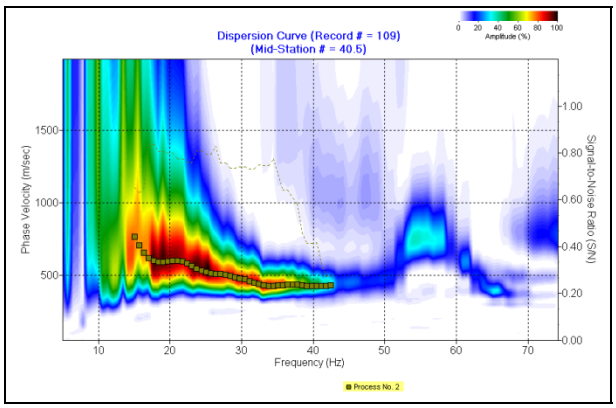

Velocity model:

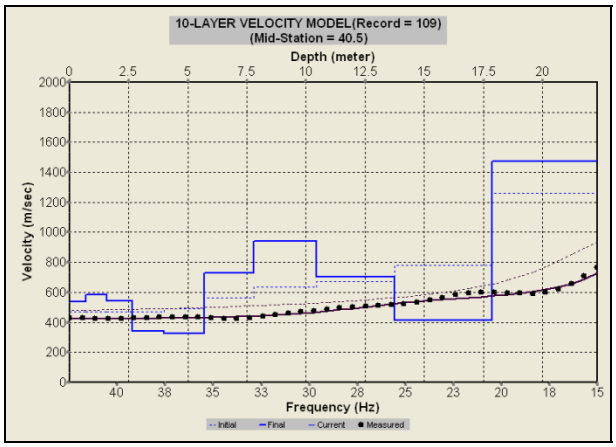

SITE NUMBER: 210(3+)

Site description: Grass covered hill slope. Not possible to get +8 m offset. Not windy.

Photographs of site:

Field file numbers:
FF 112-115 -8 m offset, 4 stack, 1/2 m spacing, 46 geophone, gain 24 d

Dispersion curves:

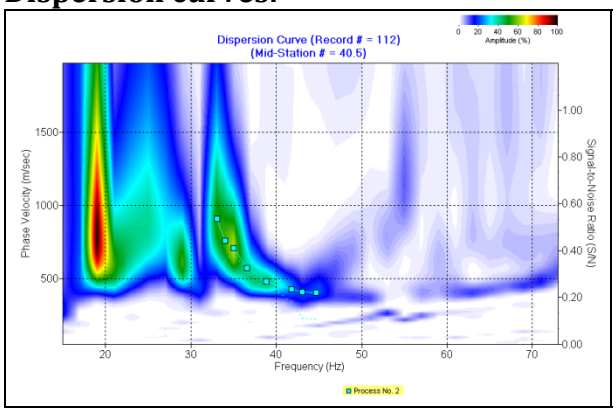

Velocity model:

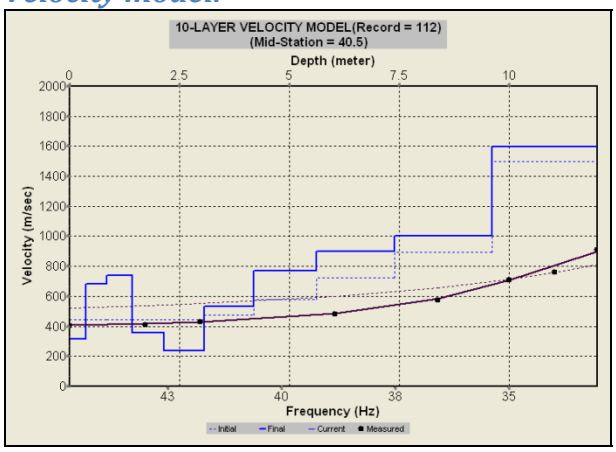

SITE NUMBER: 211(3-)

Site description: Grass covered hill slope. Light wind.

Photographs of site:

Field file numbers:

FF 116-117, -8 m offset, 4 stack, 1/2 m spacing,48 geophones, gain 24 dB.

Dispersion curves:

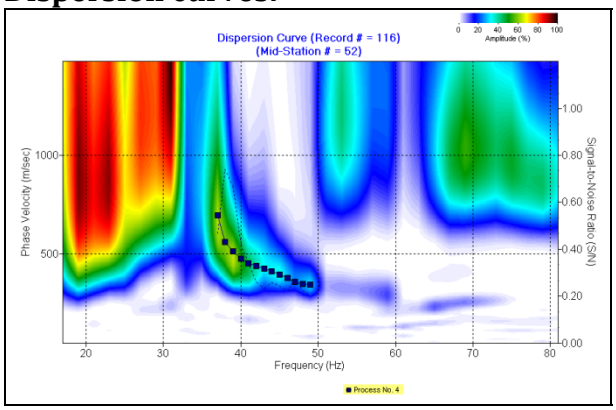

Velocity model:

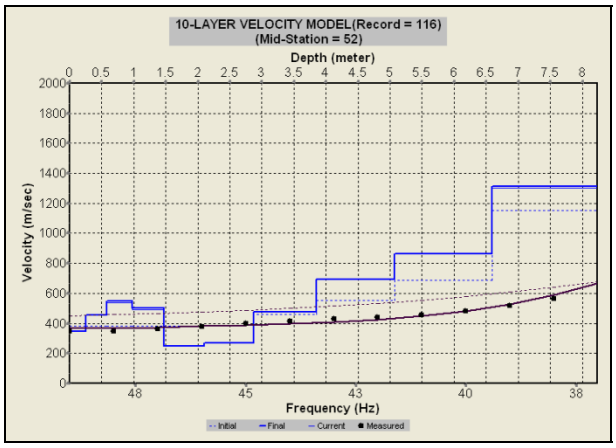

SITE NUMBER: 212(4-)

Site description: Grass covered hill slope. Light wind.

Photographs of site:

Field file numbers:

FF 118-121, -8 m offset, 4 stack, 1/2 m spacing, 48 geophones, gain 24 dB

Dispersion curves:

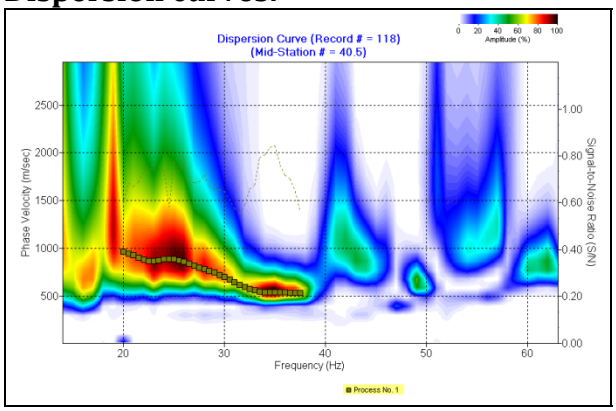

Velocity model:

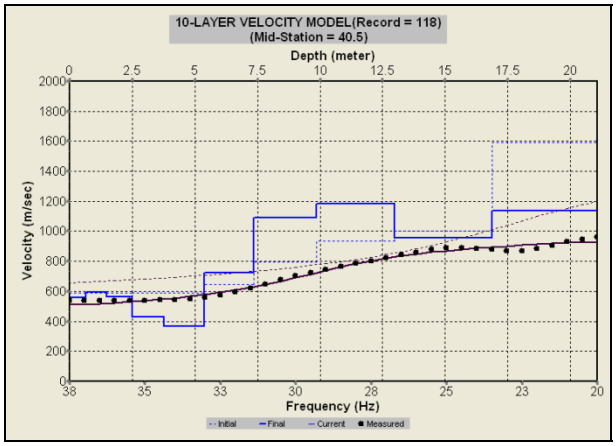

SITE NUMBER: 213(4-)

Site description: Grass covered hill slope. Light wind.

Photographs of site:

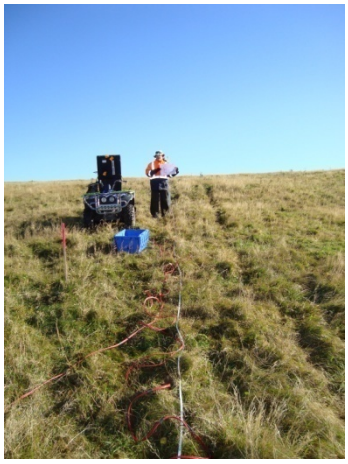

Field file numbers:

FF 122-125, -8 m offset, 4 stack, 1/2 m spacing, 48 geophones, gain 24 dB

Dispersion curves:

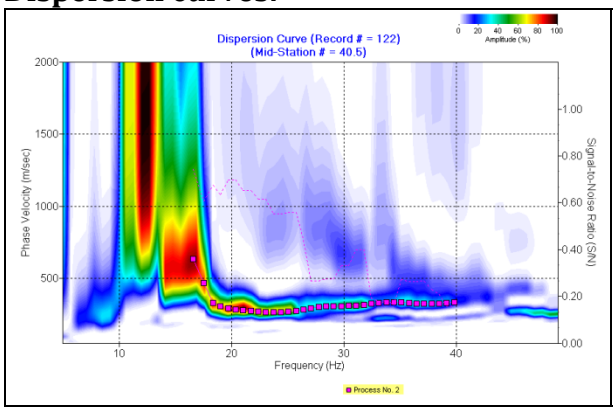

Velocity model:

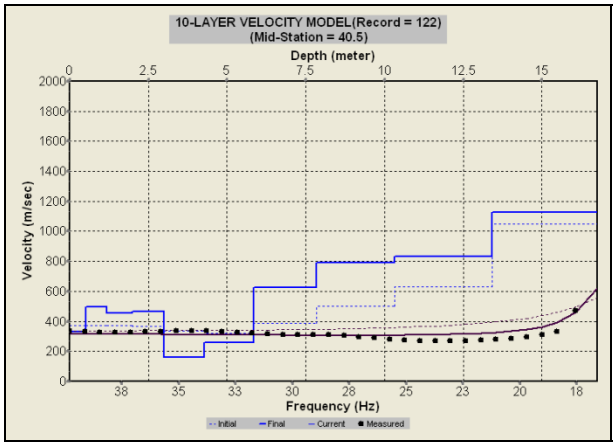

SITE NUMBER: 214(3+)

Site description: Grass covered hill slope. Light wind.

Photographs of site:

Field file numbers:

FF 127-130, -8 m offset, 4 stack, 1/2 m spacing, 48 geophones, gain 24 dB.

Dispersion curves:

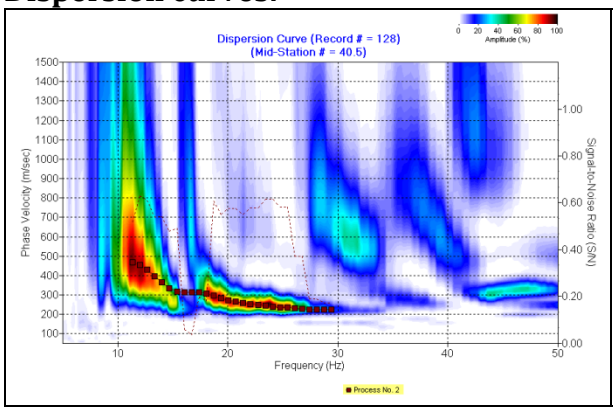

Velocity model:

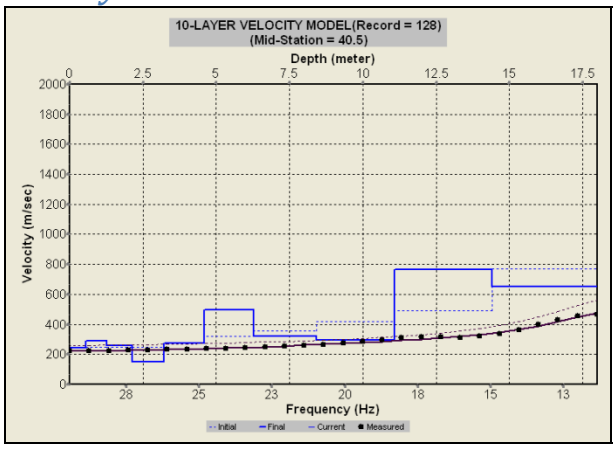

SITE NUMBER: 219(4+)

Site description: Grass covered hill slope. Light wind. Site not pegged. Position measured from plans.

Photographs of site:

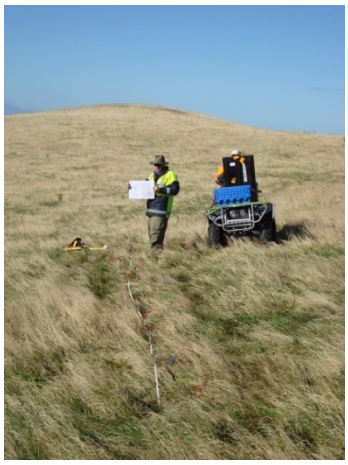

Field file numbers:

FF 132-135, -8 m offset, 4 stack, 1/2 m spacing, 48 geophones, gain 24 dB.

Dispersion curves:

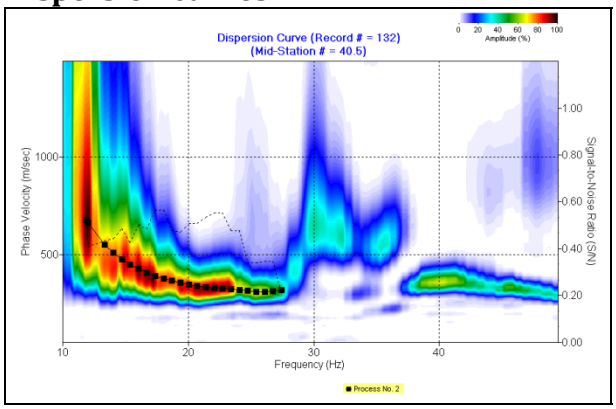

Velocity model:

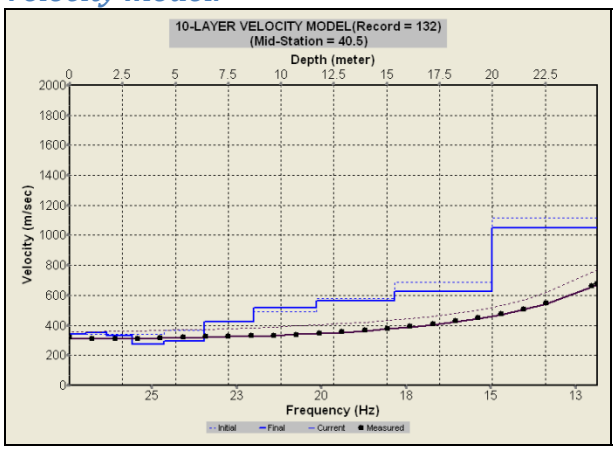

SITE NUMBER: 220(3+)

Site description: Grass covered hill slope. Light wind. Lots of surface mounds so only -8m shot possible.

Photographs of site:

Field file numbers:

FF 136-137, -8 m offset, 4 stack, 1/2 m spacing, 48 geophones, gain 24 dB.

Dispersion curves:

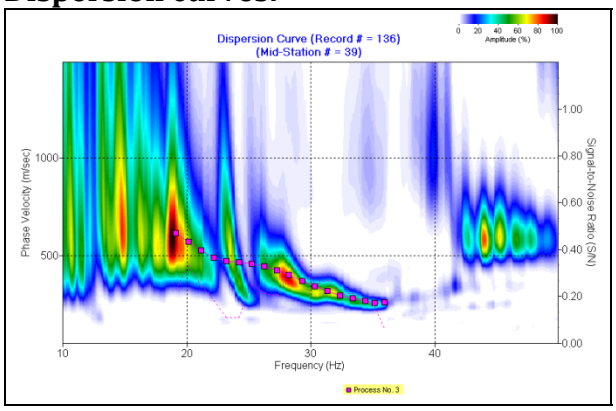

Velocity model:

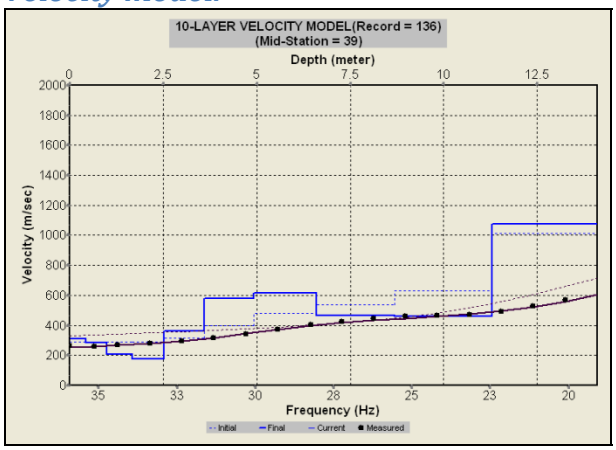

SITE NUMBER: 202(2+)

Site description: Erosional gully with extensive marsh/swamp deposits. Site not pegged, so position measured off plans. Area has many tree trunks from recently cut trees.

Photographs of site:

Field file numbers:

FF 138, +8 m offset, 4 stack, 1/2 m spacing, 24 geophones, gain 24 dB

Dispersion curves:

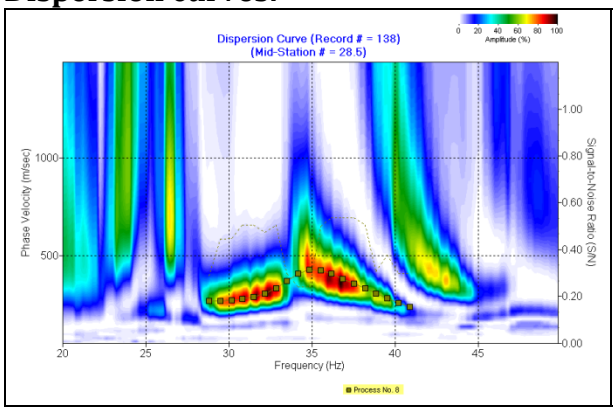

Velocity model:

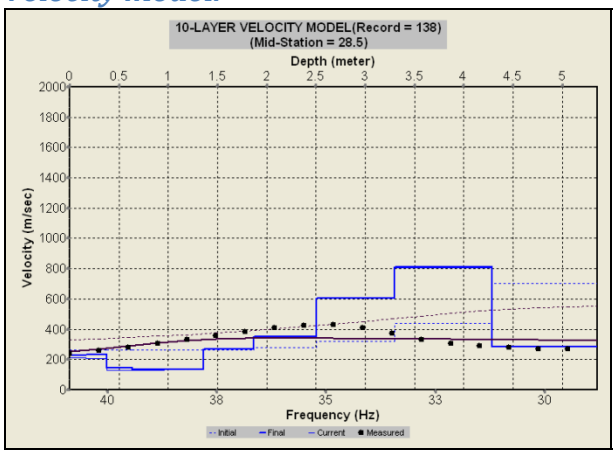

SITE NUMBER: 203(5-)

Site description: Grass covered hill slope. Light wind.

Photographs of site:

Field file numbers:

140-142, -8 m offset, 4 stack, 1/2 m spacing, 48 geophones, gain 24 dB

Dispersion curves:

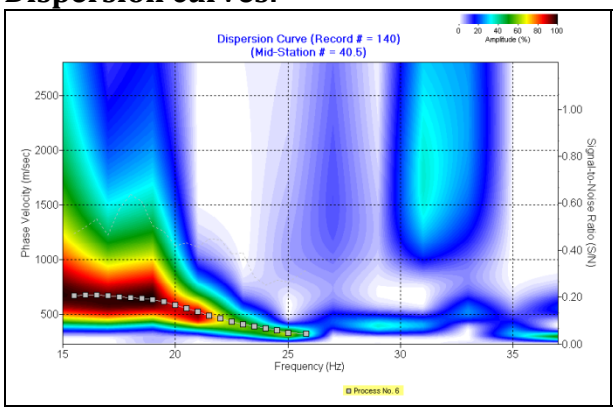

Velocity model:

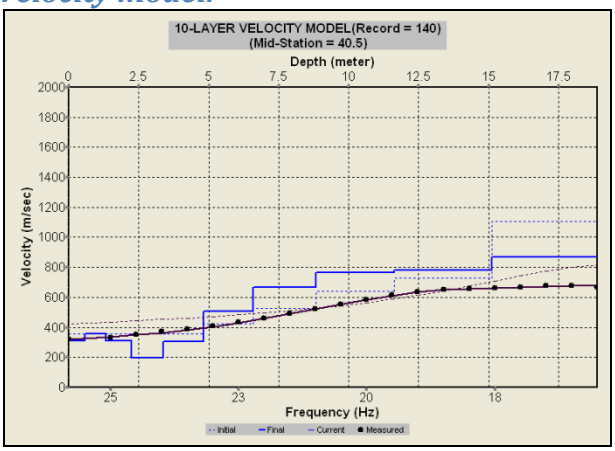

SITE NUMBER: 204(3+)

Site description: Grass covered steep hill slope. Light wind.

Photographs of site:

Field file numbers:

143-144, -8 m offset, 4 stack, 1/2 m spacing, 41 geophones, gain 24 dB.

Dispersion curves:

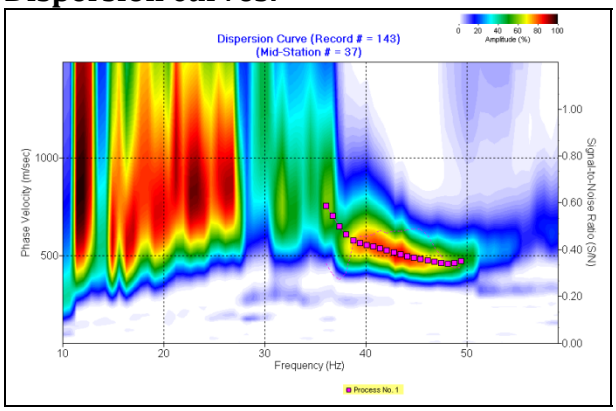

Velocity model:

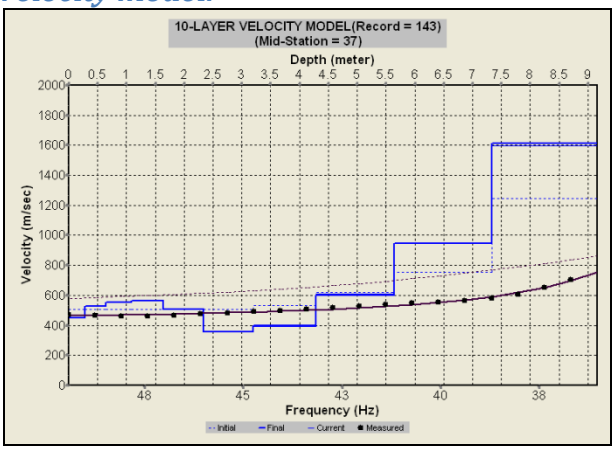

SITE NUMBER: 208(4+)

Site description: Grass covered hill spur. Survey undertaken on a small flat area between two small hills. Maximum offset for shot only 5.5 m because of slope.

Photographs of site:

Field file numbers:

145-146, +5.5 m offset, 4 stack, 1/2 m spacing, 48 geophones, gain 24 d

Dispersion curves:

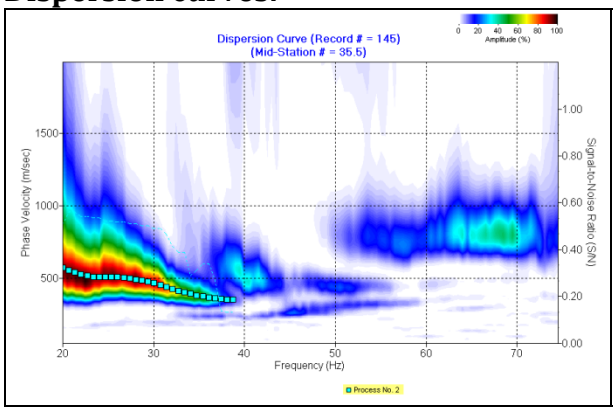

Velocity model:

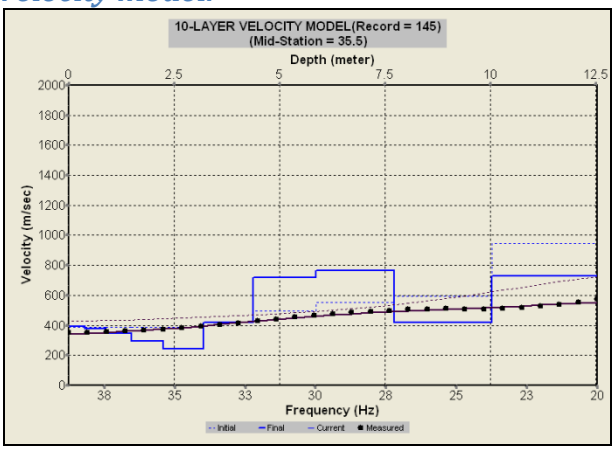

]

SITE NUMBER: 207(2+)

Site description: Grass covered flat area. Light wind. Trees to the northeast.

Photographs of site:

Field file numbers:

147-148, +8 m offset, 4 stack, 1/2 m spacing, 46 Geophones, Gain 24 dB.

Dispersion curves:

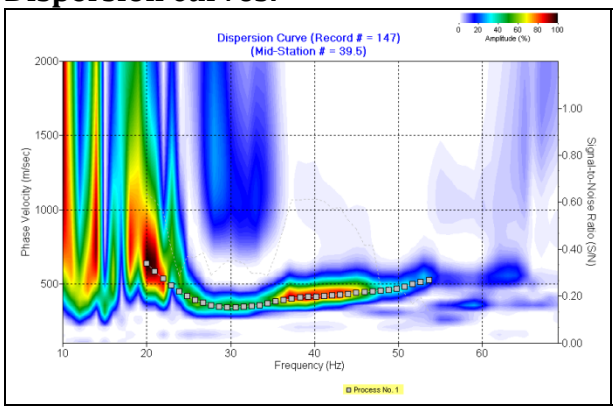

Velocity model:

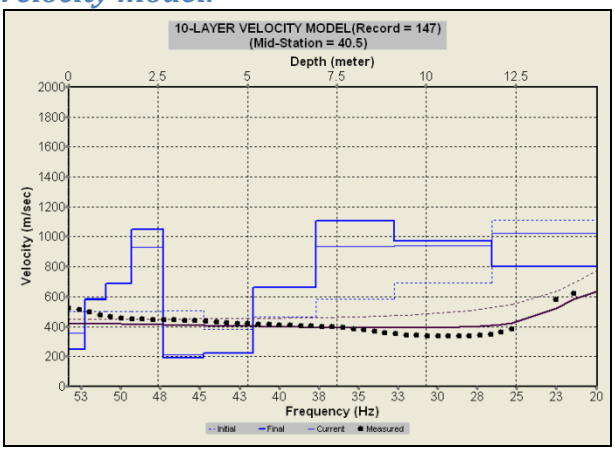

SITE NUMBER: 206(3+)

Site description: Grass covered flat area. Light wind. Trees to the northeast.

Photographs of site:

Field file numbers:

149-150, +8 m offset, 4 stack, 1/2 m spacing, 48 Geophones, Gain 24 dB.

Dispersion curves:

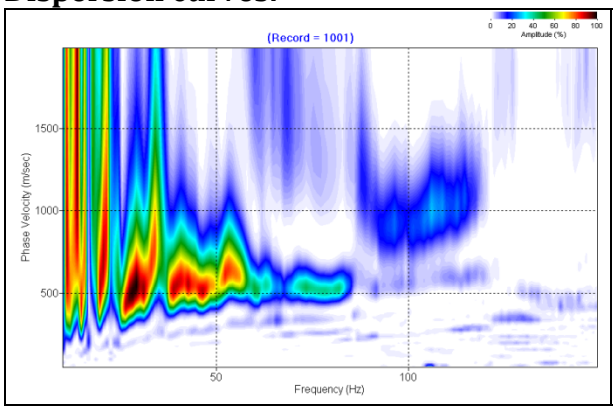

Velocity model:

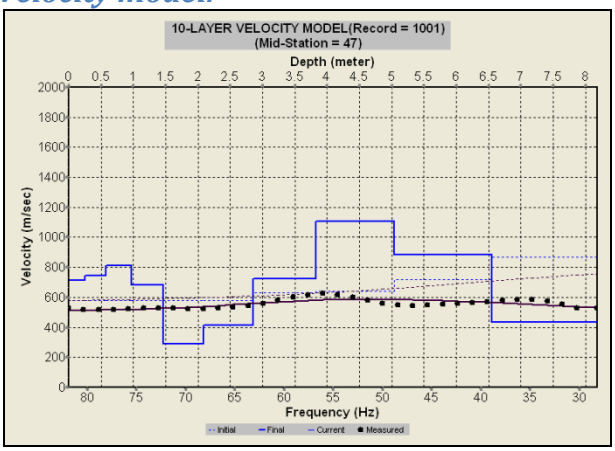

SITE NUMBER: 205(3+)

Site description: Mud/rock covered flat area. Light wind. Site cleared and flatten earlier in the day.

Photographs of site:

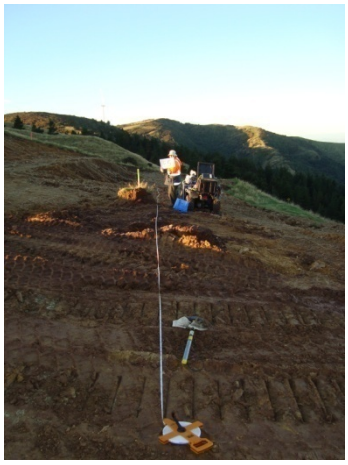

Field file numbers:

152-153, -8 m offset, 4 stack, 1/2 m spacing, 48 geophones, gain 24 dB.

Dispersion curves:

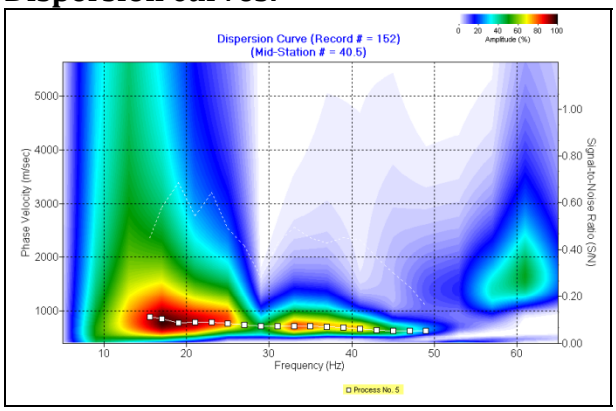

Velocity model:

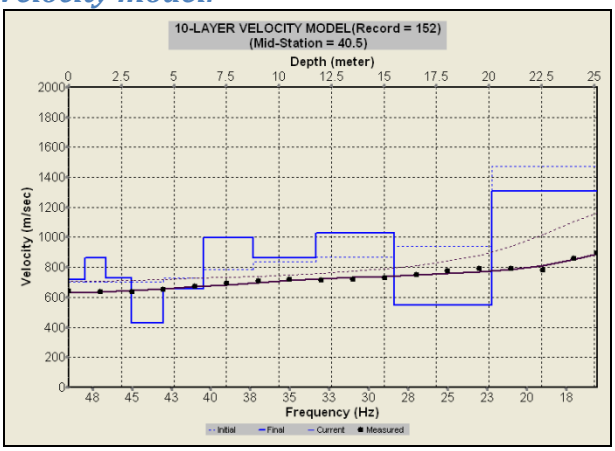

SITE NUMBER: E32(4+)

Site description: Platform cut, rock at surface. Light wind.

Photograph of site:

Field file numbers:

FF 113-114, -8 m offset, 4 stacks, 1/2 m spacing, 48 geophones, 24 dB gain.

Dispersion curves:

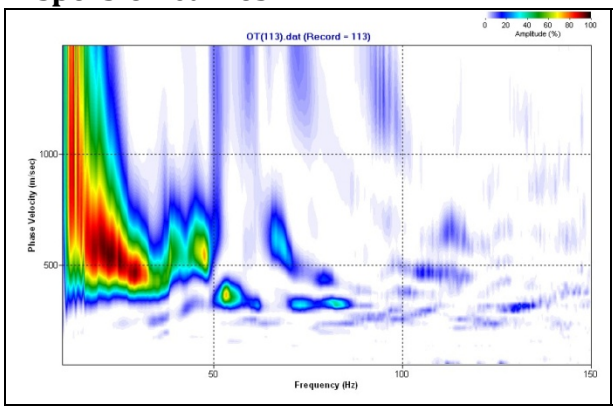

Velocity model:

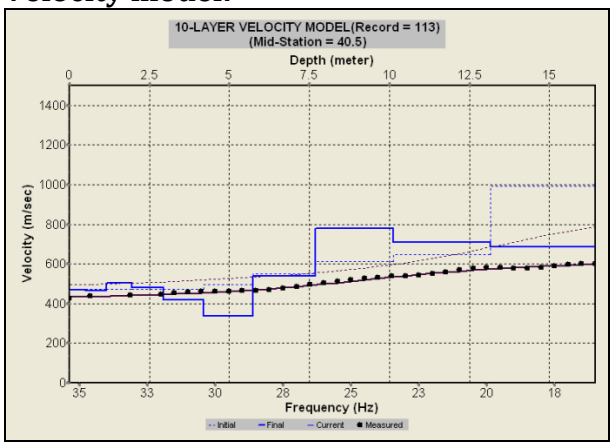

SITE NUMBER: E34(5)

Site description: Platform cut. Soil/cushed rock to surface. Light wind.

Photograph of site:

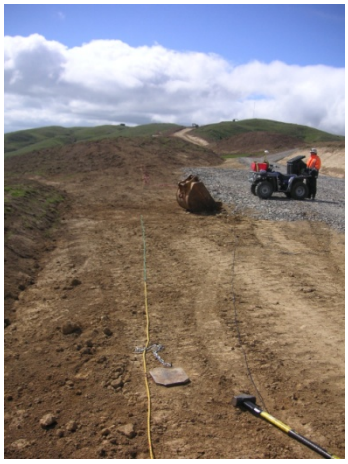

Field file numbers:

FF 117-118, -8 m offset, 4 stacks, 1/2 m spacing, 48 geophones, 24 dB gain.

Dispersion curves:

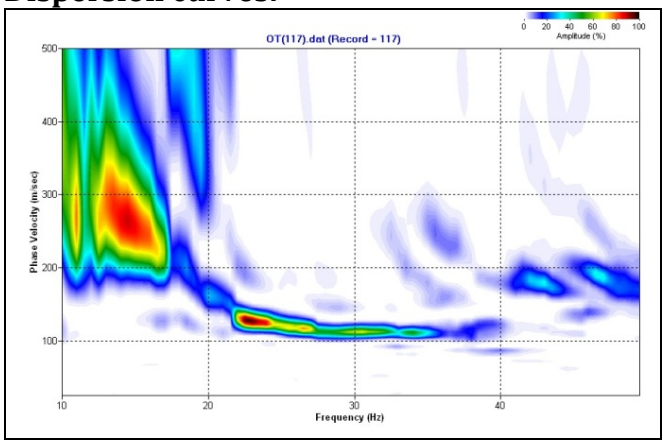

Velocity model:

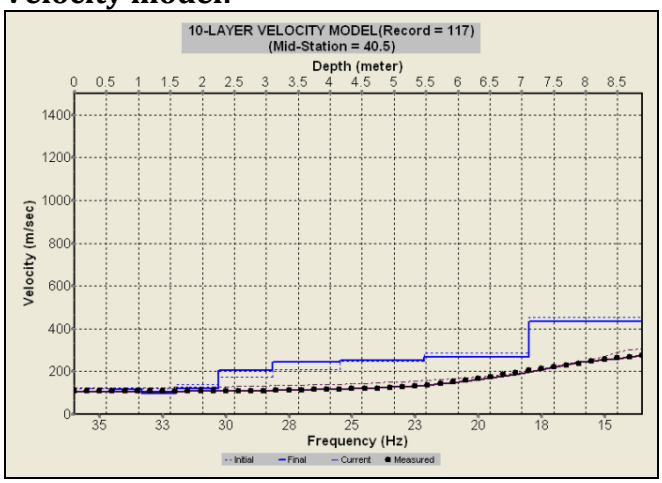

SITE NUMBER: E38(3-)

Site description: Platform cut. Crushed rock to surface. Windy.

Photographs of site:

Field file numbers:

FF 115-116, -8 m offset, 4 stacks, 1/2 m spacing, 46 geophone, 24 dB gain

Dispersion curves:

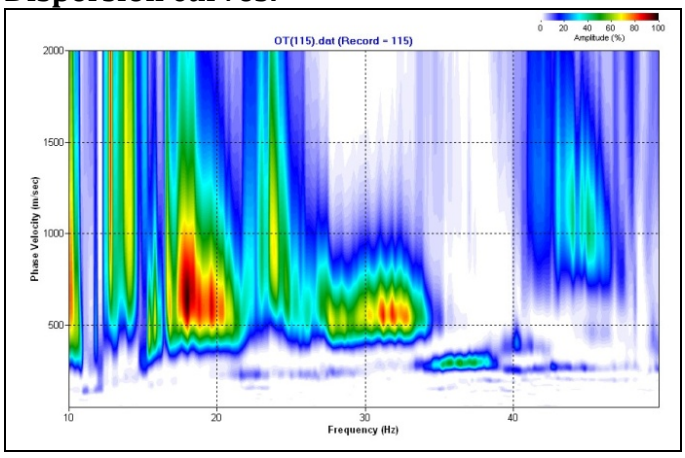

Velocity model:

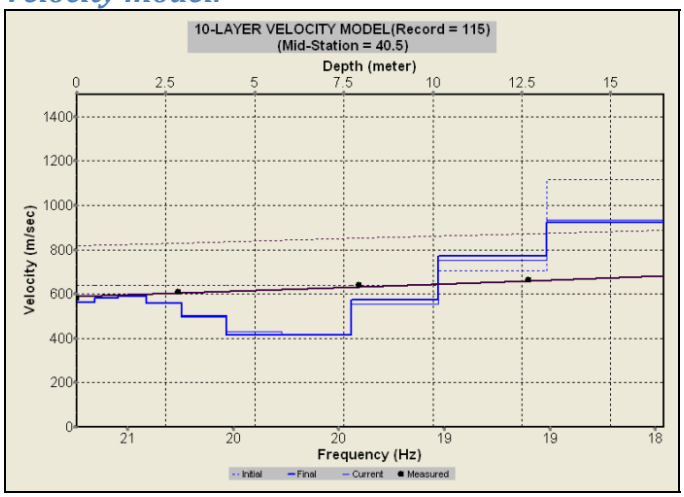

SITE NUMBER: E40(4-)

Site description: Grass-covered hill slope. Light wind.

Photograph of site:

Field file numbers:

FF 100-101, -8 m offset, 4 stacks, 1/2 m spacing,48 geophones, 24 dB gain.

Dispersion curves:

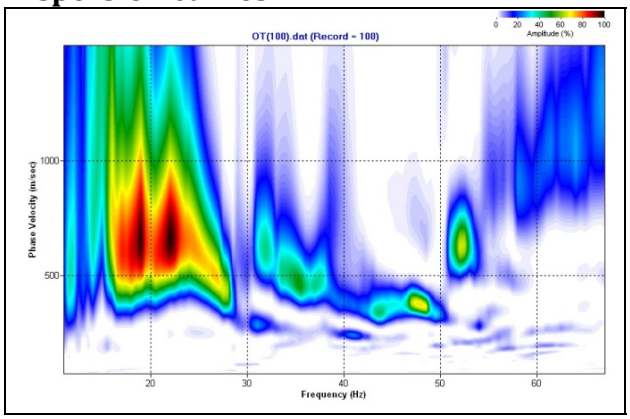

Velocity model:

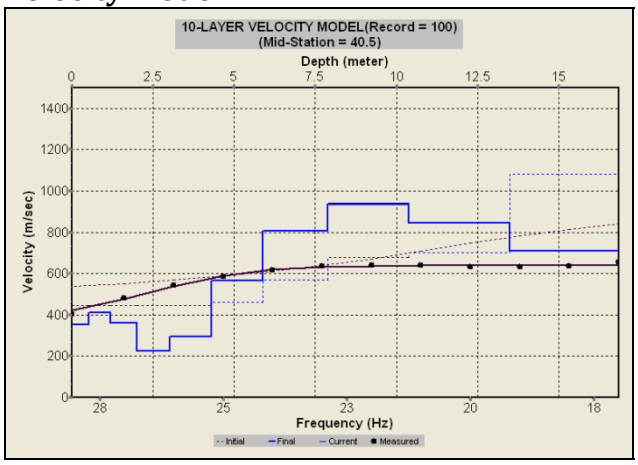

SITE NUMBER: E41(3-)

Site description: Ridge spur, grass covered no rock visible. Light wind.

Photograph of site:

Field file numbers:

FF 104-105, -8 m offset, 4 stacks, 1/2 m spacing, 48 geophones, 24 dB gain

Dispersion curves:

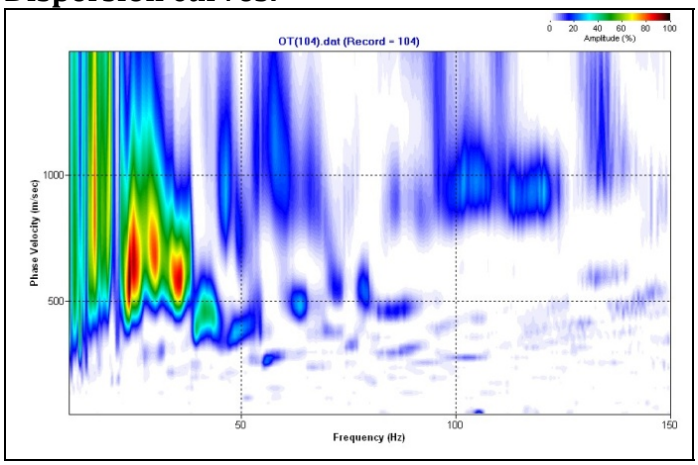

Velocity model:

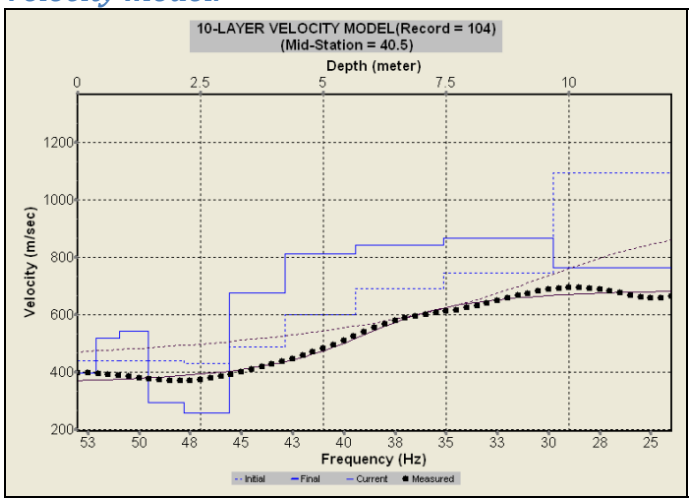

SITE NUMBER: 42(4+)

Site description: Grass-covered hill top. Light wind.

Photograph of site:

Field file numbers:

FF 102-103, -8 m offset, 4 stacks, 1/2 m spacing, 48 geophones, 24 dB gain

Dispersion curves:

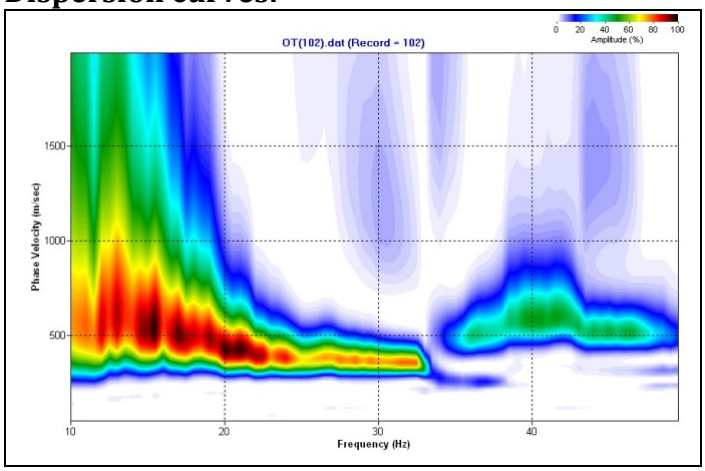

Velocity model:

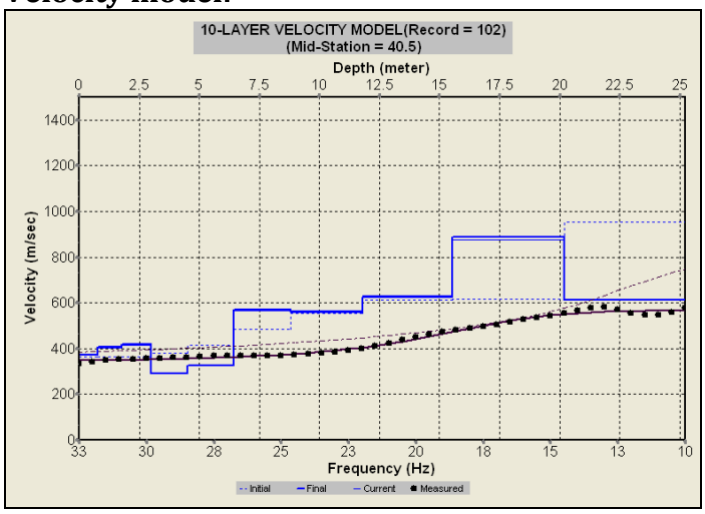

SITE NUMBER: E43(4-)

Site description: Grass-covered hill spur. Light wind.

Photograph of site:

Field file numbers:

FF 106-107, -8 m offset, 4 stacks, 1/2 m spacing, 48 geophones, 24 dB gain

Dispersion curves:

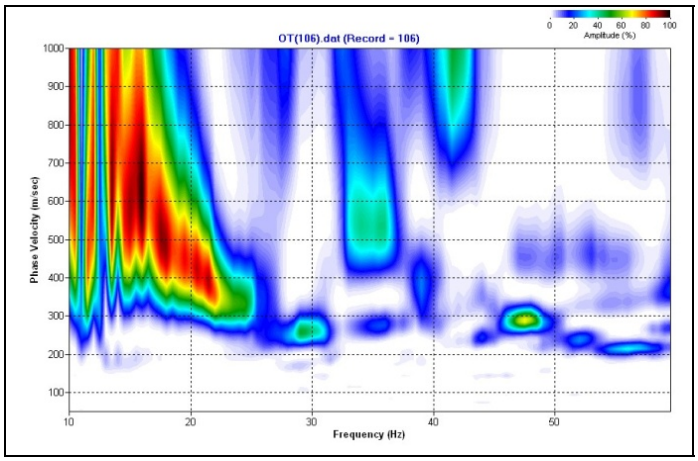

Velocity model:

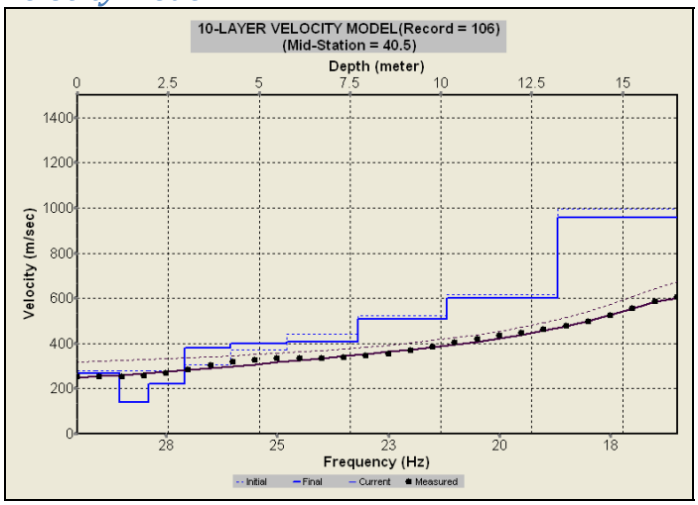

SITE NUMBER: E44(3)

Site description: Grass-covered hill top. Light wind.

Photographs of site:

Field file numbers:

FF 109-110, -8 m offset, 4 stacks, 1/2 m spacing, 48 geophones, 24 dB gain

Dispersion curves:

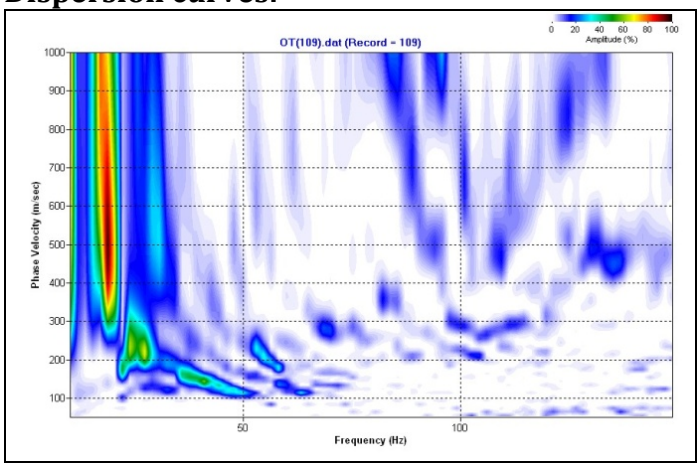

Velocity model:

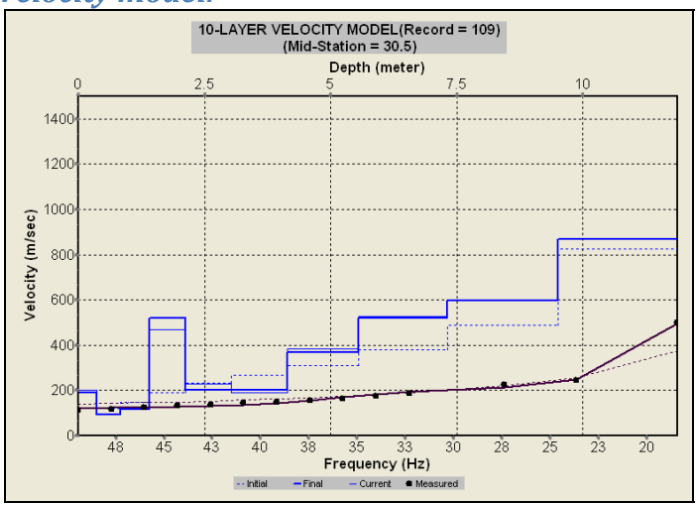

SITE NUMBER: E45(2-)

Site description: Grass-covered hill spur. Light wind.

Photograph of site:

Field file numbers:

FF 111-112, -8 m offset, 4 stacks, 1/2 m spacing, 48 geophones, 24 dB gain.

Dispersion curves:

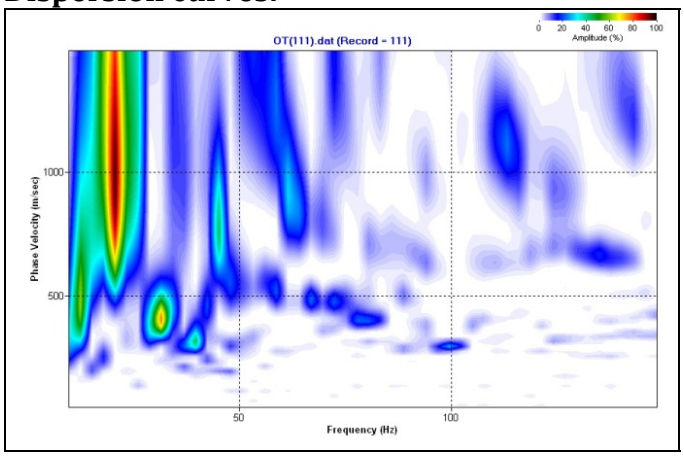

Velocity model:

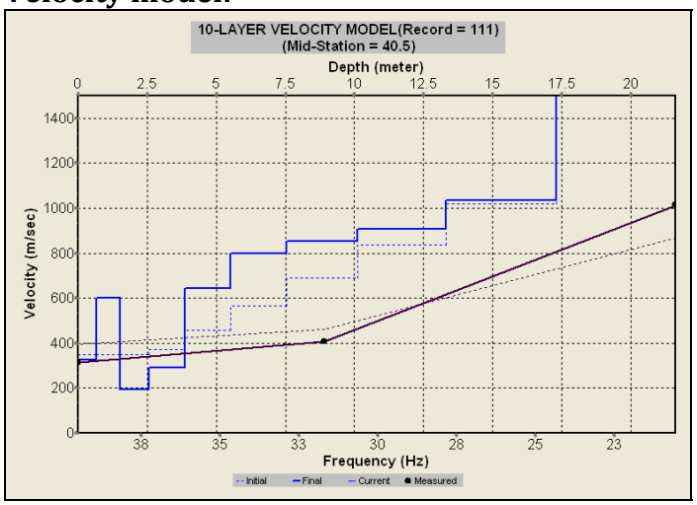

SITE NUMBER: E46(0)

Site description: Grass-covered, steeply dipping hill slope. Very bumpy.
Photograph of site:

Field file numbers:
FF 108, -8 m offset, 4 stack, **1 m spacing**, 24 geophones, 24 dB gain.

Dispersion curves:

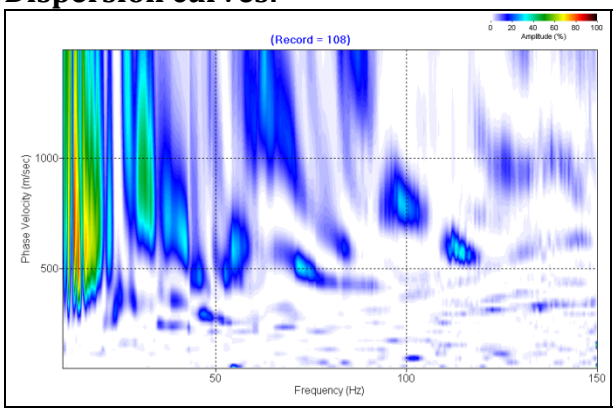

Velocity model:

No model produced because of data quality

SITE NUMBER: West Wind K04(4)

Site description: Grass-covered, flat top of hill, with downhill slopes surrounding survey area.

Photograph of site:

Field file numbers:

1003, -8 m offset, 4 stack, **0.5 m spacing**, 24 geophones, 24 dB gain

Dispersion curves:

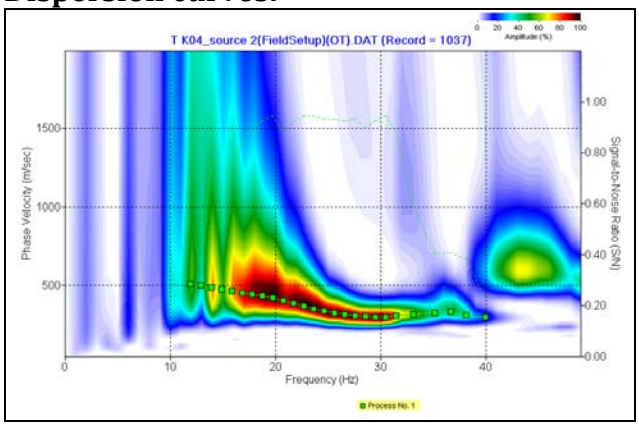

Velocity model:

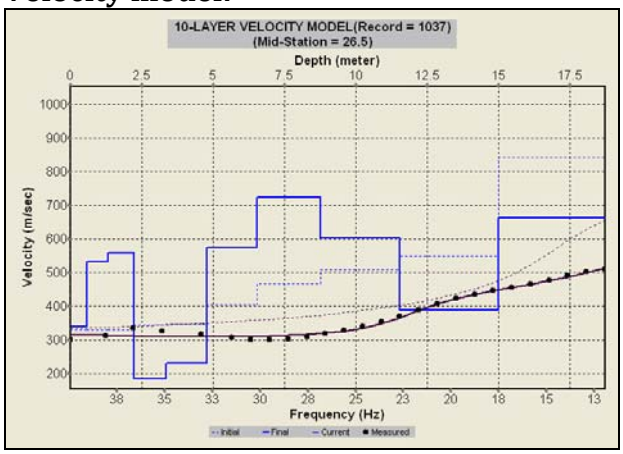

SITE NUMBER: Turitea 01(3+)

Site description: grass covered slope, flat topography.

Photograph of site:

Field file numbers:

1004/1007/1008, -8 m offset, 8 stack, **1 m spacing**, 36 geophones, 24 dB gain.

Dispersion curves:

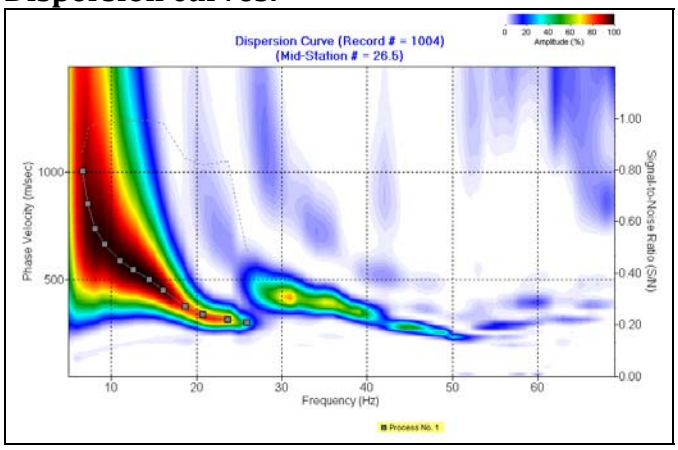

Velocity model:

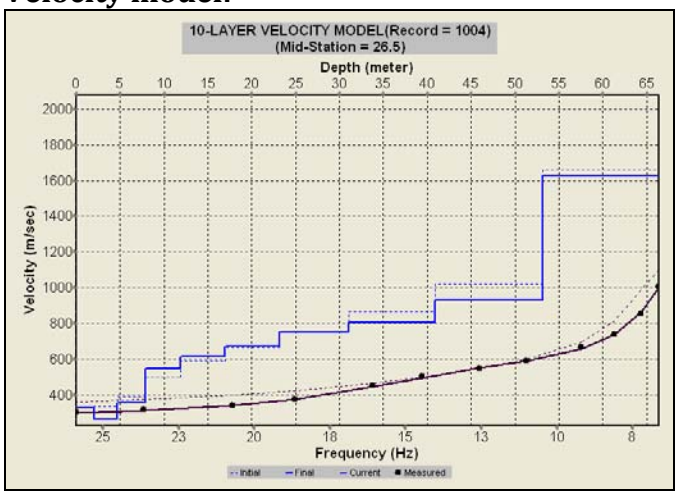

SITE NUMBER: **Turitea 02(4-)**

Site description: Along gravel road

Photograph of site:

Field file numbers:

1010/1013/1014, -8 m offset, 8 stack, **1 m spacing**, 36 geophones, 24 dB gain

Dispersion curves:

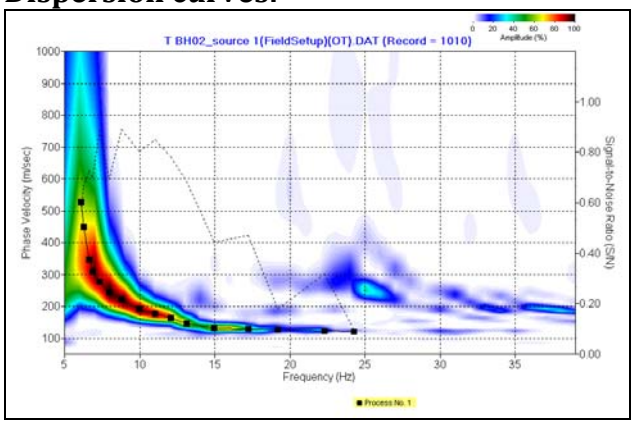

Velocity model:

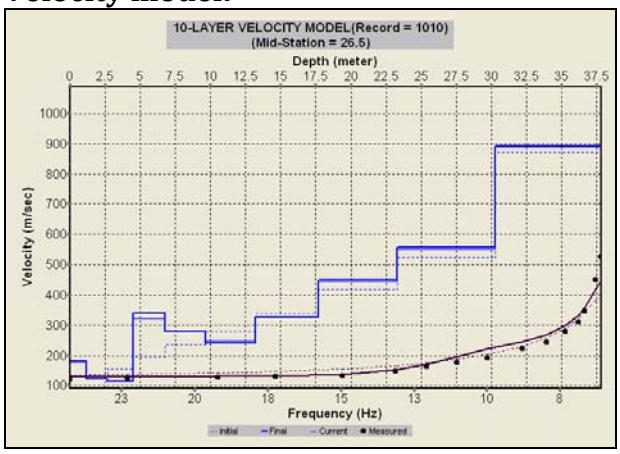

Site abandoned as an investigation site, as founded on silts and gravels, not Esk Head belt greywacke.

SITE NUMBER: Turitea 03(2)

Site description: Along gravel road.

Photograph of site:

Field file numbers:

1017/1018/1021, -8 m offset, 8 stack, **1 m spacing**, 36 geophones, 24 dB gain.

Dispersion curves:

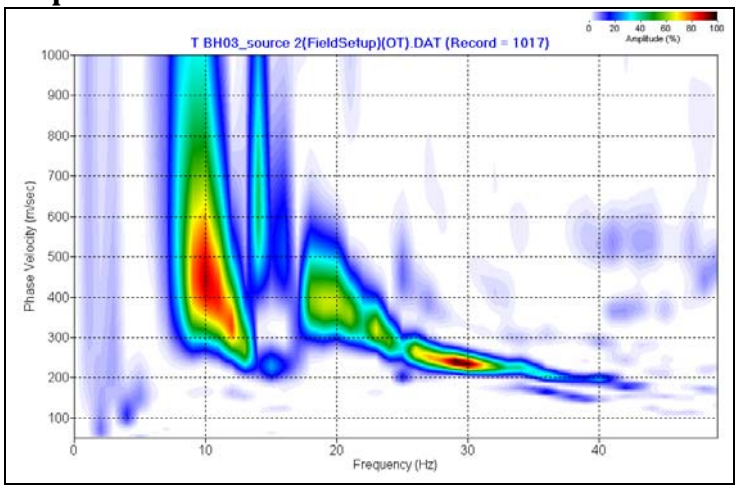

Site abandoned as investigation site, as founded on silts and gravels, not Esk Head belt greywacke.

SITE NUMBER: Turitea 05(3+)

Site description: Along gravel road.

Photograph of site:

Field file numbers:

1023/1025/1029, -8 m offset, 8 stack, **1 m spacing**, 36 geophones, 24 dB gain**Dispersion curves:**

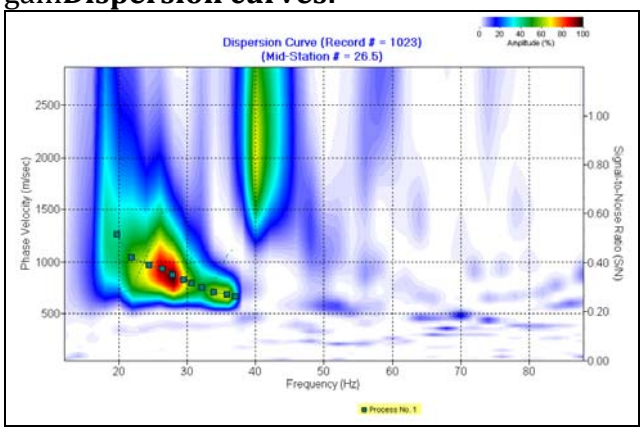

Velocity model:

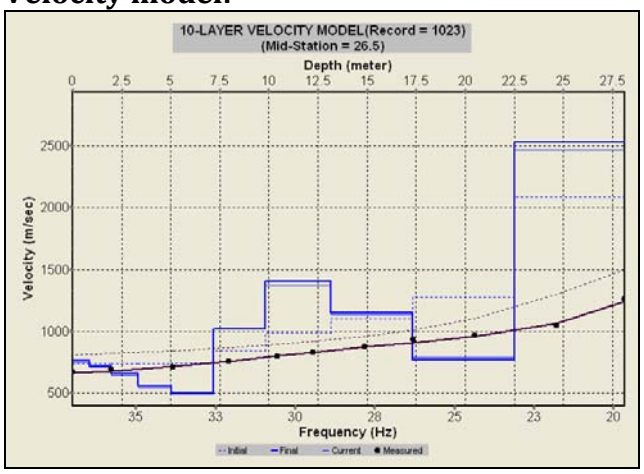

SITE NUMBER: Turitea 06(4+)

Site description: Along gravel road.

Photograph of site:

Field file numbers:

1031/1033/1034, -8 m offset, 8 stack, **1 m spacing**, 36 geophones, 24 dB gain**Dispersion curves:**

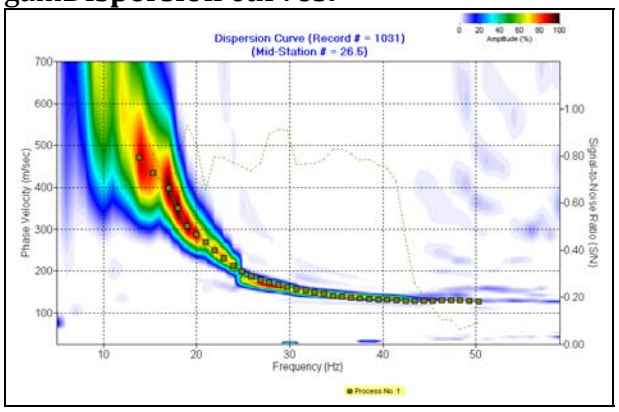

Velocity model:

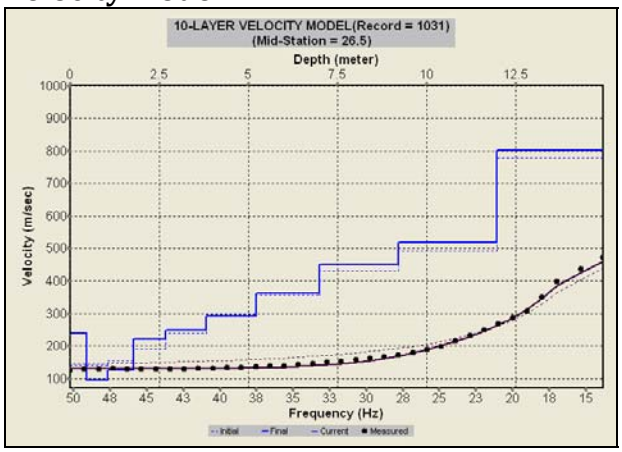

Appendix J:

Dataset Analysis: V_S Verses Depth Plots For Each Weathering Grade

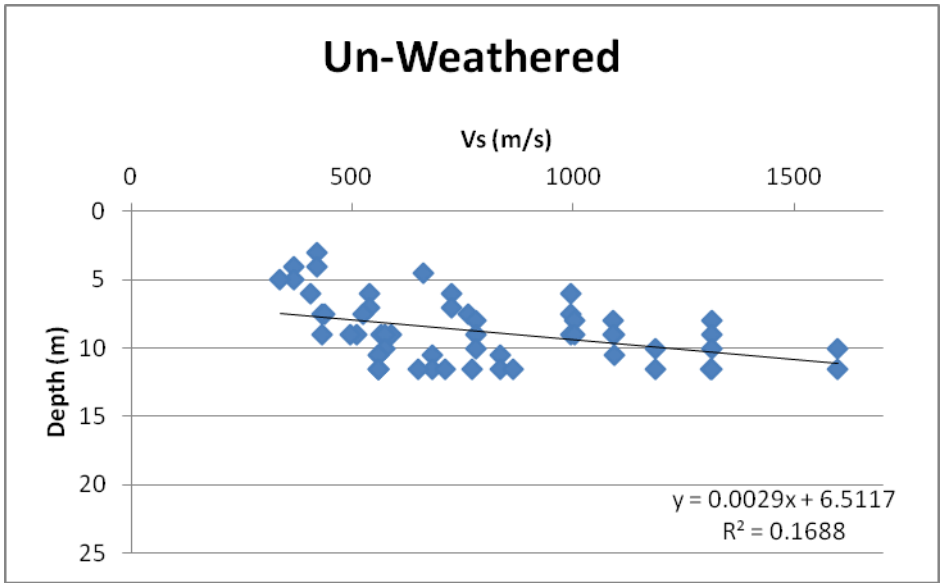
Un-Weathered
Vs (m/s)
0
500
1000
1500
Depth (m)
0
5
10
15
20
25
y = 0.0029x + 6.5117
R² = 0.1688

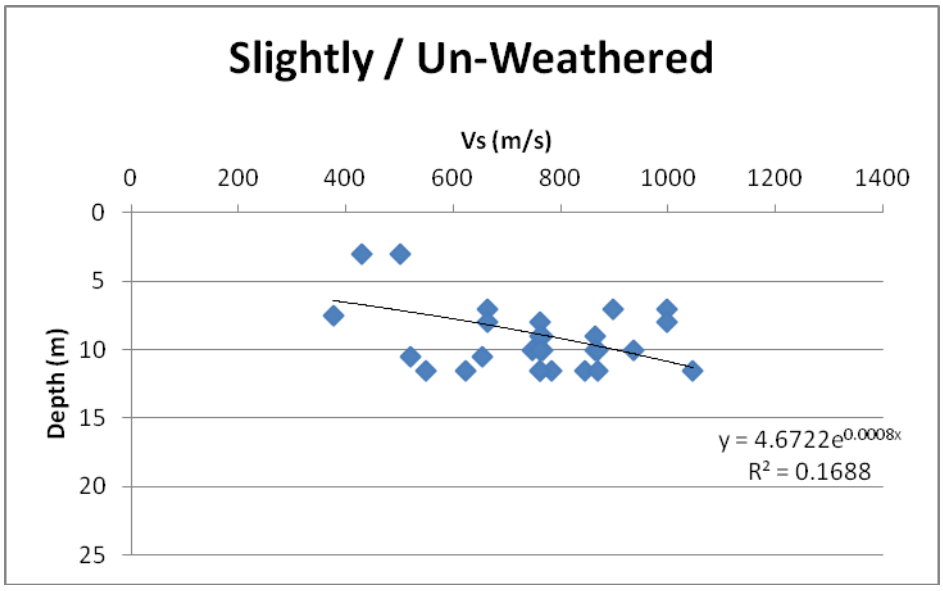
Slightly / Un-Weathered
Vs (m/s)
0
200
400
600
800
1000
1200
1400
Depth (m)
0
5
10
15
20
25
y = 4.6722e0.0008x
R² = 0.1688

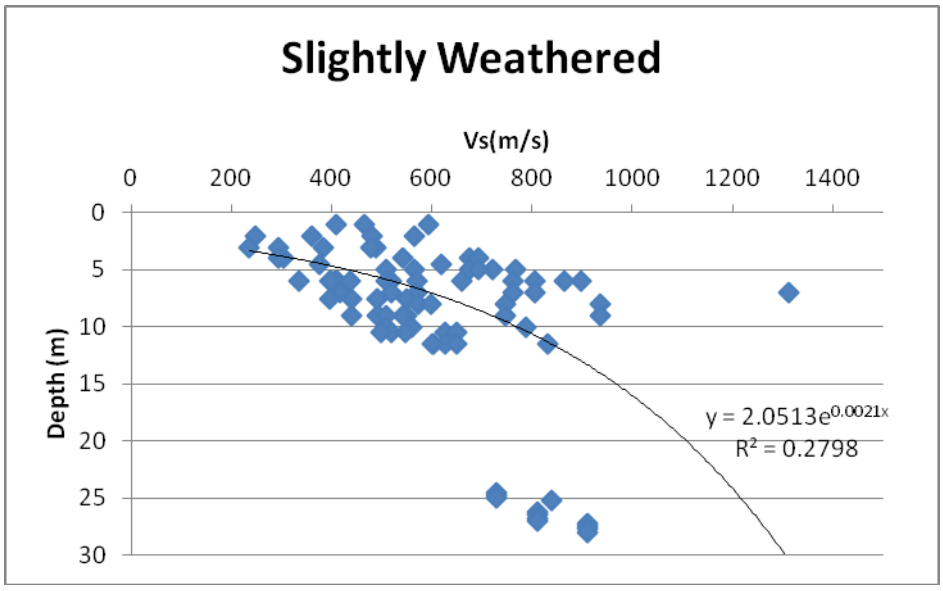
Slightly Weathered
Vs(m/s)
0
200
400
600
800
1000
1200
1400
Depth (m)
0
5
10
15
20
25
30
y = 2.0513e0.0021x
R² = 0.2798

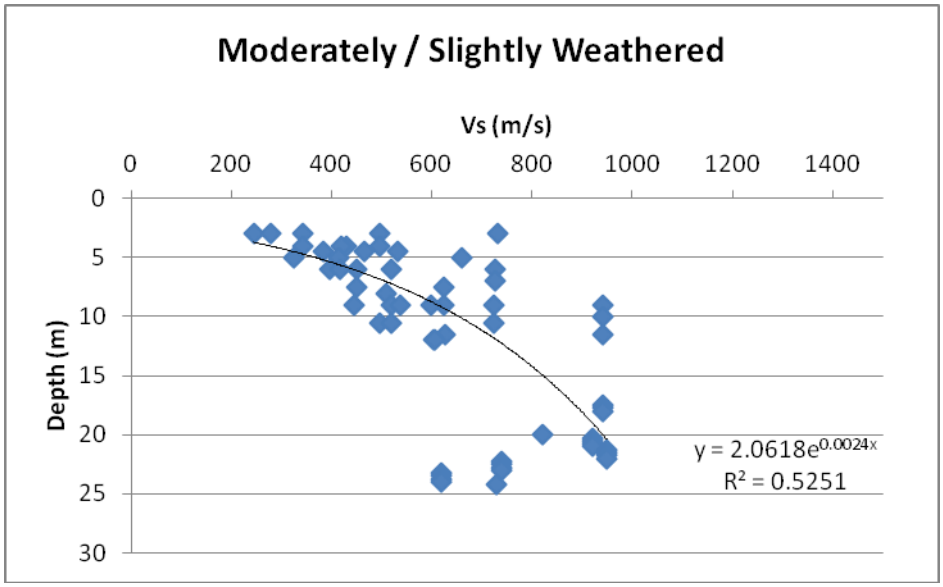
Moderately / Slightly Weathered
Vs (m/s)
0
200
400
600
800
1000
1200
1400
Depth (m)
0
5
10
15
20
25
30
y = 2.0618e0.0024x
R² = 0.5251

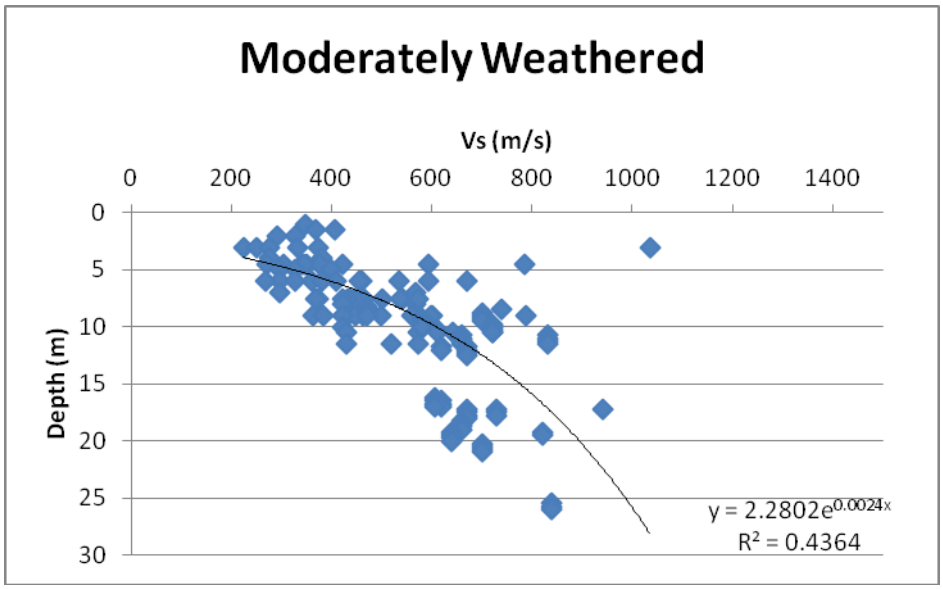
Moderately Weathered
Vs (m/s)
0
200
400
600
800
1000
1200
1400
Depth (m)
0
5
10
15
20
25
30
y = 2.2802e0.0024x
R² = 0.4364

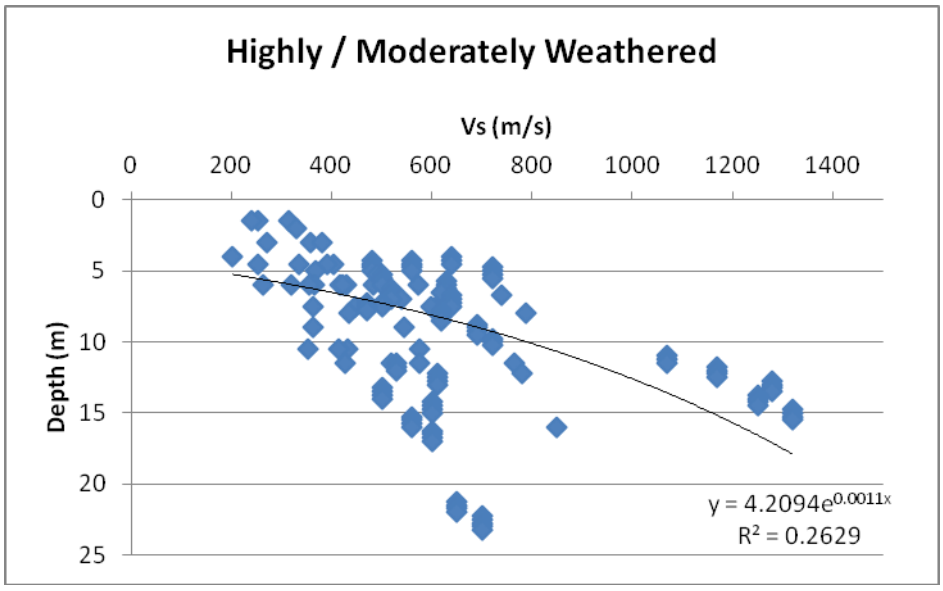
Highly / Moderately Weathered
Vs (m/s)
0
200
400
600
800
1000
1200
1400
Depth (m)
0
5
10
15
20
25
y = 4.2094e0.0011x
R² = 0.2629

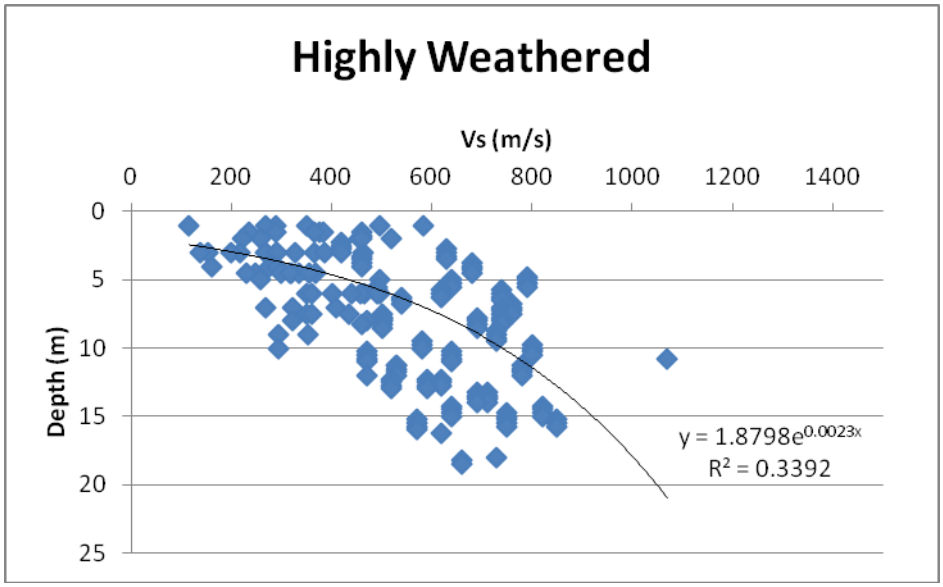
Highly Weathered
Vs (m/s)
0
200
400
600
800
1000
1200
1400
Depth (m)
0
5
10
15
20
25
y = 1.8798e0.0023x
R² = 0.3392

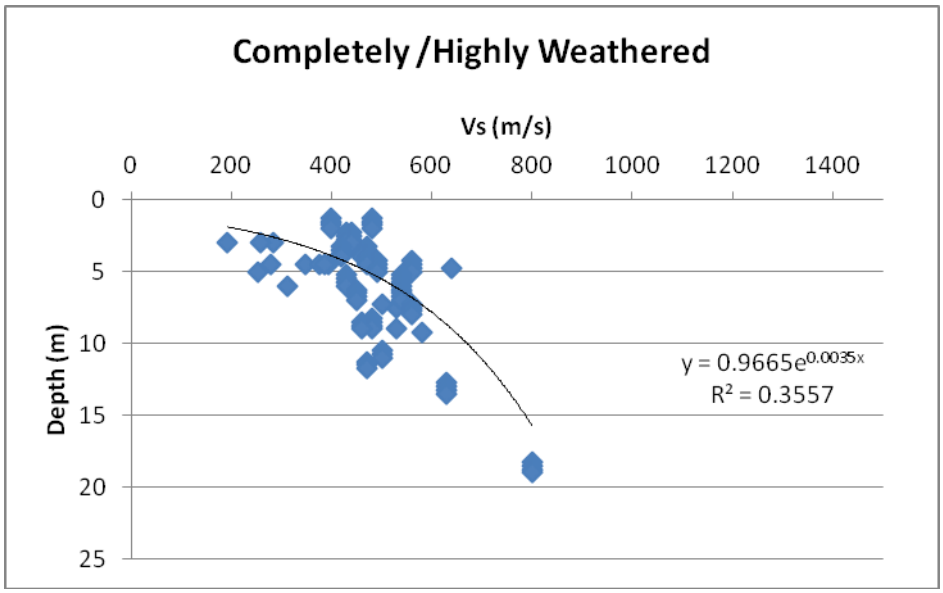
Completely /Highly Weathered
Vs (m/s)
0
200
400
600
800
1000
1200
1400
Depth (m)
0
5
10
15
20
25
y = 0.9665e0.0035x
R² = 0.3557

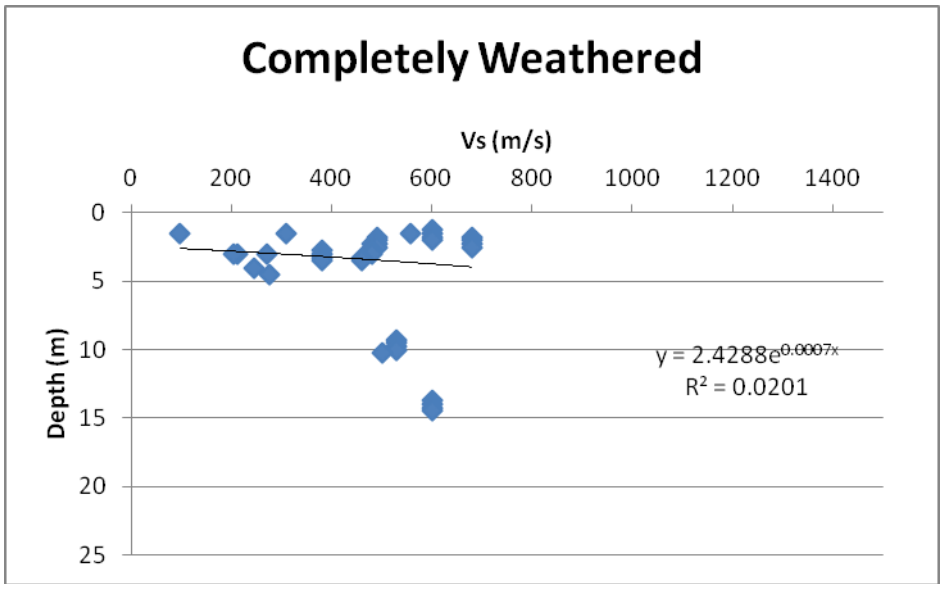
Completely Weathered
Vs (m/s)
0
200
400
600
800
1000
1200
1400
Depth (m)
0
5
10
15
20
25
y = 2.4288e0.0007x
R² = 0.0201

Appendix K:

Logarithmic Dataset Analysis

$LogV_S$ verses Depth Data Analysis:

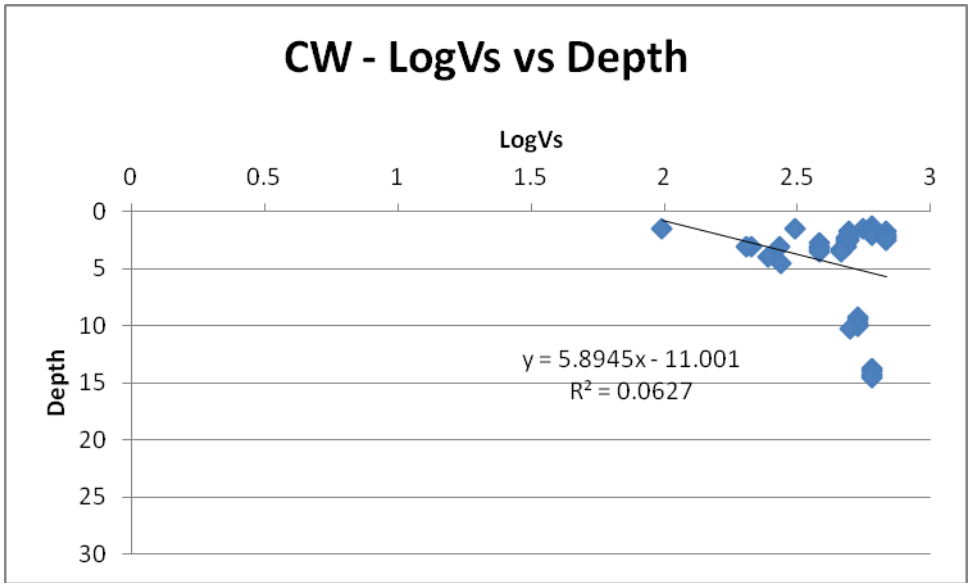

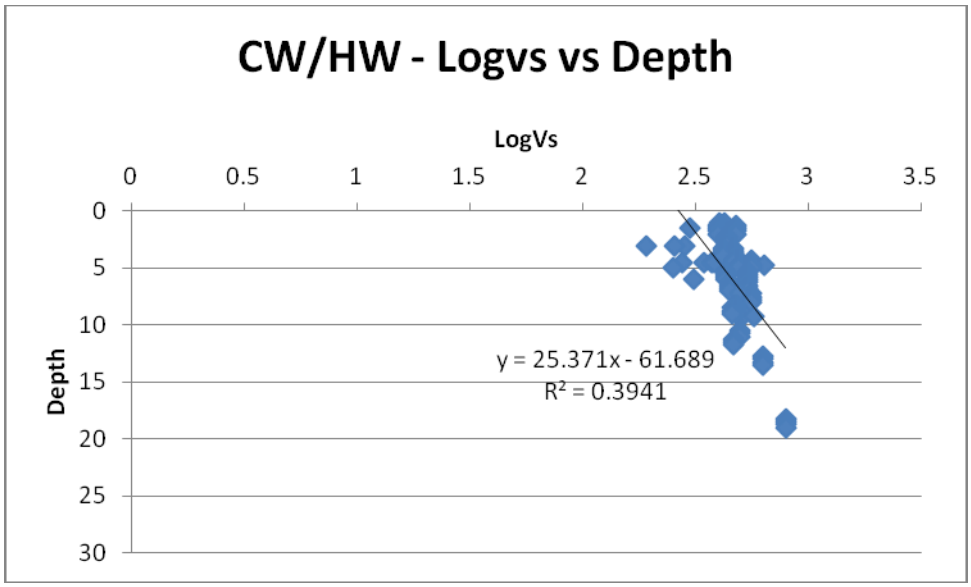

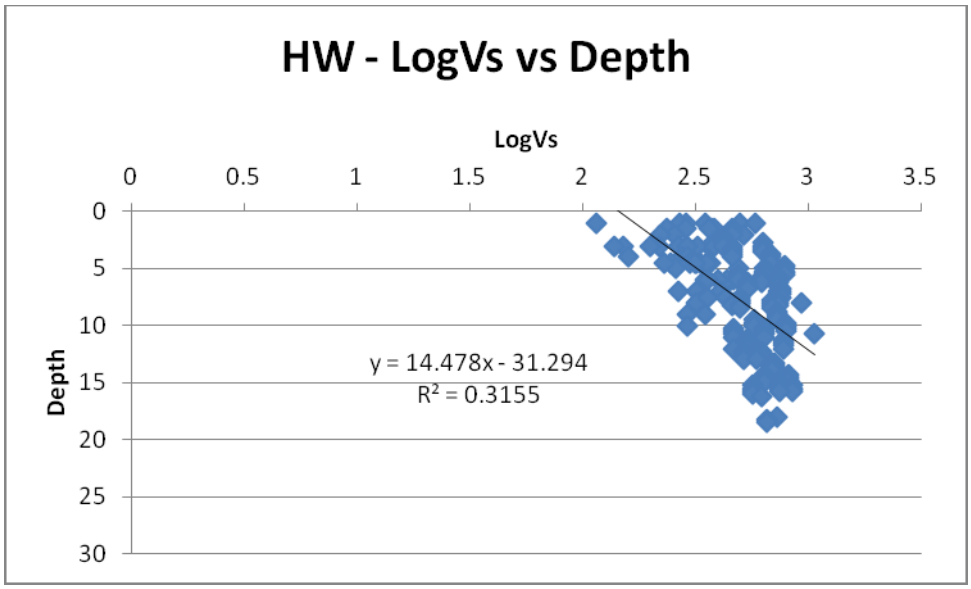

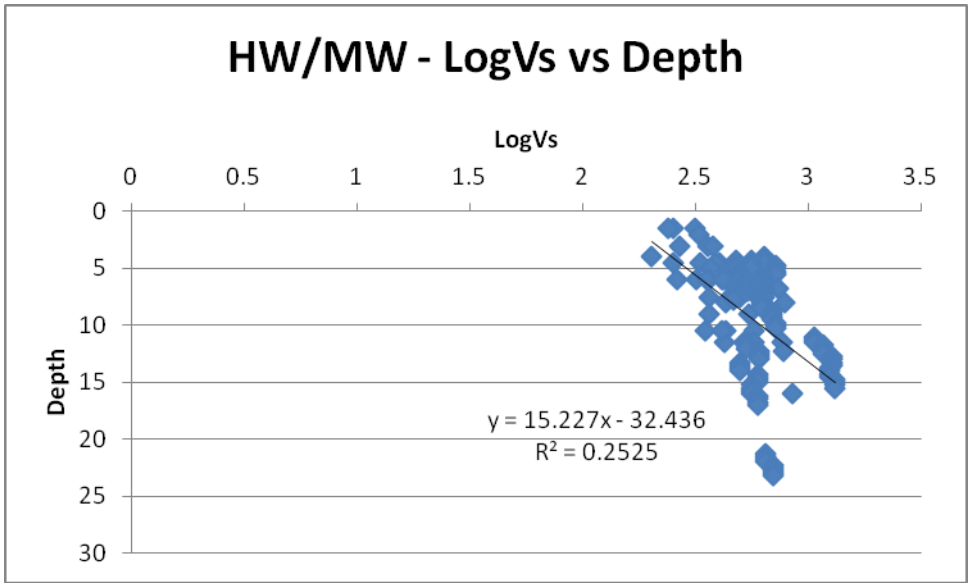
HW/MW - LogVs vs Depth
LogVs
0
0.5
1
1.5
2
2.5
3
3.5
Depth
0
5
10
15
20
25
30
y = 15.227x - 32.436
R² = 0.2525

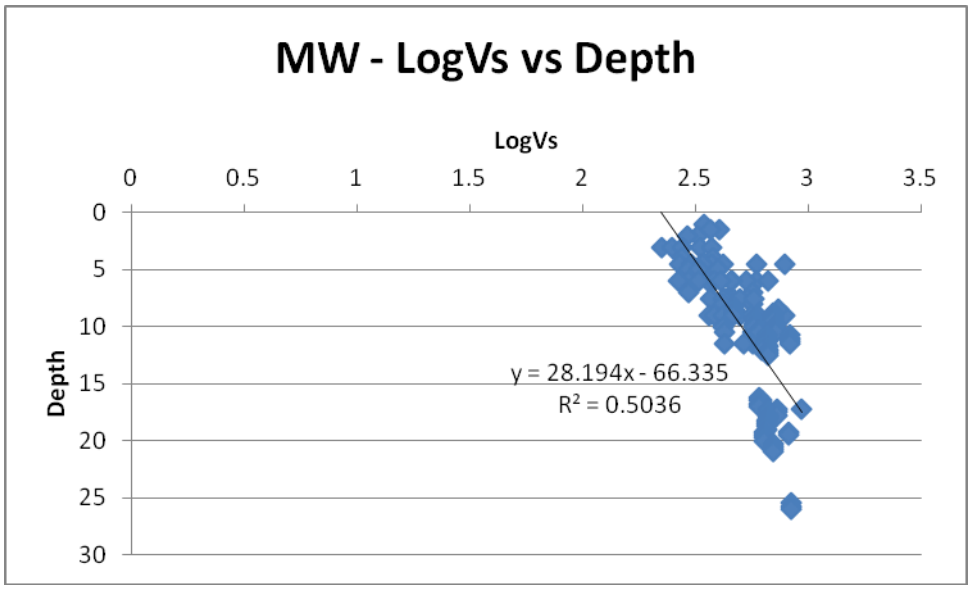
MW - LogVs vs Depth
LogVs
0
0.5
1
1.5
2
2.5
3
3.5
Depth
0
5
10
15
20
25
30
y = 28.194x - 66.335
R² = 0.5036

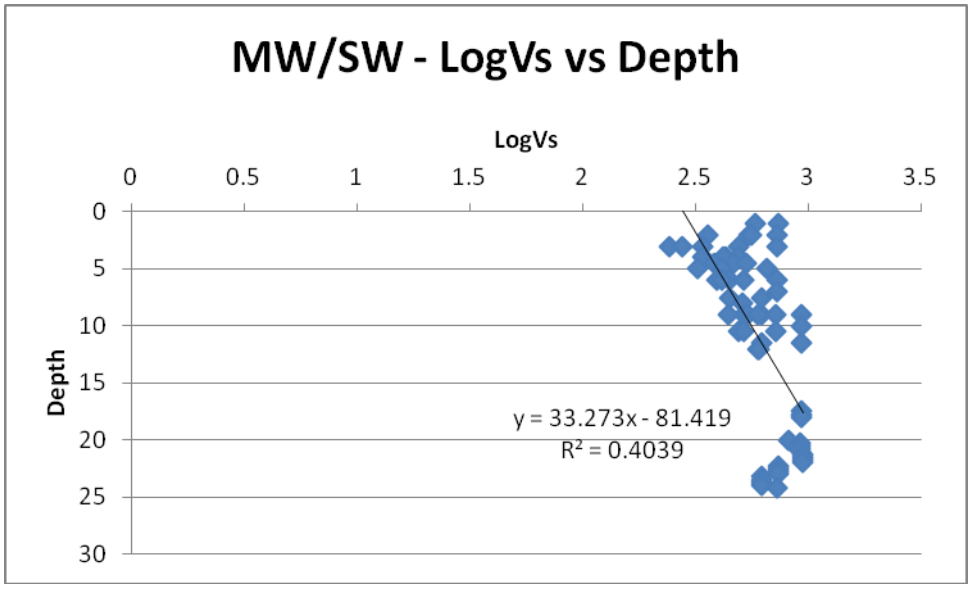
MW/SW - LogVs vs Depth
LogVs
0
0.5
1
1.5
2
2.5
3
3.5
Depth
0
5
10
15
20
25
30
y = 33.273x - 81.419
R² = 0.4039

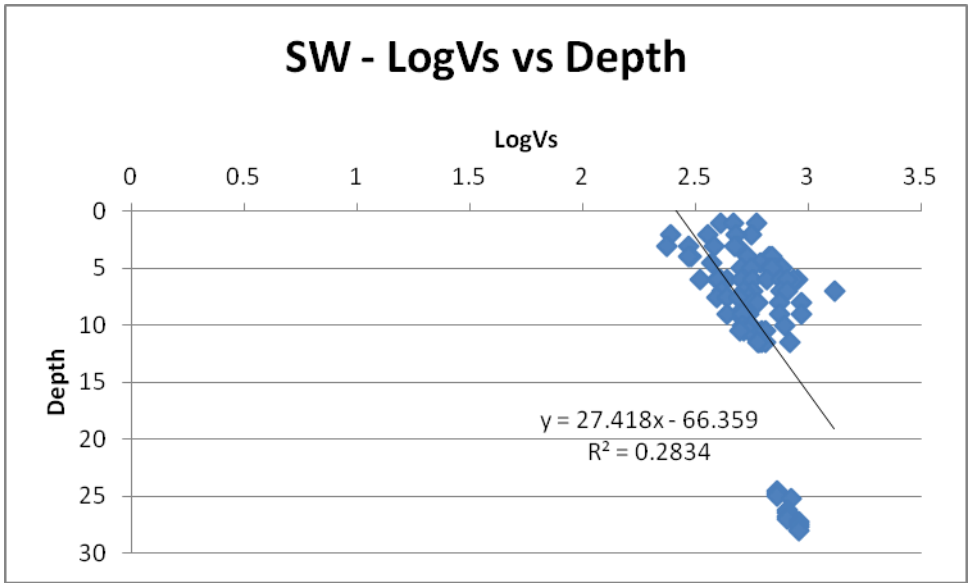
SW - LogVs vs Depth
LogVs
0
0.5
1
1.5
2
2.5
3
3.5
Depth
0
5
10
15
20
25
30
y = 27.418x - 66.359
R² = 0.2834

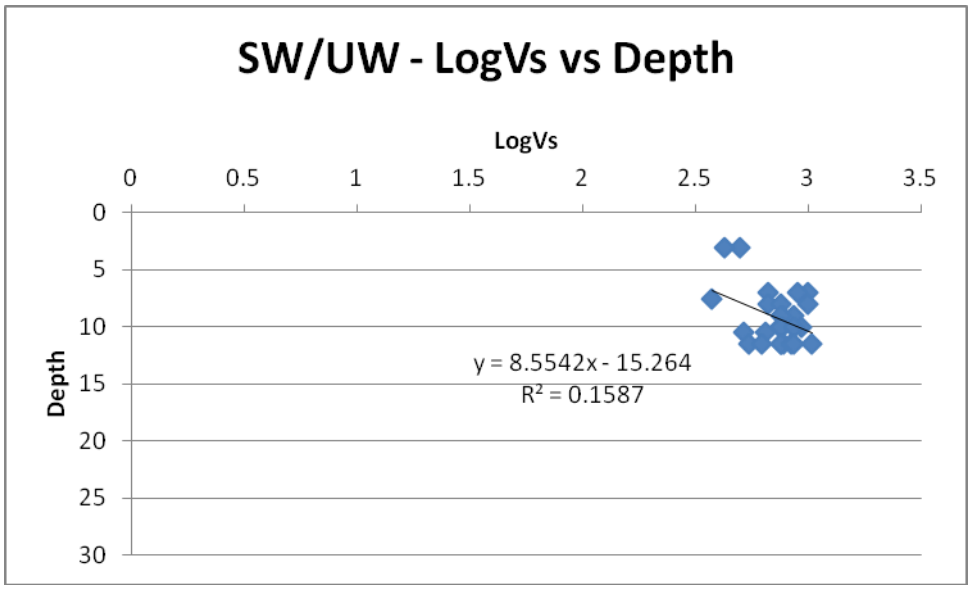
SW/UW - LogVs vs Depth
LogVs
0
0.5
1
1.5
2
2.5
3
3.5
Depth
0
5
10
15
20
25
30
y = 8.5542x - 15.264
R² = 0.1587

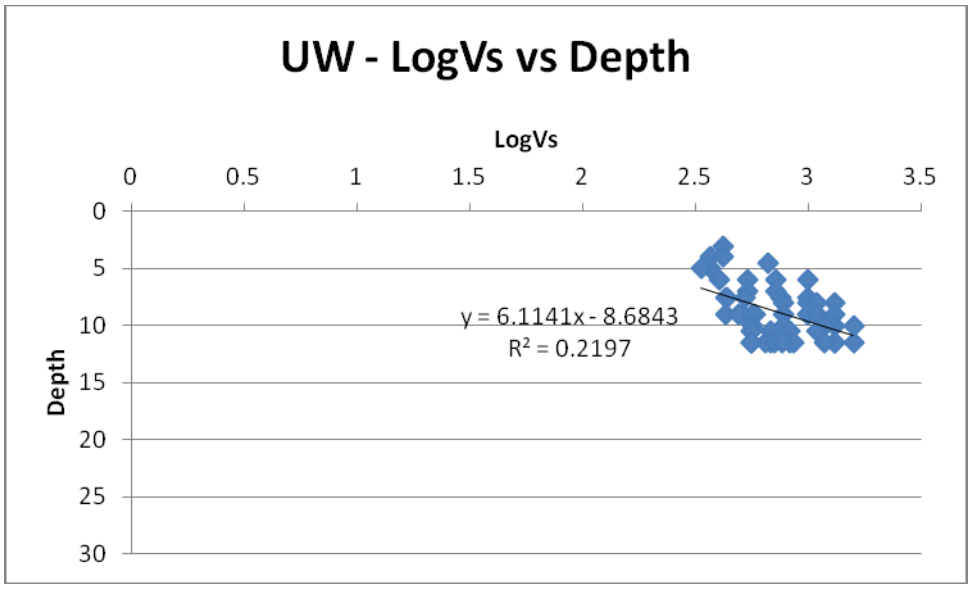
UW - LogVs vs Depth
LogVs
0
0.5
1
1.5
2
2.5
3
3.5
Depth
0
5
10
15
20
25
30
y = 6.1141x - 8.6843
R² = 0.2197

V_S verses LogDepth Data Analysis:

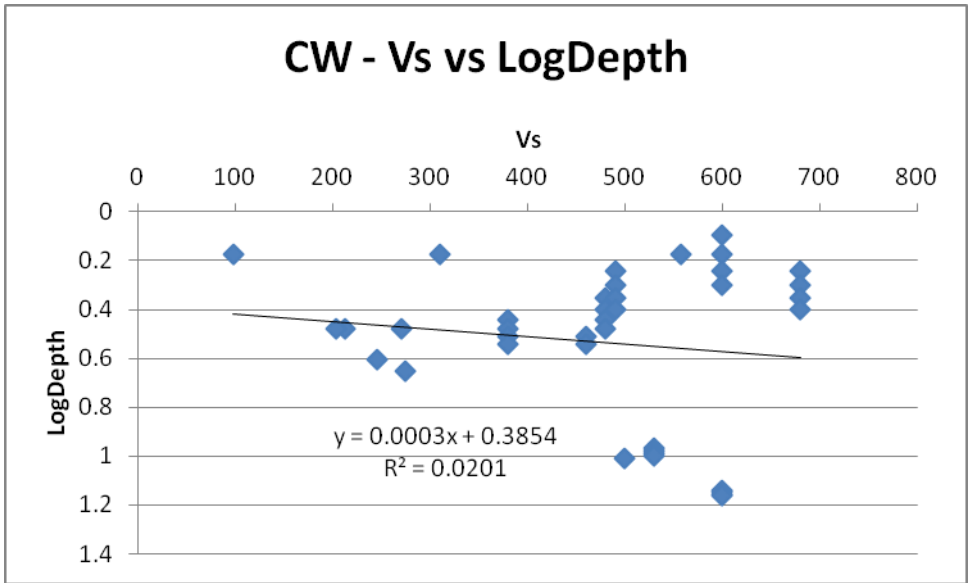

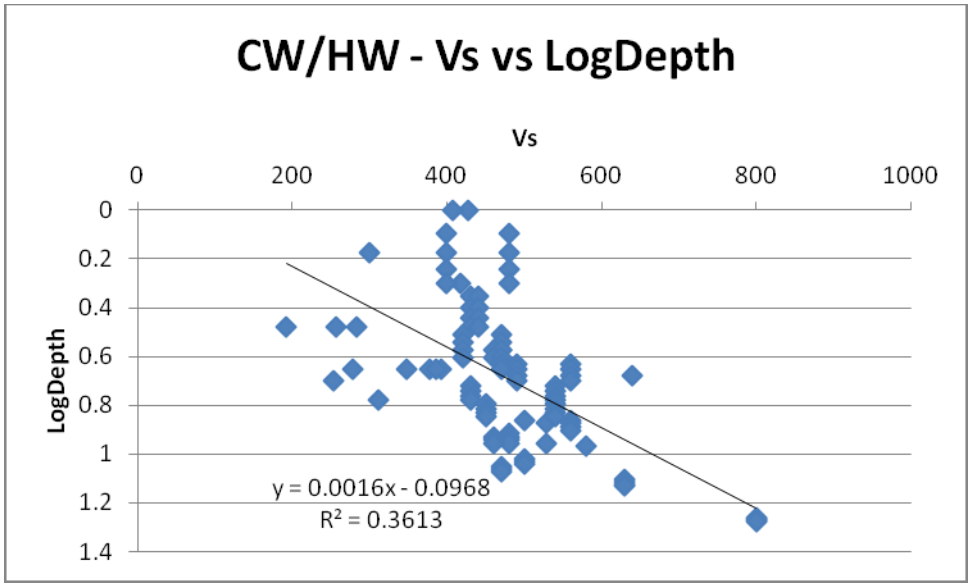

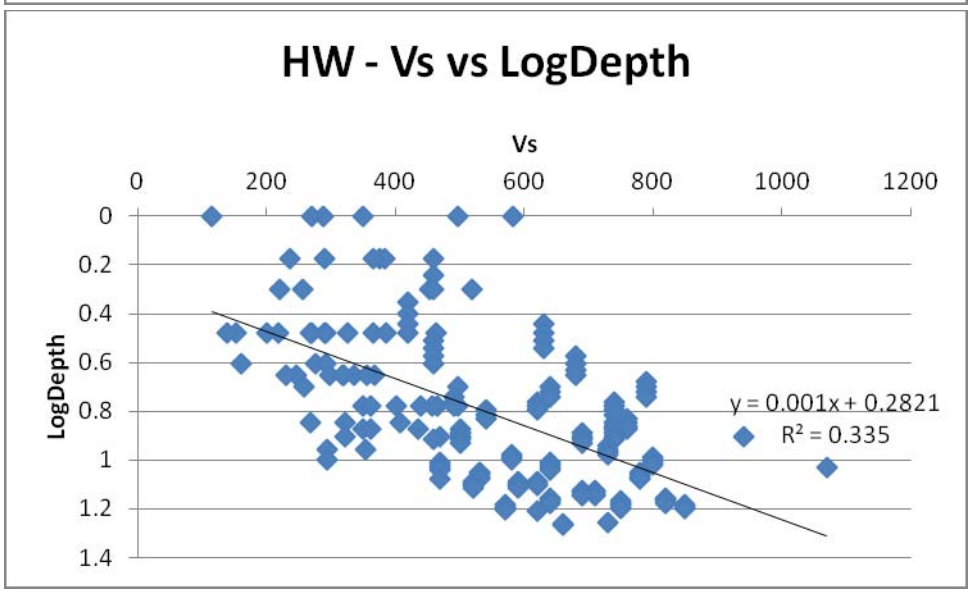

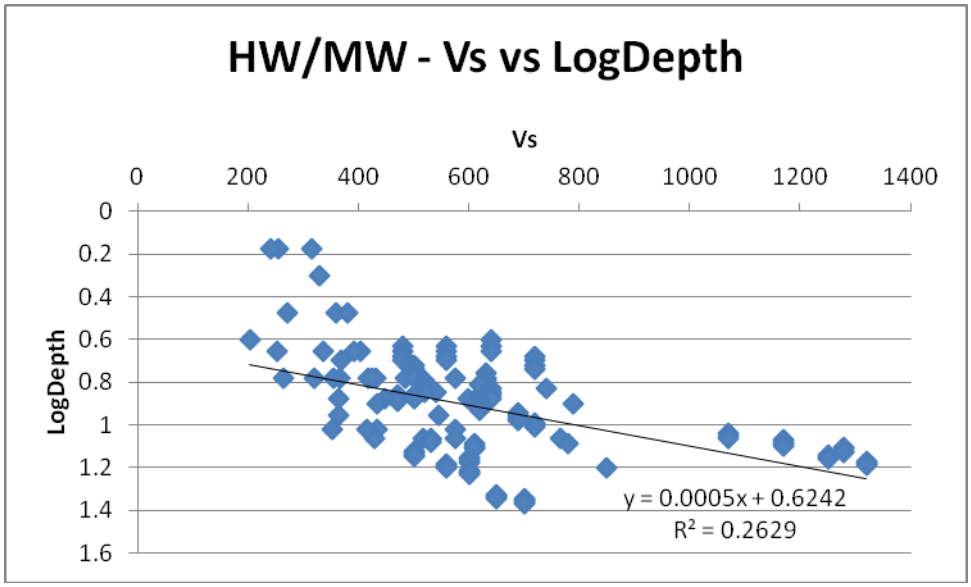
HW/MW - Vs vs LogDepth
Vs
0
200
400
600
800
1000
1200
1400
LogDepth
0
0.2
0.4
0.6
0.8
1
1.2
1.4
1.6
y = 0.0005x + 0.6242
R² = 0.2629

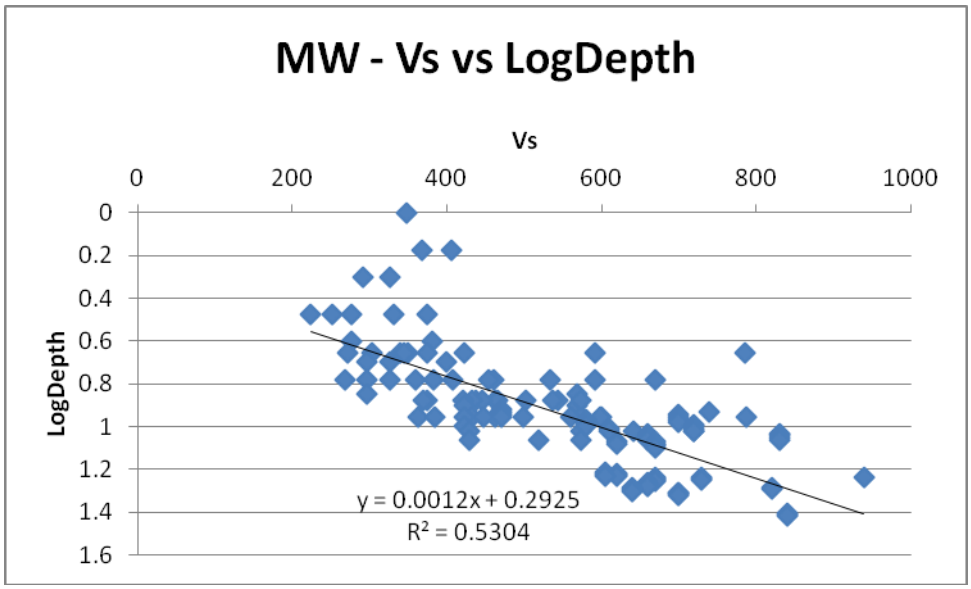
MW - Vs vs LogDepth
Vs
0
200
400
600
800
1000
LogDepth
0
0.2
0.4
0.6
0.8
1
1.2
1.4
1.6
y = 0.0012x + 0.2925
R² = 0.5304

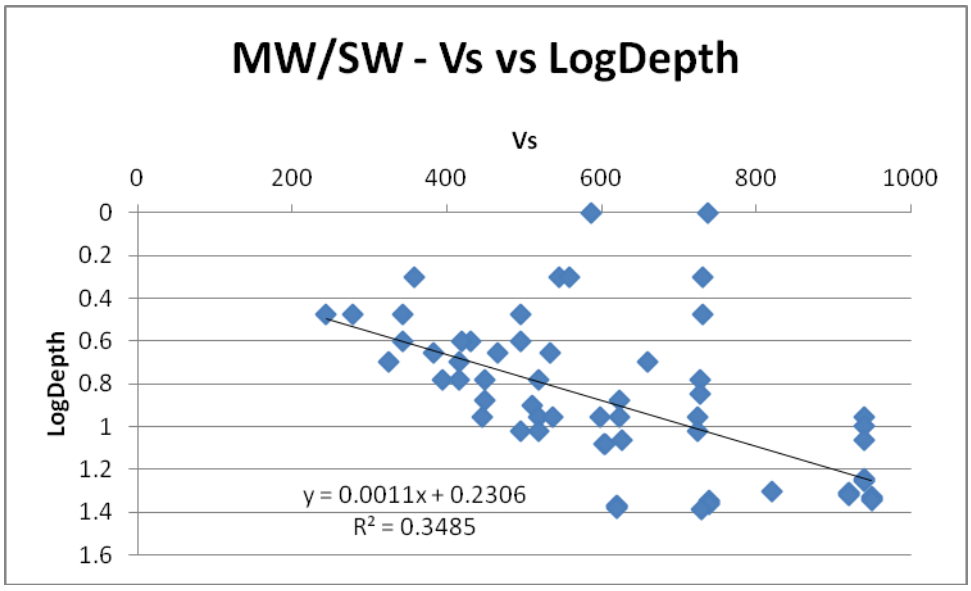
MW/SW - Vs vs LogDepth
Vs
0
200
400
600
800
1000
LogDepth
0
0.2
0.4
0.6
0.8
1
1.2
1.4
1.6
y = 0.0011x + 0.2306
R² = 0.3485

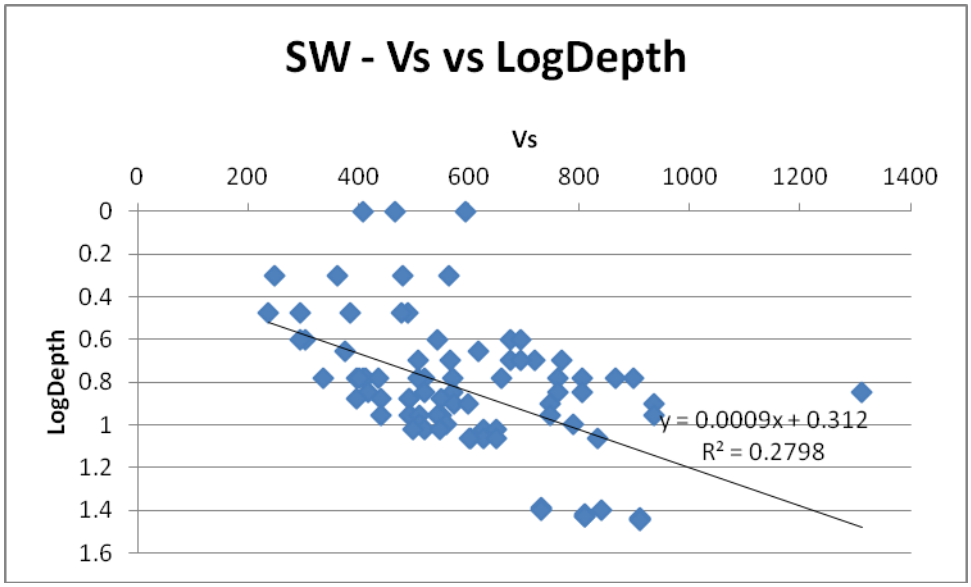
SW - Vs vs LogDepth
Vs
0
200
400
600
800
1000
1200
1400
LogDepth
0
0.2
0.4
0.6
0.8
1
1.2
1.4
1.6
y = 0.0009x + 0.312
R² = 0.2798

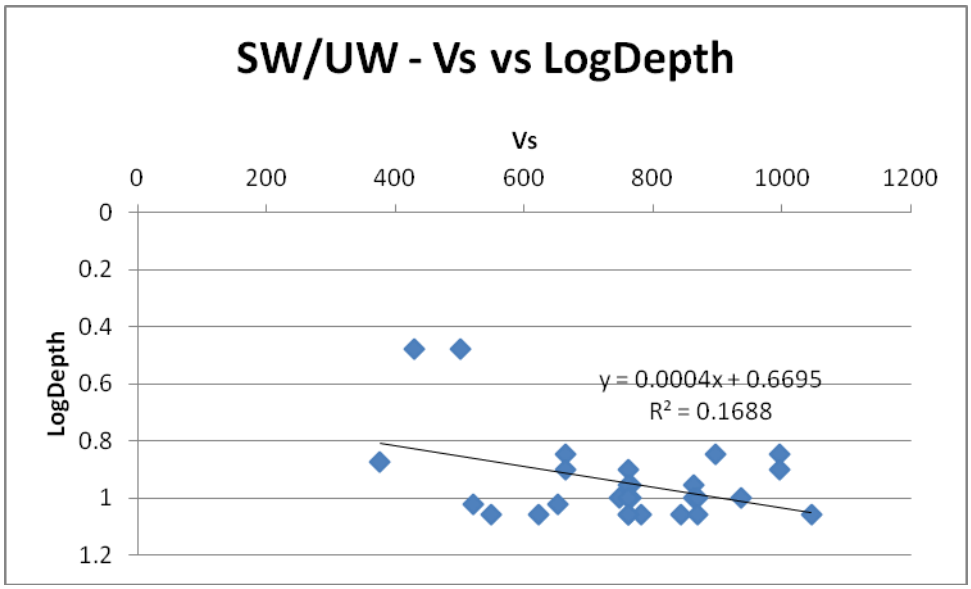
SW/UW - Vs vs LogDepth
Vs
0
200
400
600
800
1000
1200
LogDepth
0
0.2
0.4
0.6
0.8
1
1.2
y = 0.0004x + 0.6695
R² = 0.1688

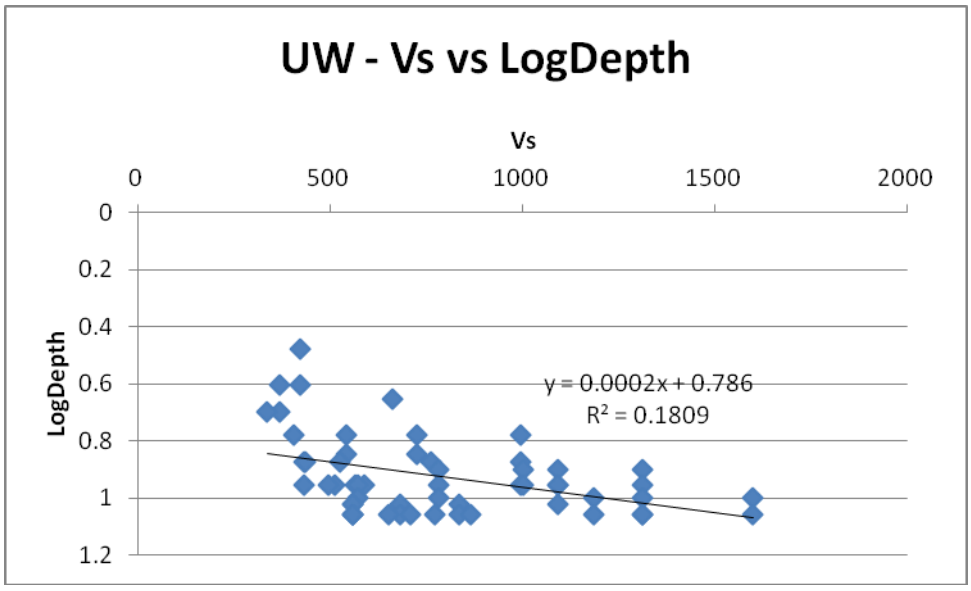
UW - Vs vs LogDepth
Vs
0
500
1000
1500
2000
LogDepth
0
0.2
0.4
0.6
0.8
1
1.2
y = 0.0002x + 0.786
R² = 0.1809

$LogV_S$ verses LogDepth Data Analysis:

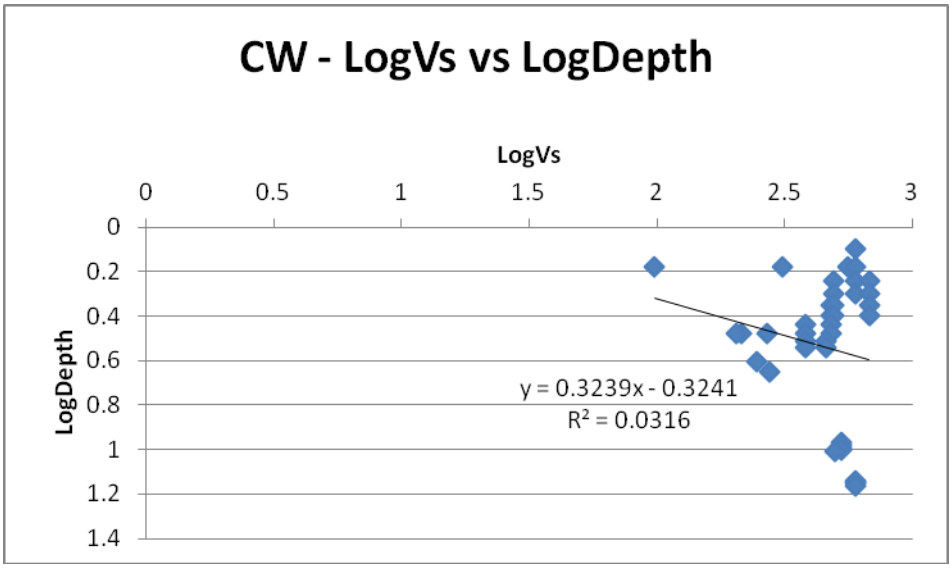

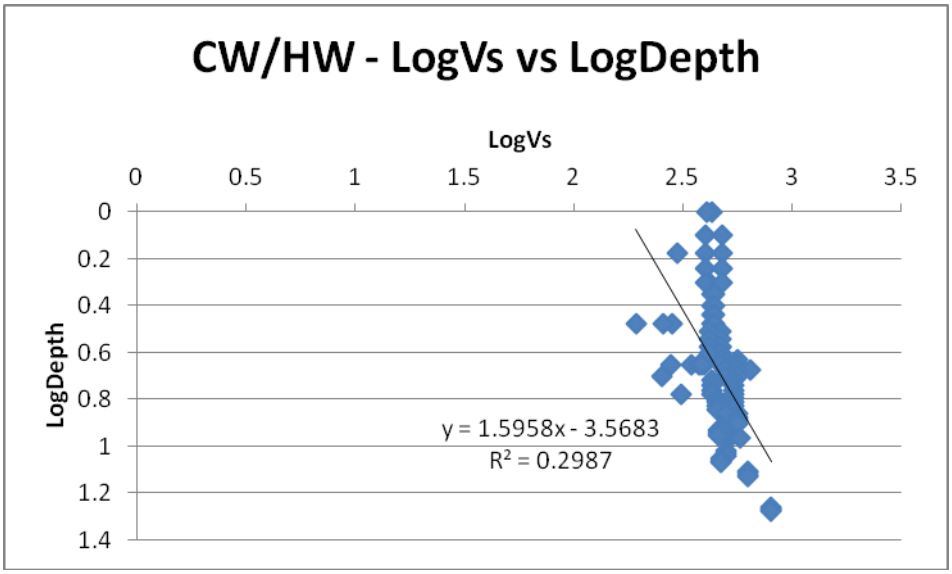

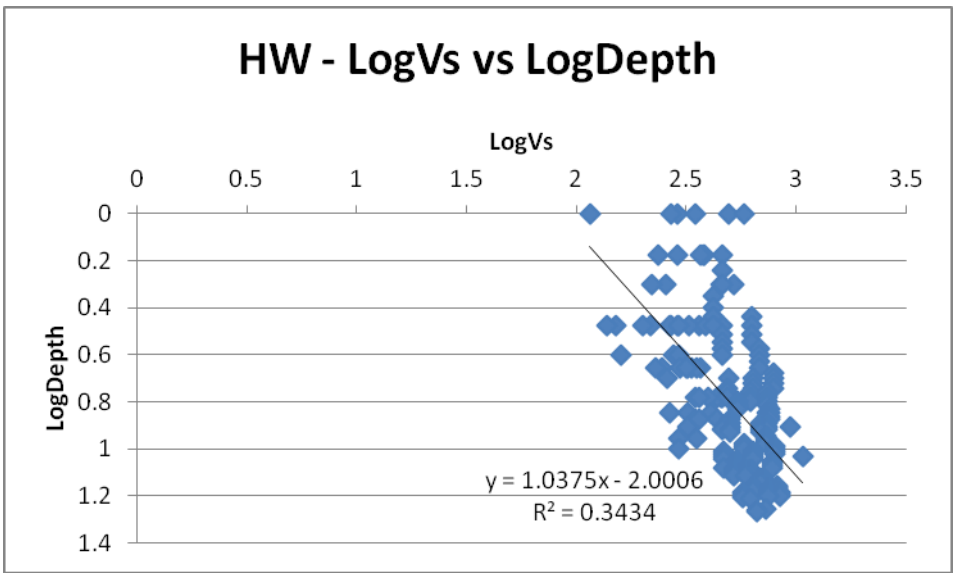

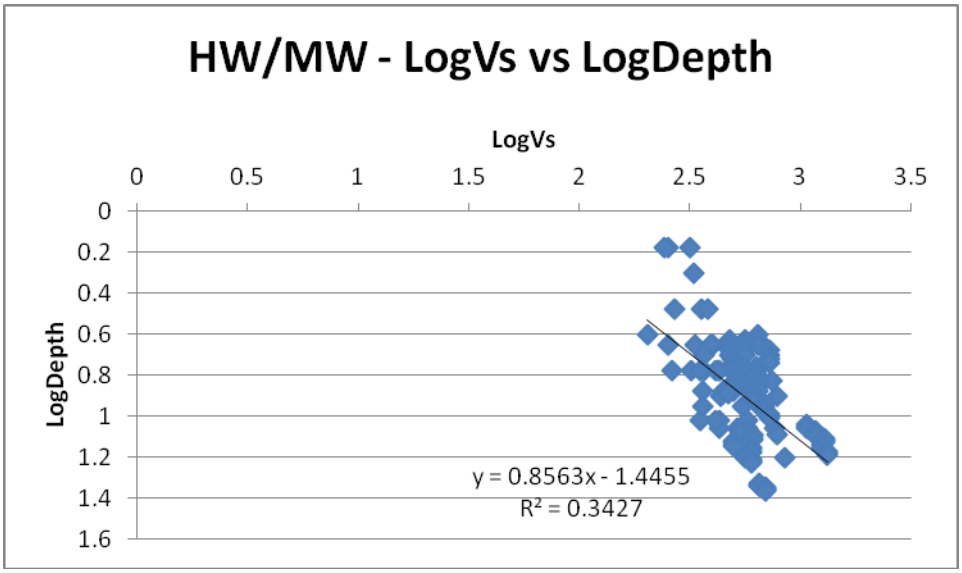
HW/MW - LogVs vs LogDepth
LogVs
0
0.5
1
1.5
2
2.5
3
3.5
LogDepth
0
0.2
0.4
0.6
0.8
1
1.2
1.4
1.6
y = 0.8563x - 1.4455
R² = 0.3427

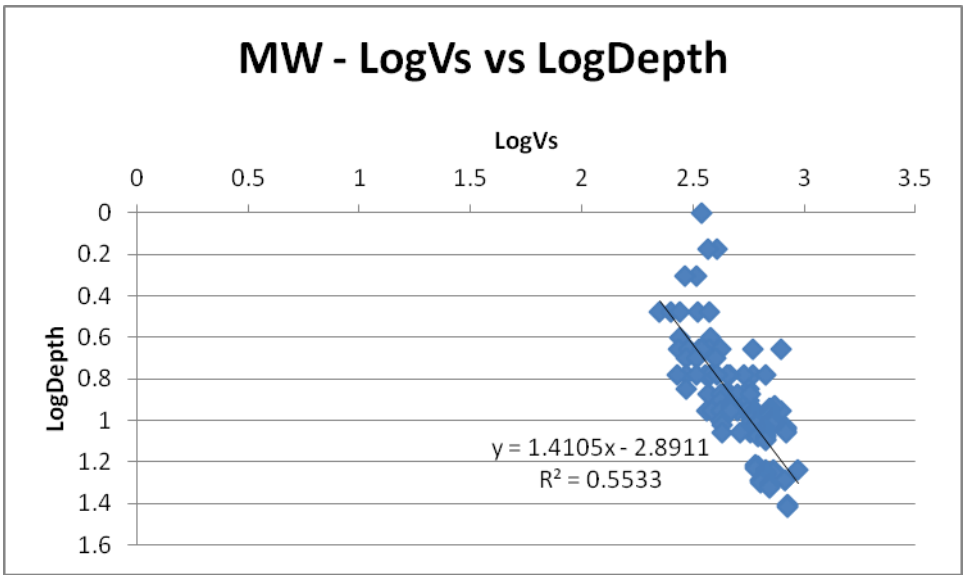
MW - LogVs vs LogDepth
LogVs
0
0.5
1
1.5
2
2.5
3
3.5
LogDepth
0
0.2
0.4
0.6
0.8
1
1.2
1.4
1.6
y = 1.4105x - 2.8911
R² = 0.5533

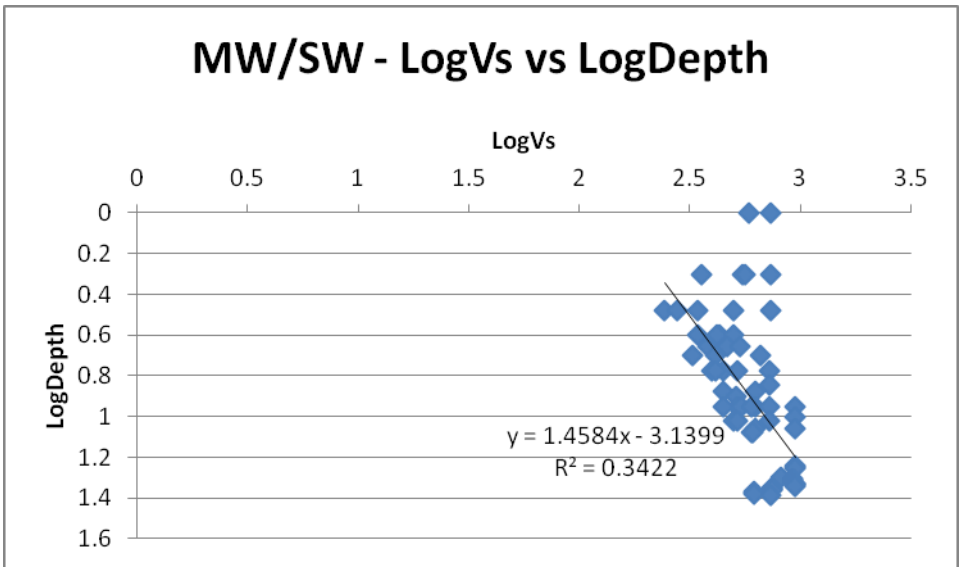
MW/SW - LogVs vs LogDepth
LogVs
0
0.5
1
1.5
2
2.5
3
3.5
LogDepth
0
0.2
0.4
0.6
0.8
1
1.2
1.4
1.6
y = 1.4584x - 3.1399
R² = 0.3422

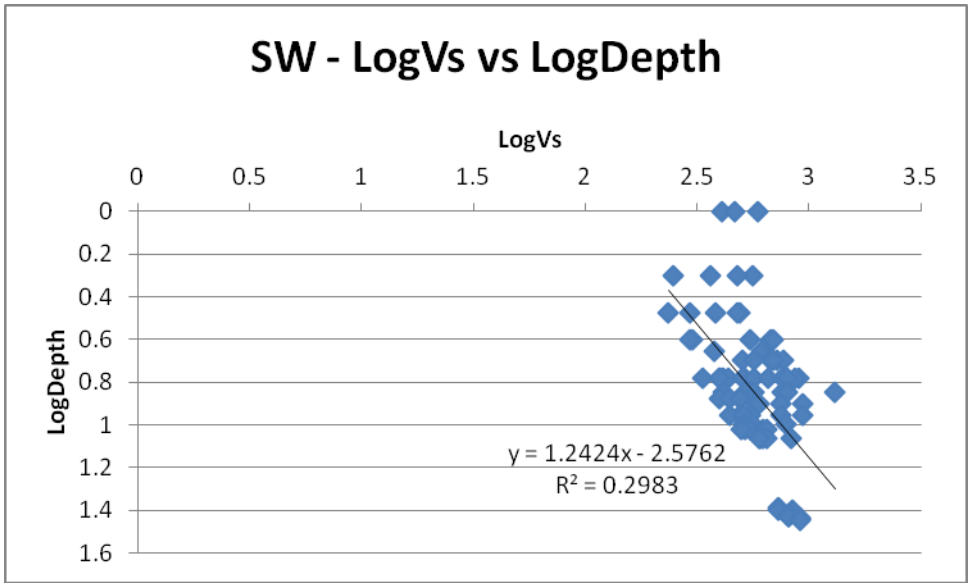
SW - LogVs vs LogDepth
LogVs
0
0.5
1
1.5
2
2.5
3
3.5
LogDepth
0
0.2
0.4
0.6
0.8
1
1.2
1.4
1.6
y = 1.2424x - 2.5762
R² = 0.2983

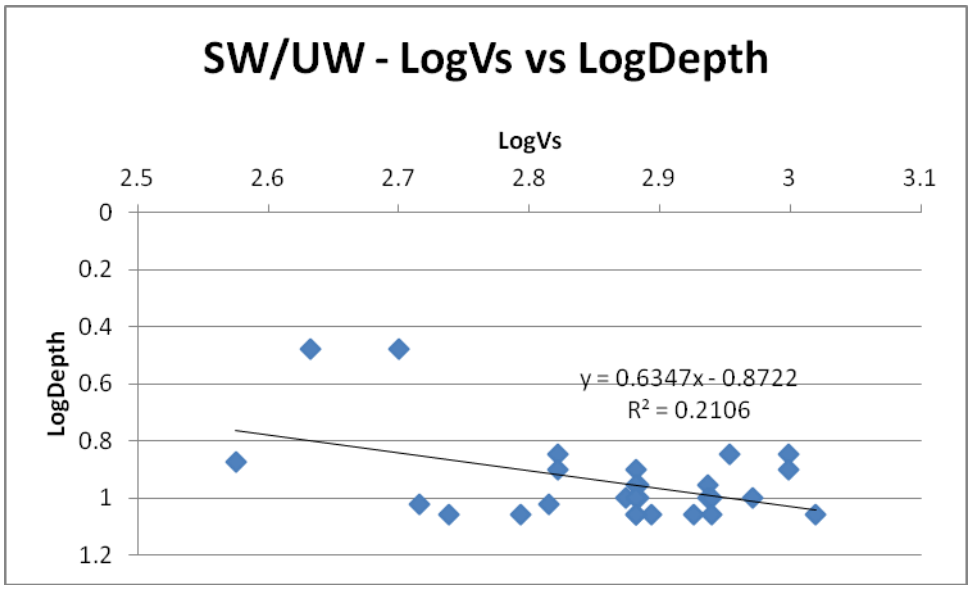
SW/UW - LogVs vs LogDepth
LogVs
2.5
2.6
2.7
2.8
2.9
3
3.1
LogDepth
0
0.2
0.4
0.6
0.8
1
1.2
y = 0.6347x - 0.8722
R² = 0.2106

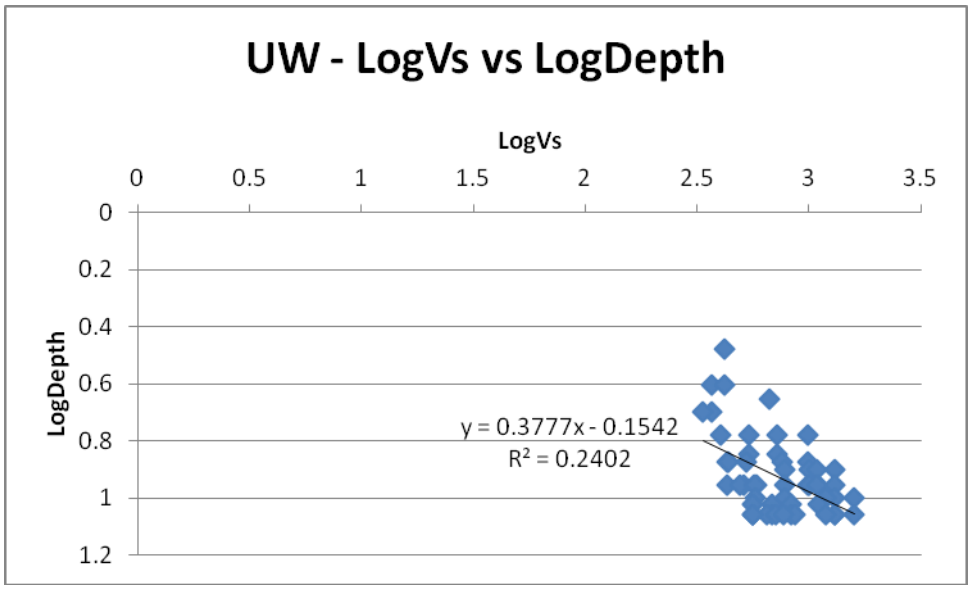
UW - LogVs vs LogDepth
LogVs
0
0.5
1
1.5
2
2.5
3
3.5
LogDepth
0
0.2
0.4
0.6
0.8
1
1.2
y = 0.3777x - 0.1542
R² = 0.2402

Appendix L:

Multi Variant Non-Linear Regression Analysis

The statistical analysis programme, R, was used to analyse the data set, and procedures and methodology are detailed in (Crawley, 2007). The entire dataset of V_S, depth and weathering grade data was converted to text file and imported into R. The data was analysed in a 3D format, effectively fitting the data to a non-linear 3D surface. This was performed using a linear model, or 'lm', along with a 'log' function applied to the V_S data. Using this combination of modelling functions, the data is effectively analysed as a non-linear multi variant model.

The input script used in R was:

- m1<-lm(log(Vs)~Depth+Weathering+factor(Turbine))

This analysis produced the following summary of results:

- summary(m1)

Call:
lm(formula = log(Vs) ~ Depth + Weathering + factor(Turbine))

Residuals:

Min	1Q	Median	3Q	Max
-0.97	-0.12	0.02	0.16	0.77

Coefficients:

	Estimate	Std. Error	t value	Pr(>|t|)
(Intercept)	5.771	0.130	44.331	< 2e-16 ***
Depth	0.077	0.007	11.902	< 2e-16 ***
Weathering	-0.035	0.011	-3.210	0.001 **
factor(Turbine)17	0.107	0.146	0.732	0.465
factor(Turbine)203	0.095	0.137	0.687	0.492
factor(Turbine)204	0.290	0.137	2.122	0.034 *
factor(Turbine)205	0.446	0.139	3.205	0.001 **
factor(Turbine)208	0.181	0.137	1.321	0.187
factor(Turbine)209	0.331	0.137	2.408	0.017 *
factor(Turbine)210	0.480	0.137	3.498	0.001 ***
factor(Turbine)211	0.551	0.137	4.024	6.89e-05 ***

factor(Turbine)212	0.345	0.138	2.494	0.013 *
factor(Turbine)213	0.206	0.140	1.475	0.141
factor(Turbine)214	-0.203	0.143	-1.423	0.156
factor(Turbine)219	-0.211	0.139	-1.521	0.129
factor(Turbine)232	0.108	0.138	0.778	0.437
factor(Turbine)234	-0.450	0.152	-2.959	0.003 **
factor(Turbine)238	0.133	0.137	0.971	0.332
factor(Turbine)240	0.241	0.137	1.761	0.079
factor(Turbine)242	0.020	0.139	0.141	0.888
factor(Turbine)243	-0.072	0.138	-0.518	0.605
factor(Turbine)244	-0.052	0.138	-0.376	0.707
factor(Turbine)30	-0.133	0.152	-0.877	0.381
factor(Turbine)32	-0.087	0.147	-0.591	0.555
factor(Turbine)33	-0.143	0.148	-0.963	0.336
factor(Turbine)35	-0.327	0.164	-1.989	0.047*
factor(Turbine)37	0.442	0.167	2.642	0.009 **
factor(Turbine)46	-0.241	0.160	-1.504	0.133
factor(Turbine)47	-0.283	0.160	-1.774	0.077
factor(Turbine)49	-0.030	0.147	-0.202	0.840
factor(Turbine)50	-0.134	0.146	-0.920	0.359
factor(Turbine)51	-0.078	0.148	-0.528	0.598
factor(Turbine)54	0.340	0.146	2.332	0.020 *
factor(Turbine)55	-0.203	0.147	-1.381	0.168
factor(Turbine)58	-0.034	0.156	-0.216	0.829
factor(Turbine)59	-0.057	0.156	-0.367	0.714
factor(Turbine)7	-0.250	0.156	-1.601	0.110
factor(Turbine)72	0.291	0.146	1.992	0.047 *

factor(Turbine)73	-0.092	0.148	-0.624	0.533
factor(Turbine)74	-0.349	0.153	-2.272	0.024 *
factor(Turbine)75	-0.251	0.152	-1.650	0.100
factor(Turbine)76	-0.278	0.158	-1.755	0.080
factor(Turbine)77	0.019	0.168	0.115	0.909
factor(Turbine)78	-0.255	0.156	-1.638	0.102
factor(Turbine)79	0.025	0.155	0.163	0.870
factor(Turbine)8	-0.116	0.163	-0.711	0.477
factor(Turbine)84	-0.063	0.163	-0.388	0.699
factor(Turbine)85	-0.293	0.165	-1.773	0.077
factor(Turbine)86	-0.198	0.151	-1.306	0.192
factor(Turbine)87	-0.133	0.148	-0.898	0.370
factor(Turbine)88	0.021	0.148	0.144	0.885
factor(Turbine)97	-0.118	0.151	-0.779	0.436
factor(Turbine)T-BH5	0.058	0.191	0.306	0.760
factor(Turbine)T-BH6	-0.367	0.152	-2.418	0.016 *
factor(Turbine)WW-K04	0.005	0.149	0.036	0.972

Signif. codes:	0 '***' 0.001 '**' 0.01 '*' 0.05 '.' 0.1 ' ' 1
Residual standard error:	0.27 on 383 degrees of freedom
Multiple R-squared:	0.74
Adjusted R-squared:	0.70
F-statistic:	19.8 on 54 and 383 DF
p-value:	< 2.2e-16